

Zentrum für Molekulare Biologie  
der Ruprecht-Karls-Universität Heidelberg

**Genome-wide analysis  
of C99-overexpressing human neuroblastoma cells:  
Effects of C99 cleavage products on gene  
expression, signal transduction and  
phosphorylation status**

**Dissertation**

submitted to the

**Combined Faculties for the Natural Sciences  
and for Mathematics of the University of Heidelberg,  
Germany**

for the degree of

**Doctor of Natural Sciences**

presented by  
Markus Uhrig

# **Dissertation**

## **Genome-wide analysis of C99-overexpressing human neuroblastoma cells: Effects of C99 cleavage products on gene expression, signal transduction and phosphorylation status**

submitted to the

**Combined Faculties for the Natural Sciences  
and for Mathematics of the Ruperto-Carola  
University of Heidelberg,  
Germany**

for the degree of

**Doctor of Natural Sciences (Dr. rer. nat.)**

presented by

Diplom-Humanbiologe Markus Uhrig  
born in: Stuttgart, Germany  
oral examination: .....

This thesis was researched and written at the Center for Molecular Biology of the  
University of Heidelberg (ZMBH) and supervised by  
Prof. Dr. Tobias Hartmann

Referees: Prof. Dr. rer. nat. Dr. h. c. Konrad Beyreuther  
Center for Molecular Biology of the  
University of Heidelberg (ZMBH)  
Heidelberg, Germany

Prof. Dr. rer. nat. Tobias Hartmann  
Institute for Neurobiology and Neurodegeneration  
Department of Neurology  
Saarland University,  
Homburg/Saar, Germany

***Es ist nicht genug zu wissen,***

***man muss auch anwenden;***

***Es ist nicht genug zu wollen,***

***man muss auch tun.***

(Johann Wolfgang von Goethe, 1749-1832)

***To my parents***

---

**TABLE OF CONTENTS**

<b>1</b>	<b>Abstract</b>	<b>1</b>
<b>2</b>	<b>Zusammenfassung</b>	<b>3</b>
<b>3</b>	<b>Introduction</b>	<b>5</b>
3.1	Overview	5
3.2	Proteolytic processing of the amyloid precursor protein (APP) and activation of transcription	9
3.3	The amyloid cascade hypothesis	12
3.4	A $\beta$ , tau and the connection in between	16
3.5	Genes associated with Alzheimer's disease	21
3.6	Selection of normalization algorithms	25
3.7	MIAME standards	29
3.8	Flow diagram of sample preparation and hybridization	30
3.9	Significance level, cut-off for fold change and normalization	31
3.10	Software	32
<b>4</b>	<b>The aim of this Ph.D. thesis</b>	<b>33</b>
<b>5</b>	<b>Results</b>	<b>35</b>
5.1	Preface	35
5.2	Flow chart of experimental steps	36
5.3	Cloning and expression of APP-fragments (C99 wildtype and -mutants)	37
5.4	Transcriptomics	39
5.4.1	Preface	39
5.4.2	Quality control	39
5.4.3	C99 as an internal control. The APP gene (overexpressed C99 respectively) was detected among the top up-regulated genes	39
5.4.4	Genes identified using different algorithms and software	41

<b>5.5</b>	<b>Transcriptomics compared to proteomics</b>	<b>43</b>
5.5.1	Preface	43
5.5.2	CRABP1 (cellular retinoic acid binding protein 1) and further genes associated with retinoic acid (RA)	43
5.5.2.1	CRABP1 was differentially expressed both on the transcript level and on the protein level	43
5.5.2.2	CRABP1 was up-regulated in mutant C99I45F ( $A\beta_{42}/A\beta_{40}\uparrow$ ) only, whereas mutant C99V50F ( $A\beta_{42}/A\beta_{40}\downarrow$ ) showed no differential expression of CRABP1	46
5.5.2.3	CRABP1 was not differentially expressed in consequence of C99-overexpression in contrast to neurofilaments	47
5.5.2.4	Increased $A\beta_{42}/A\beta_{40}$ ratio up-regulated CRABP1 and made cells less sensitive to all-trans retinoic acid	48
5.5.2.5	CRABP1 knockdown rescued the differentiation potential of $A\beta_{42}$ overexpressing human neuroblastoma cells after RA treatment	50
5.5.2.6	Three further genes, associated with RA-metabolism were differentially expressed in consequence of a changed $A\beta_{42}/A\beta_{40}$ ratio and may have influenced the effects mediated by RA	50
5.5.2.7	Further genes, located on chromosomal regions adjacent to CRABP1 (15q24), were differentially expressed	51
5.5.3	Further overlapping transcripts/proteins	51
5.5.3.1	Preface	51
5.5.3.2	PREP (prolyl endopeptidase)	52
5.5.3.3	T-cell receptor, $\alpha$ and $\delta$ locus	52
5.5.3.4	VGF (VGF nerve growth factor inducible)	52
5.5.3.5	NADH dehydrogenase (ubiquinone)	53
5.5.3.6	DNCL12 (dynein cytoplasmic light intermediate polypeptide 2)	53
<b>5.6</b>	<b>Inversely regulated genes</b>	<b>53</b>
5.6.1	Preface	53
5.6.2	Genes up-regulated in mutant C99I45F versus C99WT ( $A\beta_{42}/A\beta_{40}\uparrow$ ) and <i>at the same time</i> down-regulated in mutant C99V50F versus C99WT ( $A\beta_{42}/A\beta_{40}\downarrow$ )	54
5.6.3	Genes down-regulated in mutant C99I45F versus C99WT ( $A\beta_{42}/A\beta_{40}\uparrow$ ) and <i>at the same time</i> up-regulated in mutant C99V50F versus C99WT ( $A\beta_{42}/A\beta_{40}\downarrow$ )	57
<b>5.7</b>	<b>Increased <math>A\beta_{42}/A\beta_{40}</math> ratio down-regulated the imprinted region IGF2-H19 on chromosome 11p15.5</b>	<b>58</b>
<b>5.8</b>	<b>Phosphorylation status of proteins and total protein amounts in consequence of an altered <math>A\beta_{42}/A\beta_{40}</math> ratio detected by high throughput immunoblotting</b>	<b>59</b>
5.8.1	Immunoblots	59
5.8.2	Quantification and graphical presentation of previously shown immunoblots	69
<b>5.9</b>	<b>Models</b>	<b>77</b>
5.9.1	Preface	77
5.9.2	Model: Downregulation of IGF2/IGF1R/PKC and PI3K/AKT signaling by an increased $A\beta_{42}/A\beta_{40}$ ratio	78

5.9.3	Model: Increased $A\beta_{42}/A\beta_{40}$ ratio is expected to reduce the ATP level and to induce phosphofructokinase upregulation	85
5.9.4	Model: Transcriptional control of blood coagulation and fibrinolysis is influenced by an altered $A\beta_{42}/A\beta_{40}$ ratio	86
<b>5.10</b>	<b>Candidates for tau or GSK3 phosphorylation</b>	<b>89</b>
5.10.1	Preface	89
5.10.2	Kinases	90
5.10.3	Phosphatases	91
<b>5.11</b>	<b>Genes co-regulated with APLP1 and APLP2</b>	<b>91</b>
<b>5.12</b>	<b>Identification of altered signal transduction pathways and molecular functions</b>	<b>92</b>
5.12.1	Preface	92
5.12.2	Over and under-representation of transcripts in signal transduction and metabolic pathways	93
5.12.3	Over and under-representation of transcripts involved in certain molecular functions	96
<b>5.13</b>	<b>Cluster analysis</b>	<b>105</b>
<b>5.14</b>	<b>Quantitative real-time PCR</b>	<b>108</b>
5.14.1	Preface	108
5.14.2	Normalisation	108
5.14.3	Relative quantification with the $\Delta\Delta CT$ Method	109
5.14.4	Direct comparison of data derived from oligonucleotide microarrays and quantitative real-time PCR	112
<b>5.15</b>	<b>“Chromeron-Effect” on chromosomal loci 1q23 and 1p36</b>	<b>114</b>
<b>5.16</b>	<b>Agreement of differentially expressed genes with genes found in linkage and association studies</b>	<b>115</b>
<b>5.17</b>	<b>Agreement of differentially expressed genes with genes of the “Alzforum database”</b>	<b>119</b>
<b>5.18</b>	<b>Intersection of genes identified in this thesis as a consequence of an altered <math>A\beta_{42}/A\beta_{40}</math> ratio and genes identified as a result of PS1/PS2 knockdown in murine embryonic fibroblasts</b>	<b>119</b>
<b>5.19</b>	<b>Intersection of genes identified in this thesis as a consequence of an altered <math>A\beta_{42}/A\beta_{40}</math> ratio and genes identified in response to AICD overexpression in human neuroblastoma cells</b>	<b>120</b>
<b>6</b>	<b>Discussion</b>	<b>122</b>
6.1	Preface	122
6.2	Data analysis with different algorithms	127
6.3	An altered $A\beta_{42}/A\beta_{40}$ ratio has a strong impact on gene expression	128

<b>6.4</b>	<b>Retinoic acid, AD and neurogenesis</b>	<b>128</b>
6.4.1	Retinoic acid, APOE4, APOE2	128
6.4.2	Association between AD and RA	129
6.4.3	Linkage of the chromosomal locus 15q24 to mental retardation	130
6.4.4	Neurofilaments were inversely regulated by C99 and $A\beta_{42}$ , $A\beta_{40}$	131
6.4.5	Role of neurogenesis in AD	131
6.4.6	Sensitive balance between proliferation and differentiation is influenced by an altered $A\beta_{42}/A\beta_{40}$ ratio via CRABP1	131
6.4.7	Overlapping results obtained from different laboratories and different technologies increased reliability of the data	132
6.4.8	Target genes of retinoic acid indicate low levels of RA for $A\beta_{42}/A\beta_{40}\uparrow$ , but high levels for $A\beta_{42}/A\beta_{40}\downarrow$	133
<b>6.5</b>	<b>Downregulation of the IGF2/IGF1R/PKC and PI3K/AKT survival pathways as a result of an increased <math>A\beta_{42}/A\beta_{40}</math> ratio</b>	<b>133</b>
<b>6.6</b>	<b>Downregulation of the IGF2-H19 imprinted region on chromosome 11p15.5 as a result of an increased <math>A\beta_{42}/A\beta_{40}</math> ratio</b>	<b>136</b>
<b>6.7</b>	<b>The <i>non-catalytic</i> TrkB receptor was strongly up-regulated in response to an increased <math>A\beta_{42}/A\beta_{40}</math> ratio and might have suppressed the effects of neurotrophins on cell survival and LTP in a competitive manner</b>	<b>138</b>
<b>6.8</b>	<b>Up-regulated ATP7A, a copper transporting ATPase is expected to dys-regulate copper levels in consequence of an increased <math>A\beta_{42}/A\beta_{40}</math> ratio</b>	<b>140</b>
<b>6.9</b>	<b>Proteases and protease inhibitors</b>	<b>142</b>
6.9.1	Preface	142
6.9.2	ADAMTS9 was the most inversely regulated gene in response to a changed $A\beta_{42}/A\beta_{40}$ ratio and it was found to be clustered with other proteases	142
6.9.3	Further proteases and protease inhibitors	143
<b>6.10</b>	<b>Extracellular matrix proteins like fibronectin-domain containing proteins, collagen, heparan sulfate proteoglycan and reelin may play a fundamental role in gene expression incuded by a changed <math>A\beta_{42}/A\beta_{40}</math> ratio</b>	<b>147</b>
<b>6.11</b>	<b>ACTA2 is assumed to be a pivotal protein in gene expression induced by altered C99 cleavage products</b>	<b>153</b>
<b>6.12</b>	<b>Transcriptional control of blood coagulation and fibrinolysis was influenced by a changed <math>A\beta_{42}/A\beta_{40}</math> ratio</b>	<b>153</b>
<b>6.13</b>	<b>Kinases/phosphatases as possible candidates for tau or GSK3 phosphorylation</b>	<b>158</b>
6.13.1	Kinases	158
6.13.2	Phosphatases	161
<b>6.14</b>	<b>Changed phosphorylation status of GSK3<math>\alpha/\beta</math>, tau, proteinkinase C and further molecules</b>	<b>162</b>
6.14.1	GSK3 $\alpha$ and GSK3 $\beta$	162

6.14.2	Tau _____	163
6.14.3	Inverse phosphorylation of PKC as a result of a changed $A\beta_{42}/A\beta_{40}$ ratio _____	163
6.14.4	Differential phosphorylation of PKB (AKT1), PKA and FAK as a result of a changed $A\beta_{42}/A\beta_{40}$ ratio _____	164
6.14.5	Probable activation of MAPkinase/ERK signaling due to strong phosphorylation of MEK1 and ERK1 in response to an increased $A\beta_{42}/A\beta_{40}$ ratio _____	164
<b>6.15</b>	<b>APLP1 and APLP2 were differentially affected by a changed <math>A\beta_{42}/A\beta_{40}</math> ratio _____</b>	<b>165</b>
<b>6.16</b>	<b>APLP1/APLP2 co-regulated genes _____</b>	<b>166</b>
<b>6.17</b>	<b>Axonal outgrowth, synaptogenesis, neurotransmitter release _____</b>	<b>167</b>
<b>6.18</b>	<b>Axonal transport _____</b>	<b>173</b>
<b>6.19</b>	<b>Oxidative stress is expected to be increased by upregulation of the mitochondrial respiratory chain in consequence of an increased <math>A\beta_{42}/A\beta_{40}</math> ratio _____</b>	<b>175</b>
<b>6.20</b>	<b>Strong dysregulation of cytochromes by a changed <math>A\beta_{42}/A\beta_{40}</math> ratio _____</b>	<b>177</b>
<b>6.21</b>	<b>Enzymes regulating neurotransmitter metabolism were strongly affected by a changed <math>A\beta_{42}/A\beta_{40}</math> ratio on the transcriptional level and so might be neurotransmitter levels _____</b>	<b>178</b>
<b>6.22</b>	<b>Changed glutamine synthase and glutaminase expression in response to a changed <math>A\beta_{42}/A\beta_{40}</math> ratio _____</b>	<b>181</b>
6.22.1	Glutamine synthase was down-regulated exclusively in consequence of a decreased $A\beta_{42}/A\beta_{40}$ ratio and is assumed to couple ATP synthesis to neurotransmitter levels _____	181
6.22.2	Glutaminase was up-regulated exclusively in response to an increased $A\beta_{42}/A\beta_{40}$ ratio _____	182
<b>6.23</b>	<b>Two enzymes of the urea cycle were affected by a changed <math>A\beta_{42}/A\beta_{40}</math> ratio: argininosuccinate synthase and argininosuccinate lyase _____</b>	<b>182</b>
<b>6.24</b>	<b>Exocytosis _____</b>	<b>183</b>
<b>6.25</b>	<b>New assignment of a functional relationship between neurogenin 2 and KIAA0125 _____</b>	<b>184</b>
<b>6.26</b>	<b>Receptors were strongly differentially affected by a changed <math>A\beta_{42}/A\beta_{40}</math> ratio _____</b>	<b>185</b>
<b>6.27</b>	<b>Prostaglandin E receptor 2 was up-regulated exclusively by a decreased <math>A\beta_{42}/A\beta_{40}</math> ratio _____</b>	<b>188</b>
<b>6.28</b>	<b>Nicotinic acetylcholine receptor <math>\alpha 7</math> was inversely regulated by a changed <math>A\beta_{42}/A\beta_{40}</math> ratio _____</b>	<b>189</b>

<b>6.29</b>	<b>Excitatory and inhibitory neurotransmitter receptors were affected by a changed <math>A\beta_{42}/A\beta_{40}</math> ratio</b>	<b>190</b>
6.29.1	Glutamate-receptors were differentially expressed in response to an increased $A\beta_{42}/A\beta_{40}$ ratio and might influence $Ca^{2+}$ transport and LTP	190
6.29.2	GABA and glycine receptors were up-regulated exclusively in response to an increased $A\beta_{42}/A\beta_{40}$ ratio and might exert inhibitory effects	192
<b>6.30</b>	<b>Upregulation of Notch-signaling was triggered by an increased <math>A\beta_{42}/A\beta_{40}</math> ratio and might contribute to prevention of terminal cell differentiation</b>	<b>193</b>
<b>6.31</b>	<b>Upregulation of TGF<math>\beta</math>-signaling was triggered by an increased <math>A\beta_{42}/A\beta_{40}</math> ratio</b>	<b>196</b>
<b>6.32</b>	<b>Wnt-signaling might be inversely regulated by a changed <math>A\beta_{42}/A\beta_{40}</math> ratio</b>	<b>197</b>
<b>6.33</b>	<b>Strong and significant downregulation of RGS4 by an increased <math>A\beta_{42}/A\beta_{40}</math> ratio argues for activation of G-protein signaling</b>	<b>198</b>
<b>6.34</b>	<b>The <math>\alpha</math> and <math>\delta</math> loci of the T-cell receptor were up-regulated in response to increased and decreased <math>A\beta_{42}/A\beta_{40}</math> ratios, whereas C99 overexpression led to their downregulation</b>	<b>199</b>
<b>6.35</b>	<b>Dysregulated LRP4 is assumed to influence transcription together with Fe65</b>	<b>200</b>
<b>6.36</b>	<b>Indications of dysregulated <math>Ca^{2+}</math> levels in consequence of a changed <math>A\beta_{42}/A\beta_{40}</math> ratio</b>	<b>201</b>
<b>6.37</b>	<b>CREB1 is assumed to be less active in consequence of an increased <math>A\beta_{42}/A\beta_{40}</math> ratio</b>	<b>202</b>
<b>6.38</b>	<b>Further inversely regulated genes by a changed <math>A\beta_{42}/A\beta_{40}</math> ratio</b>	<b>203</b>
<b>6.39</b>	<b>Miscellaneous genes</b>	<b>205</b>
<b>6.40</b>	<b>Chromosomal susceptibility loci</b>	<b>206</b>
<b>6.41</b>	<b>Intersection of genes identified in this thesis as a consequence of altered C99 cleavage products and genes identified as a result of PS1/PS2 knockdown in murine embryonic fibroblasts</b>	<b>207</b>
<b>6.42</b>	<b>Intersection of genes identified in this thesis as a consequence of altered C99 cleavage products and genes identified as a result of AICD overexpression in human neuroblastoma cells</b>	<b>208</b>
<b>6.43</b>	<b>Concluding remarks and outlook</b>	<b>208</b>
<b>7</b>	<b><i>Materials and Methods</i></b>	<b>212</b>
<b>7.1</b>	<b>Materials</b>	<b>212</b>
7.1.1	Cell lines	212
7.1.2	Gene Chips <sup>®</sup> (Affymetrix whole genome oligonucleotide arrays)	212

---

7.1.3	TaqMan <sup>®</sup> Human Endogenous Control Plate _____	212
7.1.4	Primer sequences for quantitative real-time PCR _____	213
7.1.5	siRNAs _____	214
7.1.6	Plasmids _____	214
7.1.7	Chips for the Bioanalyzer 2100 <sup>™</sup> (Agilent) _____	214
7.1.8	Kits _____	215
7.1.9	Antibodies _____	215
7.1.9.1	Primary antibodies _____	215
7.1.9.2	Secondary antibodies _____	215
7.1.10	Oligonucleotides _____	216
7.1.11	Chemicals _____	216
7.1.12	Buffers and solutions _____	217
7.1.13	Enzymes _____	219
7.1.14	Antibiotics _____	219
7.1.15	Cell culture _____	219
7.1.16	Devices _____	220
7.1.17	Nucleic acid and protein molecular weight markers _____	220
<b>7.2</b>	<b>Methods _____</b>	<b>221</b>
7.2.1	DNA methods _____	221
7.2.1.1	Transformation of competent E. coli _____	221
7.2.1.2	Small scale preparation of plasmid DNA (Mini Prep) _____	221
7.2.1.3	Large scale preparation of plasmid DNA (Maxi Prep) _____	221
7.2.1.4	Purification and concentration of DNA _____	222
7.2.1.5	Determination of DNA concentration _____	222
7.2.1.6	Restriction digestion of DNA _____	222
7.2.1.7	Analysis of DNA fragments on agarose gels _____	222
7.2.1.8	Sequencing of plasmids _____	223
7.2.2	Cell culture methods _____	223
7.2.2.1	Cultivation of eukaryotic cell lines _____	223
7.2.2.2	Freezing and thawing of eukaryotic cell lines _____	224
7.2.2.3	Stable transfection of human neuroblastoma cells _____	224
7.2.2.4	RNA interference _____	225
7.2.2.4.1	Transient knockdown by siRNAs _____	225
7.2.2.4.2	Transfection of the human neuroblastoma cell line SH-SY5Y with siRNAs _____	226
7.2.3	RNA methods _____	227
7.2.3.1	Transcriptome analysis using Affymetrix screening _____	227
7.2.3.1.1	Total RNA preparation from cultured cells _____	227
7.2.3.1.2	Quantification of RNA _____	228
7.2.3.1.3	Precipitation of total-RNA _____	228
7.2.3.1.4	Reverse transcription of total RNA into cDNA by oligo (dT) primers _____	229
7.2.3.1.5	Purification of cDNA _____	229
7.2.3.1.6	In vitro transcription of cDNA into cRNA _____	229
7.2.3.1.7	Purification of cRNA _____	229
7.2.3.1.8	Fragmentation of cRNA _____	229
7.2.3.1.9	Hybridisation of fragmented cRNA onto the arrays _____	230
7.2.3.1.10	Washing and staining of the arrays _____	230

---

7.2.3.1.11	Scanning of the arrays	231
7.2.3.1.12	Data analysis	231
7.2.3.2	Quantitative real-time PCR	231
7.2.3.2.1	Preface	231
7.2.3.2.2	Reverse transcription of total RNA into cDNA by using random hexamer primers	231
7.2.3.2.3	Real-time detection of amplified cDNA by using an ABI cyclor 5700 and Taqman probes (Applied Biosystems)	232
7.2.3.3	RNA interference (siRNAs)	235
7.2.4	Quality control of cells, total-RNA, cRNA and Chips®	235
7.2.4.1	Screening of cells for mycoplasma contamination	235
7.2.4.2	Assessment of RNA purity by measuring the 260 nm/280 nm ratio	235
7.2.4.3	Agarose gel electrophoresis	235
7.2.4.4	Checking quality of unfragmented cRNA with the Bioanalyzer 2100 (Agilent)	236
7.2.4.5	Assessment of RNA integrity with the Bioanalyzer 2100 (Agilent)	236
7.2.4.6	Assessment of Gene Chip® quality, hybridisation efficiency and RNA quality by certain parameters	237
7.2.5	Protein methods	237
7.2.5.1	Protein expression in mammalian cells	237
7.2.5.2	Whole cell protein extraction from mammalian cells	237
7.2.5.2.1	Extraction of non-phosphorylated proteins	237
7.2.5.2.2	Extraction of phosphorylated proteins	238
7.2.5.3	Determination of protein concentrations	239
7.2.5.4	SDS Polyacrylamide Gel Electrophoresis (SDS-PAGE)	239
7.2.5.5	Western blotting	240
7.2.5.6	Immunoprecipitation	243
7.2.6	Differentiation of human neuroblastoma cells by retinoic acid	243
7.2.7	Immunocytochemistry	244
7.2.7.1	Immunostaining of cultured cells	244
7.2.7.2	Immunofluorescence microscopy	245
7.2.8	Light microscopy	245
<b>8</b>	<b>References</b>	<b>246</b>
<b>9</b>	<b>Acknowledgements</b>	<b>281</b>
<b>10</b>	<b>Abbreviations</b>	<b>282</b>
<b>11</b>	<b>Declaration</b>	<b>286</b>

---

<b>12</b>	<b>Supplementary Information</b>	<b>S1</b>
<b>12.1</b>	<b>Preface</b>	<b>S1</b>
<b>12.2</b>	<b>Genes identified using different algorithms</b>	<b>S1</b>
12.2.1	Genes identified using the PLIER-algorithm (Array Assist, Stratagene)	S1
12.2.2	Genes identified using the GC-RMA algorithm (Language R, Bioconductor)	S18
12.2.3	Genes identified using the MAS 5 algorithm (Array Assist, Stratagene)	S25
<b>12.3</b>	<b>Gene annotations</b>	<b>S40</b>
12.3.1	Preface	S40
12.3.2	Annotations for differentially expressed genes (volcano plots)	S40
12.3.3	Annotations for inversely regulated genes	S66
12.3.4	Annotations for clustered genes	S71
<b>12.4</b>	<b>Mathematical background</b>	<b>S76</b>
12.4.1	Preface	S76
12.4.2	Background calculation	S76
12.4.3	Noise calculation	S76
12.4.4	Match/Mismatch system™ of Affymetrix	S77
12.4.5	Normalisation algorithms	S78
12.4.5.1	Absolute analysis algorithms	S78
12.4.5.2	Relative analysis algorithms	S80
12.4.6	Derivation of the $2^{-\Delta\Delta CT}$ Method	S80
<b>12.5</b>	<b>Quality control</b>	<b>S84</b>
12.5.1	Quality control of cells, target-RNA and arrays	S84
12.5.2	Quality control of RNA by a test Chip prior to the whole genome Chip	S84
12.5.3	RNA-quality assessed using the Agilent 2100 Bioanalyzer	S85
<b>12.6</b>	<b>Extended view of connectivities</b>	<b>S87</b>
<b>12.7</b>	<b>CRABP1 knockdown, larger scale of Figure 5.9 D</b>	<b>S88</b>

# 1 Abstract

The human genome comprises approximately 20,000-25,000 genes. The genes known to be involved in Alzheimer's disease (AD) are the amyloid precursor protein (A $\beta$ PP), presenilin 1 (PS1), presenilin 2 (PS2) and apolipoprotein E (APOE). However, which additional genes are involved in its etiology is a controversial topic. C99, the C-terminal cleavage product of A $\beta$ PP is the direct, *in vivo* occurring, precursor of A $\beta$ -peptides. It is proteolytically processed, resulting in the generation of several A $\beta$ -peptides. In contrast to the form with 40 amino acids (A $\beta_{40}$ ), which is regarded as the physiological form, the variant with 42 amino acids (A $\beta_{42}$ ) is thought to be the pathogenic form triggering the pathophysiological cascade in AD. In order to produce different A $\beta_{42}$  and A $\beta_{40}$  levels, the A $\beta$  precursors C99I45F and C99V50F (two C99 mutants, known to generate different amounts of A $\beta_{42}$  and A $\beta_{40}$ ) were overexpressed in human neuroblastoma cells. This resulted, due to varying intracellular cleavage by  $\gamma$ -secretase, in different A $\beta_{42}$  and A $\beta_{40}$  levels accompanied by the generation of their respective APP intracellular domains (AICDs). The goal of this thesis was to obtain information about effects of the different C99 cleavage products. Therefore different C99 mutants were overexpressed in the human neuroblastoma cell line SH-SY5Y resulting in different A $\beta_{42}$ /A $\beta_{40}$  levels and a genome-wide transcriptomic (Affymetrix) and proteomic response of these cells was monitored. As was expected, many genes previously reported to be associated with AD were found to be differentially expressed. Importantly, further genes, not yet linked to AD, have been identified and new cross-talk between genes/proteins has been suggested. The genes assumed to play a predominant role in response to altered C99 cleavage products are indicated in brackets and full gene names are to be found in Chapter 10, Abbreviations. In this thesis, it was demonstrated that an increased A $\beta_{42}$ /A $\beta_{40}$  ratio, but not a decreased A $\beta_{42}$ /A $\beta_{40}$  ratio, induced upregulation of the retinoic acid binding protein CRABP1 on the transcript level and on the protein level. This, in turn, reduced the responsiveness of SH-SY5Y cells to retinoic acid, which reduced their differentiation potential. Knockdown of the increased CRABP1 levels by siRNA rescued the differentiation potential of these cells. These findings, in conjunction with known functional properties of CRABP1, suggest that up-regulated CRABP1 might, possibly also *in vivo*, prevent the terminal differentiation of neural precursor cells into functional neurons (disturbed neurogenesis). Furthermore, the phosphorylation status of proteins was determined providing further insights into signal transduction pathways. The IGF2/IGF1R/PKC together with the PI3K/AKT survival pathway was found to be inversely regulated by an altered A $\beta_{42}$ /A $\beta_{40}$  ratio (IGF2, IGFBP5, PKC, AKT1). The chromosomal locus 11p15.5 was identified as a hot spot: an increased A $\beta_{42}$ /A $\beta_{40}$  ratio, in contrast to a decreased one, down-regulated the IGF2-H19 imprinted region (chr.11p15.5) indicating that imprinting may play a role in AD. In consequence of an increased A $\beta_{42}$ /A $\beta_{40}$  ratio, GSK3 $\beta$  was *hyperphosphorylated* on the activating site Y216, and tau<sub>441</sub> showed stronger phosphorylation on S199/S202, two sites reported to turn tau, upon phosphorylation, into a protein with possible toxic properties. APLP2 was found to be up-regulated as a consequence of an increased A $\beta_{42}$ /A $\beta_{40}$  ratio, whereas APLP1 was up-regulated in response to a decreased A $\beta_{42}$ /A $\beta_{40}$  ratio, indicating inverse A $\beta$ -dependent regulation

of APLP1/2 expression. In response to an increased  $A\beta_{42}/A\beta_{40}$  ratio, expression levels of a set of genes were altered in such a way that a tendency towards faster blood coagulation and reduced fibrinolysis could be recognized on the transcript level (PLAT, TFPI2, FGB, SERPINF1, SERPINE2). This view is supported by observations in AD patients who have a greater risk of strokes and diminished cerebral perfusion. As  $A\beta$ -inducible candidate kinases possibly involved in tau-phosphorylation, DYRK1, CDKL1, CDKL5, CDK6, DCAMKL1, ERK1 and PFKP were identified due to their altered expression levels (or phosphorylation status for ERK1). Indeed, previous studies demonstrated that  $A\beta_{42}$  induces tau *hyper*phosphorylation in animal models. PFKP, which plays a key role in glycolysis, was found to be dysregulated in consequence of a changed  $A\beta_{42}/A\beta_{40}$  ratio and could possibly reflect disturbed regulation of glucose and ATP metabolism in brains of AD patients. A potential function was assigned to the hitherto uncharacterized KIAA0125, namely to be a counter player of neurogenin 2, which was co-regulated with C99 and neuronatin. Furthermore, the following areas were distinctly affected by a changed  $A\beta_{42}/A\beta_{40}$  ratio (for most genes determined on the transcript level and for some additionally on the protein level): Copper transport/metabolism with special regard to ATP7A, several (metallo) proteases (ADAMTS9, ADAMTS3, MMP8, PREP, ECEL1, CTSD, PRSS12), metalloprotease inhibitors (TIMP3, TIMP1), extracellular matrix proteins or related enzymes thereof (RELN, COL4A1, COL4A2, HS3ST2), cytoskeletal proteins (ACTA2, ACTN1), mitochondrial respiratory chain components (NDUFB9), cytochromes (b-561 and b-245), dopamine, serotonin and glutamate -metabolism with special regard to DDC, HMP19 and GAD1. Effects of BDNF (non-catalytic isoform of TRKB), membrane fusion of neurotransmitter containing vesicles (STX3A, SYN2),  $Ca^{2+}$  influx (AMPA2), acetylcholine receptors (CHRNA7), Notch signaling (DNER, TLE1, TLE2, JAG1, CUTL2), TGF $\beta$  signaling (TGFB2, TGFB2, BAMBI, BMP7), WNT signaling (DKK2, DKK4), G protein signaling (RGS4) and ERK/MEK signaling (ERK1, MEK1). Growth cone guidance, synaptogenesis and dendritic branching are expected to be impaired as consequence of an increased  $A\beta_{42}/A\beta_{40}$  ratio but improved as a result of a decreased one (SEMA3A, SEMA3C, L1CAM, PTN, SLIT1). Further genes involved in the following areas were distinctly influenced by a changed  $A\beta_{42}/A\beta_{40}$  ratio: Glutamate/ammonia metabolism (GLUL, GLS), urea cycle (ASS), cell cycle regulation (CCND1, CDKN1A), glucocorticoid regulated kinase (SGK), receptors (PTGER2, EGFR, AMPA2, AMPA3, GRM7, GRM8c, GLRB, GABRB3), long term potentiation (CREB1), axonal transport (DNCL12), angiogenesis (HGF, VEGF), T-cell receptors and connected transcription factors (T-cell receptor  $\alpha$  and  $\delta$  locus, GATA3), lipoprotein associated proteins or adaptor proteins hereof (LRP4, PDZK1), vesicular transport of organelles and microtubule association (VMP), transcription factors (PBX1, SHOX2) and stress-related factors (ADRB1). Taken together, the identified genes, proteins and pathways have given new and deeper insight into the effects of different C99 cleavage products and they have provided new hypotheses for the pathological mechanisms of AD. Furthermore they are possible candidates for genetic risk factors and may be helpful in explaining the mechanisms of non-genetic risk factors. The gene expression pattern, specific for an increased  $A\beta_{42}/A\beta_{40}$  ratio, could be useful, together with clinical data, for the diagnosis of AD. Finally, some of the identified transcripts, proteins and pathways might turn out to be suitable drug targets.

## 2 Zusammenfassung

Das humane Genom umfasst ca. 20.000-25.000 Gene. Die Gene, für die eine Beteiligung an der Alzheimer Krankheit (AK) bekannt ist, sind das Amyloid Precursor Protein (A $\beta$ PP), Presenilin 1 (PS1), Presenilin 2 (PS2) und Apolipoprotein E (APOE). Es wird kontrovers diskutiert, welche weiteren Gene an der Ätiologie der AK beteiligt sind. C99, das C-terminale Spaltprodukt von A $\beta$ PP, ist das direkte, *in vivo* vorkommende Vorläufer-Protein der A $\beta$ -peptide. Es wird proteolytisch prozessiert, wobei verschiedene A $\beta$ -peptide gebildet werden. Im Gegensatz zu der Form mit 40 Aminosäuren (A $\beta$ <sub>40</sub>), die als physiologische A $\beta$ -Form betrachtet wird, glaubt man von der Variante mit 42 Aminosäuren (A $\beta$ <sub>42</sub>), dass es sich um die pathogene Form handelt, welche die pathophysiologische Kaskade der AK auslöst. Um verschiedene A $\beta$ <sub>42</sub> und A $\beta$ <sub>40</sub> Mengen zu bilden, wurden die A $\beta$ -Vorläufer C99I45F und C99V50F (zwei C99-Mutanten, die dafür bekannt sind, verschiedene A $\beta$ <sub>42</sub> und A $\beta$ <sub>40</sub> Mengen zu bilden) in humanen Neuroblastomzellen überexprimiert. Daraus resultierten, in Folge variierender intrazellulärer Spaltung durch die  $\gamma$ -Sekretase, unterschiedliche A $\beta$ <sub>42</sub>- und A $\beta$ <sub>40</sub>-Mengen und die miteinhergehende Bildung der entsprechenden intrazellulären Domänen (AICD). Das Ziel dieser Arbeit war es, neue Einsichten in die pathologischen Mechanismen der AK als Konsequenz der veränderten C99-Spaltprodukte zu erhalten. Deshalb wurde die Reaktion der humanen Neuroblastomzelllinie SH-SY5Y auf verschiedene, überexprimierende A $\beta$ <sub>42</sub>/A $\beta$ <sub>40</sub> Mengen genomweit auf Transkriptom-Ebene (Affymetrix) und auf Proteom-Ebene untersucht. Wie zu erwarten war, wurde eine Vielzahl von Genen als differentiell exprimiert identifiziert, die zuvor in anderen Studien als AK-assoziiert gefunden wurden. Entscheidend war jedoch die Entdeckung weiterer Gene, für die bisher noch keine Verbindung zur AK hergestellt wurde. Hierdurch wurden neue Wechselwirkungen („Cross-Talk“) zwischen Genen/Proteinen ersichtlich. Die Gene, für die eine vorherrschende Rolle als Antwort auf veränderte C99 Spaltprodukte angenommen wird, sind in Klammern angegeben und deren vollständige Gennamen sind in Kapitel 10, Abkürzungsverzeichnis, zu finden. In dieser Arbeit wurde gezeigt, dass das Retinsäure-bindende Protein CRABP1 in Folge eines erhöhten, jedoch nicht in Folge eines erniedrigten A $\beta$ <sub>42</sub>/A $\beta$ <sub>40</sub>-Verhältnisses, auf Transkript- und Proteinebene heraufreguliert wurde. Dies wiederum erniedrigte die Ansprechbarkeit der SH-SY5Y Zellen auf Retinsäure, wodurch deren Differenzierungspotential reduziert wurde. „Knockdown“ des heraufregulierten CRABP1 stellte das Differenzierungspotential dieser Zellen wieder her. Diese Entdeckung, in Verbindung mit den bisher bekannten funktionellen Eigenschaften von CRABP1, könnte möglicherweise auch *in vivo* ein wichtiger Mechanismus sein, bei dem CRABP1 die terminale Differenzierung von neuronalen Vorläuferzellen in funktionelle Neuronen verhindern könnte (gestörte Neurogenese). Weiterhin wurde der Phosphorylierungsstatus von Proteinen bestimmt, wodurch weitere Einsichten in Signaltransduktionswege ersichtlich wurden. Der IGF2/IGF1R/PKC- zusammen mit dem PI3K/AKT-Signaltransduktionsweg wurde durch ein verändertes A $\beta$ <sub>42</sub>/A $\beta$ <sub>40</sub>-Verhältnis invers reguliert (IGF2, IGF1R, PKC, AKT1). Der chromosomale Lokus 11p15.5 wurde als „hot spot“ identifiziert: ein erhöhtes A $\beta$ <sub>42</sub>/A $\beta$ <sub>40</sub>-Verhältnis, im Gegensatz zu einem erniedrigten, regulierte die „IGF2-H19 imprinted region“ (chr.11p15.5) herunter, was darauf hindeutet, dass genomische Prägung (Imprinting) bei der AK eine Rolle spielen könnte. In Folge eines erhöhten A $\beta$ <sub>42</sub>/A $\beta$ <sub>40</sub>-Verhältnisses wurde GSK3 $\beta$  an der aktivierenden Stelle Y216 hyperphosphoryliert und Tau<sub>441</sub> zeigte stärkere Phosphorylierung an S199/S202 zwei Stellen, von denen angenommen wird, Tau durch Phosphorylierung, in ein Protein mit evtl. toxischen Eigenschaften zu überführen. APLP2 wurde in Folge eines erhöhten A $\beta$ <sub>42</sub>/A $\beta$ <sub>40</sub>-Verhältnisses heraufreguliert, wohingegen APLP1 in Folge eines erniedrigten A $\beta$ <sub>42</sub>/A $\beta$ <sub>40</sub>-Verhältnisses heraufreguliert wurde, was auf eine inverse, A $\beta$ -abhängige

Regulation von APLP1/2 hindeutet. Als Antwort auf ein erhöhtes  $A\beta_{42}/A\beta_{40}$ -Verhältnis änderte sich die Expression einer Gruppe von Genen so, dass eine Tendenz zu schnellerer Blutgerinnung, bei gleichzeitig verlangsamter Fibrinolyse (PLAT, TFPI2, FGB, SERPINF1, SERPINE2) auf Transkriptebene zu erkennen war. Diese Sichtweise wird durch Beobachtungen an Alzheimer Patienten unterstützt, die ein größeres Risiko für Schlaganfälle und verminderte cerebrale Durchblutung aufweisen. Als  $A\beta$ -induzierbare Kandidaten für Kinasen, die Tau phosphorylieren könnten, wurden DYRK1, CDKL1, CDKL5, CDK6, DCAMKL1, ERK1 und PFKP identifiziert, für die veränderte Expressionswerte (oder ein veränderter Phosphorylierungsstatus für ERK1) gefunden wurden. In der Tat haben vorhergehende Studien gezeigt, dass  $A\beta_{42}$  Tau-Hyperphosphorylierung in Tiermodellen induziert. PFKP, ein Schlüsselenzym der Glykolyse, wurde in Folge eines veränderten  $A\beta_{42}/A\beta_{40}$ -Verhältnisses unterschiedlich reguliert und könnte möglicherweise einen gestörten Glukose- und ATP-Metabolismus in Gehirnen von AK-Patienten widerspiegeln. Dem bisher uncharakterisierten KIAA0125 wurde die mögliche Funktion zugewiesen, ein Gegenspieler von Neurogenin 2 zu sein, welches mit C99 und Neuronatin als gemeinsam reguliert identifiziert wurde. Weiterhin wurden folgende Bereiche durch ein verändertes  $A\beta_{42}/A\beta_{40}$ -Verhältnis deutlich beeinflusst (für die meisten Gene auf Transkriptebene bestimmt und für manche zusätzlich auf Proteinebene): Kupfertransport/Kupferstoffwechsel mit speziellem Hinblick auf ATP7A, verschiedene (Metallo)proteasen (ADAMTS9, ADAMTS3, MMP8, PREP, ECEL1, CTSD, PRSS12), Metalloproteaseinhibitoren (TIMP3, TIMP1), extrazelluläre Matrixproteine oder hiermit verwandte Enzyme (RELN, COL4A1, COL4A2, HS3ST2), Proteine des Zytoskeletts (ACTA2, ACTN1), Komponenten der mitochondrialen Atmungskette (NDUFB9), Zytochrome (b-561 und b-245), Dopamin-, Serotonin- und Glutamatstoffwechsel mit spezieller Hinsicht auf DDC, HMP19 and GAD1. Effekte durch BDNF (nicht-katalytische TRKB-Isoform), Membranfusionen von Neurotransmitter-enthaltenden Vesikeln (STX3A, SYN2),  $Ca^{2+}$ -Einstrom (AMPA2), Azetylcholinrezeptoren (CHRNA7), Notch-Signalweg (DNER, TLE1, TLE2, JAG1, CUTL2), TGF $\beta$ -Signalweg (TGFB2, TGFB2, BAMBI, BMP7), WNT-Signalweg (DKK2, DKK4), G-Protein-Signalweg (RGS4) und ERK/MEK-Signalweg (ERK1, MEK1). Die Orientierung axonaler Wachstumskegel, die Synaptogenese und die Tendenz dendritische Verzweigungen zu bilden, waren auf Transkriptebene in Folge eines erhöhten  $A\beta_{42}/A\beta_{40}$ -Verhältnisses vermindert, aber als Resultat eines erniedrigten  $A\beta_{42}/A\beta_{40}$ -Verhältnisses verstärkt (SEMA3A, SEMA3C, L1CAM, PTN, SLIT1). Deutlich beeinflusst durch ein verändertes  $A\beta_{42}/A\beta_{40}$ -Verhältnis waren Gene, die an folgenden Bereichen beteiligt waren: Glutamat/Ammoniak Stoffwechsel (GLUL, GLS), Harnstoff-Zyklus (ASS), Zellzyklusregulation (CCND1, CDKN1A), Glukokortikoid regulierte Kinase (SGK), Rezeptoren (PTGER2, EGFR, AMPA2, AMPA3, GRM7, GRM8c, GLRB, GABRB3), Langzeitpotenzierung (CREB1), axonaler Transport (DNCL12), Angiogenese (HGF, VEGF), T-Zellrezeptoren und assoziierte Transkriptionsfaktoren (T-Zellrezeptor  $\alpha$  und  $\delta$  Lokus, GATA3), Lipoprotein-assoziierte Proteine oder Adapterproteine hiervon (LRP4, PDZK1), vesikulärer Organellen Transport und Mikrotubuli Assoziation (VMP), Transkriptionsfaktoren (PBX1, SHOX2) und stressverwandte Faktoren (ADRB1). Zusammengefasst haben die identifizierten Gene, Proteine und Signaltransduktionswege neue und tiefere Einblicke in die Effekte veränderter C99-Spaltprodukte gewährt and stellen neue Hypothesen für die pathologischen Mechanismen der Alzheimer Krankheit zur Verfügung. Weiterhin sind sie mögliche Kandidaten für genetische Risikofaktoren und könnten dabei hilfreich sein, Mechanismen nicht-genetischer Risikofaktoren zu erklären. Das für ein erhöhtes  $A\beta_{42}/A\beta_{40}$ -Verhältnis spezifische Genexpressionsmuster könnte, zusammen mit klinischen Daten, für die Diagnose der AK nützlich sein. Letztendlich könnten sich einige der identifizierten Transkripte, Proteine und Signalwege als geeignete Angriffsstellen für Medikamente erweisen.

## 3 Introduction

### 3.1 Overview

Alzheimer's disease (AD) is the most common form of dementia in the elderly population. Alois Alzheimer, a German physician, was the first to link brain pathology with cognitive dysfunction of his patients [1]. AD is a progressive neurodegenerative disorder with a long preclinical phase that can take several decades. It is manifested by cognitive and memory deterioration, a variety of neuropsychiatric symptoms and behavioral disturbances [2]. One of the most important risk factors is the *age of the patients*. Apart from the less frequent early onset of the disease, which can start from <65 years of age, most of the patients manifest symptoms over 65 years (late onset Alzheimer's disease, LOAD). With the increasing longevity of our population, it is assumed that AD will approach epidemic proportions in the future with no cure yet available. Its prevalence rises dramatically with age. Its prevalence approximately doubles every five years for those between 65 and 85 years of age, representing 5-10% of the population over 65 years of age and more than 20% over age 80. One hallmark of AD are extracellular deposits (amyloid plaques found in the patients' brains), consisting, apart from other proteins, of amyloid  $\beta$ -peptides. These peptides, of about 40 amino acids in length, are derived from cleavage of the amyloid precursor protein (APP), a transmembrane protein [3]. The proportion of two major amyloid  $\beta$ -peptides,  $A\beta_{40}$  and  $A\beta_{42}$  is approximately 90% to 10% in the amyloid plaques, however, the less abundant  $A\beta_{42}$  is regarded as the critical component for the progression of the disease.  $A\beta_{42}$  differs from  $A\beta_{40}$  by two amino acids (isoleucine and alanine). Mc Laurin and co-workers examined the folding properties of  $A\beta_{42}$  and  $A\beta_{40}$ . At pH 6.0 and in the presence of phosphatidylinositol vesicles, both  $A\beta_{42}$  and  $A\beta_{40}$  adopted an amyloidogenic  $\beta$ -structure. In contrast, at neutral pH only  $A\beta_{42}$  folded into a  $\beta$ -structure in the presence of phosphatidylinositol vesicles [4]. Anti-parallel  $\beta$ -structures contribute to reduce the water-solubility of proteins.

AD is a genetically heterogeneous disorder because mutations and polymorphisms occur in multiple genes and might together contribute to the disease. Moreover, non-genetic factors are involved [5]. Early onset familial AD is caused by rare and highly penetrant mutations which manifest in an autosomal dominant fashion, whereas late onset (>65 years of age) AD proceeds from common polymorphisms with relatively low penetrance but high prevalence [6]. In addition to APOE, a well established risk factor for AD, which is localized on chromosome 19, linkage has been found on other chromosomes. During the last years many new candidate genes have been found in genetic and biochemical approaches. The number of chromosomal regions,

assumed to be associated with AD, has grown. The genetic risk of a complex disease such as AD may be determined by the combined effects of numerous loci, some of which may produce only minor contributions to the overall risk. Linkage and association studies suggested candidate genes on nearly all chromosomes according to the overview at [www.alzforum.org](http://www.alzforum.org). The fact that nearly all chromosomes appear to be affected questions the accuracy of linkage and association studies. To narrow down putative candidate genes, more attention should be drawn onto the lod score. Most of the previously described chromosomal regions do not exceed the commonly accepted lod score of 3.0 for significant linkage and therefore true linkage is questionable. Recently, systematic meta-analyses were performed for each polymorphism with available genotype data [7].

Mutations in APP, PS1 and PS2 cause the autosomal dominant form of early onset AD. The APOE  $\epsilon$ 4 allele has been associated with an increased risk of developing both early and late onset AD [8, 9]. These genes are assumed to be responsible for approximately 50% of the genetic background of the disease, suggesting that further susceptibility genes exist.

APP is a ubiquitous protein found in all cell types of all species, suggesting a basic and important role: APP-family members were suggested to be involved in neuronal development, a crosstalk to Notch has been observed and Numb was identified as a potential target for APP-family members [10]. Furthermore, Soba and colleagues provided evidence that homo- and heterocomplexes of APP/APLPs promote trans-cellular adhesion *in vivo* and that APLP2 is required for cell-cell adhesion in mouse embryonic fibroblasts [11]. A neurotrophic function for APP and secreted APP (sAPP) is often discussed [12]. Therefore, a loss of function of APP rather than a gain of toxic function of A $\beta$  could also be a possible hypothesis to explain the stimulation of tau pathology and neurodegeneration. APP-C-terminal fragments (APP-CTFs) decrease unexpectedly during the course of AD and are well correlated with the progression of tau pathology [12]. This decrease could be explained by these observations: Firstly, loss of APP-C-terminal fragments (CTFs) could result from a modification of secretase activities, and especially from an activation of  $\gamma$ -secretase, and therefore a transformation of APP-CTFs into  $\gamma$ -CTFs and other smaller fragments. Secondly, targeting of APP in subcellular compartments might be dysregulated. Furthermore, proteasomal degradation of APP-CTFs could be involved [13]. Beta, alpha and gamma-stubs were also significantly decreased in the brain tissue of patients having an inherited form of AD linked to mutations of PS1. An important role of the gamma stub, also named AICD (APP intracellular domain), as a gene regulator could explain its involvement in the disease if these fragments are lacking [14].

A $\beta$  is a normal product of cellular metabolism throughout life and circulates as a soluble peptide in biological fluids. It is secreted by neural and non-neural cells and also primary neurons from fetal brain produce A $\beta$  [15]. A $\beta$  is also present in the cerebrospinal fluid and plasma of normal humans [16, 17]. It was hypothesized that chronically enhanced production and/or decreased clearance of soluble, diffusible A $\beta$  could lead to the gradual precipitation of aggregated non-diffusible A $\beta$  in the form of spherical plaques and vascular deposits in AD and Down's syndrome. In cerebrospinal fluid (CSF) decreases in the level of A $\beta_{42}$  correlated with the presence of AD and might be diagnostically meaningful [18]. A $\beta_{42}$  is the more fibrillogenic A $\beta$  species, whereas A $\beta_{40}$  is the physiological and more abundantly secreted A $\beta$  [19].

APOE is likely to be involved in the transport or clearance of A $\beta$ . The fact that all four known AD genes (APP, PS1, PS2, APOE) implicate A $\beta$ , and that APOE implicates fibrillogenesis directly provides support for the hypothesis that A $\beta$  accumulation is central to the disease. There are three human APOE alleles. The three common isoforms of the APOE gene on chromosome 19q13.2 are encoded by alleles  $\epsilon 2$ ,  $\epsilon 3$  and  $\epsilon 4$ . The APOE  $\epsilon 4$ -allele is considerably over-represented in AD subjects (approximately 40% versus 15% in the general population). It was observed that ApoE2 prevented the development of fibrillar plaques in transgenic mice. However, the protective  $\epsilon 2$ -allele can only be found in 2% of all AD cases, compared to 10% in the general population. The absence or presence of one or two  $\epsilon 4$ -alleles was found to correlate in a dose-dependent manner with the relative density of amyloid plaques [20]. The mean age of onset of AD is less than 70 years among the  $\epsilon 4/\epsilon 4$  population, but over 90 years for the  $\epsilon 2/\epsilon 3$  population.

The APOE gene is the only robustly replicated risk factor for the common form of AD with onset after 65 years of age. Twin studies found a concordance rate for AD among monozygotic twins to be 78%, indicating a strong genetic influence [21]. More than 95% of AD cases are sporadic with onset after 65 years of age. 25 different AD-associated mutations in the APP gene have been published (including the duplications of the APP locus), which affect more than 71 families with the age-of-onset ranging between 30 and 65 years (<http://www.molgen.ua.ac.be/AD.Mutations/>). The most frequent pathological APP-mutation is the V717I substitution, which is found in approximately 50% of APP-linked families. Some of these APP-mutations are related to hereditary cerebral hemorrhage with amyloid (conophilic) angiopathy (HCHWAD) [22, 23].

Although A $\beta$  is the major constituent of the amyloid deposits, there are other components such as P-component [24], APOE [25], APOJ [26], proteoglycans [27], lysosomal proteinases [28, 29] and the proteinases inhibitors  $\alpha_1$ -antichymotrypsin

[30],  $\alpha_1$ -antitrypsin [31],  $\alpha_2$ -macroglobulin [32, 33] and cystatin C [34-38]. These components could also contribute to (or prevent when regarded as a counter regulation in order to get rid of deposits) the development of AD.

Vascular risk factors, such as hypertension and hypercholesterolemia, may play an important role in the development of AD. Since neurodegenerative processes of AD might begin 20 to 30 years before manifestation of dementia it is crucial to identify early risk factors. Antihypertensive medication may protect against AD [39-41]. High serum cholesterol in middle age increases the risk of late-life AD [42]. Using statins as cholesterol reducing drugs has been shown to significantly reduce rates of AD [43-45]. Studies revealed that using simvastatin decreased A $\beta$  levels in the CSF and slowed the progression of AD [46]. Participants with elevated systolic blood pressure (BP,  $\geq 160$  mmHg) or high serum cholesterol ( $\geq 6.5$  mmol/l) in middle age had a significantly higher risk of AD in later life, even after normalisation for age, body mass index, education, vascular events, smoking status and alcohol consumption, than those with normal systolic BP or serum cholesterol. Both risk factors in middle age together had a significantly higher risk of developing AD than those with either of the risk factors alone. Diastolic blood pressure in middle age had no significant effect on the risk of AD. Presence of the APOE  $\epsilon 4$  allele, which is involved in cholesterol metabolism, is the most important genetic risk factor for AD. The APOE  $\epsilon 4$  allele is an independent risk factor for AD, even after adjustment for midlife vascular risk factors and other confounders. Similarly, elevated midlife cholesterol level and systolic BP were independent risk factors for AD, even after adjustment for APOE genotype and other confounding factors. APOE has a central role in lipid metabolism and the APOE  $\epsilon 4$  allele is associated with increased serum cholesterol levels. The APOE  $\epsilon 4$  allele is also associated with an adverse prognosis in other diseases of the brain in the elderly, such as stroke and brain trauma. Thus, the APOE  $\epsilon 4$  allele is not specific for AD and there is some evidence that the risk related with the APOE  $\epsilon 4$  allele could be reduced or modified by interventions to treatable risk factors. Some recent studies have suggested that the APOE  $\epsilon 4$  allele is a significant risk factor for AD only among hypertensive individuals who have not used antihypertensive drugs [47]. Searching susceptibility genes for AD has turned out to be complicated, as it is known for all other diseases with complex inheritance, due to combined effects of numerous trait loci. Microarray techniques are promising tools in order to unravel the complex interplay of numerous genes. Population based studies of patients that subsequently developed AD show a significant decrease in plasma cholesterol levels preceding development of cognitive symptoms [48], potentially obscuring the past effects of higher cholesterol levels earlier in life. Finally, subjects with the highest levels of plasma cholesterol generally die at younger ages from cardiovascular

events and are lost from the sample of elderly subjects, introducing a “survivorship effect” into the population. It is therefore important that a relationship between AD and cholesterolemia in human subjects is established at the neuropathological level during the early stages of amyloid accumulation and before development of cognitive symptoms later in life. Furthermore, autopsy of human brains showed a strong association between total plasma cholesterol levels and presence of *early* amyloid deposits in a young subgroup of subjects (40-55 years).

### **3.2 Proteolytic processing of the amyloid precursor protein (APP) and activation of transcription**

Proteolytic processing of APP plays a central role in AD (Fig. 3.1). Due to variable APP processing, several  $\beta$ -amyloid peptides are generated. In contrast to the form with 40 amino acids, the variant with 42 amino acids has a higher tendency to form protease resistant aggregates and is thought to be the pathogenic form triggering the pathophysiological cascade in AD (amyloidogenic pathway; APP can also be processed at the  $\alpha$ -site, which precludes  $A\beta$ -generation and is therefore called the non-amyloidogenic pathway). APP is cleaved by  $\beta$ -secretase within its ectodomain resulting in generation of the C-terminal fragment C99, which is further cleaved within its transmembrane domain by the  $\gamma$ -secretase complex (presumably sequentially) first at the  $\epsilon$ -, than at the  $\zeta$ -cleavage site and finally at the  $\gamma$ -cleavage site (the  $\zeta$ -cleavage site is located between the  $\gamma$ -cleavage and  $\epsilon$ -cleavage site). Due to variable processing by the  $\gamma$ -secretase complex, cleavage at the  $\gamma$ -cleavage site generates  $A\beta_{42}$  and  $A\beta_{40}$  and the AICD<sub>50-99</sub> and AICD<sub>49-99</sub> [49, 50]. Cleavage at the  $\epsilon$ -cleavage site occurs at  $A\beta_{49}$  [51] and cleavage at the  $\zeta$ -cleavage site at  $A\beta_{46}$  (APP717 mutation site=London mutation) [52]. Proceeding from the carboxyl terminus toward the N-terminus, the cleavages generate successively shorter  $A\beta$  peptides, from 49/48 to 46/45, to 43/40 and 42 [53].

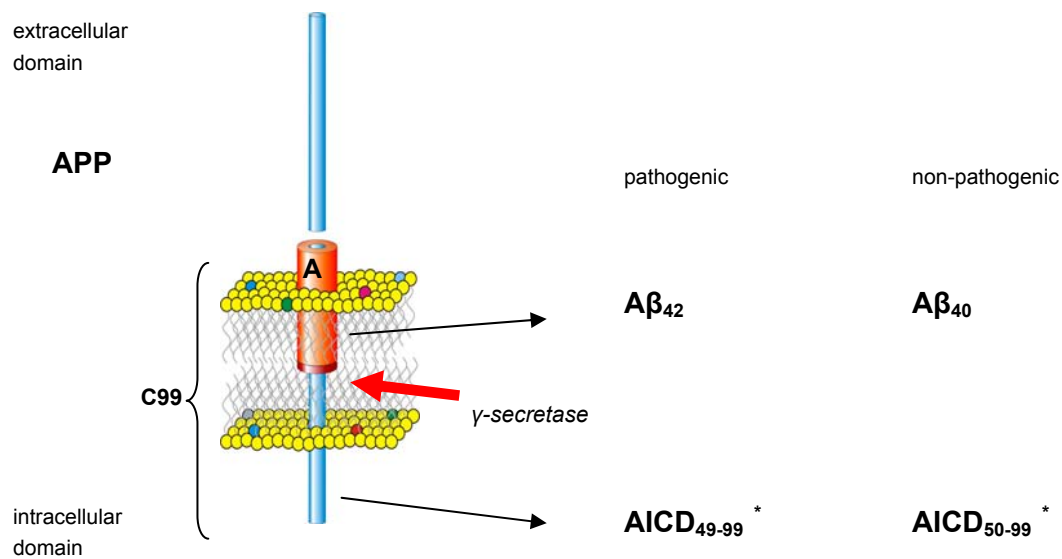


**Figure 3.1 Model of proteolytic processing of C99 by  $\gamma$ -secretase.** While knowledge of A $\beta$ <sub>42</sub> and A $\beta$ <sub>40</sub> generation is well established, knowledge of the AICD is limited by its inherent quick degradation and hence difficulties in its detection. C99 is generated as a result of APP cleavage by  $\beta$ -secretase (not shown) and undergoes further cleavage by  $\gamma$ -secretase. On the one hand A $\beta$ <sub>40</sub> is generated and accompanied by the generation of the APP C-terminal fragment AICD<sub>50-99</sub> [49]. This process is regarded as non-pathogenic. In contrast to this, due to varying processing by  $\gamma$ -secretase, the less abundant A $\beta$ <sub>42</sub> is also generated, accompanied by generation of AICD<sub>49-99</sub>. This process is regarded as pathogenic (pathogenic effects are assumed to be mediated by A $\beta$ <sub>42</sub>, while effects of the AICD<sub>49-99</sub> have not been well investigated yet). A link between the production of A $\beta$ <sub>42</sub> and the AICD<sub>49-99</sub> was suggested [50]. It has been shown that equimolar amounts of A $\beta$  and AICD are produced [49]. \*Gene expression could also be triggered by the as yet unidentified AICD<sub>57</sub> and AICD<sub>59</sub>, the two species which should theoretically remain after cleavage of A $\beta$ <sub>42</sub> and A $\beta$ <sub>40</sub> from the precursor C99. Furthermore, it has to be taken into consideration that the AICDs themselves are cleaved and that their cleavage products may also induce or repress gene expression.

How transcription is activated/repressed after APP-processing is a controversial issue. The question of whether the AICD, like the Notch intracellular domain, is involved in nuclear signaling is highly controversial [14, 54, 55] and, apart from the AICD as the transcription-activating peptide, other mechanisms are imaginable: intracellular A $\beta$ , even if present in only tiny amounts, could trigger transcription via cross-talk with other proteins, or secreted A $\beta$  could influence transcription by docking from outside of the cell to transmembrane receptors and transduce a signal to the nucleus. Moreover, AICD fragments, derived after cleavage, might activate or repress transcription.

A suggested function of the AICD is the formation of a complex together with Fe65 and TIP60, a histone-acetyl-transferase, translocation to the nucleus (after cytosolic degradation of the AICD). APP may anchor Fe65 in the cytosol, while the release of

AICD from APP by  $\gamma$ -cleavage may allow the AICD-Fe65 complex to translocate to the nucleus where it may act as a transcription factor [55, 56].

Some reports suggest that the AICD regulates the expression of KAI1, glycogen synthase kinase-3 $\beta$ , neprilysin and APP. However, no consistent effects on the expression levels of these genes were found in cells and tissues by using gamma-secretase inhibitors or by genetic deficiencies in the gamma-secretase complex. Furthermore, it was demonstrated that Fe65, an important AICD-binding protein, transactivates a wide variety of different promoters independent of AICD co-expression. It was concluded that the four previously proposed target genes are at best indirectly and weakly influenced by APP processing [54]. This is supported by a gene expression profiling study of the human neuroblastoma cell line SHEP-SF transfected with a tetracycline-inducible system, in which no differential expression was observed for KAI1 and glycogen synthase kinase-3 beta in response to AICD overexpression [57].

JNK (c-Jun N-terminal kinase)-interacting protein 1 (JIP1) may promote transcription different from the mechanism mediated by Fe65 [58]. Many proteins have been described to interact with the NPTY motif of APP: Disabled-1 (Dab1) [59], Shc [60, 61], JIP1 [62], X11 [63] and FE65 [64-67]. It has been reported that a transcriptionally active complex of APP with Fe65 and histone acetyltransferase can be formed [55]. Tarr et al. identified Shc A and Shc C, PTB containing adaptor proteins cross-talking with cellular differentiation and survival pathways, as APP interacting proteins [68]. The FE65s (FE65, FE65L1, and FE65L2) are a family of multidomain adaptor proteins that form multiprotein complexes with a range of functions. FE65 is brain-enriched, whereas FE65L1 and FE65L2 are more widely expressed. All three members contain two PTB domains and a WW domain. Through the PTB2 domain, they all interact with the AICD of APP and can alter APP processing [69].

There is *in vivo* evidence of transcriptional activation of the KAI1 gene by a complex consisting of the C-terminal cleavage product of APP, Fe65 and TIP60, which corroborates the function of APP in nuclear signaling [70], although there is some controversy in regard to nuclear translocation of the AICD [14, 71, 72].

It was shown that a caspase-mediated cleavage releases the last 31 amino acids from the C-terminus of APP. This C31 peptide causes apoptosis in cultured cells and can be found in brain samples from AD patients but not in samples from control brains. Daniel Lu, Edward Koo and colleagues reported that the 31 amino-acid peptide from the C-terminus of APP could be involved in AD neuronal death, maybe in conjunction with A $\beta$ . Their results indicate that both caspase-8 and caspase-9 cleave APP to form the C31 peptide, which is cytotoxic to cultured cells. They also

determined that the previously demonstrated cytotoxicity of the C100 peptide is dependent on that final 31-amino-acid fragment. Finally, in AD brains, but not in control tissue, they found evidence of intracytoplasmic APP cleavage (presumed to be caspase-mediated) and activation of caspase-9 [73].

### 3.3 The amyloid cascade hypothesis

Genetic analysis of kindred with AD has pointed to A $\beta$  as the initiating molecule in the development of the disease. Biochemical work on APP processing revealed that all pathogenic mutations altered processing in such a way that A $\beta_{42}$  was more likely to be produced. Such genetic and biochemical data together suggested that A $\beta_{42}$  accumulation was the primary event in the pathogenesis of AD. These data together led to the formulation of the amyloid cascade hypothesis (Fig. 3.2).

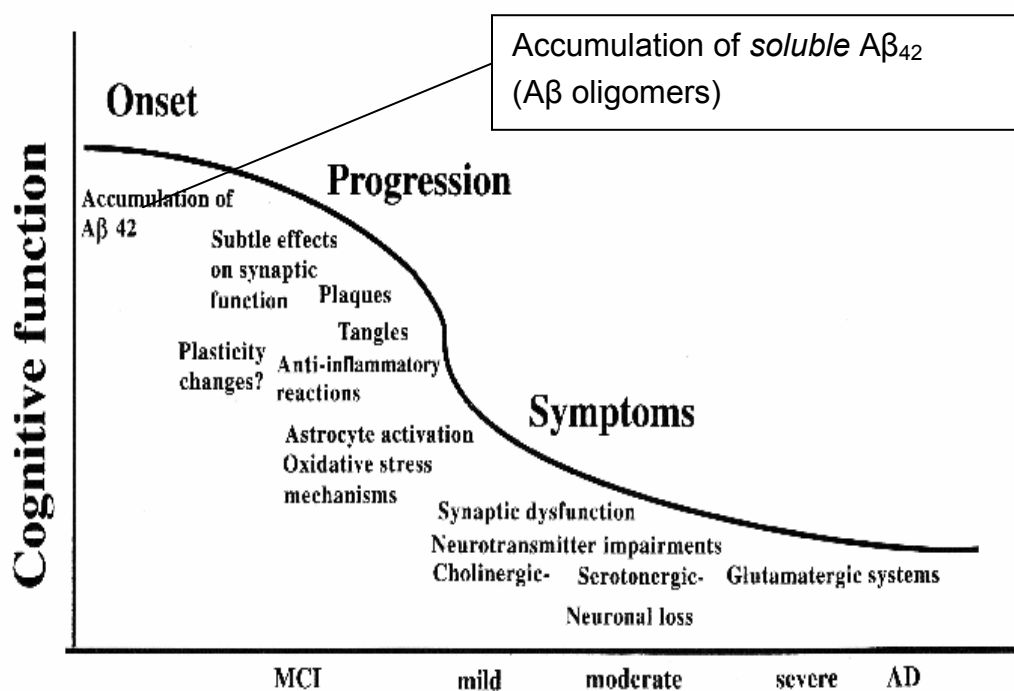


**Figure 3.2 Pathophysiological cascade in Alzheimer's disease.** Figure was taken and modified from "Alzheimer's Disease and Related Disorders" (Agneta Nordberg).

Soluble A $\beta$ , secreted *in vitro*, forms SDS-insoluble oligomers [74]. These A $\beta$  oligomers secreted by cells cause neuronal dysfunction *in vivo* [75, 76] and it was demonstrated that they are more neurotoxic than A $\beta$  fibrils [77]. The *soluble and diffusible A $\beta$  oligomers were identified as the actual trigger of AD pathogenesis. A $\beta$  is produced under normal conditions but in brain tissue it is immediately sequestered or*

*rapidly catabolized. When this A $\beta$  removal mechanism is overwhelmed by overproduction, as in Down's syndrome, or by impaired removal, A $\beta$  deposition and plaque formation start.* The A $\beta$  species associated with AD form oligomers more quickly, are more toxic to neurons and produce more severe membrane damage than the A $\beta$  species associated with normal brain aging. The combination of different A $\beta$  species leads to differently conformed A $\beta$  soluble aggregates that exhibit a large spectrum of toxicity.

There is a large body of evidence that A $\beta_{42}$ , but not A $\beta_{40}$ , triggers the pathophysiological cascade in AD. Some recent publications discuss whether the ratio of A $\beta_{40}$  to A $\beta_{42}$  is responsible for triggering this cascade [78]. Furthermore, it turned out that A $\beta$  was derived from the transmembranous part of the type 1 integral membrane protein APP after cleavage by proteases. Research on HCHWAD revealed further associations between A $\beta$  deposition in cerebral blood vessels and mutations at the APP locus coding for the middle of the A $\beta$  part of the molecule [23]. Since mutations in the APP locus have been shown to be responsible for only a very small percentage of AD familial cases it was obvious that other genes had to be involved; linkage studies in families who had an onset age from approximately 30-40 years revealed a locus on chromosome 14 [79]. Further work identified the presenilin 1 gene on chromosome 14. Genetic analysis of pedigrees of Russian-German origin revealed a further locus on chromosome 1, which was shown to correspond to presenilin 2, a presenilin 1 homologue [80]. In the presenilin 2 gene a small number of mutations which cause AD have also been found. While APP/PS transgenic mice generate amyloid plaques they develop no tangle pathology and only little cell loss. Data on amyloid plaque pathology relate directly only to the early onset familial forms of the disease, a direct connection to late onset (>65 years of age) cases is less clear. The fact that APP/PS transgenic animals do not develop either tangles or cell loss has questioned the accuracy of the amyloid cascade hypothesis. However, the fact that a perfect animal model for AD does not exist must also be considered. Furthermore, data obtained from transgenic animals are not directly transferable to humans.

These observations support the hypothesis that A $\beta$  is crucial for the initiation of the disease:

Adverse effects were recognized after the injection of 20  $\mu$ l of picomolar solutions of A $\beta$  oligomers into the cerebral ventricles of young rats, for instance disorientation in the Morris water maze [81]. Amyloid deposited in the cerebrovasculature of transgenic mice (APP: E693Q) consists predominantly of A $\beta_{1-40}$ . Cross-breeding such mice with mice expressing a PS1 variant that increases A $\beta_{1-42}$  production

resulted in early (starting at 3 months of age) accumulation of brain-parenchymal amyloid plaques and reduced cerebral amyloid angiopathy [82]. Thus, similarly to humans, the main component of blood vessels amyloid is  $A\beta_{1-40}$ . Increasing the  $A\beta_{42}/A\beta_{40}$  ratio favours parenchymal amyloid deposition with higher  $A\beta_{1-42}$  content. *The presence of a mechanism rapidly binding or breaking down  $A\beta_{42}$ , for instance by extracellular proteases (neprylisin, IDE, plasmin, etc.) was suggested [83-85].*

The APP gene, located on chromosome 21q21, consists of 19 exons that are alternatively spliced into eight mRNA forms. Several mutations in the APP gene have been discovered. Although the APP mutations account for less than 0.1% of all AD cases, they result in complete penetrance leading to AD between the fourth to seventh decades of life [86]. Although the mutations in the APP-gene in several familial AD (FAD) pedigrees were expected to alter quantitative  $A\beta$  production by a changed  $\beta$ -secretase or  $\gamma$ -secretase cleavage only in the K670N/M671L double mutation, secreted peptide amounts were affected. This mutation is located aminoterminally to  $A\beta$  and was found in a Swedish kindred [87]. Cultured cells expressing mutated APP secrete higher levels of  $A\beta$  compared to cells expressing the normal sequence [88].  $A\beta_{42}$  contains two more hydrophobic residues (isoleucine, alanine) than the  $A\beta_{40}$  form, making  $A\beta_{42}$  more fibrillogenic and enhances aggregation [89]. *Insufficient proteolytic removal of  $A\beta$  by proteases such as neprylisin, endothelin-converting enzymes, insulin-degrading enzyme, angiotensin-converting enzyme, the plasmin system and matrix metalloproteases, also has been proposed as a mechanism that leads to  $A\beta$  accumulation in the brain.*

While it is clear that familial Alzheimer's disease (FAD) mutations in APP result in increased  $A\beta$  deposition, it is unclear whether the deposition itself is pathogenic. Apart from the view that deposited  $A\beta$  is neurotoxic, more recently it has been suggested that the neurodegeneration observed in AD is caused by either soluble oligomers of  $A\beta$ , the build up of C-terminal fragments of APP or abnormal signaling by the intracellular domain of APP [90, 91].

The so-called Swedish mutation, located at the N-terminus of  $A\beta$ , results in an APP molecule that is a better substrate for  $\beta$ -site APP cleaving enzyme1 (BACE1) resulting in higher levels of  $A\beta$  [87]. In contrast FAD mutations located between APP714 and APP723 result in altered cleavage by  $\gamma$ -secretase [92]. The amounts of the different  $A\beta$  species ( $A\beta_{37}$ -  $A\beta_{43}$ ) vary with each mutation [93]. *Interestingly a common feature of all mutations causing AD seems to be an increase in  $A\beta_{42}$ .* Five mutations have been reported within the  $A\beta$  sequence at residues APP692-694. These mutations are often associated with cerebral hemorrhage rather than AD [94]. Unlike humans, transgenic mice with these mutations do not develop obvious

neurodegeneration or neurofibrillary tangles. However,  $A\beta_{42}$  overexpression primarily leads to parenchymal  $A\beta$  deposition (such as that observed in AD), whereas  $A\beta_{40}$  overexpression leads to  $A\beta$  deposition primarily in the cerebral vessels [82]. APP mutations, which result in higher levels of both  $A\beta_{40}$  and  $A\beta_{42}$  lead to both pathologies [95], while mutations, like APPV717F, lead to parenchymal  $A\beta$  deposition [96] and APPA692G leads to  $A\beta$  deposition in the cerebral vessels [82].

Analysis of families suffering from dementia and Parkinson's disease revealed linkage to chromosome 17, at the chromosomal locus where the tau gene is localized. Especially intronic mutations which influence the alternate splicing of exon 10 lead to heavy deposits of mutant tau, which in turn lead to tangle formation and neurodegeneration but *not to amyloid deposition*. This information makes it probable that  *$A\beta$  is upstream of tau dysfunction* and tau dysfunction and tangle formation is proximal to cell death. Mice with the tau-P301L-transgene, under the control of the prion promoter, develop tangle formation and cell death in the spinal cord and midbrain. However, when these mice were crossed with APP transgenic mice, enhanced tangle formation and degeneration occurred in the cortex and midbrain. The production of  $\alpha$ -synuclein, a component of Lewy bodies, which are characteristic for Parkinson's disease (PD), is enhanced by crossing  $\alpha$ -synuclein transgenic mice with APP transgenic mice.

Brains of 22 subjects with Down's syndrome (DS) were examined for the presence of soluble  $A\beta_{42}$ . Soluble  $A\beta_{42}$  was detected in half of the fetal brains and in all postnatal cases, even in the young cases (from 4 days up to 14 years old) where diffuse amyloid plaques had not yet formed. Soluble  $A\beta_{1-40}$  and  $A\beta_{x-40}$  were not detected in any of the Down's syndrome cases examined [97]. From this study it was concluded that the overproduction of total  $A\beta_{42}$  is due to APP overexpression in Down's syndrome and that the initial seeding of  $A\beta_{42}$  may begin more than a decade before amyloid fibrils are formed. Nearly all middle-aged DS patients develop AD pathology [98]. However, DS individuals with partial trisomy 21, who are not trisomic for the APP gene, do not develop AD neuropathology. AD pathology in Down's syndrome is associated with three copies of the APP gene [99].

The presence of  $A\beta$  in patients suffering from Mild Cognitive Impairment (MCI), as well as a decrease of  $A\beta_{x-42}$  in the CSF [100] is an important marker of incipient AD.

The amyloid cascade hypothesis is a controversial one and the following features are not in line with it (However, it should be borne in mind that data from mice are not always directly transferable to humans):

In cognitively intact individuals, aging of the brain is very often associated with A $\beta$  deposition but not with neurofibrillary tangles (NFT), suggesting that in these individuals A $\beta$  accumulation does not produce neuronal damage [101]. Transgenic mice expressing APP have age-related neurological deficits in the absence of plaques (however, in these studies *soluble* A $\beta$  was not tested for pathogenic effects) or neurodegenerative changes [102]. A 56 kDa soluble complex of A $\beta$ , called A $\beta$  56, in the brains of the Tg2576 mouse model of AD impairs memory in the absence of amyloidosis or neuronal loss [81].

Tau pathology is more closely related to cognitive impairment than is A $\beta$ . Moreover, tau pathology can be found in the hippocampal area without A $\beta$  deposits [99].

### **3.4 A $\beta$ , tau and the connection in between**

Neurofibrillary tangles, one pathological hallmark of AD, are composed of the highly phosphorylated microtubule-associated protein tau. Tau is involved in the assembly and stabilization of microtubules (MTs). The affinity of tau for MT is actively regulated by phosphorylation and by changes in the ratio of its isoforms, containing either three or four MT binding domains (tau-3R, tau-4R) [103, 104]. Electron microscopy revealed that the substructure of these tangles were paired helical (twisted) filaments [105]. Tangles contain 10-20 nm paired helical filaments (PHF). Phosphorylated tau was recognized as the major, if not the only, component of PHF [106].

Neurofibrillary tangles appear in the entorhinal cortex of 20 % of people with an average age of 25 years. At the age of 50 years 50% of the people are affected and at 75 years all people are affected. The extent varies greatly among individuals. Since 100% of patients have a tau pathology at the age of 75 years, tau pathology can be regarded as an inevitable degenerating process that occurs in the human brain. On the other hand, the brains of non-demented centenarians have been analyzed and a few of these patients had only a very mild entorhinal tauopathy, demonstrating the absence of a direct link with aging. Tau pathology is more closely related to cognitive impairment than A $\beta$  is, but the presence of A $\beta$  in patients suffering from Mild Cognitive Impairment, as well as a decrease of A $\beta$  x-42 in the CSF is an important marker of incipient AD. Spreading of tau is likely to start in a specific vulnerable neuronal population (presumably in layer II of the entorhinal formation in AD). Then this local tauopathy will destabilize the connected neuronal populations. This degenerating process will extend, as a kind of domino effect, to other neuronal populations along a neuron-to neuron propagation phenomenon. It is not surprising that tau pathology is well correlated with cognitive impairment, since it shows the neurodegenerative process and its extent. A $\beta$ x-42 aggregates are

observed at the early stages of tau pathology in non-demented patients and all along AD pathology. During the progression of the disease, A $\beta$ <sub>x-42</sub> aggregates increase in quantity in close parallel to the extension of tau pathology. Tau pathology can be found in the hippocampal area without A $\beta$  deposits. In contrast to this the extension of tau pathology in polymodal association areas was systematically found in the presence of A $\beta$  deposits, as if these A $\beta$  species were necessary to stimulate the progression of tau pathology.

Tau is a phosphoprotein and even normal adult tau is phosphorylated to some degree. Many kinases are able to generate phosphorylation sites on tau proteins *in vitro*. Among the most promising candidates are GSK-3 $\beta$  and cdk5. Tau phosphorylation modulates its binding to microtubules [107] and its ability to stabilize them. Hyperphosphorylated tau species do not bind well to microtubules and this decreased biological function would cause a “loss of function” in affected neurons. Phosphorylation of tau could favour the aggregation of tau in PHF. Soluble or oligomeric forms of phosphorylated tau could also be toxic by themselves, leading to a “toxic gain of function”. On the other hand, tau phosphorylation/aggregation might also be a protective response of neurons submitted to various damaging influences. According to the amyloid cascade hypothesis, tau-phosphorylation is a downstream event of amyloid accumulation. However, it was unexpectedly observed that animals developing A $\beta$  amyloid deposits did not develop NFT, including animals also expressing a human wild-type tau protein. On the other hand, in double transgenic (mutant tau and APP) animals, neurofibrillary degeneration was observed. Tau contains six isoforms [108]. PHF can also be found in entorhinal and hippocampal regions in patients aged over 75 years who are non-demented. Since 100% of people at the age of over 75 have neurofibrillary tangles, means that tau pathology is an inevitable degenerating process that occurs in the human brain. At the age of 25, 20% of people show tau pathology. NFT formation in the entorhinal cortex precedes A $\beta$ -deposition, whereas NFTs appear in the limbic and neocortical areas only after A $\beta$ -deposition [109]. Presumably NFT formation in the entorhinal cortex develops as a result of normal brain aging and only in the disease state of AD does it spread into limbic and neocortical areas.

In human SH-SY5Y cells, tau has been shown to be hyperphosphorylated at several of the same sites as in AD brains. As in AD, the hyperphosphorylated tau accumulated in the cultured cells and did not bind to microtubules [110]. Inhibition of protein phosphatase 2A (PP2A) and protein phosphatase 1 (PP1) activities by okadaic acid up-regulated the activities of MAPK and CDK5 and resulted in abnormal hyperphosphorylation of tau, a decrease in stable microtubules, and an increase in cell death. It was shown *in vitro* that protein phosphatase 2A and 2B

dephosphorylated neurofibrillary tangles/PHF and stimulated assembly of tubulin into microtubules. The state of phosphorylation of a phosphoprotein is a function of the balance between the activities of protein kinases and phosphatases that regulates its phosphorylation. Tau, which is phosphorylated at more than 30 serine/threonine residues in AD [111], is a substrate for several protein kinases. Among these kinases there are:

- glycogen-synthase kinase-3 (GSK-3)
- cyclin-dependent protein kinase 5 (CDK5)
- protein kinase A (PKA)
- calcium-calmodulin-dependent protein kinase-II (CaMKII)
- mitogen-activated protein kinase ERK1/2
- stress-activated protein kinases

It has been shown that phosphorylation of tau by non-proline-dependent protein kinases PKA, PKC, CaMKII, and casein-kinase 1 (CK1) primed it for subsequent phosphorylation by proline directed protein kinases (PDPK) cdk5 and and GSK3. Ser262 and Thr231 are the two major sites at which phosphorylation inhibits the binding of tau to microtubules [112].

Among the involved phosphatases there are for instance:

- protein phosphatase 2A (PP2A)
- protein phosphatase 1 (PP1)

PP2A also regulates the activities of several kinases in the brain:

- CaMKII
- PKA
- MAP kinase kinase (MEK1/2)
- Extracellular regulated kinase (ERK1/2)
- P70S6 kinase

PP1 activity is mainly regulated by inhibitor-1 (I-1) [113]. I-1 and DARPP32 (dopamine and cAMP-regulated phosphoprotein of a molecular weight of 32.000) are activated on phosphorylation by protein kinase A and inactivated at basal calcium levels by PP2A. Thus, inhibition of PP2A activity would keep I-1 and DARPP32 in an active form and thereby result in a decrease in PP1 activity.

PP2A is inhibited by I1<sup>PP2a</sup> (cytosolic protein, synonyms: putative and histocompatibility leukocyte antigen class II-associated protein (PHAP1), mapmodulin, pp32, LANP) and I2<sup>PP2a</sup> (nuclear protein, synonyms: TAF1 $\beta$ , PHAP2) [114]. Other conditions also influence tau phosphorylation: phosphorylation depends on whether tau contains three or four repeat domains (conserved sequence repeats) and whether it contains zero, one or two N-terminal inserts [115]. Tau can also be abnormally glycosylated, which can promote tau phosphorylation. Hyperphosphorylation of tau at the level of 4-6 moles phosphate/mole of the protein induces the toxic property. Not all of the 30 phosphorylation sites may be involved in converting normal tau into a toxic molecule. The following phosphorylation sites are among the critical ones to convert tau into a protein with toxic properties: S199/202/205, T212, T231/S235, S262/356 and S404 [116].

Glycogen synthase kinase (GSK-3 $\beta$ ) was first identified from the microtubule fraction of bovine brain. It can phosphorylate tau in vivo. GSK-3 was identified as a calcium- and cyclic nucleotide-independent kinase of glycogen synthase, which is a rate limiting enzyme for glycogen biosynthesis and a substrate for several kinases. GSK-3 $\alpha$  and GSK-3 $\beta$  are encoded by different genes but they share 85% homology [117]. GSK-3 $\beta$  consists of 482 amino acids and has a molecular weight of 47 kDa. Its promoter has putative binding sites for: AP1, AP2, c-Myb, Cre, MZF1, Sp1 and Tst1. GSK-3 $\beta$  is expressed in all tissues, its levels are highest in the brain. GSK-3 $\beta$  has also been detected in mitochondria and in nuclei [118]. The GSK-3 $\beta$  homolog in *Drosophila*, shaggy, is involved not only in glycogen homeostasis but also in cellular signaling cascades. *GSK-3 $\beta$  activity is regulated by Ser9 (inhibitory site) phosphorylation for instance by protein kinase A (PKA), protein kinase B (PKB, synonym: AKT), protein kinase C (PKC), p90Rsk and p70S6kinase [119]. Cell survival signals activate PKA, PKB, and PKC, thereby deactivating GSK-3 $\beta$ . Thus, GSK-3 $\beta$  is activated in response to reduced cell survival signals, such as the reduction of growth factors.* GSK-3 $\beta$  is able to phosphorylate many substrates and is part of several cellular events including metabolism, signaling and transcription [119]. GSK-3 is categorized as a proline-directed kinase. Most GSK-3 $\beta$  targets are phosphorylated by another kinase before they can be phosphorylated by GSK-3 $\beta$ . GSK-3 $\beta$  is the major tau kinase in vivo [120-125]. 4 moles of phosphate can be incorporated into each mole of tau. Tau is phosphorylated by GSK-3 $\beta$  at Ser199,

Thr231, Ser396 and Ser413 [126], Ser 202/Thr205, Ser396/Ser404 and Ser235 [127]. There is evidence that in total 15 sites are phosphorylated by GSK-3 $\beta$ . Among these only Ser400, Ser404 and Ser413 are non-proline-directed sites. To test whether GSK-3 $\beta$  is activated by A $\beta$ , neuronal death was induced in rat hippocampal cultures by introducing A $\beta$  to the cultures. It was found that GSK-3 $\beta$  was activated approximately two-fold over controls, and that the activation induced hyperphosphorylation of tau and that these events preceded neuronal cell death [128]. *A $\beta$  was found to inhibit phosphatidylinositol-3 (PI3K) kinase and this in turn resulted in activation of GSK-3 $\beta$ .* In hippocampal cultures, treatment of A $\beta$  resulted in cytoplasmic accumulation of the secreted form of APP. Inhibiting GSK-3 $\beta$  prevented this accumulation [129]. APP is metabolized during its transport from the endoplasmic reticulum (ER) to the synaptic regions [130]. When axonal transport is impaired, APP becomes trapped between the Golgi and synaptic regions. Thus trapped, it is metabolized, prematurely releasing the secreted form of APP into the cytoplasm. From these results it was concluded that axonal transport is disrupted by GSK-3 $\beta$ . Disruption of axonal transport could be caused by microtubule destabilization resulting from hyperphosphorylation of tau or by kinesin, a motor protein which is a substrate of GSK-3 $\beta$ . Pathways leading to cell death may be influenced by A $\beta$  accumulation, for instance by increasing intracellular Ca<sup>2+</sup> levels, induction of reactive oxygen species or other mechanisms. Ser422 of tau cannot be phosphorylated by GSK-3 $\beta$ , suggesting there are further kinases involved in phosphorylation of tau, since Ser422 was found to be phosphorylated in AD brains.

Ser422 of tau can be phosphorylated by c-Jun N-terminal kinase (JNK). Hyperphosphorylation of tau by GSK-3 $\beta$  and JNK was shown to induce NFT formation. Recently it was reported that GSK-3 $\beta$  can phosphorylate mitogen-activated protein kinase /ERK kinase kinase (MEKK) and consequently activate JNK.

Thus, A $\beta$  might activate JNK indirectly through activation of GSK-3 $\beta$  [131]. Kinesin, a substrate of GSK-3 $\beta$ , loses its ability to bind to the cargo protein of vesicles after it is phosphorylated by GSK-3 $\beta$ , impairing axonal transport.

Cyclic AMP response element binding protein (CREB), which is a further substrate of GSK-3 $\beta$ , modulates the gene expression of promoters containing cyclic AMP response elements [132]. CREB is involved in processes like long-term memory and the maintenance of synaptic plasticity. CREB is activated when it is phosphorylated at Ser133 by PKA. However, after phosphorylation of CREB at Ser133, GSK-3 $\beta$  recognizes this phosphorylation and phosphorylates CREB at Ser129, which inhibits CREB's transcriptional activity. Thus, the cell's ability to produce long term potentiation (LTP), and in consequence memory formation, is reduced.

LiCl, a known inhibitor of GSK-3 $\beta$ , protected neurons from neurotoxic influences (nerve growth factor deprivation, glutamate excitotoxicity and A $\beta$ -neurotoxicity in rat hippocampal neurons [133]. Thus GSK-3 $\beta$  might be involved in neuronal death. *The anti-apoptotic protein BCL-2 is a target of CREB. Since CREB is a substrate of GSK-3 $\beta$ , GSK-3 $\beta$  can influence BCL-2 via CREB. When GSK-3 $\beta$  is activated, it can phosphorylate CREB (previously, CREB has to be phosphorylated at SER133, for instance by PKA) and induce BCL-2 expression.*

A PS1 mutation was found in frontotemporal dementia patients. This mutation can activate GSK-3 $\beta$  [134]. GSK-3 inhibition may be a potential therapy for AD, because it may inhibit both A $\beta$ -generation and A $\beta$ -induced pathophysiological events in AD models.

### 3.5 Genes associated with Alzheimer's disease

In addition to *APOE*, the only currently established genetic risk factor for AD, linkage has been found on chromosome 12. Other linkage and association studies suggested, with less consistent results, candidate genes on chromosome 1, 2, 3, 4, 5, 6, 9, 10, 11, 12, 14, 15, 19, 21 and the X-chromosome. Recently, systematic meta-analyses were performed for each polymorphism with available genotype data. In addition to identifying the epsilon4 allele of *APOE* and related effects, over a dozen potential Alzheimer disease susceptibility genes were pinpointed (*ACE*, *CHRNA2*, *CST3*, *ESR1*, *GAPDH*, *IDE*, *MTHFR*, *NCSTN*, *PRNP*, *PSEN1*, *TF*, *TFAM* and *TNF*) with statistically significant allelic summary odds ratios (ranging from 1.11-1.38 for risk alleles and 0.92-0.67 for protective alleles) [7]. At [www.alzforum.org](http://www.alzforum.org) an effort was made to select the most promising candidate genes, which are updated regularly (Table 3.1):

1.	<i>APOE</i> ( $\epsilon$ 2/3/4)	apolipoprotein E ( $\epsilon$ 2/3/4)
2.	<i>GAB2</i>	GRB2-associated binding protein 2
3.	<i>CHRNA2</i>	cholinergic receptor, nicotinic, beta 2 (neuronal)
4.	<i>CH25H</i>	cholesterol 25-hydroxylase
5.	<i>PGBD1</i>	piggy Bac transposable element derived 1
6.	<i>LMNA</i>	lamin A/C
7.	<i>MAPT</i>	microtubule-associated protein tau
8.	<i>PCK1</i>	phosphoenolpyruvate carboxykinase 1 (soluble)
9.	<i>TFAM</i>	transcription factor A, mitochondrial
10.	<i>CST3</i>	cystatin C
11.	<i>ACE</i>	angiotensin I converting enzyme (peptidyl-dipeptidase A) 1

12.	SORCS1	sortilin-related VPS10 domain containing receptor 1
13.	hCG2039140	[predicted by Celera Genome Assembly]
14.	GALP	galanin-like peptide precursor
15.	SORL1	Sortilin-related receptor
16.	TNK1	tyrosine kinase, non-receptor, 1
17.	GWA_14q32.13	protein unknown
18.	IL1B	interleukin 1, beta
19.	TF	transferrin
20.	LOC651924	similar to Ubiquitin-like 1-activating enzyme E1B
21.	GWA_7p15.2	protein unknown
22.	LOC439999	similar to ribosomal protein S3a
23.	DAPK1	death-associated protein kinase 1
24.	GAPDHS	glyceraldehyde-3-phosphate dehydrogenase, spermatogenic
25.	PRNP	prion protein
26.	MYH13	myosin, heavy chain 13, skeletal muscle
27.	MTHFR	5,10-methylenetetrahydrofolate reductase (NADPH)
28.	BDNF	brain-derived neurotrophic factor

**Table 3.1 Top candidate genes assumed to be involved in the pathogenesis of AD (www.alzforum.org, February 2008).**

'Suggestive' linkage according to Lander & Kruglyak was observed using several programme packages including USERM13, FASTLINK and GENEHUNTER-PLUS. Multipoint lod scores and two-point lod scores give an estimation how significant a result is. *Lod scores above 3.0 are usually regarded as significant.* One of the identified regions, on chromosome 19q13, fulfills Lander & Kruglyak's criteria of "highly significant" linkage. This is presumably caused by the nearby APOE locus, localized in the same chromosomal region. Further suggestive linkage has been reported for a region between 10q22 and 10q26 close to the *insulin degrading enzyme (IDE)*. The chromosomal region 9q21-22 has also been found in linkage analyses and an association with AD on this chromosome has been reported for the *very low density lipoprotein receptor (VLDL-R)*. Three chromosomal regions are of particular interest because of their proximity to proposed AD candidate genes (1q23, 11q25) or established AD genes (14q22). The linkage region on chromosome 1q23 lies within 3 Mb of the *nicastrin* gene, which is part of the  $\gamma$ -secretase complex which liberates A $\beta$  from APP. The *beta-secretase cleavage enzyme (BACE)* is a further candidate gene and is located approximately 20 Mb upstream of the region 11q25. The strong linkage signal on chromosome 14q22 lies within 20 Mb of the *presenilin 1*

gene (14q24.3), which is responsible for the majority of all early-onset familial AD cases. Families with AD-causing PSEN1 mutations have an average onset age of about 45 years. Recently new PSEN1 mutations were found causing an onset age of 60 years or older.

Genetic and environmental factors contribute to the pathogenesis of AD which is characterized, apart from other features, by amyloid accumulation, tau hyperphosphorylation, inflammation, apoptosis and oxidative stress. Some of the genetic and environmental risk factors are *high age, a history of AD cases in the family, apolipoproteine E  $\epsilon$ 4 allele, high blood pressure, glucose intolerance, high homocysteine, low vitamine B12, B6 and folate levels, smoking, hypothyreosis, low level of education and others*. Protective factors might be *use of estrogens, antioxidants, anti-inflammatory agents, statins, apolipoproteine E  $\epsilon$ 2 allele, high level of education, physical exercise, a supporting social network*. Mutations in APP, PS1 and PS2 cause the autosomal dominant form of early onset AD. The APOE  $\epsilon$ 4 allele has been associated with an increased risk of developing both early and late onset AD. These genes are assumed to be responsible for approximately 50% of the genetic background of the disease, suggesting that further susceptibility genes exist. Fine mapping of chromosomal susceptibility regions using single nucleotide polymorphism (SNP) have been used to identify candidate genes in the most promising targets. Among many other candidate genes, which can be found on the web site [www.alzforum.org](http://www.alzforum.org), polymorphisms in the myeloperoxidase (MPO)-and alpha-2-macroglobulin (A2M)-gene have been detected in Finnish AD patients. In order to find new susceptibility loci for late onset AD, a linkage disequilibrium analysis was performed in a Finnish population [135, 136]. Forty-seven patients with late-onset AD and 51 age-matched control subjects were chosen from the same geographic area in eastern Finland, where the population is descendent mainly from a small group of original founders. These subjects were initially genotyped with 366 polymorphic microsatellite markers and a follow-up analysis was performed with additional microsatellite markers for those chromosome loci found to be associated with AD. This analysis revealed 8 chromosomal loci where more than one microsatellite marker was associated with AD: 1p36.12, 2p22.2, 3q28, 4p13, 10p13, 13q12, 18q12.1 and 19p13.3. Genes in close proximity to these loci will provide targets for future genetic and functional studies of AD.

Mutations in the PS1 gene, located on chromosome 14q24.3, account for 18-50% of all early onset AD cases and lead to the onset of the disease ranging from 16 to 65 years [137]. 155 different PS1 mutations (most of them are missense substitutions) have been found in more than 315 AD families (<http://www.molgen.ua.ac.be/ADMutations/>). The most frequent PS1 mutation is G206A observed in 18 unrelated

Caribbean Hispanic families [138].

PS2 is located on chromosome 1q31-q42. In contrast to PS1, mutations of the PS2 gene are rare and associated with a later age of onset [139]. 10 different PS2 mutations have been reported in 18 families with age of onset ranging between 40 and 85 years (<http://www.molgen.ua.ac.be/ADMutations/>).

Mutations in the PS1-and PS2 genes cause the overproduction of A $\beta$ <sub>42</sub>. In addition to APP processing, PS1 and PS2 are essential for the proteolytic cleavage of several other proteins including Notch.

The strongest support for linkage has been described for chromosomes 10 and 12. The identified regions are rather broad (>30Mb). Whether true linkage for the following genes really exists is questionable, since LOD scores are quite small (approximately up to 1.2): VR22 ( $\alpha$ -3-catenin; CTNNA3,  $\alpha$ -T-catenin), IDE (insulin degrading enzyme), CH25H (cholesterol 25-hydroxylase), plasminogen activator urokinase (PLAU), Glutathione S-Transferase Omega1 (GSTO1). Higher LOD scores (approximately up to 4.0) have been found for M6PR (mannose-6-phosphate receptor), A2M ( $\alpha$ 2-macroglobulin), and LRP1 (lipoprotein receptor-related protein 1,  $\alpha$ 2-macroglobulin receptor A2MR, APOE receptor). Recently glyceraldehyde-3-phosphate dehydrogenase (GAPD) and pregnancy zone protein (a homologue of A2M) have been discussed as candidate genes. Since in linkage studies relatively broad chromosomal regions are identified, it is probable that genes (further genes identified within this region) that have not yet been considered may play a crucial role. In recent years many genes have been reported to be associated with AD (<http://www.alzforum.org/re/com/Alzforum>) but none of these have shown the same replicable association like the one between AD and the APOE  $\epsilon$ 4-allele.

Some of the APP mutations are close to the  $\alpha$ -secretase cleavage site (for instance the following mutations: Dutch APP693, Flemish APP692, Arctic E693G, Italian E693K and Iowa D694N). Alpha-secretase cleavage prevents the generation of A $\beta$ . Thus, these mutations confirmed the expected change of the fibrillogenic potential of the generated A $\beta$  species. This was strong support for the belief that APP is central in the disease mechanism. Cerebrovascular amyloid deposits are mainly composed of A $\beta$ <sub>40</sub>, the less fibrillogenic A $\beta$  form.

### 3.6 Selection of normalization algorithms

For further information about the Affymetrix Match/Mismatch system and background calculation etc. refer to Chapter 12.4, Mathematical background.

*Microarray analysis provides the ability to measure several thousands of transcripts in parallel with the advantage of giving insight into the interplay between genes.* Here, approximately 40,000 transcripts (the human genome comprises 20,000-25,000 genes), were analyzed. Analyzing so much data in parallel requires a certain normalization strategy.

Normalization of data is necessary to make it possible to compare the output of microarrays. Even if all conditions for sample preparation and hybridization are kept constant as good as possible, there is an inevitable extent of variation of the conditions. Due to variations in sample preparation, reagents, different lot-numbers of used kits, quality of Chips and many more, the output of microarrays will vary. To equalize these differences a suitable normalization strategy is necessary.

There are several normalization strategies available, all of which can strongly influence the detection of transcripts. Some algorithms use Affymetrix's 'perfect match signals' *and* 'mismatch signals', for instance the Probe Logarithmic Intensity Error Estimate (PLIER) algorithm, others only use 'perfect match signals' (GC-RMA). Background correction using mismatch signals has shown to improve accuracy but worsen precision. GC-RMA and PLIER algorithms provided the best balance of accuracy and precision [140], PLIER appeared to be superior to other algorithms in avoiding false positives with poorly performing probe sets [141]. The variability in performance of probe set algorithms is more dependent on assumptions regarding 'background', than on calculations of 'signal'. It was argued that 'background' is an enormously complex variable that can only be vaguely quantified, and thus the optimal probe set algorithm will vary from project to project [141]. It has to be taken into consideration that raw data should be calculated with more than one normalization algorithm and with a certain filtering strategy. Data have to be filtered in such a way that also certain hidden data, for instance false-negatives (differentially expressed data not to be realized as differentially expressed due to an insufficient filtering strategy) are discovered. It is necessary to use more than one algorithm in order to pinpoint the highest number of truly differentially expressed genes (Fig. 3.3).

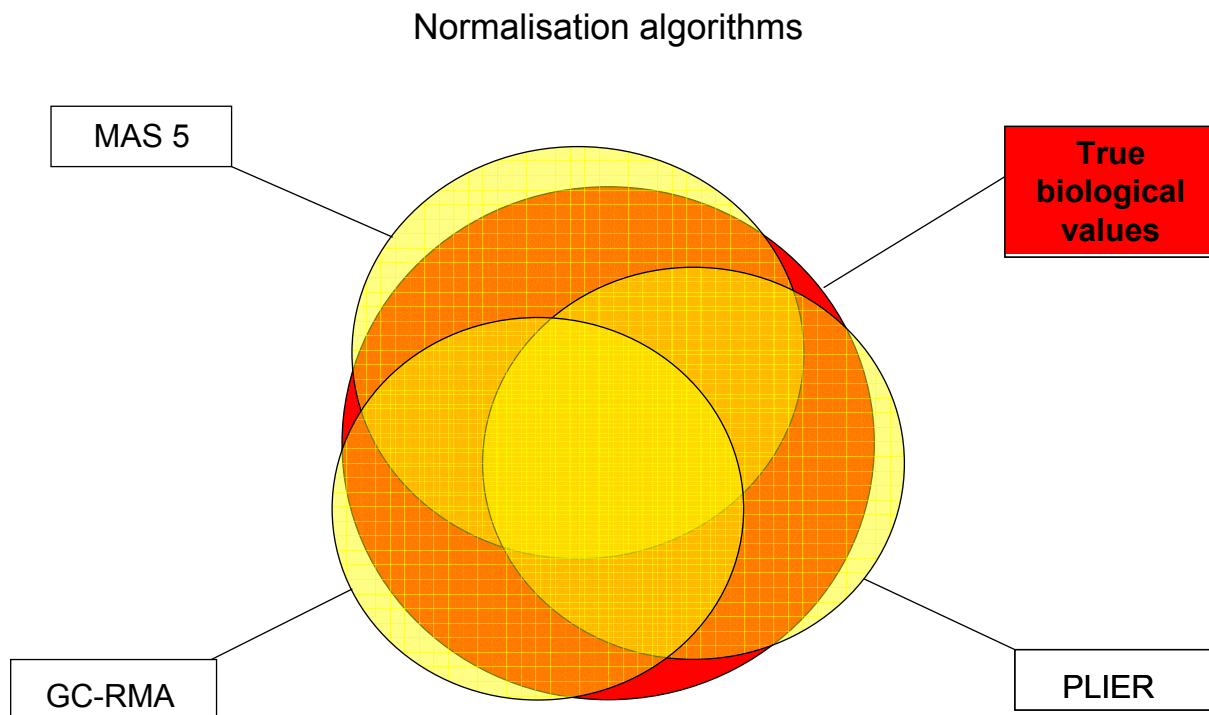


**Figure 3.3 Diagram showing unknown, truly differentially expressed genes (true values, red circle) and hypothetical intersection with normalization algorithms.** An algorithm finding 100% of true values does not exist for very big datasets, for instance when the whole genome, like here, is analyzed. In order to find the highest number of truly differentially expressed genes, a combination of three algorithms was used. Each algorithm has advantages and disadvantages concerning accuracy and precision. Some algorithms are known to detect nearly a similar set of genes. Here however, a combination of algorithms was chosen, to detect the highest number of truly differentially expressed genes, neglecting a big overlap. Some genes are detected by all 3 algorithms, others by two or by one. A few genes might be left which are not detected by any of these 3 algorithms. The genes found by only one algorithm should *not* be regarded as less important as the ones detected by two or three algorithms. The intersection in this Figure is hypothetical and provides a rough estimate of detected genes.

It was shown that the overlap of data using 6 different algorithms was only 27 to 36% [142] or 60-70% when 3 algorithms were compared [143, 144]. MAS 5 usually generates higher signal variability for low expressed genes and similar detection sensitivity at higher expression levels. It is important to remember that the numerical outputs for signal intensity are complex patterns of hybridization across numerous oligonucleotides, representing both specific (PM) and non-specific (MM) signals, in addition to local background signal from non-probe surfaces. *RMA* (*Robust Multiple Array Analysis*) uses probeset information *across several microarrays* to determine specific signal from background or non-specific hybridization, while *MAS 5 analyzes*

*one array at a time*. Here, four normalization strategies are shown that were used for the calculation of the data presented in this thesis:

**Scale factor:** This factor is used to make different intensities (measured fluorescence intensities derived from phycoerythrin-labeled targets) comparable. Different intensities are related to a common target intensity. Hybridization of a sample of bad RNA-quality (or bad hybridization conditions or low amounts of cRNA) will result in low intensities. This in turn results in an increased scale factor, because all measured intensities have to be multiplied by this factor to reach the same target intensity. Good RNA-quality usually results in high intensities. This in turn reduces the scale factor, because only a small factor is necessary to reach the same target intensity. *The absolute values for the scale factor for each Chip should be lower than 3.0. The relative values for the scale factor should not differ more than three-fold from Chip to Chip, otherwise the bias in the data becomes too big.* A scale factor of approximately 1.0 is regarded as optimal. For these reasons the scale factor is a rough estimate of sample quality. Chips with a scale factor bigger than 3 should be omitted from data analysis according to Affymetrix.

#### **GC-RMA (Robust Multichip Averaging, regarding GC content)**

This algorithm was introduced by Wu et al. [145, 146] and has a special background correction step. The goal behind its design was to reduce the bias caused by not subtracting MM (MisMatches) in the RMA algorithm. The GC-RMA algorithm uses a rather technical procedure to reduce this bias and is based on the fact that the non-specific affinity of a probe is related to its base sequence. The algorithm computes a background value to be subtracted from each probe using its base sequence and leaves the MM unconsidered.

**PLIER (Probe Logarithmic Intensity Error Estimate):** This algorithm has been shown to be the most stringent with the lowest likelihood for false positives in poorly performing probe sets [141]. The results presented by Seo et al. indicate that the new dynamic weighting and error model for PLIER signal calculation is effective in reducing the influence of noise. The PLIER method produces an improved signal by accounting for experimentally observed patterns in probe behavior and handling error.

Resulting benefits include:

- Higher reproducibility of signal (lower coefficient of variation) without loss of accuracy.
- Higher sensitivity to changes in abundance of targets near background.
- Dynamic estimation of the most informative features in an experiment to determine signal.

PLIER produces a more accurate probe set signal by utilizing inherent probe feature response values, empirical probe performance, and handling error appropriately across low and high expressors. Feature response is calculated using experimental data *across multiple arrays*. PLIER also utilizes an error model that assumes *error is proportional to the raw intensity, rather than to the background adjusted intensity*. This ensures that the error model can adjust appropriately for relatively low and high abundance of target nucleic acids.

**MAS 5:** Ordinary name for a frequently used algorithm implemented in the MAS 5.0 software (Affymetrix). The expression values are calculated according to the 'one-step Tukey's biweight algorithm'. This is a method for calculating cumulative probe set signal values. It is important to note that the MAS 5 algorithm occurs on a *Chip-by-Chip basis and is not applied across an entire set of chips*. The signal value is calculated from the combined, background-adjusted PM and MM values of the probes in the probe set. It represents the amount of transcript in the solution. The signal is calculated as follows:

- Cell intensities are pre-processed for global background.
- An ideal mismatch value is calculated and subtracted to adjust the PM intensity.
- The adjusted PM intensities are log-transformed to stabilize the variance.
- The biweight estimator is used to provide a robust mean of the resulting values. Signal is output as the antilog of the resulting value.
- Finally, the signal is scaled using a trimmed mean.

### **3.7 MIAME standards**

MIAME (Minimal Information About A Microarray Experiment) is the minimal information about a microarray experiment that is necessary to make it understandable for other researchers and to enable them to share the data and to repeat the experiment. The records of a certain experiment should be provided so that the data can be fully understood and the experiment fully reproduced by other researchers. MIAME is regarded as a guideline rather than a strict rule that has to be followed. However, MIAME has become the standard for many microarray software packages and databases, so it is highly recommended that the recorded data of the experiments are compliant with MIAME. MIAME is arranged into two broad areas: array design description and experiment description. Experiment description is further subdivided into: Experimental design, sample preparations and labelings, hybridization procedures, parameters and description of the data itself, together with any information about normalization or transformation of the data. Further details are described in Brazma et al. (2001) [147]. The microarray experiments in this thesis were carried out following MIAME guidelines.

### 3.8 Flow diagram of sample preparation and hybridization

#### Eukaryotic Target Labeling for GeneChip® Probe Arrays

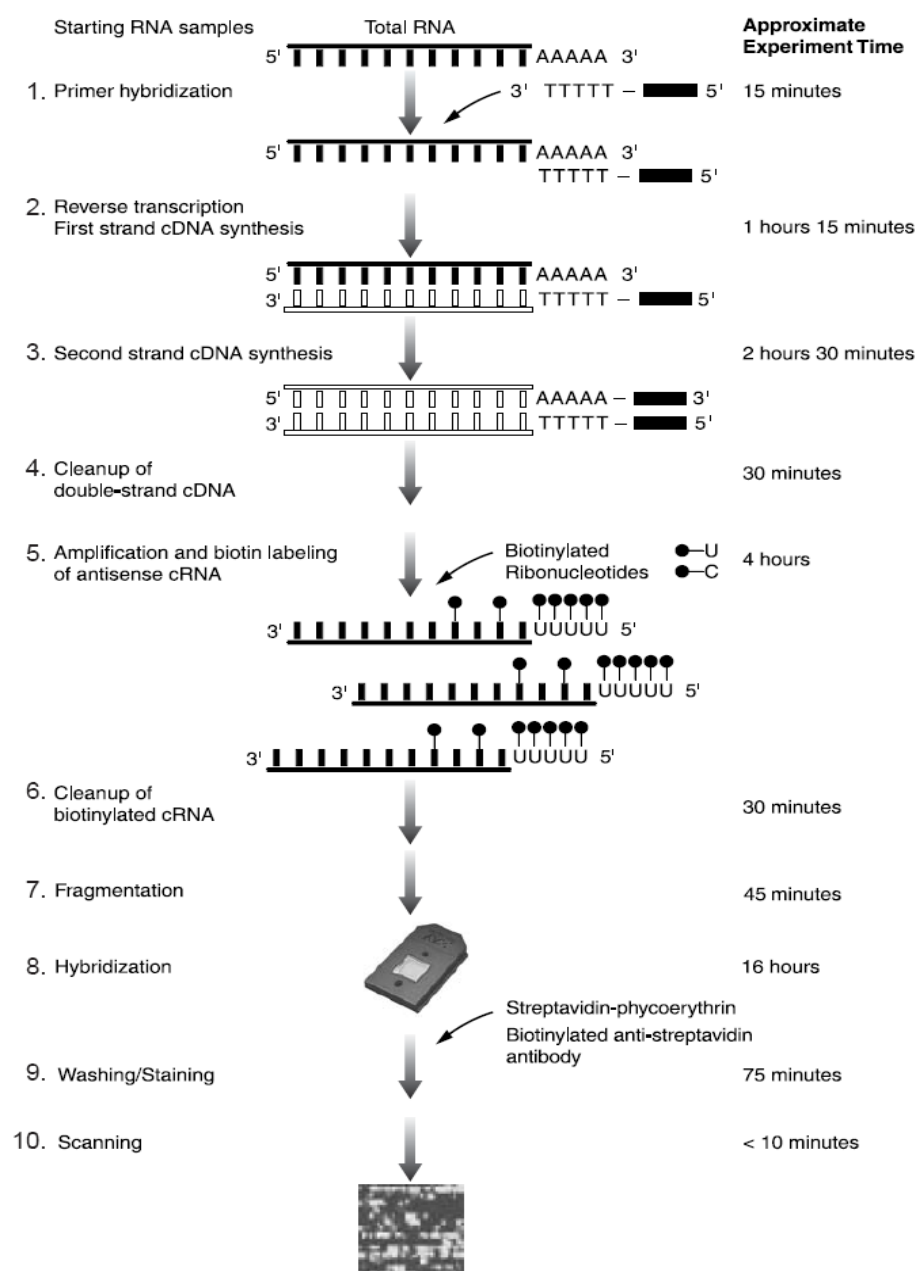


**Figure 3.4 Flow diagram of sample preparation and hybridization.** Total-RNA, extracted from cells, was reverse transcribed into cDNA, in vitro transcribed (and biotin-labeled) into cRNA. After fragmentation, cRNA was labelled with streptavidin-phycoerythrin and hybridized onto Gene Chips®. Gene Chips® were washed, scanned and data analysis was subsequently performed (Figure taken from www.Affymetrix.com).

### 3.9 Significance level, cut-off for fold change and normalization

The selection of a 'suitable' significance level in combination with a 'suitable' threshold for the fold change of expression is crucial for microarray experiments. The commonly accepted p-value of 0.05 might, especially if a large amount of data is analyzed in parallel, not be stringent enough, *if one wants to rule out any false-positive data*. This problem is known as the problem of '*multiplicity of testing*'. On the other hand, the number of obtained up and down-regulated genes could become too small if the selected threshold for the p-value is  $<0.05$ . Moreover, it has to be considered that the number of obtained genes depends crucially on the normalization algorithm used. To circumvent such problems and to obtain the most useful data the following strategy was used:

All the data were calculated with at least three different normalization algorithms (PLIER, GC-RMA, MAS 5). The thresholds for the p-values were finally adjusted to  $p < 0.05$  (PLIER), to  $p < 0.005$  (GC-RMA) and to  $p < 0.05$  (MAS 5). Fold changes  $>2$ -fold or  $>3$ -fold were regarded as biologically meaningful (strongly depending on the algorithm used). However, it should be emphasized that smaller fold changes were also regarded to be important, for instance when weakly expressed genes, like transcription factors, were analyzed. *There is no real agreement on which fold change is 'biologically meaningful', therefore, several combinations of fold changes and p-values were initially used to filter genes. Finally a combination thereof was chosen which best balanced accuracy and precision. Selected genes were confirmed by real-time PCR and proteomics.* In parallel, no threshold for the fold change was fixed; instead, a fixed number of the most up or down-regulated genes was selected (for instance the 20 most down-regulated genes with a p-value  $<0.05$ ). This approach is more applicable for some data sets, because there is no agreement on a 'suitable' cut-off for the fold change. Moreover, fold changes for relatively highly expressed genes, like the ones for structural proteins, do not have the same meaning as identical fold changes for weakly expressed genes, like transcription factors. In other words, the *absolute* intensity values have also to be considered whenever fold changes (relative intensity values) are calculated.

### 3.10 Software

Apart from standard software, like Excel (Microsoft) and others, the following software was used for data analysis:

- Microarray Suite 5.0 (Affymetrix)
- Gene Chip Operating Software (GCOS) 1.2 (Affymetrix)
- Data Mining Tool (Affymetrix)
- Array Assist 3.3 (Stratagene)
- Pathway Assist 3.0 (Stratagene)
- Pathway Architect 3.0.1 (Stratagene)
- Ingenuity Pathway Analysis (Ingenuity Systems)
- Language R (open source software) <sup>1</sup>

---

<sup>1</sup> The open source software R (<http://www.r-project.org>) has revolutionized the statistical data analysis for most bioscience disciplines. The required time to learn the R software is well invested, since the R environment covers an unmatched spectrum of statistical tools including an efficient programming language for automating time-consuming analysis routines. The fully integrated BioConductor project contains many additional R packages, in particular for the analysis of functional transcriptomics and microarray data. Due to their popularity, R and BioConductor are continuously updated and extended with the latest analysis tools that are available in the different research fields. The R environment is completely free and runs on all common operating systems.

## 4 The aim of this Ph.D. thesis

There is a large body of evidence showing that  $A\beta_{42}$ , in contrast to  $A\beta_{40}$ , triggers a chain of harmful events in the development of AD. In order to elucidate the different mechanisms of  $A\beta_{42}$  and  $A\beta_{40}$  action, expression profiles of both  $A\beta_{42}$  and  $A\beta_{40}$ -overexpressing human neuroblastoma cells should be performed. In order to produce different  $A\beta_{42}$  and  $A\beta_{40}$  levels, the  $A\beta$  precursors C99I45F and C99V50F (two C99 mutants, known to generate different amounts of  $A\beta_{42}$  and  $A\beta_{40}$ , due to their point mutations) should be overexpressed in human neuroblastoma cells. This should result, due to varying intracellular cleavage by  $\gamma$ -secretase, in different  $A\beta_{42}$  and  $A\beta_{40}$  levels accompanied by the generation of their respective APP intracellular domains (AICDs) [49, 50]. The overall goal of this thesis was to obtain information about effects of the different C99 cleavage products. Whenever in this thesis the term “ $A\beta_{42}/A\beta_{40}$  ratio” is used for reasons of simplicity, it also implies all further possible C99 cleavage products generated by  $\gamma$ -secretase. Human neuroblastoma cells should be stably transfected with constructs bearing point mutations that increase or decrease the  $A\beta_{42}/A\beta_{40}$  ratio. Whole genome gene expression profiles (Affymetrix Gene Chip Technology™) of these cells were planned to be performed and to be compared to each other. A proteomic approach to the same cells should be compared with the transcriptomic approach. Overlapping transcripts/proteins should be further characterized. The function of promising candidates was intended to be elucidated by RNA interference. Therefore, CRABP1, which turned out to be up-regulated in consequence of an increased  $A\beta_{42}/A\beta_{40}$  ratio, both on the transcript and protein-level, should be knocked down in order to evaluate its effect on the differentiation behavior of the cells. Pharmacological treatments with retinoic acid should provide further insights into the reactions of the cells. For elucidating signal transduction pathways, I intended to determine the phosphorylation status of interesting proteins belonging to those pathways, which I had previously determined by gene expression profiling.

The specific goals were to:

- Identify genes that are differentially expressed by  $A\beta_{42}$  and  $A\beta_{40}$  overexpression.
- Identify genes that are inversely regulated by  $A\beta_{42}$  and  $A\beta_{40}$  overexpression.
- Validate important genes by quantitative real-time PCR.
- Identify signal transduction pathways affected by  $A\beta_{42}$  and  $A\beta_{40}$ .

- Identify molecular functions affected by  $A\beta_{42}$  and  $A\beta_{40}$ .
- Identify chromosomal susceptibility regions which might be associated with AD.
- Analyze the phosphorylation status of proteins in consequence of  $A\beta_{42}$  and  $A\beta_{40}$  overexpression.
- Compare transcriptomic and proteomic data in order to obtain new insights into the pathological mechanisms of AD.
- Identify candidate genes for kinases phosphorylating the microtubule-associated protein tau.
- Identify the most suitable algorithm for microarray analysis.
- Discover specific gene/protein functions.
- Establish models for the genes/proteins assumed to play predominant roles in response to altered  $A\beta_{42}$  and  $A\beta_{40}$  levels.

## 5 Results

### 5.1 Preface

The main goal of this thesis was to obtain information about how the different  $A\beta_{42}$  and  $A\beta_{40}$  levels differ from each other in regard to their effect on gene expression. To generate different  $A\beta_{42}$  and  $A\beta_{40}$  levels, two C99 mutants were overexpressed in human neuroblastoma cells utilizing their ability to strongly shift the  $A\beta_{42}/A\beta_{40}$  ratio in either direction, as previously demonstrated in detail [148, 149] and also shown in this thesis. C99I45F and C99V50F had opposite effects on the  $A\beta$  species generated: C99I45F is mainly processed to  $A\beta_{42}$ , resulting in a dramatic increase of the secreted  $A\beta_{42}/A\beta_{40}$  levels, whereas C99V50F is mainly processed to  $A\beta_{40}$ . Since, due to a point mutation, the constructs expressed peptides only differing in a single amino acid outside the  $A\beta$  domain (at position 45 or 50, C99I45F and C99V50F respectively) compared to the wild type construct (C99WT), they were ideal for gene expression profiling, and potential technical variation influencing gene expression could be minimized. C99 is cleaved by  $\gamma$ -secretase resulting on the one hand in the release of  $A\beta_{42}$  and  $A\beta_{40}$  and on the other hand in the release of different AICD species. In the two C99 mutants (C99I45F and C99V50F) a strong shift in the amount of generated  $A\beta_{42}$  and  $A\beta_{40}$  levels was observed resulting from varying cleavage by  $\gamma$ -secretase. This is assumed to inherently be accompanied by production of two AICDs differing in length [49]. It has been shown that in cells overexpressing  $A\beta_{42}$  more AICD<sub>49-99</sub> is produced than in cells overexpressing  $A\beta_{40}$  in which more AICD<sub>50-99</sub> is produced [49, 50]. AICD<sub>57</sub> and AICD<sub>59</sub>, the two species which should theoretically be left over after cleavage of  $A\beta_{42}$  and  $A\beta_{40}$  from the precursor C99, have not yet been unambiguously identified [150].

Furthermore, the effects of C99-overexpression (C99WT versus mock) were evaluated and served as a control. The comparison C99I45F versus C99WT in this thesis is indicated by an increased  $A\beta_{42}/A\beta_{40}$  ratio ( $A\beta_{42}/A\beta_{40}\uparrow$ ) whereas the comparison C99V50F versus C99WT is indicated by a decreased  $A\beta_{42}/A\beta_{40}$  ratio ( $A\beta_{42}/A\beta_{40}\downarrow$ ).

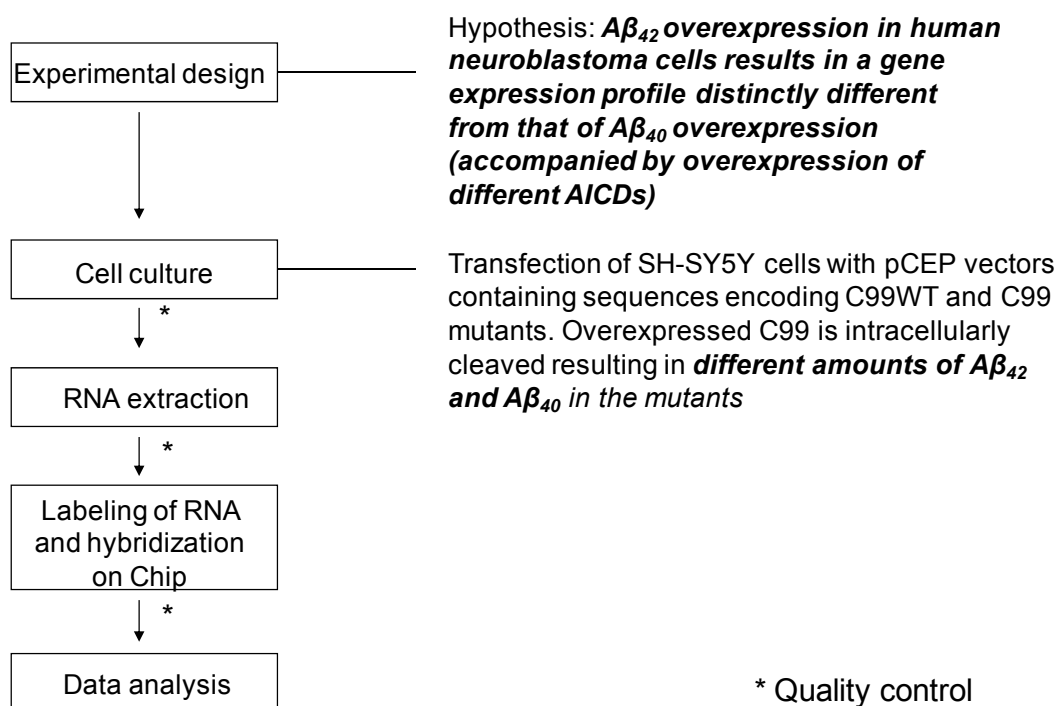
The observed alterations in gene expression may be triggered by  $A\beta_{42}/A\beta_{40}$  or their respective AICDs (or cleavage products thereof, for instance through cleavage by caspases [151]). For reasons of simplicity the term “changed  $A\beta_{42}/A\beta_{40}$  ratio” is used in this thesis but it also implies a change of the AICDs and all further possible C99 cleavage products. It is assumed, even though no experimental evidence is provided here that the AICDs change similarly to  $A\beta_{42}$  and  $A\beta_{40}$ . Currently, we are

investigating this issue together with our collaboration partner Stefan Lichtenthaler.

Genome-wide analyses, phosphorylation screenings and functional assays were performed. These data were supported by a proteomic approach and real-time PCR data. Data from all approaches were combined to identify affected signal transduction pathways (Fig. 5.1).

## 5.2 Flow chart of experimental steps

What makes  $A\beta_{42}$  putative pathogenic compared to the physiological  $A\beta_{40}$  ?



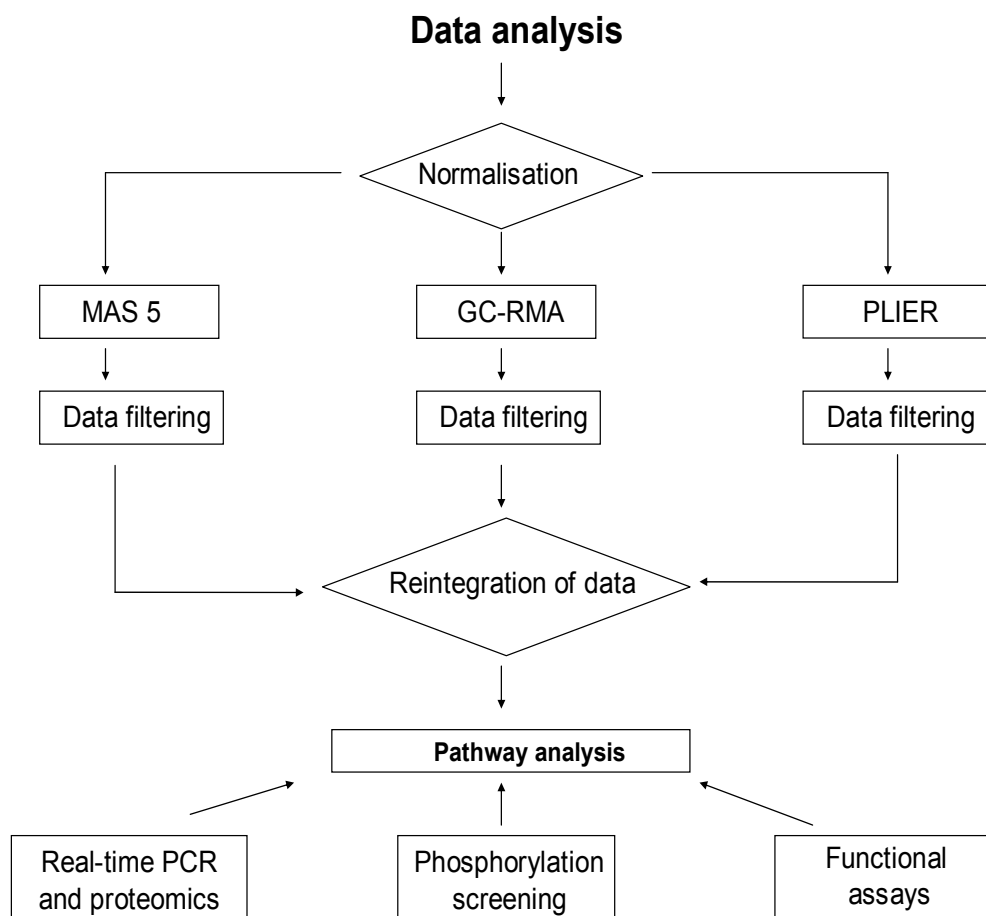


**Figure 5.1** Flow diagram showing experimental steps from setting up the experimental design to the final data analysis.

### 5.3 Cloning and expression of APP-fragments (C99 wildtype and -mutants)

To analyze altered A $\beta$  expression in a controlled manner, C99-overexpression constructs encoding the C-terminal part of A $\beta$ PP (C99) were used, together with an N-terminal signal peptide [148, 149]. This peptide is correctly cleaved by signal peptidase and thus is identical to the A $\beta$ PP-derived C99, the ultimate precursor for A $\beta$  generation. C99 is processed by  $\gamma$ -secretase in the same manner as A $\beta$ PP-derived C99, making it an ideal substrate to study  $\gamma$ -secretase function or its cleavage products A $\beta_{42}$  and A $\beta_{40}$  without the influence of  $\beta$ -secretase. Since, due to a point mutation, the constructs express peptides only differing in a single amino acid outside the A $\beta$  domain (at position 45 or 50, C99I45F and C99V50F respectively)

compared to the wild type construct (C99WT), they were ideal for gene expression profiling, enabling me to minimize potential technical variation influencing gene expression.

Single independent clones of the human neuroblastoma cell line SH-SY5Y, overexpressing C99, were selected and checked for A $\beta$ <sub>42</sub> and A $\beta$ <sub>40</sub>-expression.

SH-SY5Y cells were stably transfected with constructs coding for the A $\beta$ PP C-terminal fragment C99WT and also for constructs bearing the point mutations C99I45F and C99V50F and the vector only (negative control) (Fig. 5.2).<sup>2</sup>

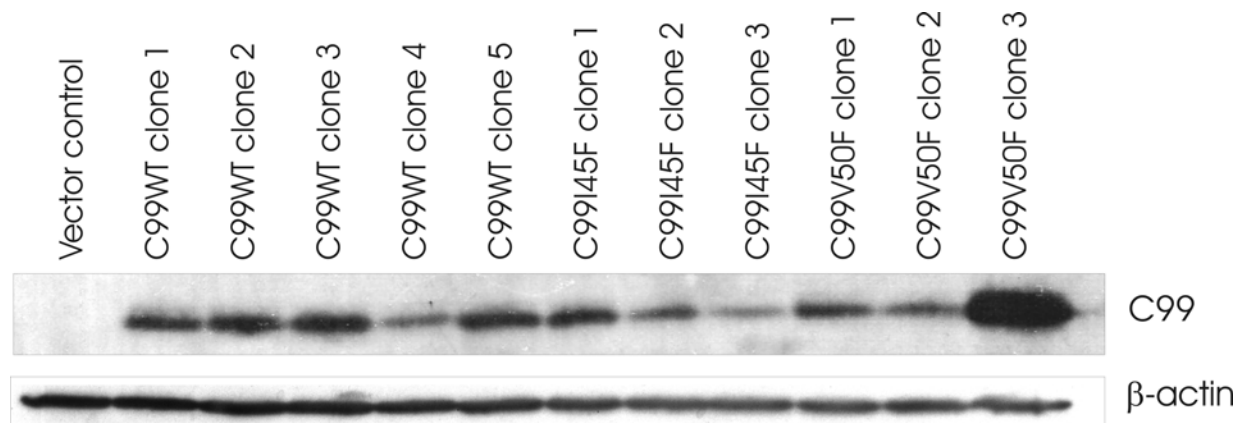


**Figure 5.2** SH-SY5Y cells were stably transfected with a pCEP-vector containing the A $\beta$ PP C-terminal fragment C99WT, and constructs bearing the point mutations C99I45F and C99V50F. The same cell line was transfected with an empty vector (negative control). Eight clones (clone 1-3 for C99WT, clone 1-3 for C99I45F and clone 1-2 for C99V50F) with approximately similar expression levels and C99V50F clone 3, showing stronger expression, were selected and used for transcriptome and proteome analysis. Apart from analyzing the complete set of 3 clones, data analysis for the transcriptomic approach was also performed by excluding clone 3 (C99V50F), resulting in no significant difference compared with the triplicates.

The purpose for using these mutations was their ability to strongly shift the A $\beta$ <sub>42</sub>/A $\beta$ <sub>40</sub> ratio in either direction, as previously demonstrated in detail [148]. This was confirmed here (Fig. 5.3).

### C99 mutants expressed different amounts of A $\beta$ <sub>42</sub> and A $\beta$ <sub>40</sub>

Overexpressed C99 is processed resulting in different amounts of A $\beta$ <sub>42</sub> and A $\beta$ <sub>40</sub> in the corresponding cell clones. To verify this, one clone of each triplicate was checked for the appropriate expression (Fig. 5.3).

<sup>2</sup> Western-blot was performed in collaboration with my colleague Kamran Honarnejad.

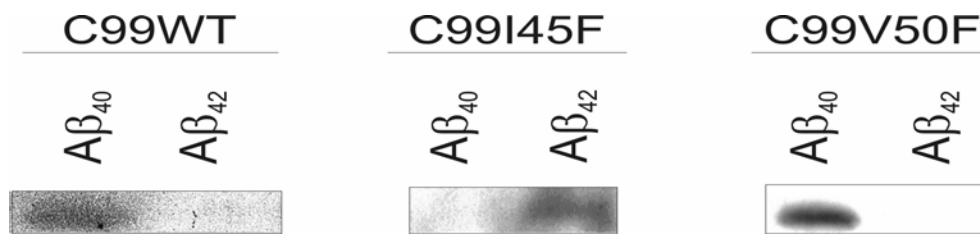


**Figure 5.3 Western blot showing secreted  $A\beta_{42}$  and  $A\beta_{40}$ .**  $A\beta_{42}$  and  $A\beta_{40}$  were immunoprecipitated from conditioned media of the human neuroblastoma cell line SH-SY5Y, overexpressing C99, using the G2-11 antibody, specific for  $A\beta_{42}$  and G2-10, specific for  $A\beta_{40}$ . Both  $A\beta$  species were detected by Western blotting using antibody W02. C99 is intracellularly cleaved, generating different amounts of  $A\beta_{42}$  and  $A\beta_{40}$  in mutant C99I45F and C99V50F. Mutant C99I45F expresses more  $A\beta_{42}$  than  $A\beta_{40}$ , whereas C99V50F expresses more  $A\beta_{40}$  than  $A\beta_{42}$ .

As expected and described in detail [148, 149] C99I45F and C99V50F had opposite effects on the  $A\beta$  species generated: C99I45F is mainly processed to  $A\beta_{42}$ , resulting in a dramatic increase of the secreted  $A\beta_{42}/A\beta_{40}$  levels (relative ratio approximately 20.4 compared to the  $A\beta_{42}/A\beta_{40}$  ratio in C99WT); C99V50F is mainly processed to  $A\beta_{40}$  (relative ratio approximately 0.3 compared to C99WT) [148].

## 5.4 Transcriptomics

### 5.4.1 Preface

In a genome-wide approach in SH-SY5Y human neuroblastoma cells, both mutants (C99I45F and C99V50F) were compared to each other and compared to C99WT with the goal of obtaining information about the effects triggered by an increased (C99I45F) or decreased (C99V50F)  $A\beta_{42}/A\beta_{40}$  ratio. Furthermore, the effects mediated by C99 were determined by comparing C99WT to a mock-control.

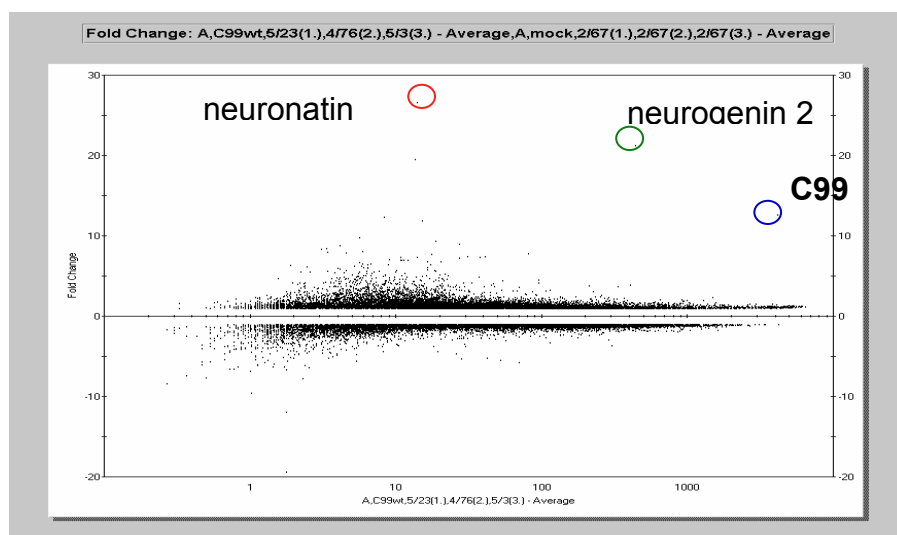
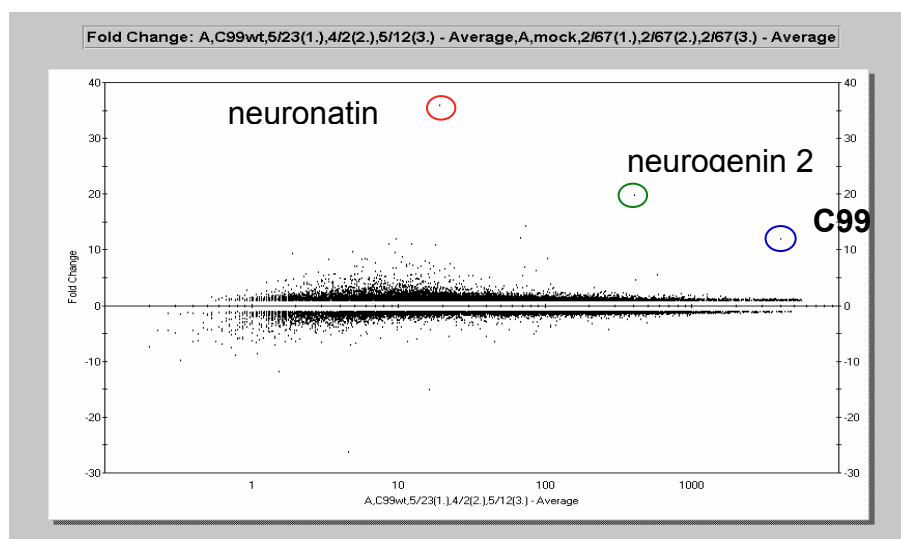
### 5.4.2 Quality control

Refer to Chapter 12.5, Supplementary Information.

### 5.4.3 C99 as an internal control. The APP gene (overexpressed C99 respectively) was detected among the top up-regulated genes

The fold changes of the data were calculated (C99WT versus vector control) and were plotted against the scanned intensity values (derived from hybridization of target-RNA to the probes on the Chip). In Figure 5.4 B another set of triplicates for C99WT was used compared to Figure 5.4 A: Comparable distributions of the

transcripts in Figure A and B show consistency of the data, especially for strongly differentially expressed genes. C99 here served as an *internal positive control* for *overexpressed* C99, which was detected by the probe on the Chip, originally designed for detecting APP (probes selected by Affymetrix are usually taken from the 3' end and so able to detect the C-terminal fragment of APP). The analysis of another comparison (C99WT versus C99I45F) in which C99 was expected to be present in similar amounts showed that C99 was not differentially expressed. However, it has been reported that the AICD regulates the transcription of its own precursor [152] and consequently upregulation of endogenous APP cannot be excluded completely.

**A****B**

**Figure 5.4 Graphs show up and down-regulated genes.** Each dot represents one transcript (calculated with the Data Mining Tool, Affymetrix). A) A set of three single clones (corresponding to three replicates) for C99WT were used for Chip analysis; the mean of these replicates was used to calculate the fold change compared to the mock control. B) One clone (C99WT) used in Fig. A was combined with two other C99WT clones (clone 4 and 5, see Fig. 5.2). The position of the transcripts indicates the fold change (y-axis) and the intensity (x-axis). Encircled transcripts showed similar positions in Fig. A and B. Comparable distributions of the transcripts in Figure A and B showed consistency of the data especially for strongly differentially expressed genes (red encircled transcript: neuronatin, green: neurogenin 2, blue: C99).

Performing data analysis with different sets of clones provided more information and a deeper insight into the spectrum of differentially expressed genes. C99 here served as an internal positive control for overexpressed C99. C99 is among the strongest up-regulated genes, reflecting the overexpression compared to the vector control (relative values). Furthermore, it is among the transcripts showing strong intensity values (absolute values), which was expected due to high abundance caused by overexpression.

#### **5.4.4 Genes identified using different algorithms and software**

The same set of raw data was analyzed with three different algorithms to obtain as much significant information as possible:

- PLIER algorithm (Array Assist, Stratagene)
- GC-RMA algorithm (Language R, Bioconductor)
- MAS 5 algorithm (one-step Tukey's biweight algorithm) (Array Assist, Stratagene)

Refer to Chapter 12.2, Supplementary Information, for gene lists analyzed with PLIER, GC-RMA and MAS 5.

Volcano plots were created with Array Assist, using the PLIER algorithm for normalization. Graphs show differentially expressed genes plotted against the p-value. Approximately 40,000 transcripts were analyzed.



**Figure 5.5 Volcano plots showing differentially expressed genes (logarithmic scale to the base 2) plotted against the p-value.** Graph A: C99I45F/C99WT1 (increased  $A\beta_{42}/A\beta_{40}$  ratio), Graph B: C99V50F/C99WT1 (decreased  $A\beta_{42}/A\beta_{40}$  ratio). Data were calculated with the PLIER algorithm. The PLIER algorithm appeared to be superior to other algorithms in avoiding false positives with poorly performing probe sets [141]. The threshold was set to  $p < 0.05$  ( $n=3$ ) and  $\log_2$  ratio  $> 1$  (fold change  $> 2$ ) (lower left and right highlighted rectangle). A  $\log_2$  ratio  $= 0$  corresponds to a fold change of 1 (not differentially expressed); a  $\log_2$  ratio  $< 0$  means downregulation; a  $\log_2$  ratio  $> 0$  means upregulation. The adjustment of a threshold for statistical and biological significance has to be regarded with care when a huge amount of data (here 44,000 data points corresponding to approximately 40,000 transcripts) are analyzed. Also data with p-values bigger than 0.05 or fold changes smaller than 2.0 may be biologically meaningful. Red colored CRABP1 and PREP were also found (along with others: INA, NEFL, NEF3 etc.) in a proteomic approach among the 20 most up-regulated proteins. The proteomic approach was performed blind by an independent laboratory of the University of Göttingen, Germany. For fold changes of expression, p-values (page S1-S11) and gene annotations (page S40-S65) refer to Chapters 12.2 and 12.3, Supplementary Information.

## 5.5 Transcriptomics compared to proteomics

### 5.5.1 Preface

The proteomic approach was performed to get information about differences on the protein level, because dysregulation on the transcript level does not necessarily mean that such a dysregulation also occurs on the protein level. Furthermore, genes from the transcriptomic approach overlapping with proteins from the proteomic approach validated each other increasing the reliability of the data.

### 5.5.2 CRABP1 (cellular retinoic acid binding protein 1) and further genes associated with retinoic acid

#### 5.5.2.1 CRABP1 was differentially expressed both on the transcript level and on the protein level

The transcriptomic and proteomic responses to an altered  $A\beta_{42}/A\beta_{40}$  ratio in human neuroblastoma cells were studied. An increased or decreased  $A\beta_{42}/A\beta_{40}$  ratio revealed differentially expressed transcripts, of which the 60 most up-regulated were used here. For the corresponding proteomic approach the 20 most up-regulated proteins were selected to validate altered protein expression. Only the overlap of transcriptomic and proteomic data was used for further analysis (Fig. 5.6).

## CRABP1 was up-regulated exclusively in the mutant cell line with an increased $A\beta_{42}/A\beta_{40}$ ratio

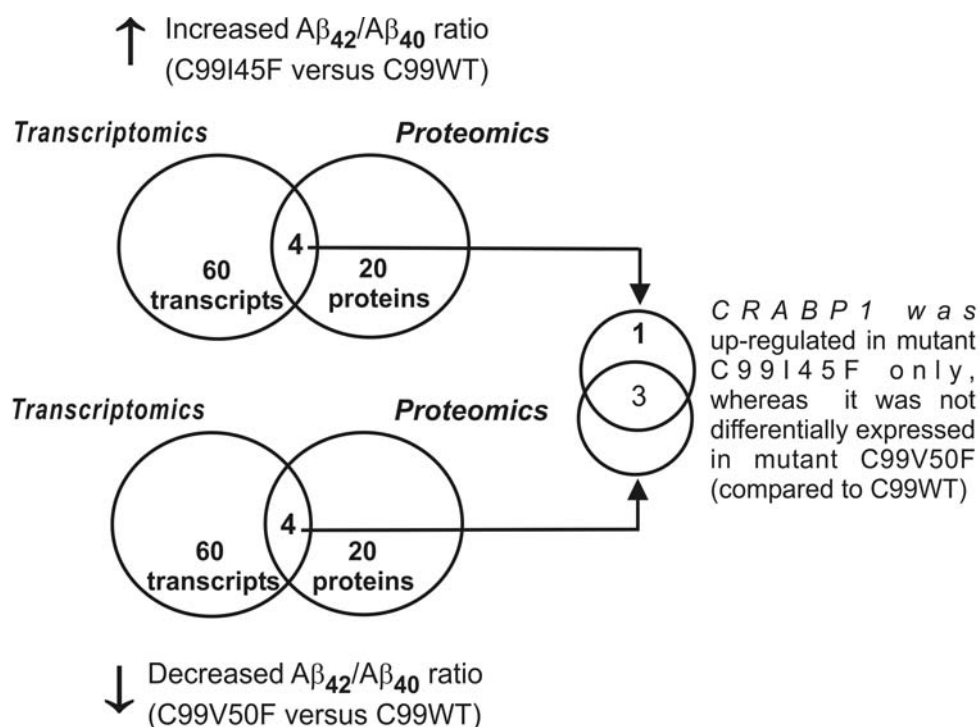


**Figure 5.6 Differentially expressed transcripts and proteins.** Comparison of C99I45F or C99V50F versus C99WT revealed differentially expressed transcripts, of which each of the 60 most up-regulated were used here. The 20 most up-regulated proteins each were selected for the corresponding proteomic approach. An intersection of the transcriptomic and proteomic data was subsequently performed. Only the intersection of both approaches (4 transcripts and proteins respectively) was used for further analysis. Out of these 4, only CRABP1 was up-regulated in C99I45F, whereas no differential expression was found in C99V50F (both mutants compared to C99WT). The remaining 3 transcripts and proteins were differentially expressed in both mutants. The proteomic approach was performed blind by an independent laboratory. The term “differentially expressed” was applied when the fold change exceeded a threshold of  $\geq 1.9$  either on the transcript or the protein level.

Three single independent clones each from C99WT, C99I45F and C99V50F (Fig. 5.2) were used for transcriptomic and proteomic analyses (mock-transfected cells as negative control):

For transcriptomics whole genome HG-U133 A and B Chips were used. Replicates were prepared and hybridized on different days and were derived from different independent clones. Data analysis was performed by calculating the means of three independent single clones.

For proteomics three clones each from C99WT, C99I45F and C99V50F were pooled, then proteins were extracted, CyDye labeled and analyzed by two-dimensional differential fluorescence intensity gel electrophoresis (2D-DIGE, Fig. 5.7). Up-regulated proteins were identified by mass spectrometry [153].

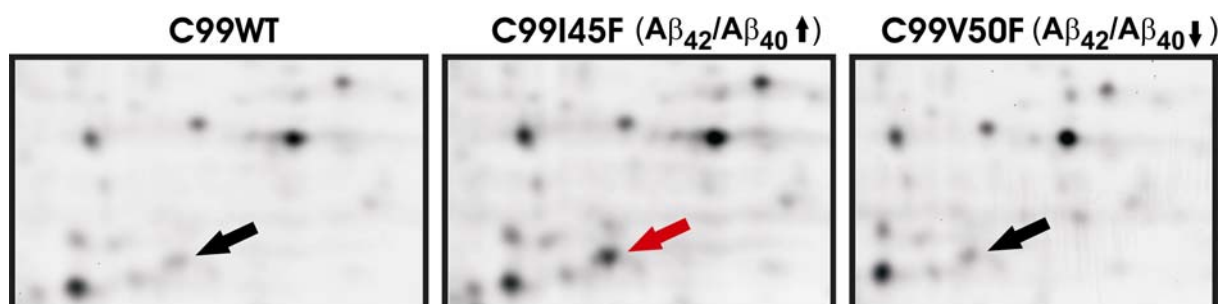


**Figure 5.7 2D-PAGE of CyDye-labeled proteins, extracted from SH-SY5Y cells.** C99I45F and C99V50F were compared with C99WT. Differentially expressed proteins, evaluated by intensity of merged colors (Cy5, Cy3), were identified by mass spectrometry. Arrows indicate CRABP1. The proteomic approach was performed in collaboration with Dr. Peter Brechlin, Prof. Dr. Markus Otto (2D-PAGE, University of Göttingen) and Dr. Olaf Jahn (mass spectrometry, Max Planck Institute for Experimental Medicine, Göttingen).

Data analysis (transcriptomics and proteomics): For testing significance, analysis of variance (ANOVA) was performed for C99WT, C99I45F and C99V50F. For direct comparison of the two mutants (C99I45F and C99V50F) an unpaired t-test was performed. For further analysis, only the intersection of the transcriptomic and proteomic approach was used, increasing the reliability of the data.

Immunocytochemistry confirmed the results of the transcriptomic and proteomic approach: CRABP1 was up-regulated in the mutant with an increased  $A\beta_{42}/A\beta_{40}$  ratio (Fig. 5.8).

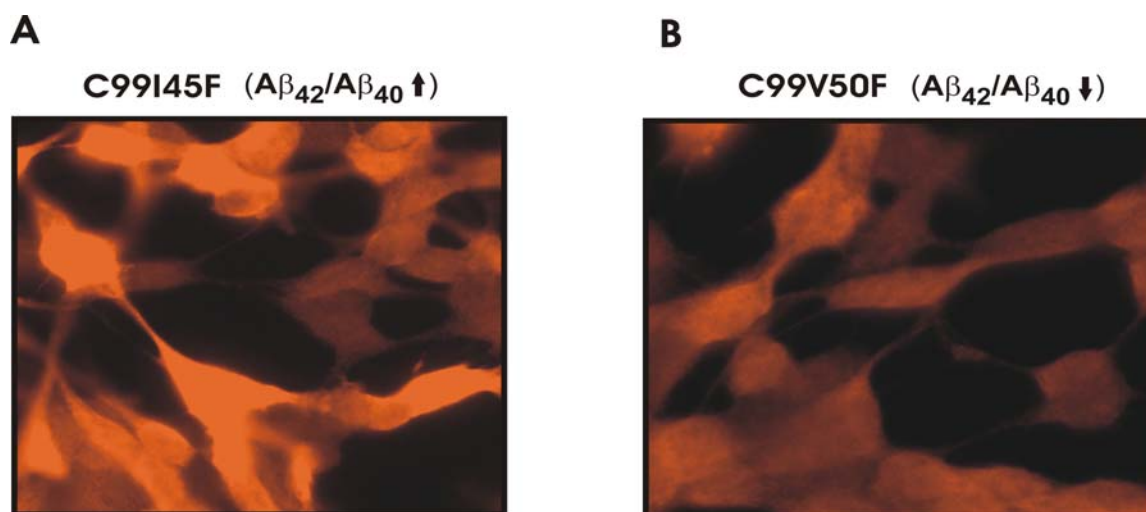


**Figure 5.8 Immunocytochemistry of human neuroblastoma cells (SH-SY5Y).** CRABP1

expression was detected with an anti-CRABP1 antibody (see Materials and Methods) . A) Mutant C99I45F showed strong CRABP1 staining. B) Mutant C99V50F showed only a weak signal close to background staining.

### 5.5.2.2 CRABP1 was up-regulated in mutant C99I45F ( $A\beta_{42}/A\beta_{40}\uparrow$ ) only, whereas mutant C99V50F ( $A\beta_{42}/A\beta_{40}\downarrow$ ) showed no differential expression of CRABP1

Name	Fold change (Transcriptomics) C99I45F/C99WT	Fold change (Proteomics) C99I45F/C99WT	Fold change (Transcriptomics) C99V50F/C99WT	Fold change (Proteomics) C99V50F/C99WT	P-value (Transcriptomics)	P-value (Proteomics)
<b>CRABP1</b>	<b>2.7</b>	<b>2.6</b>	<b>1.3</b>	<b>-1.1</b>	<b>0.123</b>	<b>0.032</b>
NEF3	2.6	3.1	2.3	2.7	0.038	0.01
NEFL	2.2	2.3	2.2	2.5	0.032	0.004
INA	1.8	1.8	1.6	1.9	0.056	0.002

**Table 5.1 Comparisons of both mutants with C99WT. The overlay of transcriptomics and proteomics revealed four differentially expressed transcripts and proteins respectively.** Out of these four, only CRABP1 was differentially expressed in C99I45F whereas C99V50F showed no differential expression of CRABP1 (compared to C99WT). Analysis of variance (One-Way ANOVA) was performed for C99WT, C99I45F and C99V50F. Cellular retinoic acid binding protein 1 (NCBI accession number of the protein identified by proteomics: gi|48146151); NEF3, Neurofilament 3 (gi|67678152); NEFL, Neurofilament, light polypeptide 68kDa (gi|105990539); INA, Internexin neuronal intermediate filament protein, alpha (gi|14249342).

CRABP1 was the second most up-regulated protein of the whole proteome and the second most up-regulated transcript of approximately 20,000 tested transcripts when only Chip A was considered (22,283 probe sets).

Direct comparison of both mutants revealed CRABP1 as up-regulated in C99I45F compared to C99V50F. In contrast to this, neurofilaments were not differentially expressed. This comparison revealed an effect mediated by a changed  $A\beta_{42}/A\beta_{40}$  ratio, because both mutants expressed inverse levels of  $A\beta_{42}$  and  $A\beta_{40}$  respectively (Table 5.2).

Direct comparison between the two mutants (C99I45F versus C99V50F) showed CRABP1 as up-regulated in mutant C99I45F ( $A\beta_{42}/A\beta_{40}\uparrow$ ) whereas neurofilaments were not differentially expressed.

Name	Fold change (Transcriptomics) C99I45F/C99V50F	Fold change (Proteomics) C99I45F/C99V50F	P-value (Transcriptomics)	P-value (Proteomics)
<b>CRABP1</b>	<b>2.3</b>	<b>2.8</b>	<b>0.188</b>	<b>0.059</b>
NEF3	1.1	-1.1	0.790	0.56
NEFL	1.1	-1.1	0.640	0.51
INA	1.1	-1.1	0.679	0.24

**Table 5.2** Direct comparison of C99I45F and C99V50F; C99V50F was the baseline experiment) revealed effects mediated by an altered  $A\beta_{42}/A\beta_{40}$  ratio for CRABP1 by a fold change distinctly deviating from 1.0, and an effect mediated by C99 for NEF3, NEFL and INA by a fold change close to 1.0, because C99 was expressed approximately equally in both mutants. Significance was determined by performing an unpaired t-test for the direct comparison of both mutants. As to be expected, p-values were high for not differentially expressed genes [154, 155].

NEF3, NEFL and INA were not differentially expressed. I regard this unaltered expression of neurofilaments as mediated by C99, since C99 was expressed in similar amounts in both mutants and hence a comparison between these two mutants resulted in a fold change close to 1.0 (not differentially expressed).

Comparison of SH-SY5Y cells transfected with the C99WT encoding construct versus SH-SY5Y cells transfected with the empty vector (mock) provides information about the effects mediated by C99 (Table 5.3).

### 5.5.2.3 CRABP1 was not differentially expressed in consequence of C99-overexpression in contrast to neurofilaments

Name	Fold change (Transcriptomics) C99WT/mock	Fold change (Proteomics) C99WT/mock	P-value (Transcriptomics)	P-value (Proteomics)
<b>CRABP1</b>	<b>1.0</b>	<b>1.4</b>	<b>0.979</b>	<b>0.042</b>
NEF3	-3.4	-1.8	0.024	0.086
NEFL	-3.0	-1.3	0.039	0.11
INA	-1.9	-1.3	0.069	0.029

**Table 5.3** Comparison between C99WT and mock-transfected cells revealed effects mediated by C99. NEF3, NEFL, INA were down-regulated in consequence of C99-overexpression. CRABP1 was not differentially expressed (cut-off for differential expression  $\geq 1.9$  on the transcript or protein level respectively).

Neurofilaments (NEF3, NEFL, INA) were down-regulated in consequence of C99-overexpression. CRABP1 was not differentially expressed, supporting the view that C99 is not responsible for CRABP1 dysregulation.

#### **Differential expression of CRABP1 was confirmed by real-time PCR**

Expression of CRABP1 was measured by quantitative real-time PCR with cyclophilin A as endogenous normalization control. Measurements reflect the mean of three independent clones, measured in triplicate. The fold change for CRABP1 of mutant C99I45F ( $A\beta_{42}/A\beta_{40}\uparrow$ ) compared to C99WT was 4.1 (stdev<sub>fold change</sub>: +/-2.3). In contrast to this, CRABP1 was only up-regulated 1.7 fold (stdev<sub>fold change</sub>: +/-0.8) in C99V50F compared to C99WT ( $A\beta_{42}/A\beta_{40}\downarrow$ ) and was up-regulated 1.3 fold (stdev<sub>fold change</sub>: +/-0.8) in C99WT compared to mock-transfected cells.

#### **5.5.2.4 Increased $A\beta_{42}/A\beta_{40}$ ratio up-regulated CRABP1 and made cells less sensitive to all-trans retinoic acid**

CRABP1 is involved in RA-metabolism and transport [156] and I found it to be up-regulated in consequence of an increased  $A\beta_{42}/A\beta_{40}$  ratio. This raised the question of whether cells with an increased  $A\beta_{42}/A\beta_{40}$  ratio show altered responses to RA treatment. SH-SY5Y cells were stably transfected with the constructs increasing or lowering the  $A\beta_{42}/A\beta_{40}$  ratio (Fig. 5.2 and 5.3). These cells were treated with 0.1-1000 nM RA in the absence or presence of serum. After 6 days, differentiation was evaluated by observing the length and number of outgrowing protrusions by phase contrast microscopy (Fig. 5.9, 1A and 1B).

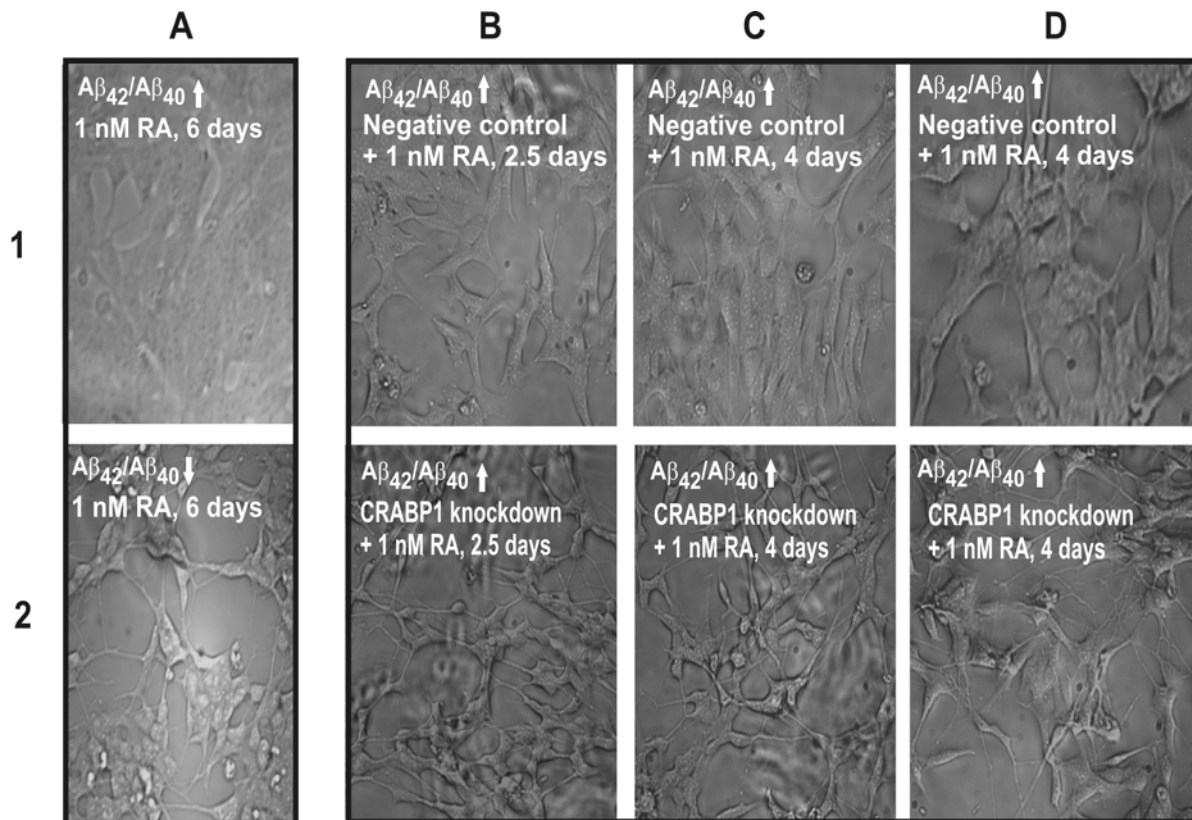


**Figure 5.9** Phase contrast images showing living human neuroblastoma cells (SH-SY5Y), grown on collagen coated glass cover slips and treated with 1 nM RA. Differentiation was evaluated by the number, shape and length of outgrowing protrusions. 1A) C99I45F ( $A\beta_{42}/A\beta_{40}\uparrow$ ). 2A) C99V50F ( $A\beta_{42}/A\beta_{40}\downarrow$ ). Differentiation was evaluated after RA-treatment for 6 days. Both cultures were 50% confluent when RA was added (day zero). C99I45F reached 90-100% confluency after 4-6 days without any signs of differentiation, whereas C99V50F did not exceed more than 60-70% confluency (after 6-10 days) and showed strong differentiation. C99I45F was also evaluated at 60-70% of confluency showing no signs of differentiation (data not shown), thus strong confluency of C99I45F (shown here) does not conceal putative signs of differentiation. B) C99I45F ( $A\beta_{42}/A\beta_{40}\uparrow$ ). 30 nM siRNA was administered to the cells for 24 h in combination with a treatment of 1 nM RA for 2.5 days. After 2.5 days, the effects of >50% knockdown of CRABP1 (2B) was compared to a nonsense sequence (negative control, 2A). C) C99I45F, same conditions as in B) except that RA was administered for 4 days. Differentiation was evaluated after 4 days. Knockdown of CRABP1 (2C) was compared to a nonsense sequence (negative control, 1C). D) C99I45F, same conditions as in C, but with another preparation from the same experiment as in C. B) and C) show preparations from different experiments. Experiments were repeated three times with consistent results. See Chapter 12.7 (page S88, Fig. 12.4), Suppl. Information, for an enlarged picture of fig 5.9 D).

Furthermore, the cell shape and number of cells were evaluated. 1 nM RA was selected for the subsequent functional validation and C99I45F-transfected cells were treated with 1 nM RA for 6 days (Fig. 5.9, 1A). No signs of differentiation were observed, irrespective of the cell confluency and duration of RA-treatment (cells were checked daily by light microscopy up to 10 days). In contrast to this, the cells expressing C99V50F (Fig. 5.9, 2A) showed differentiation at 1 nM RA treatment for 6 days: the cells were approximately 30-60% confluent and did not reach 100% confluency after 10 days. Cells had an average of 2-4 protrusions. This differentiation

was observed from 0.1-10 nM RA, which approximately corresponds to physiological plasma concentrations [157, 158]. At concentrations  $\geq 100$  nM RA, differentiation could also be observed for the C99I45F transfected cell line.

#### **5.5.2.5 CRABP1 knockdown rescued the differentiation potential of $A\beta_{42}$ overexpressing human neuroblastoma cells after RA treatment**

If an increased  $A\beta_{42}/A\beta_{40}$  exerts the diminished differentiation behavior via CRABP1, a CRABP1 knockdown in C99I45F-transfected cells should rescue this effect. 30 nM siRNA was administered to C99I45F-transfected SH-SY5Y cells for 24h in combination with a treatment of 0.1-1000 nM (1 nM shown in Fig. 5.9) for 2.5-4 days in the absence (data not shown) or presence of serum. Serum withdrawal can mimic differentiation (“pseudo differentiation”) and was therefore excluded from further analysis. A  $>50\%$  knockdown of CRABP1 was detected by quantitative real-time PCR ( $p=0.0002$ ,  $n=3$ ). Differentiation was evaluated after 2.5 days and 4 days. Knockdown of CRABP1 in combination with 1 nM RA (Fig. 5.9, 2B-2D) resulted in a strong change of cell shape, whereas transfection with a nonsense sequence, combined with 1 nM RA (negative control, Fig. 5.9, 1B-1D) did not alter the shape of the cells. The strongest differentiation was observed at 1 nM RA. No differentiation could be observed for treatment with siRNA but without RA, or treatment with 1 nM RA but without siRNA (data not shown). After CRABP1 knockdown and RA-treatment, the cells were approximately 30-80% confluent (Fig. 5.9, 2B-2D) and did not reach 100% confluency after 10 days. The extent of interconnections between cells was clearly increased (Fig. 5.9, 2D) compared to the negative control (Fig. 5.9, 1D).

#### **5.5.2.6 Three further genes, associated with RA-metabolism were differentially expressed in consequence of a changed $A\beta_{42}/A\beta_{40}$ ratio and may have influenced the effects mediated by RA**

Three further genes may influence the effects mediated by RA. Chip analysis revealed the following differential expression: Cytochrome P450 family 26 subfamily B polypeptide 1 (Cyp26B1), a RA-metabolizing enzyme [156], was found to be up-regulated 1.8 fold ( $p=0.01$ ,  $n=3$ ) in C99I45F ( $A\beta_{42}/A\beta_{40}\uparrow$ ), whereas C99V50F ( $A\beta_{42}/A\beta_{40}\downarrow$ ) showed no differential expression (compared to C99WT). Direct comparison of both mutants (C99I45F/C99V50F) revealed a 2.6 fold upregulation for Cyp26B1 in mutant C99I45F ( $p=0.02$ ,  $n=3$ ). RAR-related orphan receptor B (RORB)

was down-regulated 2.0-fold ( $p=0.049$ ,  $n=3$ ) in C99V50F (compared to C99WT), whereas it was not differentially expressed in C99I45F. RA receptor beta (RARβ) was not differentially regulated in C99V50F, whereas it was up-regulated 1.4 fold ( $p=0.05$ ,  $n=3$ ) in C99I45F (compared to C99WT).

### **5.5.2.7 Further genes, located on chromosomal regions adjacent to CRABP1 (15q24), were differentially expressed**

CRABP1 is located on the same chromosomal locus (15q24) as alpha polypeptide 3, 4 and 5 of the nicotinic cholinergic receptor and cytochrome P450, subfamily XIA (cholesterol side chain cleavage, Cyp11A1). Linkage of the chromosomal locus 15q24 to AD is explainable by the presence of alpha polypeptide 3, 4 and 5 of the nicotinic cholinergic receptor. However, this linkage actually could also be based on CRABP1, located on the same chromosomal locus. CRABP1 is in close chromosomal proximity to the  $\gamma$ -aminobutyric acid (GABA) A receptor, beta 3 (chr15q11.2-q12), which I found to be 2.6 fold up-regulated ( $p=0.03$ ,  $n=3$ ) in mutant C99I45F, whereas it was not differentially expressed in C99V50F (compared to C99WT). Furthermore, I found the insulin-like growth factor 1 receptor (IGF1R) (15q25-q26) 1.8 fold up-regulated ( $p=0.28$ ,  $n=3$ ) in mutant C99I45F whereas it was not differentially expressed in C99V50F (compared to C99WT).

### **5.5.3 Further overlapping transcripts/proteins**

#### **5.5.3.1 Preface**

Using less stringent criteria (for instance using an increased number of transcripts/proteins to be overlaid) for transcriptomics and proteomics revealed the following genes and proteins as differentially expressed. The 20 most up and down-regulated proteins were compared with the 100 most (for PREP the 200 most) up and down-regulated transcripts ( $p<0.05$ ). P-values were calculated from three independent experiments for the transcriptomic approach (each experiment with a different clone, so that the probability of clonal effects was minimized); although p-values are not yet determined for the proteomic approach (but will be calculated prior to publication as a paper), and could turn out to exceed the generally accepted level of significance ( $p\text{-value}=0.05$ ), the results are assumed to be reliable because two different technologies (transcriptomics and proteomics) validated each other and were carried out in two independent laboratories (transcriptomics: University of Heidelberg, Germany; proteomics: University of Göttingen, Germany). The probability that among a relatively small number of proteins analyzed by proteomics (20 most

up-regulated and 20 most down-regulated proteins) an overlap can be found with the most dysregulated transcripts just by chance is very low.

### 5.5.3.2 PREP (prolyl endopeptidase)

- C99I45F/C99WT ( $A\beta_{42}/A\beta_{40}\uparrow$ ): 1.6 fold up-regulated,  $p=0.0025$  (transcriptomics), 1.2 fold up-regulated (proteomics)
- C99V50F/C99WT ( $A\beta_{42}/A\beta_{40}\downarrow$ ): 1,1 fold down-regulated,  $p=0.41$  (transcriptomics, as to be expected  $p$ -values were high for not differentially expressed genes), 1.2 fold down-regulated (proteomics).
- C99I45F/C99V50F (direct comparison between the two mutants): 2.2 fold up-regulated ,  $p=0.0075$  (transcriptomics), 1.4 fold up-regulated (proteomics).

### 5.5.3.3 T-cell receptor, $\alpha$ and $\delta$ locus

- C99WT/mock ( $C99\uparrow$ ):  $\alpha$ -locus: 5.0 fold down-regulated,  $p=0.02490$  (transcriptomics),  $\alpha$  and  $\delta$  loci of the T-cell receptor were among the 20 most dysregulated proteins (proteomics).
- C99I45F/C99WT ( $A\beta_{42}/A\beta_{40}\uparrow$ ):  $\alpha$ -locus: 5.0 fold up-regulated,  $p=0.00219$  (transcriptomics),  $\delta$ -locus: 4.0 fold up-regulated,  $p=0.02572$  (transcriptomics),  $\alpha$  and  $\delta$  loci of the T-cell receptor were among the 20 most dysregulated proteins (proteomics).
- C99V50F/C99WT ( $A\beta_{42}/A\beta_{40}\downarrow$ ):  $\alpha$ -locus: 6.3 fold up-regulated 0.00132 (transcriptomics),  $\alpha$  and  $\delta$  loci of the T-cell receptor were among the 20 most dysregulated proteins (proteomics).

### 5.5.3.4 VGF (VGF nerve growth factor inducible)

- C99I45F/WT ( $A\beta_{42}/A\beta_{40}\uparrow$ ): not differentially expressed
- C99V50F/WT ( $A\beta_{42}/A\beta_{40}\downarrow$ ): 2.0 fold up-regulated (transcriptomics), VGF was among the 20 most dysregulated proteins (proteomics).

### 5.5.3.5 NADH dehydrogenase (ubiquinone)

NDUFB9 (NADH dehydrogenase (ubiquinone) 1 beta subcomplex, 22kDa) was differentially expressed on the transcript level:

- C99I45F/WT ( $A\beta_{42}/A\beta_{40}\uparrow$ ): 1.3 fold up-regulated,  $p=0.063$  (transcriptomics)
- C99V50F/WT ( $A\beta_{42}/A\beta_{40}\downarrow$ ): 2.3 fold down-regulated,  $p=0.132$  (transcriptomics)

On the protein level the ubiquinone precursor was detected:

- The NADH dehydrogenase (ubiquinone) Fe-S protein 1, 75kDa, precursor was identified among the 20 most dysregulated proteins (proteomics).

### 5.5.3.6 DNCL12 (dynein cytoplasmic light intermediate polypeptide 2)

- C99I45F/WT ( $A\beta_{42}/A\beta_{40}\uparrow$ ): 1.5 fold down-regulated  $p=0.0066$  (transcriptomics)
- DNCL12 was among the 20 most dysregulated proteins (proteomics).
- C99V50F/WT ( $A\beta_{42}/A\beta_{40}\downarrow$ ): not differentially expressed

## 5.6 Inversely regulated genes

### 5.6.1 Preface

Genes regulated in this manner are regarded in particular as *specific* for a changed  $A\beta_{42}/A\beta_{40}$  ratio, because the direction of regulation (which is inverse for  $A\beta_{42}/A\beta_{40}\uparrow$  and for  $A\beta_{42}/A\beta_{40}\downarrow$ ) point to a process expected to *depend on the ratio itself*. More  $A\beta_{42}$  /less  $A\beta_{40}$  has the opposite effect (on the direction of gene regulation) as more  $A\beta_{40}$  /less  $A\beta_{42}$ . If the ratio itself (increased ratio) up-regulated a certain gene, then the same gene should be found among the most down-regulated ones (and vice versa) for an inverted (decreased ratio). Indeed such genes could be found.

### 5.6.2 Genes up-regulated in mutant C99I45F versus C99WT ( $A\beta_{42}/A\beta_{40}\uparrow$ ) and at the same time down-regulated in mutant C99V50F versus C99WT ( $A\beta_{42}/A\beta_{40}\downarrow$ )

Most up-regulated genes (C99I45F versus C99WT( $A\beta_{42}/A\beta_{40}\uparrow$ )) which were *simultaneously* the most down-regulated ones according to the comparison C99V50F versus C99WT ( $A\beta_{42}/A\beta_{40}\downarrow$ ):

Inversely regulated genes were identified by calculating the differences ( $\Delta$  fold change) of the fold changes, derived from the comparisons of C99I45F versus C99WT1 and C99V50F versus C99WT1.  $\Delta$  fold changes were sorted descendingly. The cut off  $\Delta$  fold change was set to  $\geq 2.5$  (below  $\Delta$  fold change=2.5, differential expression here was questionable, because at least one value was close to 1.0 and thus not differentially expressed).

**Table 5.4 Most up-regulated genes (C99I45F versus C99WT( $A\beta_{42}/A\beta_{40}\uparrow$ )) which were at the same time the most down-regulated ones according to the comparison C99V50F versus C99WT**

Probe set ID	Gene Symbol	Gene name	p-value	fold change C99I45F/C99WT1	p-value	fold change C99V50/C99WT1	$\Delta$ fold change	Chromosomal location
226814_at	ADAMTS9	a disintegrin-like and metalloprotease (reprolysin type) with thrombospondin type 1 motif 9	0.003	2.0	0.066	-5.0	<b>7.0</b>	chr3p14.3-p14.2
225627_s_at	KIAA1573	KIAA1573 protein	0.044	1.6	0.149	-2.7	<b>4.3</b>	chr1p31.3
225990_at	BOC	brother of CDO	0.081	1.6	0.072	-2.5	<b>4.2</b>	chr3q13.2
225081_s_at	RAM2	transcription factor RAM2	0.160	1.4	0.157	-2.6	<b>4.0</b>	chr7p15.3
221796_at	NTRK2	neurotrophic tyrosine kinase receptor type 2, non-catalytic isoform	0.023	2.2	0.086	-1.7	<b>3.9</b>	chr9q22.1
229831_at	CNTN3	contactin 3 (plasmacytoma associated)	0.176	2.3	0.163	-1.6	<b>3.8</b>	chr3p26
228978_at	LOC440450	LOC440450	0.083	1.6	0.003	-2.2	<b>3.8</b>	chr17q23.2
223721_s_at	DNAJC12	DnaJ (Hsp40) homolog	0.036	1.7	0.170	-2.0	<b>3.7</b>	chr10q22.1

		subfamily C member 12						
228053_s_at	C9orf105	chromosome 9 open reading frame 105	0.074	1.3	0.168	-2.3	<b>3.6</b>	chr9p 13.1
221795_at	NTRK2	neurotrophic tyrosine kinase receptor type 2, non- catalytic isoform	0.193	1.9	0.058	-1.7	<b>3.6</b>	chr9q 22.1
222992_s_at	NDUFB9	NADH dehydrogenase (ubiquinone) 1 Beta subcomplex 9 22kDa	0.063	1.3	0.132	-2.3	<b>3.6</b>	chr8q 13.3
228080_at	LOC14390 3	layilin	0.149	1.6	0.182	-2.0	<b>3.6</b>	chr11 q23.1
229400_at	HOXD10	homeo box D10	0.065	1.6	0.128	-2.0	<b>3.6</b>	chr2q 31.1
241872_at	DKFZp761 D221	Hypothetical protein DKFZp761D221	0.032	1.8	0.191	-1.8	<b>3.6</b>	chr1p 31.2
221933_at	NLGN4X	neuroligin 4 X- linked	0.030	1.9	0.149	-1.5	<b>3.4</b>	chrXp 22.32- p22.3 1
236308_at	LOC28587 8	hypothetical protein LOC285878	0.081	1.9	0.151	-1.5	<b>3.4</b>	chr7p 11.2
237563_s_at	LOC44073 1	LOC440731	0.052	1.5	0.117	-1.8	<b>3.3</b>	chr1q 42.2
234472_at	GALNT13	UDP-N-acetyl- alpha-D- galactosamine: polypeptide N- acetylgalactosa minyltransferase 13 (GalNAc-T13)	0.084	1.5	0.167	-1.8	<b>3.2</b>	chr2q 23.3- q24.1
219697_at	HS3ST2	heparan sulfate (glucosamine) 3- O- sulfotransferase 2	0.012	1.7	0.137	-1.5	<b>3.2</b>	chr16 p12
224407_s_at	MASK	Mst3 and SOK1- related kinase /// Mst3 and SOK1- related kinase	0.026	1.3	0.142	-1.8	<b>3.1</b>	chrXq 26.2
209238_at	STX3A	syntaxin 3A	0.159	1.4	0.044	-1.8	<b>3.1</b>	chr11 q12.1
225626_at	PAG	phosphoprotein associated with glycosphingolipid -enriched microdomains	0.037	1.5	0.078	-1.6	<b>3.1</b>	chr8q 21.13
210123_s_at	CHRNA7	cholinergic receptor nicotinic alpha polypeptide 7	0.061	1.8	0.152	-1.3	<b>3.0</b>	chr15 q14 /// chr15 q13.1

203640_at	MBNL2	muscleblind-like 2 (Drosophila)	0.037	1.5	0.126	-1.5	<b>3.0</b>	chr13 q32.1
205151_s_at	KIAA0644	KIAA0644 gene product	0.107	1.4	0.145	-1.5	<b>2.9</b>	chr7p 15.1
205150_s_at	KIAA0644	KIAA0644 gene product	0.127	1.4	0.195	-1.5	<b>2.9</b>	chr7p 15.1
214680_at	NTRK2	neurotrophic tyrosine kinase receptor type 2, non-catalytic isoform	0.062	1.6	0.165	-1.3	<b>2.9</b>	chr9q 22.1
205380_at	PDZK1	PDZ domain containing 1	0.115	1.3	0.058	-1.6	<b>2.9</b>	chr1q 21
212148_at	PBX1	Pre-B-cell leukemia transcription factor 1	0.121	1.3	0.143	-1.6	<b>2.9</b>	chr1q 23
223734_at	OSAP	ovary-specific acidic protein	0.117	1.3	0.187	-1.5	<b>2.8</b>	chr4q 31.1
213068_at	DPT	dermatopontin	0.167	1.3	0.106	-1.4	<b>2.7</b>	chr1q 12-q23
219501_at	FLJ10094	hypothetical protein FLJ10094	0.073	1.3	0.111	-1.4	<b>2.7</b>	chr13 q14.1 1
216985_s_at	STX3A	syntaxin 3A <sup>3</sup>	0.130	1.3	0.072	-1.4	<b>2.7</b>	chr11 q12.1
210247_at	SYN2	synapsin II	0.072	1.3	0.102	-1.3	<b>2.6</b>	chr3p 25
216268_s_at	JAG1	jagged 1 (Alagille syndrome)	0.095	1.3	0.187	-1.3	<b>2.6</b>	chr20 p12.1-p11.2 3

**Table 5.4 Most up-regulated genes (C99I45F versus C99WT(A $\beta$ <sub>42</sub>/A $\beta$ <sub>40</sub>↑)) which were at the same time the most down-regulated ones according to the comparison C99V50F versus C99WT (A $\beta$ <sub>42</sub>/A $\beta$ <sub>40</sub>↓).  $\Delta$  fold change indicates the extent of differential expression between both mutants. For gene annotations see Chapter 12.3 (pages S66-S70), Supplementary Information.**

### Syntaxin 3

Syntaxin 3 was of special interest, due to its involvement in neurotransmitter release. Syntaxin 3a together with its splice product syntaxin 3b were found to be inversely regulated.

C99I45F versus C99WT (A $\beta$ <sub>42</sub> /A $\beta$ <sub>40</sub> ↑)	C99V50F versus C99WT (A $\beta$ <sub>42</sub> /A $\beta$ <sub>40</sub> ↓)
Syntaxin 3a up-regulated	Syntaxin 3a down-regulated
Syntaxin 3b up-regulated	Syntaxin 3b down-regulated

<sup>3</sup> Erroneously named (by Affymetrix) syntaxin 3A (216985\_s\_at) is a spliced form of syntaxin 3A and its correct name is syntaxin 3B. Syntaxin 3B is identical to syntaxin 3A but lacks 37 amino acid residues, from amino acid 226 to amino acid 262.

**Table 5.5 Syntaxin 3a and its splice product syntaxin 3b were inversely regulated in both mutants.** Syntaxin 3a/b were up-regulated in consequence of an increased  $A\beta_{42}/A\beta_{40}$  ratio, whereas they were down-regulated in consequence of a decreased  $A\beta_{42}/A\beta_{40}$  ratio. The fact that both isoforms (3a and 3b) were regulated in the same direction, to the same extent and belong to the transcripts with high absolute values (highly abundant transcripts), strongly increases the reliability of a real differential expression of syntaxin 3.

Intriguingly, we (together with our colleague Laura Busia) also found Syntaxin 3 to be among the most significantly down-regulated genes in embryonic mouse fibroblasts in consequence of PS2 knockdown with siRNA. In this approach  $A\beta$  levels may be speculated to be decreased. This is in line with the observation of syntaxin 3 down-regulation in mutant C99V50 compared to C99WT ( $A\beta_{42}/A\beta_{40}\downarrow$ ) and argues for an effect mediated by a decreased  $A\beta_{42}$  expression. If a decreased  $A\beta_{42}$  level exerts this effect, then an increased  $A\beta_{42}$  level should regulate syntaxin3a in the opposite direction. Indeed, this appears to be true, because it was found to be up-regulated for an increased  $A\beta_{42}/A\beta_{40}$  ratio.

### 5.6.3 Genes down-regulated in mutant C99I45F versus C99WT ( $A\beta_{42}/A\beta_{40}\uparrow$ ) and at the same time up-regulated in mutant C99V50F versus C99WT ( $A\beta_{42}/A\beta_{40}\downarrow$ )

Most down-regulated genes (C99I45F versus C99WT ( $A\beta_{42}/A\beta_{40}\uparrow$ )), which were *simultaneously* most up-regulated for the comparison C99V50F versus C99WT ( $A\beta_{42}/A\beta_{40}\downarrow$ ):

Inversely regulated genes were identified by calculating the differences ( $\Delta$  fold change) of the fold changes, derived from the comparisons C99I45F versus C99 WT1 and C99V50F versus C99 WT1.  $\Delta$  fold changes were sorted descending. The cut off  $\Delta$  fold change was set to  $\geq 2.5$  (below  $\Delta$  fold change=2.5, differential expression here was questionable, because at least one value was close to 1.0 and thus not differentially expressed).

probe set ID	Gene symbol	Gene name	p-value C99I45F/C99WT1	Fold change C99I45F/C99WT1	p-value C99V50F/C99WT1	Fold change C99V50F/C99WT1	$\Delta$ fold change	Chromosomal location
209604_s_at	GATA3	GATA binding protein 3	0.1625	-2.7	0.0780	1.2	<b>3.9</b>	chr10p15
210135_s_at	SHOX2	short stature homeobox 2	0.1886	-2.1	0.0023	1.2	<b>3.3</b>	chr3q25-q26.1
209164_s_at	CYB561	cytochrome b-561	0.0602	-1.9	0.0884	1.3	<b>3.2</b>	chr17q11-qter
209163_at	CYB561	cytochrome	0.0736	-1.8	0.0651	1.3	<b>3.1</b>	chr17q1

		b-561						1-qter
210816_s_at	CYB561	cytochrome b-561	0.0343	-1.6	0.0951	1.3	<b>2.9</b>	chr17q11-qter
217200_x_at	CYB561	cytochrome b-561	0.0370	-1.7	0.1908	1.2	<b>2.9</b>	chr17q11-qter
210134_x_at	SHOX2	short stature homeobox 2	0.1240	-1.4	0.1722	1.1	<b>2.5</b>	chr3q25-q26.1

**Table 5.6 Most down-regulated genes (C99I45F versus C99WT ( $A\beta_{42}/A\beta_{40}\uparrow$ )) which were at the same time the most up-regulated ones according to the comparison C99V50F versus C99WT ( $A\beta_{42}/A\beta_{40}\downarrow$ ).  $\Delta$  fold change indicates the extent of differential expression between both mutants. *TFPI2*, which belongs to the strongest differentially expressed genes, is not listed here, because of a rather high p-value which is beyond a threshold of 0.05. Nevertheless, it should be taken into consideration that *TFPI2* was detected by two independent probe sets as down-regulated (C99I45F versus C99WT), but strongly up-regulated in C99V50F versus C99WT, also detected by two independent probe sets and a p-value <0.05 (compare with Fig. 5.5).**

For gene annotations see Chapter 12.3.3 (pages S66-S70), Supplementary Information.

## 5.7 Increased $A\beta_{42}/A\beta_{40}$ ratio down-regulated the imprinted region IGF2-H19 on chromosome 11p15.5

Among the strongest down-regulated genes, as a consequence of an increased  $A\beta_{42}/A\beta_{40}$  ratio, were the following four genes, all of which are known to be regulated by imprinting. All are localized on the same chromosomal locus and were down-regulated to the same extent (IGF2, p=0.05, fold change= -2.6; CDKN1C, p= 0,06, fold change=-1.98; putative IGF2 associated protein, p=0.1, fold change=-1.84; H19, p=0.21, fold change=-2.0). Detection of transcripts by several probe sets make down-regulation highly reliable: downregulation was confirmed by 2 different probe sets for IGF2, by 2 different probe sets for H19, by 3 different probe sets for CDKN1C and by 1 probe set for putative IGF2 associated protein.

Gene symbol	Gene name	Chromosomal locus	Silencing
IGF2	insulin-like growth factor 2 (somatomedin A)	chr11p15.5	imprinted gene
H19	H19 imprinted maternally expressed untranslated mRNA	chr11p15.5	imprinted gene
CDKN1C	cyclin-dependent kinase inhibitor 1C (p57, Kip2)	chr11p15.5	imprinted gene
LOC492304	putative IGF2 associated protein	chr11p15.5	imprinted gene

**Table 5.7 Genes, known to be regulated by imprinting localized on the same chromosomal locus (chr.11p15.5) and down-regulated to the same extent.**

In contrast to this, a decreased  $A\beta_{42}/A\beta_{40}$  ratio did not result in dysregulation of the previously described genes. The fact that cathepsin D, one of the top candidate genes for AD, is localized on the same locus (chr.11p15.5) make this region a top candidate region for AD. Cathepsin D was among the 10 most down-regulated genes as a result of a decreased  $A\beta_{42}/A\beta_{40}$  ratio (C99V50F/C99WT1,  $p=0.09$ , fold change = -2.9). Cathepsin D, located 230 kb from H19, is among a set of candidate imprinted genes in mice [159].

## **5.8 Phosphorylation status of proteins and total protein amounts in consequence of an altered $A\beta_{42}/A\beta_{40}$ ratio detected by high throughput immunoblotting**

### **5.8.1 Immunoblots**

High throughput immunoblotting was performed using Kinetworks™, a screening procedure from the Canadian company Kinexus. Antibodies directed against phosphorylated proteins were extensively tested for specificity by Kinexus. Out of 3000 commercially available antibodies, Kinexus selected approximately the 650 most potent and specific ones for their phosphorylation screening. The Kinetworks™ analysis has been specially optimized to reveal band shifts in signaling proteins on SDS-PAGE gels that may arise from their phosphorylation. A high-resolution scanner was used by Kinexus to detect chemoluminescence. The relative abundance of each detected immunoreactive protein was quantified: The intensities of the enhanced chemoluminescence (ECL) signals were quantified (counts per minute) from the multiple immunoblots.

At first the KPSS-9.0 Phospho-Site Neurobiology screen was used to pre-select interesting proteins. For further detailed analysis the KCPS-1.0 custom screens were used twice.

The phosphorylation status of proteins extracted from the human neuroblastoma cell line SH-SY5Y, transfected with mutant C99I45F ( $A\beta_{42}/A\beta_{40}\uparrow$ ), C99V50F ( $A\beta_{42}/A\beta_{40}\downarrow$ ), and C99WT was checked by Western-blotting. C99WT served as a reference (baseline experiment). Subsequently, relative (to C99WT) percentage of phosphorylation was calculated (by densitometry of the bands and normalized to a set of normalization controls). These data were compared to each other, providing insights into differentially phosphorylated proteins. For some proteins the *total* protein expression was measured using a *pan-specific (directed against phosphorylated and non-phosphorylated binding sites)* antibody. *This provides the possibility to*

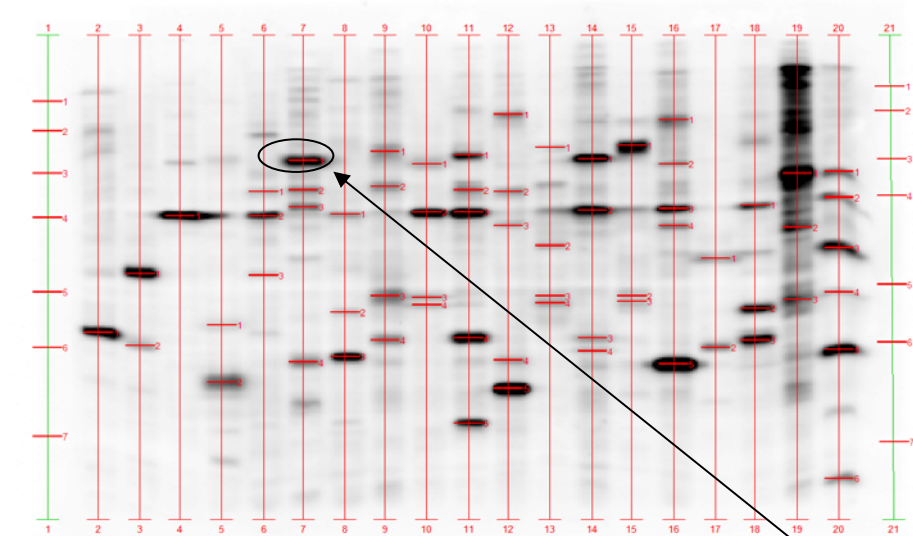
---

*discriminate between a real change in the phosphorylation status and a change in total protein expression of the corresponding protein.* For the remaining proteins, a change in the phosphorylation status was observed, however, total protein expression was not tested by Western-blotting. Gen expression data (transcript-level) for these proteins provide limited estimations of how these proteins are regulated (the protein-levels for many proteins, measured by a proteomic approach, were mostly consistent with mRNA-levels). For these proteins it can be concluded that a difference in the phosphorylation status exists or that a difference in total protein expression exists, which might simulate hyper/hypo-phosphorylation. However, differences in total protein expression were not probable (but cannot be totally excluded, due to putative regulatory processes on the protein-level, like proteasomal degradation and others), since m-RNA levels were monitored by gene expression data showing no altered transcript expression, if not indicated elsewhere. Further validation of total protein expression will provide further insights into the phosphorylation status. According to Kinexus, *only differences of expression or phosphorylation of >25% (between two samples) can be regarded as a real change in expression or phosphorylation.* Only proteins showing a *distinct difference* of expression or phosphorylation between C99WT and C99-mutants compared to each other (after normalization) were selected for further analysis (see diagrams below). Apart from a change of expression or phosphorylation (relative values between two samples presented in %), absolute values (band intensities of one sample) have to be taken into account, to evaluate data reliability.

**KPSS-9.0 - Phospho-Site Neurobiology screen:**

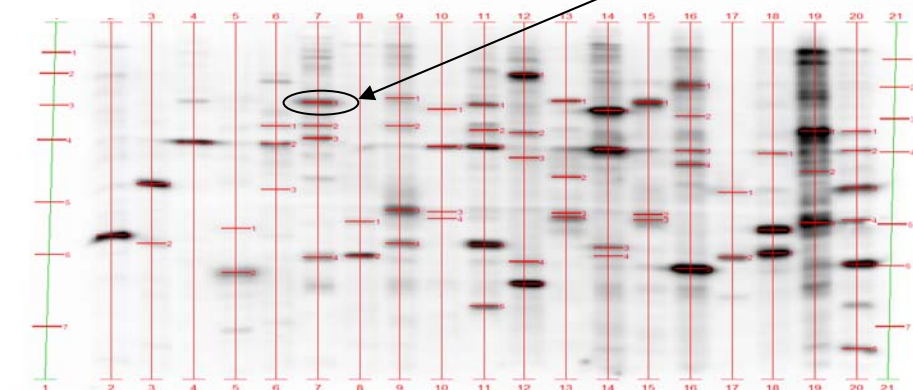
A

C99WT:



B

C99I45F:



Example:  
FAK shows less  
phosphorylation  
in C99I45F than  
in C99WT  
(normalisation  
not considered  
here)

**Figure 5.10** Immunoblots of proteins from SH-SY5Y cells. Phospho-specific antibodies were used to determine the phosphorylation status. A) Cells transfected with C99WT and B) Cells transfected with C99I45F.

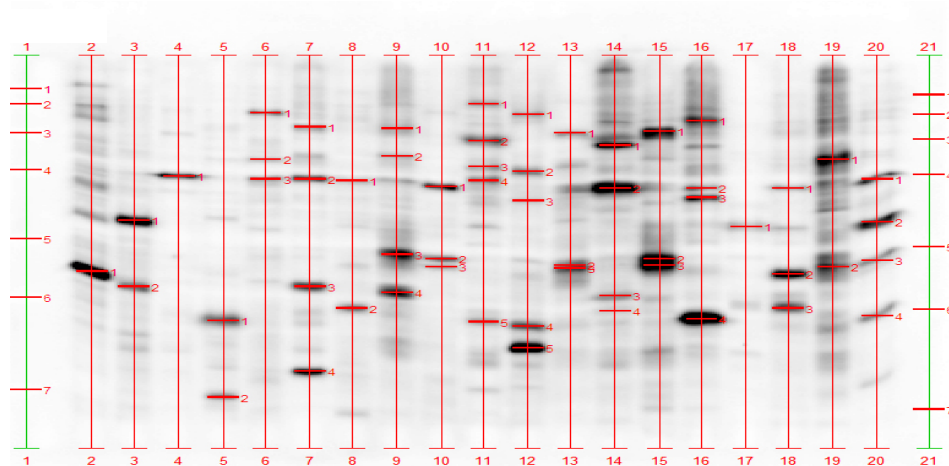
LANE	BAND	FULL NAME OF PROTEIN [EPITOPE]	ABBREVIATION	NORMALIZED COUNTS PER MINUTE	
				C99WT	C99I45F
2	1	MAPK/ERK protein-serine kinase 1 (MKK1) [T385]	MEK1	5635	5928
4	1	Protein-serine kinase C delta [S664]	PKCd	6421	3195
5	1	cAMP response element binding protein 1 [S129+S133]	CREB1	606	342
6	1	Protein-serine kinase C epsilon [S729]	PKCe	627	622
6	3	Microtubule-associated protein tau [S720] (55)	Tau	509	257
7	1	Focal adhesion protein-tyrosine kinase [S722]	FAK	4864	3048
9	3	Microtubule-associated protein tau [S515/S518] (46)	Tau	2650	4241
9	4	MAPK/ERK protein-serine kinase 1 (MKK1) [S297]	MEK1	1490	2188
10	2	Protein-serine kinase C eta [S674]	PKCh	5885	1972
11	3	Protein-serine kinase C gamma [T514]	PKCg	7009	4135
11	4	MAPK/ERK protein-serine kinase 1 (MKK1) [T291]	MEK1	5028	5832
12	3	G protein-coupled receptor-serine kinase 2 (BARK1) [S670] (70)	GRK2	652	744
13	2	Microtubule-associated protein tau [S515] (63)	Tau	742	1028
13	3	Microtubule-associated protein tau [S515] (46)	Tau	446	971
13	4	Microtubule-associated protein tau [S515] (44)	Tau	1175	2541
14	3	Extracellular regulated protein-serine kinase 1 (p44 MAP kinase) [T202+Y204]	Erk1	929	1503
15	2	Microtubule-associated protein tau [S712] (46)	Tau	677	942
15	3	Microtubule-associated protein tau [S712] (44)	Tau	789	2213
16	3	Protein-serine kinase C eta [T655]	PKCh	3631	1369
16	5	cAMP-dependent protein-serine kinase catalytic subunit beta [S338]	PKA Cb	16110	12100
17	1	Protein-serine kinase B alpha (Akt1) [S473]	PKBa (Akt1)	1401	1008
18	1	Protein-serine kinase C beta 2 [T641]	PKCb2	1917	1104
18	2	Glycogen synthase-serine kinase 3 alpha [Y279] (44)	GSK3a	4069	9008
18	3	Glycogen synthase-serine kinase 3 beta [Y216] (39)	GSK3b	4365	7390
19	3	Microtubule-associated protein tau [S518] (46)	Tau	2550	5662
20	5	cAMP-dependent protein-serine kinase catalytic subunit alpha/beta [T197]	PKA Ca/b	5858	7168
Reprobed*	Reprobed*	Protein-serine kinase C beta 1/2 [T500]	PKCb1/2	324	146

**Table 5.8** The phosphorylation status of proteins extracted from the human neuroblastoma cell line SH-SY5Y, transfected with mutant C99I45F ( $A\beta_{42}/A\beta_{40}\uparrow$ ) and C99WT was checked by Western-blotting using phospho-specific antibodies. C99WT served as a reference (base-line experiment). Subsequently, relative (to C99WT) percentage of phosphorylation was calculated. \* Due to problems with immunoblotting, the sample C99WT and C99I45F had to be reprobed with an antibody for protein-serine kinase C beta 1/2 [T500].

### KPSS-9.0 - Phospho-Site Neurobiology screen:

**A**

C99WT:



**B**

C99V50F:

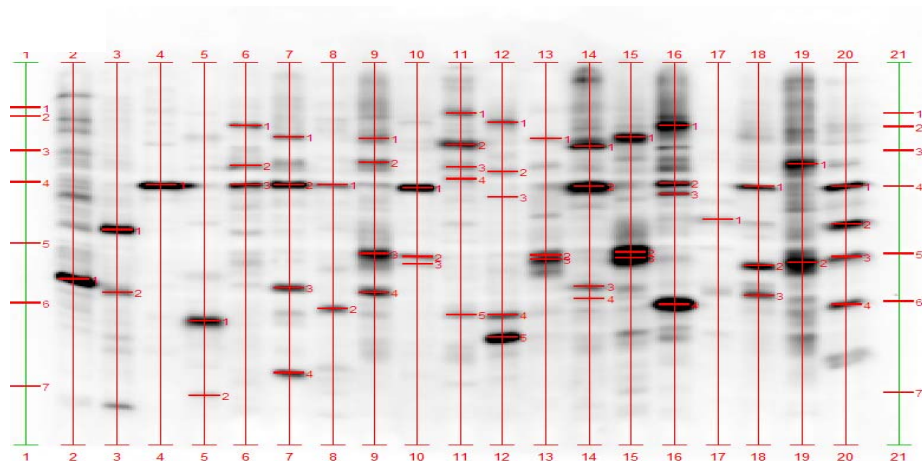


**Figure 5.11** Immunoblots of proteins from SH-SY5Y cells. Phospho-specific antibodies were used to determine the phosphorylation status. A) Cells transfected with C99WT and B) Cells transfected with C99V50F.

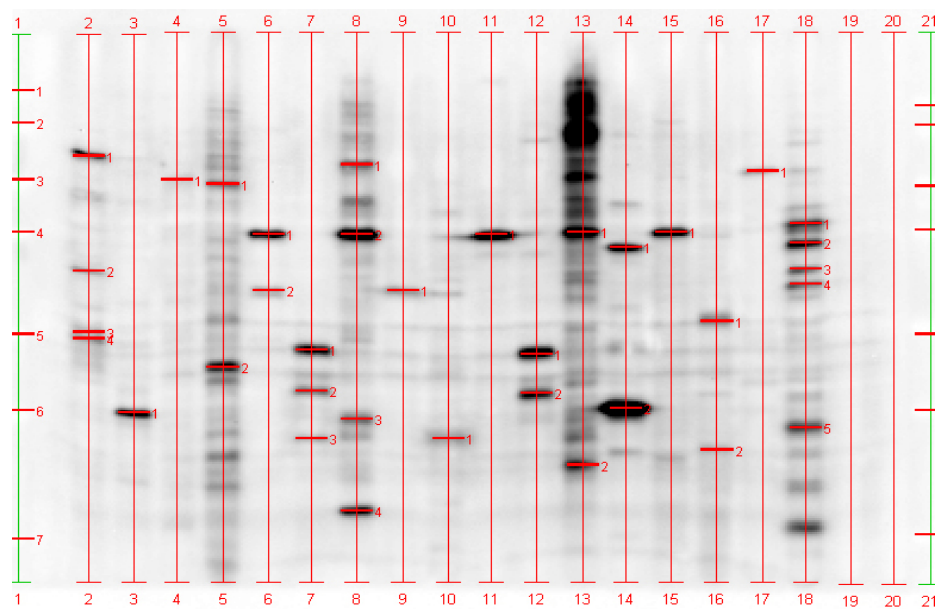
LANE	BAND	FULL NAME OF PROTEIN [EPITOPE]	ABBREVIATION	NORMALIZED COUNTS PER MINUTE	
				C99WT	C99V50F
2	1	MAPK/ERK protein-serine kinase 1 (MKK1) [T385]	MEK1	9367	7195
4	1	Protein-serine kinase C delta [S664]	PKCd	2533	5086
6	2	Protein-serine kinase C epsilon [S729]	PKCe	621	1077
7	2	Protein-serine kinase C gamma [T514]	PKCg	2122	3563
7	3	MAPK/ERK protein-serine kinase 1 (MKK1) [T291]	MEK1	3078	2229
8	1	Protein-serine kinase C beta 1/2 [T500]	PKCb1/2	731	1148
9	3	Microtubule-associated protein tau [S515/S518] (46)	Tau	4006	3784
9	4	MAPK/ERK protein-serine kinase 1 (MKK1) [S297]	MEK1	3486	2390
10	1	Protein-serine kinase C eta [S674]	PKCh	2433	4848
11	2	Focal adhesion protein-tyrosine kinase [S722]	FAK	2386	2473
12	3	G protein-coupled receptor-serine kinase 2 (BARK1) [S670] (70)	GRK2	448	277
13	2	Microtubule-associated protein tau [S720] (46)	Tau	1412	1255
13	3	Microtubule-associated protein tau [S720] (44)	Tau	2138	2499
15	2	Microtubule-associated protein tau [S712] (46)	Tau	4636	5918
15	3	Microtubule-associated protein tau [S712] (44)	Tau	4884	6751
16	2	Protein-serine kinase C eta [T655]	PKCh	990	2667
16	4	cAMP-dependent protein-serine kinase catalytic subunit beta [S338]	PKA Cb	13301	13079
17	1	Protein-serine kinase B alpha (Akt1) [S473]	PKBa (Akt1)	1113	889
18	1	Protein-serine kinase C beta 2 [T641]	PKCb2	867	1866
20	1	Protein-serine kinase C gamma [T655]	PKCg	2009	3224
20	4	cAMP-dependent protein-serine kinase catalytic subunit alpha/beta [T197]	PKA Ca/b	1712	2107

**Table 5.9** The phosphorylation status of proteins extracted from the human neuroblastoma cell line SH-SY5Y, transfected with mutant C99V50F ( $A\beta_{42}/A\beta_{40}\downarrow$ ) and C99WT was checked by Western-blotting using phospho-specific antibodies. C99WT served as a reference (base-line experiment). Subsequently, relative (to C99WT) percentage of phosphorylation was calculated.

**KCPS-1.0 custom screen:**

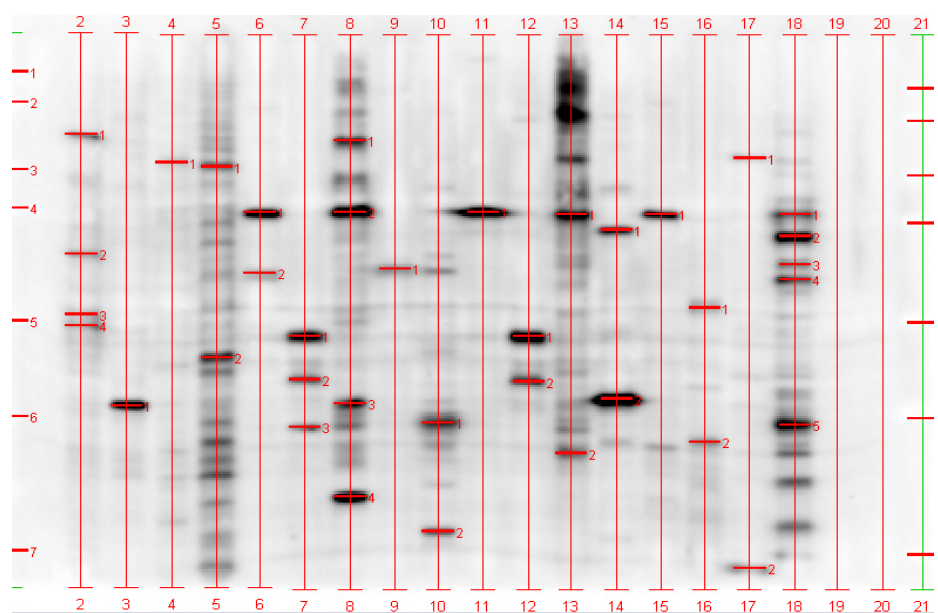
A

C99WT:



B

C99I45F:



C

C99V50F:

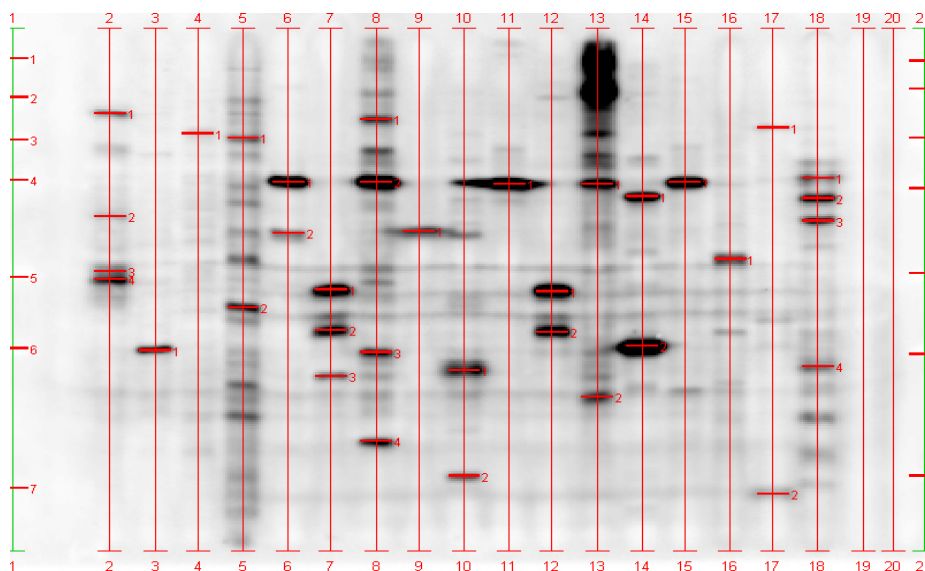


**Figure 5.12 Immunoblots of proteins from SH-SY5Y cells. Pan-specific and phospho-specific antibodies were used to determine the phosphorylation status. A) Cells transfected with C99WT and B) Cells transfected with C99I45F and C) Cells transfected with C99V50F.**

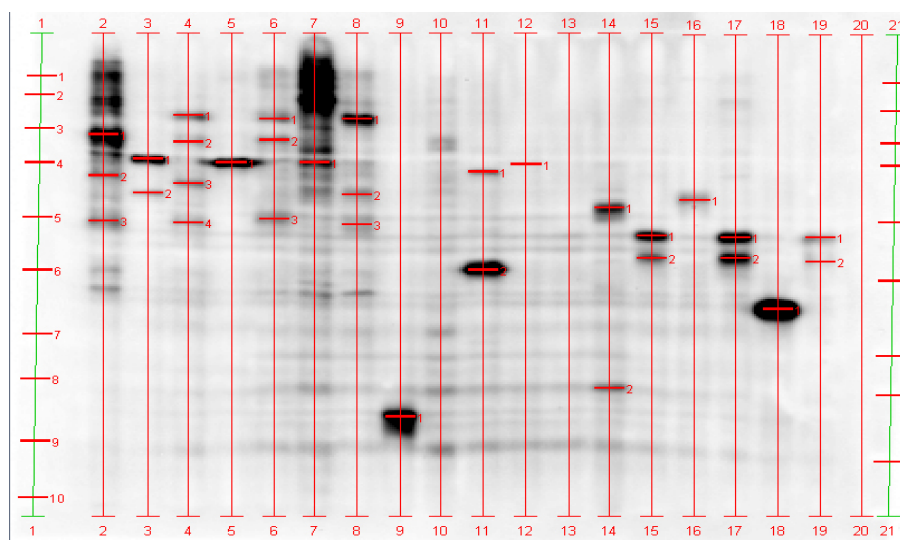
LANE	BAND	FULL NAME OF PROTEIN [EPIPE]	ABBREVIATION	NORMALIZED COUNTS PER MINUTE		
				C99WT	C99I45F	C99V50F
6	1	Protein-serine kinase C alpha/beta 2 [T638/T641]	PKCa/b2 [T638/T641]	1928	2254	3530
7	1	Glycogen synthase-serine kinase 3 alpha, pan-specific	GSK3a	1836	1906	2235
7	2	Glycogen synthase-serine kinase 3 beta, pan-specific	GSK3b	723	894	1126
8	2	Protein-serine kinase C gamma [T514]	PKCg	3822	3176	4776
11	1	Protein-serine kinase C delta [S664]	PKCd	3132	3460	5099
12	1	Glycogen synthase-serine kinase 3 alpha [Y279]	GSK3a	2741	2590	3282
14	2	cAMP-dependent protein-serine kinase catalytic subunit beta [S338]	PKA Cb	8662	4891	6923
15	1	Protein-serine kinase C eta [S674]	PKCh	2255	1550	3439
16	1	Serum/glucocorticoid regulated kinase 3,	SGK3	966	612	941

		pan-specific				
18	2	Protein-serine kinase C delta, pan-specific	PKCd	1506	2271	1064

**Table 5.10** The total protein expression level and phosphorylation status of proteins extracted from the human neuroblastoma cell line SH-SY5Y, transfected with mutant C99I45F ( $A\beta_{42}/A\beta_{40}\uparrow$ ), C99V50F ( $A\beta_{42}/A\beta_{40}\downarrow$ ) and C99WT was checked by Western-blotting using pan-specific and phospho-specific antibodies. C99WT served as a reference (base-line experiment). Subsequently, relative (to C99WT) percentage of phosphorylation was calculated.

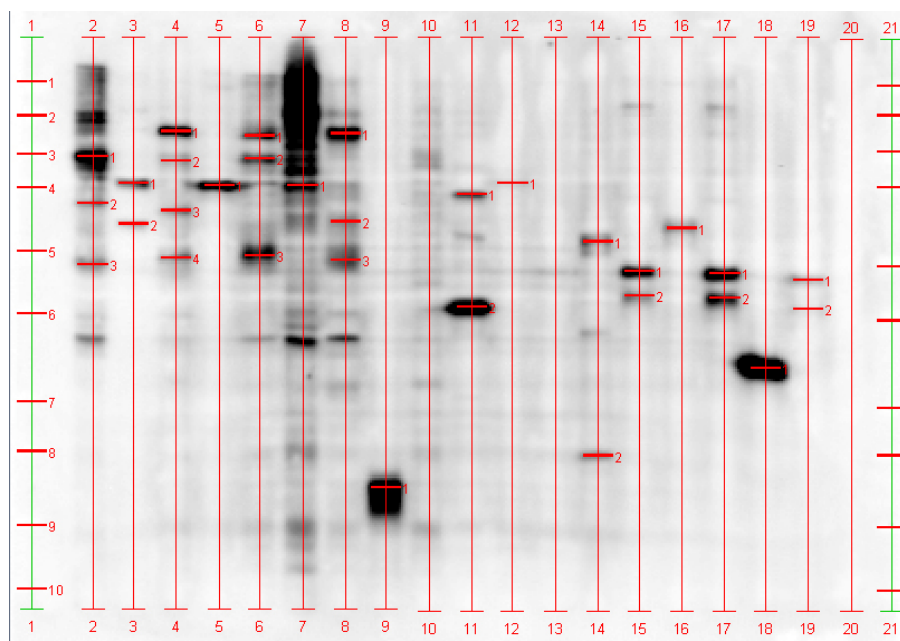
A

C99WT:



B

C99I45F:



C

C99V50F:

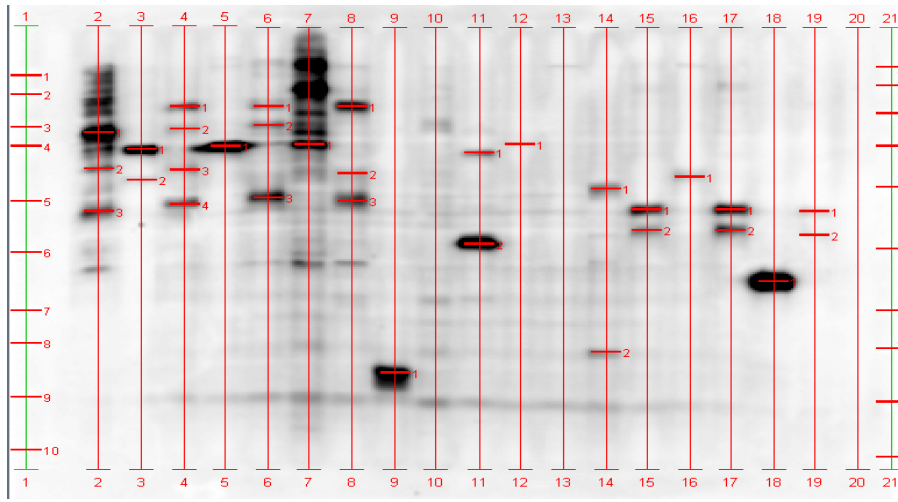


**Figure 5.13 Immunoblots of proteins from SH-SY5Y cells. Pan-specific and phospho-specific antibodies were used to determine the phosphorylation status. A) Cells transfected with C99WT and B) Cells transfected with C99I45F and C) Cells transfected with C99V50F.**

LANE	BAND	FULL NAME OF PROTEIN [EPITOPE]	ABBREVIATION	NORMALIZED COUNTS PER MINUTE		
				C99WT	C99I45F	C99V50F
3	1	Protein-serine kinase C alpha/beta 2 [T638/T641]	PKCa/b2	1516	746	2092
4	4	Microtubule-associated protein tau [S515] (46)	Tau	343	524	797
5	1	Protein-serine kinase C delta [S664]	PKCd	2331	1723	4497
6	3	Microtubule-associated protein tau [S515+S518] (46)	Tau	602	1927	1606
7	1	Protein-serine kinase C eta [T655]	PKCh	595	679	1077
9	1	Superoxide dismutase 1, pan-specific	SOD (Cu/Zn)	4761	7110	3570
11	2	cAMP-dependent protein-serine kinase catalytic subunit beta [S338]	PKA Cb	3958	4055	3720
12	1	Serine/threonine-protein kinase DCAMKL1, pan-specific	CPG16/CaMK VI	57	130	51
14	1	Serum/glucocorticoid regulated kinase 3, pan-specific	SGK3	1481	794	768
18	1	Cyclin D1 (PRAD1), pan-specific	Cyclin D1	11253	7990	10013
19	1	Glycogen synthase-serine kinase 3 alpha, pan-specific	GSK3a	521	385	224

19	2	Glycogen synthase-serine kinase 3 beta, pan-specific	GSK3b	210	149	78
----	---	--	-------	-----	-----	----

**Table 5.11** The total protein expression level and phosphorylation status of proteins extracted from the human neuroblastoma cell line SH-SY5Y, transfected with mutant C99I45F ( $A\beta_{42}/A\beta_{40}\uparrow$ ), C99V50F ( $A\beta_{42}/A\beta_{40}\downarrow$ ) and C99WT was checked by Western-blotting using pan-specific and phospho-specific antibodies. C99WT served as a reference (base-line experiment). Subsequently, relative (to C99WT) percentage of phosphorylation was calculated.

## 5.8.2 Quantification and graphical presentation of previously shown immunoblots

Immunoblots were performed in triplicates, duplicates or single experiments. Since a large number of proteins was examined, it was not possible to perform any experiments in triplicates for financial reasons. So triplicates were restricted to those proteins that were expected to reveal the most useful information.

### Protein kinase C $\beta$ 1/2:

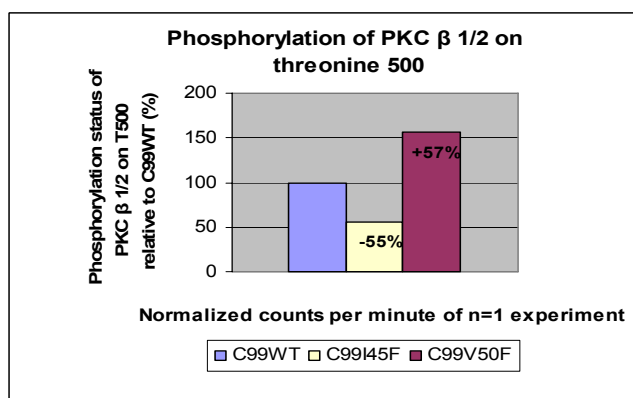


**Figure 5.14** Protein kinase C  $\beta$  1/2 showed weaker phosphorylation on threonine 500 in mutant C99I45F compared to C99V50F and C99WT.

### Protein kinase C $\alpha/\beta$ 2:

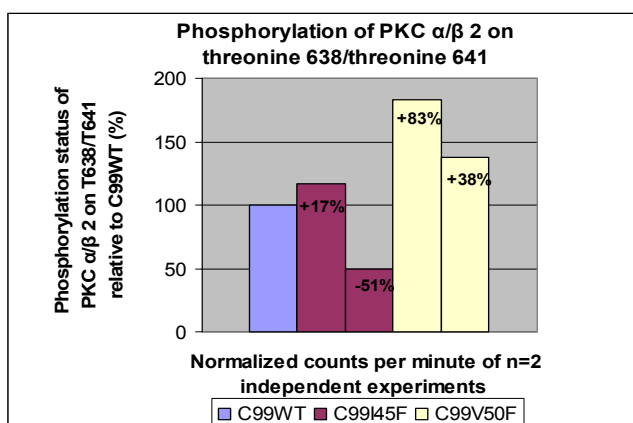


**Figure 5.15** Protein kinase C  $\alpha/\beta$  2 showed weaker phosphorylation on threonine 638/641 in mutant C99I45F compared to C99V50F.

### Protein kinase C $\beta$ 2:

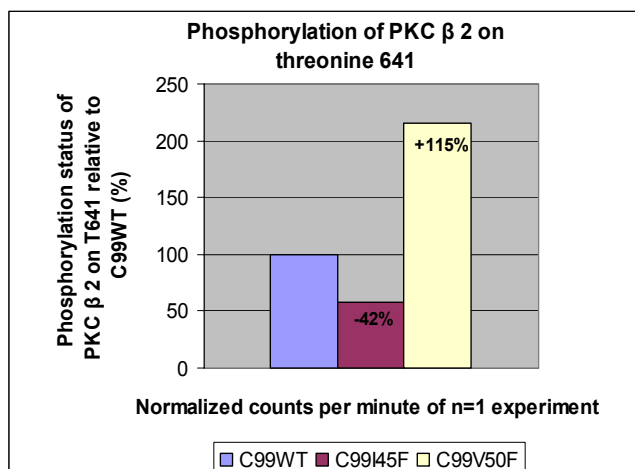


Figure 5.16 Protein kinase C  $\beta$ 2 showed weaker phosphorylation on threonine 641 in mutant C99I45F compared to C99V50F and C99WT.

### Protein kinase C $\delta$ :

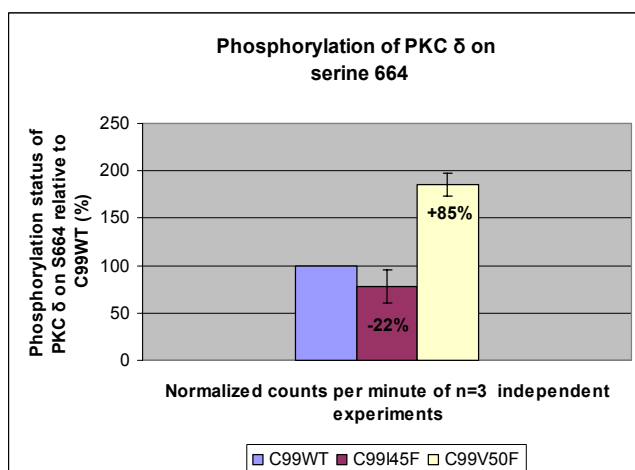


Figure 5.17 Protein kinase C  $\delta$  showed weaker phosphorylation on serine 664 in mutant C99I45F compared to C99V50F and C99WT (n=3, p=0.007).

### Protein kinase C $\epsilon$ :

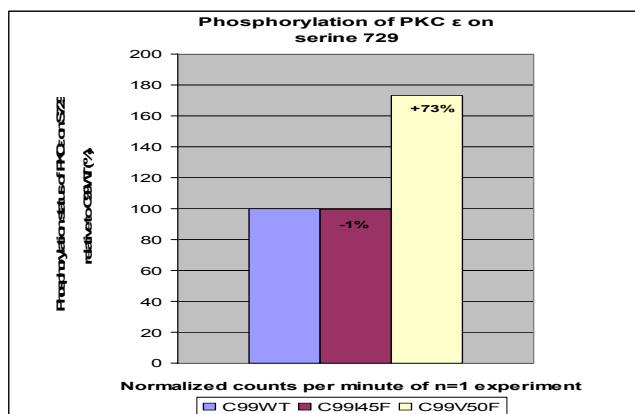


Figure 5.18 Protein kinase C  $\epsilon$  showed weaker phosphorylation on serine 729 in mutant C99I45F compared to C99V50F.

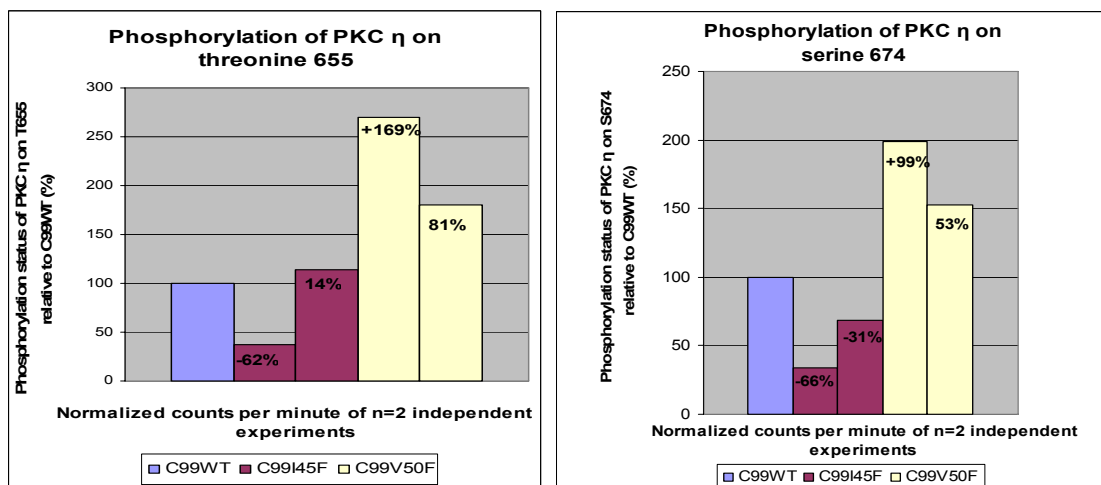
Protein kinase C  $\eta$ :

Figure 5.19 Protein kinase C  $\eta$  showed weaker phosphorylation on threonine 655 and on serine 674 in mutant C99I45F compared to C99V50F.

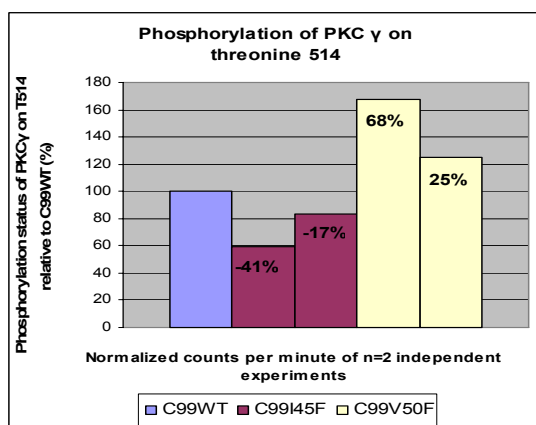
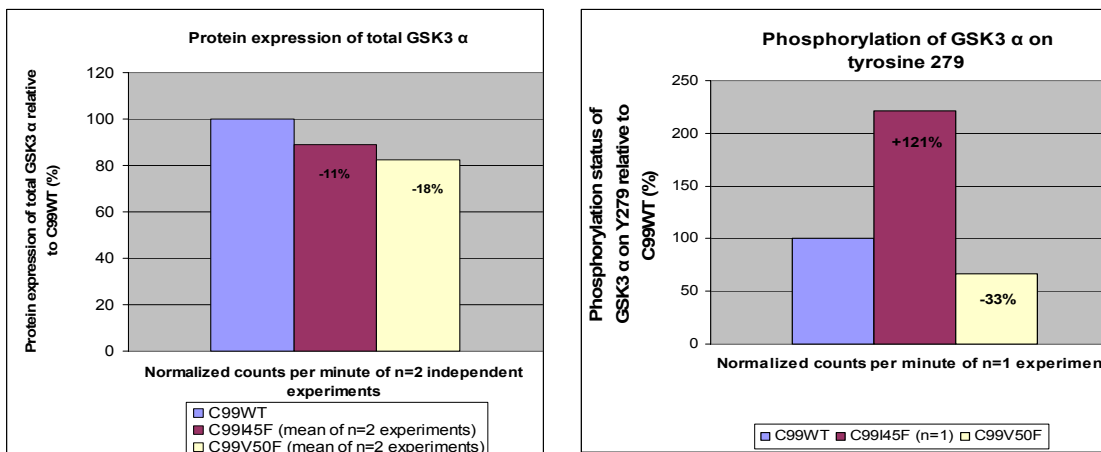
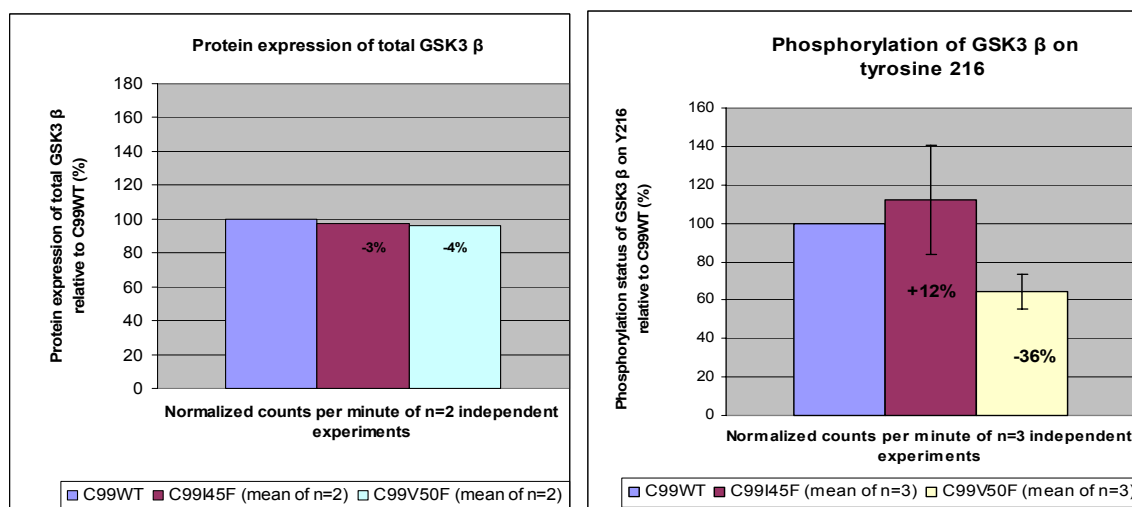
Protein kinase C  $\gamma$ :

Figure 5.20 Protein kinase C  $\gamma$  showed weaker phosphorylation on threonine 514 in mutant C99I45F compared to C99V50F and to C99WT.

GSK3 $\alpha$ :

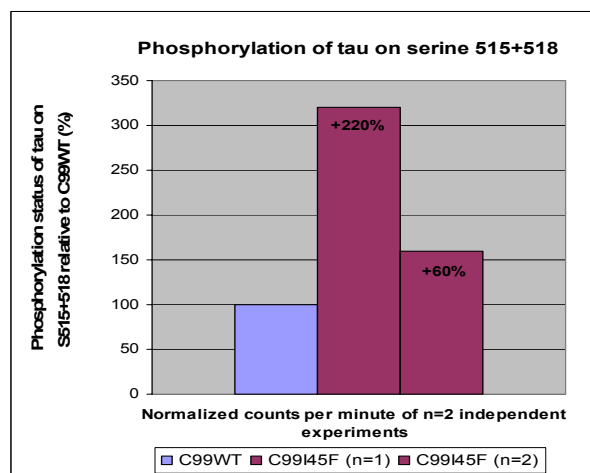
**Figure 5.21 Expression of total-GSK3 $\alpha$  (left Figure) and phosphorylation on tyrosine 279 (right Figure).** Total GSK3 $\alpha$  was not more strongly expressed in mutant C99I45F and C99V50F than in C99WT, but showed *hyper*-phosphorylation on tyrosine 279 in mutant C99I45F compared to C99V50F and C99WT. Due to a change in the antibody-panel of Kinexus, it was not possible to repeat the experiment with the same (anti-GSK3 $\alpha$  tyrosine 279) antibody. Another anti-GSK3 $\alpha$  tyrosine 279 antibody, provided by Kinexus, did not allow reproducing the previous results. Further replicates, with diverse antibodies recognizing the same phosphorylation-site, are necessary to clarify this issue.

### GSK3 $\beta$ :



**Figure 5.22 Total GSK3 $\beta$  expression and phosphorylation on tyrosine 216.** Total GSK3 $\beta$  was approximately equally expressed in mutant C99I45F, C99V50F and in C99WT (diagram on the left), but showed *hyper*phosphorylation on tyrosine 216 in mutant C99I45F compared to C99WT and *hypophosphorylation* on tyrosine 216 in mutant C99V50F compared to C99WT. In addition direct comparison of both mutants showed stronger phosphorylation on tyrosine 216 in mutant C99I45F compared to C99V50F (diagram on the right).

### Tau:



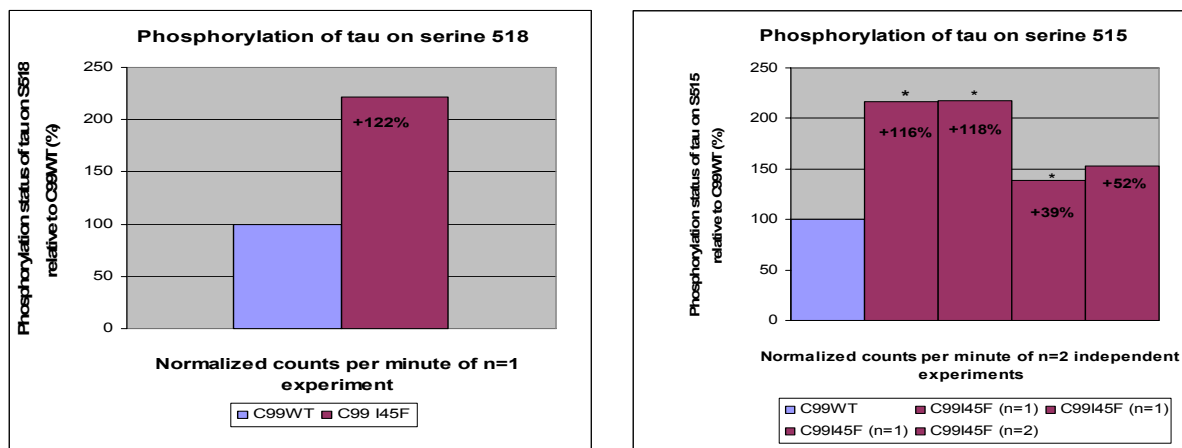


**Figure 5.23** Tau showed stronger phosphorylation on serine 515<sup>♦</sup> and 518<sup>♦</sup> in mutant C99I45F compared to C99WT. Stronger phosphorylation detected by an antibody recognizing both serine 515 and 518 (diagram on page 72) was confirmed by two specific antibodies recognizing either serine 518 (corresponding to serine 202 of tau isoform 2=tau<sub>441</sub>, diagram on the left) or serine 515 (corresponding to serine 199 of tau isoform 2, diagram on the right). \*Different splice forms of tau, detected with the same antibody.

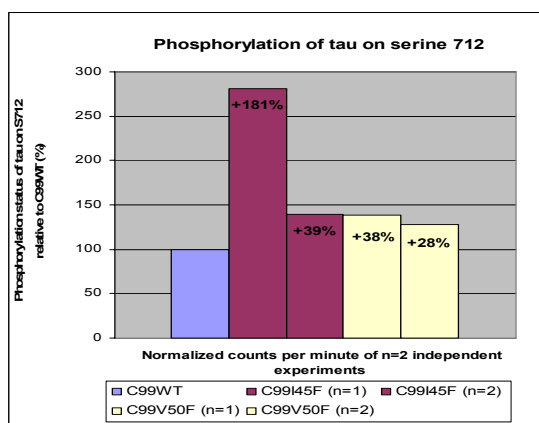


**Figure 5.24** Tau showed stronger phosphorylation on serine 712<sup>♦</sup> (corresponding to serine 396 of tau isoform 2=tau<sub>441</sub>) in mutant C99I45F compared to C99WT and a weak tendency towards a stronger phosphorylation compared to C99V50F.

### CREB1:

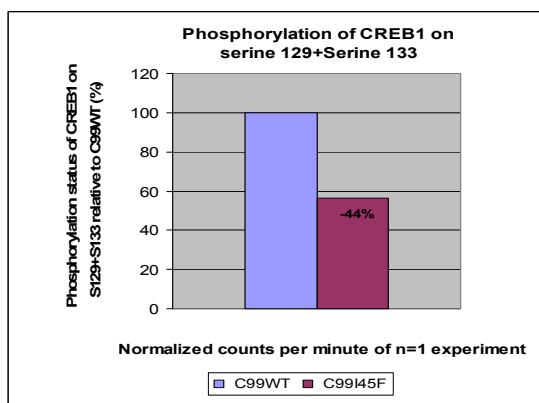


**Figure 5.25** CREB1 appeared to be less phosphorylated on serine 129 and 133 in mutant C99I45F compared to C99WT. Microarray data revealed that CREB1 was among the most 20 down-regulated transcripts (C99I45F versus C99WT1).

♦ Numbering refers to the full length (unspliced) form of tau

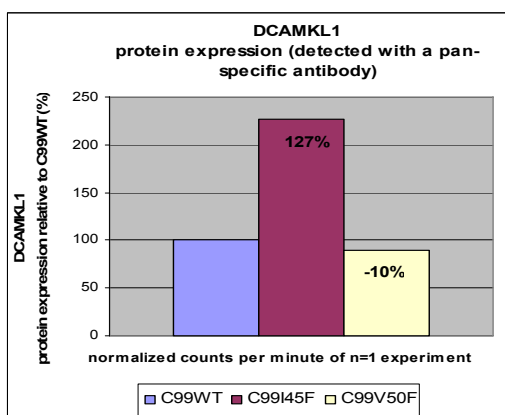
**DCAMKL1:**

Figure 5.26 DCAMKL1 was more strongly expressed in mutant C99I45F compared to C99WT and C99V50F.

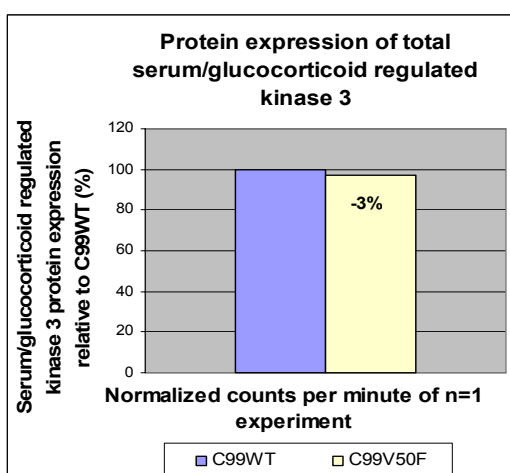
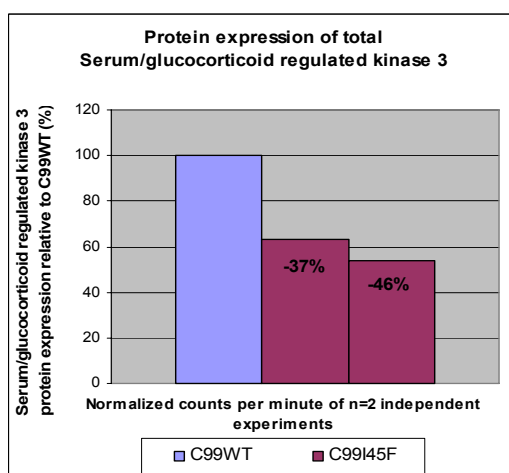
**Serum/glucocorticoid regulated kinase 3 (SGK3):**

Figure 5.27 SGK3 was more weakly expressed in mutant C99I45F compared to C99WT (Figure on the left). This was corroborated by microarray data in which SGK was down-regulated on the transcript-level (C99I45F versus C99WT1). Interestingly SGK was among the 16 most up-regulated transcripts in mutant C99V50F compared to C99WT (shown by microarray analysis). This inverse regulation indicates that SGK was regulated by a changed  $A\beta_{42}/A\beta_{40}$  ratio.

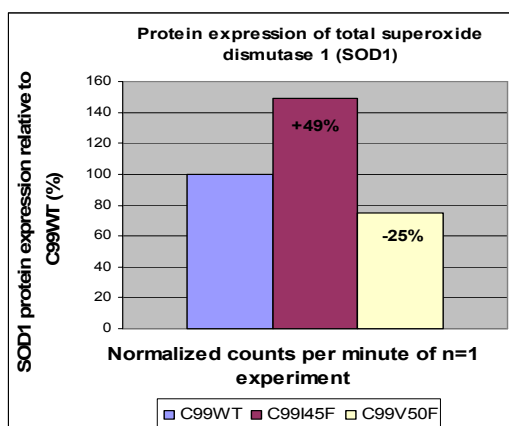
**Superoxide dismutase 1 (SOD1):**

Figure 5.28 SOD1 was more strongly expressed in mutant C99I45F whereas it was more weakly expressed in mutant C99V50F (compared to C99WT).

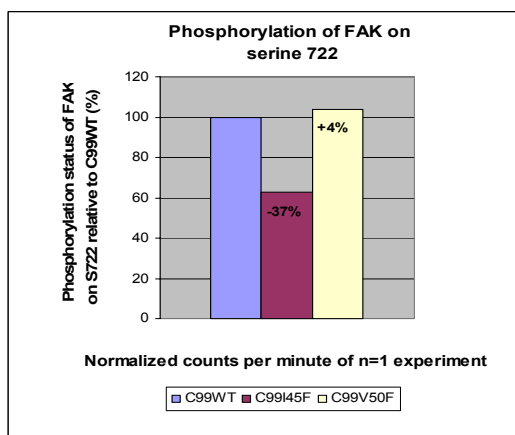
**FAK:**

Figure 5.29 Focal adhesion protein-tyrosine kinase (FAK) showed weaker phosphorylation on serine 722 in mutant C99I45F compared to C99WT and C99V50F.

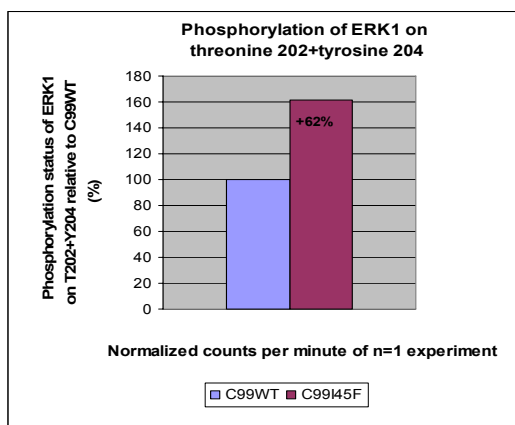
**ERK1 :**

Figure 5.30 ERK1 showed stronger phosphorylation on threonine 202/tyrosine 204 in mutant C99I45F compared to C99WT.

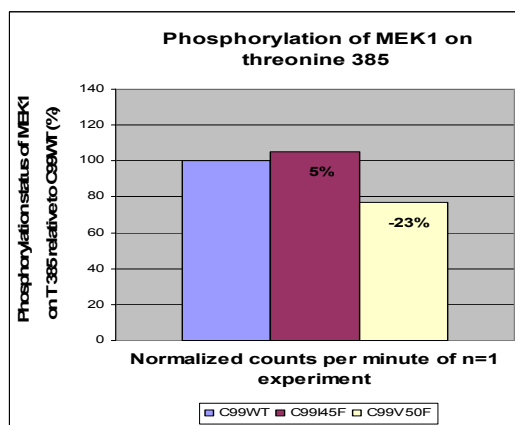
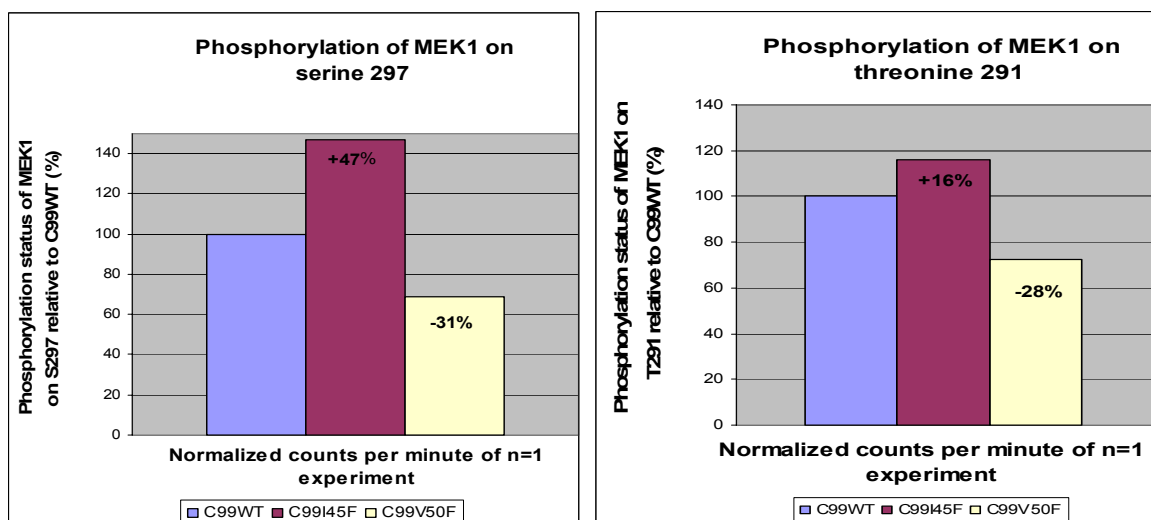
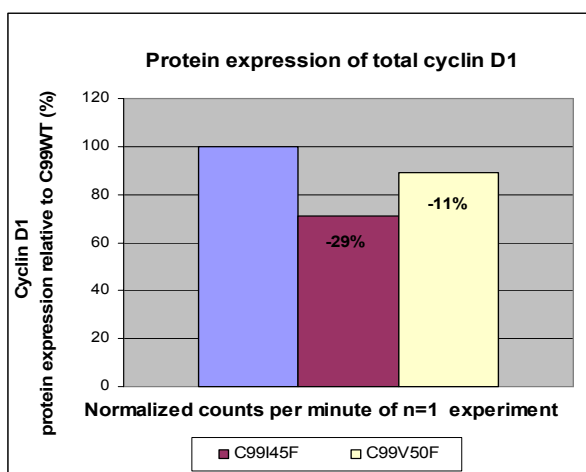
**MEK1:**

Figure 5.31 MEK1 showed stronger phosphorylation on threonine 385 in mutant C99I45F compared to C99V50F.



**Figure 5.32** MEK1 showed stronger phosphorylation on serine 297 in mutant C99I45F and weaker phosphorylation in mutant C99V50F compared to C99WT (Figure on the left). The same might be true, although less evident, for threonine 291 (Figure on the right).

### Cyclin D1:



**Figure 5.33** Cyclin D1 was more weakly expressed in mutant C99I45F compared to C99WT and C99V50F.

### PKA $\beta$ :

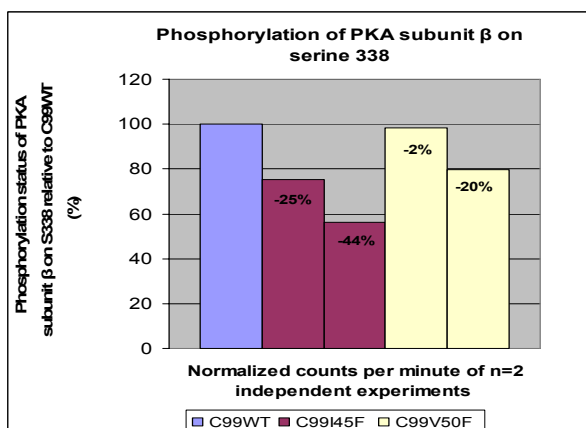


**Figure 5.34** PKA $\beta$  (Protein kinase A  $\beta$ ) showed weaker phosphorylation on serine 338 in mutant C99I45F compared to C99WT. Direct comparison of both mutants showed weaker phosphorylation on serine 338 in mutant C99I45F compared to mutant C99V50F.

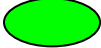
## 5.9 Models

### 5.9.1 Preface

Data derived from the transcriptomic approach and from the output of the phosphorylation status were used for pathway analysis. Moreover, some genes were validated on the protein level by immunoblotting. Analysis was performed with Pathway Architect™ (Stratagene).

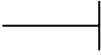
 not differentially expressed

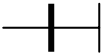
 up-regulated transcript

 down-regulated transcript

 activation

 inhibited activation

 inhibition

 inhibited inhibition

P↑ *hyperphosphorylation*\*

P↓ *hypophosphorylation*\*

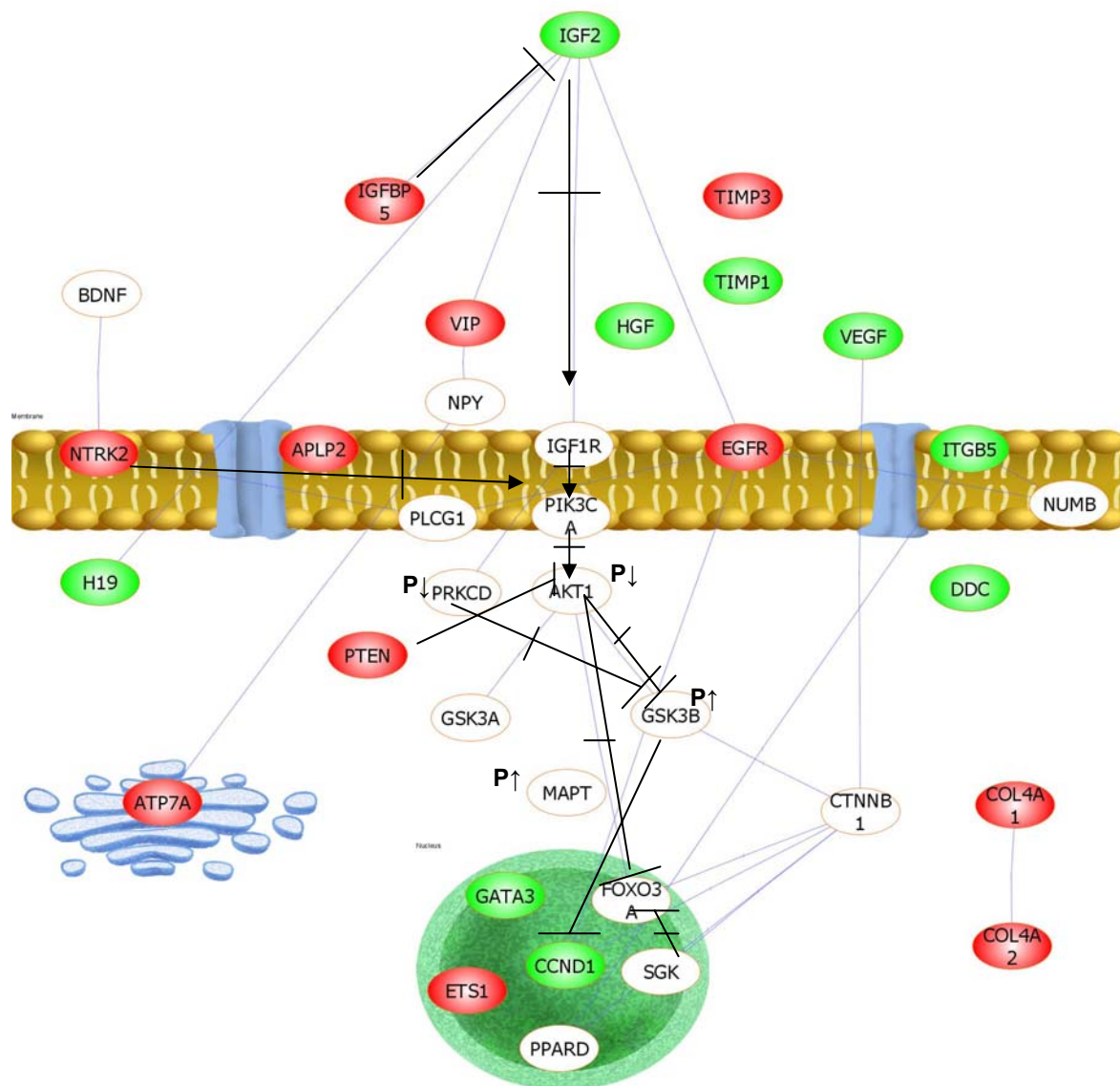
---

\* For proteins whose total protein expression was not tested and thus an apparent *hypo/hyperphosphorylation* (tested with phospho-specific antibodies by immuno-blotting) may be a result of altered protein levels rather than a real change in the phosphorylation status, the term “showed weaker or stronger phosphorylation” was used instead of “*hypo/hyperphosphorylation*”.

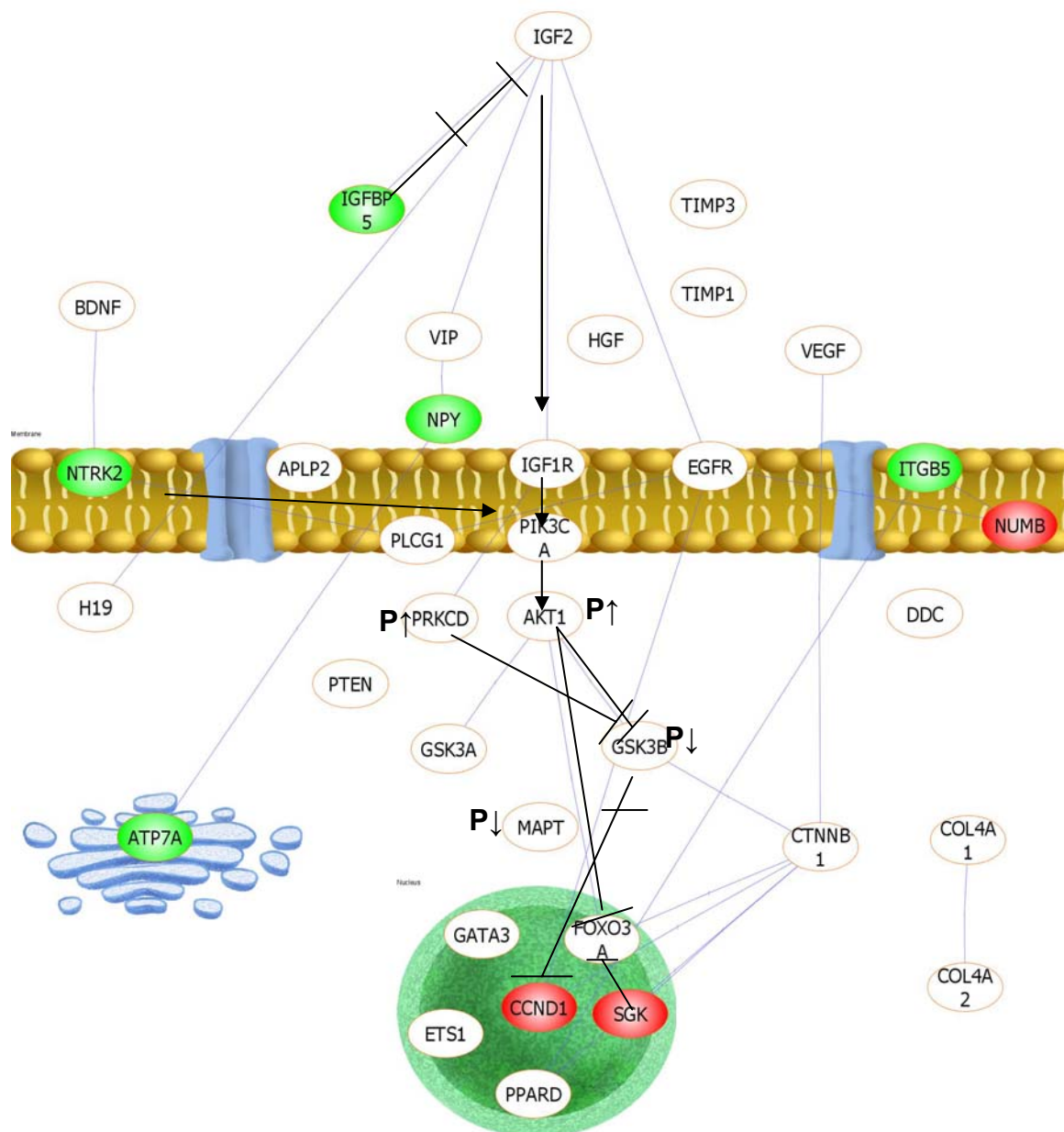
## 5.9.2

Model: Downregulation of IGF2/IGF1R/PKC and PI3K/AKT signaling by an increased  $A\beta_{42}/A\beta_{40}$  ratio

A

 $A\beta_{42}/A\beta_{40} \uparrow$ 

B

 $A\beta_{42}/A\beta_{40}\downarrow$ 

**Figure 5.35 IGF2/IGF1R/PKC and PI3K/AKT signaling are influenced by an altered  $A\beta_{42}/A\beta_{40}$  ratio.** Crucial differentially expressed genes were selected and integrated into the Pathway Architect software (Stratagene). By a complex filtering procedure this pathway was created in which all transcripts/proteins (except for DDC) were found to be connected in a network. Only direct bindings (gray faint lines) are shown for simplicity. A Figure with all interconnectivities can be found in the Supplementary Information (Chapter 12.6, Fig. 12.3, page S87). Crucial activating or inhibiting interactions are illustrated (black bold lines). For most of the shown transcripts/proteins there is more than one localization (for instance transcription factors, here shown in the nucleus, are also localized in the cytoplasm). See Table 5.12 after this Figure legend (page 83), for fold changes, p-values and gene names.

**A) An increased  $A\beta_{42}/A\beta_{40}$  ratio down-regulates IGF2/IGF1R/PKC and PI3K/AKT signaling.**

A plethora of inhibiting/activating molecules converge towards PI3K and AKT. PI3K/AKT activating molecules like IGF2 were significantly down-regulated (4.0 fold down-regulated, determined by real-time PCR). This downregulation was corroborated by the simultaneous downregulation of H19 and may have been triggered by imprinting (IGF2-H19 imprinted region on chromosome 11p15.5). The insulin-like growth factor 2 (IGF2) is essential for development; bioavailable IGF2 is tightly regulated by 6 related IGFbps of which IGFBP5 is the most conserved. Up-regulated IGFBP5 binds IGF2 directly with a high association rate and is expected to reduce unbound levels of IGF2 [161]. IGF2 is known to exert its effects by binding to the IGF1 Receptor<sup>4</sup> (IGF2 may also bind to the IGF2 Receptor which acts as a signaling antagonist preventing IGF2 responses; the IGF2 Receptor specifically binds IGF2 but is devoid of signal transduction capability, and its primary function with respect to IGF action is as a clearance receptor that can modulate the bioavailability of extracellular IGF2) [164]. Although the IGF1 Receptor is regarded as the main receptor for IGF2 action, it has been discovered that IGF2 also binds to the insulin receptor [165, 166] and important information can be expected from further study of this binding (binding competition between IGF2 and insulin to the insulin receptor may be of importance). Direct bindings between IGF2 and VIP, VIP and NPY, NPY and ATP7A are known. This builds up an axis starting from IGF2 and ending up in ATP7A. *IGF2 might thus influence copper transport via ATP7A*. It can be speculated that APLP2 influences this pathway via VIP because interactions between APLP2 and VIP have been reported and VIP was strongly increased in brains of a Down's syndrome mouse model [167] (NPY was insignificantly ( $p=0.569$ ) down-regulated); *thus APLP2 could influence copper homeostasis by affecting the IGF2/VIP/NPY/ATP7A axis*. The effects of BDNF, known to activate this pathway via NTRK2 (synonym: TrkB) [160], are expected to be reduced because the *non-catalytic* isoform of NTRK2 was strongly *up-regulated*. Consequently the catalytic isoform (not up-regulated) is expected to compete with the non-catalytic isoform for BDNF binding so that *less BDNF is expected to be available for pathway activation*. Down-regulated HGF and ITGB5 target PI3K (PIK3CA: catalytic subunit of PI3K, PI3K: phosphoinositide-3-kinase) and may further contribute to downregulation of PI3K/AKT signaling. TIMP1 and TIMP3, two metalloproteinase inhibitors, may target different metalloproteinases, because of their inverse regulation. TIMPs (synonym: collagenase inhibitors) are natural inhibitors of the matrix metalloproteinases (MMPs), a group of proteinases involved in degradation of the extracellular matrix. Transcription of TIMPs is highly inducible in response to many cytokines and hormones. TIMP1 is located within intron 6 of the synapsin I gene and is transcribed in the opposite direction. TIMP genes and synapsin genes are interlocked: SYN1-TIMP1, SYN2-TIMP4 and SYN3 with TIMP3. Interestingly differential expression was found for synapsins together with TIMPs. Thus proteolytic cleavage (TIMPs are protease inhibitors) and neurotransmitter release (mediated by synapsins) are expected to interact and play a crucial role in  $A\beta$  induced cellular processes. TIMP3 has specifically been shown to inhibit the actions of ADAM10 and ADAM17 [168, 169], two APP  $\alpha$ -secretases [170]. Very recently it has been demonstrated that TIMP3 immunoreactivity is increased in AD brains [171] and that TIMP3 treatment reduces  $\alpha$ -cleavage of APP and promotes  $\beta$ -cleavage, with significant increases in  $A\beta$  production [169]. The authors emphasized that there is a striking increase in TIMP3 in AD brains (but not in other tested neurodegenerative diseases) which raises the possibility that TIMP3 contributes to the elevated  $A\beta$  levels in AD, making its inhibition a potential target for therapeutic approaches to reducing  $A\beta$ . It may be speculated that up-regulated TIMP3, apart from  $\alpha$ -secretase inhibition, also inhibits the metalloproteinase MMP8 (MMP8:  $A\beta_{42}/A\beta_{40}\uparrow$ :  $p=0.00219$ , fold change= -5.0;  $A\beta_{42}/A\beta_{40}\downarrow$ : not differentially expressed). MMP8, a collagenase, may be involved in plaque formation. Collagenous Alzheimer amyloid plaque component/collagen XXV (CLAC) [172] was observed in brains from subjects with AD. CLAC is derived from a type II transmembrane collagen protein [173]. VEGF might exert its influence on PI3K/AKT signaling via direct binding to CTNNB1 ( $\beta$ -catenin) or via diverse other molecules, since VEGF is currently the gene/protein with the most known

<sup>4</sup> Interestingly, IGF1R/EGFR heterodimerization has been reported in epithelial cancers. Stimulation of head and neck cancer cells with either IGF or EGF resulted in IGF1R and EGFR heterodimerization, but only IGF caused activating phosphorylation of both receptors [162]. Insulin receptor (IR) and insulin-like growth factor I receptor (IGF1R) are both from the same subgroup of receptor tyrosine kinases that exist as covalently bound receptor dimers at the cell surface. For both IR and IGF-IR, the most described forms are homodimer receptors. However, hybrid receptors consisting of one-half IR and one-half IGF-IR are also present at the cell surface [163].

interconnectivities to other molecules (only for AKT1 more interconnectivities have been reported). VEGF is the protein with strongest known angiogenic effects and it is also involved in neurodegeneration. Even if here ( $A\beta_{42}/A\beta_{40}\uparrow$ ) only weakly (fold change=-1.3) and insignificantly (0.2343) down-regulated it may, synergistically with down-regulated HGF (also a well-known promoter of angiogenesis), reduce vascularisation [174]; (this effect may be supported by upregulation of flj13710, an uncharacterized gene, 37% similarity to ADAMTS1 precursor, found in the cluster analysis as significantly up-regulated for  $A\beta_{42}/A\beta_{40}\uparrow$  but not for  $A\beta_{42}/A\beta_{40}\downarrow$ , which is assumed to have angiogenic inhibitor activity). Low VEGF levels cause neurodegeneration in part by impairing neural tissue perfusion. Perfusion deficits have also been documented, apart from AD, in other neurodegenerative disorders like amyotrophic lateral sclerosis (ALS) and Huntington disease. Mice with reduced VEGF levels develop motoneuron degeneration [175]. DOPA decarboxylase (DDC) is an enzyme synthesizing 2 important neurotransmitters, dopamine and serotonin. DDC catalyzes the decarboxylation of dihydroxyphenylalanine (dopa) to dopamine, and hydroxytryptophan to serotonin. Downregulation of DDC in consequence of an increased  $A\beta_{42}/A\beta_{40}$  ratio (but no differential expression for  $A\beta_{42}/A\beta_{40}\downarrow$ ) *argues for decreased dopamine and serotonin levels (for  $A\beta_{42}/A\beta_{40}\uparrow$ )*. The up-regulated EGFR might play a crucial role in the regulation of PI3K/AKT signaling due to its direct bindings to IGF2, CCND1, PLCG1 and NUMB. Crosstalk between the IGF1R and the EGFR has often been described [176]. The EGFR directly binds to IGF2, PLCG1, NUMB and CCND1 making it a putative key factor in this pathway. Mutations in the mouse Col4a1 gene, encoding procollagen type IV alpha 1, predisposes both newborn and adult mice to intracerebral hemorrhage [177] and cause perinatal cerebral hemorrhage and porencephaly [178]. Col4a1 gene transcription is mediated by TGF- $\beta$  [179]. This is in line with the later mentioned (see discussion) activation of TGF- $\beta$  signaling in response to an increased  $A\beta_{42}/A\beta_{40}$  ratio. PRKCD, normally known to inhibit GSK3 $\beta$ , was *hypophosphorylated*, so its inhibiting influence on GSK3 $\beta$  is expected to be diminished. Inhibiting action of PTEN onto PIP3 (PIP3 is a substrate of PI3K, not shown here) may further contribute to inactivation of PI3K/AKT signaling. Furthermore, AKT1 received inhibiting input via the IGF2/IGF1R/PIK3CA axis. Consequently AKT1 was found to be less phosphorylated, resulting in less inhibition of GSK3 $\beta$ . AKT1 (synonym: protein kinase B) as well as protein kinase A and C (known inhibitors of GSK3 $\beta$ ), all of which showed a decreased phosphorylation status compared to C99WT, are expected to exert reduced kinase activity and consequently contribute to GSK3 $\beta$  activation. Especially protein kinase C, for which a very strong and most reliable (shown for many subunits, many different phosphorylation sites, partially demonstrated with n=3 independent experiments) differential phosphorylation status has been demonstrated, is expected to contribute to downregulation of PI3K/AKT signaling. PKC and AKT1 (presumably in concert with protein kinase A) may synergistically activate GSK3 $\beta$  (due to reduced inhibitory effects), and due to the very strong inverse phosphorylation, PKC could have the stronger effect on GSK3 $\beta$  (apart from this, cross-talk from Wnt-signaling, in which GSK3 $\beta$  is a pivotal protein, may be expected). In this study, GSK3 $\beta$  was found to be activated by *hyperphosphorylation* on tyrosine 216. This in turn enables GSK3 $\beta$  to phosphorylate tau (synonym: MAPT). Indeed, tau showed stronger phosphorylation on serine 199/202 (numbering refers to tau isoform 2), two sites reported to convert tau into a molecule with toxic properties [116]. GSK3 $\beta$  phosphorylates the cell cycle regulators  $\beta$ -catenin, cyclin D1, cyclin E, p21CIP1 and c-Myc, leading to their ubiquitin-dependent destruction. GSK3 $\beta$  phosphorylates cyclin D1 on Thr286 and induces its rapid turnover [118]. Indeed, cyclinD1 was found to be down-regulated on the transcript and on the protein-level. Cyclins function as regulators of CDK kinases. Cyclin D1 forms a complex with and functions as a regulatory subunit of CDK4 and CDK6, whose activity is required for cell cycle G1/S transition. Brisken et al. found that IGF2 induced cyclin D1 protein expression in mouse mammary epithelial cultures [180]. Downregulation of cyclin D1, which is also a target gene of Wnt-signaling, is in line with the previously mentioned downregulation (off-state) of the Wnt-signaling pathway. Cyclin D1 became predominantly cytoplasmic as primary cortical progenitor cells underwent cell cycle withdrawal and terminal differentiation whereas it efficiently entered the nucleus of proliferating progenitor cells [181]. GATA3 is a transcriptional activator which binds to the enhancer of the T-cell receptor alpha and delta genes [187]. Interestingly the expression of the T-cell receptor genes was significantly down-regulated in consequence of C99 overexpression (C99WT/mock), while both increased and decreased  $A\beta_{42}/A\beta_{40}$  ratios resulted in strong and significant upregulation of these genes. Since this cannot be a consequence of GATA3 dysregulation (if so, T-cell receptors would be expected to be down-regulated for  $A\beta_{42}/A\beta_{40}\uparrow$ , because GATA3 was down-regulated here), GATA3 downregulation is rather assumed to be a consequence than the cause of differential T-cell

receptor expression, which maybe limits its own expression by GATA3 downregulation (negative feedback loop). The transcription factor ETS1 regulates the transcription of matrix metalloproteinase (MMP) genes and tissue inhibitors of metalloproteinases (TIMPs), the activities of which regulate matrix degradation and the migration of endothelial cells [188]. Up-regulated ETS1 might thus participate in regulating the differential expression of TIMP1, TIMP3 and MMP8 ( $A\beta_{42}/A\beta_{40}\uparrow$ ). This view is corroborated by the fact that these 3 proteins (together with ETS1) were not differentially expressed for a decreased  $A\beta_{42}/A\beta_{40}$  ratio. Foxo3A can be assumed to be activated (for  $A\beta_{42}/A\beta_{40}\uparrow$ ) because two effects derived from AKT1 and SGK, known to directly inhibit FoxoA, were expected to be inhibited (AKT1 showed less phosphorylation and thus was expected to be less active, total SGK3 was lower expressed in C99I45F than in C99WT (shown by immunoblotting) and consequently its inhibiting actions were expected to be diminished compared to  $A\beta_{42}/A\beta_{40}\downarrow$  where SGK was demonstrated to be up-regulated on the transcript level and where hyperphosphorylated AKT1 was able to inhibit Foxo3A.

**B) A decreased  $A\beta_{42}/A\beta_{40}$  ratio up-regulates IGF2/IGF1R/PKC and PI3K/AKT signaling.**

Compared to an increased  $A\beta_{42}/A\beta_{40}$  ratio IGF2 was not down-regulated for a decreased  $A\beta_{42}/A\beta_{40}$  ratio, so no inactivating effect was derived from IGF2. The effect of BDNF, known to activate this pathway via NTRK2 (synonym: TrkB), is expected to be increased because the non-catalytic isoform of NTRK2 was down-regulated. Since the catalytic isoform (not dysregulated) is expected to compete with the non-catalytic isoform for BDNF binding, *more BDNF is expected to be available for pathway activation*. IGFBP5 binds IGF2 directly and may, due to its downregulation, increase unbound levels of IGF2. Thus, although not up-regulated on the transcript level, a higher IGF2 protein level may be expected. *The IGF2/VIP/NPY/ATP7A axis may influence copper transport via downregulation of ATP7A*. Numb is a Notch antagonist, it functions during asymmetric cell division to determine alternative cell fates. Numb upregulation indicates downregulation of Notch signaling. Distinct Notch isoforms inhibit proliferation of stem cells and promote neuronal differentiation [189]. Thus, a stronger tendency towards neuronal differentiation for  $A\beta_{42}/A\beta_{40}\downarrow$  may be expected. This view is supported by CDK6 down-regulation: CyclinD1 was found to be up-regulated. Cyclins function as regulators of CDK kinases. Cyclin D1 forms a complex with and functions as a regulatory subunit of CDK4 and CDK6, whose activity is required for cell cycle G1/S transition. Apart from its role in cell cycle progression, a new role for CDK6 has recently been described in differentiation [182]. Exit from the cell cycle is a necessary step in terminal differentiation and may be triggered by down-regulation of CDK6. It was shown that CDK6 blocks differentiation [183]. CDK6 expression must be reduced to allow proper osteoblast and osteoclast differentiation; enforced CDK6 expression blocked differentiation of mouse embryo fibroblasts, and CDK6 expression in primary astrocytes favored the expression of progenitor cell markers [183-186]. Strong and significant down-regulation of CDK6 (validated by three different probe sets, not shown in Fig. 5.35) for  $A\beta_{42}/A\beta_{40}\downarrow$  (but not for  $A\beta_{42}/A\beta_{40}\uparrow$ ) argues for an enhanced tendency of mutant C99V50F ( $A\beta_{42}/A\beta_{40}\downarrow$ ) to differentiate. PRKCD was hyperphosphorylated, so its inhibitory influence on GSK3 $\beta$  can be expected to be enhanced. Furthermore, AKT1 can be expected to not receive inhibiting input via the IGF2/IGF1R/PIK3CA axis (because IGF2 signaling is not down-regulated, in contrast to  $A\beta_{42}/A\beta_{40}\uparrow$ ). Consequently, AKT1 was found to be stronger phosphorylated, resulting in stronger inhibition of GSK3 $\beta$  (AKT1 is known to inhibit GSK3 $\beta$ ). GSK3 $\beta$  can be expected to be less active by hypophosphorylation on tyrosine 216. This in turn inhibits the kinase activity of GSK3 $\beta$  to phosphorylate tau (synonym: MAPT). Indeed, tau was found to be less phosphorylated (in mutant C99V50F) on serine 396 (numbering refers to tau isoform 2, phosphorylation of this site is reported to convert tau into a protein with toxic properties [116]) when directly compared to mutant C99I45F. GSK3 $\beta$  is known to inhibit Cyclin D1 (CCND1) by phosphorylation. This is in concert with upregulation of CCND1 on the transcript level. IGFBP5, known to reduce free IGF2 levels, may, by its downregulation provide more free IGF2 on the protein level. Increased IGF2 levels have been demonstrated to induce CCND1 expression [180]. Foxo3A can be assumed to be less active because of the inhibiting effects derived from activated AKT1 and up-regulated SGK.

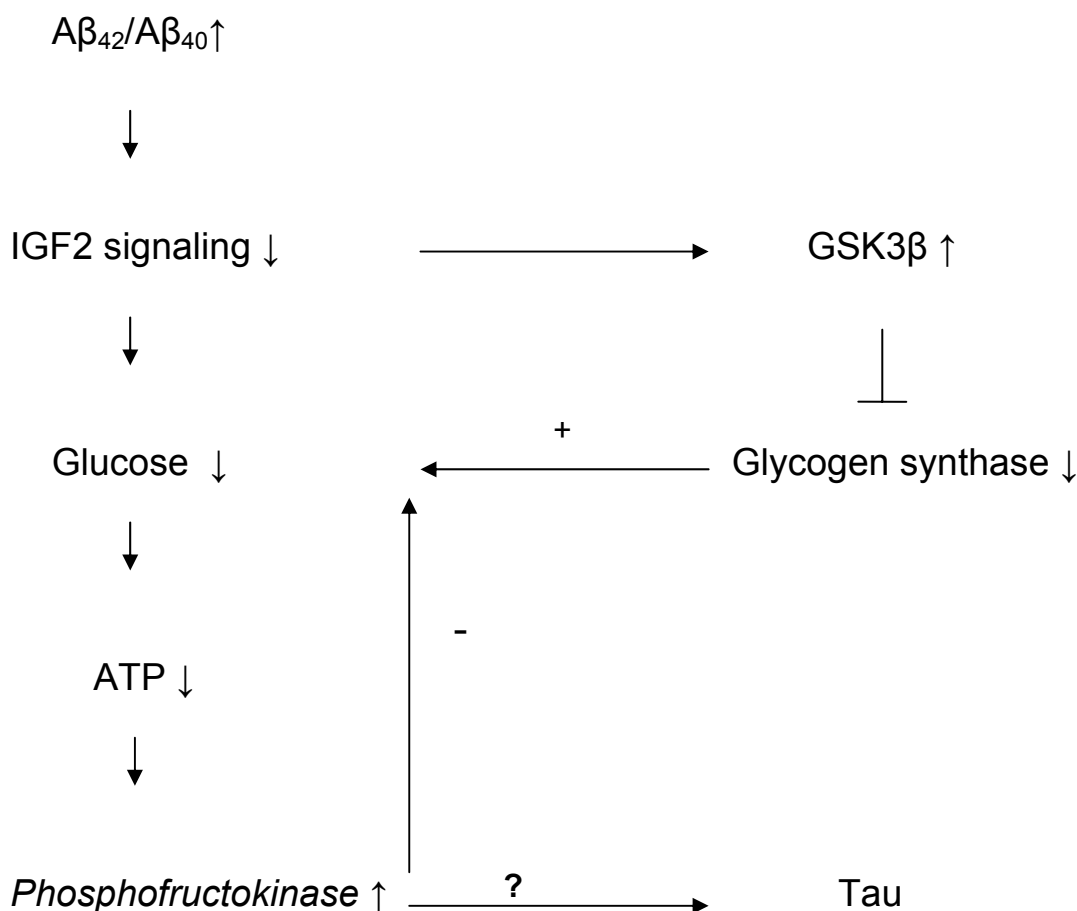
**Table 5.12 Differentially expressed transcripts or differentially phosphorylated proteins found in the PI3K/AKT pathway and interconnected pathways (only differential expression is shown here. For a change in the phosphorylation status see Chapter 5.8, pages 59-76).**

Gene symbol	Name	fold change C99I45F/C99WT	p-value	fold change C99V50F/C99WT	p-value	Connectivities	Ranking of connectivities
NTRK2	neurotrophic tyrosine kinase, receptor, type 2 (non-catalytic isoform)	2.2	0.0231	-1.7	0.0581	303	26.
IGFBP5	insulin-like growth factor binding protein 5	1.9	0.0905	-1.7	0.1694	428	20.
ETS1	v-ets erythroblastosis virus E26 oncogene homolog 1 (avian)	1.9	0.0876	-	-	611	17.
IGF1R	insulin-like growth factor 1 receptor	1.8	0.2803	-	-	603	18.
VIP	vasoactive intestinal peptide	1.8	0.0361	-	-	2450	4.
EGFR	epidermal growth factor receptor (erythroblastic leukemia viral (v-erb-b) oncogene homolog, avian)	1.8	0.0733	-	-	3574	3.
TIMP3	TIMP metalloproteinase inhibitor 3	1.7	0.0263	-	-	231	28.
COL4A1	collagen, type IV, alpha 1	1.6	0.1167	-	-	214	29.
APLP2	amyloid beta (A4) precursor-like protein 2	1.5	0.0080	-	-	1065	15.
COL4A2	collagen, type IV, alpha 2	1.5	0.1163	-	-	28	35.
ATP7A	ATPase, Cu <sup>++</sup> transporting, alpha polypeptide (Menkes syndrome)	1.5	0.0222	-2.0	0.0621	484	19.
VEGF	vascular endothelial growth factor	-1.3	0.2343	-	-	4281	2.
CCND1	cyclin D1 (PRAD1: parathyroid adenomatosis 1)	-1.4	0.1325	1.5	0.0249	2267	6.
ITGB5	integrin, beta 5	-2.0	0.0477	-1.7	0.2	34	34.
H19	H19, imprinted maternally expressed	-2.1	0.2135	-	-	111	32.

	untranslated mRNA						
DDC	dopa decarboxylase (aromatic L-amino acid decarboxylase)	-2.1	0.1295	-	-	123	31.
IGF2	insulin-like growth factor 2 (somatomedin A)	-2.6 (-4.0 by real-time PCR, standard error <sub>fold change</sub> =1.55)	0.0522	-1.7 (-1.2 by real-time PCR, standard error <sub>fold change</sub> =0.2)	0.2	2351	5.
GATA3	GATA binding protein 3	-2.7	0.1625	-	-	290	27.
HGF	hepatocyte growth factor (hepapoietin A; scatter factor)	-3.0	0.1571	-	-	2166	7.
TIMP1	TIMP metalloproteinase inhibitor 1	-3.5	0.1275	-	-	1203	12.
PTEN	phosphatase and tensin homolog	4.0	0.02572			902	16.
PRKCD	protein kinase C, delta	-	-	-	-	1286	10.
PPARD	peroxisome proliferative activated receptor, delta	-	-	-	-	396	22.
PLCG1	phospholipase C, gamma 1	-	-	-	-	1249	11.
NUMB	numb homolog (Drosophila)	-	-	3.2	0.00749	65	33.
SGK	serum/glucocorticoid regulated kinase	-	-	1.9	0.0291	369	23.
PIK3CA (subunit of PI3K)	phosphoinositide-3-kinase, catalytic, alpha polypeptide	-	-	-	-	201	30.
NPY	neuropeptide Y	-	-	-1.4	0.1161	1840	8.
MAPT	microtubule-associated protein tau	-	-	-	-	304	25.
GSK3B	glycogen synthase kinase 3 beta	-	-	-	-	1120	13.
GSK3A	glycogen synthase kinase 3 alpha	-	-	-	-	397	21.
FOXO3A	forkhead box O3A	-	-	-	-	322	24.
CTNNB1	catenin (cadherin-associated protein), beta 1, 88kDa	-	-	-	-	1114	14.
BDNF	brain-derived neurotrophic factor	-	-	-	-	1757	9.
AKT1	v-akt murine thymoma viral oncogene homolog1	-	-	-	-	6459	1.

**Table 5.12 Differentially expressed transcripts or differentially phosphorylated proteins for the comparisons C99I45F/C99WT ( $A\beta_{42}/A\beta_{40}\uparrow$ ) and C99V50F/C99WT ( $A\beta_{42}/A\beta_{40}\downarrow$ ) found in the PI3K/AKT pathway and interconnected pathways.**

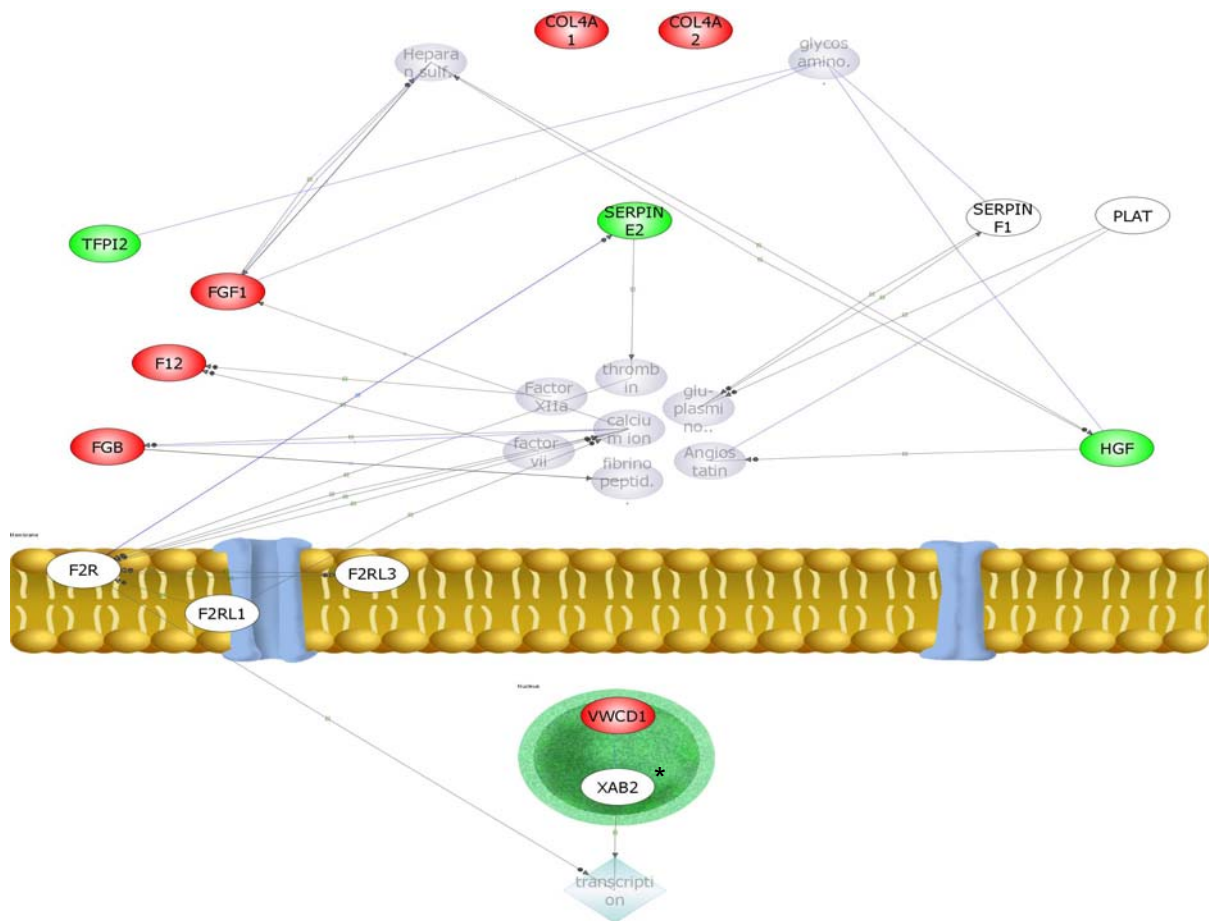
### 5.9.3 Model: Increased $A\beta_{42}/A\beta_{40}$ ratio is expected to reduce the ATP level and to induce phosphofructokinase upregulation



**Figure 5.36 Hypothetical model: Low glucose and ATP levels as pacemakers for dysregulation of glycolytic enzymes.** Parallel effects of insulin-like growth factor 2 (IGF2) and insulin on glucose metabolism have been described: IGF2 and insulin stimulate the glucose uptake and incorporation into glycogen and stimulate the activity of glycogen synthase [190]. Here, due to downregulation of IGF2 signaling (which has also been described in the brain of Alzheimer patients [191]), glucose uptake by the cells is expected to be impaired. Thus, intracellular glucose cannot be replenished due to down-regulated IGF2 signaling and is followed by low intracellular glucose levels. In consequence there is no feed forward production of ATP. A low ATP level (high AMP level) is the best known inductor for phosphofructokinase (ATP inhibits, AMP induces phosphofructokinase; upregulation of phosphofructokinase is a typical indicator for reduced energy levels). Phosphofructokinase is the most important regulatory enzyme of glycolysis. If phosphofructokinase turns out to be a possible kinase for tau phosphorylation, then tau phosphorylation would be inherently caused by low glucose/ATP levels. While possibly resulting in higher ATP levels, up-regulated phosphofructokinase ( $A\beta_{42}/A\beta_{40}\uparrow$ : 2.1 fold up-regulated,  $p=0.0023$ , but not differentially expressed for  $A\beta_{42}/A\beta_{40}\downarrow$ ) may contribute to reduce glucose levels. Inhibited glycogen synthase by phosphorylation through GSK3 $\beta$  can be regarded as an 'attempt' (self-regulated by feedback loops) of the cells to restore sufficient glucose/ATP levels by down-regulating glycogen synthesis. Phosphofructokinase generates fructose 1,6 bisphosphate from fructose 6-phosphate. There is also the possibility that an increased  $A\beta_{42}/A\beta_{40}$  ratio directly up-regulates phosphofructokinase (not mediated by IGF2 signaling, glucose and ATP).

### 5.9.4 Model: Transcriptional control of blood coagulation and fibrinolysis is influenced by an altered $A\beta_{42}/A\beta_{40}$ ratio

A

 $A\beta_{42}/A\beta_{40} \uparrow$ Blood coagulation  $\uparrow$ (Fibrinolysis  $\downarrow$ )

B

$A\beta_{42}/A\beta_{40}\downarrow$

Blood coagulation ↓

Fibrinolysis ↑

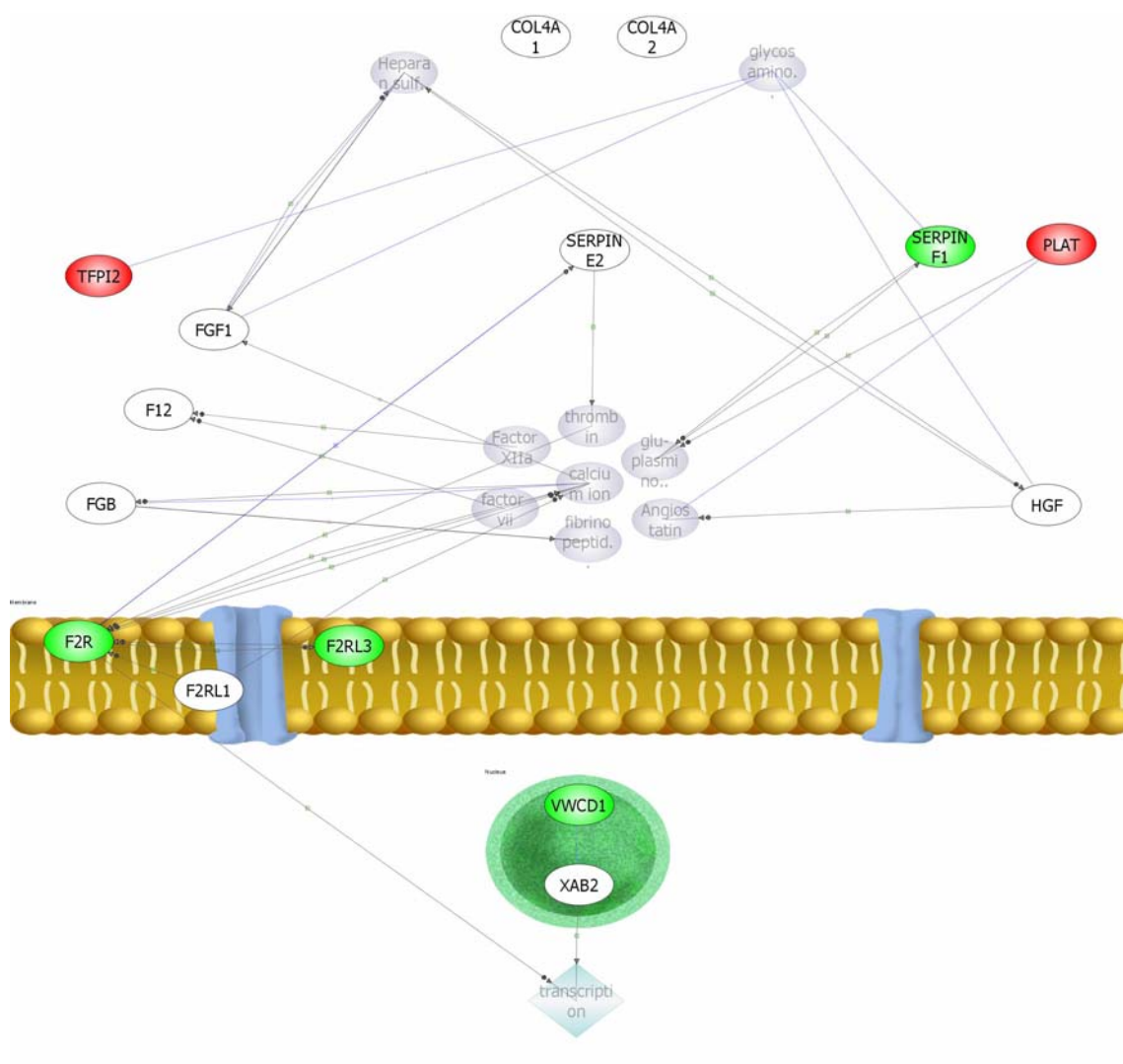


**Figure 5.37 Transcriptional control of blood coagulation and fibrinolysis is influenced by an altered  $A\beta_{42}/A\beta_{40}$  ratio.** A) An increased  $A\beta_{42}/A\beta_{40}$  ratio results in upregulation of F12 and FGB, well-known factors for the activation of blood clotting (up-regulated FGF1 may also contribute to blood clotting, see Chapter 6.12, page 156). Moreover, inhibitors of blood clotting, like TFPI2, are down-regulated. Both factors might synergistically enhance blood coagulation in consequence of an increased  $A\beta_{42}/A\beta_{40}$  ratio. Serpin E2 affects both, blood coagulation and fibrinolysis. Interestingly, in presence of collagen 4 (Col4A1, Col4A2), serpin E2 has a much stronger tendency to affect blood coagulation than fibrinolysis (see discussion, Chapter 6.12). In presence of collagen 4, serpin E2 (if expression is increased, which is not the case here) tends to inhibit thrombin and thus coagulation. However, here, this inhibiting effect may be abolished by serpin E2 downregulation. This might result in increased blood clotting. HGF was found to inhibit thrombin-dependent platelet aggregation. Thus, down-regulation of HGF might support platelet aggregation and in consequence blood clotting. The function of the uncharacterized VWCD1 is not well understood, but it may influence transcription (via XAB2, \*XAB2 could be regarded as weakly up-regulated, 1.3 fold,  $p=0.104$ ) in concert with F2R. Increased intracellular  $Ca^{2+}$  levels, a well studied consequence of increased  $A\beta_{42}$  levels and a hallmark of AD, may contribute to enhance blood coagulation (for instance after disruption of cells and release of  $Ca^{2+}$  into the extracellular space and uptake into adjacent blood vessels).

B) A decreased  $A\beta_{42}/A\beta_{40}$  ratio results in upregulation of TFPI2 (inhibitor of blood clotting), so blood clotting might be inhibited and downregulation of the thrombin receptor F2R and F2RL3 (thrombin receptor-like 3), may further reduce the tendency towards coagulation. In parallel to this, strong down-regulation of serpin F1, an anti-plasmin, might result in higher plasmin levels, which in turn accelerates fibrinolysis. *One of the most prominent activators of fibrinolysis (and a candidate gene for AD according to the Alzforum database, [www.alzforum.org](http://www.alzforum.org)) is PLAT (plasminogen activator, tissue). Due to its upregulation enhanced fibrinolysis may be expected.*

**Table 5.13 Differentially expressed transcripts found in blood coagulation and fibrinolysis**

Gene symbol	Name	fold change C99I45F/C99WT	p-value	fold change C99V50F/C99WT	p-value
-	Angiostatin	-	-	-	-
-	calcium ion	presumably increased levels <sup>♦</sup>	-	presumably decreased levels <sup>♦</sup>	-
COL4A1	collagen, type IV, alpha 1	1.6	0.1167	not differentially expressed <sup>■</sup>	-
COL4A2	collagen, type IV, alpha 2	1.5	0.1163	not differentially expressed <sup>■</sup>	-
F12	coagulation factor XII (Hageman factor)	1.3	0.036	not differentially expressed <sup>■</sup>	-
F2R	coagulation factor II (thrombin) receptor	-	-	-1.2	0.0266
F2RL1	coagulation factor II (thrombin) receptor-like 1	not differentially expressed <sup>■</sup>	-	not differentially expressed <sup>■</sup>	-
F2RL3	coagulation factor II (thrombin) receptor-like 3	not differentially expressed <sup>■</sup>	-	-3.2	0.04742
-	factor vii	-	-	-	-
-	Factor XIIa	1.3	0.0723	-	-
FGB	fibrinogen beta chain	2.5	0.0161	-	-

FGF1	fibroblast growth factor 1 (acidic)	1.6	0.0036	-	-
-	fibrinopeptide a	-	-	-	-
-	glu-plasminogen	-	-	-	-
-	glycosaminoglycan	-	-	-	-
-	Heparan sulfate	-	-	-	-
HGF	hepatocyte growth factor (hepapoietin A; scatter factor)	-3.0	0.157	-	-
PLAT	plasminogen activator, tissue	not differentially expressed <sup>■</sup>	-	2.1	0.0047
SERPINE2	serpin peptidase inhibitor, clade E, member 2	-2.3	0.174	not differentially expressed <sup>■</sup>	-
SERPINF1	serpin peptidase inhibitor, clade F (alpha-2 antiplasmin), member 1	not differentially expressed <sup>■</sup>	-	-3.1	0.00362
TFPI2	tissue factor pathway inhibitor 2	-3.1	0.365*	2.6	0.027
-	thrombin	-	-	-	-
VWCD1	von Willebrand factor type A and cache domain containing 1	1.6	0.044	-2.7	0.149
XAB2	XPA binding protein 2	1.3	0.104	not differentially expressed <sup>■</sup>	-

**Table 5.13 Differentially expressed transcripts found in blood coagulation and fibrinolysis.**

Hyphen (-): no information available because not regulated on the transcript level but derived from the cells' metabolism or because not probed on the microarray.

◆ see Chapter 6.36, page 201, for further explanation

■ the term "not differentially expressed" was used when fold changes were close to 1.0 (0.9-1.1) or exceeded a threshold of  $p > 0.2$

\*TFPI2 could be regarded as not differentially expressed due to its high p-value (for the comparison C99I45F/C99WT). It is listed here despite the high p-value, because it was detected as down-regulated with more than one probe set, increasing the probability of a true downregulation. In contrast to this, TFPI2 was significantly up-regulated for C99V50F/C99WT.

## 5.10 Candidates for tau or GSK3 phosphorylation

### 5.10.1 Preface

The state of phosphorylation of a phosphoprotein is a function of the balance between the activities of protein kinases and phosphatases that regulates its phosphorylation. Tau, which is phosphorylated at more than 30 serine/threonine residues in AD [111, 192], is a substrate for several protein kinases. Not all of the 30 phosphorylation sites may be involved in converting normal tau into a toxic molecule. Hyperphosphorylation of tau at the level of 4-6 moles phosphate/mole of the protein induces the toxic property.

GSK3 $\beta$  is able to phosphorylate many substrates and is part of several cellular events including metabolism, signaling and transcription [119]. GSK-3 $\beta$  is the major tau kinase in vivo [120-125]. There is evidence that in total 15 sites are phosphorylated by GSK3 $\beta$ . GSK3 $\beta$  itself can also be phosphorylated/dephosphorylated by several kinases/phosphatases. This is crucial for its functional state. For these reasons candidate kinases/phosphatases for tau and GSK3 $\beta$  were identified.

### 5.10.2 Kinases

Even if activation of kinases is often regulated on the protein level (for instance by phosphorylation) kinases are also regulated on the transcript level. Here, only kinases showing distinctly stronger expression for A $\beta_{42}$ /A $\beta_{40}$  $\uparrow$  than for A $\beta_{42}$ /A $\beta_{40}$  $\downarrow$  were selected.

Gene symbol	Name	differentially expressed kinases				Chromosomal location
		A $\beta_{42}$ /A $\beta_{40}$ $\uparrow$		A $\beta_{42}$ /A $\beta_{40}$ $\downarrow$		
		p-value	Fold change	p-value	Fold change	
GRK5	G protein-coupled receptor kinase 5	0.0167	2.0	-	-	chr10q24-qter
PFKP	phosphofructokinase platelet	0.00230	2.1	-	-	chr10p15.3-p15.2
RPS6KA5	ribosomal protein S6 kinase, 90kDa, polypeptide 5	-	-	0.018	-1.2	chr14q31-q32.1
PHKG1	phosphorylase kinase gamma 1 (muscle)	-	-	0.0441	-1.3	chr7p12-q21
PKN2	Protein kinase N2	-	-	0.0215	-1.4	chr1p22.2
CDK6	cyclin-dependent kinase 6	-	-	0.00749	-3.2	chr7q21-q22
CDKL5	cyclin-dependent kinase-like 5	0.02490	4.0	-	-	chrXp22
<b>CDKL1</b>	<b><i>cyclin-dependent kinase-like 1 (CDC2-related kinase)</i></b>	0.01613	2.5	-	-	<b><i>chr14q21.3</i></b>
<b>DYRK1A</b>	<b><i>Dual-specificity tyrosine-(Y)-phosphorylation regulated kinase 1A</i></b>	-	-	0.03517	-6.3	<b><i>chr21q22.13 (according to Affymetrix) chr21q22.22 (according to other sources)</i></b>

Table 5.14 Differentially expressed genes encoding kinases as candidates that could phosphorylate tau or GSK3

A further kinase, DCAMKL1 (doublecortin and CaM kinase-like 1), was up-regulated for  $A\beta_{42}/A\beta_{40}\uparrow$  and slightly down-regulated for  $A\beta_{42}/A\beta_{40}\downarrow$  on the protein level, shown by immunoblotting. DCAMKL1 might be a further candidate for tau or GSK3 phosphorylation. Moreover ERK1 showed stronger phosphorylation on threonine 202 and tyrosine 204 (two activating sites, making ERK1 a further possible candidate kinase for tau or GSK3 phosphorylation) in consequence of an increased  $A\beta_{42}/A\beta_{40}$  ratio. However, no data are available for a decreased  $A\beta_{42}/A\beta_{40}$  ratio.

### 5.10.3 Phosphatases

Here, the focus was on phosphatases showing weaker expression (except for PPP2R2C which showed stronger expression) for  $A\beta_{42}/A\beta_{40}\uparrow$  than for  $A\beta_{42}/A\beta_{40}\downarrow$ .

Gene symbol	Name	differentially expressed phosphatases (or their subunits)				Chromosomal location
		$A\beta_{42}/A\beta_{40}\uparrow$		$A\beta_{42}/A\beta_{40}\downarrow$		
		p-value	Fold change	p-value	Fold change	
	protein phosphatase 2A, regulatory subunit B' (PR 53)	-	-	0.0069	1.2	chr9q34
PPP2R2C	protein phosphatase 2 (formerly 2A) regulatory subunit B (PR 52) gamma isoform	0.0201	2.4	-	-	chr4p16.1
PHACTR2	Phosphatase and actin regulator 2	0.02572	-3.2	-	-	chr6q24.2

**Table 5.15 Differentially expressed genes encoding phosphatases as candidates that could dephosphorylate tau or GSK3.** PPP2R4, PPP2R2C were differentially expressed and are important regulatory subunits for protein phosphatase 2A. PHACTR2 is a family member of proteins that binds protein phosphatase 1 and cytoplasmic actin; it may play a role in regulation of the actin cytoskeleton.

### 5.11 Genes co-regulated with APLP1 and APLP2

APP is a member of a larger gene family including amyloid precursor-like proteins APLP1 and APLP2. Mice deficient in the nervous system-specific APLP1 protein showed a postnatal growth deficit as the only obvious abnormality. In contrast to this minor phenotype, APLP2(-)/APLP1(-) and APLP2(-)/APP(-) mice die early postnatally. Surprisingly, APLP1(-)/APP(-) mice were viable, apparently normal, and showed no compensatory upregulation of APLP2 expression. These data indicate a key physiological role for APLP2. This view gains further support by the

observation that APLP1(-)/APP(-)/APLP2(+/-) mice die early postnatally [193]. In order to shed light on the redundancy between APLP2 and both other family members, co-regulated genes (which are speculated as having an important common function) to APLP1 and APLP2 were identified.

APLP2 appeared among the most up-regulated genes from the comparison C99I45F versus C99WT ( $A\beta_{42}/A\beta_{40}\uparrow$ ), whereas APLP1 appeared among the most up-regulated genes from the comparison C99V50F versus C99WT ( $A\beta_{42}/A\beta_{40}\downarrow$ ). The genes found in close vicinity (and thus co-regulated) with APLP2 *and* APLP1 (if gene lists were compared in which genes were sorted according to fold changes), were:

- Catenin (cadherin-associated protein)  $\alpha$  2 (CTNNA2), chr2p12-p11.1
- Neural cell adhesion molecule 1 (NCAM1), chr11q23.1
- Actinin alpha 1 (ACTN1), chr14q22-q24
- Rho GTPase activating protein 26 (ARHGAP26), chr5q31
- KIAA1102, chr4p13

## 5.12 Identification of altered signal transduction pathways and molecular functions

### 5.12.1 Preface

PANTHER (Protein Analysis Through Evolutionary Relationships, Applied Biosystems) is a classification system for genes and proteins. It delivers information about the under or over-representation of transcripts in certain pathways or provides information about which molecular functions are under or over-represented. It is crucial to evaluate these data with special regard to the kind of data integrated (most up or down-regulated transcripts, number of integrated transcripts etc.). Most important was to find a suitable number of transcripts which reflects a balance between acceptable sensitivity (all affected pathways should be discovered, so the number of integrated transcripts should not be too small) and specificity (only strong up or downregulation is likely to be meaningful, therefore, the number of transcripts should not be too big, otherwise weakly dysregulated transcripts could possibly falsify the results). Here in this analysis, PANTHER delivers information about the *representation* of transcripts in certain pathways which *must not be mixed up with the extent of up and downregulation*: The most up and down-regulated genes were

integrated into PANTHER. (For pathway analysis making use of the extent of up and downregulation, see Fig. 5.35 (pages 78, 79), Fig. 5.37 (page 86) and Fig. 12.3 (page S87), which were created with Pathway Architect; for this, the gene *expression values* of up and down-regulated genes were used). Using both approaches together, *over/under-representation* and the *extent of up and downregulation (gene expression values)*, provides more reliable information than one approach alone.

When a certain pathway is meant to be evaluated for activation or inhibition, there are crucial considerations, which ***must be seen in the whole context***:

- Were the integrated data the most up or down-regulated ones?
- Do the transcripts that were found to be differentially expressed have *inhibitory* or *activating* functions within the pathway?
- What was the cut-off for the p-value?
- How big was the fold change of the integrated data?
- How many transcripts were integrated?

Due to similarities of names of integrated gene symbols and 'matching' gene names, PANTHER very occasionally erroneously recognizes genes to be affected, so PANTHER's analysis was manually checked and corrected.

### **5.12.2 Over and under-representation of transcripts in signal transduction and metabolic pathways**

The two mutants C99I45F and C99V50F were compared to C99WT. *Differentially represented pathways might be key regulators in the pathogenesis of AD.*

#### **Top fifty up-regulated transcripts**

The top fifty up-regulated transcripts, selected by using the Array Assist software and the PLIER algorithm, derived from the comparisons C99I45F versus C99WT and C99V50F versus C99WT ( $p < 0.05$ ,  $n=3$ ), were integrated into the PANTHER™ gene and protein classification system.

Out of 130 tested *signal transduction and metabolic pathways*, 43 pathways were *differentially represented (data not shown)* in consequence of a changed  $A\beta_{42}/A\beta_{40}$  ratio. These 43 pathways, in turn, were used for further analysis. The distribution of transcripts into these pathways was examined and those pathways, which showed

the *strongest difference in the number of transcripts*, were selected. The most differentially represented pathways were these 7:

Pathways	Transcripts		Δ Number of transcripts
	C99V50F versus C99WT (Aβ <sub>42</sub> /Aβ <sub>40</sub> ↓):	C99I45F versus C99WT (Aβ <sub>42</sub> /Aβ <sub>40</sub> ↑):	
Wnt signaling pathway	<ul style="list-style-type: none"> <li>• cyclin D1 CCND1</li> <li>• catenin (cadherin-associated protein), alpha 2 CTNNA2</li> <li>• protein kinase C, alpha PRKCA</li> </ul>	–	3
Apoptosis signaling pathway	<ul style="list-style-type: none"> <li>• cAMP responsive element modulator CREM</li> <li>• protein kinase C, alpha PRKCA</li> <li>• B-cell CLL/lymphoma 2 BCL2</li> </ul>	–	3
Endothelin signaling pathway	<ul style="list-style-type: none"> <li>• protein kinase C, alpha PRKCA</li> <li>• endothelin converting enzyme-like 1 ECEL1</li> </ul>	–	2
Interleukin signaling pathway	<ul style="list-style-type: none"> <li>• forkhead box C1 FOXC1</li> <li>• cyclin-dependent kinase inhibitor 1A (p21, Cip1) CDKN1A</li> </ul>	–	2
PDGF signaling pathway	<ul style="list-style-type: none"> <li>• protein kinase C, alpha PRKCA</li> <li>• FEV (ETS oncogene family) FEV</li> <li>• Rho GTPase activating protein 26 ARHGAP26 GRAF-RELATED</li> </ul>	<ul style="list-style-type: none"> <li>• Rho GTPase activating protein 26 ARHGAP26 GRAF-RELATED</li> </ul>	2
PI3K kinase pathway	<ul style="list-style-type: none"> <li>• forkhead box C1 FOXC1</li> <li>• cyclin D1 CCND1</li> </ul>	–	2
TGF-beta signaling pathway	<ul style="list-style-type: none"> <li>• jun D proto-oncogene JUND</li> <li>• forkhead box C1 FOXC1</li> <li>• BMP and activin</li> </ul>	<ul style="list-style-type: none"> <li>• bone morphogenetic protein 7 (osteogenic protein 1) BMP7</li> </ul>	2

	membrane-bound inhibitor homolog ( <i>Xenopus laevis</i> ) BAMBI		
--	--	--	--

**Table 5.16 PANTHER™ gene and protein classification system: The analysis of the fifty most up-regulated transcripts from the comparison C99V50F/C99WT and C99I45F/C99WT ( $p < 0.05$ ,  $n=3$ ) revealed these 7 most differentially represented pathways.**

The remaining pathways differed only in one transcript. Nevertheless, it cannot be concluded that they are unimportant, because the single transcript might fulfill important functions, like having a key position within a pathway, cross-talk to other pathways etc. An example for this was:

Pathways	Transcripts		$\Delta$ Number of transcripts
	C99V50F versus C99WT ( $A\beta_{42}/A\beta_{40}\downarrow$ ):	C99I45F versus C99WT ( $A\beta_{42}/A\beta_{40}\uparrow$ ):	
Inflammation mediated by chemokine and cytokine signaling pathway	<ul style="list-style-type: none"> <li>• jun D proto-oncogene JUND</li> <li>• protein kinase C, alpha PRKCA</li> <li>• doublecortin and CaMkinase-like 1 DCAMKL1</li> </ul>	<ul style="list-style-type: none"> <li>• G protein-coupled receptor kinase 5 GRK5</li> <li>• tenascin C (hexabrachion) TNC</li> </ul>	1
Axon guidance mediated by semaphorins	<ul style="list-style-type: none"> <li>• collapsin response mediator protein 1 CRMP1</li> </ul>	–	1

The total difference in transcripts here is one, but *different* transcripts are affected (*in the upper example*). Especially if they fulfill contrary functions in the cell (e.g. inhibitory/activating when both mutants are compared), this might be an important pathway. Hence, the pathways differing only in one transcript were examined manually and, if regarded as important, they were taken into account and listed in this thesis.

### The twenty most down-regulated transcripts

The twenty most down-regulated transcripts, selected by the Array Assist software and the PLIER algorithm, derived from the comparisons C99I45F versus C99WT and C99V50F versus C99WT ( $p < 0.05$ ,  $n=3$ ), were integrated into the PANTHER™ gene and protein classification system.

Out of 130 tested *signal transduction and metabolic pathways*, 21 pathways were *differentially represented (data not shown)* in consequence of a changed  $A\beta_{42}/A\beta_{40}$  ratio. Out of these 21 pathways, the strongest difference in the number of transcripts ( $\Delta$  transcripts), and hence the most differentially represented pathways were these 3:

Pathways	Transcripts		$\Delta$ Number of transcripts
	C99V50F versus C99WT ( $A\beta_{42}/A\beta_{40}\downarrow$ ):	C99I45F versus C99WT ( $A\beta_{42}/A\beta_{40}\uparrow$ ):	
Alzheimer disease-amyloid secretase pathway	<ul style="list-style-type: none"> <li>protein kinase N2 PKN2</li> <li>cholinergic receptor, muscarinic 3 CHRM3<sup>5</sup></li> </ul>	–	2
Angiogenesis	<ul style="list-style-type: none"> <li>ephrin-B2 EFNB2</li> <li>transcription factor 7-like 2 (T-cell specific, HMG-box) TCF7L2</li> </ul>	–	2
Endothelin signaling pathway	<ul style="list-style-type: none"> <li>adenylate cyclase 1 (brain) ADCY1</li> <li>protein kinase N2 PKN2</li> </ul>	–	2

**Table 5.17 PANTHER™ gene and protein classification system: The analysis of the twenty most down-regulated transcripts from C99I45F/C99WT and C99V50F/C99WT ( $p < 0.05$ ,  $n=3$ ) revealed these 3 most differentially represented pathways.**

### 5.12.3 Over and under-representation of transcripts involved in certain molecular functions

The same data set used in 5.12.2 was integrated into PANTHER in order to obtain information about affected molecular functions.

#### Top fifty up-regulated transcripts

Out of 254 tested *molecular functions*, 52 were *differentially represented (data not shown)* in consequence of a changed  $A\beta_{42}/A\beta_{40}$  ratio:

Out of these molecular functions, the strongest difference in the number of transcripts ( $\Delta$  transcripts), and hence, the most differentially represented, were these:

<sup>5</sup> In a less stringent ( $p < 0.075$  instead of  $< 0.05$ ) analysis, CHRM3 appeared also as down-regulated in mutant C99I45F, so  $\Delta$  Number of transcripts was finally = 1, which makes a real differential representation of this pathway less probable.

Molecular functions	Transcripts		Δ Number of transcripts
	C99V50F versus C99WT (Aβ <sub>42</sub> /Aβ <sub>40</sub> ↓):	C99I45F versus C99WT (Aβ <sub>42</sub> /Aβ <sub>40</sub> ↑):	
Receptors	<ul style="list-style-type: none"> <li>• (slit homolog 1 (Drosophila) SLIT1)<sup>6</sup></li> <li>• prostaglandin E receptor 2 (subtype EP2), 53kDa PTGER2</li> </ul>	<ul style="list-style-type: none"> <li>• delta/Notch-like EGF repeat containing DNER</li> <li>• gamma-aminobutyric acid (GABA) A receptor, beta 3 GABRB3</li> <li>• G protein-coupled receptor 64 GPR64</li> <li>• glutamate receptor, ionotropic, AMPA 2 GRIA2</li> <li>• neurotrophic tyrosine kinase, receptor, type 2 NTRK2, non-catalytic isoform</li> <li>• odz, odd Oz/ten-m homolog 4 (Drosophila) ODZ4</li> <li>• protease, serine, 12 (neurotrypsin, motopsin) PRSS12</li> <li>• protein tyrosine phosphatase, receptor type, M PTPRM</li> </ul>	7
Other transcription factors	<ul style="list-style-type: none"> <li>• jun D proto-oncogene JUND</li> <li>• inhibitor of DNA binding 4, dominant negative helix-loop-helix protein ID4</li> <li>• forkhead box C1 FOXC1</li> <li>• FEV (ETS oncogene family) FEV</li> </ul>	–	4
Actin binding cytoskeletal proteins	<ul style="list-style-type: none"> <li>• tropomodulin 1 TMOD1</li> <li>• spectrin, beta, non-erythrocytic 1 SPTBN1</li> <li>• ectodermal-neural cortex (with BTB-like domain) ENC1</li> <li>• catenin (cadherin-associated protein), alpha 2 CTNNA2</li> <li>• actinin, alpha 1</li> </ul>	<ul style="list-style-type: none"> <li>• ectodermal-neural cortex (with BTB-like domain) ENC1</li> <li>• troponin C type 1 (slow) TNNC1</li> </ul>	3

<sup>6</sup> Slit1 was erroneously recognized as a receptor by PANTHER analysis. Correctly, it is a *secreted* protein involved in axon guidance.

	ACTN1		
Non-motor actin binding proteins	<ul style="list-style-type: none"> <li>• spectrin, beta, non-erythrocytic 1 SPTBN1</li> <li>• ectodermal-neural cortex (with BTB-like domain) ENC1</li> <li>• catenin (cadherin-associated protein), alpha 2 CTNNA2</li> <li>• actinin, alpha 1 ACTN1</li> </ul>	<ul style="list-style-type: none"> <li>• ectodermal-neural cortex (with BTB-like domain) ENC1</li> </ul>	3
Nucleic acid binding	<ul style="list-style-type: none"> <li>• single-stranded DNA binding protein 2 SSBP2</li> <li>• REV3-like, catalytic subunit of DNA polymerase zeta (yeast) REV3L</li> <li>• jun D proto-oncogene JUND</li> <li>• forkhead box C1 FOXC1</li> <li>• cAMP responsive element modulator CREM</li> </ul>	<ul style="list-style-type: none"> <li>• ELAV (embryonic lethal, abnormal vision, Drosophila)-like 4 (Hu antigen D) ELAVL4</li> <li>• Scm-like with four mbt domains 2 SFMBT2</li> </ul>	3
Transcription factors	<ul style="list-style-type: none"> <li>• jun D proto-oncogene JUND</li> <li>• inhibitor of DNA binding 4, dominant negative helix-loop-helix protein ID4</li> <li>• forkhead box C1 FOXC1</li> <li>• FEV (ETS oncogene family) FEV</li> <li>• cAMP responsive element modulator CREM</li> </ul>	<ul style="list-style-type: none"> <li>• delta/Notch-like EGF repeat containing DNER</li> <li>• Scm-like with four mbt domains 2 SFMBT2</li> </ul>	3
Ion channels	–	<ul style="list-style-type: none"> <li>• glutamate receptor, ionotropic, AMPA 2 GRIA2</li> <li>• gamma-aminobutyric acid (GABA) A receptor, beta 3 GABRB3</li> <li>• calcium channel, voltage-dependent, L type, alpha 1D subunit CACNA1D</li> </ul>	3
Membrane-bound signaling molecules	–	<ul style="list-style-type: none"> <li>• sema domain, immunoglobulin domain (Ig), short basic domain, secreted, (semaphorin) 3C SEMA3C</li> <li>• odz, odd Oz/ten-m homolog 4 (Drosophila)</li> </ul>	3

		<ul style="list-style-type: none"> <li>ODZ4</li> <li>delta/Notch-like EGF repeat containing DNER</li> </ul>	
Other receptors	–	<ul style="list-style-type: none"> <li>protein tyrosine phosphatase, receptor type, M PTPRM</li> <li>protease, serine, 12 (neurotrypsin, motopsin) PRSS12</li> <li>protein tyrosine phosphatase, receptor type, M PTPRM</li> </ul>	3
Signaling molecules	<ul style="list-style-type: none"> <li>VGF nerve growth factor inducible VGF</li> <li>FEV (ETS oncogene family) FEV</li> <li>B-cell CLL/lymphoma 2 BCL2</li> </ul>	<ul style="list-style-type: none"> <li>bone morphogenetic protein 7 (osteogenic protein 1) BMP7</li> <li>delta/Notch-like EGF repeat containing DNER</li> <li>neuroligin 4, X-linked NLGN4X</li> <li>odz, odd Oz/ten-m homolog 4 (Drosophila) ODZ4</li> <li>sema domain, immunoglobulin domain (Ig), short basic domain, secreted, (semaphorin) 3C SEMA3C</li> <li>vasoactive intestinal peptide VIP</li> </ul>	3
Protein kinases	<ul style="list-style-type: none"> <li>tribbles homolog 2 (Drosophila) TRIB2</li> <li>serum/glucocorticoid regulated kinase SGK</li> <li>protein kinase C, alpha PRKCA</li> <li>polo-like kinase 2 (Drosophila) PLK2</li> <li>doublecortin and CaM kinase-like 1 DCAMKL1</li> </ul>	<ul style="list-style-type: none"> <li>neurotrophic tyrosine kinase, receptor, type 2 NTRK2, non-catalytic isoform</li> <li>G protein-coupled receptor kinase 5 GRK5</li> <li>polo-like kinase 2 (Drosophila) PLK2</li> </ul>	2

Cytoskeletal proteins	<ul style="list-style-type: none"> <li>tropomodulin 1 TMOD1</li> <li>spectrin, beta, non-erythrocytic 1 SPTBN1</li> <li>neurofilament, medium polypeptide 150kDa NEFM</li> <li>neurofilament, light polypeptide 68kDa NEFL</li> <li>ectodermal-neural cortex (with BTB-like domain) ENC1</li> <li>doublecortin and CaM kinase-like 1 DCAMKL1</li> <li>catenin (cadherin-associated protein), alpha 2 CTNNA2</li> <li>actinin, alpha 1 ACTN1</li> </ul>	<ul style="list-style-type: none"> <li>dynein, cytoplasmic 1, intermediate chain 1 DYNC111</li> <li>ectodermal-neural cortex (with BTB-like domain) ENC1</li> <li>neurofilament, light polypeptide 68kDa NEFL</li> <li>neurofilament, medium polypeptide 150kDa NEFM</li> <li>septin 9 SEPT9</li> <li>troponin C type 1 (slow) TNNC1</li> </ul>	2
Hydrolases	<ul style="list-style-type: none"> <li>phosphodiesterase 2A, cGMP-stimulated PDE2A</li> <li>collapsin response mediator protein 1 CRMP1</li> </ul>	–	2
Kinase modulators	<ul style="list-style-type: none"> <li>cyclin-dependent kinase inhibitor 1A (p21, Cip1) CDKN1A</li> <li>cyclin D1 CCND1</li> </ul>	–	2
Non-receptor serine/threonine protein kinases	<ul style="list-style-type: none"> <li>protein kinase C, alpha PRKCA</li> <li>serum/glucocorticoid regulated kinase SGK</li> <li>polo-like kinase 2 (Drosophila) PLK2</li> <li>doublecortin and CaM kinase-like 1 DCAMKL1</li> </ul>	<ul style="list-style-type: none"> <li>polo-like kinase 2 (Drosophila) PLK2</li> <li>G protein-coupled receptor kinase 5 GRK5</li> </ul>	2
Ligand-gated ion channels	–	<ul style="list-style-type: none"> <li>glutamate receptor, ionotropic, AMPA 2 GRIA2</li> <li>gamma-aminobutyric acid (GABA) A receptor, beta 3 GABRB3</li> </ul>	2
Other signaling molecules	<ul style="list-style-type: none"> <li>B-cell CLL/lymphoma 2 BCL2</li> <li>FEV (ETS oncogene family) FEV</li> </ul>	<ul style="list-style-type: none"> <li>bone morphogenetic protein 7 (osteogenic protein 1) BMP7</li> <li>neuroligin 4, X-linked NLGN4X</li> <li>odz, odd Oz/ten-m homolog</li> </ul>	2

		4 (Drosophila) ODZ4 <ul style="list-style-type: none"> <li>• sema domain, immunoglobulin domain (Ig), short basic domain, secreted, (semaphorin) 3C SEMA3C</li> </ul>	
Oxidoreductases	–	<ul style="list-style-type: none"> <li>• ubiquinol-cytochrome c reductase, Rieske iron-sulfur polypeptide 1 UQCRFS1</li> <li>• cytochrome P450, family 26, subfamily B, polypeptide 1 CYP26B1</li> </ul>	2
Phosphatases	–	<ul style="list-style-type: none"> <li>• protein phosphatase 2 (formerly 2A), regulatory subunit B (PR 52), gamma isoform PPP2R2C</li> <li>• protein tyrosine phosphatase, receptor type, M PTPRM</li> </ul>	2
Protein phosphatases	–	<ul style="list-style-type: none"> <li>• protein phosphatase 2 (formerly 2A), regulatory subunit B (PR 52), gamma isoform PPP2R2C</li> <li>• protein tyrosine phosphatase, receptor type, M PTPRM</li> </ul>	2

**Table 5.18 PANTHER™ gene and protein classification system: The analysis of the *fifty most up-regulated* transcripts from the comparisons C99V50F/C99WT and C99I45F/C99WT ( $p < 0.05$ ,  $n=3$ ) revealed these differentially represented molecular functions.**

The total difference of the following transcripts was one, *but different transcripts were affected*. Especially if they fulfill contrary functions in the cell (e.g. inhibitory/activating), these molecular functions might play an important role:

Molecular functions	Transcripts		$\Delta$ Number of transcripts
	C99V50F versus C99WT ( $A\beta_{42}/A\beta_{40}\downarrow$ ):	C99I45F versus C99WT ( $A\beta_{42}/A\beta_{40}\uparrow$ ):	
Kinases	<ul style="list-style-type: none"> <li>• tribbles homolog 2 (Drosophila) TRIB2</li> <li>• serum/glucocorticoid regulated kinase SGK</li> <li>• protein kinase C, alpha PRKCA</li> <li>• polo-like kinase 2 (Drosophila) PLK2</li> <li>• doublecortin and CaM kinase-like 1 DCAMKL1</li> </ul>	<ul style="list-style-type: none"> <li>• G protein-coupled receptor kinase 5 GRK5</li> <li>• neurotrophic tyrosine kinase, receptor, type 2 NTRK2, non-catalytic isoform</li> <li>• phosphofructokinase, platelet PFKP</li> <li>• polo-like kinase 2 (Drosophila) PLK2</li> </ul>	1
Select calcium binding proteins	<ul style="list-style-type: none"> <li>• protein kinase C, alpha PRKCA</li> <li>• sarcoglycan, epsilon SGCE</li> </ul>	<ul style="list-style-type: none"> <li>• troponin C type 1 (slow) TNNC1</li> </ul>	1
Proteases	<ul style="list-style-type: none"> <li>• endothelin converting enzyme-like 1 ECEL1</li> </ul>	<ul style="list-style-type: none"> <li>• ADAM metallopeptidase with thrombospondin type 1 motif, 9 ADAMTS9</li> <li>• protease, serine, 12 (neurotrypsin, motopsin) PRSS12</li> </ul>	1

### The twenty most down-regulated transcripts

Out of 254 tested molecular functions, 47 (data not shown) were differentially represented in consequence of a changed  $A\beta_{42}/A\beta_{40}$  ratio. Out of these molecular functions, the strongest difference in the number of transcripts ( $\Delta$  transcripts), and hence, most differentially represented, were these:

Molecular function	Transcripts		$\Delta$ Number of transcripts
	C99V50F versus C99WT ( $A\beta_{42}/A\beta_{40}\downarrow$ ):	C99I45F versus C99WT ( $A\beta_{42}/A\beta_{40}\uparrow$ ):	
Receptors	<ul style="list-style-type: none"> <li>transferrin receptor (p90, CD71) TFRC</li> <li>cholinergic receptor, muscarinic 3 CHRM3</li> <li>G protein-coupled receptor 176 GPR176</li> <li>RAR-related orphan receptor B RORB</li> </ul>	<ul style="list-style-type: none"> <li>integrin, beta 5 ITGB5</li> </ul>	3
G-protein coupled receptors	<ul style="list-style-type: none"> <li>cholinergic receptor, muscarinic 3 CHRM3</li> <li>G protein-coupled receptor 176 GPR176</li> </ul>	–	2
Kinases	<ul style="list-style-type: none"> <li>protein kinase N2 PKN2</li> <li>cyclin-dependent kinase 6 CDK6</li> </ul>	–	2
Non-receptor serine/threonine protein kinases	<ul style="list-style-type: none"> <li>protein kinase N2 PKN2</li> <li>cyclin-dependent kinase 6 CDK6</li> </ul>	–	2
Protein kinases	<ul style="list-style-type: none"> <li>protein kinase N2 PKN2</li> <li>cyclin-dependent kinase 6 CDK6</li> </ul>	–	2
Nucleic acid binding	<ul style="list-style-type: none"> <li>transcription factor 4 TCF4</li> <li>prospero-related homeobox 1 PROX1</li> <li>neurogenin 2 NEUROG2</li> <li>v-myc myelocytomatosis viral related oncogene, neuroblastoma derived (avian) MYCN</li> <li>transcription factor 7-like 2 (T-cell specific, HMG-box) TCF7L2</li> <li>RAR-related orphan receptor B RORB</li> </ul>	<ul style="list-style-type: none"> <li>heart and neural crest derivatives expressed 1 HAND1</li> <li>cAMP responsive element binding protein 1 CREB1</li> <li>ribosomal protein S2 RPS2</li> <li>nuclear receptor coactivator 6 NCOA6</li> <li>endothelial PAS domain protein 1 EPAS1</li> <li>homeobox A7 HOXA7</li> <li>poly(A) binding protein, cytoplasmic 1 PABPC1</li> <li>ELAV (embryonic lethal, abnormal vision, Drosophila)-like 1 (Hu antigen R) ELAVL1</li> </ul>	2
Other	–	<ul style="list-style-type: none"> <li>matrix Gla protein</li> </ul>	2

signaling molecules		<ul style="list-style-type: none"> <li>MGP</li> <li>golgi apparatus protein 1 GLG1</li> </ul>	
Select regulatory molecules	<ul style="list-style-type: none"> <li>serpin peptidase inhibitor, clade F (alpha-2 antiplasmin, pigment epithelium derived factor), member 1 SERPINF1</li> </ul>	<ul style="list-style-type: none"> <li>protein kinase C substrate 80K-H PRKCSH</li> <li>dynein, cytoplasmic 1, light intermediate chain 2 DYNC1LI2</li> <li>regulator of G-protein signaling 4 RGS4</li> </ul>	2
Transferases	–	<ul style="list-style-type: none"> <li>tetratricopeptide repeat domain 5 TTC5</li> <li>COX10 homolog, cytochrome c oxidase assembly protein, heme A: farnesyltransferase (yeast) COX10</li> </ul>	2

**Table 5.19 PANTHER™ gene and protein classification system: The analysis of the *twenty most down-regulated* transcripts from the comparisons C99V50F/C99WT and C99I45F/C99WT ( $p < 0.05$ ,  $n=3$ ) revealed these differentially represented molecular functions.**

The total difference in the following transcripts was one, *but different transcripts were affected*. Especially if they have contrary functions in the cell (e.g. inhibitory/activating when both mutants are compared), they could fulfill important functions:

Molecular function	Transcripts		Δ Number of transcripts
	C99V50F versus C99WT ( $A\beta_{42}/A\beta_{40}\downarrow$ ):	C99I45F versus C99WT ( $A\beta_{42}/A\beta_{40}\uparrow$ ):	
CREB transcription factor	–	cAMP responsive element binding protein 1 CREB1	1
Protease inhibitor	<ul style="list-style-type: none"> <li>serpin peptidase inhibitor, clade F (alpha-2 antiplasmin, pigment epithelium derived factor), member 1 SERPINF1</li> </ul>	–	1



See Chapter 12.3.4 (pages S71-S75), Supplementary Information, for gene annotations.

In order to extract maximum information out of the data, data analysis was performed in parallel with another set of triplicates for C99WT (here named C99WT2: C99WT clone 1 was combined with C99WT clone 4 and 5, refer to Fig. 5.2, page 38) and used as a baseline experiment. This procedure revealed further genes and expression patterns (Fig. 5.39). See also annotations for clustered genes, Chapter 12.3.4 (pages S73-S75), Supplementary Information:

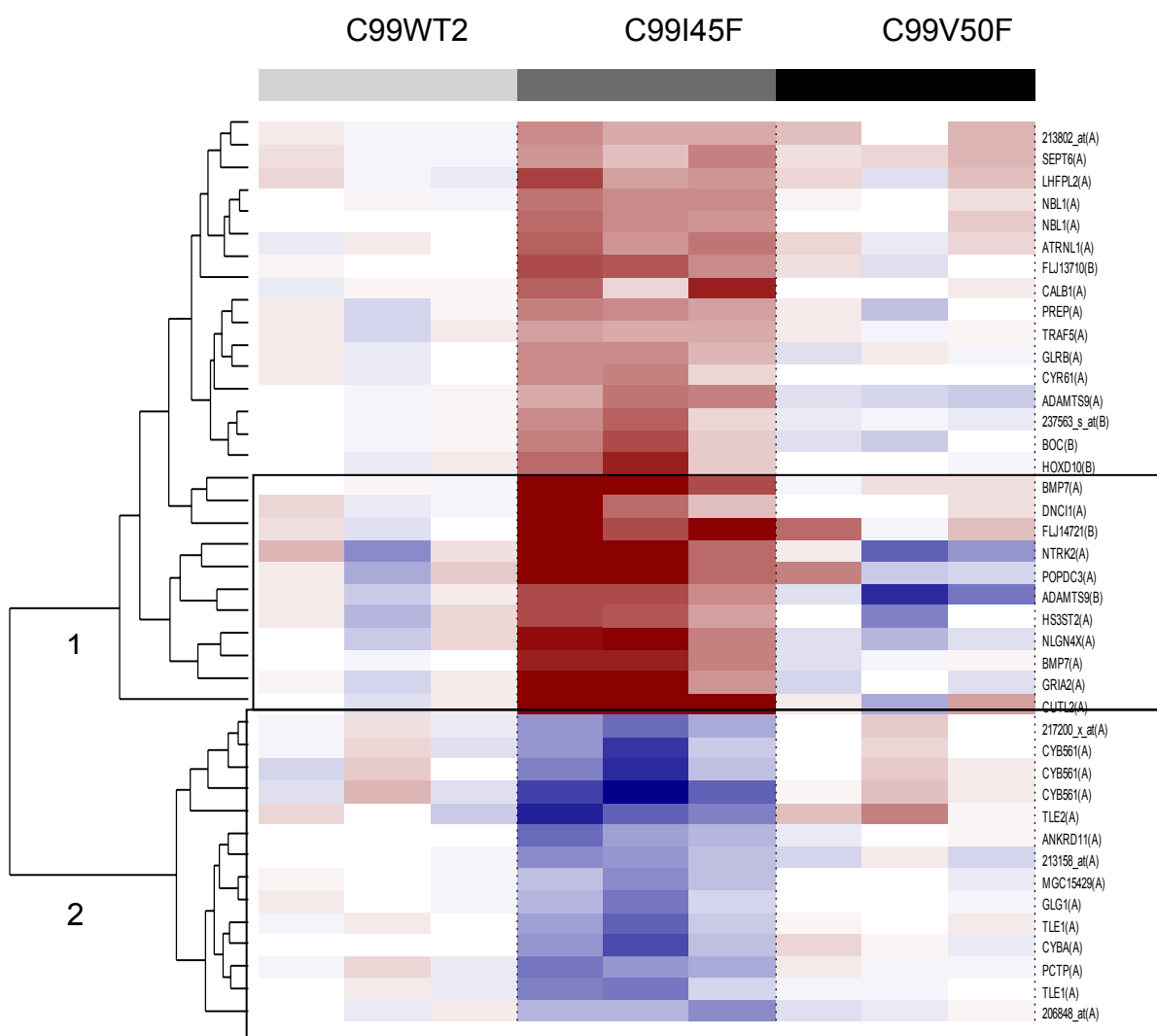


**Figure 5.39 Hierarchical clustering according to gene expression values. Gene expression values of three independent replicates of C99WT and C99-mutants were clustered in order to obtain information about expression patterns in wildtype and mutants. C99WT2 (clone 1, 4 and 5, see Fig. 5.2, page 38) was used as a baseline experiment. Using a different set of replicates for the baseline experiment provides further information about affected genes and provides insight into variability from clone to clone. Two main clusters were identified.**

In order to utilize maximum information out of the data, data derived from C99WT1, C99WT2, C99 mutants and the mock control was used providing information about overall gene regulation.

This procedure revealed a hitherto unknown relationship between neurogenin 2 and the uncharacterized KIAA0125. Interestingly both genes were the most strongly differentially expressed genes, and secondly, they were inversely regulated in *all* measured cell clones.

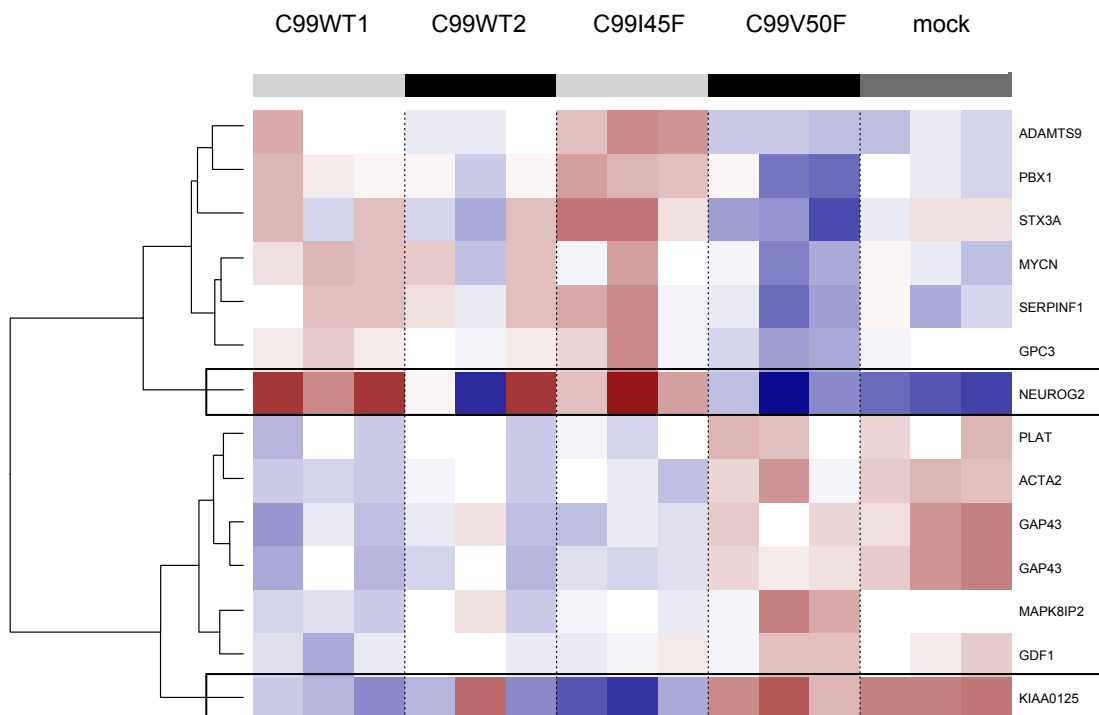


**Figure 5.40 Hierarchical clustering according to gene expression values.** Gene expression values of three independent replicates of C99WT1, C99WT2, C99-mutants and mock transfected cells were clustered in order to obtain information about expression patterns. This procedure revealed a so far unknown relationship between neurogenin 2 (Neurog2) and the until now uncharacterized KIAA0125: Neurogenin 2 and KIAA0125 were inversely regulated. Here, no baseline experiment was defined. Instead, for each probe set the mean was calculated over all Chips and was subtracted from every single value (centering of data).

Interestingly, KIAA0125 (chr14q32.33) is localized close to the PS1 locus (chr14q24.3). There might be a functional relationship between PS1, KIAA0125 and neurogenin 2.

---

## 5.14 Quantitative real-time PCR

### 5.14.1 Preface

The advantage of using microarrays to measure thousands of transcripts in parallel is accompanied by a certain imprecision of the measurements. Calculated fold changes for microarray experiments can vary greatly depending on the used normalisation algorithms. Quantitative real-time PCR is a suitable tool to verify microarray data and provide more precise results. The fold changes determined by real-time PCR better reflect true expression levels and hence was used here to validate microarray data. To obtain reliable results, measurements need to be normalized, thus a normalisation control was selected out of ten different normalisation controls and used for all measurements. All fold changes determined by real-time PCR validated the microarray data. As to be expected [194] microarray data calculated with the PLIER algorithm slightly underestimated true fold changes of expression (as determined by real-time PCR).

### 5.14.2 Normalisation

These 10 candidate controls were used to select a suitable endogenous control for normalisation:

- Acidic ribosomal protein
- $\beta$ -actin
- CyclophilinA
- Glyceraldehyde-3-phosphate dehydrogenase
- Phosphoglycerokinase
- $\beta_2$ -Microglobulin
- $\beta$ -Glucuronidase
- Hypoxanthine ribosyl transferase
- Transcription factor IID, TATA binding protein
- Transferrin receptor

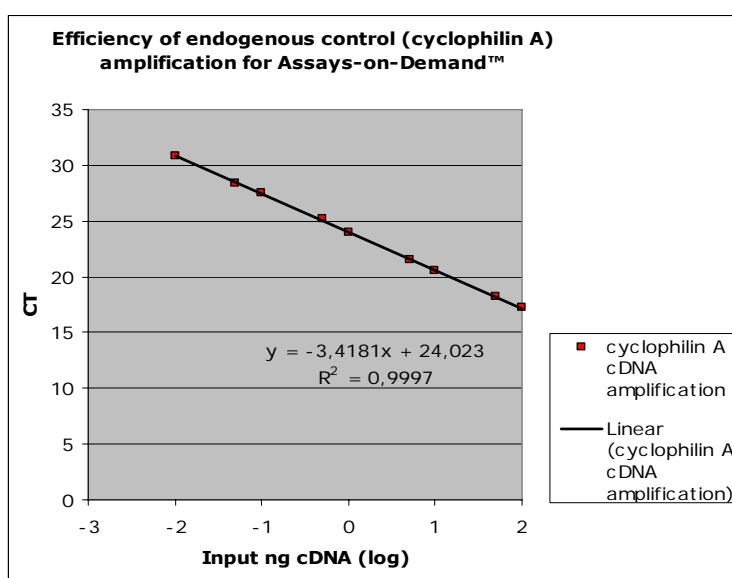
Suitable controls were those providing *equal* and high expression in all tested cell clones. *Cyclophilin A*,  $\beta$ -actin and acidic ribosomal protein turned out to be suitable for normalisation. Detailed analysis of these 3 normalisation controls, in turn, showed that *cyclophilin A* was insignificantly more favorable than the other two, due to *equal expression in all cell clones*. Thus, *cyclophilin A* was chosen as the normalisation control.

### 5.14.3 Relative quantification with the $\Delta\Delta C_T$ Method

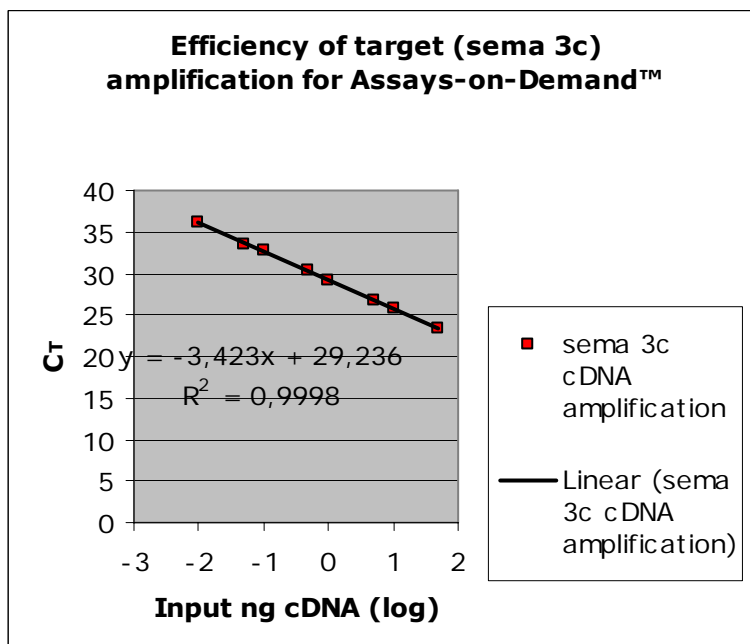
#### Validation of an equal amplification efficiency of the genes of interest and the endogenous control for Assays-on-Demand™

For the  $\Delta\Delta C_T$ –Method to be valid, the efficiency of the target amplification and the efficiency of the reference amplification must be approximately equal. A suitable method to assess this, is to look at how  $\Delta C_T$  varies with template dilution. As an example, the amplification efficiencies of the endogenous control and two target genes (sema3c and ecel1) are shown (Fig. 5.41, A-C). Furthermore, the amplification efficiencies of endogenous control and one target gene were directly compared to assess equal efficiencies (Fig. 5.42).

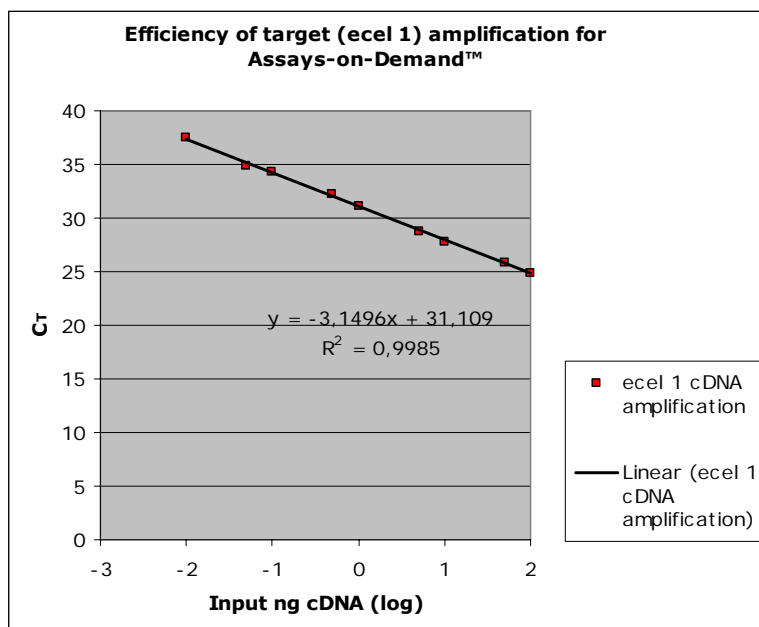
**A**



Efficiency: 0.96 (96%)

**B**

Efficiency: 0.96 (96 %)

**C**

Efficiency: 1.01 (101%)

**Figure 5.41 A-C** Diagrams show cDNA amplification determined by measuring the threshold cycle ( $C_T$ ) at different input cDNA amounts by real-time PCR. For calculating the amplification efficiencies (E) the equation used was:  $E = 10^{(-1/\text{slope})} - 1$ .

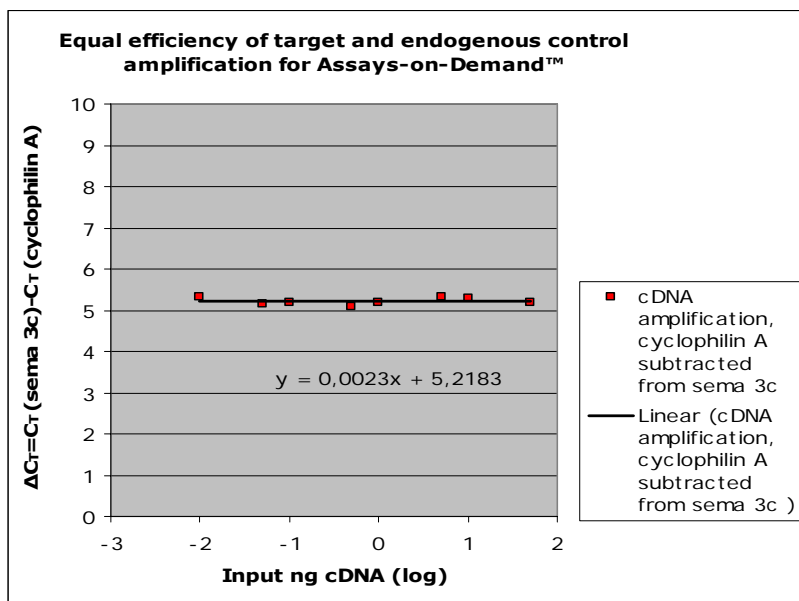


**Figure 5.42** Input cDNA is plotted against the differences ( $\Delta C_T$ ) of the  $C_T$  values between gene of interest and reference. If the efficiencies of the two amplicons are approximately equal, the slope tends towards zero and should be  $<0.1$ .

The *amplification efficiencies of target (gene of interest) and reference were found to be equal and close to 100% (90%-110%) in all tested assays*. Apart from this, Applied Biosystems guarantees the same efficiencies of target and reference amplification for all Assays-on Demand™ when measuring at a range from 1-100 ng cDNA) so the  $\Delta\Delta C_T$  Method could be used for calculating fold changes of gene expression. Apart from this, efficiency curves delivered information about the *range in which reliable measurements were possible*: It turned out that it was possible to measure from 0.01-100 ng input cDNA for high and medium abundant transcripts and from 1-100 ng for low abundant transcripts. Finally 50 ng was chosen to be sure to measure in a linear range (at th is amount one is able to detect low abundant transcripts while inhibition by overexcess of cDNA can be excluded).

### 5.14.4 Direct comparison of data derived from oligonucleotide microarrays and quantitative real-time PCR

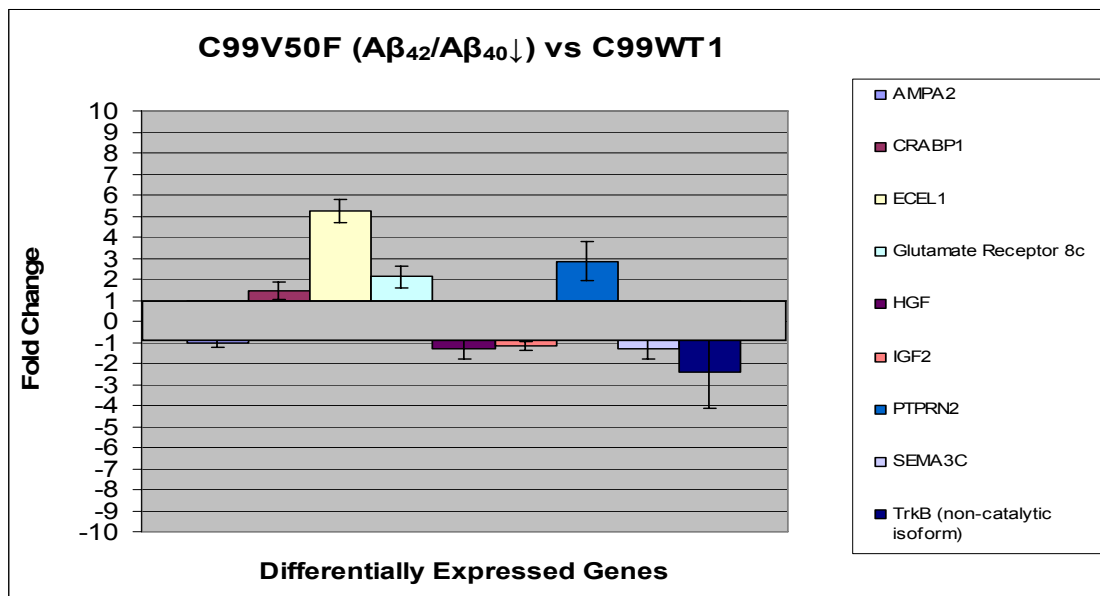
#### Oligonucleotide microarrays

	C99V50F/C99WT1		C99I45F/C99WT1		C99I45F/C99V50F		C99WT1/mock	
	Fold change	p-value	Fold change	p-value	Fold change	p-value	Fold change	p-value
AMPA2	not differentially expressed		6.5	0.033	4.8	0.025	not differentially expressed	
CRABP1	not differentially expressed		2.7	0.116	2.3	0.188	not differentially expressed	
ECEL1	1.9	0.037	not differentially expressed		-4.0	0.137	-2.0	0.3238
Glutamate Receptor 8c	not differentially expressed		1.5	0.247	-2.6	0.198	not differentially expressed	
HGF	not differentially expressed		-3.0	0.157	-2.5	0.219	not differentially expressed	
IGF2	not differentially expressed		-2.6	0.05	-3.8	0.082	1.9	0.1030
PTPRN2	1.6	0.095	1.8	0.041	1.9	0.027	not differentially expressed	
Sema3c	not differentially expressed		1.8	0.032	2.6	0.027	not differentially expressed	
<b>TrkB, different splice products:</b>								
214680_at ( <i>non-catalytic isoform</i> )	-1.3	0.165	1.6	0.062	2.8	0.030	1.6	0.0721
221796_at ( <i>non-catalytic isoform</i> )	-1.7	0.086	2.2	0.023	5.4	0.013	3.3	0.0111
221795_at ( <i>non-catalytic isoform</i> )	-1.7	0.058	1.9	0.193	5.2	0.047	2.7	0.0038
207152_at ( <i>catalytic isoform</i> )	not differentially expressed		not differentially expressed		1.4	0.142	not differentially expressed	

**Table 5.20 Selected genes from whole genome microarray experiments.** Data were derived from three independent experiments. All replicates (n=3) were performed at different days and from independent single clones. Data were normalized with the PLIER algorithm. The complete coding sequence of TrkB (NTRK2) consists of 24 exons (207152\_at, longest isoform, contains the carboxyterminal catalytic domain (exon 20-24) and the carboxyterminal phospholipase C  $\gamma$  binding site (exon 23-24). The non-catalytic isoforms of TrkB end after exon 16, so that they lack both the catalytic domain and the phospholipase C  $\gamma$  binding site. All (non-catalytic and catalytic isoforms) transcripts were sufficiently abundant (absolute values) to ensure reliable results. (The direct comparison of both mutants (C99I45F/C99V50F) and the comparison C99WT1/mock are shown here to give an impression of their regulation but are not shown by Real-Time PCR).

## Quantitative Real-Time PCR

A



B

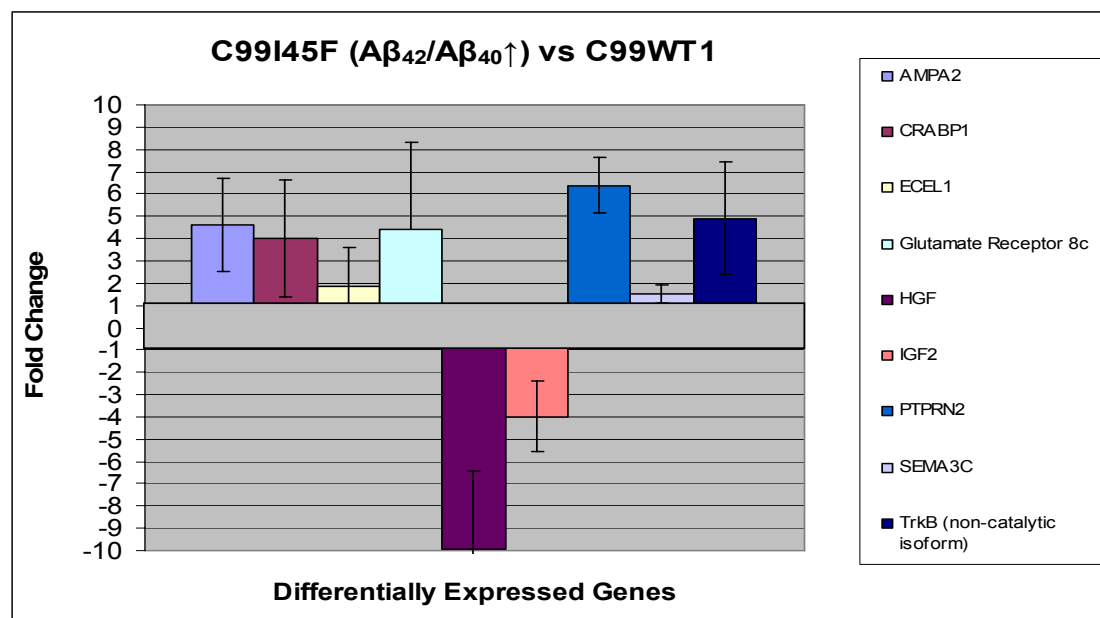


**Figure 5.43 Differentially expressed genes validated by Real-Time PCR.** Columns represent the mean of the fold change of three *independent single clones*. Each clone was measured once and the mean was calculated from three clones ( $n=3$ ). Thus biological clone to clone variation is not concealed and can be seen from error bars representing the S.E.M. (standard error of the mean).

Data derived from Real-Time PCR showed agreement with microarray data in all tested cell clones. Real-Time PCR delivers more precise data than the microarray analysis (in which thousands of transcripts are measured in parallel) due to the concentration onto one transcript.

### 5.15 “Chromeron-Effect” on chromosomal loci 1q23 and 1p36

*Equally regulated genes, localized on the same chromosomal locus* may have important functional relations. Such a regulation, resembling the “Operon” in prokaryotes, was named “*Chromeron*” in eukaryotes [195, 196]. I observed this effect for the chromosomal loci 1q23 and 1p36:

Gene Name	Gene Symbol	C99I45F versus C99WT (A $\beta$ <sub>42</sub> /A $\beta$ <sub>40</sub> ↑)	Chromosomal locus
neural cell adhesion molecule 1	NCAM1	1.7 fold up-regulated	1q23
regulator of G-protein signaling 7	RGS7	1.5 fold up-regulated	1q23
(regulator of G-protein signaling 4)	(RGS4)	(2.7 fold down-regulated)	(1q23)
kinesin family member 1B	Kif1B	1.6 fold up-regulated	1p36
neuroblastoma suppression of tumorigenicity 1	NBL1	1.7 fold up-regulated	1p36

**Table 5.21 “Chromeron-Effect” on chromosomal loci 1q23 and 1p36 (n=3, p<0.05 for all listed genes).** Equally regulated NCAM1 and RGS7 show the chromeron effect on chromosome 1q23. Kif1B and NBL1 show this effect on chromosome 1p36. RGS4, localized on 1q23, was one of the most *downregulated* genes (C99I45F versus C99WT) and is discussed as a top candidate gene for schizophrenia.

Further genes that are regulated in the same direction and to the same extent (co-regulated genes), but are localized *on different chromosomal regions* were:

*APLP2* (1.6 fold up-regulated in C99I45F versus C99WT, chr11q23-q25|11q24),  $\alpha$ -catenin (1.8 fold up-regulated in C99I45F versus C99WT, chr2p12), *PREP* (1.5 fold up-regulated in C99I45F versus C99WT, chr6q22), *Sema3c* (1.8 fold up-regulated in C99I45F versus C99WT, chr7q21).

## 5.16 Agreement of differentially expressed genes with genes found in linkage and association studies

Two genes or markers that are so close together on a chromosome that they are rarely separated by recombination are said to be linked. Linkage analysis is a statistical method for detecting linkage between a disease and markers of known location by following their inheritance in families. Two genes that are near each other on the same chromosome are said to be linked. If one gene is inherited, the probability is high that the other one will also be inherited. Linkage usually means that a gene contributing partially or completely to the phenotype (a genetic disease, for instance) maps in the vicinity of the markers. The tendency of certain genes to be inherited together due to their physical proximity on the chromosome provides important information. This information (chromosomal loci identified by linkage analysis) was compared to the identified susceptibility loci identified here in this thesis. Genes identified in overlapping loci (identified by linkage analysis and gene expression profiling in consequence of altered  $A\beta_{42}/A\beta_{40}$  ratios) are expected to provide more promising candidates for AD than one approach alone.

Chromosomal regions of most differentially expressed genes (as a result of a changed  $A\beta_{42}/A\beta_{40}$  ratio) were selected and compared with chromosomal regions identified in linkage analyses (lod score > 2). Only overlapping results are shown here. This procedure was used in order to narrow down important candidate genes.

Gene Symbol	Gene Name	Differentially expressed in these compared clones	Fold change	p-value	Chromosomal location, lod score > 2
RGS4	regulator of G-protein signaling 4	C99I45F/C99WT1	>3- fold down - regulated	<0.005	chr1q23.3
LPAL2	LPAL2 Lipoprotein, Lp(a)-like 2	C99I45F/C99WT1	>3- fold down - regulated	<0.005	chr6q26-q27
FGF21	FGF21 fibroblast growth factor 21	C99I45F/C99WT2	>3- fold down - regulated	<0.005	chr19q13.1-qter
NTRK2	neurotrophic tyrosine kinase, receptor, type 2 (non-catalytic isoform)	C99I45F/C99V50F	>3-fold up-regulated	<0.005	chr9q22.1
NTRK2	neurotrophic tyrosine kinase, receptor, type	C99I45F/C99WT2	>3-fold up-regulated	<0.005	chr9q22.1

	2 (non-catalytic isoform)				
DPT	dermatopontin	C99I45F/C99V50F	>3-fold up-regulated	<0.005	chr1q12-q23
DPT	dermatopontin	C99I45F/C99WT2	>2-fold up-regulated	<0.005	chr1q12-q23
ITPR2	inositol 1,4,5-trisphosphate receptor, type 2	C99I45F/C99V50F	>3-fold up-regulated	<0.005	chr12p11

**Table 5.22** Overlap of chromosomal regions, identified by localization of differentially expressed genes (identified in this thesis), with chromosomal susceptibility loci identified by linkage analysis. Chromosomal loci, in which the most strongly differentially expressed genes were found, were compared to chromosomal loci in which relatively strong (lod score >2) linkage to AD was found. Lod (logarithm of the odds) score 2 is a rather stringent cut-off for true linkage. Data were derived from calculation with several algorithms.

The same procedure was used for the following genes and linkage was also found for these regions, but with a lod score <2.0, reducing the reliability of true linkage compared to lod scores >2.0:

Gene Symbol	Gene Name	Differentially expressed in these compared clones	Fold change	p-value	Chromosomal location
WNT9A	Wingless-type MMTV integration site family, member 9A	C99V50F/C99WT1	>3-fold up-regulated	<0.005	chr1q42
WNT9A	Wingless-type MMTV integration site family, member 9A	C99I45F/C99V50F	>3-fold down-regulated	<0.005	chr1q42
GRM7	glutamate receptor, metabotropic 7	C99I45F/C99WT2	>3-fold up-regulated	<0.005	chr3p26
ENPP5	ectonucleotide pyrophosphatase/phosphodiesterase 5 (putative function)	C99I45F/C99WT1	>3-fold down-regulated	<0.005	chr 6p21.1-p11.2
PAX2	paired box gene 2	C99V50F/C99WT1	>3-fold up-regulated	<0.005	chr 10q24
ADRB1	adrenergic, beta-1-, receptor	C99V50F/C99WT1	>3-fold up-regulated	<0.005	chr 10q24-q26
ADRB1	adrenergic, beta-1-, receptor	C99V50F/C99WT2	>3-fold up-regulated	<0.005	chr 10q24-q26
ADRB1	adrenergic, beta-1-, receptor	C99I45F/C99V50F	>3-fold down-regulated	<0.005	chr 10q24-q26
CMKLR1	chemokine-like receptor 1	C99I45F/C99WT1	>3-fold down-regulated	<0.005	chr 12q24.1
CUTL2	cut-like 2 (Drosophila)	C99I45F/C99WT2	>3-fold up-regulated	<0.005	chr 12q24.11-q24.12

FLT1	Fms-related tyrosine kinase 1 (vascular endothelial growth factor/vascular permeability factor receptor) , spliced form	C99V50F/C99WT1	>3-fold up-regulated	<0.005	chr13q12
TC9	tetratricopeptide repeat domain 9	C99I45F/C99WT1	>3-fold up-regulated	<0.005	chr14q24.2
TTC9	tetratricopeptide repeat domain 9	C99I45F/C99WT2	>3-fold up-regulated	<0.005	chr14q24.2
CYP2B6	cytochrome P450, family 2, subfamily B, polypeptide 6	C99I45F/C99V50F	>3-fold up-regulated	<0.005	chr19q13.2
NCR1	natural cytotoxicity triggering receptor 1	C99I45F/C99V50F	>3-fold up-regulated	<0.005	chr19q13.42
GRIA3	glutamate receptor, ionotropic, AMPA 3	C99I45F/C99WT2	>3- fold down - regulated	<0.005	chrXq25-q26

**Table 5.23** Overlap of chromosomal regions, identified by localization of differentially expressed genes (identified in this thesis), with chromosomal susceptibility loci identified by linkage analysis. Chromosomal loci, in which strong differentially expressed genes were found, were compared to chromosomal loci in which linkage (lod score <2.0) was found. Data were derived from calculation with several algorithms.

Genetic association studies are performed to determine whether a genetic variant is associated with a disease or trait: if association is present, a particular allele, genotype or haplotype of (a) polymorphism(s) will be seen more often than expected by chance in an individual carrying the trait. Thus, a person carrying one or two copies of a high-risk variant is at an increased risk of developing the associated disease or having the associated trait. Genetic association is the occurrence together in a population, more often than can be readily explained by chance, of two or more traits of which at least one is known to be genetic. This can be between phenotypes, e.g. visible characteristics such as height or eye colour, between a phenotype and a genetic polymorphism, such as a single nucleotide polymorphism, or between two genetic polymorphisms.

Linkage disequilibrium (LD) is a term used in the study of population genetics for the non-random association of alleles at two or more loci, not necessarily on the same chromosome. It is not the same as linkage, which describes the phenomenon whereby two or more loci on a chromosome have reduced recombination between them because of their physical proximity to each other. LD describes a situation in which some combinations of alleles or genetic markers occur more or less frequently in a population than would be expected from a random formation of haplotypes from alleles based on their frequencies.

In order to find new susceptibility loci for late onset AD a linkage disequilibrium analysis was performed in a Finnish population [135, 136]. Forty-seven patients with late-onset AD and 51 age-matched control subjects were chosen from the same geographic area in eastern Finland, where the population is descended mainly from a small group of original founders. These subjects were initially genotyped with 366 polymorphic microsatellite markers and a follow-up analysis was performed with additional microsatellite markers for those chromosome loci found to be associated with AD. This analysis revealed 8 chromosomal loci where more than one microsatellite marker was associated with AD: 1p36.12, 2p22.2, 3q28, 4p13, 10p13, 13q12, 18q12.1 and 19p13.3. Genes in close proximity to these loci (Table 5.24) will provide targets for future genetic and functional studies of AD.

Gene Symbol	Gene Name	Differentially expressed in these compared clones	Fold change	p-value	Chromosomal location
NBL1	neuroblastoma, suppression of tumorigenicity 1	C99I45F/C99WT1	2.6 fold up-regulated	0.00002	chr1p36.13-p36.11
KIAA1026	KIAA1026 protein	C99I45F/C99WT1	1.7 fold up-regulated	0.0021	chr1p36.21
KIF1B	kinesin family member 1B	C99I45F/C99WT1	1.6 fold up-regulated	0.0371	chr1p36.2
VAMP3	vesicle-associated membrane protein 3 (cellubrevin)	C99I45F/C99WT1	1.1 fold down-regulated	0.0327	chr1p36.23
NPPA	natriuretic peptide precursor A	C99V50F/C99WT1	1.3 fold up-regulated	0.0488	chr1p36.21
NPD014	NPD014 protein	C99V50F/C99WT2	1.2 fold up-regulated	0.0163	chr1p36.13-p35.1
KIAA1102	KIAA1102 protein	C99I45F/C99WT1	2.1 fold up-regulated	0.0038	chr4p13
CCDC3	coiled-coil domain containing 3	C99I45F/C99WT1	2.5 fold up-regulated	0.01613	chr10p13
TLE2	transducin-like enhancer of split 2 (E(sp1) homolog, Drosophila)	C99I45F/C99WT1	2.8 fold down-regulated	0.00253	chr19p13.3
EML4	echinoderm microtubule associated protein like 4	C99V50F/C99WT1	1.6 fold up-regulated	0.0224	chr2p22-p21
SOS1	Son of sevenless homolog 1 (Drosophila)	C99V50F/C99WT1	4.0 fold down-regulated	0.02572	chr2p22-p21
SLC14A2	Solute carrier family 14	C99I45F/C99WT1	5.0 fold	0.00219	chr18q12.1

	(urea transporter), member 2		up- regulated		
SLC14A2	Solute carrier family 14 (urea transporter), member 2	C99V50F/C99WT1	4.0 fold up- regulated	0.02572	chr18q12.1

**Table 5.24** Overlap of chromosomal regions, identified by localization of differentially expressed genes (identified in this thesis) with chromosomal susceptibility loci identified by genotyping and subsequent use of microsatellite markers (publications of other working groups). Chromosomal loci, in which strongly differentially expressed genes were found, were compared to chromosomal susceptibility loci identified in a Finnish population. No overlap was found for chromosomal region 3q28.

### 5.17 Agreement of differentially expressed genes with genes of the “Alzforum database”

The Alzforum database, containing candidate genes for AD, is updated regularly and thus varies with time. For this reason, here only a small selection of genes is shown: Gene lists presented in Chapter 12.2 (Supplementary Information) can be compared with the gene list presented at [www.alzforum.org](http://www.alzforum.org) from time to time in order to identify further candidate genes.

Gene Name	Gene Symbol	Differentially expressed in these compared clones	Fold change	p-value
CD14	CD14	C99I45F/C99WT1	>3-fold down-regulated	<0.005
CD14	CD14	C99V50F/C99WT1	>3-fold up-regulated	<0.005
neurotrophic tyrosine kinase, receptor, type 2 (non-catalytic isoform)	NTRK2	C99I45F/C99WT2	>3-fold up-regulated	<0.005
plasminogen activator, tissue	PLAT	C99V50F/C99WT1	>2-fold up-regulated	<0.005

**Table 5.25** Genes found to be differentially expressed as a result of a changed  $A\beta_{42}/A\beta_{40}$  ratio, were compared to putative candidate genes presented at [www.alzforum.org](http://www.alzforum.org). Only overlapping genes are listed here. Data were derived from calculation with several algorithms.

### 5.18 Intersection of genes identified in this thesis as a consequence of an altered $A\beta_{42}/A\beta_{40}$ ratio and genes identified as a result of PS1/PS2 knockdown in murine embryonic fibroblasts

Differentially expressed genes derived from the comparison C99I45F/C99WT ( $A\beta_{42}/A\beta_{40}\uparrow$ ) and C99V50F/C99WT ( $A\beta_{42}/A\beta_{40}\downarrow$ ) in human neuroblastoma cells were

compared with differentially expressed genes from embryonic mouse fibroblasts in which presenilin 1 and presenilin 2 were knocked down by siRNA (carried out by my colleague Laura Busia; data are available in her Master thesis). Here, the 100 most up and down-regulated transcripts in either datasets were compared. Both approaches have one common mechanism, namely the processing by the  $\gamma$ -secretase complex. If processing by the  $\gamma$ -secretase complex is the pivotal common step, genes dependent on this process should be identified in *both* approaches. Indeed I found such genes by overlaying both datasets:

Gene symbol	Name
ACTA2	actin, alpha 2, smooth muscle, aorta
CDKN1A	cyclin-dependent kinase inhibitor 1A (p21, Cip1)
COL4A1	collagen type IV $\alpha$ 1
CRABP1	cellular retinoic acid binding protein 1
DKK2	dickkopf homolog 2 ( <i>Xenopus laevis</i> )
FBN1	fibrillin 1 (Marfan syndrome)
RELN	Reelin
SEMA3A	sema domain, immunoglobulin domain (Ig), short basic domain, secreted, semaphorin 3A
STX3	syntaxin 3
USP18	ubiquitin specific protease 18

**Table 5.26** Genes, found to be differentially expressed as a result of a changed  $A\beta_{42}/A\beta_{40}$  ratio (identified in this thesis) were compared with genes identified as a result of PS1/PS2 knockdown in embryonic mouse fibroblasts. Only overlapping genes are listed here.

### 5.19 Intersection of genes identified in this thesis as a consequence of an altered $A\beta_{42}/A\beta_{40}$ ratio and genes identified in response to AICD overexpression in human neuroblastoma cells

Differentially expressed genes derived from the comparison C99I45F/C99WT ( $A\beta_{42}/A\beta_{40}\uparrow$ ) and C99V50F/C99WT ( $A\beta_{42}/A\beta_{40}\downarrow$ ) in the human neuroblastoma cell line SH-SY5Y (identified in this thesis) were compared with differentially expressed genes in the human neuroblastoma cell line SHEP-SF overexpressing the AICD identified by Müller et al. [57].

Here, the 100 most up and down-regulated transcripts (identified in this thesis) were compared with the genes presented in the dissertation by Thorsten Müller (University of Münster, Germany, 2005). A selection of overlapping genes is shown in Table 5.27.

---

Gene symbol	Name
ACTA2	$\alpha$ 2-actin, smooth muscle, aorta
PTN	pleiotrophin (heparin binding growth factor 8, neurite growth-promoting factor 1)
PROX1	prospero-related homeobox 1
DOCK4	dedicator of cytokinesis 4
TFPI2	tissue factor pathway inhibitor 2

**Table 5.27 Genes, found to be differentially expressed as a result of changed C99 cleavage products (identified in this thesis) were compared with genes identified as a result of AICD overexpression. A selection of overlapping genes is listed here.**

## 6 Discussion

### 6.1 Preface

There is a large body of evidence showing that  $A\beta_{42}$ , in contrast to  $A\beta_{40}$ , triggers a chain of harmful events in the development of AD [19, 197]. Most of the scientific community generally agrees on the hypothesis that  $A\beta_{42}$  triggers or is causally involved in the malfunction of AD. However, the mechanism of how  $A\beta_{42}$  acts is unclear. It has been demonstrated that  $A\beta_{42}$  and  $A\beta_{40}$  have opposing effects on amyloid deposition. It has been shown that  $A\beta_{42}$  promotes amyloid deposition, whereas  $A\beta_{40}$  inhibits it [78].  $A\beta_{40}$  seems to have protective properties and it was suggested that selective increases in  $A\beta_{40}$  levels may actually reduce the risk for development of AD. Moreover it was suggested that the  $A\beta_{42}/A\beta_{40}$  ratio, not total  $A\beta$  levels, controls amyloid deposition in transgenic mice [78]. To shed light on this issue, gene expression profilings of human neuroblastoma cells were performed in the presence of altered  $A\beta_{42}/A\beta_{40}$  levels. One big advantage of human cells, in contrast to neurons from mice or other species, is that obtained data can be better compared to linkage and association studies from affected families suffering from AD. Furthermore, signal transduction and metabolic pathways differ between species and elucidation of the mechanism for AD feasible for mice is not necessarily beneficial to humans. The question of how transcription is activated was not directly addressed in this thesis. There is growing evidence that the APP intracellular domain (AICD) is involved in nuclear signaling. Fe65 has been shown to stabilize the intracellular domains of  $\gamma$ -secretase cleaved APP, APLP1 and APLP2, which, together with Fe65, are localized to the nuclear compartment [198, 199]. The analogy of APP processing to Notch receptor signaling suggested a possible function for the AICD in nuclear signaling [200, 201]. Nuclear signaling of the AICD is assumed to be regulated by the APP-adaptor proteins Fe65, Jip1b and X11 $\alpha$ , as well as the nuclear docking protein Tip60.

C99 is cleaved by  $\gamma$ -secretase, resulting on the one hand in the release of  $A\beta_{42}$  and  $A\beta_{40}$  and on the other hand in the release of two AICD species (AICD<sub>49-99</sub> and AICD<sub>50-99</sub>) [49]. So the observed alterations in gene expression may be triggered by  $A\beta$  or the AICD (or cleavage products thereof for instance through cleavage by caspases [151]). Further research distinguishing AICD effects from  $A\beta$  effects is necessary. Some publications about these issues already exist with the inherent problems of external  $A\beta$  supply [197, 202, 203]. Here, however,  $A\beta$  expression was analyzed in a controlled manner: C99-overexpressing constructs encoding the C-

terminal part of A $\beta$ PP (C99), together with an N-terminal signal peptide were used. This peptide is correctly cleaved by signal peptidase and thus is identical to the A $\beta$ PP-derived C99, the ultimate precursor for A $\beta$  generation. C99 is processed by  $\gamma$ -secretase in the same manner as A $\beta$ PP-derived C99, making it an ideal substrate to study  $\gamma$ -secretase function or its cleavage products A $\beta_{42}$  and A $\beta_{40}$  without influence of  $\beta$ -secretase. C99 cleavage by  $\gamma$ -secretase results in A $\beta_{42}$  and A $\beta_{40}$  production and is inherently accompanied by production of two AICDs differing in length [49]. A link between the production of A $\beta_{42}$  and the AICD49-99 has been suggested [50]. It has been shown that equimolar amounts of A $\beta$  and AICD are produced [49]. Gene expression could also be triggered by the as yet unidentified AICD<sub>57</sub> and AICD<sub>59</sub>, the two species which should theoretically be left after cleavage of A $\beta_{42}$  and A $\beta_{40}$  from the precursor C99. Furthermore, it has to be taken into consideration that the AICDs themselves are cleaved and that their cleavage products may also induce or repress gene expression.

Comparing our datasets with gene expression profiles from human neuroblastoma cells overexpressing the AICD alone (Müller et al. 2007 [57]) may indicate that some of the observed changes in gene expression are partially triggered by the AICD (or cleavage products thereof). This can be concluded from the significant overlap of identified genes by Müller et al. and genes identified here in this thesis. Further support for this view comes from the work of my colleague Laura Busia who identified genes in consequence of presenilin 1 and presenilin 2 knockdown by siRNA in murine embryonic fibroblasts (a big overlap of genes with the genes presented here in this thesis and with the genes identified by Müller et al. was observed). Processing by  $\gamma$ -secretase is expected to be influenced, with the consequence of changed A $\beta_{42}$ /A $\beta_{40}$  and AICD levels. If gene expression is triggered by the AICD, overlapping genes should be found with the genes identified by Müller et al.. Therefore, I compared this dataset with the genes identified by Müller et al. and indeed found an overlap of genes that is bigger than can be expected by chance (a selection of such genes is shown in Chapter 5.19, pages 120-121). The overlap of genes from our approaches (changed A $\beta_{42}$ /A $\beta_{40}$  and AICD levels in human neuroblastoma cells and PS1/PS2 knockdown in murine embryonic fibroblasts) was bigger, if compared to identified genes by Müller et al. in which the AICD was inducibly overexpressed in a human neuroblastoma cell line (and compared to the same non-induced cell line), than a comparison between our identified genes with several gene expression studies about A $\beta_{42}$  treated cells [197, 204]. However, it has to be taken into consideration that treating cells with A $\beta_{42}$  may be more artificial than our approach in which A $\beta_{42}$  is generated from a precursor. KAI1, which was shown to be induced by the AICD [152], was significantly differentially expressed in our PS1/PS2 knockdown approach.

However, it is noteworthy that AICD-regulated genes may be a subset of a much larger group of genes controlled by  $\gamma$ -secretase processing.

Whenever the term “ $A\beta_{42}/A\beta_{40}$  ratio” is used in this thesis for reasons of simplicity, it also implies the corresponding AICDs [49, 50] and all possible further C99 cleavage products.

Apart from relative values (equal to fold changes derived from the comparison between two groups) the absolute values from one group (absolute expression levels) have to be taken into consideration: The genes discussed in this thesis were checked for sufficiently high absolute values. However, there is no real agreement on what “sufficiently high” means. Also weakly expressed genes can be of relevance, if they belong to a group of genes which are generally weakly expressed, like for instance transcription factors. The absolute expression values of the genes were checked, but not necessarily intentionally excluded from analysis if they were below a certain threshold. Instead, genes with very low absolute values were explicitly mentioned in the text. Furthermore, it has to be taken into consideration that absolute values (as well as relative values) strongly depend on the algorithm used to calculate the data.

The terms “differentially expressed and up/down-regulated” refer to data derived from microarray analysis. If they were derived from real-time PCR, immunoblotting, immunocytochemistry, this was explicitly mentioned in the text.

Among big datasets derived from microarray analysis there is usually a portion of data which are so-called “false-positives” (genes that are not differentially expressed, but erroneously appear so). To restrict the number of false positives, while avoiding a too stringent cut-off, which would also remove genes with biologically relevant information, a balance for the stringency should be found. This was done by adjusting the threshold for the p-value to 0.05 (MAS 5 algorithm), 0.05 (PLIER algorithm) and 0.005 (GC-RMA algorithm). Nevertheless, differentially expressed genes with p-values slightly greater than 0.05 were also partially included into the data analysis, otherwise possible important biological effects would have been overlooked. The often used technique of strictly excluding such data (without any regard to their biological relevance) is a convenient way to make data analysis more simple (because a smaller data set has to be handled), but increases the risk of not recognizing crucial biological relationships. This is particularly true for signal transduction pathways in which many proteins (or their encoding genes) are components of a certain pathway: The probability that some of these proteins (genes) exceed the general accepted cut-off for significance ( $p=0.05$ ) is high; excluding such data from the beginning may conceal that this pathway is actually

affected.

Among big datasets derived from microarray analysis, the differentially expressed genes are usually a mixture of direct (primary) effects and indirect (secondary) effects derived from the original trigger (the trigger can be for instance an overexpressed protein, a knocked down gene etc.). Primary effects are caused directly by the trigger (overexpression of the trigger A leads to dysregulation of gene B). Secondary effects are caused by an indirectly dysregulated gene/protein (overexpression of the trigger A leads to dysregulation of gene C, via dysregulation of gene B). Such secondary effects are inevitable but can be biologically meaningful (for instance when gene B codes for a protein that itself has a strong impact on gene expression and influences the expression of gene C). A way to restrict such secondary effects (even if they cannot be excluded completely) is time-course experiments, in which typical “immediate early genes” (together with further directly responding genes, influenced by the trigger) can to some degree be distinguished from subsequently responding genes (secondary effects).

Gene expression profiling studies usually result in the generation of gene lists, in which genes can be listed according to their relative expression levels (fold changes), p-values or other kind of sorting criteria. Among these listed genes are some that specifically respond to the intended trigger (for instance an overexpressed protein triggering a pathological effect) and thus provide important information about the pathological mechanism. However, a subset of the listed genes, whose size is unknown, is differentially expressed in consequence of unspecific effects (these are, for instance, epiphenomena, not connected to the pathological mechanism). In order to control these unspecific effects as much as possible, a mock control (cells transfected with an empty vector) was used to recognize such effects. C99WT overexpression was compared to the mock control (dataset I) providing information about C99 effects. On the other hand the two mutants C99I45F (increased  $A\beta_{42}/A\beta_{40}$  ratio) and C99V50F (decreased  $A\beta_{42}/A\beta_{40}$  ratio) were compared with C99WT (dataset II and III). Finally all three datasets (I, II and III) were compared to each other to identify specific effects (specific especially for the AD-typical increased  $A\beta_{42}/A\beta_{40}$  ratio). Taking advantage of the knowledge about the amounts of generated  $A\beta_{42}/A\beta_{40}$  (C99I45F>C99WT>C99V50F) allowed to some degree the distinguishing between effects of different  $A\beta_{42}/A\beta_{40}$  amounts. *Of special interest were those genes which were among the most up-regulated ones for dataset II and in parallel among the most down-regulated ones for dataset III and vice versa. These genes in particular were expected to be influenced by inverse levels of  $A\beta_{42}/A\beta_{40}$ .*

It has to be taken into consideration that a small portion of  $A\beta_{42}/A\beta_{40}$  (C99 respectively) was also present in the cells, which was endogenously generated from the APP-locus (untransfected cells) with the disadvantage that expression values cannot go below endogenous levels (in contrast to APP knockout approaches). C99 was overexpressed approximately 10-fold (compared to endogenous C99 levels). This overexpression affected the comparison C99WT/mock. I regarded a 10-fold overexpression as sufficient to recognize important biological effects while it might not have been too high to cause a significant bias in the data due to unphysiological high C99 concentrations. For the comparisons C99I45F/C99WT and C99V50F/C99WT, C99-levels themselves were not expected to have an influence on gene expression, because all cells to be compared contained matched C99 expression levels. It was previously demonstrated [148, 149] and shown in this thesis that C99I45F and C99V50F express inverse  $A\beta_{42}/A\beta_{40}$  levels. Secreted  $A\beta_{42}/A\beta_{40}$  levels were 20-fold higher in C99I45F than in C99WT and intracellular  $A\beta_{42}/A\beta_{40}$  levels were 1.9-fold higher in C99I45F than in C99WT. In contrast to this, secreted  $A\beta_{42}/A\beta_{40}$  was approximately 3-fold lower in C99V50F than in C99WT and intracellular  $A\beta_{42}/A\beta_{40}$  was 1.9-fold lower in C99V50F than in C99WT [148]. These differences in  $A\beta_{42}/A\beta_{40}$  levels turned out (in this thesis) to be sufficient to see an effect on gene expression. Another possible approach would have been an APP knockout background where  $A\beta$ -expressing cells would have been compared with APP-knockout cells in which no endogenous  $A\beta$ -levels would have been expected. However, this would also have had disadvantages: APP-like proteins could have taken over APP-functions which might have caused a bias in the data. Moreover, cells from animals, instead from humans, would have been used and precious information that can possibly only be recognized in human cells would have been lost (for instance, signal transduction pathways differ between species).

According to what is currently known, the possible mechanisms identified in this thesis (synaptic dysfunction, influenced copper transport, change in protease (inhibitor) expression, etc.) are in agreement with the assumption that they are caused by increased  $A\beta_{42}$ . However this does not provide any proof that other consequences of the processing of C99I45F and C99V50F mutants (changed  $A\beta_{40}$  levels, possible changed AICD levels) are not responsible for some of the observed effects. Increased  $A\beta_{42}$  levels are usually accompanied by reduced  $A\beta_{40}$  levels. So effects of increased  $A\beta_{42}$  could also be caused by reduced  $A\beta_{40}$  levels (and vice versa). Moreover, it cannot be ruled out that increased  $A\beta_{42}$  *and* reduced  $A\beta_{40}$  levels act synergistically. For these reasons the term " $A\beta_{42}/A\beta_{40}$  ratio" is mostly used in this thesis and might be more suitable than just speaking about  $A\beta_{42}$  levels.

It has to be expected that  $A\beta_{42}/A\beta_{40}$  and the AICDs are similarly produced by processing, thus the possibility of effects being mediated by non- $A\beta$  mechanisms is rather likely.

The models presented in this thesis were derived from microarray data and real-time PCR and thus reflect changes on the transcript level. For the model “Downregulation of IGF2/IGF1R/PKC and PI3K/AKT signaling by an increased  $A\beta_{42}/A\beta_{40}$  ratio”, microarray data were supported by data about the phosphorylation status of crucial proteins (determined by immunoblotting with phospho-specific antibodies) also providing insight into the regulation on the protein-level. The models provide information about a changed C99 processing. This is comparable to C99 processing *in vivo*. However, these models are derived from cell culture experiments and are not validated *in vivo*. Thus, further *in vivo* research is necessary. The models are in line with many observations of the brains of AD patients and might reflect the molecular basis of some of the pathological mechanisms for which an explanation has been missing. The use of human cells in this thesis is an advantage over studies using cells from animals: Signal transduction pathways differ partially between mice and humans and a cure for AD that works in mice will not necessarily work in humans as well. For these reasons data on human cells are important. Moreover, the data in this thesis can be better compared with association studies of families suffering from AD than data derived from mice.

## 6.2 Data analysis with different algorithms

The use of different algorithms has an extreme impact on the data obtained. In this thesis I used three of the most frequently used algorithms (MAS 5, GC-RMA, PLIER), with the goal of obtaining complementary information, rather than to obtain a big overlap. This procedure increases the probability of getting a *maximal amount of significant data*. I favoured the recently developed PLIER-algorithm for several reasons: Most importantly, the intersection of calculated data (transcript level) with the data derived from a proteomic approach was the biggest when the data were analyzed with the PLIER-algorithm. Moreover, the PLIER-algorithm provides the best balance of accuracy and precision [140]. In addition PLIER appeared to be superior to other algorithms in avoiding false positives with poorly performing probe sets [141]. Furthermore, all genes tested by real-time PCR, which were selected by using the PLIER algorithm (9 genes), could be validated by real-time PCR in all cell clones. Nevertheless, *I emphasize that data derived from the MAS 5 and GC-RMA algorithm provide further information that could not be obtained by using the PLIER algorithm. In conclusion, the data demonstrates that it is necessary to calculate raw data with*

*more than one algorithm, in order to obtain a maximal amount of information while reducing the risk of overlooking important data. This increases the number of candidate genes.* The identified candidate genes needed to be functionally verified. Since verification of all candidate genes was not feasible, due to their large number, it cannot be excluded that some of the presented top candidate genes (which were not functionally verified) are not associated to any pathological mechanism of AD (but possibly appear dysregulated caused by unspecific effects). So further functional verification of these genes is necessary. To validate the approach, one candidate gene (CRABP1, which was also identified on the protein level through a proteomic approach) was selected and examined in detail. This showed that the approach identified the genes correctly and consequently essential cellular functions (here cellular differentiation).

### **6.3 An altered $A\beta_{42}/A\beta_{40}$ ratio has a strong impact on gene expression**

As can be seen from the distribution of differentially expressed genes (volcano plots, Fig. 5.5 A, B, page 42) the number of up-regulated genes was bigger than the number of down-regulated genes in consequence of an increased  $A\beta_{42}/A\beta_{40}$  ratio (Fig. 5.5 A). An inverse distribution could be observed if the ratio was decreased: the number of down-regulated genes was bigger than the number of up-regulated genes in consequence of a decreased  $A\beta_{42}/A\beta_{40}$  ratio (Fig. 5.5 B). These distributions provide hints about the general activation/inhibition of transcription. However, it has to be taken into consideration that among the up-regulated genes there might occur genes which have inhibiting properties, whereas among the down-regulated genes there might occur genes which have activating properties. So it was necessary to analyze every strongly differentially expressed gene separately.

## **6.4 Retinoic acid, AD and neurogenesis**

### **6.4.1 Retinoic acid, APOE4, APOE2**

Taking up retinoids, transport, storage and conversion into retinoic acid (RA) is a highly regulated process known as the “retinoid cascade” [195]. Retinoid availability is influenced by environmental factors and diet. As a nutritional vitamin necessary for life but not produced within the body, retinoid must be ingested from plants as beta-carotene, as preformed retinyl esters, and as retinol from animal origin (liver and fish oil). Vitamin A showed anti-amyloidogenic and fibril-destabilizing effects in vitro [205] and it was shown that disruption of the retinoid signaling pathway causes a

deposition of A $\beta$  in the adult rat brain [206]. RA amounts are determined by the supply of retinoids in the food, their transport to the brain and within the cells, and the production and removal of the functional end product of the retinoid cascade. Diffusion at high-retinyl ester concentrations of retinol into cells of the nervous system is enabled by other transporters, including apolipoprotein E (APOE) and apolipoprotein D (APOD). The retinyl ester/APOE complex has a crucial impact on the transcription of retinoid-regulated target genes. The APOE2 allele clears postprandial chylomicron remnants containing retinyl esters more slowly than APOE3 or APOE4 [207]. As a consequence retinyl esters are more abundant in the presence of the APOE2 allele. APOE2 is protective against late onset Alzheimer's disease (LOAD) and has been shown to protect against memory impairment in rats. APOE4 is strongly associated with an increased risk of AD of both early and late onset AD in genetic and clinical trials. APOD expression is regulated by retinoic acid receptor A (RARA) and increased in stressed neurons of LOAD patients. It was suggested that the increased expression may be the result of a feedback mechanism as a consequence of the reduced amounts of retinol in ageing individuals, particularly those at risk of LOAD. APOE2, which slowly clears retinyl esters may be a preferred carrier of retinol to brain in contrast to APOE4 which rapidly clears retinyl esters and preferentially transports low density lipoprotein cholesterol. The RBPs (retinol binding proteins) are able to carry retinol alone as well as complexed with transthyretin (TTR). TTR is probably the major carrier of retinol bound to RBP from liver stores through plasma [209, 210] and across the choroid plexus to the brain [211].

#### **6.4.2 Association between AD and RA**

Associations between AD and RA-transport and metabolism are known [196, 212]. It was shown that disruption of the retinoid signaling pathway causes a deposition of A $\beta$  in the adult rat brain [206]. RA amounts are determined by many regulatory proteins, like retinoid binding proteins, retinoid anabolizing and catabolizing enzymes [195]. *CYP26B1* has been linked to AD and psychosis [213]. One crucial mechanism whereby availability of RA is regulated is by binding to CRABP1 (cellular retinoic acid binding protein 1). CRABP1 is a protein with a molecular weight of 15.4 kDa, localized in the cytoplasm. The gene is strongly conserved in evolution and assumed to play an important role in RA-mediated differentiation and proliferation processes. It may regulate the access of RA to the nuclear RA receptors (RAR). In the adult brain the two main regions of RA signaling are the olfactory bulb and the hippocampus [214], both regions are predominantly affected in LOAD [195]. CRABP1 and RA are inversely regulated [215]. CRABP1 binds RA and prevents it from entering the

nucleus and in cells with low CRABP1 expression RA enters the nucleus and binds to RARs [216-218]. An association between CRABP1 and A $\beta$  has not yet been established. In this study I demonstrated that an increased A $\beta_{42}$ /A $\beta_{40}$  ratio resulted in CRABP1 upregulation on the transcript and on the protein-level. Furthermore, I demonstrated that up-regulated CRABP1 reduced the differentiation potential of SH-SY5Y cells. C99I45F-transfection of SH-SY5Y cells resulted in differentiation only if exposed to 100 nM or more of RA, but the same cell line already showed strong differentiation at 1 nM RA when CRABP1 was knocked down by >50%. Therefore, it was estimated that a 50% knockdown of CRABP1 makes cells more sensitive to RA by a factor of approximately  $10^1$ - $10^2$ . The physiological plasma concentration of RA in humans is approximately 10 nM and 8.4 pmol/g in the hippocampi of mice [219]. Excess of exogenous RA may oversaturate the binding capacities of CRABP1 allowing the remaining RA to bind to the RARs [220]. This provides an explanation for our finding that treatment with an excess of RA (>100 nM) makes no difference in the differentiation behavior detectable, but differences are evident at low (physiological) levels of RA. CRABP1 transfection of AMC-HN-7 cells results in an increased Cyp26-mediated catabolism of RA [156]. This decreases the RA level accessible to the nuclear receptors. Indeed I found Cyp26B1 to be up-regulated in C99I45F (A $\beta_{42}$ /A $\beta_{40}$ ↑), but not in C99V50F (A $\beta_{42}$ /A $\beta_{40}$ ↓). RORB (RAR-related orphan receptor B) was down-regulated in C99V50F, but not in C99I45F. Furthermore, RARB (RA receptor beta) was not differentially regulated in C99V50F, but up-regulated in C99I45F. These observations might reflect a response of the cells to an increased RA-level in C99V50F or a decreased RA-level in C99I45F respectively. An inverse regulation of receptors and their ligands is often observed [221].

#### **6.4.3 Linkage of the chromosomal locus 15q24 to mental retardation**

CRABP1 is located on the same chromosomal locus (15q24) as alpha polypeptide 3, 4 and 5 of the nicotinic cholinergic receptor (nAChR) and cytochrome P450, subfamily XIA (cholesterol side chain cleavage, Cyp11A1). Association of nAChR and AD has been described [222]. Moreover, there has been found to be a linkage of the chromosomal locus 15q24 to mental retardation [223] and linkage of the flanking regions (15q22 and 15q26) to AD [224, 225]. This linkage may be explained by the presence of alpha polypeptide 3, 4 and 5 of nAChR or of CRABP1, located on the same chromosomal locus.

#### **6.4.4 Neurofilaments were inversely regulated by C99 and A $\beta$ <sub>42</sub>, A $\beta$ <sub>40</sub>**

Downregulation of the neurofilaments NEF3, NEFL and INA was observed as a result of C99-overexpression. Interestingly, these three neurofilaments were up-regulated in response to A $\beta$ <sub>42</sub> and A $\beta$ <sub>40</sub>-overexpression. This may indicate a role of NEF3, NEFL and INA in the axonal “clogging” phenomenon [226-229] observed in neurons induced by A $\beta$ PP or its cleavage products [230].

#### **6.4.5 Role of neurogenesis in AD**

Neurogenesis is reported to be enhanced in the hippocampi [231] of patients with AD [232] where it may generate cells to replace neurons lost in the disease [233]. The effect of AD on neurogenesis could be reproduced in a transgenic mouse model [234] in which A $\beta$ PP mutations lead to increased incorporation of BrdU and expression of immature neuronal markers in two neuroproliferative regions: the dentate gyrus and the subventricular zone. As neurogenesis is increased in these mice in the absence of neuronal loss, it might be triggered by more subtle disease manifestations, for example the initial accumulation of the A $\beta$  peptide. In transgenic mice, overexpressing familial AD variants of A $\beta$ PP and/or PS1 dramatically diminished survival of newborn neurons *4 weeks after birth* [235]. These data hint at an increased neurogenesis in AD, but in contrast to this, also point to early detrimental events shortly after the neurons are born.

#### **6.4.6 Sensitive balance between proliferation and differentiation is influenced by an altered A $\beta$ <sub>42</sub>/A $\beta$ <sub>40</sub> ratio via CRABP1**

Treating neural stem cells with A $\beta$  increases the total number of neurons in a dose-dependent manner [236]. In our study neuroblastoma cells were used, which shared related proliferation and differentiation properties with neural stem cells. We observed increased proliferation of human neuroblastoma cells in consequence of an increased A $\beta$ <sub>42</sub>/A $\beta$ <sub>40</sub> ratio via CRABP1 and suggest that this influences neurogenesis by promoting proliferation. However, the newly generated neurons may be prevented from adopting a functional phenotype, as a consequence of CRABP1 upregulation restricting the quantity of RA. This view is supported by a study showing that RA induces neurite outgrowth in SH-SY5Y cells [237]. Theoretically, it seems possible that CRABP1 knockdown would release the block of terminal differentiation of neurons in AD and thus improve the differentiation of neural stem cells into a functional phenotype.

In summary, it was observed that an increased  $A\beta_{42}/A\beta_{40}$  ratio up-regulated CRABP1, reducing the availability of free RA. This resulted in an increased tendency towards proliferation, accompanied by a reduced potential to differentiate. This effect could be rescued by knocking down CRABP1. It can be speculated that, *in vivo*,  $A\beta_{42}$  induces the initial steps in neurogenesis by boosting neuronal precursor cell proliferation while preventing the terminal differentiation into mature neurons. This scenario may provide an explanation for why there is an increase in neurogenesis in AD and at the same time an increased risk of neurodegeneration.

The ADAM10 gene encodes a membrane-bound disintegrin-metalloproteinase, which, after overexpression in an AD mouse model, prevents amyloid pathology and improves long term potentiation and memory. RA was identified as an inducer of human ADAM10 promoter activity [238]. This finding suggests that pharmacologic inhibition of CRABP1, and hence increased availability of RA, may increase the expression of the  $\alpha$ -secretase ADAM10, with beneficial effects on AD pathology. Furthermore, RA has been shown to protect hippocampal neurons from amyloid-beta induced neurodegeneration [239]. Elevated CRABP1 levels were detected in the cerebrospinal fluid of patients with Moyamoya disease [240]. Moyamoya disease is a occlusive disease of the cerebral vasculature, in which the blood supply to the brain is affected, resulting in frequent strokes. In an effort to circumvent these blockages, the body forms abnormal blood vessels (Moyamoya vessels) to reroute blood flow to the brain.

#### **6.4.7 Overlapping results obtained from different laboratories and different technologies increased reliability of the data**

Our results were derived from several independent clones with slightly varying expression. Thus clonal effects which can only be observed in a single clone, but not in others, can be regarded as minimized. Furthermore, two independent experimental approaches, transcriptomics and proteomics, led to highly similar results (CRABP1 was found to be the second most up-regulated transcript of approximately 20,000 ones tested on Chip A, and the second most up-regulated protein of the whole proteome in consequence of an increased  $A\beta_{42}/A\beta_{40}$  ratio). Transcriptomics and proteomics were carried out by two independent laboratories and the time interval between these two approaches was nearly three years, minimizing the probability that cell culture conditions or preparation procedures caused a bias in our data. The genomic approach was performed first and the subsequent proteomic approach was performed blind.

#### 6.4.8 Target genes of retinoic acid (RA) indicate low levels of RA for $A\beta_{42}/A\beta_{40}\uparrow$ , but high levels for $A\beta_{42}/A\beta_{40}\downarrow$

A meta-analysis was performed with the goal of identifying target genes of retinoic acid [241]. Therefore, published data from 1191 papers covering 532 genes were investigated. I compared the most differentially expressed genes (from the comparisons  $A\beta_{42}/A\beta_{40}\uparrow$  and  $A\beta_{42}/A\beta_{40}\downarrow$ ) with the genes identified by Balmer et al.. There were more overlapping genes than could be expected by chance, indicating a predominant role for RA. For instance the following genes are *induced* by RA, according to Balmer et al. : PLAT, TGFBR2, ACTA2, BCL2, GAP43, TGF $\beta$ 2, ITGB5. Interestingly, I found the following genes to be *down*-regulated for  $A\beta_{42}/A\beta_{40}\uparrow$ : TGFBR2, ITGB5. In contrast to this the following genes were *up*-regulated for  $A\beta_{42}/A\beta_{40}\downarrow$ : PLAT, ACTA2, BCL2, GAP43. This is in line with my view that up-regulated CRABP1 (for  $A\beta_{42}/A\beta_{40}\uparrow$ ) suppresses the effects of RA.

#### 6.5 Downregulation of the IGF2/IGF1R/PKC and PI3K/AKT survival pathways as a result of an increased $A\beta_{42}/A\beta_{40}$ ratio

It was shown that IGF2 and insulin are normally produced in the central nervous system and that their expression levels are markedly reduced in AD. These abnormalities were associated with reduced levels of phosphatidylinositol 3-kinase and phospho-Akt (activated), increased GSK3 $\beta$  activity and APP-mRNA expression. The strikingly reduced central nervous system (CNS) expression of genes encoding insulin, IGF1, and IGF2, as well as the insulin and IGF1 receptors, suggested that AD may represent a neuro-endocrine disorder that resembles diabetes mellitus. Therefore, the name "Type 3 diabetes" was proposed for AD [191].

The PI3K/AKT survival pathway is known to be activated by insulin, growth factors, integrins and other molecules [242, 243] and crosstalk to IGF2/IGF1R/PKC signaling is known [242, 244, 245]. I identified the PI3K/AKT survival pathway and IGF2/IGF1R/PKC signaling as down-regulated in consequence of an increased  $A\beta_{42}/A\beta_{40}$  ratio. As can be seen from the model (see Fig. 5.35, pages 78-79), the PI3K/AKT pathway is activated by different molecules, most of which have been found to be down-regulated as a result of an increased  $A\beta_{42}/A\beta_{40}$  ratio (C99I45F/C99WT), whereas the same molecules were not regulated or even up-regulated as a result of a decreased  $A\beta_{42}/A\beta_{40}$  ratio (C99V50F/C99WT): Some of these molecules, HGF and several integrins (ITGB5 is a receptor for fibronectin), target the PI3-kinase [246-251]. This pathway is known to be especially activated by

insulin, IGF1 or IGF2 via the IGF1 receptor [164, 166]. IGF2 was found to activate the IGFR1 with an affinity similar to IGF1 [252] and the PI3K/AKT pathway was demonstrated to be activated by IGF2 [245]. Increasing insulin-related signals in neurons reduces GSK3 $\beta$  activity by improving PI3K/Akt activity [245]. (Furthermore, apoptosis-inducing genes were up-regulated for A $\beta$ <sub>42</sub>/A $\beta$ <sub>40</sub>↑, for instance TNFAIP6 and TRAF5, but not for A $\beta$ <sub>42</sub>/A $\beta$ <sub>40</sub>↓). IGF2 was among the 10 most down-regulated genes as a result of an increased A $\beta$ <sub>42</sub>/A $\beta$ <sub>40</sub> ratio (C99I45F/C99WT). The fact that downregulation of IGF2 was detected by two probe sets validates the downregulation. There is a plethora of further indications of PI3K/AKT downregulation not only on the transcript but also on the protein and phosphorylation level. From the view of an increased A $\beta$ <sub>42</sub>/A $\beta$ <sub>40</sub> ratio (C99I45F/C99WT), the following molecules targeting different steps of the pathway, are assumed to down-regulate it synergistically: PTEN was up-regulated and inhibits PIP3 [253, 254]. The effect of TrkB, normally known to activate AKT [160, 255, 256], can be assumed to be less active by binding of the ligands BDNF and neurotrophins 3, 4, 5 to the strongly *up-regulated non-catalytic* isoform of TrkB (a competitive binding of these ligands between catalytic and non-catalytic isoforms can be assumed; truncated TrkB receptors have been shown to inhibit BDNF-induced neurite outgrowth in vitro [257]). In contrast to this, a *decreased* A $\beta$ <sub>42</sub>/A $\beta$ <sub>40</sub> ratio *down-regulated the non-catalytic* isoform of TrkB. This up and downregulation was validated by detection of the transcript for the non-catalytic isoform of TrkB by more than one probe set (see information below). Moreover, AKT1 (protein kinase B) showed weaker phosphorylation (n=1) for mutant C99I45F than for C99WT.

I found IGFBP1 up-regulated (increased A $\beta$ <sub>42</sub>/A $\beta$ <sub>40</sub> ratio, C99I45F/C99WT), whereas no differential expression was observed for a decreased A $\beta$ <sub>42</sub>/A $\beta$ <sub>40</sub> ratio, (C99V50F/C99WT). Unlike insulin, both IGF1 and IGF2 circulate in plasma tightly bound to specific binding proteins. Two major forms of IGF-binding proteins have been identified in human plasma, a low molecular weight form and a high molecular weight form. The low molecular weight IGF-binding protein (IGFBP1) binds both IGF1 and IGF2 with high affinity [258]. In primary cultures of human fetal hepatocytes under hypoxic conditions, IGFBP1 mRNA expression increased 3 to 4-fold compared with normoxic controls. Western blot analysis of conditioned medium revealed the presence of IGFBP1, IGFBP2, IGFBP3, and IGFBP4. IGFBP1 was the most abundant IGFBP in conditioned medium. The authors concluded that hypoxia up-regulates fetal hepatocyte IGFBP1 mRNA levels and protein [259]. Using loss and gain-of-function approaches with zebrafish embryos, Kajimura et al. (2005) demonstrated that IGFBP1 mediated hypoxia-induced embryonic growth retardation and developmental delay. When tested in vitro with cultured zebrafish embryonic

cells, IGFBP1 itself had no mitogenic activity, but it inhibited IGF1 and IGF2-stimulated cell proliferation by binding to and inhibiting the activities of IGFs [258].

MBNL2 (muscleblind-like 2 (Drosophila)) was found to be inversely expressed as a result of a changed  $A\beta_{42}/A\beta_{40}$  ratio (up-regulated as consequence of an increased  $A\beta_{42}/A\beta_{40}$  ratio, C99I45F/C99WT, down-regulated as consequence of a decreased  $A\beta_{42}/A\beta_{40}$  ratio, C99V50F/C99WT). MBNL2 is a zinc finger protein that regulates alternative splicing of two pre-mRNAs that are misregulated in myotonic dystrophy. It was demonstrated that small interfering RNA-mediated downregulation of MBNL2 in myoblasts results in abnormal insulin receptor (IR) splicing [260].

Further clues for altered insulin-signaling are the inversely regulated uncharacterized gene KIAA0644. There is a relatively strong similarity (34%) to insulin-like growth factor-binding protein complex acid labile chain precursor. KIAA0644 was up-regulated as a result of an increased  $A\beta_{42}/A\beta_{40}$  ratio, but down-regulated as a result of a decreased  $A\beta_{42}/A\beta_{40}$  ratio. KIAA0644 is assumed to be a secreted protein that may have an important role in regulating the access of circulating insulin growth factors to the tissues. KIAA0644 is assumed (due to similarity to Insulin-like growth factor-binding protein complex acid labile chain) to form a ternary complex of about 140 to 150 kda with IGF2 and/or IGFBP3 [261]. I speculate that KIAA0644 binds IGF2 and keeps it in an inactive state or lowers its ability to bind to the IGF receptor.

Target genes of the PI3K/AKT-pathway were found to be down-regulated as a result of an increased  $A\beta_{42}/A\beta_{40}$  ratio (C99I45F/C99WT), for instance cyclin D1. I observed downregulation of cyclin D1 on the transcript level and on the protein level, whereas cyclin D1 was up-regulated as a result of a decreased  $A\beta_{42}/A\beta_{40}$  ratio (C99V50F/C99WT).

Finally it can be concluded that a plethora of molecules known to activate the PI3K/AKT-pathway are down-regulated and inhibiting effects or missing activation converge towards PI3K/PIP3/AKT. Many molecules known to inhibit this pathway were up-regulated. Important downstream components of this pathway, known to be inhibited by AKT1 (by reduced phosphorylation), like GSK3 ( $\alpha$  and  $\beta$ ), might be activated by downregulation of AKT1. Further components, known to inhibit GSK3 were also less active (PKC lambda/iota), which further contribute to activation of GSK3.

## 6.6 Downregulation of the IGF2-H19 imprinted region on chromosome 11p15.5 as a result of an increased A $\beta$ <sub>42</sub>/A $\beta$ <sub>40</sub> ratio

It is intriguing that these genes (IGF2, H19, CDKN1C, LOC492304) known to be imprinted (see Chapter 5.7, page 58) were especially prominent among the most down-regulated ones. The IGF2 (insulin-like growth factor 2) gene encodes a member of the insulin family of polypeptide growth factors that is involved in development and growth. It is an *imprinted* gene and is expressed only from the paternally inherited allele. Two alternatively spliced transcript variants encoding the same protein have been found for this gene. Symmetric and asymmetric DNA methylations in the human IGF2-H19 imprinted region have been detected [262]. Enhancers specifically activate *IGF2 on the paternal chromosome and H19 on the maternal chromosome* [263]. Interaction between differentially methylated regions partitions the imprinted genes IGF2 and H19 into parent-specific chromatin loops [264]. Interaction of IGF2 with multiple plasma proteins has been observed: high affinity binding of plasminogen to IGF2 and IGF binding protein 3. Transferrin binds insulin-like growth factors and affects binding properties of insulin-like growth factor binding protein 3 [380].

H19 is an imprinted maternally expressed untranslated mRNA. Mutter et al. found that H19 is expressed only from the maternal allele and IGF2 is expressed from the paternal allele. The oppositely imprinted genes H19 and IGF2 have been shown to be coexpressed in the human androgenetic trophoblast [265]. These results demonstrated that a biparental genome may be required for expression of the reciprocal IGF2/H19 imprint. In the mouse, the imprinted H19 gene, which encodes an untranslated RNA, lies at the end of a cluster of imprinted genes. Leighton et al. found that imprinting of the insulin2 (INS2) gene and the IGF2 gene, which lie about 100 kb upstream of H19, can be disrupted by maternal inheritance of a targeted deletion of the H19 gene and its flanking sequence [266]. Pfeifer et al. stated that the product of the H19 gene is an untranslated RNA that is expressed exclusively from the maternal chromosome during mammalian development. The H19 gene and its 5'-flanking sequence are required for the genomic imprinting of 2 paternally expressed genes in mice, INS2 and IGF2 that lie 90 and 115 kb 5-prime to the H19 gene, respectively [267]. Imprinted genes are expressed from only 1 of the parental alleles and are marked epigenetically by DNA methylation and histone modifications. The paternally expressed gene IGF2 is separated by approximately 100 kb from the maternally expressed noncoding gene H19 on mouse distal chromosome 7. Differentially methylated regions in IGF2 and H19 contain chromatin boundaries,

silencers, and activators, and regulate the reciprocal expression of the 2 genes in a methylation-sensitive manner by allowing them exclusive access to a shared set of enhancers. Murrell et al. used a GAL4 knock-in approach as well as the chromosome conformation capture technique to show that the differentially methylated regions in the imprinted genes IGF2 and H19 interact in mice. These interactions are genetically regulated and partition maternal and paternal chromatin into distinct loops. This generates a simple epigenetic switch for IGF2, through which it moves between an active and a silent chromatin domain [264]. It is believed that chromosomes interact with each other to regulate transcription in trans. To explore systematically the epigenetic dimension of such interactions, Zhao et al. devised a strategy termed 'circular chromosome conformation capture' (4C). This approach enabled high-throughput screening of physical interactions between chromosomes without a preconceived idea of the interacting partners. *The authors identified 114 unique sequences from all autosomes, several of which interact primarily with the maternally inherited H19 imprinting control region.* Imprinted domains were strongly overrepresented in the library of 4C sequences, further highlighting the epigenetic nature of these interactions. Moreover, Zhao et al. found that the direct interaction between differentially methylated regions was linked to epigenetic regulation of transcription in trans. They found that the patterns of interactions specific to the maternal H19 imprinting control region underwent reprogramming during in vitro maturation of embryonic stem cells [268].

Hatada and Mukai showed that a mouse homolog of p57(KIP2) is genomically imprinted. The paternally inherited allele is transcriptionally repressed and methylated. The mouse gene maps to the distal region of chromosome 7, within a cluster of imprinted genes, including IGF2 and H19 [269]. Matsuoka et al. demonstrated that the p57(KIP2) gene is imprinted in humans as well. It is situated 500 kb centromeric to the IGF2 gene. The maternal allele is preferentially expressed; However, the imprint is not absolute, as the paternal allele is also expressed at low levels in most tissues and at levels comparable to the maternal allele in fetal brain and some embryonal tumors. It appears to lie in a domain containing other imprinted genes [270]. Matsuoka et al. commented that establishment of an imprint may be coordinately regulated throughout the entire domain, as suggested by similar tissue-specific expression and imprinting patterns of IGF2, H19, and p57(KIP2) genes, while loss of imprinting may not necessarily affect the entire region [270]. Du et al. confirmed the existence of insulators in the differentially methylated region (DMR) of the H19 gene and reported 2 insulators in the IGF2 gene. They also found 2 novel silencer sequences: one in KvDMR, a region that is thought to contain the promoter for the KCNQ1OT1 transcript, and the other in CDKN1C. The authors demonstrated

binding of the zinc finger protein CTCF in vitro to all the insulators and sequences detected [271]. Using primary human hematopoietic cells and microarray analysis, Scandura et al. identified p57 (KIP2) as the only cyclin-dependent kinase inhibitor induced by TGF- $\beta$ . Upregulation of p57 mRNA and protein occurred before TGF- $\beta$ -induced G1 cell cycle arrest, required transcription, and was mediated via a highly conserved region of the proximal p57 promoter. Upregulation of p57 was essential for TGF- $\beta$ -induced cell cycle arrest in these cells, since 2 different small interfering RNAs that prevented p57 upregulation blocked the cytostatic effects of TGF- $\beta$  on hematopoietic cells [272]. The putative insulin-like growth factor 2 associated gene (LOC492304) encodes a member of the insulin family of polypeptide growth factors that is involved in development and growth. It is an *imprinted* gene and is expressed only from the paternally inherited allele.

### **6.7 The *non-catalytic* TrkB receptor was strongly up-regulated in response to an increased A $\beta$ <sub>42</sub>/A $\beta$ <sub>40</sub> ratio and might have suppressed the effects of neurotrophins on cell survival and LTP in a competitive manner**

NTRK2 (synonym:TrkB) is a member of the neurotrophic tyrosine receptor kinase (NTRK) family. It is a membrane-bound receptor that, upon neurotrophin binding, phosphorylates itself and members of the MAPK pathway. Signaling through this kinase leads to cell differentiation. Mutations in its gene have been associated with obesity and mood disorders. Alternate transcriptional splice variants encoding different isoforms have been found for this gene [273]. TrkB and its ligands influence neuronal survival, differentiation, synaptogenesis, and maintenance. Decreased BDNF and full-length TrkB expression accompanied by *increased truncated TrkB expression, as revealed by Western blotting, was observed in the (postmortem) frontal cortex of patients with AD*. Strong BDNF immunoreactivity was observed in dystrophic neurites surrounding senile plaques (postmortem frontal cortex). Moreover increased truncated TrkB immunoreactivity was observed in frontal cortex of patients with AD [274]. Differential regulation of catalytic and non-catalytic trkB messenger RNAs was observed in the rat hippocampus following seizures induced by systemic administration of kainate [275]. Hybridization with probes specific for the non-catalytic trkB receptor and the catalytic trkB receptor revealed that the increases at four and seven days in the molecular layers of the hippocampus reflected an upregulation of only the non-catalytic form of the receptor [276]. *Truncated TrkB receptors have been shown to inhibit BDNF-induced neurite outgrowth in vitro [257]*.

*There is growing evidence suggesting that the naturally occurring truncated TrkB receptors have dominant inhibitory effects on brain-derived neurotrophic factor signaling [277] and it was suggested that the truncated TrkB receptors negatively influence neuron survival by interfering with the function of catalytic TrkB receptors [278]. Expression of the catalytic TrkB alone conferred a BDNF survival response whereas co-expression of non-catalytic TrkB substantially reduced this response and it was suggested that BDNF responsiveness in sensory neurons during development is modulated by the relative levels of catalytic and non-catalytic TrkB [273]. BDNF, neurotrophin 3 and neurotrophin 4/5 levels in the brain are fine-tuned and kept constant. Due to the fact that these neurotrophins do not occur in excess they are ideal regulatory molecules which can be controlled by binding to their appropriate receptors: There might be competition between the catalytic and non-catalytic isoform of the TrkB-receptor for their ligands. In response to an increased  $A\beta_{42}/A\beta_{40}$  ratio, the non-catalytic isoform of TrkB was found to be strongly up-regulated. The up-regulated non-catalytic isoform is supposed to compete with the not differentially expressed catalytic isoform for their ligands. Binding of the neurotrophins to the non-catalytic isoform reduces the amount of them available for binding to the catalytic isoform. Thus the signal transduced from the receptor to the nucleus should be reduced. Diminished signaling from the TrkB receptor has been demonstrated to suppress cell survival and LTP [279-281].*

In contrast to this, a decreased  $A\beta_{42}/A\beta_{40}$  ratio down-regulated the non-catalytic isoform of TrkB (while leaving the catalytic isoform unaffected). The up and downregulation of the non-catalytic isoform of TrkB was validated by the detection of the transcripts for the non-catalytic isoform of TrkB by three different probe sets (see Table 5.20, page 112).

The effect of TrkB, normally known to activate AKT, can be assumed to be less active by binding of the ligands BDNF and neurotrophins 3, 4, 5 to the strongly up-regulated non-catalytic isoform of TrkB (for an increased  $A\beta_{42}/A\beta_{40}$  ratio; a competitive binding of these ligands between catalytic and non-catalytic isoforms can be assumed). In contrast to this, a decreased  $A\beta_{42}/A\beta_{40}$  ratio down-regulated the non-catalytic isoform of TrkB. This up and downregulation was validated by detection of the transcript for the non-catalytic isoform of TrkB by more than one probe set, thus increasing the reliability of the data.

## 6.8 Up-regulated ATP7A, a copper transporting ATPase is expected to dysregulate copper levels in consequence of an increased A $\beta$ <sub>42</sub>/A $\beta$ <sub>40</sub> ratio

It has been shown that APP modulates copper-induced toxicity and oxidative stress in primary neuronal cultures. APP can reduce copper (II) to copper (I) in a cell-free system potentially leading to increased oxidative stress in neurons, suggesting APP may interact with copper to induce a localized increase in oxidative stress through copper (I) production. Substitution of the copper coordinating histidine residues with asparagines (APP142-166, H147N, H149N, H151N) abrogates the toxic effects. These data support a role for the APP copper-binding domain in APP-mediated copper (I) generation and toxicity in primary neurons, a process that has important implications for AD and other neurodegenerative disorders [282].

High concentrations of copper are found in the vicinity of A $\beta$  amyloid deposits in AD. It was reported that Cu(II) markedly potentiates the neurotoxicity exhibited by A $\beta$  in cell culture. The potentiation of toxicity is greatest for A $\beta$ <sub>1-42</sub> > A $\beta$ <sub>1-40</sub> >> mouse/rat A $\beta$ <sub>1-40</sub>, corresponding to their relative capacities to reduce Cu(II) to Cu(I), to form H<sub>2</sub>O<sub>2</sub> in cell-free assays and to exhibit amyloid pathology [283]. It was shown that human A $\beta$  directly produces hydrogen peroxide (H<sub>2</sub>O<sub>2</sub>) by a mechanism that involves the reduction of metal ions, like Cu(II). These findings indicate that the accumulation of A $\beta$  could be a direct source of oxidative stress in AD [284].

Copper is essential for human health, however copper imbalance is a key factor in the etiology and pathology of several neurodegenerative diseases. The copper-transporting ATP7A is a key molecule required for the regulation and maintenance of mammalian copper homeostasis. Its malfunction leads to the genetically inherited disorders, Menkes and Wilson's diseases, respectively. ATP7A has a dual role in cells, namely to provide copper to essential cuproenzymes and to mediate the excretion of excess intracellular copper. A unique feature of ATP7A is its ability to sense and respond to intracellular copper levels, the latter manifested through their copper-regulated trafficking from the transGolgi network to the appropriate cellular membrane domain (basolateral or apical, respectively) to eliminate excess copper from the cells [285]. Raised copper concentrations result in the trafficking of ATP7A to the plasma membrane, where it functions in copper export.

A role for ATP7A and/or copper in axon outgrowth and synaptogenesis has been demonstrated [286].

ATP7A exports copper from cells and thus critically contributes to the homeostatic control of copper [287]. The trafficking of ATP7A from the *trans*-Golgi network to endocytic vesicles in response to various signals allows the balancing of intracellular

copper levels. ATP7A uses the energy of ATP hydrolysis to transport copper from the cytosol into the secretory pathway and thus supply the metal for subsequent biosynthetic incorporation into various copper-dependent enzymes. The localization in the *trans*-Golgi network (TGN), which is observed for ATP7A under low copper conditions, reflects its role in the delivery of copper to copper-dependent enzymes.

The exporting of copper from the cell requires trafficking of ATP7A from the TGN to vesicles. This re-localization occurs in response to copper elevation, hormone release, or other signaling and developmental events. The vesicles then fuse with the plasma membrane releasing copper into the extracellular space. The regulation of intracellular localization of ATP7A represents the key mechanism that determines whether the ATP7A performs its homeostatic or biosynthetic function at a given moment. The function of ATP7A is *to translocate copper across the membrane from the cytosol into the lumen of the appropriate intracellular compartment (either TGN or vesicles)*. This copper translocation across the membranes is driven by the hydrolysis of ATP. Copper binds to the N-terminal cytosolic sites of ATP7A in the reduced Cu(I) form and it is thought that copper is translocated across the membrane in that form. This process takes place in the lumen of the *trans*-Golgi network, i.e. at the site of copper release from the transporters. It has previously been reported that the biosynthesis of secreted copper containing enzymes, such as SOD1, correlates well with the rate of copper incorporation into these proteins (SOD1 was found to be up-regulated in consequence of an increased  $A\beta_{42}/A\beta_{40}$  ratio, shown by immunoblotting in this thesis). Although the rate of apo-protein production and secretion is not affected by copper levels, the amount of holo-protein is greatly diminished when copper is limited. The close link between the copper transporter activity and the biosynthesis of copper-dependent enzymes is also emphasized by a correlation in their expression levels and developmental co-regulation. Trafficking (from the TGN to vesicles) may be initiated when the amount of copper transported into the secretory pathway exceeds the biosynthetic needs of a cell.

ATP7A was up-regulated in consequence of an increased  $A\beta_{42}/A\beta_{40}$  ratio (and down-regulated for a decreased ratio). Further research is necessary to answer the question of whether *upregulation of ATP7A* is a direct consequence of an increased  $A\beta_{42}/A\beta_{40}$  ratio, or an indirect result of increased intracellular copper-levels, or the *reason for decreased intracellular copper-levels*. *In the latter case upregulation of ATP7A could be pathological and possibly a suitable target for a therapy (knock-down or pharmacological inhibition of ATP7A could increase copper concentrations to normal levels)*. In the other cases upregulation of ATP7A might be an attempt of the cells to expel excess copper from the cells. Copper levels are expected to be

decreased in brains of AD patients [288]. This is supported by the observation from White and colleagues who observed increased copper levels in mice brains in which APP or APLP2 was knocked out [289]. The APP and APLP2 molecules contain metal binding sites for copper and zinc. APP reduces copper (II) to copper (I) and this activity could promote copper-mediated neurotoxicity [289]. Furthermore it was demonstrated that double knockout of APP and APLP2 resulted in significant increases in copper accumulation in the primary cortical neurons of mice and embryonic fibroblasts. In contrast, over-expression of APP in transgenic mice resulted in significantly reduced copper levels in primary cortical neurons [290].

## 6.9 Proteases and protease inhibitors

### 6.9.1 Preface

Insufficient proteolytic removal of A $\beta$  by proteases such as neprilysin, endothelin-converting enzymes, insulin-degrading enzyme, angiotensin-converting enzyme, the plasmin system and matrix metalloproteases, has been proposed as a mechanism that leads to A $\beta$  accumulation in the brain [83-85]. For this reason proteases and their inhibitors were analyzed.

### 6.9.2 **ADAMTS9 was the most inversely regulated gene in response to a changed A $\beta_{42}$ /A $\beta_{40}$ ratio and it was found to be clustered with other proteases**

ADAMTS9 (a disintegrin and metalloproteinase with thrombospondin motifs) belongs to the ADAMTS family. Members of this family share several distinct protein modules, including a propeptide region, a metalloproteinase domain, a disintegrin-like domain, and a thrombospondin type 1 (TS) motif. Members of the ADAMTS family have been implicated in the *cleavage of proteoglycans*, the control of organ shape during development, and the inhibition of angiogenesis. ADAMTS9 is a secreted, cell-surface-binding metalloprotease that *cleaves the proteoglycans versican and aggrecan and binds Zn<sup>2+</sup> ions* [291]. Unlike most precursor proteins, the ADAMTS9 zymogen (pro-ADAMTS9) is resistant to intracellular processing. Instead, *pro-ADAMTS9 is processed by furin at the cell surface*. It is suggested that unlike other metalloproteases, furin processing of the ADAMTS9 propeptide reduces its catalytic activity [292]. Observations suggest that the propeptide is a key functional domain of ADAMTS9, mediating an unusual regulatory mechanism that may have evolved to ensure maximal activity of this protease at the cell surface. ADAMTS proteins are structurally homologous to ADAM proteins, but they also contain at least 1 C-terminal

thrombospondin type 1 (TSP1) repeat and are secreted rather than membrane bound.

ADAMTS9 was found to be clustered with other proteases and binding partners for APP: Here in this thesis, *NBL1* (neuroblastoma suppression of tumorigenicity 1) was found in the same cluster as prolylendopeptidase (PREP) *and it is a known binding partner for APP (770aa) and ubiquilin-1 (UBQLN1). (UBQLN1 modulates amyloid precursor protein trafficking and A $\beta$  secretion)*. PREP cleaves peptide bonds on the C-terminal side of prolyl residues within peptides that are up to approximately 30 amino acids long. Prolyl endopeptidases have been reported to be involved in the maturation and degradation of peptide hormones and neuropeptides. *PREP is believed to inactivate neuropeptides that are present in the extracellular space.* Immunocytochemical double-labelling procedures and localization of PREP-enhanced green fluorescent protein fusion proteins showed that PREP is mainly localized to the perinuclear space, and is *associated with the microtubulin cytoskeleton* in human neuroblastoma and glioma cell lines [293]. *Disassembly of the microtubules by nocodazole treatment disrupts both the fibrillar tubulin and PREP labelling. Furthermore, in a two-hybrid screen, PREP was identified as a binding partner of tubulin. These findings indicate new functions for PREP in axonal transport and/or protein secretion. In brains of young APP transgenic Tg2576 mice, hippocampal PREP activity was higher than in wild-type littermates in the pre-plaque phase but not in aged mice with beta-amyloid plaque pathology.* This "accelerated aging" with regard to hippocampal PREP expression in young APP transgenic mice might be one factor contributing to the observed cognitive deficits in these mice in the pre-plaque phase and could also explain in part the cognition-enhancing effects of PREP inhibitors in several experimental paradigms [294]. PREP is a proline-specific oligopeptidase with a reported effect on learning and memory in different rat model systems. Measuring different second-messenger concentrations revealed an inverse correlation between inositol 1,4,5-trisphosphate [Ins(1,4,5)P<sub>3</sub>] concentration and PREP expression.

### 6.9.3 Further proteases and protease inhibitors

The matrix metalloproteinase 8 (MMP8, neutrophil collagenase) was down-regulated ( $A\beta_{42}/A\beta_{40}\uparrow$ ) ( $p=0.00219$ , fold change=-5.0), but not differentially expressed when the ratio was decreased ( $A\beta_{42}/A\beta_{40}\downarrow$ ). MMP8 can degrade fibrillar type I, II, and III collagens. Collagenous Alzheimer amyloid plaque component collagen XXV (CLAC) [172] was observed in the brains of subjects with AD. CLAC is derived from a type II transmembrane collagen protein [173]. *Downregulation of the collagenase MMP8*

*may contribute to the maintenance of these plaques.*

The tissue inhibitor of metalloproteinase 3 (TIMP3) was up-regulated ( $A\beta_{42}/A\beta_{40}\uparrow$ ) ( $p=0.0263$ , fold change=1.7), but not differentially expressed when the ratio was decreased. *TIMP3 has specifically been shown to inhibit the actions of ADAM10 and ADAM17 [168, 169] two APP  $\alpha$ -secretases [170]. Very recently it has been demonstrated that TIMP3 immunoreactivity is increased in AD brains [171] and that TIMP3 treatment reduces  $\alpha$ -cleavage of APP and promotes  $\beta$ -cleavage, with significant increases in  $A\beta$  production [169].* The authors emphasized that there is a striking increase in TIMP3 in AD brains (but not in other neurodegenerative diseases) which raises the possibility that TIMP3 contributes to the elevated  $A\beta$  levels in AD, making its inhibition a potential target for therapeutic approaches to reducing  $A\beta$ . It may be speculated that up-regulated TIMP3, apart from  $\alpha$ -secretase inhibition, also inhibits the metalloprotease MMP8.

A disintegrin-like and metalloprotease (reprolysin ADAMTS3) was down-regulated ( $A\beta_{42}/A\beta_{40}\uparrow$ ,  $p=0.086$ , fold change=-2.1), but not differentially expressed when the ratio was decreased. ADAMTS3 is the major *procollagen II N-propeptidase*. ADAMTS3 induced procollagen I processing in fibroblasts, suggesting a role in procollagen I processing during musculoskeletal development [295]. The fact that ADAMTS3 was down-regulated ( $A\beta_{42}/A\beta_{40}\uparrow$ ) argues for increased collagen II and presumably collagen I levels ( $A\beta_{42}/A\beta_{40}\uparrow$ ).

ADAM22 was up-regulated ( $A\beta_{42}/A\beta_{40}\uparrow$ ,  $p=0.074$ , fold change=1.7), but not differentially expressed when the ratio was decreased. ADAM22 is one of three catalytically inactive ADAM family members highly expressed in the brain. ADAM22 has numerous splice variants and can act to inhibit cell proliferation, however, it has been suggested that it also acts as an adhesion protein. 14-3-3 protein members have been shown to bind to ADAM22. There might be a role for 14-3-3 proteins in targeting ADAM22 to the cell membrane by masking ER retention signals [296].

Protease serine 12 (PRSS12, neurotrypsin, motopsin) was up-regulated ( $A\beta_{42}/A\beta_{40}\uparrow$ ,  $p=0.00486$ , fold change=2.1) and confirmed by another probe-set ( $p=0.0008$ , fold change=2.0), but not differentially expressed when  $A\beta_{42}/A\beta_{40}$  was decreased. This gene encodes a member of the trypsin family of secreted serine proteases. Studies in mice suggest that PRSS12 may be involved in structural reorganizations associated with learning and memory and plays a role in neuronal plasticity. Molinari et al. studied the temporospatial expression of neurotrypsin by in situ hybridization in fetal human brain. Neurotrypsin was expressed from day 44 to 15 weeks of gestation. At 15 weeks the highest gene expression was detected in the cortical plate, the hippocampal formation, and the tegmental nuclei of the brainstem. In the

hippocampal formation, neurotrypsin was expressed in a spatial gradient. Staining was moderate in the subiculum and reached very high levels in areas CA3 and CA4 of the Ammon's horn. By electron microscopy, neurotrypsin was identified in the presynaptic nerve endings of cortical synapses [297].

TIMP1, previously described as an collagenase inhibitor, was down-regulated ( $A\beta_{42}/A\beta_{40}\uparrow$ ,  $p=0.127$ , fold change=-3.5), but not differentially expressed when the  $A\beta_{42}/A\beta_{40}$  ration was decreased. The TIMP1 gene is localized on chromosome Xp11.3-p11.23. Transcription of this gene is highly inducible in response to many cytokines and hormones. The proteins encoded by this gene family are natural inhibitors of the matrix metalloproteinases (MMPs), a group of peptidases involved in degradation of the extracellular matrix. Transcription of this gene is highly inducible in response to many cytokines and hormones. This gene is *located within intron 6 of the synapsin I gene and is transcribed in the opposite direction*.

Cathepsin D (CTSD), a lysosomal aspartyl protease, was previously mentioned in this thesis (because its gene is localized in an imprinted chromosomal region and is one of the top candidate genes for AD). It was not differentially expressed for  $A\beta_{42}/A\beta_{40}\uparrow$ , but it was down-regulated when the  $A\beta_{42}/A\beta_{40}$  was decreased ( $p=0.09$ , fold change=-2.9). This lysosomal aspartyl protease is composed of a dimer of disulfide-linked heavy and light chains, both produced from a single protein precursor. Transcription of this gene is initiated from several sites, including one which is a start site for an estrogen-regulated transcript. CTSD is a protease, localized in lysosomes, and active in *intracellular protein breakdown*. Mutations in this gene are possibly involved in the pathogenesis of Alzheimer disease. The val-58 allele is significantly overrepresented in demented patients compared with nondemented controls. *Carriers of the val-58 allele have a 3.1-fold increased risk for developing AD than non carriers [298]*.

Endothelin converting enzyme-like 1 (ECE1) was not differentially expressed for  $A\beta_{42}/A\beta_{40}\uparrow$ , but was *up-regulated for  $A\beta_{42}/A\beta_{40}\downarrow$*  ( $p=0.037$ , fold change=1.9 (microarray) and confirmed by the more exact real-time PCR measurement: fold change=5.3 (see Fig. 5.43, page 113). The ECE1 gene encodes a member of the neutral endopeptidase (NEP)-related family. *It is expressed specifically in the nervous system and may contribute to the degradation of peptide hormones and be involved in the inactivation of neuronal peptides. It is assumed to bind one zinc ion. In cell-based and in vitro models (ECE1) was characterized as an  $A\beta$ -degrading enzyme that appears to act intracellularly, thus limiting the amount of  $A\beta$  available for secretion. To determine the physiological significance of this activity,  $A\beta$  levels were analyzed in the brains of mice deficient for ECE1 and the closely related enzyme,*

*ECEL2. Significant increases in the levels of both  $A\beta_{40}$  and  $A\beta_{42}$  were found in the brains of these animals when compared with age-matched littermate controls. The increase in  $A\beta$  levels in the ECEL-deficient mice provided the first direct evidence for a physiological role for both ECEL1 and ECEL2 in limiting  $A\beta$  accumulation in the brain and also provides further insight into the factors involved in  $A\beta$  clearance in vivo [299]. Since I found it up-regulated for  $A\beta_{42}/A\beta_{40}\downarrow$  it may be assumed that  $A\beta$ -degradation is increased in mutant C99V50F. I observed no upregulation for  $A\beta_{42}/A\beta_{40}\uparrow$ , so the  $A\beta$ -degrading effect can be expected to be missing in mutant C99I45F.*

An uncharacterized transcribed locus (expressed sequence tag (EST), detected by the probe set 238237\_at) may be of interest, since it was found significantly and strongly down-regulated ( $A\beta_{42}/A\beta_{40}\uparrow$ ,  $p=0.023$ , fold change=-8.0, calculated with the MAS 5 algorithm) but not differentially expressed when the  $A\beta_{42}/A\beta_{40}$  ratio was decreased. Interestingly, the comparison C99WT/mock revealed that this transcript was strongly up-regulated (C99WT/mock,  $p=0.014$ , fold change=12.7). Alignment of the EST with sequences from human genomic databases by means of the Basic Local Alignment Search Tool (BLAST) showed that it is >98% similar (compared was the whole target sequence which is larger than 400 nucleotides) to human ADAM32 and ADAM28, two disintegrin and metalloproteases. I suggest that the EST, with previously unknown function, is identical to ADAM32, ADAM28 or another protease with sequence similarity. Furthermore, I suggest that the EST is functionally associated to  $A\beta_{42}/A\beta_{40}$  and to C99 (due to extreme differential expression of the EST in C99WT and C99I45F).

The rho and metalloprotease 1 motif GTPase activating protein 26 (ARHGAP26) and its splice product were significantly up-regulated for  $A\beta_{42}/A\beta_{40}\uparrow$  (215955\_x\_at:  $p=0.0074$ , fold change 1.5; 205068\_s\_at:  $p=0.0093$ , fold change=1.8). Upregulation was also found for  $A\beta_{42}/A\beta_{40}\downarrow$  (205068\_s\_at:  $p=0.0199$ , fold change=1.5). The comparison C99WT/mock showed significant downregulation of ARHGAP26 (C99WT/mock, 205068\_s\_at,  $p=0.0104$ , fold change=-2.1 and no differential expression for 215955\_x\_). FAK (tyrosine kinase, component of the integrin signaling transduction pathway) binds with its C-terminal domain to the SH3 domain of ARHGAP26. ARHGAP26 is known to stimulate the GTPase activity of the GTP-binding protein RhoA. RhoA is a GTP-binding protein and activation of its GTPase activity turns GTP into GDP, thus finally inhibiting RhoA. Since ARHGAP26 was up-regulated, RhoA is assumed to be inhibited. ARHGAP26 is part of PDGF signaling (apart from integrin signaling). Upregulation of ARHGAP26 in both  $A\beta_{42}/A\beta_{40}\uparrow$  and  $A\beta_{42}/A\beta_{40}\downarrow$  hints at upregulation of this pathway. This is especially true for

$A\beta_{42}/A\beta_{40}\downarrow$ , because here, two further components of this pathway (PKC $\alpha$  and FEV) were also significantly up-regulated and supported by strong phosphorylation (shown by immuno blotting for PKC $\alpha$ ). PKC $\alpha$  was down-regulated for  $A\beta_{42}/A\beta_{40}\uparrow$  and less phosphorylation could be observed questioning whether this pathway is really affected (for  $A\beta_{42}/A\beta_{40}\uparrow$ ). In conclusion, an upregulation of PDGF signaling can be expected for  $A\beta_{42}/A\beta_{40}\downarrow$ .

*In summary, proteases and protease inhibitors belonged to the most significantly and differentially expressed genes in consequence of a changed  $A\beta_{42}/A\beta_{40}$  ratio. Especially intriguing is the interplay between the most strongly down-regulated proteases and the top up-regulated protease inhibitors (and vice versa) and should be one of the major topics of future research.*

## **6.10 Extracellular matrix proteins like fibronectin-domain containing proteins, collagen, heparan sulfate proteoglycan and reelin may play a fundamental role in gene expression incuded by a changed $A\beta_{42}/A\beta_{40}$ ratio**

Fibronectins are adhesive proteins. They are filamentous dimers consisting of two related peptide chains linked to each other by disulfide bonds. Fibronectins have different domains enabling them to bind to cell-surface receptors, collagen, fibrin and proteoglycans (heparan sulfate, heparin, hyaluronate etc.) Fibronectin has a module that causes adhesion to cells containing the characteristic amino acid sequence Arg-Gly-Asp-Ser. These residues enable fibonectin to bind to cell surface receptors, known as integrins.

I found *fibronectin type III* domain containing 3A (FNDC3A), *fibronectin type III* domain containing 6 (FNDC6) [300] significantly down-regulated (for  $A\beta_{42}/A\beta_{40}\uparrow$ ).

L1 cell adhesion molecule (L1CAM, on chromosome Xq28), was up-regulated ( $A\beta_{42}/A\beta_{40}\downarrow$ ). L1CAM is a type I membrane protein. The protein encoded by this gene is an axonal glycoprotein belonging to the immunoglobulin supergene family. The *ectodomain*, consisting of several immunoglobulin-like domains and *fibronectin-like repeats (type III)*.

Neuronal cell adhesion molecule (NRCAM) was up-regulated ( $A\beta_{42}/A\beta_{40}\downarrow$ ) and contains *fibronectin type-III* domains and is an ankyrin-binding protein. KIAA0746 was up-regulated ( $A\beta_{42}/A\beta_{40}\downarrow$ ). KIAA0746 is a potential type I membrane protein which may play a role in Notch signaling. It has 27% similarity with Sel-1 homolog precursor (Mus musculus) and contains 1 fibronectin type-II domain. SEL-1 functions as a *negative regulator of the LIN-12/GLP-1 Notch-like signaling pathway in C.*

*elegans*.

Brother of CDO (BOC) and contactin 3 plasmacytoma associated (CNTN3) were among the most up-regulated genes ( $A\beta_{42}/A\beta_{40}\uparrow$ ) and *in parallel* the most downregulated ones in mutant C99V50F ( $A\beta_{42}/A\beta_{40}\downarrow$ ). BOC is a cell surface receptor of the immunoglobulin (Ig)/*fibronectin type III* repeat family involved in myogenic differentiation.

Contactins mediate cell surface interactions during nervous system development. CNTN3 contains 4 *fibronectin type-III* domains and 6 immunoglobulin-like domains.

Fibronectin leucine rich transmembrane protein 1 (FLRT1) was down-regulated ( $A\beta_{42}/A\beta_{40}\uparrow$ ,  $p=0.113$ , fold change=-2.4, derived from the comparison C99I45F/WT2)

These data indicate a crucial role for fibronectin type III in  $A\beta$ -mediated gene expression. Moreover, apart from the expected involvement in cell adhesion, it is striking that many of these fibronectin-associated genes are involved in axonal outgrowth and growth cone guidance.

Collagens, of which there are at least 19 different varieties, form fibers, fibrils and networks. They are quantitatively among the most abundant proteins. Collagens form water-insoluble fibers that occur as structural elements of the extracellular matrix.

I found the following collagens up-regulated in consequence of a decreased  $A\beta_{42}/A\beta_{40}$  ratio: collagen, type XII, alpha 1 (COL12A1) ( $p=0.00653$ , fold change=8.0), collagen, type XXVII, alpha 1 (COL27A1) ( $p=0.01613$ , fold change=6.3), collagen, type XI (COL11A1) ( $p=0.00313$ , fold change=6.3), collagen, type I, alpha (COL1A2), ( $p=0.02322$ , fold change=5.0). In contrast to this, none of these collagens were differentially expressed when the  $A\beta_{42}/A\beta_{40}$  ratio was increased.

In response to wounding, the expression of amyloid precursor-like protein 2 (APLP2) in the basal cells of migrating corneal epithelium is greatly up-regulated. APLP2 has been suggested to be involved in wound healing, therefore the migratory response of transfected Chinese Hamster Ovary (CHO) cells expressing APLP2 isoforms to a variety of extracellular matrix components including laminin, collagen types I, IV, and VII, fibronectin, and heparan sulfate proteoglycans (HSPGs) was measured [301]. *CHO cells overexpressing either of two APLP2 variants, differing in chondroitin sulfate attachment, exhibit a marked increase in chemotaxis toward type IV collagen and fibronectin but not to laminin, collagen types I and VII, and HSPGs.* APLP2 was suggested to contribute to re-epithelialization during wound healing by supporting epithelial cell adhesion to fibronectin and collagen IV, thus influencing their capacity to migrate over the wound bed. (Furthermore, APLP2 interactions with fibronectin and collagen IV appear to be potentiated by the addition of a chondroitin sulfate

chain to the core proteins) [301]. This is in line with co-regulation (both up-regulated to the same extent) of collagen IV and APLP2 (observed in this thesis) in consequence of an increased  $A\beta_{42}/A\beta_{40}\uparrow$  ratio, in contrast to a decreased one, for which neither of these proteins were up-regulated. I have proposed collagen IV (see Fig. 5.37) to be involved in blood coagulation. This fits to the previously mentioned data by Li et al. [301], because enhanced local blood coagulation is a prerequisite to wound healing.

Collagen type IV  $\alpha$  1 (COL4A1) has been described to influence  $A\beta$  levels in platelets, but the opposite aspect ( $A\beta_{42}$  influences collagen IV) may also be true, because I found COL4A1 up-regulated in response to an increased  $A\beta_{42}/A\beta_{40}\uparrow$  ( $p=0.03$ , fold change=2.4), but not differentially expressed when the  $A\beta_{42}/A\beta_{40}$  ratio was decreased. This could be a *vicious circle in which  $A\beta_{42}$  reinforces itself via COL4A1 expression*. Furthermore, I found COL4A2 up-regulated in response to an increased  $A\beta_{42}/A\beta_{40}\uparrow$  ( $p=0.116$ , fold change=1.5) and validated by another probe-set, but not differentially expressed when the  $A\beta_{42}/A\beta_{40}$  ratio was decreased.

Type IV collagen is associated with laminin and heparan sulfate proteoglycans to form the sheetlike basement membranes that separate epithelium from connective tissue. The genes for the alpha-1 and alpha-2 chains of type IV collagen (COL4A1 and COL4A2) map to the same chromosomal band (13q34) and have a high degree of nucleotide homology. Aligning the 2-alpha chains of type IV collagen from the N-terminus, it was concluded that the alpha-2 chain has 43 more amino acids than the alpha-1 chain. Twenty-one of these additional residues form a disulfide-bridged loop within the triple helix, which is unique among all known collagens. *The 2 subunit genes COL4A1 and COL4A2 are transcribed from a common promoter*. COL4A2 encodes one of the six subunits of type IV collagen, the major structural component of basement membranes. The C-terminal portion of the protein, known as canstatin, is an inhibitor of angiogenesis and tumor growth. Like the other members of the type IV collagen gene family, this gene is organized in a head-to-head formation with another type IV collagen gene so that each gene pair shares a common promoter.

Microfibrillar-associated protein 4 (MFAP4), which was down-regulated ( $A\beta_{42}/A\beta_{40}\downarrow$ ) has *binding specificities for both collagens* and carbohydrates. It is thought to be an extracellular matrix protein which is involved in cell adhesion or intercellular interactions. Although the precise function of this protein is not known, it has been suggested that it could be a  $Ca^{2+}$ -dependent adhesive protein that is associated with elastin microfibrils in the extracellular matrix. MFAP4 has a *fibrinogen-like domain*. The N-terminus of the protein contains an arg-gly-asp sequence that serves as the *ligand motif for cell surface receptor integrin*. The matrix metalloproteinase 8

(MMP8), a collagenase, was down-regulated ( $A\beta_{42}/A\beta_{40}\uparrow$ ,  $p=0.00219$ , fold change=-5.0, see discussion about proteases for further information). However, MMP8 was not differentially expressed when the ratio was decreased. A disintegrin-like and metalloprotease (reprolysin type) with thrombospondin type 1 motif 3 (ADAMTS3) was down-regulated ( $A\beta_{42}/A\beta_{40}\uparrow$ ,  $p=0.086$ , fold change=-2.1), however, weakly up-regulated ( $A\beta_{42}/A\beta_{40}\downarrow$ ,  $p=0.23$ , fold change=1.3). ADAMTS3 is the major procollagen II N-propeptidase.

Tissue inhibitor of metalloproteinase 1 (collagenase inhibitor) (TIMP1) was down-regulated ( $A\beta_{42}/A\beta_{40}\uparrow$ ,  $p=0.127$ , fold change=-3.5), but not differentially expressed when the  $A\beta_{42}/A\beta_{40}$  ration was decreased. The TIMP1 gene belongs to the TIMP gene family and is localized on chrXp11.3-p11.23. The proteins encoded by this gene family are natural inhibitors of the matrix metalloproteinases (MMPs), a group of peptidases involved in *degradation of the extracellular matrix*. In addition to its inhibitory role against most of the known MMPs, the encoded protein is able to promote cell proliferation in a wide range of cell types, and may also have an anti-apoptotic function. Transcription of this gene is highly inducible in response to many cytokines and hormones. In addition, the expression from some but not all inactive X chromosomes suggests that this gene inactivation is polymorphic in human females. This gene is located within intron 6 of the synapsin I gene and is transcribed in the opposite direction.

Heparan sulfate (glucosamine) 3-O-sulfotransferase 2 (HS3ST2) was among the most inversely regulated genes:  $A\beta_{42}/A\beta_{40}\uparrow$  ( $p=0.0116$ , fold change=1.7) and  $A\beta_{42}/A\beta_{40}\downarrow$  ( $p=0.137$ , fold change=-1.5). *Heparan sulfate biosynthetic enzymes are key components in generating a myriad of distinct heparan sulfate structures that carry out multiple biological activities*. HS3ST2 is a type II integral membrane protein and possesses heparan sulfate glucosaminyl 3-O-sulfotransferase activity. The HS3ST2 gene is expressed predominantly in the brain and may play a role in the nervous system.

Heparan sulfate proteoglycan 2 (HSPG2) (perlecan) was up-regulated  $A\beta_{42}/A\beta_{40}\uparrow$  ( $p=0,158$ , fold change=2, calculated with the MAS 5 algorithm) and not differentially expressed for  $A\beta_{42}/A\beta_{40}\downarrow$ .

Heparan sulfate proteoglycan 1, (syndecan 2 (SDC2), cell surface-associated, fibroglycan) was not differentially expressed for  $A\beta_{42}/A\beta_{40}\uparrow$ , but down-regulated for  $A\beta_{42}/A\beta_{40}\downarrow$  ( $p=0,116$ , fold change=1.6, calculated with the MAS 5 algorithm).

Glypican 3 (GPC3) was not differentially expressed ( $A\beta_{42}/A\beta_{40}\uparrow$ ), but was among the 6 most significantly down-regulated genes (calculated with the GC-RMA algorithm) when the  $A\beta_{42}/A\beta_{40}$  was decreased ( $p=0.00089$ , fold change=-2.5). GPC3 is a cell surface heparan sulfate proteoglycan that is composed of a membrane-associated protein core substituted with a variable number of heparan sulfate chains. Members of the glypican-related integral membrane proteoglycan family (GRIPS) contain a core protein anchored to the cytoplasmic membrane via a glycosyl phosphatidylinositol linkage. These proteins may play a role in the control of cell division and growth regulation. GPC3 may play a role in the modulation of IGF2 interactions with its receptor and thereby modulate its function. Predicted functional partners are IGF2, Insulin precursor, WNT5A, CDKN1C, WNT3A, WNT7B.

Reelin (RELN) was the *third most significantly up-regulated gene* (C99I45F/C99WT2,  $A\beta_{42}/A\beta_{40}\uparrow$ ,  $p=0,031728$ , fold change=3.3), but was not differentially expressed for  $A\beta_{42}/A\beta_{40}\downarrow$ . Reelin is up-regulated in the brain and CSF of AD patients [302]. Intriguingly, we (together with our colleague Laura Busia) also found reelin to be among the most significantly dysregulated genes in embryonic mouse fibroblasts in consequence of PS1 knockdown with siRNA.

The encoded protein resembles extracellular matrix proteins involved in cell adhesion [303] thought to control cell-cell interactions critical for cell positioning and neuronal migration during brain development. RELN may be involved in schizophrenia, autism, bipolar disorder, major depression and in migration defects associated with temporal lobe epilepsy. *RELN regulates microtubule functions in neurons and neuronal migration. RELN is an extracellular matrix serine protease [304] that plays a role in layering of neurons in the cerebral cortex and cerebellum and its enzymatic activity is important for the modulation of cell adhesion. RELN binds to the extracellular domains of lipoprotein receptors VLDLR and APOER2 [305, 306] induces tyrosine phosphorylation of Dab1 and modulation of tau phosphorylation [306]. Very recently it has been shown that APOER2 and X11 alpha/beta mediate apolipoprotein E-induced endocytosis of APP and  $\beta$ -secretase, leading to amyloid- $\beta$  production [307].* RELN is abundantly produced during brain ontogenesis by the Cajal-Retzius cells and other pioneer neurons located in the telencephalic marginal zone and by granule cells of

the external granular layer of the cerebellum. In adult brains, it is preferentially expressed in GABAergic interneurons of prefrontal cortices, temporal cortices, hippocampi and glutamatergic granule cells of cerebellum. It is also expressed in fetal and adult liver.

Taken together, collagen IV levels might be increased (for  $A\beta_{42}/A\beta_{40}\uparrow$ ) through down-regulation of collagenases and by up-regulation on the transcript level (for  $A\beta_{42}/A\beta_{40}\uparrow$ ). On the other hand, collagen-levels (for type 11 $\alpha$ 1, 12  $\alpha$ 1, 27 $\alpha$ 1 and type 1 $\alpha$ 2) might be increased for  $A\beta_{42}/A\beta_{40}\downarrow$  by upregulation of collagen-coding genes. *Collagen type IV  $\alpha$  may play a crucial role in  $A\beta$  induced pathology supported by the observation that collagen type IV and fibronectin are present in Alzheimer deposits [308].* Furthermore, the data indicate increased generation of heparan sulfate proteoglycans as a result of an increased  $A\beta_{42}/A\beta_{40}$  ratio and reduced generation in consequence of a decreased  $A\beta_{42}/A\beta_{40}$  ratio. *RELN may be involved, by its extracellular matrix serine protease activity in the break down of the extracellular matrix (for  $A\beta_{42}/A\beta_{40}\uparrow$ ).*

### 6.11 ACTA2 is assumed to be a pivotal protein in gene expression induced by altered C99 cleavage products

ACTA2 (actin, alpha 2, smooth muscle, aorta) is one of six different actin isoforms. Actins are highly conserved proteins that are involved in cell motility, structure and cell integrity. They are ubiquitous proteins involved in the formation of filaments that are major component of the cytoskeleton. Interaction with myosin provides the basis of muscular contraction and many aspects of cell motility.

ACTA2, localized on chromosome chr10q23.3, was the third most strongly up-regulated gene for  $A\beta_{42}/A\beta_{40}\downarrow$  but it was not differentially expressed for  $A\beta_{42}/A\beta_{40}\uparrow$ . It was *co-regulated with GAP43, PLAT, GDF1 and MAPK8IP2*. Co-regulation with GAP43 was further supported by the observation that ACTA2 and GAP43 were also co-regulated for the comparison C99WT/mock in which both transcripts were found to be down-regulated. Intriguingly, we (together with our colleague Laura Busia) also found ACTA2 among the most strongly and most significantly up-regulated genes in embryonic mouse fibroblasts in consequence of PS1 and PS2 knockdown with siRNA. In this approach  $A\beta$  levels were expected to be decreased. This is in line with the observation of ACTA2 upregulation in mutant C99V50F compared to C99WT ( $A\beta_{42}/A\beta_{40}\downarrow$ ) and argues for an effect mediated by a decreased  $A\beta_{42}$  or increased  $A\beta_{40}$  expression or for a change in the corresponding AICD levels. Müller et al. found ACTA2 among the most up-regulated genes in consequence of AICD overexpression [57]. This argues for an effect mediated by the AICD (or further cleavage products hereof). ACTA2 has been described as being involved in vascularisation and vascular branching [309, 310, 311]. *Furthermore, impaired vascular contractility and blood pressure homeostasis in smooth muscle  $\alpha$ -actin null mice has been observed [312]; The major function of vascular smooth muscle cells is contraction to regulate blood pressure and flow [311]. It can be speculated that a decreased  $A\beta_{42}/A\beta_{40}$  up-regulates ACTA2, a mechanism that might also occur in smooth muscle cells, which in turn could lead to improved vascularisation and could regulate blood pressure. This positive effect might be missing for an increased  $A\beta_{42}/A\beta_{40}$  ratio where no differential ACTA2 expression was observed.*

### 6.12 Transcriptional control of blood coagulation and fibrinolysis was influenced by a changed $A\beta_{42}/A\beta_{40}$ ratio

See Model, Fig. 5.37, pages 86-87. Clinical data as well as immunohistochemical and electron microscopy data of cerebral cortex and brain microvessels hint at an altered regulation of blood coagulation and fibrinolysis in Alzheimer's patients [313,

314]. Here, information is available about the transcriptional control of blood coagulation and fibrinolysis, however, blood coagulation and fibrinolysis were not tested directly. The tissue factor pathway inhibitor 2 (TFPI2) was significantly ( $p=0.027$ ) up-regulated (fold change=2.6) in consequence of a decreased  $A\beta_{42}/A\beta_{40}$  ratio (and confirmed by another probe-set), however, it was down-regulated for  $A\beta_{42}/A\beta_{40}\uparrow$  ( $p=0.365$ , fold change=-3.1); this downregulation was confirmed with another probe-set making a real downregulation more probable. Using another set of triplicates as a baseline experiment (C99WT2) revealed TFPI2 as the most down-regulated gene ( $A\beta_{42}/A\beta_{40}\uparrow$ , 10-fold down-regulated,  $p=0.241034$ ). This result was also confirmed with another probe set. Direct comparison between both mutants (C99I45F/C99V50F) indicated strong downregulation in mutant C99I45F ( $A\beta_{42}/A\beta_{40}\uparrow$ ,  $p=0.132$ , fold change=-10.1) and another probe set for detection of TFPI2 delivered similar results ( $A\beta_{42}/A\beta_{40}\uparrow$ ,  $p=0.158$ , fold change=-32.0). TFPI2 was the most inversely regulated gene (by a changed  $A\beta_{42}/A\beta_{40}$  ratio). Even if TFPI2 does not pass the generally accepted cut-off for significant differential expression for  $A\beta_{42}/A\beta_{40}\uparrow$  ( $p<0.05$ ), TFPI2 can be regarded as important, because of the fact that it was the *most inversely* regulated gene and *only 3 replicates* ( $n=3$ ) were measured: a few outliers (for instance one replicate shows diverse expression compared to the other two) could have increased the p-value. It can be assumed that increasing the number of replicates would reduce the p-value for this gene. Further measurements with further clones (for instance  $n=6$  instead of  $n=3$ ) may reduce the p-value.

Tissue factor pathway inhibitor is an important regulator of the *extrinsic pathway of blood coagulation* through its ability to *inhibit factor Xa and factor VIIa-tissue factor activity*. It was originally identified by Siiteri et al. [315] and Butzow et al. [316] as a placental glycoprotein that inhibits blood coagulation [317]. After a 22-residue signal peptide, the mature TFPI2 protein contains 213 amino acids with 18 cysteines and 2 canonical N-linked glycosylation sites. The deduced sequence of mature TFPI2 revealed a short acidic N-terminal region, 3 tandem Kunitz-type domains, and a C-terminal tail highly enriched in basic amino acids. It may also play a role in the regulation of plasmin-mediated matrix remodeling.

Taken together, there are strong indications that *blood coagulation is increased (decreased blood flow) for  $A\beta_{42}/A\beta_{40}\uparrow$* , due to downregulation of inhibiting properties of TFPI2 onto blood clotting. *In vivo, a decreased cerebral blood flow may be assumed to be a consequence of an increased  $A\beta_{42}/A\beta_{40}$  ratio*. Here, information about the transcriptional control of blood coagulation is available. Future research should focus on the direct analysis of blood coagulation.

The gene *plasminogen activator, tissue* (PLAT) was not differentially expressed for  $A\beta_{42}/A\beta_{40}\uparrow$ , but significantly ( $p=0.0047$ ) up-regulated (fold change=2.1) when the  $A\beta_{42}/A\beta_{40}$  was decreased. Even if only shown on the transcript-level in cell culture, this points to *increased fibrinolysis, and thus augmented blood flow when the  $A\beta_{42}/A\beta_{40}$  was decreased*. In contrast to this, fibrinogen, B beta polypeptide (FGB) was significantly ( $p=0.01613$ ) up-regulated ( $A\beta_{42}/A\beta_{40}\uparrow$ , fold change= 2.5), but no differential expression was observed when the  $A\beta_{42}/A\beta_{40}$  was decreased. This indicates *increased generation of fibrin in consequence of an increased  $A\beta_{42}/A\beta_{40}$* .

A plethora of proteins with fibronectin domains were found to be differentially expressed (previously discussed in this thesis). Fibronectin was shown to enhance thrombocyte aggregation, which may further influence blood coagulation or fibrinolysis.

SERPINE2 (synonyms: Nexin plasminogen activator inhibitor type 1, protease nexin I (PN1), protease inhibitor 7, glial-derived neurite promoting factor p) was down-regulated ( $A\beta_{42}/A\beta_{40}\uparrow$ ). SERPINE2 shares several features with antithrombin III, an abundant plasma thrombin inhibitor. Both SERPINE2 and AT-III have high affinities for heparin; heparin accelerates their rate of thrombin inhibition and it is the most important physiologic regulator of alpha-thrombin in tissues [318]. SERPINE2 is highly expressed and developmentally regulated in the nervous system where it is concentrated at neuromuscular junctions and also at central synapses in the hippocampus and striatum. Approximately 10% of identified proteins at mammalian neuromuscular junctions are serine protease inhibitors, consistent with their central role in balancing serine protease activity to develop, maintain, and remodel synapses. *Pericyte expression of SERPINE2 may provide endogenous anticoagulant activity [319]. SERPINE2 in solution forms inhibitory complexes with thrombin or urokinase, which have opposing effects on the blood coagulation cascade. An initial report provided data supporting the idea that SERPINE2 properties are under the influence of collagen type IV. SERPINE2 binds tightly to and is regulated by the extracellular matrix. This interaction accelerates the inhibition of thrombin by SERPINE2 and blocks urokinase and plasmin inhibition by SERPINE2. Previous work showed that heparan sulfate proteoglycan is largely responsible for the acceleration of thrombin inhibition by SERPINE2. It has been shown that collagen type IV decreased the formation of SDS-stable complexes between urokinase or plasmin and SERPINE2 without affecting formation of complexes between thrombin and SERPINE2.* Other extracellular matrix components (collagen type I, vitronectin, fibronectin, and heat-denatured collagen type IV) did not affect complex formation or the rate of inhibition of proteases by SERPINE2, indicating that these effects were

*specific to collagen type IV. Collagen type IV was also copurified with SERPINE2 from fibroblast-conditioned medium [320]. This has led to the generally accepted idea that the primary role of SERPINE2 in the brain is to act as a rapid thrombin inhibition mechanism during trauma. Due to the down-regulation of SERPINE2 (for  $A\beta_{42}/A\beta_{40}\uparrow$ ) the inhibiting properties of SERPINE2 on thrombin can be expected to be reduced. In consequence thrombin may be more active leading to faster blood coagulation.*

The serine proteinase inhibitor, clade F, member 1 (SERPINF1,  $\alpha$ -2 anti-plasmin) was the third *most significantly down-regulated* transcript ( $A\beta_{42}/A\beta_{40}\downarrow$ ,  $p=0.00362$ , fold change=-3.1, GC-RMA algorithm), whereas it was not differentially expressed when the  $A\beta_{42}/A\beta_{40}$  was increased. Generated fibrin (the end product of blood coagulation) can be converted into soluble fragments (fibrinolysis). Plasmin, a protease, converts fibrin into soluble fragments by cleavage. SERPINF1 is an *anti-plasmin* and it was strongly down-regulated ( $A\beta_{42}/A\beta_{40}\downarrow$ ). This means that more plasmin is expected to be available, which in turn would accelerate fibrinolysis (for a decreased  $A\beta_{42}/A\beta_{40}$  ratio).

Heparin strongly inhibits blood coagulation, for instance by binding to anti-thrombin III, factor IXa and Xa. FGF1, a heparin-binding growth factor, was up-regulated for  $A\beta_{42}/A\beta_{40}\uparrow$  ( $p=0.02$ , fold change=1.6), whereas it was not differentially expressed when the  $A\beta_{42}/A\beta_{40}$  was decreased. Superoxide dismutase 1 (SOD1) was reported to bind heparin [321] and immunoblotting showed its upregulation for  $A\beta_{42}/A\beta_{40}\uparrow$ , but its downregulation when the  $A\beta_{42}/A\beta_{40}$  ratio was decreased. I speculate that FGF1 and SOD1 could retain heparin by binding it, so that the free level of heparin may be reduced. Consequently, it may be no longer available in sufficient amounts to inhibit blood coagulation (for  $A\beta_{42}/A\beta_{40}\uparrow$ ).

Binding of the weakly, but significantly up-regulated coagulation factor XII (Hageman factor; for  $A\beta_{42}/A\beta_{40}\uparrow$ ,  $p=0.036$ , fold change 1.3) to *collagens, triggers the intrinsic blood coagulation cascade*. The Hageman factor was not differentially expressed when the  $A\beta_{42}/A\beta_{40}$  was decreased. KIAA1573 was among the most inversely regulated genes. It was up-regulated (for  $A\beta_{42}/A\beta_{40}\uparrow$ ,  $p=0.044$ , 1.6 fold), but down-regulated ( $p=0.149$ , -2.7 fold) when the  $A\beta_{42}/A\beta_{40}$  was decreased. KIAA1573 (Von Willebrand factor type A and cache domain containing 1), is assumed, due to sequence similarity, to be a L-type calcium channel. It contains a VWFA (Von Willebrand factor A) domain. Von Willebrand factor mediates thrombocyte aggregation to collagen.  $Ca^{2+}$  ions were shown to be a co-factor for local clotting ( $Ca^{2+}$  supports triggering the extrinsic clotting cascade) and  $Ca^{2+}$  can be assumed to be increased ( $A\beta_{42}/A\beta_{40}\uparrow$ , see information about  $Ca^{2+}$ -levels, Chapter 6.36, pages 201-202). Coagulation factor II (thrombin) receptor-like 3 (F2RL3) was down-

regulated ( $A\beta_{42}/A\beta_{40}\downarrow$ ,  $p=0.04742$ , fold change=-3.2) and coagulation factor II (thrombin) receptor was weakly down-regulated ( $A\beta_{42}/A\beta_{40}\downarrow$ ,  $p=0.0266$ , fold change=-1.2), whereas no differential expression was observed when the  $A\beta_{42}/A\beta_{40}$  was increased. I speculate that down-regulated thrombin receptors support the downregulation of the blood coagulation cascade ( $A\beta_{42}/A\beta_{40}\downarrow$ ) and thus increase blood flow. Interestingly, the inversely regulated JAG1 ( $A\beta_{42}/A\beta_{40}\uparrow$ : up-regulated,  $A\beta_{42}/A\beta_{40}\downarrow$ : down-regulated) is a type I membrane-protein and contains in its extracellular part a von Willebrand factor type C domain. HGF was one of the most down-regulated genes ( $A\beta_{42}/A\beta_{40}\uparrow$ ). At physiological concentrations HGF was found to inhibit thrombin-dependent platelet aggregation in a dose- and time-dependent manner. These results suggest that circulating HGF may counteract thrombogenesis by negatively modulating platelet functions [322]. Thus, down-regulation of HGF might support platelet aggregation (for  $A\beta_{42}/A\beta_{40}\uparrow$ ).

In summary, there are indications of increased blood coagulation and presumably decreased fibrinolysis as a consequence of an increased  $A\beta_{42}/A\beta_{40}$  ratio, while a decreased  $A\beta_{42}/A\beta_{40}$  ratio may result in enhanced fibrinolysis, while blood coagulation might be reduced. All differentially expressed genes (described in Figure 5.37, pages 86-89), except for F2R, F2RL3 and VWCD1, code for secreted proteins. Theoretically it seems possible that *in vivo* (in brains of AD patients) an increased  $A\beta_{42}/A\beta_{40}$  ratio triggers the release of the previously mentioned factors into the extracellular space and into blood vessels, in which a shift towards increased blood coagulation and decreased fibrinolysis may take place. Indeed, clinical data on blood coagulation and fibrinolysis as well as immunohistochemical and electron microscopy data of cerebral cortex and brain microvessels hint at such a regulation in Alzheimer's patients [313, 314]. Such a regulation would result in decreased cerebral blood flow and a stronger tendency towards stroke and mental dysfunction.

Further research directly focusing on blood coagulation and fibrinolysis is necessary to demonstrate that the changes, identified here on the transcriptional level, hold true.

Platelets contain both APP and  $A\beta$  and may contribute to the perivascular amyloid deposition seen in AD [323]. APP is abundantly expressed in the platelet  $\alpha$ -granule where its role remains unclear. A study described a function for APP in regulating human platelet activation. Secreted APP (sAPP) potently inhibited platelet aggregation [324]. *Secreted APP*, which contains a KPI (Kunitz protease inhibitor) domain, has been identified as the serine protease inhibitor, protease nexin II (PNII), which *inhibits the serine protease factor XIa in the blood coagulation cascade* [325, 326]. These studies indicate an association of APP and  $A\beta$  with blood coagulation. Furthermore,  $A\beta$  was detected in human atherosclerotic plaques suggesting a link

between A $\beta$  and strokes [327].

Taken together, previously publications hint at inhibition of blood coagulation by secreted APP. Here in this thesis, altered C99 processing accompanied by an increased A $\beta_{42}$ /A $\beta_{40}$  ratio seemed to enhance blood coagulation via its transcriptional control.

## 6.13 Kinases/phosphatases as possible candidates for tau or GSK3 phosphorylation

### 6.13.1 Kinases

See results, Table 5.14 (Chapter 5.10.2, page 90). The state of phosphorylation of a phosphoprotein is a function of the balance between the activities of protein kinases and phosphatases that regulates its phosphorylation. For these reasons candidate kinases/phosphatases for tau and GSK3 $\beta$  were identified.

Of special interest was CDKL1 (cyclin-dependent kinase-like 1, synonyms: CDC2-related kinase, p42), due to its location on chromosome chr14q21.3, which is in very close vicinity to the presenilin 1 gene (chr14q24). This gene product is a member of a large family of CDC2-related serine/threonine protein kinases. CDKL1 is known to regulate important transitions in the eukaryotic cell cycle.

Another *top candidate* was *DYRK1A* (dual-specificity tyrosine-(Y)-phosphorylation regulated kinase 1A), *located on chromosome chr21q22.13, which is directly adjacent to the APP locus (chr21q21.2|21q21.3)*. Song et al. mentioned that DYRK1A may be involved in the abnormal neurogenesis found in Down's syndrome. They considered DYRK1A a good candidate to mediate some of the pleiotropic effects of Down's syndrome [328]. DYRK1A is activated by tyrosine phosphorylation in the activation loop between subdomains VII and VIII of the catalytic domain. The human gene for DYRK1A is located in the "*Down's syndrome critical region*" of chromosome 21 and is therefore a *candidate gene for mental retardation in Down syndrome*. An *unusual enzymatic property of Dyrk-related kinases is their ability to catalyze tyrosine-directed autophosphorylation as well as phosphorylation of serine/threonine residues in exogenous substrates* [329]. Using fluorescence in situ hybridization and regional mapping data, Song et al. localized the DYRK gene between markers D21S336 and D21S337 in the 21q22.2 region [328]. Altafaj et al. generated transgenic mice *overexpressing the full-length cDNA of DYRK1A*. DYRK1A mice exhibited delayed craniocaudal maturation with functional consequences in neuromotor development. Dyrk1A mice also showed altered motor skill acquisition

and hyperactivity, which was maintained to adulthood. *In the Morris water maze, DYRK1A mice showed a significant impairment in spatial learning and cognitive flexibility, indicative of hippocampal and prefrontal cortex dysfunction.* In the more complex repeated reversal learning paradigm, this defect was specifically related to reference memory, whereas working memory was almost unimpaired. The authors suggested a causative role of DYRK1A in mental retardation and in motor anomalies of Down's syndrome [330].

For both loci (chr14q21.3 and chr21q21.2|21q21.3) a “*Chromeron regulation*” [195] can be assumed: *APP would then be co-regulated with DYRK1A and presenilin 1 would be co-regulated with CDKL1.* Overexpressed APP would be accompanied by DYRK1A upregulation (and low expressed APP would be accompanied by DYRK1A downregulation). Consequently, as a result of increased APP processing, more  $A\beta_{42}$  would be produced and *at the same time* DYRK1A would be increased, which in turn could phosphorylate downstream targets like GSK3 $\beta$  or tau. Overexpressed presenilin 1 would be accompanied by up-regulated CDKL1. Consequently, as a result of changed APP processing (due to overexpressed presenilin 1), more  $A\beta_{42}$  would be produced while CDKL1 would be increased. CDKL1, in turn, could then phosphorylate downstream targets like GSK3 $\beta$  or tau.

PFKP (phosphofructokinase platelet) catalyzes the irreversible conversion of fructose-6-phosphate to fructose-1,6-bisphosphate and is *the key regulatory enzyme of glycolysis* ( $ADP + D\text{-fructose -1,6-bisphosphate} = ATP + D\text{-fructose -6-phosphate}$ ). PFKP was up-regulated for  $A\beta_{42}/A\beta_{40}\uparrow$ , but not differentially expressed for  $A\beta_{42}/A\beta_{40}\downarrow$ . This form of PFK is called the 'platelet' type because it is the only form made by platelets, whereas for instance fibroblasts have more than one form of phosphofructokinase. The 'platelet' type is abundant in the brain. This allosteric enzyme is activated by ADP, AMP, or fructose bisphosphate and is inhibited by ATP or citrate.

Up-regulated PFKP ( $A\beta_{42}/A\beta_{40}\uparrow$ , see Model Chapter 5.9.3, Fig. 5.36, page 85) may contribute to reduce glucose levels observed in brains of AD patients [331] and its induction on the transcript level is in line (PFKP is activated by ADP and AMP, but inhibited by ATP) with reduced ATP levels observed in brains of AD patients [332]. Phosphofructokinase activity in brains from patients with Alzheimer's disease was significantly increased in frontal and temporal cortex when compared with control brains [332]. There is a long lasting debate about “metabolic insufficiency” in AD. Since PFKP was found to be up-regulated (for  $A\beta_{42}/A\beta_{40}\uparrow$ ), this may be a response to, rather than the cause of reduced glucose metabolism and could be regarded as the attempt of the cells to restore sufficient ATP levels. Another explanation might be

reduced glucose levels in the brains of AD patients that triggers upregulation of glycolysis by PFKP upregulation. The observation that glucose metabolism is reduced in AD brains might rather reflect reduced levels of substrates (as part of the glycolysis pathway, reduced feed-forward stimulation) than decreased expression of glycolytic enzymes. This would mean that glucose is missing in the brain (possibly due to a changed insulin/IGF2 metabolism) resulting in reduced ATP levels (increased ADP and AMP levels), which in turn would cause PFKP to produce more ATP. Thus, missing glucose/ATP could be inherently connected to GSK3/tau phosphorylation (provided PFKP turns out to be a possible GSK or tau-kinase) via PFKP upregulation, so GSK3/tau phosphorylation would be an inherent byproduct of reduced glucose/ATP levels. In Tg2576 mice, overexpressing the Swedish mutation of APP, reduced PFKP levels were detected [333]. Bigl et al. found increased levels in astrocytes localized in frontal and temporal cortex from AD patients compared to healthy controls [331] and phosphofructokinase activity in brains from patients with Alzheimer's disease was significantly increased in the frontal and temporal cortex [332].

Further protein kinases were dysregulated for a changed  $A\beta_{42}/A\beta_{40}$  ratio and thus possible GSK/tau kinases:

Cyclin-dependent kinase-like 5 (CDKL5), localized on chrXp22, was up-regulated for  $A\beta_{42}/A\beta_{40}\uparrow$  ( $p=0.02490$ , fold change=4.0), but not differentially expressed for  $A\beta_{42}/A\beta_{40}\downarrow$ . CDKL5 (cyclin-dependent kinase-like 5, synonym: STK9 serine/threonine kinase 9). CDKL5 belongs to the ser/thr protein kinase family. Defects in CDKL5 are a cause of Rett syndrome. Rett syndrome is an X-linked dominant disease. It is a progressive neurologic disorder accompanied by brain atrophy and is one of the most common causes of mental retardation in females.

GRK5 (G protein-coupled receptor kinase 5) plays an important role in phosphorylating and regulating the activity of a variety of G protein-coupled receptors.

Rps6ka5 (ribosomal protein S6 kinase, polypeptide 5, synonym: mitogen- and stress-activated protein kinase1, MSK1). Rps6ka5 is directly activated by MAPK and SAPK2/p38, and may mediate activation of CREB [334].

PHKG1 (phosphorylase kinase gamma 1 (muscle)) is a crucial *glycogenolytic* regulatory enzyme. The holoenzymes are composed of 16 subunit proteins containing equimolar ratios of 4 subunit types known as alpha, beta, gamma, and delta. Skeletal muscles contain the highest amount of phosphorylase kinase enzymatic activity, although activity is also observed in the liver, cardiac muscle,

brain and several other tissues. PHKG1 was not differentially expressed in C99I45F. However, it was slightly down-regulated in C99V50F compared to C99WT ( $p=0.0441$ , fold change=-1.3). This could be a weak sign of sufficient ATP levels for  $A\beta_{42}/A\beta_{40}\downarrow$  because glucose generation (to produce ATP) by glycogenolysis may not be needed, so the glycogenolytic enzyme PHKG1 is down-regulated.

PKN2 (protein kinase N2, synonym: PAK2) belongs to the serine/threonine protein kinase family. This phospholipid-regulated protein kinase phosphorylates ribosomal protein S6 and is activated by lipids, particularly by cardiolipin and to a lesser extent by other acidic phospholipids and unsaturated fatty acids.

CDK6 (cyclin-dependent kinase 6) regulates cell cycle transitions in eukaryotic cells. Vulnerable neurons in the AD brain show activation of cell cycle markers [335]. This observation is supported by the recent demonstration that hypoxia/ischemia in the mouse and rat brain may also result in activation of the cell cycle and DNA replication prior to neuronal death [336, 337].

DCAMKL1 (synonym: CPG16) is highly expressed in the brain and may mediate calcium signaling in neural cells. DCAMKL1 has *microtubule polymerizing activity* that is independent of its protein kinase activity [338]. Overexpression of DCAMKL1 seems to partially inhibit cAMP-stimulated activity of the transcription factor CREB (cAMP response element-binding protein), suggesting its involvement in the down-regulation of cAMP-induced transcription [339].

DCAMKL1 was found up-regulated on the protein-level for  $A\beta_{42}/A\beta_{40}\uparrow$  and slightly down-regulated for  $A\beta_{42}/A\beta_{40}\downarrow$ , shown by immunoblotting ( $n=1$ ). Thus, it could be a possible candidate kinase for GSK3 or tau-phosphorylation. In this regard its microtubule polymerizing activity is of special interest and should be a focus in future research.

### 6.13.2 Phosphatases

See results, Table 5.15 (Chapter 5.10.3, page 91). Protein phosphatase 2A (PP2A) is a serine/ threonine protein phosphatase regulating mainly cell growth and division. It comprises three subunits, A, B, and C. All PP2A holoenzymes have a catalytic subunit C and a structural scaffolding subunit A in common. These subunits assemble with regulatory and targeting B subunits to form functionally distinct heterotrimers which are likely to have different functions in the cell [340]. PPP2R4 (protein phosphatase 2A activator, regulatory subunit 4) belongs to the B' family. This gene encodes a specific phosphotyrosyl phosphatase activator of the dimeric form of protein phosphatase 2A and might severely affect PP2A activities [341, 342].

Recently it has been suggested to be a peptidyl-prolyl cis/trans-isomerase [343]. The B-subunit is involved in enzyme activity and substrate specificity. The B-subunit family is of great diversity and is divided into three classes, the B1, B2, and B3 subfamilies. The putative protein B1 gamma (PPP2R2C) shares 81 and 85% identity with B1alpha (PPP2R2A) and B1beta (PPP2R2B), respectively. One remarkable characteristic of PPP2R2C is that it is highly expressed in the brain with a 4.7-kb transcript while it is nearly undetectable in other tissues [344]. Interestingly, in contrast to its significant upregulation (for  $A\beta_{42}/A\beta_{40}\uparrow$ ), it was significantly ( $p=0.0198$ ) down-regulated (-2.2 fold) in C99WT compared to mock-transfected cells.

*The often cited protein phosphatase 2A (as a candidate for tau dephosphorylation) is strongly regulated by its regulatory subunit B [341, 342]. Interestingly, PPP2R4 and the more recently discovered PPP2R2C (for which less information is available in the literature and in databases) are differentially affected by an altered  $A\beta_{42}/A\beta_{40}$  ratio. Further research focusing on these two subunits, with special regard to their regulation shown here, may help to gain further insight into the function of PP2A.*

A further phosphatase dysregulated by a changed  $A\beta_{42}/A\beta_{40}$  ratio was PHACTR2 (Phosphatase and actin regulator 2). PHACTR2 is a family member of proteins that binds protein phosphatase 1 and cytoplasmic actin; it may play a role in regulation of the actin cytoskeleton. PHACTR2 was -3.2 fold down-regulated ( $p=0.02572$ ) for  $A\beta_{42}/A\beta_{40}\uparrow$  but not differentially expressed for  $A\beta_{42}/A\beta_{40}\downarrow$ . This downregulation could contribute to increased phosphorylation of tau and GSK3 for  $A\beta_{42}/A\beta_{40}\uparrow$ .

## **6.14 Changed phosphorylation status of GSK3 $\alpha/\beta$ , tau, proteinkinase C and further molecules**

### **6.14.1 GSK3 $\alpha$ and GSK3 $\beta$**

Signal transduction pathways are especially activated/inhibited by *phosphorylation or dephosphorylation*, thus the phosphorylation status of key molecules was checked. Phosphorylation on tyrosine 279 and/or 216 activates GSK3 $\alpha$  and GSK3 $\beta$ . GSK3 $\alpha$  was found to be *hyperphosphorylated* on tyrosine 279 ( $n=1$ ) as result of an increased  $A\beta_{42}/A\beta_{40}$  ratio, whereas a decreased  $A\beta_{42}/A\beta_{40}$  ratio (C99V50F/C99WT) led to *hypophosphorylation* ( $n=1$ ) on tyrosine 279. GSK3 $\beta$  was *hyperphosphorylated* on tyrosine 216 ( $n=3$ ;  $A\beta_{42}/A\beta_{40}\uparrow$ , C99I45F/C99WT), whereas a decreased  $A\beta_{42}/A\beta_{40}$  ratio led to *hypophosphorylation* ( $n=3$ ) on tyrosine 279. GSK3 is known to inhibit glycogen synthase, cyclin D1, p21. These 3 genes were down-regulated (increased  $A\beta_{42}/A\beta_{40}$  ratio, C99I45F/C99WT), and thus in line with GSK3 activation.

### 6.14.2 Tau

Tau *hyper*phosphorylation of certain phosphorylation sites is a hallmark of AD and consequence of  $A\beta$  overproduction. Indeed, I found tau more strongly phosphorylated on serine 515 and serine 518 (corresponding to S199 and S202 of tau isoform 2= $\tau_{441}$ ) while it was not differentially expressed on the transcript level ( $A\beta_{42}/A\beta_{40}\uparrow$ ). This was validated by 3 antibodies: one directed against phosphorylated serine 515/518, one specifically against phosphorylated serine 515 and one specifically against phosphorylated serine 518. Serine 712 (corresponding to S396 of tau isoform 2= $\tau_{441}$ ) showed stronger phosphorylation in C99I45F than in C99V50F. Further repetitions with other antibodies (directed against serine 712) are necessary to validate this result. The following phosphorylation sites are among the critical sites to convert tau into a protein with toxic properties: S199/202/205, T212, T231/S235, S262/356 and S404 [116]. Furthermore, phosphorylation on T231, S396, and S422 promotes self-assembly of tau into filaments. *Taken together, serine 199, serine 202 and presumably serine 396 showed stronger phosphorylation in consequence of an increased  $A\beta_{42}/A\beta_{40}$  ratio than in consequence of a decreased  $A\beta_{42}/A\beta_{40}$  ratio. This strong phosphorylation possibly converts tau into a protein with toxic properties.*

### 6.14.3 Inverse phosphorylation of PKC as a result of a changed $A\beta_{42}/A\beta_{40}$ ratio

PKC showed a clear difference in the phosphorylation status as a consequence of a changed  $A\beta_{42}/A\beta_{40}$  ratio: PKC showed weaker phosphorylation as a result of an increased  $A\beta_{42}/A\beta_{40}$  ratio (mutant C99I45F/C99WT), whereas a decreased  $A\beta_{42}/A\beta_{40}$  ratio (mutant C99V50F/C99WT) led to stronger phosphorylation. This was observed for many subunits of PKC:  $\beta 1/2$  (threonine 500, n=1),  $\alpha/\beta 2$  (threonine 638/ threonine 641, n=2),  $\beta 2$  (threonine 641, n=1),  $\delta$  (serine 664, n=3),  $\eta$  (serine 674, n=2), strongly indicating inverse phosphorylation of PKC. *Hypophosphorylation for C99I45F ( $A\beta_{42}/A\beta_{40}$  ratio $\uparrow$ ) at the sites mentioned above is known to decrease activity of PKC. PKC, as well as protein kinases A and B, are reported to inhibit GSK3. For an increased  $A\beta_{42}/A\beta_{40}$  ratio, due to the expected reduced activity of PKC, the inhibiting effect on GSK3 is expected to be reduced which may contribute to GSK3 activation.*

#### **6.14.4 Differential phosphorylation of PKB (AKT1), PKA and FAK as a result of a changed $A\beta_{42}/A\beta_{40}$ ratio**

AKT1 showed weaker phosphorylation on serine 473 in mutant C99I45F than in C99WT. Hence, in mutant C99I45F the known inhibiting effects from AKT1 onto GSK3 $\beta$  might be reduced. This should result in increased GSK3 $\beta$  activity in C99I45F. AKT normally activates SGK. SGK was found to be down-regulated on the transcript (n=3) and protein level (n=1) and is in agreement with AKT-downregulation (for  $A\beta_{42}/A\beta_{40}$   $\uparrow$ ).

FAK (Focal adhesion protein-tyrosine kinase) is known to activate AKT (via further proteins). FAK showed weaker phosphorylation on S722 and is expected to be less active (for C99I45F compared to C99WT,  $A\beta_{42}/A\beta_{40}$   $\uparrow$ ), which might contribute to reduced activity of AKT.

PKA $\beta$  (on serine 338) showed weaker phosphorylation in mutant C99I45F than in mutant C99V50F which might lead to reduced PKA activity, so that inhibiting effects from PKA onto GSK3 $\beta$  might be reduced. This should contribute to increased GSK3 $\beta$  activity.

#### **6.14.5 Probable activation of MAPkinase/ERK signaling due to strong phosphorylation of MEK1 and ERK1 in response to an increased $A\beta_{42}/A\beta_{40}$ ratio**

Raf1 or other upstream proteins activate the MAP2 kinases, MEK1 and MEK2 (MEK1/2). MEK1/2, in turn, activates ERK1/2. The extracellular signal-regulated kinases 1 and 2 (ERK1 and ERK2) are pleiotropic mitogen activated serine/threonine protein (MAP) kinases with over 160 known substrates, found throughout the cell that include other protein kinases, membrane receptors, cytoskeletal proteins, downstream effector kinases and transcription factors. ERK1/2 regulates proliferation, differentiation, cell cycle processes, and survival, as well as many other cell processes. Excessive ERK1/2 activation induces apoptosis. ERK1/2 activate a plethora of transcription factors including but not limited to CREB, c-Myc, c-Jun, c-Fos, and STAT. In response to an increased  $A\beta_{42}/A\beta_{40}$  ratio MEK1 was stronger phosphorylated on serine 297, but less phosphorylated on the same site for  $A\beta_{42}/A\beta_{40}$   $\downarrow$ . The same phosphorylation pattern could be found for threonine 291. ERK1 was more strongly phosphorylated on threonine 202 or/and tyrosine 204 in mutant C99I45F than in C99WT. This argues for an activation of both MEK1 and ERK1. Since ERK1 is a downstream target of MEK1 the whole pathway seems to be activated (in response to an increased  $A\beta_{42}/A\beta_{40}$ ).

## 6.15 APLP1 and APLP2 were differentially affected by a changed A $\beta$ <sub>42</sub>/A $\beta$ <sub>40</sub> ratio

Amyloid precursor-like protein 1 (APLP1) is a membrane-associated glycoprotein cleaved by secretases in a manner similar to APP cleavage. This cleavage liberates an intracellular cytoplasmic fragment that may act as a transcriptional activator. The encoded protein may also play a role in synaptic maturation during cortical development. Alternatively spliced transcript variants encoding different isoforms have been described. It may play a role in postsynaptic function. APLP1 may interact with cellular G-protein signaling pathways. It can regulate neurite outgrowth through binding to components of the extracellular matrix such as heparin and collagen I. APLP1 is a cell membrane; single-pass type I membrane protein, C-terminally processed in the golgi complex. It is assumed to bind, via its C-terminus, to several cytoplasmic proteins, including MAPK8IP1 and DAB1. Binding to DAB1 inhibits its serine phosphorylation and it is assumed to interact with CPEB1. It is expressed in the cerebral cortex where it is localized to the postsynaptic density. It binds zinc and copper in the extracellular domain, zinc-binding increases heparin binding. APLP1 influences endocytosis and proteolytic processing of the amyloid precursor protein. APLP1 affects the endocytosis of APP and makes more APP available for  $\alpha$ -secretase cleavage [345]. Interaction of APLP1 with the  $\alpha$ 2A-adrenergic receptor increases agonist-mediated inhibition of adenylate cyclase [346]. The proteolytic processing of the amyloid precursor protein gene family members APLP1 and APLP2 involves  $\alpha$ ,  $\beta$ ,  $\gamma$ , and  $\epsilon$ -like cleavages; APLP1 processing is modulated by n-glycosylation [347].

The human amyloid precursor-like protein 2 (APLP2) is a highly conserved single-pass type I membrane protein. APLP2 may interact with cellular G-protein signaling pathways. *The intracellular domains of APLP2 interact with the CP2 transcription factor in the nucleus and induce glycogen synthase kinase 3 $\beta$  expression* [348, 349].

It has been shown that APP/APLP2-deficient mice die shortly after birth [350]. APLP2(-)/APLP1(-) and APLP2(-)/APP(-) mice died at an early postnatal stage. Surprisingly, APLP1(-)/APP(-) mice were viable, apparently normal, and showed no compensatory upregulation of APLP2 expression. These data indicate a key physiological role for APLP2. This view gains further support by the observation that APLP1(-)/APP(-)/APLP2(+/-) mice died early postnatally. However, none of the lethal double mutants displayed obvious histopathological abnormalities in the brain or any other organ examined. Moreover, cortical neurons from single or combined mutant mice showed unaltered survival rates under basal culture conditions and

unaltered susceptibility to glutamate excitotoxicity *in vitro* [193].

As a consequence of an increased  $A\beta_{42}/A\beta_{40}$  ratio I found APLP2 significantly ( $n=3$ ,  $p=0.0179$ , fold change=1.6) up-regulated, whereas APLP1 was not differentially expressed. There is *in vivo* evidence for increased immunoreactivities of the nuclear C-terminal fragments of APLP2 in the brains of AD patients [348].

In contrast to this APLP1 was significantly ( $n=3$ ,  $p=0.0188$ , fold change=1.7) up-regulated as a result of a decreased  $A\beta_{42}/A\beta_{40}$  ratio, whereas APLP2 was not differentially expressed. APP was not differentially expressed in either of the mutants (compared to C99WT).

I speculate that upregulation of APLP2 as a consequence of an increased  $A\beta_{42}/A\beta_{40}$  ratio could either be a putative physiological function of  $A\beta_{42}$  or a survival signal of the cells, which are stressed by  $A\beta_{42}$ . Furthermore, it can be argued that APLP2 up-regulation is a counter-reaction of the cell to protect itself from toxic  $A\beta_{42}$ . APLP2 has been reported to be involved in apoptosis [351].

Further characterisation of the promoters of APLP2/APLP1 is necessary to address the question of whether  $A\beta_{42}/A\beta_{40}$  directly bind to their promoters (even if only small intracellular amounts of  $A\beta$  are expected to be available) or if APLP2/APLP1 expression is triggered via further factors. Glypican 3 was among the genes with smallest p-values and so it was significantly down-regulated as a result of a decreased  $A\beta_{42}/A\beta_{40}$  ratio. Colocalisation in perinuclear compartments of neuroblastoma cells of APLPs and glypicans has been shown [352], so it can be speculated that there is a functional relationship between the up-regulated APLP1 (for  $A\beta_{42}/A\beta_{40}\downarrow$ ) and the down-regulated cell adhesion molecule glypican 3. Further functional interaction partners for APLP1/APLP2 may be the following cell adhesion molecules, which were found to be dysregulated in consequence of a changed  $A\beta_{42}/A\beta_{40}$  ratio: integrin beta 5, tetraspanin 7, neural cell adhesion molecule 1, neural cell adhesion molecule 2, CD99 antigen, catenin alpha 2, reelin, microfibrillar-associated protein 4, neurofascin, L1 cell adhesion molecule and neuronal cell adhesion molecule.

## 6.16 APLP1/APLP2 co-regulated genes

Genes coding for catenin  $\alpha$  2, NCAM1, ACTN1, Rho GTPase activating protein 26 and KIAA1102 were found to be co-regulated with APLP1 *and* APLP2. Since these genes were found to be co-regulated with *both* APP-like genes, a functional relationship can be assumed between APP-like genes and these five genes. Furthermore, it can be assumed to not be by chance that actinin alpha 1 (ACTN1,

chr14q24) is localized on the same chromosomal locus as presenilin 1 (chr14q24). There might be a feedback mechanism between presenilin 1 and actinin alpha 1, possibly via processing of APLPs/APP or another kind of regulation.

### **6.17 Axonal outgrowth, synaptogenesis, neurotransmitter release**

Axonal outgrowth, synaptogenesis and neurotransmitter release have been shown to be affected in AD [353-355].

L1CAM (synonym: L1) was found to be up-regulated ( $A\beta_{42}/A\beta_{40}\downarrow$ ). L1CAM is a cell adhesion molecule which plays an important role in nervous system development, including neuronal migration and differentiation. L1CAM is involved in neuron-neuron adhesion, neurite fasciculation, outgrowth of neurites, etc.. It binds to axonin on neurons. Mutations in the gene cause three X-linked neurological syndromes known by the acronym CRASH (corpus callosum hypoplasia, retardation, aphasia, spastic paraplegia and hydrocephalus). Defects in hydrocephalus due to stenosis of the aqueduct of sylvius are characterized by mental retardation and enlarged brain ventricles. Kenrick et al. reviewed the various functions of L1CAM, including guidance of neurite outgrowth in development, neuronal cell migration, axon bundling, synaptogenesis, myelination, neuronal cell survival, and long-term potentiation [356]. On differentiated neurons L1 is found at regions of contact between neighbouring axons and on the growth cones, the structures at the leading tip of axons that are responsible for sensing extracellular growth and guidance cues. This distribution supports the suggestion from in vitro studies that L1 adhesive interactions may mediate axon bundling (fasciculation) and that L1 acts as a growth cone receptor for signals that induce the extension of processes (neurites) from neurons in culture.

Neuronal cell adhesion molecule (NRCAM) was up-regulated ( $A\beta_{42}/A\beta_{40}\downarrow$ ). This ankyrin-binding protein is involved in neuron-neuron adhesion and promotes directional signaling during axonal cone growth. This gene is also expressed in non-neural tissues and may play a general role in cell-cell communication via signaling from its intracellular domain to the actin cytoskeleton during directional cell migration. Allelic variants of this gene have been associated with autism and vulnerability to addiction.

Contactin 3 (CNTN3) was up-regulated in mutant C99I45F ( $A\beta_{42}/A\beta_{40}\uparrow$ ) and *in parallel* downregulated in mutant C99V50F ( $A\beta_{42}/A\beta_{40}\downarrow$ ). Contactins mediate cell surface interactions during nervous system development. CNTN3 is assumed to have neurite outgrowth-promoting activity.

Semaphorin 3C (SEMA3C) was up-regulated ( $A\beta_{42}/A\beta_{40}\uparrow$ ,  $p=0.0106$ , fold change=1.9), but not differentially expressed when the  $A\beta_{42}/A\beta_{40}$  was decreased. Semaphorins, constitute a family characterized by the presence of a conserved semaphorin domain at the N-terminus. SEMA3C may be involved in diverse cell survival mechanisms. All glioma cell lines are reported to express SEMA3A and SEMA3C and exhibit SEMA3A binding sites.

SEMA3A was up-regulated, which was confirmed by another probe-set ( $A\beta_{42}/A\beta_{40}\downarrow$ ,  $p=0.025$ , fold change=4.0), but not differentially expressed when the  $A\beta_{42}/A\beta_{40}$  was increased. Intriguingly, we (together with our colleague Laura Busia) also found SEMA3A to be among the most strongly and significantly up-regulated genes in embryonic mouse fibroblasts in consequence of PS1 and PS2 knockdown with siRNA. In this approach  $A\beta$  levels were expected to be decreased. This is in line with the observation of SEMA3A upregulation in mutant C99V50F compared to C99WT ( $A\beta_{42}/A\beta_{40}\downarrow$ ) and argues for an effect mediated by decreased  $A\beta_{42}$ .

The SEMA3A gene is a member of the semaphorin family and encodes a protein with an Ig-like C2-type (immunoglobulin-like) domain, a PSI domain and a sema domain. It is a secreted protein which can function as a *chemoattractive* agent, stimulating the growth of apical dendrites. The protein is vital for normal neuronal pattern development. Associations with Alzheimer's disease have been found [357]. SEMA3A could serve as a ligand that guides specific growth cones by a motility-inhibiting mechanism, it binds to the complex neuropilin-1/plexin-1. Polleux et al. demonstrated that the growth of apical dendrites toward the pial surface is regulated by a diffusible chemoattractant present at high levels near the marginal zone. A major component of this signal was SEMA3A. Soluble guanylate cyclase is asymmetrically localized to the developing apical dendrite, and is required for the chemoattractive effect of SEMA3A. Thus, the asymmetric localization of soluble guanylate cyclase confers distinct SEMA3A responses to axons and dendrites. Polleux et al. concluded that these observations reveal a mechanism by which a single chemotropic signal can pattern both axons and dendrites during development [358]. Loss of neuropilin function increases the number of interneurons that migrate into the striatum. Marin et al. concluded that their observations reveal a mechanism by which neuropilins (semophorin-neuropilin interaction were studied) mediate sorting of distinct neuronal populations into different brain structures, and provide evidence that, in addition to guiding axons, these receptors also control neuronal migration in the central nervous system [359].

Growth associated protein 43 (GAP43) has been termed a 'growth' or 'plasticity' protein because it is expressed at high levels in neuronal growth cones during development and axonal regeneration. GAP43 is considered to be a crucial component of an effective regenerative response in the nervous system. GAP43 binds calmodulin with a greater affinity in the absence of  $\text{Ca}^{2+}$  than in its presence. Aberrant GAP43 gene expression in Alzheimer's disease has been observed [360].

Nuclear receptor subfamily 2, group F, member 1 (NR2F1) was not differentially expressed (for  $\text{A}\beta_{42}/\text{A}\beta_{40}\uparrow$ ), but up-regulated when the  $\text{A}\beta_{42}/\text{A}\beta_{40}$  was decreased ( $p=0.064$ , fold change=1.4). NR2F1, a transcription factor, is an orphan member of the nuclear receptor superfamily. It is an important regulator of neurogenesis, cellular differentiation and cell migration. NR2F1 is required for *proper axonal growth and guidance* of all major forebrain commissures. Moreover, *hippocampal neurons lacking NR2F1 have a defect in neurite outgrowth and show an abnormal axonal morphology* [359].

Pleiotrophin (heparin binding growth factor 8, neurite growth-promoting factor 1 (PTN) was not differentially expressed (insignificantly down-regulated,  $\text{A}\beta_{42}/\text{A}\beta_{40}\uparrow$ ,  $p=0.69$ , fold change=-1.2), but up-regulated when the  $\text{A}\beta_{42}/\text{A}\beta_{40}$  ratio was decreased,  $p=0.152$ , fold change=1.6). PTN is a heparin binding mitogenic protein. It has neurite extension activity. PTN is a member of a highly conserved human gene family of proteins. It exhibits neurite outgrowth-promoting activity and may play a role in nervous tissue development and/or maintenance. Expression of this factor is developmentally regulated, increasing in the brain during embryogenesis and reaching its maximum expression at the time of birth. In a spinal cord explant system, PTN caused increased outgrowth of spinal motor axons and protected spinal motor neurons against chronic excitotoxic injury. In neonatal mice, PTN protected facial motor neurons against cell death induced by deprivation of growth factors. In adult rats, PTN enhanced regeneration of myelinated axons across a graft in transected sciatic nerve. Pleiotrophin is a neurotrophic factor for spinal motor neurons [361].

HGF was down-regulated ( $\text{A}\beta_{42}/\text{A}\beta_{40}\uparrow$ ,  $p=0.157$ , fold change=-3.0), but not differentially expressed when the  $\text{A}\beta_{42}/\text{A}\beta_{40}$  was decreased. Two further probe-sets confirmed the downregulation, however, with  $p$ -values  $>0.05$ .

HGF induces signal transduction through the receptor tyrosine kinase c-Met [362]. It activates the urokinase-type plasminogen activator promoter (PLAU) [363] and thus accelerates fibrinolysis. Gene transfer of the HGF gene into rat brains improved learning and memory in the chronic stage of cerebral infarction; immunohistochemical analysis for Cdc42 and synaptophysin in the peri-infarct region revealed that HGF enhanced the neurite extension and increased the number of

synapses. These data demonstrated that HGF has a pivotal role for the functional recovery after cerebral infarction through neurogenesis and improved microcirculation [364]. HGF antagonizes TGF- $\beta$ 1 by stabilizing SMAD transcriptional co-repressor TGIF [365]. Human platelets express the HGF receptor (the tyrosine kinase encoded by the c-MET gene). At physiological concentrations HGF was found to inhibit both glycoprotein  $\alpha$ 2 $\beta$ 3 activation and thrombin-dependent platelet aggregation in a dose and time-dependent manner. These results suggest that circulating HGF may counteract thrombogenesis by negatively modulating platelet functions [322]. Exogenous HGF promoted a highly significant increase in dendritic growth and branching of layer 2 pyramidal neurons, whereas deactivation of endogenous HGF with function-blocking anti-HGF antibodies caused a marked reduction in size and complexity of the dendritic arbors of these neurons. Furthermore, pyramidal neurons transfected with an MET dominant-negative mutant receptor likewise had much smaller and less complex dendritic arbors than control transfected neurons did. These results indicate that HGF plays a role in regulating dendritic morphology in the developing cerebral cortex [366]. Expression of c-Met in developing rat hippocampus provided evidence for HGF as a neurotrophic factor for calbindin D-expressing neurons [367]. It is known that HGF induces in vitro expression of vascular endothelial growth factor (VEGF), a key agonist of tumor angiogenesis; by contrast, thrombospondin 1 (TSP-1) is a negative regulator of angiogenesis. It was shown that, in the very same tumor cells, in addition to inducing VEGF expression, HGF down-regulated TSP-1 expression.

Amyloid beta (A $\beta$ ) precursor-like protein 1 (APLP1) was not differentially expressed (for A $\beta$ <sub>42</sub>/A $\beta$ <sub>40</sub>↑) but was up-regulated when the A $\beta$ <sub>42</sub>/A $\beta$ <sub>40</sub> was decreased (p=0.0188, fold change=1.7). Accumulation of APLP2 and reduction of APLP1 in retinoic acid-differentiated human neuroblastoma cells has been observed upon curcumin-induced neurite retraction [368].

Ectodermal-neural cortex (with BTB-like domain) (ENC1) was up-regulated both when the A $\beta$ <sub>42</sub>/A $\beta$ <sub>40</sub> ratio was increased (p=0.0079, fold change=2.2) and when the A $\beta$ <sub>42</sub>/A $\beta$ <sub>40</sub> ratio was decreased (p=0.0089, fold change=1.7). Kim et al. showed that expression of ENC1 induced neuronal process formation, whereas antisense treatment inhibited neurite development. Immunoblot analysis showed that ENC1 is a nuclear matrix protein and can be phosphorylated and binds to the functionally active hypophosphorylated form of the nuclear matrix protein RB1 during neuronal differentiation [369]. The fact that ENC1 was up-regulated in consequence of an increased A $\beta$ <sub>42</sub>/A $\beta$ <sub>40</sub> ratio *as well as* a decreased A $\beta$ <sub>42</sub>/A $\beta$ <sub>40</sub> ratio hints at it not being a good candidate gene for axonal outgrowth due to a changed A $\beta$ <sub>42</sub>/A $\beta$ <sub>40</sub> ratio.

SERPINE2 (synonyms: glial-derived *neurite promoting* factor p, nexin plasminogen activator inhibitor type 1, protease nexin I (PN1), protease inhibitor 7), previously mentioned in this thesis as being involved in blood coagulation, was down-regulated ( $A\beta_{42}/A\beta_{40}\uparrow$ ,  $p=0,174$  fold change=-2.3), but not differentially expressed when the  $A\beta_{42}/A\beta_{40}$  was decreased. SERPINE2 is highly expressed and developmentally regulated in the nervous system where it is concentrated at neuromuscular junctions and central synapses in the hippocampus and striatum. Approximately 10% of identified proteins at mammalian neuromuscular junctions are, like SERPINE2, serine protease inhibitors, consistent with their central role in balancing serine protease activity to develop, maintain, and remodel synapses.

TIMP1, previously described as an collagenase inhibitor, was down-regulated ( $A\beta_{42}/A\beta_{40}\uparrow$ ,  $p=0.127$ , fold change=-3.5), but not differentially expressed when the  $A\beta_{42}/A\beta_{40}$  ratio was decreased. *This gene is located within intron 6 of the synapsin I gene and is transcribed in the opposite direction. TIMP1 is mentioned here, because of its location within an intron of the synapsin I gene. So there might be a functional relationship between synaptogenesis/neurotransmitter release (mediated by synapsins) and inhibition of metalloproteases (function of TIMPs).*

SynapsinI (SYN1) could only be found to be significantly down-regulated for the comparison C99WT/mock ( $p=0.00194$ , fold change= -3.0), but it was not differentially expressed when both mutants were compared to the wildtype (C99I45F/C99WT and C99V50F/C99WT). This argues, in contrast to the results obtained for synapsinII, for an effect mediated by C99 rather than by  $A\beta_{42}$  or  $A\beta_{40}$ .

SynapsinII was among the most inversely regulated genes by an altered  $A\beta_{42}/A\beta_{40}$  ratio:  $A\beta_{42}/A\beta_{40}\uparrow$ ,  $p=0.072$ , fold change=1,3 ;  $A\beta_{42}/A\beta_{40}\downarrow$ ,  $p=0.102$ , fold change=-1,3. These data demonstrated that SynapsinII (SYN2) was regulated by  $A\beta_{42}/A\beta_{40}$ .

Synapsins encode neuronal phosphoproteins which associate with the cytoplasmic surface of synaptic vesicles. They are implicated in synaptogenesis and the *modulation of neurotransmitter release*, suggesting a potential role in several neuropsychiatric diseases. The synapsins are a family of 4 synaptic vesicle-associated proteins, synapsins Ia, Ib, IIa, and IIb that have been implicated in modulation of neurotransmitter release and in synaptogenesis [370]. They are products from alternative splicing of 2 distinct genes, SYN1 and SYN2. SYN2 encodes a neuron-specific phosphoprotein that *selectively binds to small synaptic vesicles in the presynaptic nerve terminal. The TIMP4 gene is located within an intron of this gene and is transcribed in the opposite direction. Mutations in this gene may be associated with abnormal presynaptic function and schizophrenia.* Alternative splicing of this gene results in two transcripts. SYN2 coats synaptic vesicles, binds to

the cytoskeleton, and is believed to function in the *regulation of neurotransmitter release*. Mirnics et al. found that transcripts encoding proteins involved in the regulation of presynaptic function were decreased in all subjects with schizophrenia [371]. Predicted functional partners (predicted by computational calculations) of SYN2 are: TIMP2, 3 and 4. Using a cDNA microarray representing 6794 distinct human genes, Ho et al. identified candidate genes whose expression is altered in cerebral cortex of cases of early AD; among these was the synaptic vesicle protein SYN2, which plays an important role in neurotransmitter release. A selective decrease in the expression of the SYN2 splice variants I-III of the a-type isoform was found in the entorhinal but not visual cortex characterized by the earliest clinically detectable stage of AD. In contrast, Ho et al. found no changes in synapsin splice variant II of the b-type isoform. Alteration of synapsin expression at the earliest clinical stage of AD may suggest new strategies for improved treatment [372].

SLIT1, a human homolog of the *Drosophila* SLIT gene, encodes a secreted protein, which contains conserved protein-protein interaction domains including leucine-rich repeats and epidermal growth factor-like motifs. Slit proteins have been shown to regulate axon guidance, branching, and neural migration. It was reported that SLIT1 regulates dendritic development. Slit1 is expressed in the developing cortex, and *exposure to SLIT1 leads to increased dendritic growth and branching*. Conversely, inhibition of Slit-Robo interactions (Slit is the ligand and Robo the corresponding receptor) by a dominant-negative Robo attenuates dendritic branching. Stimulation of neurons transfected with a Met-Robo chimeric receptor with Hepatocyte growth factor leads to a robust induction of dendritic growth and branching, suggesting that Robo-mediated signaling is sufficient to induce dendritic remodeling. These experiments indicated that Slit-Robo interactions may exert a significant influence over the specification of cortical neuron morphology by regulating both axon guidance and dendritic patterning [373]. SLIT1 was found to be up-regulated for a decreased  $A\beta_{42}/A\beta_{40}$  ratio, *but not for an increased one*.

*In summary, these data strongly indicate inhibited axonal outgrowth in consequence of an increased  $A\beta_{42}/A\beta_{40}$  ratio, but a strong tendency to enhanced axonal outgrowth in consequence of a decreased  $A\beta_{42}/A\beta_{40}$  ratio. Furthermore, there are signs of reduced dendritic sprouting and synaptogenesis ( $A\beta_{42}/A\beta_{40}\uparrow$ ) in contrast to promoted dendritic sprouting and synaptogenesis for a decreased  $A\beta_{42}/A\beta_{40}$  ratio. The genomic localisation of TIMP genes within introns of synapsin genes and its transcription in the opposite direction is interesting. This mechanism may turn out to be crucial, because TIMP and synapsin genes belong to the most differentially expressed genes in this thesis.*

## 6.18 Axonal transport

Axonal transport has been shown to be affected in AD (reviewed in [374]).

Dynein cytoplasmic *light* intermediate polypeptide 2 (DNCL12) was down-regulated ( $A\beta_{42}/A\beta_{40}\uparrow$ ,  $p=0.0066$ , fold change=-1.5). The corresponding protein (DNCL12) was *also found to be among the 20 most down-regulated proteins in blind samples (proteomic approach: 2D-gel with subsequent mass spectrometry)*. DNCL12 was not differentially expressed when the  $A\beta_{42}/A\beta_{40}$  was decreased. It may play a role in regulating interactions between dynein and p150-glued, and the cellular substrates for dynein-mediated motility (such as organelles). *Downregulation of DNCL12 could explain the “clogging phenomenon” in axons, due to aggravated retrograde cargo transport.*

Dynein cytoplasmic intermediate polypeptide 1 (DNC11) was up-regulated ( $A\beta_{42}/A\beta_{40}\uparrow$ ,  $p=0.0111$ , fold change=1.8), but not differentially expressed when the  $A\beta_{42}/A\beta_{40}$  was decreased. The intermediate chains seem to help dynein bind to the dynactin 150 kDa component. It may play a role in mediating the interaction of cytoplasmic dynein with membranous organelles and kinetochores. *There is experimental evidence for an association between DNC11 and internexin neuronal intermediate filament protein, alpha (INA) [375]. INA was found to be among the 20 most up-regulated and significant ( $p<0.05$ ) transcripts and proteins ( $A\beta_{42}/A\beta_{40}\uparrow$ , C99I45F/C99WT) but also when the  $A\beta_{42}/A\beta_{40}$  ratio was decreased (C99V50F/C99WT).*

The following kinesin family members were up-regulated ( $A\beta_{42}/A\beta_{40}\uparrow$ ), but not differentially expressed when the  $A\beta_{42}/A\beta_{40}$  was decreased. Kinesin family member 1A (KIF1A) ( $p=0.15$ , fold change=2.2), KIF21A ( $p=0.074$ , fold change=1.8), KIF5c ( $p=0.01$ , fold change=1.7), KIF1B ( $p=0.0371$ , fold change=1.6). In contrast to this Kinesin 2 (KNS2, 60/70kDa) was not differentially expressed ( $A\beta_{42}/A\beta_{40}\uparrow$ ), but weakly and significantly up-regulated ( $p=0.027$ , fold change=1.3) when the  $A\beta_{42}/A\beta_{40}$  was decreased. KIF1A is an anterograde motor protein that transports membranous organelles along axonal microtubules. Its cargo includes a subset of precursors for synaptic vesicles: synaptophysin, synaptotagmin, and Rab3A. The phenotype of KIF1A knockout mice includes motor and sensory disturbances, a reduction in the density of synaptic vesicles in nerve terminals, and accumulation of vesicles in nerve cell bodies [376]. It can be hypothesized that KIF1A may play a critical role in the development of axonal neuropathies resulting from impaired axonal transport. Kinesin family member 21A (KIF21A). It was demonstrated that mouse KIF21A bound strongly to microtubules in the presence of a nonhydrolyzable ATP analog. They found that KIF21A accumulated on the proximal side of a sciatic nerve ligation,

consistent with KIF21A being a plus end-directed motor protein. Nangaku et al. found that mouse KIF1B works as a monomer, having a microtubule plus-end-directed motility. Immunocytochemically, KIF1B was colocalized with mitochondria in vivo. A subcellular fractionation study showed that KIF1B was concentrated in the mitochondrial fraction, and purified KIF1B could transport mitochondria along microtubules in vitro. These data suggested that *KIF1B works as a monomeric motor for anterograde transport of mitochondria. KIF1B up-regulation may be a counter-regulation of the cells (due to possible reduced energy in consequence of an increased  $A\beta_{42}/A\beta_{40}$  ratio), with the goal of providing more ATP to regions where energy is needed. ATP might be involved, which is also suggested by the previously discussed KIF21A, which binds strongly to microtubules in the presence of a nonhydrolyzable ATP analog [377].*

Weak upregulation of Kinesin 2 (synonyms: KLC, KLC1, KNS2A) could be interpreted as an augmented anterograd axonal transport, in consequence of a decreased  $A\beta_{42}/A\beta_{40}$  ratio.

Prolyl endopeptidase (PREP) was found to be up-regulated on the transcript level and on the protein level for  $A\beta_{42}/A\beta_{40}\uparrow$  but not for  $A\beta_{42}/A\beta_{40}\downarrow$ . Immunocytochemical double-labelling procedures and localization of PREP-enhanced green fluorescent protein fusion proteins showed that PREP is mainly localized to the perinuclear space, and is associated with the microtubulin cytoskeleton in human neuroblastoma and glioma cell lines. Disassembly of the microtubules by nocodazole treatment disrupts both the fibrillar tubulin and PREP labelling. *Furthermore, in a two-hybrid screen, PREP was identified as binding partner of tubulin [293].* These findings indicate novel functions for PREP in axonal transport and/or protein secretion.

Vesicular membrane protein p24 (VMP) was the second most significantly up-regulated gene (for  $A\beta_{42}/A\beta_{40}\uparrow$ ,  $p=0.0055$ , fold change=2.8), but no differential expression was observed for  $A\beta_{42}/A\beta_{40}\downarrow$ . VMP contains two putative membrane spanning domains and a hydrophilic tail homologous to the microtubule-binding domain of MAPs. So it can be speculated that VMP may be associated with microtubules through its C-terminus and may play an important role in vesicular organelles transport and nerve signals.

## 6.19 Oxidative stress is expected to be increased by up-regulation of the mitochondrial respiratory chain in consequence of an increased $A\beta_{42}/A\beta_{40}$ ratio

Accumulation of reactive oxygen species (ROS) results in damage to major components of cells: nucleus, mitochondrial DNA, membranes, and cytoplasmic proteins. The imbalance between the generation of free radicals and ROS may be involved in the pathogenesis of most of the neurodegenerative disorders, including AD, as suggested by many authors for many years. The fact that age is a key risk factor in AD provides considerable support for the “free radical hypothesis” because effects of the attacks by free radicals, particularly those produced by ROS, can accumulate over the years [378].

The respiratory chain is influenced by a changed  $A\beta_{42}/A\beta_{40}$  ratio. NDUFB9 (NADH dehydrogenase (ubiquinone) 1 beta subcomplex) was 1.3 fold up-regulated ( $p=0.063$ , for  $A\beta_{42}/A\beta_{40}\uparrow$ ) and *in parallel* 2.3 fold down-regulated ( $p=0.132$ , for  $A\beta_{42}/A\beta_{40}\downarrow$ ). NDUFB9 transfers electrons from NADH to the respiratory chain. The immediate electron acceptor for the enzyme is believed to be ubiquinone. NDUFB9 is localized in the inner mitochondrial membrane on the matrix side. It transfers electrons to the following reaction:  $NADH + ubiquinone = NAD^+ + ubiquinol$ .

SDHAL2 (Succinate dehydrogenase complex, subunit A, flavoprotein-like 2, localized on chr3q29) was not differentially expressed (for  $A\beta_{42}/A\beta_{40}\uparrow$ ) but 3.2 fold down-regulated ( $p=0.04742$ , for  $A\beta_{42}/A\beta_{40}\downarrow$ ). This regulations might reflect a response of the cells to reduced ATP levels for  $A\beta_{42}/A\beta_{40}\uparrow$  and sufficient ATP levels for  $A\beta_{42}/A\beta_{40}\downarrow$ . ADAM11 (a disintegrin and metalloproteinase domain 11) was exactly co-regulated (not differentially expressed for  $A\beta_{42}/A\beta_{40}\uparrow$ , but down-regulated for  $A\beta_{42}/A\beta_{40}\downarrow$ ,  $p=0.04742$ , fold change=-3.2) with SDHAL2. Moreover, ADAM11 is located on the same chromosomal locus as tau (chr17q21.3), thus it can be speculated that there is a functional relationship between the respiratory chain (ATP-levels respectively), metalloproteases and tau. Another functional relationship can be assumed for the dysregulated transferrin receptor (p90, CD71), localized on the same locus as SDHAL2 (chr3q29). The transferrin receptor was not differentially expressed (for  $A\beta_{42}/A\beta_{40}\uparrow$ ) but 1,4 fold down-regulated for  $A\beta_{42}/A\beta_{40}\downarrow$  ( $p=0.0361$ ). Due to the same tendency of regulation on the same chromosomal locus a “Chromeron regulation” is probable. Cellular uptake of iron occurs via receptor-mediated endocytosis of ligand-occupied transferrin receptors into specialized endosomes and endosomal acidification leads to iron release. *The transferrin receptor is required for iron delivery from transferrin to cells.* There is a bidirectional

relationship between iron metabolism and type 2 diabetes: Iron affects glucose metabolism and glucose metabolism influences several iron metabolic pathways. Both insulin sensitivity and glucose tolerance are closely associated with serum transferrin receptor concentrations [379]. Furthermore, transferrin binds insulin-like growth factors and affects binding properties of insulin-like growth factor binding protein 3 [380].

The above proposed ATP-dependent regulation of components of the respiratory chain is supported by the observation of upregulation of UQCRC1 (ubiquinol-cytochrome c reductase, Rieske iron-sulfur polypeptide 1, localized at the mitochondrial inner membrane) for  $A\beta_{42}/A\beta_{40}\uparrow$ , but the lack of differential expression for  $A\beta_{42}/A\beta_{40}\downarrow$  (detected by PANTHER analysis in which the 50 most up-regulated genes were integrated with a p value  $<0.05$ ).

The hypothetical protein FLJ10094 shows strong similarity to hydroquinone (NADH) oxidase. Hydroquinone (NADH) oxidase is assumed to be localized at the plasma membrane. It probably acts as a terminal oxidase of electron transport from cytosolic NAD(P)H via hydroquinones to acceptors at the cell surface. FLJ10094 was up-regulated for  $A\beta_{42}/A\beta_{40}\uparrow$  ( $p=0.073$ , fold change=1.3) and down-regulated for  $A\beta_{42}/A\beta_{40}\downarrow$  ( $p=0.111$ , fold change=-1.4).

*Taken together, the results indicate an upregulation of the respiratory chain for  $A\beta_{42}/A\beta_{40}\uparrow$ , but a downregulation for  $A\beta_{42}/A\beta_{40}\downarrow$ , which might reflect the attempt of the cells to restore sufficient ATP-levels for  $A\beta_{42}/A\beta_{40}\uparrow$ . This may be inherently connected with increased oxidative stress by the release of reactive oxygen species (ROS) like the superoxide radical ( $\cdot O_2^-$ ), the peroxide anion ( $O_2^{2-}$ ) or the hydroxy radical ( $\cdot OH$ ). Hydrogen peroxide levels were found to be significantly increased in Tg2576 mice when compared with age-matched WT littermates and directly correlated with levels of soluble A $\beta$  in Tg2576 mice, suggesting that soluble A $\beta$  may be responsible for the production of hydrogen peroxide in AD progression in Tg2576 mice [381]. In parallel to this, the superoxide dismutase 1 (SOD1) was up-regulated for  $A\beta_{42}/A\beta_{40}\uparrow$  (shown by immuno blot,  $n=1$ ). Intracellular copper levels might be decreased (extracellular copper levels could be increased, depending at least in part on basal extracellular copper levels) because the copper-transporting ATP7A (exports copper from the cells) was increased for  $A\beta_{42}/A\beta_{40}\uparrow$  ( $p=0.0222$ , fold change=1.5) and decreased for  $A\beta_{42}/A\beta_{40}\downarrow$  ( $p=0.0621$ , fold change=-2.0). The driving force for these regulatory processes might be low ATP-levels caused by an increased  $A\beta_{42}/A\beta_{40}$  ratio.*

## 6.20 Strong dysregulation of cytochromes by a changed $A\beta_{42}/A\beta_{40}$ ratio

The cytochrome b-245, alpha polypeptide (Cyba, synonyms: Nox2, *superoxide-generating* NADPH oxidase light chain subunit) is an essential component of NADPH-oxidase (for instance in phagocytes), a membrane-bound enzyme complex that generates large quantities of microbicidal superoxide and other oxidants upon activation. NADPH oxidase of phagocytic cells is important for the efficient killing and digestion of ingested microbes. Cyba is a flavocytochrome containing FAD and the NADPH-binding site of the microbicidal oxidase of phagocytes [382]. Cyba was found in the plasma membrane, cytosol and granules of neutrophil granulocytes [383, 384], but was also suggested to be located in other intracellular structures [385].

Jackson et al. reported that activated mouse T-cells deficient in Cyba showed enhanced activation of ERK and MEK and diminished expression of phagocyte-type NADPH oxidase and that *T cell receptor stimulation induces rapid generation of reactive oxygen species* by an yet unclear mechanism [386].

The cytochrome b-245, alpha polypeptide was among the most significantly down-regulated ( $p=0.00028$ , fold change=-2.5) genes for  $A\beta_{42}/A\beta_{40}\uparrow$  but was not differentially expressed for  $A\beta_{42}/A\beta_{40}\downarrow$ . Interestingly the expression (detected on the transcript level by microarray analysis and on the protein level by a proteomics approach) of the T-cell receptor alpha and delta locus was significantly up-regulated in consequence of both increased *and* decreased  $A\beta_{42}/A\beta_{40}$  ratios. MEK1 and ERK1 were more strongly phosphorylated in response to an increased  $A\beta_{42}/A\beta_{40}$  ratio (compared to a decreased ratio) and thus most probably activated (described elsewhere in this thesis). This underlines the observation of Jackson et al. of a relationship between T-cells (or T-cell receptors), Cyba and ERK/MEK.

Cyba downregulation for  $A\beta_{42}/A\beta_{40}\uparrow$  might be a secondary effect of increased  $A\beta_{42}$ . I suggest that in our approach,  $A\beta_{42}$  overexpression triggers oxidative stress (for instance via upregulation of the mitochondrial respiratory chain, discussed in the previous Chapter). The cells may counter-regulate this by downregulating the *superoxide-generating* Cyba, so that superoxide radicals do not rise too extremely.

Cyp561 (cytochrome b561) is a functional ferric reductase presumed to be regulated by iron [387]. It is a major transmembrane protein that is found in catecholamine and neuropeptide secretory vesicles of the adrenal medulla, pituitary gland, and other neuroendocrine tissues. This cytochrome is present in both the small synaptic vesicles and the large dense core vesicles (chromaffin granules) of the tissues. Its role is to supply reducing equivalents to 2 monooxygenases, dopamine beta-

hydroxylase in chromaffin granules and monooxygenases in neurosecretory vesicles. Cyp561 was among the most significantly down-regulated ( $p=0.00129$ , fold change=-2.8) genes for  $A\beta_{42}/A\beta_{40}\uparrow$  and *validated by 4 different probe sets* on the microarray, but it was not differentially expressed for  $A\beta_{42}/A\beta_{40}\downarrow$ . Interestingly, the expression of MAOA (monoamine oxidase A) was strongly down-regulated for the comparison C99WT1/mock ( $p=0.02572$ , fold change=-4.0) and validated by three different probe sets on the microarray. In contrast to this MAOA was not found differentially expressed for  $A\beta_{42}/A\beta_{40}\uparrow$  and  $A\beta_{42}/A\beta_{40}\downarrow$ . Since Cyp561 is a functional ferric reductase and down-regulated in consequence of an increased  $A\beta_{42}/A\beta_{40}$  ratio, I assume that the reduction of  $Fe^{3+}$  to  $Fe^{2+}$  may be impaired. *This could lead to abnormal  $Fe^{3+}$  accumulation.* Basal ganglia ferritin is increased in AD. Similarly in Parkinson's disease patients' iron is increased by approximately 35% in the substantia nigra, mainly due to a rise in *insoluble* Fe[III] rather than *soluble* Fe[II] iron [388]. *Iron Fe[II] is necessary for the conversion of norepinephrine (noradrenaline) into dopamine and serves as a cofactor of tyrosine hydroxylase, thus increasing of Fe[III] at the expense of Fe[II] may result in reduced dopamine levels. This is supported by the observation of decreased dopa decarboxylase (DDC) levels in response to an increased  $A\beta_{42}/A\beta_{40}$  level.  $Fe^{3+}$  induces the deposition of "fibrillar" amyloid plaques at neutral pH [389].*

## **6.21 Enzymes regulating neurotransmitter metabolism were strongly affected by a changed $A\beta_{42}/A\beta_{40}$ ratio on the transcriptional level and so might be neurotransmitter levels**

Altered Neurotransmitter metabolism has been shown to be involved in AD [390] and clinical data hint at changed neurotransmitter levels [391]. Glutamate decarboxylase 1 (GAD1, brain, 67kDa) was not differentially expressed (for  $A\beta_{42}/A\beta_{40}\uparrow$ ), but it was significantly and strongly up-regulated when the  $A\beta_{42}/A\beta_{40}$  ratio was decreased ( $p=0.0048$ , fold change=5.0). Interestingly, GAD1 was strongly down-regulated for the comparison C99WT/mock ( $p=0.02572$ , fold change=-4.0). In conclusion, *reduced glutamate levels for a decreased  $A\beta_{42}/A\beta_{40}$  ratio can be assumed.*

Glutamate decarboxylase (GAD; L-glutamate-1-carboxylase; EC 4.1.1.15) catalyzes the conversion of *glutamate, the major excitatory neurotransmitter, to gamma-aminobutyric acid (GABA), the major inhibitory neurotransmitter in the vertebral central nervous system.* The GAD1 gene encodes one of several forms of glutamic acid decarboxylase, identified as a *major autoantigen in insulin-dependent diabetes.*

The enzyme encoded is responsible for catalyzing the production of gamma-aminobutyric acid from L-glutamic acid. A pathogenic role for this enzyme has been identified in the human pancreas since it has been identified as an autoantigen and an autoreactive *T cell target in insulin-dependent diabetes*. Alternative splicing of this gene results in two products, the predominant 67-kD form and a less-frequent 25-kD form. *Autoantibodies to insulin and GAD are features of preclinical type 1 diabetes in children. For insulin autoantibodies, the antibody affinity and epitope specificity predict which children progress to diabetes [392]*.

HMP19 is a D1 dopamine receptor-interacting protein and it was the most up-regulated gene for the comparison  $A\beta_{42}/A\beta_{40}\uparrow$  ( $p=0.003$ , fold change=3.0), however, it was also up-regulated when the  $A\beta_{42}/A\beta_{40}$  was decreased ( $p=0.0139$ , fold change=2.1).

Dopa decarboxylase (DDC, aromatic L-amino acid decarboxylase) was down-regulated ( $A\beta_{42}/A\beta_{40}\uparrow$ ,  $p=0.00496$ , fold change=-3.1), but not altered when the  $A\beta_{42}/A\beta_{40}$  was decreased.

DDC catalyzes the decarboxylation of dihydroxyphenylalanine (dopa) to dopamine, and hydroxytryptophan to serotonin and tryptophan to tryptamine. Defects in DDC are the cause of *aadc* (aromatic L-amino acid decarboxylase deficiency). *Aadc* deficiency is an inborn error in neurotransmitter metabolism that leads to combined serotonin and catecholamine deficiency. It causes developmental and psychomotor delay, poor feeding and lethargy. The onset is early in infancy and inheritance is autosomal recessive. Dopa decarboxylase (EC 4.1.1.28) is an enzyme implicated in 2 metabolic pathways, synthesizing 2 important neurotransmitters, dopamine and serotonin [393]. Tyrosine is hydroxylated by tyrosine hydroxylase (tyrosine-3-monooxygenase) to form L-dihydroxyphenylalanine (L-DOPA), which in turn is converted into dopamine by DDC. DDC is found in different areas of the brain and is particularly abundant in basal ganglia. Dopamine is also produced by DDC in the sympathetic nervous system and is the precursor of the catecholaminergic hormones, noradrenaline and adrenaline in the adrenal medulla. In the nervous system, tryptophan hydroxylase produces 5-OH tryptophan, which is decarboxylated by DDC, giving rise to serotonin. DDC is a homodimeric, pyridoxal phosphate-dependent enzyme.

Cytochrome b-561 (CYB561, mentioned before in Chapter 6.20) was down-regulated ( $A\beta_{42}/A\beta_{40}\uparrow$ ,  $p=0.00333$ , fold change=-2.3). Two spliced isoforms were also among the 10 most significantly down-regulated genes ( $A\beta_{42}/A\beta_{40}\uparrow$ , CYB561, 209164\_s\_at:  $p=0.00129$ , fold change=-2.8 and 210816\_s\_at,  $p=0.00018$ , fold change=-4.8; data normalized with the GC-RMA algorithm). Data normalized with the PLIER algorithm

resulted in similar results and revealed that *these most down-regulated ( $A\beta_{42}/A\beta_{40}\uparrow$ ) transcripts, where in parallel among the most up-regulated ones for the comparison  $A\beta_{42}/A\beta_{40}\downarrow$ . The fact that CYB561 and two of its spliced isoforms were regulated in the same way, moreover, were among the most inversely regulated genes and among the most significant ones, make CYB561 a major candidate for  $A\beta_{42}$  induced pathology.*

Cytochrome b561 is a major transmembrane protein that is *specific to catecholamine and neuropeptide secretory vesicles* of the adrenal medulla, pituitary gland, and other neuroendocrine tissues. This 30-kDa *cytochrome* is present in both the small synaptic vesicles and the large dense core vesicles (chromaffin granules) of the tissues. Its role is to *supply reducing equivalents to 2 monooxygenases, dopamine beta-hydroxylase (dopamine  $\beta$  monooxygenase, copper-dependent !)* in chromaffin granules and *peptidylglycine monooxygenase in neurosecretory vesicles*. The cytochrome fulfills this role by catalyzing the transfer of electrons from a cytoplasmic donor, ascorbate, across a phospholipid bilayer to the luminal acceptor, semidehydroascorbate, in the interior of the vesicles. The continuously regenerated ascorbate within these vesicles is the immediate donor of the monooxygenases within the neuroendocrine secretory vesicles. Thus cytochrome b561 is a transmembrane electron channel. B561 is assumed to bind 2 heme groups non-covalently.

The gene for RAM2, a transcription factor, was up-regulated ( $A\beta_{42}/A\beta_{40}\uparrow$ ,  $p=0.160$ , fold change=1.4) and *in parallel among* the most downregulated genes according to the comparison  $A\beta_{42}/A\beta_{40}\downarrow$ ,  $p=0.157$ , fold change -2.6.

The transcription factor RAM2 (R1/CDCA7L/JPO2) inhibits the Monoamine oxidase A (MAOA) promoter and enzymatic activities. MAOA degrades serotonin, norepinephrine, and dopamine and produces reactive oxygen that may cause neuronal cell death. Using R1 overexpression, R1 small interfering RNA, and a MAOA inhibitor, it was found that R1 and MAOA act upstream of cyclin D1 and E2F1. In summary, this study demonstrated the functions of MAOA and its repressor R1 in apoptotic signaling pathways [394].

MAOA was only found to be strongly down-regulated for the comparison C99WT/mock ( $p=0.00017$ , fold change=-6.5, validated by another probe set:  $p=0.00001$ , fold change=-6.5, also a spliced isoform, 204388\_s\_at, revealed similar results:  $p=0.00008$ , fold change=-7.0, calculated with the GC-RMA algorithm), but neither for  $A\beta_{42}/A\beta_{40}\uparrow$  nor for  $A\beta_{42}/A\beta_{40}\downarrow$  MAOA dysregulation was observed. This indicates increased serotonin, norepinephrine, and dopamine-levels in consequence of C99-overexpression. This effect may get lost after C99-cleavage, because

differential expression of MAOA was observed neither for  $A\beta_{42}/A\beta_{40}\uparrow$  nor for  $A\beta_{42}/A\beta_{40}\downarrow$ . This, in turn, is a sign of both  $A\beta_{42}$  and  $A\beta_{40}$ -overexpression, leading to reduced serotonin, norepinephrine, and dopamine-levels (compared to C99-overexpression) due to the “missing effect” of down-regulated MAOA (C99WT/mock).

Taken together, I conclude that dopamine, serotonin and tryptamine-levels might be reduced due to DDC downregulation in consequence of an increased  $A\beta_{42}/A\beta_{40}$  ratio, but not altered when the  $A\beta_{42}/A\beta_{40}$  was decreased. Furthermore, the data indicate that the supply of reducing equivalents to 2 monooxygenases like dopamine  $\beta$ -hydroxylase is reduced due to downregulation ( $A\beta_{42}/A\beta_{40}\uparrow$ ) of CYB561, and thus the conversion of dopamine to norepinephrine (noradrenaline) might be impaired. Reduced noradrenaline levels, apart from reduced serotonin and dopamine levels, are well-known for causing mood disorders and may explain the often observed symptoms of depression in AD. CYB561 downregulation could be a counter-regulation of the cells to keep up sufficient dopamine levels while accepting reduced noradrenaline levels.

## **6.22 Changed glutamine synthase and glutaminase expression in response to a changed $A\beta_{42}/A\beta_{40}$ ratio**

### **6.22.1 Glutamine synthase was down-regulated exclusively in consequence of a decreased $A\beta_{42}/A\beta_{40}$ ratio and is assumed to couple ATP synthesis to neurotransmitter levels**

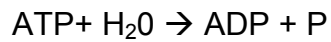
Changed glutamate levels have been claimed to be involved in AD [395, 396] presumably accompanied by altered ATP levels [397, 398]. The underlying mechanism, however is unclear. Here, an explanation is provided by the changed expression of glutamine synthase.

Glutamine synthase (synonym: Glutamate-ammonia ligase, GLUL) catalyzes an *energetic coupled reaction*<sup>8</sup>:



This reaction is coupled to:

<sup>8</sup> Direct transfer of  $\text{NH}_3$  to glutamate is endergonic and can therefore only take place coupled to an exergonic reaction like ATP hydrolysis. In the cell, the reaction is divided into two exergonic steps: First, the  $\gamma$ -phosphate residue is transferred from ATP to glutamate and forms an energy-rich mixed acid anhydride. In the second step the phosphate residue from the intermediate is substituted by  $\text{NH}_3$ , and glutamine and free phosphate are produced.



-31 kJ/mol

---

This results in the following total reaction:



-17 kJ/mol

Since GLUL was *down*-regulated in consequence of a decreased  $A\beta_{42}/A\beta_{40}$  ratio ( $p=0.01613$ , fold change=-2.5), whereas an increased  $A\beta_{42}/A\beta_{40}$  ratio did not lead to differential expression of glutamine synthase, *ATP levels may be assumed to be increased in mutant C99V50F* (due to the downregulation of glutamine synthase the ATP-consuming reaction is expected to be reduced, so that more ATP may be available). In parallel the expected increase in glutamate levels may be limited by up-regulation ( $A\beta_{42}/A\beta_{40}\downarrow$ ,  $p=0.0048$ , fold change=5.0) of glutamate decarboxylase 1 (GAD1).

### 6.22.2 Glutaminase was up-regulated exclusively in response to an increased $A\beta_{42}/A\beta_{40}$ ratio

*Changed glutamate and ammonia levels are neurotoxic in larger amounts* [353, 390]. The underlying mechanism for increased levels, however is unclear. Here, an explanation is provided by changed expression of glutaminase.

Glutaminase (GLS) hydrolyzes glutamine by desamination so that glutamate and ammonia are generated. GLS was up-regulated ( $n=0.02589$ , fold change=1.5) in response to an increased  $A\beta_{42}/A\beta_{40}$  ratio, whereas a decreased  $A\beta_{42}/A\beta_{40}$  ratio did not lead to differential expression of GLS. Due to GLS upregulation more glutamate and  $\text{NH}_3$  are expected to be produced while GAD1 is not up-regulated ( $A\beta_{42}/A\beta_{40}\uparrow$ ). *This may contribute to increased glutamate and  $\text{NH}_3$  levels (for  $A\beta_{42}/A\beta_{40}\uparrow$ ).* However, ammonia levels may be restricted by other metabolic reactions (see Chapter 6.23).

### 6.23 Two enzymes of the urea cycle were affected by a changed $A\beta_{42}/A\beta_{40}$ ratio: argininosuccinate synthase and argininosuccinate lyase

Argininosuccinate synthase (ASS) converts citrulline (mitochondria) into argininosuccinate (cytoplasm) in an ATP consuming step. ASS was up-regulated ( $n=0.0047$ , fold change=2.6, calculated with the GC-RMA algorithm) in response to an increased  $A\beta_{42}/A\beta_{40}$  ratio, whereas a decreased  $A\beta_{42}/A\beta_{40}$  ratio did not lead to differential expression of ASS. *This might contribute to increased ATP consumption*

*and might reduce total ATP levels in mutant C99I45F ( $A\beta_{42}/A\beta_{40} \uparrow$ ).*

Argininosuccinate lyase (ASL) converts argininosuccinate into arginine and fumarate in a non-ATP consuming step. ASL was up-regulated ( $n=0,06$  fold change=1.4, calculated with the GC-RMA algorithm) in response to an increased  $A\beta_{42}/A\beta_{40}$  ratio, and a decreased  $A\beta_{42}/A\beta_{40}$  ratio led to a 1.8 fold upregulation ( $n=0.032$ ) of ASL.

ASS upregulation exclusively in response to an increased  $A\beta_{42}/A\beta_{40}$  ratio might drive the following reaction circle in the cytoplasm: argininosuccinate (which may play a key role here, because it participates in both ASS and ASL-mediated, reactions)  $\rightarrow$  fumarate  $\rightarrow$  malate  $\rightarrow$  oxaloacetate  $\rightarrow$  aspartate  $\rightarrow$  argininosuccinate. The steps malate  $\rightarrow$  oxaloacetate  $\rightarrow$  aspartate are accompanied by *glutamate production* (from 2-oxoglutarate and  $NH_4^+$ ) and  *$NH_4^+$  consumption* (glutamate is also used for aspartate production from oxaloacetate).

*In summary it can be speculated that for an increased  $A\beta_{42}/A\beta_{40}$  ratio, ATP levels and  $NH_4^+$  levels could be reduced and glutamate levels could possibly be increased. Maybe this can be interpreted as an 'attempt' (via feedback loops) of the cells to reduce neurotoxic  $NH_4^+$  levels.*

## 6.24 Exocytosis

Neurotransmission has been reported to be influenced in AD [399] and impaired exocytosis was observed [400].

I found syntaxin 3A and its splice product syntaxin 3B to be up-regulated as a result of an increased  $A\beta_{42}/A\beta_{40}$  ratio. I conclude that the pre-m-RNA of syntaxin 3 is up-regulated as a result of an increased  $A\beta_{42}/A\beta_{40}$  ratio. Syntaxin 3, in turn, is spliced subsequently to generate syntaxin 3B. In contrast to this a decreased  $A\beta_{42}/A\beta_{40}$  ratio led to downregulation of both syntaxin 3A and 3B. I regard this as an important regulatory mechanism for several reasons: Out of about 40,000 measured transcripts the unspliced form (syntaxin 3A) together with the spliced form (syntaxin 3B) were inversely regulated as a result of a changed  $A\beta_{42}/A\beta_{40}$  ratio. The probability that this strong inverse regulation of *the same gene* occurs by chance is extremely low ! Moreover, both transcripts (syntaxin 3A and its splice product 3B) were regulated in the same direction, to the same extent and belong to those with high absolute values (highly abundant transcripts), increasing the reliability of the results. *Syntaxins (t-SNAREs) interact with synaptotagmin and are responsible for membrane fusions of transmitter containing vesicles. Synaptotagmin XIII was up-regulated in consequence of an increased  $A\beta_{42}/A\beta_{40}$  ratio and could possibly be an interaction partner for*

*syntaxin 3A/B*<sup>9</sup>. I speculate that neurotransmitter release is influenced by dysregulation of *syntaxin 3A/B*.

## 6.25 New assignment of a functional relationship between neurogenin 2 and KIAA0125

Neurogenin 2 (Ngn2, synonym: Math4A) and the so far completely uncharacterized KIAA0125 were the most extremely and inversely regulated genes when genes were hierarchically clustered (see Chapter 5.13, Fig. 5.40, page 107) in consequence of a decreased  $A\beta_{42}/A\beta_{40}$  ratio: While KIAA0125 was the most up-regulated gene ( $p=0.00142$ , fold change=5.3, calculated with the GC-RMA algorithm), Ngn2 was the most down-regulated one ( $p=0.00166$ , fold change=-12.5, calculated with the GC-RMA algorithm), (KIAA0125 and Ngn2 were not differentially expressed as a result of an increased  $A\beta_{42}/A\beta_{40}$  ratio). This pattern was not only seen for a decreased  $A\beta_{42}/A\beta_{40}$  ratio but also for the comparison C99/mock. Interestingly, for this comparison the expression was inverted: Ngn2 was the second most up-regulated gene, whereas KIAA0125 was strongly down-regulated. *Most interestingly, Ngn2 was co-expressed with C99 (and neuronatin) as revealed by the comparison C99/mock while KIAA0125 was co-regulated with APLP1 (and BCL2) as revealed by the comparison C99V50F/C99WT1. This argues for an effect associated with C99 and APP like proteins respectively. Ngn2 and KIAA0125 respond inversely to decreased  $A\beta_{42}$  and/or increased  $A\beta_{40}$  expression (concluded from the observation that a decreased  $A\beta_{42}/A\beta_{40}$  ratio strongly influences their expression), while they do not respond to increased  $A\beta_{42}$  and/or decreased  $A\beta_{40}$  expression (concluded from the observation that an increased  $A\beta_{42}/A\beta_{40}$  ratio does not influence their expression).* It may be speculated that there is, due to the close chromosomal vicinity, a relationship between KIAA0125 (chr.14q32-33) and presenilin 1 (chr.14q24). Ngn2 is a member of the neurogenin subfamily of basic helix-loop-helix (bHLH) transcription factor genes that play an important role in neurogenesis. *During mouse neurogenesis, Ngn2 and Ngn1 are expressed in distinct progenitor populations in the central and peripheral nervous systems [401].* Yan et al. observed that in the developing chick retina, Ngn2 was expressed in a subpopulation of proliferating progenitor cells [402]. Scardigli et al. hypothesized that Ngn2 is both responsive to, and a regulator, of

<sup>9</sup> Affymetrix uses the gene name for target sequences, so the name of splice products can differ from the gene name. Unprecisely named *syntaxin 3A* (216985\_s\_at) is a spliced form of *syntaxin 3A*; its correct name is *syntaxin 3B*. *Syntaxin 3B* is identical to *syntaxin 3A* but lacks 37 amino acid residues, from amino acid 226 to amino acid 262. *Syntaxin 3A* has one potential target sequence of phosphorylation by cAMP/cGMP-dependent protein kinase in Thr-161 and four potential sites of phosphorylation by protein kinase C at the residues S124, T156, S207, and T250, *this last one being absent in syntaxin 3B*. *Syntaxins are involved in vesicle transport to the apical plasma membrane.*

genetic pathways that *specify neuronal fates* in the ventral spinal cord [403]. It was reported that in the developing ventral mesencephalon the *proneural gene neurogenin 2 is expressed exclusively in the part of the ventricular zone that gives rise to the migrating mesencephalic dopamine neuroblasts, but not in the differentiated mesencephalic dopamine neurons. It was shown that Ngn2 is involved in the generation of mesencephalic dopamine neurons and that the development of mesencephalic dopamine neurons is severely compromised in Ngn2-null mutant mice.* It was reported that proneural genes have an intricate pattern of expression in the ventricular zone of the ventral midbrain, where mesencephalic dopaminergic neurons are generated. Neurogenin 2 (Ngn2) and Mash1 are expressed in the ventral midline, while Ngn1, Ngn2 and Mash1 are co-localized more laterally in the ventricular zone. Ngn2 is also expressed in an intermediate zone, immediately adjacent to the ventricular zone at the ventral midline. *Ngn2 is required for the differentiation of ventricular zone progenitors into postmitotic dopaminergic neuron precursors in the intermediate zone. It was concluded that Ngn2 is required for the development of midbrain dopaminergic neurons [404].* Ngn2 was immunohistochemically detected in a certain cycling population during G1 phase and was further restricted during G2-M phases to the subventricular zone-directed population. Ngn2 may further be involved in the asymmetric cell divisions of progenitor cells [405]. *Furthermore, it has been reported that inhibition of proneural bHLH factors, like Ngn2, in cortical progenitors promotes the formation of astrocytes [406].*

I assign the following property/function to KIAA0125: Firstly, that KIAA0125 has a functional relationship to Ngn2 (KIAA0125 probably acts as an antagonist of Ngn2), secondly that KIAA0125 and Ngn2 are dependent on a decreased  $A\beta_{42}/A\beta_{40}$  ratio, C99 or/and APLP1, thirdly that KIAA0125 plays a role in neurogenesis (maybe in preventing the generation of dopaminergic neurons or it could be involved in inducing astrocytosis).

## **6.26 Receptors were strongly differentially affected by a changed $A\beta_{42}/A\beta_{40}$ ratio**

The number of dysregulated receptors was greatly affected *for the 50 most up-regulated transcripts (for  $A\beta_{42}/A\beta_{40}\uparrow$ )*. Many more receptors or subunits thereof (8 receptors; 8 out of 50 is a high proportion for receptors) were up-regulated as a result of an increased  $A\beta_{42}/A\beta_{40}$  ratio compared to a decreased  $A\beta_{42}/A\beta_{40}$  ratio: delta/Notch-like EGF repeat containing (DNER); gamma-aminobutyric acid (GABA) A receptor,

---

beta 3 (GABRB3); G protein-coupled receptor 64 (GPR64); glutamate receptor, ionotropic, AMPA 2 (GRIA2); neurotrophic tyrosine kinase, receptor, type 2 (NTRK2, non-catalytic isoform); odd Oz/ten-m homolog 4 (Drosophila) (ODZ4); protease serine 12 (neurotrypsin, motopsin) (PRSS12) and protein tyrosine phosphatase, receptor type, M (PTPRM). In contrast to this, only 1 receptor, the prostaglandin E receptor 2, subtype EP2 (PTGER2) was up-regulated for  $A\beta_{42}/A\beta_{40}\downarrow$ .

*The difference between the number of up-regulated receptors (8 for  $A\beta_{42}/A\beta_{40}\uparrow$  and only 1 for  $A\beta_{42}/A\beta_{40}\downarrow$ ) was 7. This strong difference indicates a regulatory process on the receptor/ligand level. Up-regulation of receptors is often found accompanied by low-levels of ligands and vice versa [221]. This is a well-known mechanism of the cells to keep up the cells' homeostasis. However, other mechanisms, like feedback loops or cross talk between receptors or pathways may also play a role here.*

*Among the 20 most down-regulated genes ( $A\beta_{42}/A\beta_{40}\uparrow$ ), the only affected receptor was integrin  $\beta$  5 (ITGB5): ITGB5 is a type I membrane protein. It is a heterodimer of an  $\alpha$  and a  $\beta$  subunit. Subunit  $\beta$ -5 associates with  $\alpha$ -v integrin;  $\alpha$ -v/ $\beta$ -5 is a receptor for fibronectin. This is of interest because fibronectin-associated genes were among the most differentially expressed genes and the number of them was much higher than could be expected by chance.*

ITGB5 downregulation is in agreement with PKC downregulation (shown on the transcript and protein-level), because ITGB5 is known to activate PKC. Taken together, ITGB5 is a further component playing in concert with many other molecules to down-regulate PKC, and hence contribute to the upregulation of GSK3, since PKC is known to inhibit GSK3.

Among the 20 most down-regulated genes (for  $A\beta_{42}/A\beta_{40}\downarrow$ ) were:

The transferrin receptor (p90, CD71) (TFRC), the cholinergic receptor, muscarinic 3 (CHRM3), (CHRM3 was also found down-regulated for an increased  $A\beta$  ratio ( $A\beta_{42}/A\beta_{40}\uparrow$ ) when the stringency of significance was reduced from  $p < 0.05$  to  $p < 0.075$ , so *downregulation of CHRM3 does not appear to be specific for  $A\beta_{42}$* ), the G protein-coupled receptor 176 (GPR176), the RAR-related orphan receptor B (RORB). RA is assumed to be the ligand for RORB. Presumably RA is present in excess ( $A\beta_{42}/A\beta_{40}\downarrow$ ), leading to downregulation of its receptor on the transcript-level. This is in line with the observation that many RA target genes were found to be induced ( $A\beta_{42}/A\beta_{40}\downarrow$ ), indicating presence of RA. To name a few: PKC, PLAT, STRA6, ACTA2, BCL2, p21.

---

*Furthermore, I would like to emphasize the involvement of transferrin receptors in insulin metabolism, dynein-mediated transport processes and gatekeeper function for regulating iron uptake by most cells:*

Cellular uptake of iron occurs via receptor-mediated endocytosis of the ligand-occupied transferrin receptor into specialized endosomes, endosomal acidification leads to iron release. The apotransferrin-receptor complex is then recycled to the cell surface with a return to neutral pH and the simultaneous loss of affinity of apotransferrin for its receptor. The transferrin receptor is necessary for the development of erythrocytes and the nervous system. The relationships between iron metabolism and type 2 diabetes are bidirectional: iron affects glucose metabolism and glucose metabolism influences several iron metabolic pathways. Both insulin sensitivity and glucose tolerance status are significantly linked with serum transferrin receptor concentrations [379]. The early endosome is organized into domains to ensure the separation of cargo. Activated mitogenic receptors, such as epidermal growth factor (EGF) receptor, are concentrated into vesicles enriched for the small GTPase Rab5, which progressively exclude nutrient receptors, such as transferrin receptor, into neighbouring tubules. These vesicles become enlarged, increase their content of intraluminal vesicles as EGF receptor is sorted from the limiting membrane, and eventually mature to late endosomes. Maturation is governed by the loss of Rab5 and is accompanied by the movement of endosomes along microtubules towards the cell centre. It has been shown that EGF relocates to the cell center in a dynein-dependent fashion, simultaneously with the sorting away of transferrin receptor, although it remains in Rab5-positive early endosomes. When dynein function is acutely disrupted, efficient recycling of transferrin from EGF-containing endosomes is retarded, loss of Rab5 is slowed and endosome enlargement is reduced [407]. *Transferrin receptor 1 is required for iron delivery from transferrin to cells.* It was established as a gatekeeper for regulating iron uptake by most cells. TFRC is regulated by cellular iron levels through binding of the iron regulatory proteins, Irf1 and Irf2, to iron-responsive elements in the 3'-UTR. Down-regulation of the transferrin receptor for a decreased A $\beta$ <sub>42</sub>/A $\beta$ <sub>40</sub> ratio could be a counter-regulation of the cells in response to increased iron availability.

## 6.27 Prostaglandin E receptor 2 was up-regulated exclusively by a decreased $A\beta_{42}/A\beta_{40}$ ratio

PTGER2 (Prostaglandin E receptor 2, subtype EP2) was up-regulated ( $p=0.011$ , fold change=1.8) as a consequence of a decreased  $A\beta_{42}/A\beta_{40}$  ratio whereas an increased  $A\beta_{42}/A\beta_{40}$  ratio did not differentially express PTGER2.

The activity of prostaglandin receptors is mediated by G-proteins that stimulate adenylate cyclase. The subsequent rise in intracellular cAMP is responsible for the relaxing effect of this receptor on smooth muscle. How cyclooxygenase-2 (COX-2) and its proinflammatory metabolite prostaglandin E2 (PGE2) enhance colon cancer progression remains poorly understood. It has been shown that PGE2 stimulates colon cancer cell growth through its heterotrimeric guanine nucleotide-binding protein (G protein)-coupled receptor, EP2, by a signaling route that involves the activation of phosphoinositide-3-kinase and the protein kinase AKT by free G protein  $\beta$ ,  $\gamma$ -subunits and the direct association of the G protein alpha subunit with the regulator of G protein signaling (RGS) domain of axin. *This leads to the deactivation and release of glycogen synthase kinase 3  $\beta$  from its complex with axin, thereby relieving the inhibitory phosphorylation of  $\beta$ -catenin and activating its signaling pathway [408]. Recent studies suggest a neuroprotective function of the PGE2 EP2 receptor in excitotoxic neuronal injury. The function of the EP2 receptor was examined at certain time intervals after excitotoxicity in an organotypic hippocampal model of N-methyl-D-aspartate (NMDA) challenge and in a permanent model of focal forebrain ischemia. Activation of EP2 led to significant neuroprotection in hippocampal slices up to 3 hours after a toxic NMDA stimulus. Genetic deletion of EP2 resulted in a marked increase in the number of strokes in the permanent middle cerebral artery occlusion model. These findings support further investigation into therapeutic strategies targeting the EP2 receptor in stroke [409]. Neuroprotective function of the PGE2 EP2 receptor was observed in cerebral ischemia [408].* Cyclo-oxygenases (COXs) catalyze the first committed step in the synthesis of the prostaglandins PGE(2), PGD(2), PGF(2 $\alpha$ ), PGI(2) and thromboxane A(2). Expression and enzymatic activity of COX-2, the inducible isoform of COX, are observed in several neurological diseases and result in significant neuronal injury. The neurotoxic effect of COX-2 is believed to occur through downstream effects of its prostaglandin products. The function of PGD(2) and its two receptors DP1 and chemo-attractant receptor-homologous molecule expressed on Th2 cells (CRTH2) (DP2) was studied in neuronal survival. PGD(2) is the most abundant prostaglandin in brain and regulates sleep, temperature and nociception. It signals through two distinct G protein-coupled receptors, DP1 and DP2 that have opposite effects on cyclic AMP (cAMP)

production. *Physiological concentrations of PGD(2) potently and unexpectedly rescued neurons in paradigms of glutamate toxicity in cultured hippocampal neurons and organotypic slices [410].*

*Interestingly, the PTGER2 gene (chr.14q22) is located in close proximity to the PS1 gene (chr.14q24). There could be a (functional) relationship between PTGER2 and PS1 (probably via a decreased  $A\beta_{42}/A\beta_{40}$  ratio).*

## **6.28 Nicotinic acetylcholine receptor $\alpha 7$ was inversely regulated by a changed $A\beta_{42}/A\beta_{40}$ ratio**

The nicotinic acetylcholine receptors (nAChRs) are members of a superfamily of ligand-gated ion ( $\text{Na}^+$ ,  $\text{K}^+$ ,  $\text{Ca}^{2+}$ ) channels that mediate fast signal transmission at synapses. The protein encoded by this gene forms a homo-oligomeric channel, displays marked *permeability to calcium ions* and is a major component of brain nicotinic receptors that are blocked by, and highly sensitive to,  $\alpha$ -bungarotoxin. *Once this receptor binds acetylcholine, it undergoes an extensive change in conformation that affects all subunits and leads to opening of an ion-conducting channel across the plasma membrane.* This gene (encoding nicotinic acetylcholine receptor  $\alpha 7$ ) is located in a region identified as a major susceptibility locus for juvenile myoclonic epilepsy and *schizophrenia*.  $A\beta_{1-42}$  interacts with the  $\alpha 7$  subtype of the nicotinic acetylcholine receptor subunit ( $\alpha 7$  nAChR, synonym: *CHRNA7*), which is widely expressed throughout the central and peripheral nervous systems, as well as in several non-neuronal loci, such as epithelial cells, lymphoid tissues, and peripheral blood lymphocytes. Western blot and autoradiographic analyses indicate that the  *$\alpha 7$  nAChR subunit protein is up-regulated in human brain samples from Alzheimer's patients, as well as in animal models of AD [411-413].* Nordberg and colleagues investigated the expression of nicotinic acetylcholine receptors (nAChRs) on astrocytes and neurons in the hippocampus and temporal cortex of subjects carrying the Swedish amyloid precursor protein (APP) 670/671 mutation (APP<sup>swe</sup>) and in patients with sporadic Alzheimer's disease (AD), and age-matched control subjects. *Significant increases in the total number of astrocytes and of astrocytes expressing the  $\alpha 7$  nAChR subunit, along with significant decreases in the levels of  $\alpha 7$  and  $\alpha 4$  nAChR subunits on neurons, were observed in the hippocampus and temporal cortex of both APP<sup>swe</sup> and sporadic AD brains. Furthermore, the number of 125I- $\alpha$ -BTX (125I- $\alpha$  bungarotoxin) binding sites ( $\alpha 7$  nAChR) in the temporal cortex of the APP<sup>swe</sup> brain was significant lower than in the younger control group, reflecting the lower neuronal level of  $\alpha 7$  nAChR. The increase in the level of expression of  $\alpha 7$  nAChR on astrocytes was positively correlated with the extent of neuropathological alternations,*

*especially the number of neuritic plaques, in the AD brain. The elevated expression of  $\alpha 7$  nAChR on astrocytes might participate in the  $A\beta$  cascade and formation of neuritic plaques, thereby playing an important role in the pathogenesis of AD [414]. Fodero and colleagues demonstrated that  $A\beta_{42}$  was more potent than  $A\beta_{40}$  in its ability to increase AChE (acetylcholinesterase) in primary cortical neurons [415].*

The muscarinic 3 cholinergic receptor (CHRM3) was found to be down-regulated by both increased *and* decreased  $A\beta_{42}/A\beta_{40}$  ratios. Thus, this regulation can be assumed to be non-specific for  $A\beta_{42}$ . In contrast to this, the *nicotinic acetylcholine receptor  $\alpha 7$  (CHRNA7) was found among the most inversely expressed genes as response to a changed  $A\beta_{42}/A\beta_{40}$  ratio: an increased  $A\beta_{42}/A\beta_{40}$  ratio led to 1.8 fold upregulation ( $p=0.061$ ), whereas a decreased  $A\beta_{42}/A\beta_{40}$  ratio led to 1.3 fold downregulation ( $p=0.152$ ) of CHRNA7.* Further investigation of the CHRNA7 might provide additional useful information about effects mediated by acetylcholine.

## **6.29 Excitatory and inhibitory neurotransmitter receptors were affected by a changed $A\beta_{42}/A\beta_{40}$ ratio**

### **6.29.1 Glutamate-receptors were differentially expressed in response to an increased $A\beta_{42}/A\beta_{40}$ ratio and might influence $Ca^{2+}$ transport and LTP**

Glutamate receptors, like the  $\alpha$ -amino-3-hydroxy-5-methylisoxazole-4-propionic acid (AMPA) receptors mediate the majority of excitatory synaptic transmission in the central nervous system (CNS) and are essential for the induction and maintenance of long-term potentiation and long-term depression, two cellular models of learning and memory.

The AMPA receptors are ionotropic transmembrane receptors for glutamate that mediate fast synaptic transmission in the CNS. The name is derived from their ability to be activated by the artificial glutamate analog AMPA. AMPA receptors are found in many parts of the brain and are the most commonly found receptors in the nervous system. AMPA receptors are composed of four types of subunits, designated as GLUR1 (GRIA1), GLUR2 (GRIA2), GLUR3 (GRIA3), and GLUR4 (GRIA4), which combine to form tetramers [416, 417]. Most AMPA receptors are either homo-tetramers of GluR1 or GluR4, or symmetric 'dimer of dimers' of GluR2 and either GluR1, GluR3 or GluR4.

The gene encoding the ionotropic glutamate receptor AMPA2 subunit (synonyms: GLUR2, GRIA2) was the most strongly up-regulated gene for an increased  $A\beta_{42}/A\beta_{40}$  ratio ( $p=0.00034$ , fold change=8.7, calculated with the GC-RMA algorithm, and the third most up-regulated gene,  $p=0.0331$ , fold change=2.7, calculated with the PLIER algorithm). A decreased ratio did not differentially express AMPA2. It has been demonstrated that calcium entry into cells is prevented by activation of AMPA receptors containing GLUR2. This was proposed to protect the cells against excitotoxicity [418]. I conclude that the increased  $A\beta_{42}/A\beta_{40}$  ratio triggers an increase in intracellular  $Ca^{2+}$  levels, which in turn is limited by upregulation of AMPA2. However, a direct upregulation of AMPA2 by an increased  $A\beta_{42}/A\beta_{40}$  ratio cannot be excluded.

The ionotropic glutamate receptor AMPA3 subunit (synonyms: GLUR3, GRIA3) has been shown to be involved in cognitive impairment. Mutations in AMPA3 alter ion channel properties and are associated with moderate cognitive impairment in humans [419]. Moreover, AMPA3 has been suggested as a candidate for bipolar disorders and X-linked mental retardation [420]. AMPA3 was down-regulated ( $A\beta_{42}/A\beta_{40}\uparrow$ , C99I45F/C99WT2,  $p<0.005$ , more than 3-fold down-regulated), but not differentially expressed for a decreased  $A\beta_{42}/A\beta_{40}$  ratio.

The inverse regulation of the AMPA2 and AMPA3 subunits of the AMPA receptor is interesting. This regulation is not expected to be just by chance because the probability of two genes encoding proteins for subunits of the *same* receptor type showing such a *strong inverse regulation* is low. It can rather be expected that there is a functional relationship, for instance an antagonistic one, between AMPA2 and AMPA3 subunits. An explanation for such a relation could be increased  $Ca^{2+}$  levels. It can be hypothesized that an increased  $A\beta_{42}/A\beta_{40}$  ratio up-regulates intracellular  $Ca^{2+}$  levels. The cells may counter regulate this to keep up the  $Ca^{2+}$  homeostasis by up-regulating the  $Ca^{2+}$  *blocking* AMPA2 subunit while down-regulating the  $Ca^{2+}$  *conducting* AMPA3 subunit.

The metabotropic glutamate receptors are a family of G protein-coupled receptors that have been divided into 3 groups on the basis of sequence homology, putative signal transduction mechanisms and pharmacological properties. Group I includes GRM1 and GRM5 and these receptors have been shown to activate phospholipase C. Group II includes GRM2 and GRM3 while Group III includes GRM4, GRM6, GRM7 and GRM8c. The activities of group II and III receptors are mediated by G-proteins that *inhibit adenylate cyclase activity*.

The metabotropic glutamate receptor 7 (GRM7), was 1.5 fold up-regulated ( $p=0.005$ ) for an increased  $A\beta_{42}/A\beta_{40}$  ratio and validated by another probe set on the microarray. Moreover, using another set of triplicates as a baseline experiment (comparison C99I45F/C99WT2 instead of C99I45F/C99WT1) confirmed these results ( $p=0.008$ , fold change=1.6). In contrast to this a decreased  $A\beta_{42}/A\beta_{40}$  ratio did not result in differential expression of GRM7.

The metabotropic glutamate Receptor 8c (GRM8c), measured by real-time PCR, appeared to be up-regulated for an increased  $A\beta_{42}/A\beta_{40}$  ratio (fold change=4.4, standard error<sub>fold change</sub>=3.875,) and less up-regulated for a decreased  $A\beta_{42}/A\beta_{40}$  ratio (fold change=2.1, standard error<sub>fold change</sub>=0.52,) However, a stronger differential expression for  $A\beta_{42}/A\beta_{40}\uparrow$ , due to its high standard error, is questionable and could be caused by a clonal effect of one of the three measured independent single clones.

In summary, *GRM7 and possibly GRM8 were up-regulated exclusively in consequence of an increased  $A\beta_{42}/A\beta_{40}$  ratio. They are known to inhibit adenylate cyclase. Adenylate cyclase normally activates CREB1. CREB1 was found less (-44%) phosphorylated on the activating sites S129 and S133 as a result of an increased  $A\beta_{42}/A\beta_{40}$  ratio. CREB1 could be less active by up-regulated GRM7 and possibly GRM8 (which could act synergistically) to inhibit adenylate cyclase. However, there are further ways of how the activity of CREB1 may be reduced. To name a few: cAMP also exerts its function via PKA to induce CREB1 and downregulation of the PI3K/AKT/CREB1 axis may also contribute to reduce CREB1 activity.*

### **6.29.2 GABA and glycine receptors were up-regulated exclusively in response to an increased $A\beta_{42}/A\beta_{40}$ ratio and might exert inhibitory effects**

The  $\gamma$ -aminobutyric acid (GABA) A receptor beta 3 (GABRB3) was 2.6 fold up-regulated ( $p=0.0256$ ) for  $A\beta_{42}/A\beta_{40}\uparrow$  and validated by another probe set (fold change=2.4,  $p=0.0076$ ) but not differentially expressed for  $A\beta_{42}/A\beta_{40}\downarrow$ . Moreover, the glycine receptor, beta (GLRB) was 2.1 fold up-regulated ( $p=0.00018$ ) for  $A\beta_{42}/A\beta_{40}\uparrow$ , but not differentially expressed for  $A\beta_{42}/A\beta_{40}\downarrow$ . Both GABA and glycine receptors, the typical inhibitory neurotransmitter receptors, were up-regulated exclusively in response to an increased  $A\beta_{42}/A\beta_{40}$  ratio. This argues for inhibitory effects which could occur (for instance in neurons of brains from AD patients) on postsynaptic membranes: Anion influx (mainly  $Cl^-$ ) into the cells induce hyperpolarization, which would make the generation of postsynaptic action potentials more difficult.

### **6.30 Upregulation of Notch-signaling was triggered by an increased $A\beta_{42}/A\beta_{40}$ ratio and might contribute to prevention of terminal cell differentiation**

The Notch signaling pathway controls cellular interactions important for the specification of a variety of cell fates in both invertebrates and vertebrates. I identified Notch-signaling as up-regulated in consequence of an increased  $A\beta_{42}/A\beta_{40}$  ratio. The Delta/Notch-like EGF-related receptor (DNER) was found among the 10 most up-regulated genes in response to an increased  $A\beta_{42}/A\beta_{40}$  ratio. Furthermore, the Notch ligand *jagged1* was among the most inversely regulated genes (upregulation in consequence of an increased  $A\beta_{42}/A\beta_{40}$  ratio, downregulation as response to a decreased  $A\beta_{42}/A\beta_{40}$  ratio). The Co-repressors of Notch-signaling TLE1 and TLE2 were down-regulated ( $A\beta_{42}/A\beta_{40}\uparrow$ ). Cut-expression was shown to be induced by Notch-signaling [421]. Cut-like 2 (CUTL2) was the second most up-regulated gene (increased  $A\beta_{42}/A\beta_{40}$  ratio,  $p<0.005$ ). The Notch-signaling target-gene CD44 was up-regulated. None of the previously mentioned genes (except for *jagged1*, which was down-regulated for  $A\beta_{42}/A\beta_{40}\downarrow$ ) were differentially expressed when the  $A\beta_{42}/A\beta_{40}$  ratio was decreased. There were even signs indicating that Notch-signaling was down-regulated in consequence of a decreased  $A\beta_{42}/A\beta_{40}$  ratio, because the Notch inhibitor NUMB was up-regulated when the  $A\beta_{42}/A\beta_{40}$  ratio was decreased.

DNER was identified as a new epidermal growth factor (EGF)-like repeat-containing single-pass *transmembrane protein* that is specifically expressed in the developing and mature central nervous system. Thus, it was named Delta/Notch-like EGF-related receptor (DNER). The DNER protein is strongly expressed in several types of post-mitotic neurons, including cortical and hippocampal pyramidal neurons, cerebellar granule cells, and Purkinje cells. DNER protein is localized to the *dendritic plasma membrane and endosomes and is excluded from the axons, even when overexpressed*. The tyrosine-based sorting motif in the cytoplasmic domain is required for dendritic targeting of DNER. DNER also has a single transmembrane region and an intracellular C-terminal region containing potential tyrosine kinase phosphorylation sites, a typical tyrosine-based sorting signal (YEEF), and a dileucine-type sorting signal (LI). Differentiation of glia in the central nervous system is regulated by Notch1 signaling through neuron-glia interaction. *Eiraku et al. identified DNER as a ligand of Notch during cellular morphogenesis of Bergmann glia in the mouse cerebellum. DNER bound to Notch1 at cell-cell contacts and activated Notch signaling in vitro* [422].

Human jagged1 (JAG1) is the ligand for the receptor Notch 1. Mutations that alter the jagged1 protein cause Alagille syndrome. Binding of jagged 1 to Notch triggers a cascade of proteolytic cleavage that eventually leads to the release of the intracellular part of the receptor from the membrane, allowing it to translocate to the nucleus and activate transcription factors that play key roles in cell differentiation and morphogenesis [423]. Loomes et al. found that JAG1 is expressed in cells adjacent to those expressing Notch2, suggesting a possible ligand receptor interaction [424]. Wild-type JAG1 is inhibitory for HGF expression and mutant JAG1 relieves the inhibition. Downregulation of jagged 1 induces cell growth inhibition and S phase arrest in prostate cancer cells [425]. Overexpression of the Notch ligand jagged1 induces human regulatory T-cells [426]. The Notch ligands, jagged and delta, are sequentially processed by  $\alpha$ -secretase and presenilin/ $\gamma$ -secretase and release signaling fragments [427].

The TLE genes are human homologs of the *Drosophila* 'groucho' gene and their products belong to this pathway. The transcriptional *co-repressor Groucho/TLE1 (TLE1)* is expressed in virtually all major cortical subdivisions, hippocampus, amygdala, and thalamus, as well as in the cerebellum of the adult rat brain. Transcriptional co-repressors of the Groucho (Gro)/TLE family play important roles during a variety of developmental pathways, including neuronal differentiation. In particular, they *act as* negative regulators of neurogenesis, together with Hairy/Enhancer of split (Hes) DNA-binding proteins.

Analysis of mutant alleles of members of the Notch cascade showed that Notch signaling extends the differentiation-competent state of developmentally immature precursor cells, thereby preventing or delaying their differentiation until the correct morphogenetic signals become available (reviewed by Artavanis-Tsakonas et al. [428]). A number of pathologies resulting from incomplete cellular differentiation due to this general inhibitory action during cell determination were shown to be the result of alterations in Notch signaling, including both lymphoblastic and epithelial neoplasms. Liu et al. studied the expression of individual TLE genes during epithelial differentiation. By a combination of *in situ* hybridization and immunohistochemical studies, they showed that *TLE1, TLE2, and TLE3 are coexpressed in a number of tissues* [429]. Sestan et al. demonstrated inhibition of cortical neurite growth mediated by upregulation of Notch signaling [430]. This is in line with my observation that many genes promoting neurite outgrowth (previously described in this thesis) were repressed as a response to an increased  $A\beta_{42}/A\beta_{40}$  ratio. Furthermore, there are hints indicating a shift towards glial differentiation of the human neuroblastoma cells as a consequence of an increased  $A\beta_{42}/A\beta_{40}$  ratio, but towards neuronal

differentiation as a result of a decreased  $A\beta_{42}/A\beta_{40}$  ratio: morphologically the cells, treated with retinoic acid ( $A\beta_{42}/A\beta_{40}\uparrow$ ) slightly resembled preparations of astrocytes (Fig. 5.9, 1D), whereas cells with a decreased  $A\beta_{42}/A\beta_{40}$  ratio treated the same way adopt a more neuronal shape with budding protrusions. An expression profile of such treated cells or search for glial/neuronal markers would help to clarify this issue. *Increased truncated TrkB immunoreactivity (I observed upregulation of the truncated, non-catalytic isoform in consequence of an increased  $A\beta_{42}/A\beta_{40}$  ratio) was observed in reactive glial cells in the cerebral cortex and white matter in AD [274].* The glial cell line-derived neurotrophic factor receptor  $\alpha$ -3 (GDNF $\alpha$ -3) was down-regulated ( $A\beta_{42}/A\beta_{40}\downarrow$ ) possibly arguing at least for a weak tendency of the cells not to differentiate into the glial direction. *DNER has been shown to bind to Bergmann glial cells promoting their glial fate in cell culture [422]. I found DNER among the 10 most up-regulated genes ( $A\beta_{42}/A\beta_{40}\uparrow$ ), but no differential expression was observed in cells with reduced  $A\beta_{42}/A\beta_{40}$  ratio. Similar processes might occur for neural stem cells in the human brain surrounded by diverse  $A\beta_{42}/A\beta_{40}$  levels which could shift them towards a glial or a neuronal cell fate depending on  $A\beta_{42}$  and  $A\beta_{40}$  levels.*

NR2F1 (Nuclear receptor subfamily 2, group F, member 1) was not differentially expressed (for  $A\beta_{42}/A\beta_{40}\uparrow$ ), but up-regulated when the  $A\beta_{42}/A\beta_{40}$  ratio was decreased ( $p=0.064$ , fold change=1.4). NR2F1 controls Notch regulation of hair cells and supports cell differentiation. Notch regulation of hair cell differentiation in NR2F1 (-/-) mice was investigated and misregulation of Notch signaling components was confirmed. Reduced Notch signaling correlated with increases hair cell differentiation [431].

It has been suggested that Notch signaling is essential for the development of T lineage cells [432, 433], whereas it prevents B cell development [434, 435]. Notch signaling may influence the survival and lineage commitment of T cell progenitors at several discrete stages. Pre-T- $\alpha$ -chain (preT $\alpha$ ) mRNAs have been demonstrated to be up-regulated upon activated Notch signaling [436]. This is in line with the observation that the T-cell receptor  $\alpha$  locus was up-regulated in response to an increased  $A\beta_{42}/A\beta_{40}$  ratio (shown by transcriptomics and proteomics) and supports the view that up-regulated Notch signaling is a consequence of an increased  $A\beta_{42}/A\beta_{40}$  ratio.

*Taken together there are strong indications of up-regulated Notch signaling in consequence of an increased  $A\beta_{42}/A\beta_{40}$  ratio. In contrast to this, Notch signaling might be down-regulated, possibly accompanied by an increased tendency of the cells to differentiate when the  $A\beta_{42}/A\beta_{40}$  ratio was decreased.*

### 6.31 Upregulation of TGF $\beta$ -signaling was triggered by an increased A $\beta_{42}$ /A $\beta_{40}$ ratio

TGF $\beta$ -signaling has been shown to be involved in AD [437]. In humans with AD, transforming growth factor- $\beta$ 1 (TGF $\beta$ 1) mRNA levels in the midfrontal gyrus correlate positively with the relative degree of cerebrovascular amyloid deposition in that brain region, suggesting a possible role for TGF $\beta$ 1 in human cerebrovascular abnormalities. Transgenic mice overexpressing TGF $\beta$ 1 in astrocytes develop AD-like cerebrovascular abnormalities, including perivascular astrogliosis, microvascular basement membrane thickening, and accumulation of thioflavin S-positive amyloid. Mice overexpressing TGF $\beta$ 1 alone or in addition to human APP show selective accumulation of human A $\beta$  in blood vessels and develop cerebral hemorrhages in old age. In TGF $\beta$ 1 transgenic mice, cerebral blood flow in the limbic system was significantly lower than in non-transgenic littermate controls. Aged TGF $\beta$ 1 mice also showed overall reduced cerebral glucose uptake as a measure of brain activity [438]. However, TGF $\beta$ 1 was also reported to promote microglial A $\beta$  clearance and reduces plaque burden in transgenic mice [439].

There were signs that TGF $\beta$ -signaling was up-regulated by an increased A $\beta_{42}$ /A $\beta_{40}$  ratio. The ligand BMP7 was strongly up-regulated (A $\beta_{42}$ /A $\beta_{40}$  $\uparrow$ ) and known to activate TGF $\beta$ -signaling (TGF $\beta$ -induced signaling and BMP induced-signaling are known to converge in the common signaling transducer smad 4, strong crosstalk and feedback loops have been described for these pathways). In contrast to this, BAMBI, an inhibitor of this pathway, was strongly up-regulated as a result of a decreased A $\beta_{42}$ /A $\beta_{40}$  ratio. BAMBI is a transmembrane glycoprotein related to the type I receptors of the transforming growth factor- $\beta$  (TGF $\beta$ ) family, whose members play important roles in signal transduction in many developmental and pathological processes. BAMBI is known to negatively regulate TGF $\beta$  signaling. BAMBI is a *pseudoreceptor, lacking an intracellular serine/threonine kinase domain required for signaling*. Similar proteins in frogs, mice and zebrafish function as negative regulators of TGF $\beta$ , which has led to the suggestion that the encoded protein may function to limit the signaling range of the TGF $\beta$  family during early embryogenesis.

TGF $\beta$  signaling is involved in A $\beta$ -induced gene expression, which can be seen from strong and significant upregulation (A $\beta_{42}$ /A $\beta_{40}$  $\uparrow$ ) of transforming growth factor  $\beta$ 2 (TGF $\beta$ 2) ( $p=0.00219$ , fold change=4.0) and TGF $\beta$ -inducible nuclear protein 1 (TINP1) ( $p=0.01324$ , fold change=3.2) and *in parallel* strong and significant downregulation (A $\beta_{42}$ /A $\beta_{40}$  $\uparrow$ ) of transforming growth factor  $\beta$  receptor II (70/80kDa) (TGFB2) ( $p=0.00219$ , fold change= -5.0). *Inverse, significant and strong differential expression of ligand and its receptor is a strong indication of an affection of the corresponding*

*pathway !* Downregulation of the receptor is assumed to be a response of the cells to increased availability of the ligand (on the other hand it cannot be excluded that up-regulation of the ligand is a response to downregulation of the receptor). Since activation of pathways is usually regulated by the binding of a ligand to its receptor and subsequent autophosphorylation of the receptor, I regard the TGF $\beta$  pathway as up-regulated in consequence of an increased A $\beta_{42}$ /A $\beta_{40}$  ratio (due to strong ligand upregulation and plenty of further data, like upregulation of TGF $\beta$ -inducible genes and proteins). Hepatocyte growth factor (HGF) was strongly down-regulated (A $\beta_{42}$ /A $\beta_{40}$ ↑). HGF antagonizes TGF $\beta$ 1 by stabilizing SMAD transcriptional co-repressor TGIF [365]. Dermato-pontin was found to be among the most up-regulated genes (for A $\beta_{42}$ /A $\beta_{40}$ ↑) and *in parallel, among* the most down-regulated ones (for A $\beta_{42}$ /A $\beta_{40}$ ↓). Dermato-pontin augmented the biological activity of TGF $\beta$ 1, as analysed by the expression of luciferase in mink lung epithelial cells transfected with a plasminogen activator inhibitor-promoter-luciferase construct [441].

*Taken together, the results demonstrated that TGF $\beta$  signaling and BMP-signaling are affected by a changed A $\beta_{42}$ /A $\beta_{40}$  ratio on the transcript level. There are strong indications, that both pathways are up-regulated in consequence of an increased A $\beta_{42}$ /A $\beta_{40}$  ratio and down-regulated in consequence of a decreased A $\beta_{42}$ /A $\beta_{40}$  ratio. However, further work is necessary, focusing on smad proteins, which are components of both pathways. This might help to answer unsolved questions about feedback loops and cross-talk between TGF $\beta$  signaling and BMP-signaling.*

### **6.32 Wnt-signaling might be inversely regulated by a changed A $\beta_{42}$ /A $\beta_{40}$ ratio**

The Wnt pathway is suggested to be involved in AD [442]. Wnt9a and Wnt6 were found to be down-regulated in consequence of an increased A $\beta_{42}$ /A $\beta_{40}$  ratio. They are known to signal through the canonical Wnt/beta-catenin signaling pathway [443]. In contrast to this Wnt5a was up-regulated (for an increased A $\beta_{42}$ /A $\beta_{40}$  ratio). Wnt5a inhibits the Wnt pathway by promoting GSK3-independent  $\beta$ -catenin degradation [444]. Interestingly, in breast cancer cells the activation/inhibition pattern was reversed (Wnt9a, Wnt6 up-regulated, Wnt5a down-regulated), so it can be speculated that proliferation (a hallmark of cancer cells) and differentiation processes could be involved in this regulation. DKK2 (p=0.05, 2.2 fold up-regulated, increased A $\beta_{42}$ /A $\beta_{40}$  ratio) and DKK4 (p=0.016, 2.5 fold up-regulated, increased A $\beta_{42}$ /A $\beta_{40}$  ratio), both inhibitors of Wnt-signaling [445] were up-regulated, but were not found to be differentially expressed when the A $\beta_{42}$ /A $\beta_{40}$  ratio was decreased. Interestingly, WNT antagonist DKK2 is a Notch signaling target in intestinal stem cells [446], supporting

the previously provided data of upregulation of Notch signaling in consequence of an increased  $A\beta_{42}/A\beta_{40}$ . *This might trigger a vicious circle starting from an increased  $A\beta_{42}/A\beta_{40}$  ratio, leading to activation of Notch-signaling which, in turn, expresses the WNT-signaling inhibitor DKK2. Suppressed WNT-signaling may lead to decreased inhibition of GSK3 $\beta$ , which in turn might lead to stronger tau phosphorylation. Targeting this regulation could turn out to be a suitable drug target for interrupting the link between  $A\beta_{42}$  overproduction and tau-hyperphosphorylation.*

There were signs indicating an *upregulation of Wnt-signaling triggered by a decreased  $A\beta_{42}/A\beta_{40}$  ratio*: A large number of target genes were induced as a result of an increased  $A\beta_{42}/A\beta_{40}$  ratio. These, included: cyclin D1, catenin  $\alpha 2$ , PKC  $\alpha$ , NRCAM, Runx2 and Stra6. Interestingly many of these genes were suppressed in consequence of an increased  $A\beta_{42}/A\beta_{40}$  ratio, supporting the previously mentioned data, arguing for a *downregulation of Wnt-signaling in consequence of an increased  $A\beta_{42}/A\beta_{40}$  ratio*.

*Taken together there are many indications of downregulation (off-state) of Wnt signaling in consequence of an increased  $A\beta_{42}/A\beta_{40}$  ratio, but upregulation (on-state) of Wnt signaling as a result of a decreased  $A\beta_{42}/A\beta_{40}$  ratio.*

### **6.33 Strong and significant downregulation of RGS4 by an increased $A\beta_{42}/A\beta_{40}$ ratio argues for activation of G-protein signaling**

See Chapter 5.4.4, Fig. 5.5 (Volcano plots, pages 42-43). Regulator of G-protein signaling 4 (RGS4) showed decreased mRNA levels in AD in a large collection of human brain autopsies from prefrontal cortex. It was shown that all splice variants were down-regulated in AD patients [447]. In AD parietal cortex, total levels of RGS4 proteins were significantly lower than age-matched control cases by 40% and 53%, respectively [448].

Regulator of G-protein signaling 4 (RGS4) was found to be the most significantly down-regulated gene (for  $A\beta_{42}/A\beta_{40}\uparrow$ ), but it was not found to be differentially expressed when the  $A\beta_{42}/A\beta_{40}$  ratio was decreased. Furthermore, downregulation was confirmed by three probe sets, all of which had a p-value <0.05 (see Volcano plots, Chapter 5.4.4, Fig. 5.5, pages 42-43) strongly increasing the reliability of downregulation. Most importantly RGS4 also belongs to the genes that were down-regulated in hippocampi of 22 subjects with AD of varying severity (compared to healthy controls) with the *downregulation having already started at incipient AD stages* [449]. *This makes RGS4 a promising candidate (especially in combination*

*with further susceptibility genes) for early diagnosis of AD.* RGS4 is also discussed as one of the top candidate genes for schizophrenia [450] and might be the link between clinical symptoms occurring in schizophrenic as well as in AD patients (problems with copying of drawings, cognitive impairment, mood disorders etc.). The down-regulation of RGS4, a G-protein signaling inhibitor, indicates activation of G-protein signaling. At the same time, G-protein signaling *activators* (G protein-coupled receptor 64) were *up*-regulated ( $A\beta_{42}/A\beta_{40}\uparrow$ ). On the other hand GPR176, another G protein-coupled receptor, was down-regulated ( $A\beta_{42}/A\beta_{40}\downarrow$ ). Taken together, these data indicate upregulation of G-protein signaling in consequence of an increased  $A\beta_{42}/A\beta_{40}$  ratio and presumably downregulation in consequence of a decreased  $A\beta_{42}/A\beta_{40}$  ratio. This might be true, at least for some G-protein signaling pathways in which the previously mentioned genes participate. Further research is necessary including the investigation of the phosphorylation status of kinases belonging to these pathways.

#### **6.34 The $\alpha$ and $\delta$ loci of the T-cell receptor were up-regulated in response to increased and decreased $A\beta_{42}/A\beta_{40}$ ratios, whereas C99 overexpression led to their downregulation**

The genes coding for the T-cell receptor (TCR) polypeptide chains are located on different chromosomes. The TCR consists of two polypeptide chains. Most of the TCRs possess a  $\beta$  and  $\gamma$ -chain. Only a few consist of a  $\alpha$  and  $\delta$ -chain. The  $\alpha$  and  $\delta$  locus of the T-cell receptor was significantly down-regulated in consequence of C99 overexpression (C99WT/mock). Interestingly an increased *and* decreased  $A\beta_{42}/A\beta_{40}$  ratio resulted in *strong and significant upregulation of these genes* (transcript level, microarray analysis). This was validated on the protein level by a proteomic approach, in which the  $\alpha$  and  $\delta$  locus of the T-cell receptor was found among the first 20 most differentially expressed proteins. The  $\alpha$  and  $\delta$  genes (both located on chr14q11.2) are located in vicinity of the PS1 gene (chr14q24). The genes for the  $\beta$  and  $\gamma$  chain are located on chromosome 7. The fact that those TCR genes, which are in vicinity of the PS1 gene, were differentially expressed hint at a regulatory process between a changed  $A\beta_{42}/A\beta_{40}$  ratio, PS1 and the  $\alpha$  and  $\delta$  genes of the TCR.

Furthermore, it might be of importance that only a few TCRs consist of an  $\alpha$  and  $\delta$ -chain. This argues for a distinct regulatory process rather than a broad regulation. It can be speculated that  $\alpha$  and  $\delta$  genes of the TCR participate in immunological processes involved in AD and might contribute to explain hitherto open questions about the immune response (participation of microglial cells, T cell activation, B lymphocytes, cytokines) in brains of AD patients.

### **6.35 Dysregulated LRP4 is assumed to influence transcription together with Fe65**

There are a plenty of imaginable ways of how  $A\beta$  or the AICD could trigger gene expression. To name but a few: Extracellular  $A\beta_{42}$  or  $A\beta_{40}$  could bind to a receptor, transducing a signal to the nucleus, which in turn could activate transcription. On the other hand, intracellular  $A\beta_{42}$  or  $A\beta_{40}$  (even if only present in small amounts intracellularly) could be transported to the nucleus, in order to activate transcription. More publications, however, point to the AICD as the transcription inducing molecule. The intracellular domains cleaved from the membrane-bound precursors APLP1, APLP2 and APP translocate to the nucleus and activate transcription [55, 62, 199, 200]. Nuclear signaling of the AICD is regulated by the APP-adaptor proteins Fe65, Jip1b and X11 $\alpha$ , as well as the nuclear docking protein Tip60 that might be involved in chromatin remodelling. It has been discussed that the AICD regulates the expression of its precursor APP and therefore acts as a signal of APP cleavage, leading to the replenishment of full-length APP levels [152]. Furthermore, cleavage products of the AICD could activate transcription [73, 151, 208]. *It is noteworthy that AICD-regulated genes may be a subset of a much larger group of genes controlled by  $\gamma$ -secretase processing.*

In this thesis I observed downregulation ( $p=0.05$ , 1.5 fold) of low density lipoprotein receptor-related protein 4 (LRP4) in consequence of a decreased  $A\beta_{42}/A\beta_{40}$  ratio, whereas LRP4 was not differentially expressed in consequence of an increased  $A\beta_{42}/A\beta_{40}$  ratio. LRP4 is a potential cell surface endocytic receptor, which binds and internalizes extracellular ligands for degradation by lysosomes (reviewed in [451]). *Importantly, LRP4 and APOE were co-immunoprecipitated in Cos7 cells and it has been suggested that APOE is an endogenous ligand for LRP4.* Moreover it has been suggested that LRP4 may play a role as a receptor for extracellular signals, including those from glial cells, in the maintenance of the viability of neurons [451]. Low density lipoprotein receptor-related proteins have been demonstrated to bind to FE65, translocates to the nucleus and activates/inhibits transcription [69, 452-454]. I speculate that decreased  $A\beta_{42}$  or increased  $A\beta_{40}$  (or the corresponding AICDs) down-

regulates LRP4 and that, consequently, less extracellular LDL binds to LRP4; less LDL is then internalized and degraded in lysosomes, which may have an influence on gene expression. Since LRP4 was down-regulated ( $A\beta_{42}/A\beta_{40}\downarrow$ ), there might have been less LRP4-FE65 which could have activated transcription, so that transcription was assumed to be inhibited. This is in line with the observation that a decreased  $A\beta_{42}/A\beta_{40}$  ratio led to general transcriptional downregulation (see Volcano plots, Chapter 5.4.4, Fig. 5.5, pages 42-43).

### 6.36 Indications of dysregulated $Ca^{2+}$ levels in consequence of a changed $A\beta_{42}/A\beta_{40}$ ratio

Nicotinic acetylcholine receptors are known to increase intracellular  $Ca^{2+}$  concentrations. An increased  $A\beta_{42}/A\beta_{40}$  ratio led to upregulation of CHRNA7 whereas a decreased  $A\beta_{42}/A\beta_{40}$  ratio led to downregulation of CHRNA7. Moreover, the T-cell receptor has been reported to increase intracellular  $Ca^{2+}$  concentrations [455]. The alpha locus of the T cell receptor was up-regulated ( $A\beta_{42}/A\beta_{40}\uparrow$ ,  $p=0.00219$ , fold change=5.0). The calcium channel voltage-dependent L type alpha 1D subunit (CACNA1D) conducts  $Ca^{2+}$ -influx and was found to be up-regulated ( $A\beta_{42}/A\beta_{40}\uparrow$ ). Also the AMPA2 (GLUR2) subunit of the AMPA receptor was strongly up-regulated ( $A\beta_{42}/A\beta_{40}\uparrow$ ), however, it was shown to rather inhibit  $Ca^{2+}$  influx [418]. Increased intracellular  $Ca^{2+}$  concentrations have been reported to induce apoptosis [456]. AMPA2 upregulation might be a counter-regulation of the cells as response to increased intracellular  $Ca^{2+}$  concentrations and in order to protect themselves from  $Ca^{2+}$  induced apoptosis. *Enhanced LTP has been observed in AMPA receptor GluR2-deficient mice [457-459] and long term depression (LTD) has been associated with the presence of AMPA2 containing AMPA receptors [460]*. Further indications of increased intracellular  $Ca^{2+}$  concentrations are differential expression of specific  $Ca^{2+}$  binding proteins: actinin alpha 1 (ACTN1) was up-regulated ( $A\beta_{42}/A\beta_{40}\uparrow$ ), but not specifically for  $A\beta_{42}$ , since it was also found up-regulated when the  $A\beta_{42}/A\beta_{40}$  ratio was decreased. Calbindin was found up-regulated in consequence of an increased  $A\beta_{42}/A\beta_{40}$  ratio only, whereas it was not differentially expressed when this ratio was decreased. Calbindin is a *calcium-binding protein* belonging to the troponin C superfamily. *Calbindin contains 4 active calcium-binding domains*, and 2 modified domains that presumably have lost their calcium-binding capacity. Taken together there are indications of increased intracellular  $Ca^{2+}$  levels in consequence of an increased  $A\beta_{42}/A\beta_{40}$  ratio. However, it is not clear (since  $Ca^{2+}$  levels were not measured directly,  $Ca^{2+}$  levels could also be decreased) whether the genes mentioned above were directly dysregulated in consequence of an increased

$A\beta_{42}/A\beta_{40}$  ratio or if an increased  $A\beta_{42}/A\beta_{40}$  ratio first dysregulates  $Ca^{2+}$  levels, which in turn dysregulate the genes. The latter case is assumed to be slightly more probable (however the direct regulation of the genes cannot be excluded), because of observations made in AD brains: In AD brains, both frontal and temporal cortex vesicles show elevated  $Ca^{2+}$  content, most evident as an increased peak  $Ca^{2+}$  content at 2 min (after stimulation). The AD cerebellar cortex time course was similar to controls and did not show an elevated peak at 2 min [461]. This regulation takes place within a few minutes. Such a short duration cannot be mediated via gene expression but must be directly regulated on the protein level. Increased intracellular  $A\beta_{42}$ -induced  $Ca^{2+}$  levels have been observed [462]. If an increased  $A\beta_{42}/A\beta_{40}$  ratio directly up-regulated AMPA2 (not via dysregulated  $Ca^{2+}$  levels), then  $Ca^{2+}$  influx would be expected to be blocked (at least through the AMPA receptor) and decreased rather than increased intracellular  $Ca^{2+}$  levels would be expected.

### **6.37 CREB1 is assumed to be less active in consequence of an increased $A\beta_{42}/A\beta_{40}$ ratio**

Long term potentiation (LTP) has been shown to be involved in AD. LTP was accompanied by robust phosphorylation of the cAMP-responsive element binding protein 1 (CREB1) in tissue prepared from entorhinal cortex of both young and old rats [281].

CREB1 was found among the 20 most significantly down-regulated transcripts, only in consequence of an increased  $A\beta_{42}/A\beta_{40}$  ratio, whereas a decreased  $A\beta_{42}/A\beta_{40}$  ratio did not effect CREB1 expression. However, CREB1 was found to be only very weakly down-regulated which questions a real downregulation. However, it has to be taken into consideration that the PLIER algorithm, used here to calculate the fold change, is known to slightly underestimate the true fold change, so that a slightly stronger downregulation can be expected. Moreover, two different probe sets on the microarray showed this very weak but significant downregulation (probe set 204314\_s\_at: fold change=-1.1,  $p=0.0072$ , 204313\_s\_at: fold change=-1.1,  $p=0.0144$ ) which make a real down-regulation more probable (the fold change of -1.1 was calculated with the PLIER algorithm, that is known to slightly underestimate true fold changes [194]. Furthermore, CREB1 showed *weaker phosphorylation on S129+S133* (for  $A\beta_{42}/A\beta_{40}\uparrow$ ), two sites known to induce transcriptional activation of CREB1 upon phosphorylation. Phosphorylation on S133 is accomplished by different kinases, like PKB (synonym: AKT; for instance via PI3K/AKT signaling) and PKC. PKA, PKB and PKC were *hypophosphorylated* at distinct sites (shown elsewhere in this thesis) and in consequence were expected to be less active (for  $A\beta_{42}/A\beta_{40}\uparrow$ ).

This may have contributed to reduced phosphorylation and activity of CREB1.

It can be concluded that for an increased  $A\beta_{42}/A\beta_{40}$  ratio CREB1 might be less active either via its downregulation on the transcript level or/and its reduced phosphorylation status at the activating phosphorylation sites. Both effects have been shown to aggravate long term potentiation (LTP) [463].

### **6.38 Further inversely regulated genes by a changed $A\beta_{42}/A\beta_{40}$ ratio**

Associations to AD or crucial neural processes were found for the following genes and deserve further investigation. Up-regulated (for  $A\beta_{42}/A\beta_{40}\uparrow$ ) and *in parallel* down-regulated (for  $A\beta_{42}/A\beta_{40}\downarrow$ ) were: PDZK1, PBX1.

PDZK1 (PDZ domain containing 1), a multi-PDZ domain containing adaptor protein, interacts with various membrane proteins, including the high density lipoprotein (HDL) receptor scavenger receptor class B type I (SRBI, synonym: CD36L1). Targeted disruption of the PDZK1 gene in mice causes tissue-specific depletion of SRBI and altered lipoprotein metabolism [464]. SRBI mediates the selective uptake of cholesteryl esters from high density lipoprotein. By coexpressing SRBI with PDZK1 in Chinese Hamster Ovary cells, Ikemoto et al. observed an increase in the expression level of SRBI, a reduction in the deacylation rate of the cholesteryl esters taken up from HDL and a change in the intracellular distribution of a fluorescent lipid taken up from HDL. Taken together, these data suggest that PDZK1 is associated with SRBI and may modulate intracellular transport and metabolism of cholesteryl esters taken up from HDL [465].

*In vitro* studies have shown that PBX1 (Pre-B-cell leukemia transcription factor 1) regulates the activity of IPF1 (insulin promoter factor 1; IPF1 is a para-Hox homeodomain transcription factor required for the development and function of the pancreas in mice and humans). To investigate *in vivo* roles of PBX1 in pancreatic development and function, Kim et al. examined pancreatic PBX1 expression, and morphogenesis, cell differentiation, and function in mice deficient for PBX1. PBX1 *-/-* embryos had pancreatic hypoplasia and marked defects in exocrine and endocrine cell differentiation prior to death at embryonic day 15 or 16. In these embryos, expression of ISL1 and ATOH5, essential regulators of pancreatic morphogenesis and differentiation, was severely reduced. PBX1 *+/-* adults had pancreatic islet malformations, impaired glucose tolerance, and hypoinsulinemia. Thus, Kim et al. concluded that PBX1 is essential for normal pancreatic development and function. Analysis of trans-heterozygous PBX1 *+/-* and IPF1 *+/-* mice revealed *in vivo* genetic

interactions between PBX1 and IPF1 that are essential for postnatal pancreatic function. Mutations affecting the IPF1 protein promote diabetes mellitus in mice and humans. Kim et al. concluded that perturbation of PBX1 activity may also promote susceptibility to diabetes mellitus [466, 467]. Retinoic acid regulates the expression of PBX1, PBX2, and PBX3 in P19 cells both transcriptionally and post-translationally [468].

GATA3, SHOX2 and ADRB1 were down-regulated (for  $A\beta_{42}/A\beta_{40}\uparrow$ , comparison C99I45F/C99WT1) and *in parallel* up-regulated (for  $A\beta_{42}/A\beta_{40}\downarrow$ , comparison C99V50F/C99WT1).

GATA3 (GATA binding protein3) is a transcriptional activator which binds to the enhancer (to the consensus sequence 5'-agatag-3') of the T-cell receptor alpha and delta genes [187]. Interestingly the expression (detected on the transcript level by microarray analysis and on the protein level by a proteomics approach) of the T-cell receptor alpha and delta locus was significantly down-regulated in consequence of C99 overexpression (C99WT/mock), while increased *and* decreased  $A\beta_{42}/A\beta_{40}$  ratios resulted in strong and significant upregulation of these genes. Since this cannot be a consequence of GATA3 dysregulation (if so, T-cell receptors would be expected to be *down*-regulated for  $A\beta_{42}/A\beta_{40}\uparrow$ , because GATA3 was down-regulated for  $A\beta_{42}/A\beta_{40}\uparrow$ ), GATA3 downregulation is assumed to be a consequence of, rather than the cause of differential T-cell receptor expression, which maybe limits its own expression by GATA3 downregulation (negative feedback loop).

The SHOX2 (short stature homeobox 2) gene is a member of the homeobox family of genes that encodes proteins with a DNA binding domain. Homeobox genes have been characterized extensively as transcriptional regulators involved in pattern formation in both invertebrate and vertebrate species. Several human genetic disorders are caused by aberrations in human homeobox genes. SHOX is thought to be responsible for short stature and is implicated in the short stature phenotype of Turner syndrome patients. This gene is considered to be a candidate gene for Cornelia de Lange syndrome (a disease with strong mental retardation).

Recent publications associate AD with a dysbalanced stress-response or dysfunction of noradrenergic regulation [469]. Dysregulated ADRB1 (adrenergic  $\beta$ -1 receptor, direct comparison of both mutants, C99I45F/C99V50F, showed >3-fold down-regulation for  $A\beta_{42}/A\beta_{40}\uparrow$ ,  $p < 0.005$ ) may play a role here. However, ADRB1 was expressed at low absolute values (expression values in one group). So relative values (fold changes, comparisons between two groups), which are usually more reliable when absolute values are high, have to be regarded with care.

### 6.39 Miscellaneous genes

The following genes were found to be significantly ( $p < 0.05$ ) and differentially (fold change  $> 2.0$ ) expressed and deserve further investigation in future projects. For these genes, an association with AD or a connection to important cellular processes or important cerebral functions were found. Depending on the nature of research, the opinions about which genes play crucial roles change over the course of time. So the genes listed below only represent a small selection of interesting targets or projects for future research. It is noteworthy that *all* the differentially expressed genes identified in this thesis (which can be found in Chapter 12, Supplementary Information), should be compared with the latest publications and with updated databases from time to time.

The comparison between C99I45F and C99WT ( $A\beta_{42}/A\beta_{40}\uparrow$ ) revealed the following genes as *up*-regulated: TNC (Tenascin C), NLGN4X (neuroligin 4, X-linked), PAG (phosphoprotein associated with glycosphingolipid-enriched microdomains)\*, TNFAIP6 (tumor necrosis factor, alpha-induced protein 6) and TRAF5 (tumor necrosis factor receptor-associated factor 5).

In contrast to this the following genes were *down*-regulated (for  $A\beta_{42}/A\beta_{40}\uparrow$ ): GJA1 (gap junction protein, alpha 1, synonym: connexin 43) and CD99 (CD99 antigen).

The comparison between C99V50F and C99WT ( $A\beta_{42}/A\beta_{40}\downarrow$ ) revealed the following genes as *up*-regulated: SGK (serum/glucocorticoid regulated kinase), CDKN1A (cyclin-dependent kinase inhibitor 1A, synonyms: p21, Cip1), VGF (VGF nerve growth factor inducible), ID4 (inhibitor of DNA binding 4, dominant negative helix-loop-helix protein), FOXC1 (forkhead box C1), BCL2 (B-cell CLL/lymphoma 2), GAP43 (growth associated protein 43), GDF1 (growth differentiation factor 1), MAPK8IP2 (mitogen-activated protein kinase 8 interacting protein 2).

In contrast to this, the following genes were *down*-regulated (for  $A\beta_{42}/A\beta_{40}\downarrow$ ): NAV2 (neuron navigator 2), PAG\*

*\*Of special interest are those genes that were inversely regulated by a changed  $A\beta_{42}/A\beta_{40}$  ratio, like PAG and other genes listed in Chapter 5.6 (Inversely regulated genes).*

## 6.40 Chromosomal susceptibility loci

The following loci were selected according to various criteria. Further association studies, like analyses of SNPs (single nucleotide polymorphisms) in affected families (families in which AD occurs more often than seems likely to be just by chance) should be carried out with special regard to these loci. Focusing on these loci might be also beneficial for linkage analyses. Numbering refers to *human* chromosomes. The chromosomal locus and a short description why it was selected are shown:

- chr11p15.5, several genes were found to be co-regulated in this imprinted region (down-regulated for an increased  $A\beta_{42}/A\beta_{40}$  ratio, presumably by imprinting).
- chr3p14.3-p14.2, ADAMTS9, the most inversely metalloprotease expressed (in consequence of a changed  $A\beta_{42}/A\beta_{40}$  ratio).
- chr6q22, PREP, prolylendopeptidase, independently identified by two laboratories (University of Heidelberg and University of Göttingen) by two different methods (transcriptomics, proteomics).
- chr14q32.33, KIAA0125, see Chapter 6.25.
- chr1q23 and 1p36, “Chromeron“ effect on this locus, see Chapter 5.15.
- chr15q24, CRABP1, might have a crucial effect on neurogenesis, independently identified by two laboratories (University of Heidelberg and University of Göttingen) by two different methods (transcriptomics, proteomics).
- chr2q36, co-regulated genes: DNER (delta-Notch-like EGF repeat-containing transmembrane), SGPP2 (Sphingosine-1-phosphate phosphatase 2), IGFBP5 (insulin-like growth factor binding protein 5).
- chr10q24.33, co-regulated genes: GRK5 (G protein-coupled receptor kinase 5), INA (internexin neuronal intermediate filament protein alpha).
- chr10q23.3, ACTA2, see Chapter 6.11.
- chr7q21-q22, HGF (hepatocyte growth factor) and TFPI2 (tissue factor pathway inhibitor 2), both co-regulated and found in the same signal transduction pathway.
- chr9q22.1, NTRK2, non-catalytic isoform, assumed to inhibit BDNF signaling.

- chr11q12.1, syntaxin3, among the most inversely regulated genes, also found in a PS1/PS2 knockdown approach in our laboratory and as a consequence of AICD overexpression [57].
- chr10p15, GATA3, dysregulated transcription factor in a pathway that turned out to be important (IGF2 signaling).
- chr17q11, CYB561, cytochrome b-561, transmembrane protein, electron transport, among the most strongly down-regulated genes (in consequence of an increased  $A\beta_{42}/A\beta_{40}$  ratio), CYB561 supplies electrons to monooxygenases (for instance to dopamine beta-hydroxylase).
- chr22q12.1-q13.2|22q12.3, TIMP3 (tissue inhibitor of metalloproteinase 3), inhibits  $\alpha$ -secretases.
- chr8p12, PLAT (plasminogen activator, tissue), altered transcriptional control of fibrinolysis.
- chr17p13.1, SERPINF1 (serine proteinase inhibitor, clade F), altered transcriptional control of fibrinolysis.
- chr14q21.3, CDKL1, cyclin-dependent kinase-like 1 (CDC2-related kinase), candidate kinase for tau or GSK3 phosphorylation.
- chr21q22.13 DYRK1A Dual-specificity tyrosine-(Y)-phosphorylation regulated kinase 1A, candidate kinase for tau or GSK3 phosphorylation.

#### **6.41 Intersection of genes identified in this thesis as a consequence of altered C99 cleavage products and genes identified as a result of PS1/PS2 knockdown in murine embryonic fibroblasts**

The overlapping genes of both approaches are assumed to be differentially expressed due to one common mechanism, namely *processing by the  $\gamma$ -secretase complex*. The probability that the same genes occur by chance in both approaches among the 100 most up or 100 most down-regulated genes when such big data sets (40,000 transcripts in the human neuroblastoma cells, 12,000 in the murine fibroblasts) are compared is extremely low. Here (see Chapter 5.18), 9 genes were identified as overlapping genes. Although data from two species (human and mouse) were compared, more overlapping genes were found than could be expected just by chance, increasing the reliability of a common regulatory process.

## **6.42 Intersection of genes identified in this thesis as a consequence of altered C99 cleavage products and genes identified as a result of AICD overexpression in human neuroblastoma cells**

See Chapter 5.19, page 120. The overlapping genes of both approaches are assumed to be differentially expressed by the AICD or cleavage products thereof. C99 was overexpressed in the human neuroblastoma cell line SH-SY5Y: A $\beta$ <sub>42</sub>/A $\beta$ <sub>40</sub> and their respective APP intracellular domains (AICDs) were liberated by processing. This special comparison with an approach in which the AICD was overexpressed alone and also together with FE65 [57], argues, at least *for this small overlapping subset of genes*, for a mechanism triggered by the AICD. Intriguingly, *ACTA2* was found to be among the *three most dysregulated genes (all with a p-value <0.05)* by Müller et al. (in the human neuroblastoma cell line SHEP-SF, in consequence of AICD overexpression), by our PS1/PS2 knockdown approach with siRNA in murine embryonic fibroblasts (presented in the Master thesis of my colleague Laura Busia) and by changed C99 cleavage products in the human neuroblastoma cell line SH-SY5Y (presented in this thesis). Common to all three approaches is the AICD, either released by processing (our two approaches: PS1/PS2 knockdown, altered C99 processing) or overexpressed in human neuroblastoma cells [57]. The fact that Müller et al. found the same gene (*ACTA2*) as a consequence of AICD-overexpression argues for an effect triggered by the AICD.

## **6.43 Concluding remarks and outlook**

In summary, it was shown that C99 cleavage products had a strong impact on gene expression. In contrast to many other studies in which A $\beta$ <sub>42</sub>/A $\beta$ <sub>40</sub> is added artificially from outside the cells, here, the naturally occurring precursor C99 was overexpressed and A $\beta$ <sub>42</sub>/A $\beta$ <sub>40</sub> (and their respective APP intracellular domains) were liberated by processing. The goal of this thesis was to obtain information about effects of the changed C99 processing, due to point mutations in two C99 mutants which resulted in different A $\beta$ <sub>42</sub>/A $\beta$ <sub>40</sub> levels, together with the inherently produced AICDs. This approach does not allow distinguishing between effects mediated by A $\beta$ <sub>42</sub>/A $\beta$ <sub>40</sub> and the AICDs. Furthermore, it has to be taken into consideration that the AICD is further processed and its cleavage products themselves could also influence gene expression.

It was demonstrated that in mutants with an increased  $A\beta_{42}/A\beta_{40}$  ratio CRABP1 was up-regulated on the transcript level and on the protein level which reduced responsiveness of human neuroblastoma cells to retinoic acid. The knockdown of CRABP1 rescued the differentiation potential of these cells and could also be an important mechanism *in vivo*, where CRABP1 might prevent the terminal differentiation of neural precursor cells into functional neurons.

IGF2 signaling, via the IGF-Receptor 1, was shown to be down-regulated in consequence of an increased  $A\beta_{42}/A\beta_{40}$  ratio and is most probably caused in part by imprinting processes. This is in line with previously published *in vivo* data in which IGF2 levels were found to be decreased in the brains of AD patients. The presented model (see Chapter 5.9.2, Fig. 5.35, pages 78-79) was created using Pathway Architect (Stratagene), a literature mining program used to build biological interaction networks among genes/proteins of interest. It accesses over 2 million biological facts from the current literature. By a complex filtering procedure this pathway (Fig. 5.35) was created, in which all transcripts (except for DDC) were found to be connected in a network. Nodes (transcripts and/or proteins) are connected via interconnectivities (lines). These lines represent direct interactions, regulatory processes or other kinds of associations that have been published. The presented model reveals a hitherto unknown network of interactions triggered by a changed  $A\beta_{42}/A\beta_{40}$  ratio. PI3K/AKT activating molecules like IGF2 were significantly down-regulated. This downregulation was corroborated by the simultaneous downregulation of H19 and may have been triggered by imprinting (IGF2-H19 imprinted region on chromosome 11p15.5). Furthermore, effects mediated by other molecules (effects via the non-catalytic TrkB-receptor, inhibiting effects by IGFBP5 etc.) may act synergistically to down-regulate this pathway (for  $A\beta_{42}/A\beta_{40}\uparrow$ ). Imprinting may exert a key role here, due to the fact that not only IGF2, but also further molecules belonging to the imprinted region, were simultaneously down-regulated. Future experiments (for instance functional assays, in which insulin or insulin like growth factors are added to the cells or using inhibitors for this pathway) will provide further insight into insulin/IGF2 signaling.

There are indications of increased blood coagulation and presumably decreased fibrinolysis as a consequence of an increased  $A\beta_{42}/A\beta_{40}$  ratio, while a decreased  $A\beta_{42}/A\beta_{40}$  ratio may result in enhanced fibrinolysis, while blood coagulation might be reduced. All differentially expressed genes (described in Figure 5.37, except for F2R, F2RL3 and VWCD1) code for secreted proteins. Theoretically, it seems possible that *in vivo* (in brains of AD patients) an increased  $A\beta_{42}/A\beta_{40}$  ratio triggers the release of the previously mentioned factors into the extracellular space and into blood vessels, in which a shift towards increased blood coagulation and decreased fibrinolysis may

take place. Indeed, clinical data on blood coagulation and fibrinolysis hint at such a regulation in Alzheimer patients [313] as well as immunohistochemical and electron microscopy data of cerebral cortex and brain microvessels [314]. Such a regulation would result in decreased cerebral blood flow and a stronger tendency towards having strokes and mental dysfunction. Further research focusing on blood coagulation and fibrinolysis is necessary.

The model “Increased  $A\beta_{42}/A\beta_{40}$  ratio is expected to reduce ATP levels and to induce phosphofructokinase upregulation” (see Model, Chapter 5.9.3, Fig. 5.36, page 85) provides an explanation for changed glucose and ATP levels in brains of AD patients. Up-regulated (for  $A\beta_{42}/A\beta_{40}\uparrow$ ) phosphofructokinase, which plays a key role in glycolysis, may contribute to reduce glucose levels by inducing glycolysis. This could be regarded as the ‘attempt’ (by feedback loops) of the cells to restore sufficient ATP levels. Phosphofructokinase activity in brains from patients with Alzheimer's disease was significantly increased in frontal and temporal cortex when compared with control brains [332]. Thus, missing glucose could be inherently connected to GSK3/tau phosphorylation (provided PFKP turns out to be a possible tau kinase) via PFKP upregulation, so GSK3/tau phosphorylation would be an inherent byproduct of reduced glucose/ATP levels. Further research is necessary, which focuses on phosphofructokinase, its relation to GSK3 $\beta$  and glucose/ATP levels in brains of AD patients.

As candidate genes encoding kinases possibly phosphorylating tau, I identified DYRK1, CDKL5, CDK6, DCAMKL1, ERK1 and PFKP (furthermore, PPP2R4 and PPP2R2C two regulatory subunits of protein phosphatase 2A, which may influence its phosphatase activity on tau). Concentrating on these candidates might help to interrupt the harmful connection between  $A\beta$  and tau. Further research should also focus on the following areas which were distinctly differentially affected by a changed  $A\beta_{42}/A\beta_{40}$  ratio: (metallo) proteases (especially ADAMTS9 and MMP8) and protease inhibitors (especially TIMP3, TIMP1), extracellular matrix proteins (especially ACTA2), mitochondrial respiratory chain (especially NDUF9), cytochromes with special regard to the cytochromes b-561 and b-245, copper transport/metabolism (with special regard to ATP7A), dopamine, serotonin and glutamate-metabolism with special regard to DDC, GLS and GLUL, effects of BDNF (non-catalytic isoform of TRKB), membrane fusion of neurotransmitter containing vesicles (especially syntaxin 3 and synapsin 2),  $Ca^{2+}$ -metabolism (especially the AMPA2 and AMPA3 subunits of AMPA receptors), synaptosomal and axonal transport events (SEMA3A, SEMA3C, L1CAM, PTN, SLIT1, DNCL12), acetylcholine receptors (CHRNA7). Furthermore, future research should focus on Notch, Wnt, TGF $\beta$  and G protein signaling which have been shown to be influenced by a changed  $A\beta_{42}/A\beta_{40}$  ratio. Moreover, strong

differential effects of a changed  $A\beta_{42}/A\beta_{40}$  ratio have been observed on receptor expression (PTGER2, EGFR, GRM7, GRM8c, GLRB, GABRB3). APP is a transmembrane protein which is expected to exert trans-cellular interactions. It can be speculated that some of the dysregulated receptors may turn out to be possible interaction partners of APP.

Further research is necessary to provide the possibility of distinguishing between effects by  $A\beta_{42}/A\beta_{40}$  and by the AICD (or its cleavage products). It is assumed, even though no experimental evidence is provided here, that the AICDs change similarly to  $A\beta_{42}$  and  $A\beta_{40}$ . Currently, we are investigating this issue together with our collaboration partner Stefan Lichtenthaler. I expect that at least some of the identified genes in our approach are differentially expressed by different AICD species. It has to be taken into consideration that AICD-induced/repressed genes may only be a subset of the genes that are regulated by  $\gamma$ -secretase cleavage. Moreover, the AICD is further cleaved. Additionally, a signalling function of its cleavage products cannot be ruled out. Finally, the possibility that both  $A\beta_{42}/A\beta_{40}$  and the AICDs synergistically influence gene expression, cannot be excluded.

Future research should focus on the most inversely (by an altered  $A\beta_{42}/A\beta_{40}$  ratio) expressed genes (Chapter 5.6), because they are expected to show the biggest differences in  $A\beta_{42}$  and  $A\beta_{40}$  effects.

RNA interference experiments (knockdown of up-regulated transcripts) and overexpression of down-regulated genes could unravel crucial signal transduction pathways and could be helpful in obtaining further insights into the behaviour of the cells. Time course experiments with an inducible system (for instance tet-off/on system) or by RNA interference would help to distinguish between primary and secondary effects initially triggered by  $A\beta$  overexpression.

The genes selected in this thesis are currently being used to generate a subarray (oligonucleotide microarray), for example in order to test primary neurons and their response to  $A\beta$  overexpression or for human post-mortem tissue. This is currently carried out in collaboration with the biotechnological company Febit, Heidelberg, Germany.

## 7 Materials and Methods

### 7.1 Materials

#### 7.1.1 Cell lines

- E.coli DH5 $\alpha$  and BL21 (DE3)
- Human neuroblastoma cell line SH-SY5Y:

This cell line was originally isolated from a metastatic bone tumor. Transformed neural tissue (neuroblastoma) from a 4 year old girl was metastasized into the bone marrow from where it was isolated. SH-SY5Y is a thrice cloned (SK-N-SH -> SH-SY -> SH-SY5 -> SH-SY5Y) subline of the neuroblastoma cell line SK-N-SH which was isolated and established in 1970. This cell line has 47 *chromosomes*. The cells possess a unique marker comprised of a chromosome 1 with a complex insertion of an additional copy of a 1q segment into the long arm, resulting in trisomy of 1q. SH-SY5Y cells are reported to exhibit moderate levels of dopamine beta hydroxylase activity. These cells grow as a mixture of floating and adherent cells. The cells grow as clusters of neuroblastic cells with multiple, short, fine cell processes (neurites). Cells tend to aggregate, form clumps and float [470, 471].

#### 7.1.2 Gene Chips<sup>®</sup> (Affymetrix whole genome oligonucleotide arrays)

- Test 3 arrays
- Gene Chip Human Genome HG-U133 A (22283 probe sets for the detection of approximately the corresponding number of transcripts)
- Gene Chip Human Genome HG-U133 B (22645 probe sets for the detection of approximately the corresponding number of transcripts)

#### 7.1.3 TaqMan<sup>®</sup> Human Endogenous Control Plate

The amplification of an endogenous control can be used to normalize the amount of sample RNA or cDNA added to a reaction. The TaqMan<sup>®</sup> Human Endogenous Control Plate is designed to identify an endogenous control for gene-expression studies. It consists of an Optical 96-well Reaction Plate loaded with TaqMan<sup>®</sup> probes and primers for 11 candidate control assays and an internal positive control (IPC) assay arranged into 12 columns of eight replicate wells. Assays for the endogenous controls included on the TaqMan<sup>®</sup> Human Endogenous Control Plate are conveniently available once an appropriate endogenous control has been selected.

Out of 11 candidate control assays one was excluded (18s rRNA-assay), due to a different preparation procedure. The remaining 10 candidate control assays were used to select a suitable endogenous control for normalisation:

- Acidic ribosomal protein
- $\beta$ -actin
- CyclophilinA
- Glyceraldehyde-3-phosphate dehydrogenase
- Phosphoglycerokinase
- $\beta_2$ -Microglobulin
- $\beta$ -Glucuronidase
- Hypoxanthine ribosyl transferase
- Transcription factor IID, TATA binding protein
- Transferrin receptor

The assay was performed according to the manufacturer's instructions ([www.appliedbiosystems.com](http://www.appliedbiosystems.com)) and measured with a GeneAmp 5700 Sequence Detection System (real-time PCR cyclor).

#### 7.1.4 Primer sequences for quantitative real-time PCR

All primers for real-time PCR were purchased from Applied Biosystems and were part of the Taq man Gene expression assays (assays-on-demand).

Gene name	Assay ID
peptidylprolyl isomerase A (cyclophilin A)	Hs99999904_m1
actin, beta	Hs99999903_m1
ribosomal protein, large, P0	Hs99999902_m1
glutamate receptor, metabotropic 7	Hs00356067_m1
hepatocyte growth factor (hepapoietin A; scatter factor)	Hs00300159_m1
protein tyrosine phosphatase, receptor type, N polypeptide 2	Hs00243067_m1
neurofilament 3 (150kDa medium)	Hs00193572_m1
endothelin converting enzyme-like 1	Hs00191400_m1
glutamate receptor, ionotropic, AMPA 2	Hs00181331_m1
neurotrophic tyrosine kinase, receptor, type 2	Hs00178811_m1
cellular retinoic acid binding protein 1	Hs00171635_m1
insulin-like growth factor 2 (somatomedin A)	Hs00171254_m1
sema domain, immunoglobulin domain (Ig), short basic domain, secreted, (semaphorin) 3C	Hs00170762_m1
glutamate receptor, metabotropic 8	Hs00168299_m1
human GAPD (GAPDH) endogenous control (FAM™ dye/MGB Probe, non-primer limited)	4333764T

### 7.1.5 siRNAs

All siRNAs were double-stranded Silencer™ siRNAs, purchased from Ambion with the following properties:

Type:	Pre-designed
Format:	Annealed
Purity:	Standard purity (column purified), the siRNAs for GAPDH, beta-actin, Cyclophilin A (positive controls) and non-targeting siRNAs (scrambled sequences=negative controls) were HPLC purified.
Amount:	5 nmol
Catalogue #:	16708
Length:	21 nucleotides

5 nmol siRNA, delivered as a powder, was reconstituted in 100 µl of nuclease-free water to come to a stock solution of 50 µM. Once reconstituted in nuclease-free water, the siRNA was ready to transfect and were used at a final concentration of 30-90 nM.

Controls:

- Negative controls: Validated, non-targeting siRNAs (scrambled sequences)
- Positive controls: Validated, siRNAs against GAPDH and cyclophilin A

Catalogue # or siRNA ID #:

- To efficiently knock-down crabp1 three siRNAs were used targeting different exons: siRNA ID # 121004 (exons 3, 4), siRNA ID # 121005 (exon 4), siRNA ID # 121006 (exon 4),
- Positive controls: directed against GAPDH: Catalogue # 4605 and cyclophilin A: Catalogue # 4616

### 7.1.6 Plasmids

- pCEP4 vector alone, negative control (Invitrogen)
- pCEP4-spA4ct-DA-WT
- pCEP4-spA4ct-DA-I45F
- pCEP4-spA4ct-DA-V50F

pCEP4-spA4ct-DA constructs were provided by colleagues and have been described previously [148, 149].

### 7.1.7 Chips for the Bioanalyzer 2100™ (Agilent)

- RNA 6000 Nano Chips Agilent Technologies.

## 7.1.8 Kits

RNA 6000 Nano Assay Reagent Kit	Agilent, Böblingen, Germany
Superscript <sup>™</sup> Double-Stranded cDNA Synthesis Kit	Invitrogen, Karlsruhe, Germany
GeneChip <sup>®</sup> Sample Clean up Module	Affymetrix, Santa Clara (California, USA)
GeneChip <sup>®</sup> Eucaryotic Hybridization Control Kit	Affymetrix, Santa Clara (California, USA)
BioArray <sup>™</sup> High Yield <sup>™</sup> RNA Labeling Kit (10rct)	Enzo Life Sciences, NY (USA)
QIAshredder <sup>™</sup> (50)	Qiagen, Hilden, Germany
RNeasy <sup>®</sup> Midi Kit (50)	Qiagen, Hilden, Germany
RNeasy <sup>®</sup> -Free DNase Set	Qiagen, Hilden, Germany
High Capacity cDNA Archive Kit	Applied Biosystems, USA
GeneChip <sup>®</sup> Eukaryotic Hybridization Control Kit	Affymetrix, Santa Clara (California, USA)

## 7.1.9 Antibodies

### 7.1.9.1 Primary antibodies

Apart from primary antibodies used for screening of phosphorylated proteins mentioned in Chapter 5.8.1, the following antibodies were used:

- W0-2, recognized epitope A $\beta$  (1-16 aa) [472].
- G-10 [472].
- G-11 [472].
- Monoclonal anti-cellular retinoic acid binding protein 1 (Sigma, product number C1608), 1:250 for immunofluorescence.
- Anti- $\beta$ -actin (Abcam, ab8227), 1:5000 as loading control for Western blot.

### 7.1.9.2 Secondary antibodies

- Western Blotting:

For Enhanced Chemical Luminescence (ECL) detection after Western Blotting, Horseradish-Peroxidase (HRP) coupled anti-mouse (Promega), anti-rabbit (Promega), anti-rat (DAKO) antibodies were used with a 1:10 000 dilution.

- Immunocytochemistry:

For immunocytochemistry Alexa 488 goat anti-mouse, Alexa 488 goat anti-rabbit, Alexa 568 goat anti-mouse and Alexa 594 goat anti-rabbit (Molecular Probes) were used with a 1:200 dilution.

### 7.1.10 Oligonucleotides

Primer name	Sequence (5'→3')	Description	Company
pCEP (forward primer)	5'-AGCAGAGCTC GTTTAGTGAACCG 3'	Primer for sequencing	MWG-Biotech, Germany
pCEP/spa4ct12 79-1260	5'-GGCGGTGTT GTCATA GCGAC-3'	Primer for sequencing	MWG-Biotech, Germany
pCEP/spa4ct95 2-933	5'-GCTGTAACAC AAGTAGATGC -3'	Primer for sequencing	MWG-Biotech, Germany
pCEP/spa4ct66 3-642	5'- GCTTCTCTTGC CTAAGTATTCC-3'	Primer for sequencing	MWG-Biotech, Germany
T7-(dT)24	5'-GGCCAGTGA ATTGTAATACGAC TCACTATAGGGAGGCGG TTTTTTTTTTTTTTTTT TTTTTTTTT-3'	Primer for cDNA-Synthesis	Proligo, Germany and France
Control oligoB2	Confidential information, not provided by Affymetrix	Biotin labelled oligonucleotide, added to the hybridization solution to provide alignment signals for image analysis	Affymetrix, England

### 7.1.11 Chemicals

Agarose (Dnase-, Rnase-free)	Serva Heidelberg
Ammoniumacetate	ApliChem, Darmstadt
Ampicillin	Serva Heidelberg
Antifoam O-30	SIGMA, Deisenhofen
Bromophenol blue	LKB. Broma, Sweeden
BSA (50 mg/ml)	Invitrogen, Karlsruhe
Complete <sup>®</sup> Protease Inhibitor Mix	Roche, Basel
Dithiothreitol (DTT)	Invitrogen, Karlsruhe
EDTA Disodium Salt	SIGMA, Deisenhofen
Ethanol (absolute)	Riedel-de-Haën Lab Chemicals, Seelze
Ethidiumbromide (10 mg/ml)	SIGMA, Deisenhofen
Ethylenediaminetetraacetic acid (EDTA)	SIGMA, Deisenhofen
Herring Sperm DNA (10 mg/ml)	Invitrogen, Karlsruhe
Isopropanol	Riedel-de-Haën Lab Chemicals, Seelze
Magnesiumchloride	Merk KGaA, Darmstadt
MES free Acid Monohydrate	SIGMA, Deisenhofen
MES Sodium Salt	SIGMA, Deisenhofen
Methanol	Merk KGaA, Darmstadt
Natriumchloride	J. T. Baker, Deventer, Holland
Potassium-Acetate	SIGMA, Deisenhofen
Retinoic acid	SIGMA, Deisenhofen
Sodium-Acetate	SIGMA, Deisenhofen

Sodium-Chloride	J. T. Baker, Deventer, Holland
Streptavidin (R-phycoerythrin conjugate)	Molecular Probes, Leiden, Holland
Tricine	Biomol, Hamburg
Tris	SIGMA, Deisenhofen
Tris-Acetate	SIGMA, Deisenhofen
Triton-X-100	Merk KGaA, Darmstadt
TRIZMA® BASE	SIGMA, Deisenhofen
Trizma® Hydrochloride	SIGMA, Deisenhofen
Tween® 20	SIGMA, Deisenhofen
β-Mercaptoethanol	SIGMA, Deisenhofen

### 7.1.12 Buffers and solutions

- 12 x MES Stock (1000 ml):  
70.4 g MES Free Acid Monohydrate  
193.3 g MES Sodium Salt  
These components were dissolved  
in 800 ml H<sub>2</sub>O and filled up to 1000 ml with H<sub>2</sub>O.  
pH was adjusted between 6,5 and 6,7.  
This solution was filtered sterile (0.2 µm filter)  
and stored at 4°C (shielded from light).
- 2 x MES hybridisation buffer (50 ml):  
8.3 ml 12 x MES Stock  
17.7 ml 5 M NaCl  
4 ml 0.5 M EDTA  
0.1 ml 10% TWEEN 20  
19.9 ml RNase-free water
- Wash-buffer A (non-stringent buffer) (1000 ml):  
300 ml 20x SSPE  
1 ml 10% TWEEN 20  
698 ml RNase-free water  
This solution was filtered sterile (0.2 µm filter)  
After filtration, 1 ml 5% antifoam was added.

- Wash-buffer B (stringent buffer) (1000 ml):
  - 83.3 ml 2x MES stock
  - 5.2 ml 5 M NaCl
  - 1 ml 10% TWEEN 20
  - 910.5 ml RNase free water

This solution was filtered sterile (0.2  $\mu$ m filter)
  
- 2 x staining buffer (250 ml):
  - 41.7 ml 12 x MES Stock
  - 92.5 ml 5 M NaCl
  - 2.5 ml 10% TWEEN 20

112.8 ml RNase-free water

This solution was filtered sterile (0.2  $\mu$ m filter)

After filtration, 0.5 ml 5% antifoam were added
  
- SAPE staining solution (1.staining, 3.staining, 1200  $\mu$ l):
  - 600  $\mu$ l 2 x stain buffer
  - 540  $\mu$ l RNase free water
  - 48  $\mu$ l 50 mg/ml acetylated BSA (final concentration: 2 mg/ml)
  - 12  $\mu$ l 1mg/ml SAPE (final concentration: 10  $\mu$ m/ml)

This solution was mixed well and centrifuged for 5 min at 14000 rpm,

The supernatant was aliquoted and stored in light-protected brown tubes.
  
- Antibody solution (for 2. staining, 600  $\mu$ l):
  - 300  $\mu$ l 2 x stain buffer
  - 266.4  $\mu$ l RNase-free water
  - 24  $\mu$ l 50 mg/ml BSA (final concentration: 2 mg/ml)
  - 6  $\mu$ l 10 mg/ml goat IgG (final concentration: 0,1 mg/ml)
  - 3.6  $\mu$ l 0.5 mg/ml biotinylated anti-streptavidin antibody (final concentration: 0.3  $\mu$ g/ml)

### 7.1.13 Enzymes

Enzymes	Company
NheI	Biolabs
BamHI	Biolabs
KpnI	Promega
XhoI	Biolabs
Bgl II	Biolabs
DNaseI	Qiagen
SuperSript II Reverse Transcriptase	Invitrogen
E.coli DNA-Ligase	Invitrogen
E.coli DNA-Polymerase I	Invitrogen
RNase H	Invitrogen
T4 Polymerase	Invitrogen
T7 RNA -Polymerase	Invitrogen

### 7.1.14 Antibiotics

Hygromycin B, (50 mg/ml) (PAA Laboratories), 300 µg/ml (final concentration)

### 7.1.15 Cell culture

- Medium for human neuroblastoma cells (SH-SY5Y):
  - 250 ml MEM (Minimum Essential Medium), without L-Glutamine (Sigma)
  - 250 ml F12 (Nutrient Mixture F-12, HAM) (Sigma)
  - 57 ml FBS (PAN)
  - 5.7 ml MEM non essential-amino acids 100x (Sigma)
  - 5.7 ml L-Glutamine (Sigma)
  - 3.0 ml Hygromycin B, 50 mg/ml (PAA Laboratories), 300 µg/ml (final concentration)
- Reagents for cell culture:

Dimethylsulfoxyde (DMSO)	SIGMA, Deisenhofen
Dulbecco's Modified Eagle's Medium	SIGMA, Deisenhofen
Fetal Bovine Serum	SIGMA, Deisenhofen
Fetal Bovine Serum	PAN™, Biotech GmbH, South America
Hygromycin B, solution (50 mg/ml)	PAA Laboratories GmbH, Pasching
Minimum Essential Medium Eagle	SIGMA, Deisenhofen
MEM Non-Essential Amino Acid Solution 100 x	SIGMA, Deisenhofen
Nutrient Mixture-F12 HAM	SIGMA, Deisenhofen
OptiMEM® + GlutaMAX™	GIBCO™ Invitrogen, Auckland N.Z.
Trypsin-EDTA-Solution (1x)	SIGMA, Deisenhofen
L-Glutamine	SIGMA, Deisenhofen

### **7.1.16            Devices**

- Agilent 2100 Bioanalyzer<sup>®</sup>
- Gene Chip<sup>®</sup> Hybridization Oven 640 (Affymetrix)
- Gene Chip<sup>®</sup> Fluidics Station 400 (Affymetrix)
- Gene Array<sup>®</sup> Scanner (Hewlett Packard)

### **7.1.17            Nucleic acid and protein molecular weight markers**

- 1 kb (+) DNA-ladder (Invitrogen)
- RNA 6000 Ladder (Ambion)
- Prestained protein ladder (Fermentas)

## 7.2 Methods

### 7.2.1 DNA methods

#### 7.2.1.1 Transformation of competent *E. coli*

Chemo-competent *E. coli* DH5 $\alpha$  cells were thawed on ice and 50 ng plasmid-DNA was added to a 100  $\mu$ l cell aliquot. After incubation on ice for 30 min, cells were heat shocked for 90 s at 42°C and further incubated on ice for 5 min. Then 900  $\mu$ l LB-medium was added to each aliquot and incubated on a roller shaker for 45 min at 37°C. Afterwards, 200  $\mu$ l were plated on agar plates and incubated over night at 37°C.

#### 7.2.1.2 Small scale preparation of plasmid DNA (Mini Prep)

For small scale preparation of plasmid DNA (Mini Prep), the Qiagen Mini Prep Kit was used:

S1: 50 mM Tris/HCl, 10 mM EDTA, 100  $\mu$ g RNase A/ml, pH 8.0

S2: 200 mM NaOH, 1% SDS

S3: 2.8 M Potassium acetate pH 5.1

70% ethanol

TE-buffer, pH 8.0: 10 mM Tris/HCl pH 8.0, 1mM EDTA pH 8.0

A single bacterial colony was picked from an agar-plate, inoculated into 3 ml LB-medium, supplemented with 3  $\mu$ l ampicillin (100mg/ml) and incubated over night at 37°C under vigorous shaking. 1-2 ml of this culture was transferred into an Eppendorf tube and centrifuged at 6.000 rpm for 5 min. The cells were resuspended in 100  $\mu$ l S1 buffer and further processed according to the manufacturer's protocol.

#### 7.2.1.3 Large scale preparation of plasmid DNA (Maxi Prep)

For large scale preparation of plasmid DNA (Maxi Prep), the Nucleobond AX-500 Kit (Macherey & Nagel) was used:

- N2: 100 mM Tris, 15% ethanol, 900 mM KCL pH 6.3
- N3: 100 mM Tris, 15% ethanol, 1150 mM KCL pH 6.3
- N5: 100 mM Tris, 15% ethanol, 1000 mM KCL pH 8.5

3 ml of LB medium (containing 3  $\mu$ l of 100mg/ml ampicillin) were inoculated with a bacterial colony and incubated at 37°C for approximately 6 hours under vigorous shaking. Then this culture was added to 400 ml (containing 400  $\mu$ l of 100mg/ml ampicillin) LB medium and incubated at 37°C over night under vigorous shaking. This culture was centrifuged for 10 min at 6000 rpm/4°C and further processed according to the manufacturer's protocol.

### 7.2.1.4 Purification and concentration of DNA

An equal volume of phenol-chloroform-isoamylalcohol (25:24:1) was added to a given volume of DNA solution and vortexed thoroughly for at least 1 min. The emulsion was centrifuged for 10 min at 13000 rpm in a common table centrifuge to achieve a separation of the phases. The aquatic, DNA-containing phase on top was carefully transferred into a new Eppendorf tube. This procedure was repeated once and the DNA was precipitated as follows: 1/10 volume of sodium acetate (3M, pH 5.2) and 2.5 volumes of 100% ethanol (-20°C) was added to the given volume of DNA solution, mixed well, and incubated for 30 min at -20°C. The precipitated DNA was centrifuged for 5 min at 4°C/13000 rpm. The supernatant was removed, the precipitated DNA was air-dried and diluted in a suitable volume of H<sub>2</sub>O.

### 7.2.1.5 Determination of DNA concentration

DNA concentrations were measured with a spectrophotometer (Biorad Smart Spec 3000) at a wavelength of 260nm. The DNA was diluted in a suitable volume of H<sub>2</sub>O so that the following measurements of absorption were in a range of 0.1 -1.0.

The following equation was used to calculate the concentration from the measured absorption:

dsDNA:  $A_{260\text{nm}}(1\text{cm})=1$  corresponds to a concentration of approximately 50 µg/ml

(ssDNA or ssRNA):  $A_{260\text{nm}}(1\text{cm})=1$  corresponds to a concentration of approximately 40 µg/ml)

The purity of the DNA was determined by measuring the absorption at 280 nm and 310 nm which corresponds to the absorption maxima of aromatic proteins and polysaccharides. For pure DNA the  $A_{260\text{nm}}/A_{280}$  ratio should be between 1.8 and 2.1, with no absorption at 310 nm.

### 7.2.1.6 Restriction digestion of DNA

A typical reaction was prepared as follows:

Plasmid-DNA	1.0 µg
10 x reaction buffer	3 µl
Restriction enzyme (5-10 U)	0.5-1.0 µl
H <sub>2</sub> O	ad 30 µl

The reaction was incubated at the appropriate temperature (generally 37 °C) for 1-2 h.

### 7.2.1.7 Analysis of DNA fragments on agarose gels

1x TAE buffer: 40 mM Tris-acetate  
1 mM EDTA ph 8.0

Ethidiumbromide stock: 10 mg/ml (diluted 1:10 000)

6x DNA sample buffer:            30 % glycerol (w/v)  
   0.25 % bromophenol-blue  
   0.25 % Xylencyanol  
   50 mM EDTA pH 8.0

1 % agarose gels were used for separation of DNA. The agarose was dissolved in 1xTAE buffer by boiling in a microwave oven. Ethidiumbromide was added to a final concentration of 1 µg/ml and the solution was poured into a gel chamber. DNA sample buffer was added to the samples. Then the samples and a 1 kb DNA ladder were loaded onto the gel and electrophoresis was performed at 100-200 V. After separation, photographs were taken of the gels under UV-light and correct cleavage was estimated by comparing the fragment sizes with the DNA ladder.

### **7.2.1.8            Sequencing of plasmids**

Plasmids mentioned in Chapter 7.1.6 were sent for sequencing to MWG-Biotech using the primers listed in Chapter 7.1.10. All constructs showed the expected sequences.

## **7.2.2            Cell culture methods**

### **7.2.2.1            Cultivation of eukaryotic cell lines**

- 1 x PBS:                            137 mM NaCl  
   2.7 mM KCl  
   10 mM Na<sub>2</sub>HPO<sub>4</sub>  
   2 mM KH<sub>2</sub>PO<sub>4</sub>

PBS was adjusted to pH 7.4

- Medium for human neuroblastoma cells (SH-SY5Y):  
250 ml MEM (Minimum Essential Medium), without L-Glutamine  
250 ml Nutrient Mixture F-12, HAM  
57 ml FBS  
5.7 ml MEM non essential-amino acids 100x  
5.7 ml L-Glutamine  
3.0 ml Hygromycin B, solution (50 mg/ml)

All cells were cultured at 37°C in cell culture medium described above in a humidified atmosphere with 5% CO<sub>2</sub>. The cells were cultivated in 10 cm cell culture dishes (Sarstedt®) and passaged with Trypsin-EDTA at 90-100% confluency. For passaging, cells were washed once with sterile 1x PBS, and trypsinized with 1 ml of Trypsin-EDTA for 2-5 min at 37°C. 9 ml fresh growth medium was added and detached cells were resuspended until a single cell suspension was obtained. Aliquots (1/20-1/3) of

the resuspended cells were plated in dishes containing 10 ml fresh medium and were equally distributed by gentle shaking.

### 7.2.2.2 Freezing and thawing of eukaryotic cell lines

- Freezing medium:

Medium for human neuroblastoma cells (previously mentioned)

15% (v/v) DMSO

10% FBS

without antibiotics

Cells at 60-90% confluency were used for freezing. Cells from a 10 cm dish were trypsinized as described and transferred into a 15 ml tube with 10 ml of fresh medium. The cells were centrifuged at 300 x g for 5 min, resuspended in 1 ml freezing medium and transferred into cryovials (Nunc). The vials were incubated in a cryobox (Nunc) containing isopropanol at -80°C, and then transferred into a liquid nitrogen tank for long-term storage.

- Thawing cells:

Cells frozen in liquid nitrogen were quickly thawed at 37°C in a water bath.

Cells were then transferred to a 10 cm dish with 10 ml fresh growth medium and equally distributed by gentle shaking. The next day the medium was replaced in order to remove residual DMSO and non-viable cells. Cells were further cultured as described above.

### 7.2.2.3 Stable transfection of human neuroblastoma cells

Human neuroblastoma cells (SH-SY5Y) were transfected with the following constructs:

- pCEP4 vector alone, negative control (Invitrogen)
- pCEP4-spA4ct-DA-WT
- pCEP4-spA4ct-DA-I45F
- pCEP4-spA4ct-DA-V50F

OptiMEM (Invitrogen)

Lipofectamine (Invitrogen)

Plus-reagent (Invitrogen)

In an Eppendorf tube, 4 µg plasmid-DNA was mixed with 750 µl OptiMEM and 20 µl Plus-reagent (mixture a). Meanwhile, 750 µl OptiMEM was mixed with 30 µl OptiMEM (mixture b). Both mixtures were separately incubated for 15 min at room temperature. Afterwards mixture a and mixture b were combined and further incubated for 15 min at room temperature. A 10 cm dish with SH-SY5Y cells at 70-80 % confluency was washed with OptiMEM twice and 5 ml OptiMEM were added. The combined

Lipofectamine/DNA mixture was added to 80% confluent cells and incubated for 3 h at 37°C and 5% CO<sub>2</sub>. Afterwards, 4 ml OptiMEM supplemented with 10% FCS was added. The next day, the transfection medium was removed and 10 ml of growth medium, described in Chapter 7.2.2.1 containing hygromycin B (final concentration 300 µg/ml), was added to the cells to select transfected cells for stable expression. Single colonies (corresponding to single clones with varying expression levels), consisting of 1-7 cells, were selected and transferred to 48 well plates and grown to 100% confluency. Then the cells were transferred to 24 well plates, grown again to 100% confluency. Afterwards the cells were transferred to 6 well plates, grown again to 100% confluency and finally cells were transferred to 10 cm dishes. Within 1-10 passages cells were checked for expression by Western-Blotting. Afterwards total-RNA and proteins were extracted from single clones producing varying or equal amounts of overexpressed C99.

C99WT, C99I45F and C99V50F were overexpressed. The same cell line was mock-transfected (negative control). Overexpressed C99 was intracellularly processed resulting in different amounts of A $\beta$ <sub>42</sub> and A $\beta$ <sub>40</sub> [148, 149]. 9 clones (3 for C99WT, 3 for C99I45F and 3 for C99V50F) with approximately similar expression levels were selected and used for transcriptome analysis and analysis of the phosphorylation status of crucial proteins.

## 7.2.2.4 RNA interference

### 7.2.2.4.1 Transient knockdown by siRNAs

Long, double-stranded RNAs (dsRNAs; typically >200 nt) can be used to silence the expression of target genes in a variety of organisms and cell types (e.g. worms, fruit flies and plants). Upon introduction, the long dsRNAs enter a cellular pathway that is commonly referred to as the RNA interference (RNAi) pathway. Firstly, the dsRNAs get processed into 20-25 nucleotide (nt) *small interfering RNAs (siRNAs)* by an RNase III-like enzyme called Dicer (initiation step)<sup>\*</sup>. Then, the siRNAs assemble into endoribonuclease-containing complexes known as RNA-induced silencing complexes (RISCs), unwinding in the process. The siRNA strands subsequently guide the RISCs to complementary RNA molecules, where they cleave and destroy the cognate RNA (effector step). Cleavage of cognate RNA takes place near the middle of the region bound by the siRNA strand. In mammalian cells, introduction of long dsRNA (>30 nt) initiates a potent antiviral response, exemplified by nonspecific inhibition of protein synthesis and RNA degradation. The mammalian antiviral response can be bypassed, however, by the introduction or expression of siRNAs.

<sup>\*</sup>Alternatively siRNAs can be directly administered to the cells. In this thesis, siRNAs with 21 nucleotides in length were used. This leads to an effective knockdown of target m-RNA while bypassing the mammalian antiviral response (473). Tuschl, T., *Functional genomics: RNA sets the standard*. Nature, 2003. **421**(6920): p. 220-1, 474. Elbashir, S.M., W. Lendeckel, and T. Tuschl, *RNA interference is mediated by 21- and 22-nucleotide RNAs*. Genes Dev, 2001. **15**(2): p. 188-200, 475. Elbashir, S.M., J. Harborth, W. Lendeckel, A. Yalcin, K. Weber, and T. Tuschl, *Duplexes of 21-nucleotide RNAs mediate RNA interference in cultured mammalian cells*. Nature, 2001. **411**(6836): p. 494-8, 476. Fire, A., S. Xu, M.K. Montgomery, S.A. Kostas, S.E. Driver, and C.C. Mello, *Potent and specific genetic interference by double-stranded RNA in *Caenorhabditis elegans**. Nature, 1998. **391**(6669): p. 806-11, 477. Tuschl, T., J.B. Thomson, and F. Eckstein, *RNA cleavage by small catalytic RNAs*. Curr Opin Struct Biol, 1995. **5**(3): p. 296-302, 478. Tuschl, T., P.D. Zamore, R. Lehmann, D.P. Bartel, and P.A. Sharp, *Targeted mRNA degradation by double-stranded RNA in vitro*. Genes Dev, 1999. **13**(24): p. 3191-7, 479. Tuschl, T., *Expanding small RNA interference*. Nat Biotechnol, 2002. **20**(5): p. 446-8.).

Optimizing transfection efficiency is crucial for *maximizing gene silencing* while *minimizing cytotoxicity*.

The following conditions were adjusted (in order of importance):

- Identification of an effective transfection agent for the used cell type
- Amount of transfection agent
- Amount of siRNA
- Cell density at the time of transfection
- Order of transfection (pre-plating cells or plating cells/transfecting in tandem)
- Length of exposure of cells to transfection agent/siRNA complexes

#### 7.2.2.4.2 Transfection of the human neuroblastoma cell line SH-SY5Y with siRNAs

The following three transfection solutions were tested for transfection efficiency of the human neuroblastoma cell line SH-SY5Y:

Transfection solution	Properties
siPORT™ NeoFX™ Transfection Agent (Ambion)	Lipid-based agent that delivers siRNA into mammalian cells with minimal cytotoxicity.
siPORT™ Amine Transfection Agent (Ambion)	Polyamines that deliver siRNA into mammalian cells with minimal cytotoxicity.
Lipofectamin plus (Invitrogen)	Cationic-lipid reagent for transfecting a broad range of cells.

The volumes and the amounts in the following protocol were for transfections in 10 cm plates.

- Cell plating

Approximately 24 h before transfection, cells were plated in normal growth medium so that they were approximately 50% confluent after 24 hours.

The cells were incubated overnight under normal cell culture conditions.

After 24 hours the normal growth medium was substituted with OPTI-MEM I without serum and the cells were incubated for 1-3 hours.

- Preparing siRNA/transfection agent complexes (si PORT Amine)

33 µl of the transfection agent siPORT Amine, was diluted in 517 µl OPTI-MEM I without serum to reach a final volume of 550 µl. The solution was mixed well and incubated at room temperature for 15 minutes.

8.25 µl of 20 µM siRNA (for a final concentration of 30 nM) was diluted in 541.75 OPTI-MEM I to reach a final volume of 550 µl. The solution was incubated for 15 minutes at room temperature.

The diluted siRNA was added to the diluted transfection agent and mixed by gently flicking the tube.

The dilution was incubated for 15 minutes at room temperature.

- Transfecting cells

12650  $\mu$ l OPTI-MEM I was added to the solution containing the transfection agent and the siRNA.

After removing the OPTI-MEM I from the plate containing the cells, the transfection agent/siRNA complex in OPTI-MEM I was added dropwise to the cells.

Without swirling, the dish was gently rocked back and forth to evenly distribute the complexes.

The cells were incubated under normal cell culture conditions for 24 hr.

After 24 h, the medium containing the transfection agent/siRNA complex was substituted with normal growth medium and the cells were incubated for 24 hours.

- Assay for target gene activity 48 h after transfection

The total RNA was extracted from the cells 48 hours after the start of transfection and the knock down of the gene of interest was measured by real-time PCR.

- Protocol for transfection with Lipofectamin Plus (6-well plate):

20  $\mu$ l of Lipofectamin Plus was diluted in 490  $\mu$ l OPTI-MEM I and the solution was incubated at room temperature for 15 minutes.

After adding 1.5  $\mu$ l of siRNA to 98.5  $\mu$ l of OPTI-MEM I, 2.7  $\mu$ l of Plus Reagent were added to the solution and incubated for 15 minutes at room temperature.

The standard protocol was not modified from this step and continues as above.

### **7.2.3 RNA methods**

#### **7.2.3.1 Transcriptome analysis using Affymetrix screening**

##### **7.2.3.1.1 Total RNA preparation from cultured cells**

Total RNA was extracted using the Qiashredder-Kit (Qiagen), RNeasy Midi-columns (Qiagen) and the RNase-free DNase set (Qiagen).

Human neuroblastoma cells (SH-SY5Y) were grown in 10 cm cell culture dishes until they reached 70% confluency. Cells were washed twice with ice-cold PBS. Then cells were lysed with 1.8 ml RLT-buffer per cell culture dish containing  $\beta$ -mercaptoethanol. After 5 min, lysed cells were scraped off and put on Qiashredder columns. The columns were centrifuged for 1 min at room temperature at 13000 rpm in a commonly used table Eppendorf centrifuge. The flow-through was mixed with an equal volume of 70% ethanol and put onto RNeasy Midi-columns. The columns were centrifuged for 5 min at room temperature at 3000-5000g in a swinging-bucket centrifuge. Directly on the columns any remaining DNA was digested by using the RNase-free DNase set (Qiagen) following the manufacturer's instructions. Then 2.5 ml RPE-buffer was put onto the columns. The columns were centrifuged for 2 min at room temperature at 3000-5000g in a swinging-bucket centrifuge. 250 $\mu$ l RNase-free water was put onto the columns in order to elute the total-RNA. After 10 min columns

were centrifuged for 2 min at room temperature at 3000-5000 g in a swinging-bucket centrifuge. The eluted total-RNA was immediately stored at -80°C.

### 7.2.3.1.2 Quantification of RNA

For quantitation the BIO-RAD spectrophotometer SmartSpec™ 3000 was used.

To determine the concentration of total RNA in an aqueous solution, total-RNA was diluted in an appropriate volume of RNase-free water (approximately 1:10, depending on RNA yield). The absorbance of this solution was measured at wavelengths of 260/280 and 320 nm.

To ensure significance, absorbance at 260 nm should be between 0.1 and 0.9. An absorbance of 1 unit at 260 nm corresponds to 40 µg of RNA per ml. This relation is valid for measurements in water only.

$$C_{RNA} = A_{260} \cdot 40 \frac{\mu\text{g}}{\text{ml}} \cdot f_{dil} \quad f_{dil} = \text{dilution factor}$$

RNA samples have to be measured in RNase-free cuvettes, especially if the RNA is to be recovered after spectrophotometry. This can be accomplished by washing cuvettes with RNase-free water. It is crucial to use the same solution (here: water) in which the RNA was diluted to blank the spectrophotometer.

An example for the calculation of RNA yield is shown below:

The total amount of RNA in µg resulting from one extraction, was calculated by multiplying the calculated concentration in µg/ml with the total volume of water in which the sample was initially dissolved.

Volume of extracted total-RNA= 1.6 ml

Dilution = 10 µl of RNA sample + 90 µl RNase-free water (1/10 dilution).

Measured absorbance of diluted sample in a 1 ml cuvette (RNase-free): A<sub>260</sub> = 0.75

Concentration of RNA sample = 40 x A<sub>260</sub> x dilution factor

$$= 40 \times 0.75 \times 10$$

$$= 296 \mu\text{g ml}^{-1}$$

Total yield = concentration x volume of sample in ml

$$= 296 \mu\text{g ml}^{-1} \times 1.6 \text{ ml}$$

$$= 473.6 \mu\text{g RNA}$$

### 7.2.3.1.3 Precipitation of total-RNA

A given volume of total-RNA (corresponding to 20 µg total-RNA) was precipitated by adding 10% (v/v) sodium-acetate (3 M, pH 5.2) and 2.5 times the volume of absolute ethanol. After mixing by finger flicking the precipitate was stored overnight (or at least 1 hour) at -20°C. Then it was centrifuged at 13000 rpm/4°C. The pellet was washed twice with 80% ice cold ethanol. Then the supernatant was carefully removed and the remaining precipitate was air-dried for 15-30 min at room temperature and dissolved in 9 µl of RNase-free water.

### **7.2.3.1.4 Reverse transcription of total RNA into cDNA by oligo (dT) primers**

20 µg of total RNA was used to generate first-strand cDNA by using the Superscript™ Double-Stranded cDNA Synthesis Kit (Invitrogen).

1.5 µl T7-linked oligo(dT)<sub>24</sub> primer (100 µM) was added to 9 µl total-RNA (precipitated from 20 µg total-RNA and dissolved in RNase-free water) and incubated for 10 min at 70°C. Then 4 µl 5x first strand cDNA buffer, 2 µl 0.1 M DTT and 1 µl 10 mM dNTP-mix were added and incubated for 2 min at 45°C. Afterwards, 3 µl Super Script II RT was added and incubated for 1 h at 45°C. Second strand synthesis was performed by adding the following substances and incubated for 2 h at 16°C: 91 µl RNase-free water, 30 µl 5 x second strand cDNA buffer, 3 µl 10 mM dNTP mix, 1 µl E.coli DNA ligase (10 U/µl), 4 µl E.coli DNA polymerase I and 1 µl RNase H (2 U/µl). Then 2 µl T4 polymerase was added and incubated for 5 min at 16°C. The reaction was stopped by adding 10 µl 0.5 M EDTA. Finally, the samples were frozen at -80°C.

### **7.2.3.1.5 Purification of cDNA**

The purification of previously synthesized cDNA was performed using the GeneChip® Sample Clean up Module (Affymetrix) by following the manufacturer's instructions.

### **7.2.3.1.6 In vitro transcription of cDNA into cRNA**

After purification of cDNA, in vitro transcription was performed with biotinylated UTP and CTP using the BioArray™ High Yield™ RNA Labeling Kit (Enzo Life Sciences).

3.3 µl of purified cDNA was mixed with appropriate volumes of reaction buffer, biotin-labeled ribonucleotides, DTT, RNase inhibitor and T7 RNA polymerase in a total volume of 40 µl according to the manufacturer's instructions. This mixture was incubated for 5 h at 37°C and stored at -80°C afterwards.

### **7.2.3.1.7 Purification of cRNA**

The purification of previously in vitro transcribed cRNA was performed using the GeneChip® Sample Clean up Module (Affymetrix) by following the manufacturer's instructions.

### **7.2.3.1.8 Fragmentation of cRNA**

The fragmentation of the cRNA was performed using the GeneChip® Eukaryotic Hybridization Control Kit (Affymetrix).

A given volume of purified cRNA (corresponding to 15 µg of purified cRNA) was mixed with 8 µl 5x fragmentation buffer and filled up with RNase-free water to a total volume of 40 µl. This mixture was incubated for 35 min at 94°C and stored afterwards at -80°C. (To confirm successful fragmentation cRNA could again be checked with the Bioanalyzer 2100™).

### 7.2.3.1.9 Hybridisation of fragmented cRNA onto the arrays

Hybridisation controls (spike controls) and the control oligonucleotide B2 (land mark for the scanner) were added to 15 µg fragmented cRNA. In detail, the following *hybridisation cocktail* was prepared:

40 µl (15 µg) fragmented cRNA, 5.1 µl control oligonucleotide B2 (3nM), 15 µl 20x Eukaryotic Hybridisation Controls, 3 µl herring sperm DNA (10 mg/ml), 3 µl BSA (50 mg/ml), 2x MES hybridisation buffer and 83.9 µl of RNase-free water.

Prior to using whole genome arrays, test arrays were used to check sample quality again. After checking sample quality with the test array, the same cRNA was hybridized to Affymetrix whole genome U-133 A and B oligonucleotide arrays:

The hybridisation cocktail was incubated for 5 min at 99°C followed by an incubation of 5 min at 45°C.

- Pre-incubation:

Meanwhile 240 µl 1x MES hybridisation buffer was filled into the Chip cartridges and the Chips were pre-incubated for 10 min/45°C at 60 rpm in a hybridisation oven (Affymetrix).

- Hybridisation:

Then the 1x MES hybridisation buffer was removed from the Chip cartridges and 240 µl of the incubated hybridisation cocktail was filled into the Chip cartridges. The Chips were incubated for 16 h/45°C at 60 rpm in the hybridisation oven.

### 7.2.3.1.10 Washing and staining of the arrays

Before washing, 240 µl of the hybridisation cocktail, used for hybridisation, was collected and stored at -20°C for eventual reuse. The arrays were then washed by filling the Chip-cartridges with wash buffer A (non-stringent wash buffer). The Chips were put into the Fluidics station (Affymetrix) and were washed according to the manufacturer's instructions:

- wash buffer A: non-stringent wash buffer
- wash buffer B: stringent wash buffer
- SAPE: streptavidin-phycoerythrin

Specification	Conditions
Post Hyb Wash#1	10 cycles of 2 mixes/cycle with wash buffer A at 25°C
Post Hyb Wash#2	8 cycles of 15 mixes/cycle with wash buffer B at 50°C
Staining	Staining of the array for 10 min with SAPE solution at 25°C
Post Stain Wash	10 cycles of 4 mixes/cycle with wash buffer A at 25°C
2nd Staining	Staining of the array for 10 min with a biotinylated anti-streptavidin antibody at 25°C
3rd Staining	Staining of the array for 10 min with SAPE solution at 25°C
Final Wash	15 cycles of 4 mixes/cycle with wash buffer A at 25°C. Holding temperature= 25°C

### **7.2.3.1.11 Scanning of the arrays**

The Chips were scanned twice with a Gene Array Scanner (Hewlett Packard) and the quality of the created dat-file images were evaluated by using the Microarray Suite MAS 5.0 (Affymetrix) and the Gene Operating Software GCOS1.2 (Affymetrix).

### **7.2.3.1.12 Data analysis**

The data analysis was performed with the Microarray Suite MAS 5.0 (Affymetrix) and the Gene Operating Software GCOS1.2 (Affymetrix). Further data analysis was performed with the Micro DB (Affymetrix), Data Mining Tool (Affymetrix), Array Assist 3.3 (Stratagene), Pathway Assist (Stratagene) 3.0, Ingenuity Pathway Analysis (Ingenuity Systems) and the PANTHER Gene and Protein Classification System (Applied Biosystems). Data analysis was performed at the same time by our collaboration partner Carina Itrich with the open source software "Language R" available at [www.r-project.org](http://www.r-project.org). Further information and R-packages are available at [www.bioconductor.org](http://www.bioconductor.org) <sup>10</sup>

## **7.2.3.2 Quantitative real-time PCR**

### **7.2.3.2.1 Preface**

Quantitative real-time PCR can be performed in a one-step reaction (reverse transcription carried out in the same tube as PCR) or in two steps (reverse transcription carried out in a separate reaction). Here I followed a two-step reverse transcription polymerase chain reaction (RT-PCR) protocol. In the first step, total-RNA, extracted from cells, is reverse transcribed into cDNA. In the second step, this cDNA acts as a template for DNA amplification, which is measured with a GeneAmp<sup>®</sup> 5700 Sequence Detection System (real-time PCR cyclers). Pre-designed and labelled primer/probe sets were selected from the Applied Biosystems' Assays-on-Demand<sup>™</sup> product line.

### **7.2.3.2.2 Reverse transcription of total RNA into cDNA by using random hexamer primers**

The High-Capacity cDNA Archive Kit (*Applied Biosystems*) was used for reverse transcription (RT) of total-RNA into single-stranded cDNA.

As a first step, a 2 X RT master mix was prepared using the kit 's components, already thawed on ice.

As a second step, a given volume of a total-RNA sample (10-50 ng) was adjusted with RNase-free water to a volume of 50 µl.

---

<sup>10</sup> Bioconductor is an open source and open development software project for the analysis and comprehension of transcriptomic data.

	Volume (µl)/Reaction
10X Reverse Transcription Buffer	10
25X dNTPs	4
10X random primers	10
MultiScribe™ Reverse Transcriptase, 50 U/µl	5
Nuclease-free H <sub>2</sub> O	21
Total volume of 2 X RT master mix	50
Total volume of total-RNA sample adjusted to 10-50 ng/50 µl	50
Total volume of reaction	100

Finally the following mix was pipetted into a 96-well reaction plate or single Eppendorf tubes:

50 µl of 2 X RT master mix was added to 50 µl of total-RNA sample (adjusted to 10-50 ng/50 µl) to come to a total volume of 100 µl. The sample was pipetted up and down twice to ensure a homogenous mixture.

The samples were incubated for 120 min at 37°C and subsequently held at 4°C using a common thermal cycler (Mastercycler® gradient (Eppendorf)). The obtained cDNA was kept at -20°C for long term storage.

#### **7.2.3.2.3 Real-time detection of amplified cDNA by using an ABI cyclor 5700 and Taqman probes (Applied Biosystems)**

The quantitative real-time PCR assay was performed using the TaqMan® Gene Expression Assays and the TaqMan® Universal PCR Master Mix. The cDNA amplification was measured with a GeneAmp® 5700 Sequence Detection System.

Principle: the special design of TaqMan probes, combined with 5'-3' nuclease activity of the polymerase allows direct detection of PCR products by the release of a fluorescent reporter during the PCR on the ABI PRISM Sequencing Detector.

TaqMan probes consist of an oligonucleotide with a 5'-reporter dye and a downstream, 3'- quencher dye. The fluorescent reporter dye, FAM (6-carboxy-fluorescein) is covalently linked to the 5' end of the oligonucleotide. This reporter is quenched by TAMRA (6-carboxy-tetramethyl-rhodamin), typically located at the 3' end. During PCR, if the target of interest is present, the probe specifically anneals between the forward and reverse primer sites. The nucleolytic activity of the polymerase only cleaves the probe between the reporter and the quencher if this region hybridizes to the target. This cleavage between the reporter and the quencher dyes results in an increase of fluorescence of the reporter that is proportional to the amount of product accumulated. This process is described in Figure 7.1

The fluorescence signal in each reaction is *measured in real time at each cycle* of the PCR by the ABI 5700 instrument. Laser light passes through optical fibres to excite the fluorochromes in the samples. Emitted fluorescence passes back through the optical fibres and is directed to a spectrograph attached to a CCD camera. Fluorescence detection between 500 and 660 nm is possible. The ABI 5700 can simultaneously measure more than one fluorescence wavelength per well. This means that endogenous controls can be run either as parallel reactions in separate wells (singleplex<sup>11</sup> PCR) or within the same well as the sample (multiplex<sup>12</sup> PCR). Here singleplex PCR was performed.

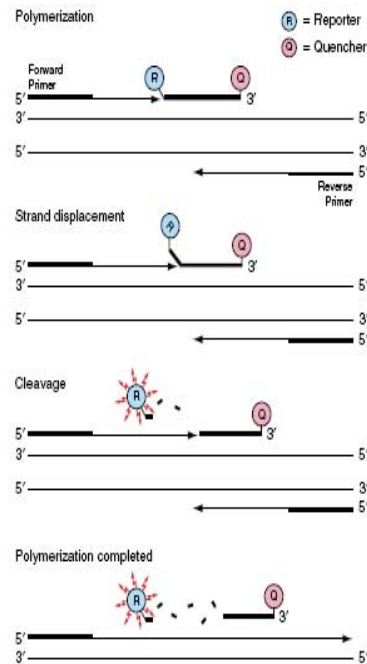


**Figure 7.1 Polymerisation-associated, 5' to 3' nuclease activity of AmpliTaq Gold DNA Polymerase during PCR.** (Figure taken from Applied Biosystems)

When the probe is intact, the proximity of the reporter dye to the quencher dye results in suppression of the reporter fluorescence primarily by Förster-type energy transfer (Förster, 1948; Lakowicz, 1983). During PCR, if the target of interest is present, the probe specifically anneals between the forward and reverse primer sites. The 5' to 3' nucleolytic activity of the AmpliTaq Gold enzyme cleaves the probe between the reporter and the quencher only if the probe hybridizes to the target. The probe fragments are then displaced from the target, and polymerization of the strand continues. The 3' end of the probe is blocked to prevent extension of the probe during PCR. This process occurs in every cycle and does not interfere with the exponential accumulation of product. Analysis of the digitized fluorescence intensity signal is done by the Sequence Detector software (Applied Biosystems). The reporter signal is plotted against the cycle number. The threshold cycle ( $c_T$ ) is the PCR cycle at which a significant increase in reporter fluorescence above baseline can be detected.

<sup>11</sup> Singleplex PCR: one primer pair is used for the reaction

<sup>12</sup> Multiplex PCR: more than one primer pair are used for the reaction

Method: The reaction was carried out in 96 well plates from Applied Biosystems.

<b>TaqMan Universal PCR Master Mix (2 x)</b>	<b>12.5 µl</b>
Assays-on-Demand™ Gene Expression Assay Mix (20x) (containing forward and reverse primers and labelled probe)	1.25 µl
RNase-free water	1.25 µl
Total volume of master mix	15 µl
Total volume of cDNA (corresponding to 10ng-100ng)	10 µl
Total volume of reaction	25 µl/well

For one well, 12.5 µl of TaqMan Universal PCR Master Mix (2 x), 1.25 µl of 20 x Assays-on-Demand™ Gene Expression Assay Mix (containing forward and reverse primers and labelled probe) and 1.25 µl RNase-free water were mixed. A total volume of 15 µl of this premix, already prepared in batch for multiple wells, was distributed in each well together with 10 µl of cDNA sample (10ng-100ng final amount) as template. Three control-wells, containing just the premix with primers and Taq Man probe but without template, were added to each plate to detect any possible contamination with non specific DNA (NTC, No-Template-Control). Amplification of an endogenous control was performed to standardize the amount of sample DNA added to the reaction. For the quantification of gene expression, cyclophilin A was used as this endogenous control. Three replicates of each sample and endogenous control were amplified.

*Relative quantification* with data from the ABI PRISM® 5700 Sequence Detection System was performed with the comparative method (the  $2^{-\Delta\Delta C_T}$  Method ).

This method is a convenient way to analyze the relative changes in gene expression from real-time quantitative PCR experiments. *For the  $\Delta\Delta C_T$  calculation to be valid, the amplification efficiencies of the target (gene of interest) and reference (in all samples equally expressed gene) must be approximately equal.* A sensitive method for assessing if two amplicons have the same efficiency is to look at how  $\Delta C_T$  varies with the template dilution. Therefore, standard curves were established for calculating the efficiency of amplification.

The  $\Delta C_T$  value is determined by subtracting the average  $C_T$  value of the endogenous control from the average  $C_T$  value of the gene of interest. The same is done for a so-called calibrator (this is for instance a user-defined baseline experiment).

$$\Delta C_{T1} = C_T \text{ gene of interest} - C_T \text{ endogenous control (calibrator=baseline experiment)}$$

$$\Delta C_{T2} = C_T \text{ gene of interest} - C_T \text{ endogenous control}$$

The *fold change* of gene expression is:

$$2^{-(\Delta C_{T2} - \Delta C_{T1})}$$

*This is the amount of target, normalized to an endogenous reference and relative to a calibrator.*

### 7.2.3.3 RNA interference (siRNAs)

Refer to Chapter 7.2.2.4, RNA interference.

## 7.2.4 Quality control of cells, total-RNA, cRNA and Chips®

### 7.2.4.1 Screening of cells for mycoplasma contamination

Each sample was screened and found to be free from mycoplasma contamination. The Mycoplasma Detection Kit (Roche) was used according to the manufacturer's recommendations. This is an enzyme immunoassay for the detection of mycoplasmas/acholeplasmas in cell culture (*M. arginini*, *M. hyorhinitis*, *M. orale*, *A. laidlawii*).

### 7.2.4.2 Assessment of RNA purity by measuring the 260 nm/280 nm ratio

The ratio of the measurements at 260 nm and 280 nm ( $A_{260}/A_{280}$ ) provides an estimate of the purity of RNA with respect to contaminants that absorb in the UV-range, such as proteins and phenol. Pure RNA has an  $A_{260}/A_{280}$  ratio of 1.9–2.1. If there is contamination with protein or phenol, the  $A_{260}/A_{280}$  will be significantly less than the values given above, and accurate quantification of the RNA will not be possible. A more exact ratio is gained by subtracting a previously measured background wavelength at 320 nm from the numerical values of  $A_{260}$  and  $A_{280}$ .

The resulting formula for the ratio is:

$$Ratio = \frac{A_{260} - Bg_{320}}{A_{280} - Bg_{320}}$$

Absorption at 280 nm is caused by aromatic amino acids, mainly by tryptophane and less strongly by tyrosine and phenylalanine, depending on their absorption maximum. Absorption at 260 nm is caused by nucleic acids. A 260 nm/280 nm ratio < 1.8 is caused by increased amounts of proteins in the sample. A 260 nm/280 nm ratio of 1.9-2.1 for Chip experiments and 1.8-2.1 for quantitative real-time PCR was accepted.

### 7.2.4.3 Agarose gel electrophoresis

Total-RNA, unfragmented cRNA and fragmented cRNA were checked on 1% agarose gels. For total-RNA two distinct bands (28s and 18s ribosomal RNA) were expected. The 28 s band should be approximately twice as strong as the 18 s band. For unfragmented cRNA a smear of bands, representing the different mRNAs, was expected with an accumulation in the centre of the smear. For fragmented cRNA bands corresponding to a size of 35-200 bases were expected.

#### 7.2.4.4 Checking quality of unfragmented cRNA with the Bioanalyzer 2100 (Agilent)

As described in Chapter 7.2.4.5 the quality of cRNA was checked using RNA Nano Chips. The quality of cRNA was evaluated by the distribution of the cRNAs which should result in a characteristic shape of the curve generated by the Bioanalyzer 2100™. If the quality was evaluated to be good, 15 µg of purified cRNA was used for fragmentation.

#### 7.2.4.5 Assessment of RNA integrity with the Bioanalyzer 2100 (Agilent)

Principle: The integrity of RNA samples is essential in the context of gene expression analysis via microarray technology or real-time PCR. Agilent provides RNA assays that enable rapid characterization of total or mRNA or cRNA samples, with unmatched sensitivity and with *minimal sample consumption*.

The quantitative range for total RNA Assay is 25-500 ng/µl, while the qualitative range is 5-500 ng/µl. The Agilent 2100 Bioanalyzer is the most successful micro fluidics-based platform for the analysis of RNA, DNA and proteins.

The system uses micro-fabrication technology to transfer laboratory processes onto miniature glass chips that contain a network of interconnected channels and reservoirs. Filling the channels with a gel matrix and the wells with buffer or sample allows electrophoresis to be carried out on a miniaturized scale. Choosing the appropriate LabChip kit (containing chips, buffer, gel, intercalating dye and standards) enables the analysis of RNA, DNA or protein samples.

The electropherogram of the sample well window for total RNA (eukaryotic) consists of 2 ribosomal peaks, the 28S and 18S and one marker peak. If the total RNA is undamaged the ratio of 28S: 18S RNA is close to the theoretical maximum of 2.5. The respective ribosomal bands should appear as sharp bands. 28S ribosomal RNA bands should be present with an intensity approximately twice that of the 18S RNA band. If the ribosomal bands in a given lane are not sharp, but appear as a smear of smaller sized RNAs, it is likely that the RNA sample suffered major degradation during preparation.

Method:

The first step in performing the RNA 6000 Nano assay consisted of centrifuging 550 µl of RNA 6000 Nano gel matrix in a spin filter at 1500 g ± 20% for 10 minutes.

65 µl of this filtered gel was mixed with 1 µl of the RNA 6000 Nano dye concentrate, already equilibrated to room temperature for 30 min and spinned down.

The solution was well vortexed and spun down at 13000 g for 10 min at room temperature. A new RNA Nano chip was placed on a device for filling the Nano chip with the samples (Chip Priming Station) and the gel-dye mix, the RNA 6000 Nano Marker, the Ladder and the samples were pipetted into the wells, following the instructions of the RNA 6000 Nano Assay Protocol.

### **7.2.4.6 Assessment of Gene Chip<sup>®</sup> quality, hybridisation efficiency and RNA quality by certain parameters**

After scanning, array images were assessed by several parameters giving information about Chip quality, hybridisation efficiency and RNA quality:

- Array images were assessed by eye to confirm the absence of bubbles or scratches.
- Scaling factors
- Background
- Noise
- Number of present transcripts
- 3'/5' ratios for GAPDH and beta-actin
- Bio spike controls

## **7.2.5 Protein methods**

### **7.2.5.1 Protein expression in mammalian cells**

Human neuroblastoma cells (SH-SY5Y) were transfected as described and C99WT, C99I45F and C99V50F were overexpressed. The same cell line was mock-transfected (negative control). Overexpressed C99 was intracellularly processed resulting in different amounts of A $\beta$ <sub>42</sub> and A $\beta$ <sub>40</sub> [148, 149].

### **7.2.5.2 Whole cell protein extraction from mammalian cells**

#### **7.2.5.2.1 Extraction of non-phosphorylated proteins**

- Cell lysis buffer:
  - 50 mM Tris-HCl pH 7.5
  - 150 mM NaCl
  - 5 mM EDTA
  - 1% Triton X
  - 1% NP40
  - 1x Complete<sup>®</sup> protease inhibitor (freshly added before use)
  - 1 X PBS
  - 4 X SDS sample buffer

To minimize protein degradation, all steps were carried out on ice. For protein extraction from cell cultures, cells were washed once with ice-cold PBS and after adding 1 ml of PBS, cells were scraped off, transferred into a 1 ml Eppendorf tube, and centrifuged at 300 g, at 4°C, for 5 min. The supernatant was removed and 200 µl of lysis buffer, containing 1x (prepared from a 25x stock solution) protease inhibitor was added to the pellet. After incubating for 20 minutes on ice, the solution was further centrifuged at 13000 rpm, at 4°C, for 10 minutes and the supernatant was stored at -80°C for later use or immediately denatured with the appropriate volume of 4xSDS sample buffer. For analyzing proteins by SDS-PAGE, the lysates were boiled for 10 min in 4xSDS sample buffer and loaded on a SDS-polyacrylamide gel.

### 7.2.5.2.2 Extraction of phosphorylated proteins

- Screening of phosphorylated proteins using the Kinexus-screening service™:

Kinexus offers different kinds of screenings for the detection of phosphorylated proteins by SDS-PAGE. Here the Kinetworks™ Biosource Phospho-Site Neurobiology Screen (KPSS-9.0) and the KCPS-1.0 Custom Screen were used. All antibodies used for these screens were intensively tested for specificity by Kinexus.

The human neuroblastoma cell line SH-SY5Y, transfected with C99-spA4CT WT, C99-spA4CT I45F or C99-spA4CT V50F was grown to 70% confluency. Protein was extracted by lysing the cell pellet, derived from three 10 cm dishes in 250 µl of the following buffer:

20 mM MOPS, pH 7.0

2 mM EGTA

5 mM EDTA

Phosphatase inhibitor cocktail II (Calbiochem), according to the manufacturer's instructions

20 mM sodium pyrophosphate

40 mM β-glycerophosphate, pH 7.2

Complete® Protease Inhibitor Mix (Roche) (1x final concentration from a 25x stock solution)

0.5% NonidetP-40

This solution was sonicated on ice for 15 seconds followed by a break of 45 seconds, sonicated again for 15 seconds and stored on ice afterwards for 20 min. Then this lysate was ultracentrifuged at 120 000 g for 30 min at 4°C. The protein concentration of the supernatant was determined using the BCA-test described elsewhere. 500 µg of protein was added to 125 µl 4x SDS-PAGE sample buffer and filled up with double-distilled water to a total volume of 500 µl. This sample was sent to Kinexus for screening of the phosphorylation status of important proteins involved in signaling processes. After approximately 4 weeks the results were provided from Kinexus as TIFF-files of the scanned Western-blots and the normalized phosphorylation status was delivered as Microsoft Excel spreadsheets. Further data analysis was performed using a student's t-test.

### 7.2.5.3 Determination of protein concentrations

Protein concentrations were measured using an ELISA-reader (microplate-reader 450, BIO-RAD) or the BIO-RAD spectrophotometer SmartSpec™ 3000 according to the BCA (Bicinchoninic acid) method. In an alkaline solution, proteins reduce Copper-ions to  $\text{Cu}^{1+}$ -ions which form a violet complex with BCA. The absorption maximum of this complex is at 562 nm.

BCA, working solution: 1 ml  $\text{CuSO}_4 \cdot 5 \text{H}_2\text{O}$  + 39 ml BCA (Sigma)(1:40 dilution)

BSA standard solutions (0, 0.1, 0.2, 0.3, 0.4, 0.5, 0.6, 0.7, 0.8, 0.9, 1.0 mg/ml)

ELISA 96-well plate (Greiner)

The proteins were diluted approximately 1:10 (dependent on protein yield) with 1 X PBS.

20  $\mu\text{l}$  of each diluted protein sample were placed in each well and 200  $\mu\text{l}$  of BCA working solution was added. 20  $\mu\text{l}$  of standard (BSA), gradual concentrations (as above), were added into each well, together with 200  $\mu\text{l}$  of BCA working solution. The plate was covered with aluminium and kept for 15 minutes at 37°C and subsequently 15 minutes at room temperature on a horizontal shaker. Absorption was measured with a microplate-reader (model 450, BIO-RAD) at 550 nm. Protein concentrations were calculated with the BSA standard curve.

### 7.2.5.4 SDS Polyacrylamide Gel Electrophoresis (SDS-PAGE)

- 4 X loading buffer for SDS-PAGE:
  - 250 mM Tris/HCl pH 6.8
  - 8% SDS
  - 30% Glycerol
  - 0.02% Bromophenol blue

Prior to use, 5%  $\beta$ -mercaptoethanol was added

- 10 X SDS-Running Buffer
  - 1.92 M Glycine
  - 0.25 M Tris-base
  - 1% (w/v) SDS
- Separating gel: 10 ml (12% Polyacrylamide):
  - 4 ml 30% Acrylamide + 0,8 ml Bisacrylamide
  - 2.5 ml 1,5 M Tris, pH 8,8
  - 0.1 ml 10% SDS
  - 0.1 ml 10% APS
  - 0.004 ml TEMED
  - 3.3 ml double-distilled  $\text{H}_2\text{O}$

- Stacking gel: 3 ml (5% Acrylamide)
  - 0.5 ml 30% Acrylamide + 0,8 ml Bisacrylamide
  - 0.38 ml 1 M Tris, pH 6,8
  - 0.03 ml 10% SDS
  - 0.03 ml 10% APS
  - 0.003 ml TEMED
  - 2.1 ml double-distilled H<sub>2</sub>O

SDS binds to hydrophobic regions of the proteins so that they become negatively charged and migrate to the anode. As the amount of SDS bound is proportional to the molecular weight of the proteins, the SDS-polypeptide complex moves in the gel according to the size of the proteins.

Pre-cut glass plates were assembled with Teflon spacers (1mm) and a silicon tube and used for casting the gel. After pouring the separating gel, a thin layer of isopropanol was added on top. As soon as the separating gel was polymerized (approximately 1 h) the isopropanol was removed, the stacking gel was poured and a comb was positioned in the polymerising stacking gel. After polymerisation was finished, protein samples were loaded (after boiling for 10 min in 4 X loading buffer) and electrophoresis was performed in 1 x running buffer for approximately 2 hours at 160 V.

### 7.2.5.5 Western blotting

#### Transfer of proteins onto nitrocellulose membranes and their immunological detection

Western blotting was used to identify a protein of interest by its size in a protein extract.

Proteins are separated by SDS-PAGE and electrophoretically transferred from the gel to a nitrocellulose membrane. Specific antibodies can detect the immobilized proteins on the membrane.

- Western Blot Transfer (Wet Blot)
  - Transferbuffer (Western blot) pH 8.4:
    - 20 mM Tris-base
    - 200 mM Glycine
    - 20% Methanol
    - ad 3000 ml H<sub>2</sub>O

After separating the proteins by SDS-PAGE the separating gel was equilibrated in transfer buffer for 5 min. Whatman sheets and a nitrocellulose membrane were cut to the size of the gel and soaked for 5 min in transfer buffer. The gel and the membrane were sandwiched between soaked pieces of sponge pads, Whatman paper, and perforated plastic plates as follows:

- Anode (+)
- Sponge pad
- 2 Whatman sheets
- Nitrocellulose
- SDS gel
- 2 Whatman sheets
- Sponge pad
- Cathode (-)

The proteins were blotted at approximately  $1\text{mA}/\text{cm}^2$

The transfer was performed in a blotting tank (Bio-Rad) for 3 hours at 400 mA, 280 V, at  $4^\circ\text{C}$ .

- Staining of immobilized proteins with Ponceau S

Ponceau S-solution:

0.2% (w/v) Ponceau-S red

3% (w/v) sulfonic acid

0.1% (w/v) glacial acid

Proteins immobilized on a membrane can be reverse stained with Ponceau S-dye to evaluate the efficiency of protein transfer after Western blotting.

The nitrocellulose membrane was incubated in Ponceau S-solution on a horizontal shaker for 5 min. The stained solution was recovered, and unspecifically bound dye was removed with dd  $\text{H}_2\text{O}$ . The efficiency of protein transfer was evaluated and subsequently the membrane staining was removed by incubation with 1 x PBS.

- Immunological detection of blotted proteins

1 x TBST:

100 mM Tris/HCl

1.5 M NaCl

0.5% Tween 20

pH 7.4

ECL-kit (Amersham)

After Western Blot transfer of proteins to the nitrocellulose membrane, the membrane was blocked for 1 h in 5% (w/v) skim-milk in 1 x TBST to prevent unspecific binding of antibodies. The primary antibody was diluted in 5% (w/v) skim-milk in 1 x TBST to a suitable concentration. The membrane

was incubated with the primary antibody either for 2-4 h at room temperature or overnight at 4°C. To remove all the traces of unspecifically bound primary antibodies the membrane was washed twice with 1 x TBST, and further incubated twice in 1 x TBST for 10 min. Incubation of the membrane with the secondary antibody conjugated to horseradish peroxidase (HRP, dilution 1:2000-10000 in TBS) was carried out for 1h at room temperature. The membrane was again washed twice with 1 x TBST, and further incubated three times in 1 x TBST for 5 min.

The protein of interest was detected by enhanced chemical luminescence (ECL) utilizing the reaction of luminol and H<sub>2</sub>O<sub>2</sub>, which is catalyzed by HRP. For this purpose, the membrane was incubated with the ECL (Amersham) reagent for exactly 1 min and the chemifluorescent signal was immediately visualized by exposure to Hyperfilm ECL films (Amersham).

- Stripping and re-probing of Western Blot membranes

Stripping buffer:

62.5 mM Tris/HCl pH 6.7

100 mM β-Mercaptoethanol

2% SDS

For reprobing the membrane with different antibodies, the previously applied antibodies first had to be removed. For this purpose, stripping buffer was preheated to 80°C. The membrane was incubated with 100-200 ml preheated stripping buffer on a horizontal shaker until room temperature was reached (30-45 min). The membrane was further incubated several times (3-5 times) with 1 x TBST, until hardly any residual β-Mercaptoethanol could be detected by smelling.

The membrane was again blocked in 5% (w/v) skim-milk in 1 x TBST for 1 h, and a new primary antibody could be applied as described.

Normalisation and relative quantification of proteins:

For normalisation of loaded protein amounts, blotted membranes were stripped as described and re-probed with an anti-β-actin antibody (Abcam), diluted according to the manufacturer's instructions. The obtained bands on Hyperfilm ECL films (Amersham) were quantified by densitometry using the Image Gauge software.

### 7.2.5.6 Immunoprecipitation

- Washing buffer A: 10 mM Tris/HCl pH 7.5, 150 mM NaCl, 2 mM EDTA, 0.2% NP40
- Washing buffer B: Like washing buffer A, but with 500 mM NaCl instead
- Washing buffer C: 10 mM Tris/HCl pH 7.5
- Protein A sepharose (Amersham)
- Protein G sepharose (Sigma)

Proteins secreted into the medium or extracted from cell lysates were precipitated with appropriate antibodies and 30  $\mu$ l Protein A sepharose (for polyclonal antibodies) or Protein G sepharose (for monoclonal antibodies). Protein samples were cleared from cell debris by centrifugation at 15.000 x g for 10 min. Samples were pre-incubated for 1 h at 4°C with 10  $\mu$ l of Protein A or G- sepharose to reduce unspecific binding. Equally, antibodies were prebound to 30  $\mu$ l of Protein A or G- sepharose in 500  $\mu$ l Washing buffer A by incubating on an overhead shaker for 1 h at room temperature. The sepharose beads were sedimented at 15.000 x g for 30 s and the supernatant was transferred to the prebound antibody beads. The samples were incubated for 2-3 h at room temperature or overnight at 4°C. The sepharose beads were centrifuged at 5000 x g for 30 s, washed three times with Washing buffer A. In case of unspecific binding, additional washing steps with Washing buffer B and C were performed. The buffer was completely removed with a Hamilton syringe and the proteins attached to the sepharose beads were denatured in 2x SDS sample buffer for 10 min at 70°C. The samples were further analyzed by SDS-PAGE and Western blotting.

### 7.2.6 Differentiation of human neuroblastoma cells by retinoic acid

A 0.5 M stock solution of all-trans retinoic acid (RA, Sigma R2625) was prepared by dissolving 1 g RA in 6.66 ml DMSO. A further stock solution was prepared by diluting the 0.5 M stock solution 1:1000 in DMSO. To reach final concentrations of 0.1-1000 nM, this stock solution was further diluted in appropriate volumes of cell culture medium in absence or presence of serum. The human neuroblastoma cell line SH-SY5Y was treated with 0.1 nM-10  $\mu$ M RA in cell culture medium, mentioned in Chapter 7.1.15, in absence or presence of serum for 2-9 days. All preparation steps of RA and cell culture experiments were performed in dim light due to light-sensitiveness of RA. Differentiation of cells was checked by light microscopy at appropriate times.

## 7.2.7 Immunocytochemistry

### 7.2.7.1 Immunostaining of cultured cells

- Preparation of coverslips:

PLL, 20 µg/ml (Sigma)

Collagen (Sigma, C7661)

Neuroclean<sup>®</sup> Coverslips (Primeglass, Neuherberg, Germany), were distributed in a 24 well plate, covered with PLL or collagen for several hours. PLL or collagen was removed and the coverslips were air-dried for approximately 30 min. Afterwards human neuroblastoma cells were plated.

- Immunostaining

Mowiol: 2.4 g Mowiol 4-88 (Sigma)

6 ml Glycerol (Sigma)

6 ml double-distilled H<sub>2</sub>O

12 ml 0.2 M Tris-HCl pH 8.5

Mowiol was incubated for 10 min at 50°C, centrifuged for 15 min at 5000 rpm in a commonly used Eppendorf centrifuge, the supernatant was collected in fresh tubes and stored at -20°C. Once defrosted, it was stable for at least one month.

4% PFA in PBS

1 x PBS

For immunocytochemistry, cells were grown on (PLL or collagen coated) coverslips in 24 well plates and fixed with 4% Paraformaldehyde in 1x PBS for 5 min. Cells were permeabilized in 1x PBS + 0.1 % NP40 for 10 min and blocked with 5% normal goat serum in 1 x PBS for 1 h. Primary antibodies were diluted in 1 x PBS + 5% goat serum (1:50-1:1000). Each coverslip was placed upside down on approximately 50 µl antibody solution and incubated at 4°C over night. The next day, cells were incubated with the appropriate secondary antibodies coupled with Alexa 488 and Alexa 594 fluorescent dyes (Molecular probes) for 0.5-1 h at room temperature and mounted with Mowiol. Embedded cells were stored, protected from light, until examination under a deconvolution fluorescence microscope.

### **7.2.7.2 Immunofluorescence microscopy**

Pictures were taken using the deconvolution microscope Leica DMRXA, equipped with suitable software (Openlab). Omission of primary antibodies was used as a control to verify specificity (expected to show only very low background staining). Embedded cells were examined with a Leica deconvolution microscope by using 10x, 40x and 100x objectives.

### **7.2.8 Light microscopy**

For checking differentiation after RA treatment, cells were cultured in a 24-well plate, treated with RA, as described, and pictures were taken of the living human neuroblastoma cell line SH-SY5Y. An inverse photo-microscope, the Zeiss Axiovert 35 was used, equipped with an Olympus DP50 digital colour camera. Pictures were taken using a 20x objective. Afterwards cells were incubated at 37°C to induce further differentiation.

## 8 References

1. Alzheimer, A., *Über eine eigenartige Erkrankung der Hirnrinde*, Allg. Z. Psychiatrie Psychisch-Gerichtl. Med., 1907, **64**,: p. 146-148.
2. Cummings, J.L., *Alzheimer's disease*. N Engl J Med, 2004. **351**(1): p. 56-67.
3. Kang, J., H.G. Lemaire, A. Unterbeck, J.M. Salbaum, C.L. Masters, K.H. Grzeschik, G. Multhaup, K. Beyreuther, and B. Muller-Hill, *The precursor of Alzheimer's disease amyloid A4 protein resembles a cell-surface receptor*. Nature, 1987. **325**(6106): p. 733-6.
4. McLaurin, J., T. Franklin, A. Chakrabarty, and P.E. Fraser, *Phosphatidylinositol and inositol involvement in Alzheimer amyloid-beta fibril growth and arrest*. J Mol Biol, 1998. **278**(1): p. 183-94.
5. Bertram, L. and R.E. Tanzi, *Of replications and refutations: the status of Alzheimer's disease genetic research*. Curr Neurol Neurosci Rep, 2001. **1**(5): p. 442-50.
6. Tanzi, R.E., *A genetic dichotomy model for the inheritance of Alzheimer's disease and common age-related disorders*. J Clin Invest, 1999. **104**(9): p. 1175-9.
7. Bertram, L., M.B. McQueen, K. Mullin, D. Blacker, and R.E. Tanzi, *Systematic meta-analyses of Alzheimer disease genetic association studies: the AlzGene database*. Nat Genet, 2007. **39**(1): p. 17-23.
8. Saunders, A.M., W.J. Strittmatter, D. Schmechel, P.H. George-Hyslop, M.A. Pericak-Vance, S.H. Joo, B.L. Rosi, J.F. Gusella, D.R. Crapper-MacLachlan, M.J. Alberts, and et al., *Association of apolipoprotein E allele epsilon 4 with late-onset familial and sporadic Alzheimer's disease*. Neurology, 1993. **43**(8): p. 1467-72.
9. Farrer, L.A., L.A. Cupples, J.L. Haines, B. Hyman, W.A. Kukull, R. Mayeux, R.H. Myers, M.A. Pericak-Vance, N. Risch, and C.M. van Duijn, *Effects of age, sex, and ethnicity on the association between apolipoprotein E genotype and Alzheimer disease. A meta-analysis. APOE and Alzheimer Disease Meta Analysis Consortium*. Jama, 1997. **278**(16): p. 1349-56.
10. Merdes, G., P. Soba, A. Loewer, M.V. Bilic, K. Beyreuther, and R. Paro, *Interference of human and Drosophila APP and APP-like proteins with PNS development in Drosophila*. Embo J, 2004. **23**(20): p. 4082-95.
11. Soba, P., S. Eggert, K. Wagner, H. Zentgraf, K. Siehl, S. Kreger, A. Lower, A. Langer, G. Merdes, R. Paro, C.L. Masters, U. Muller, S. Kins, and K. Beyreuther, *Homo- and heterodimerization of APP family members promotes intercellular adhesion*. Embo J, 2005. **24**(20): p. 3624-34.
12. Sergeant, N., J.P. David, D. Champain, A. Ghestem, A. Watzet, and A. Delacourte, *Progressive decrease of amyloid precursor protein carboxy terminal fragments (APP-CTFs), associated with tau pathology stages, in Alzheimer's disease*. J Neurochem, 2002. **81**(4): p. 663-72.
13. Nunan, J., M.S. Shearman, F. Checler, R. Cappai, G. Evin, K. Beyreuther, C.L. Masters, and D.H. Small, *The C-terminal fragment of the Alzheimer's disease amyloid protein precursor is degraded by a proteasome-dependent mechanism distinct from gamma-secretase*. Eur J Biochem, 2001. **268**(20): p. 5329-36.

14. Cao, X. and T.C. Sudhof, *Dissection of amyloid-beta precursor protein-dependent transcriptional transactivation*. J Biol Chem, 2004. **279**(23): p. 24601-11.
15. Haass, C., M.G. Schlossmacher, A.Y. Hung, C. Vigo-Pelfrey, A. Mellon, B.L. Ostaszewski, I. Lieberburg, E.H. Koo, D. Schenk, D.B. Teplow, and et al., *Amyloid beta-peptide is produced by cultured cells during normal metabolism*. Nature, 1992. **359**(6393): p. 322-5.
16. Shoji, M., T.E. Golde, J. Ghiso, T.T. Cheung, S. Estus, L.M. Shaffer, X.D. Cai, D.M. McKay, R. Tintner, B. Frangione, and et al., *Production of the Alzheimer amyloid beta protein by normal proteolytic processing*. Science, 1992. **258**(5079): p. 126-9.
17. Seubert, P., C. Vigo-Pelfrey, F. Esch, M. Lee, H. Dovey, D. Davis, S. Sinha, M. Schlossmacher, J. Whaley, C. Swindlehurst, and et al., *Isolation and quantification of soluble Alzheimer's beta-peptide from biological fluids*. Nature, 1992. **359**(6393): p. 325-7.
18. Motter, R., C. Vigo-Pelfrey, D. Kholodenko, R. Barbour, K. Johnson-Wood, D. Galasko, L. Chang, B. Miller, C. Clark, R. Green, and et al., *Reduction of beta-amyloid peptide<sub>42</sub> in the cerebrospinal fluid of patients with Alzheimer's disease*. Ann Neurol, 1995. **38**(4): p. 643-8.
19. Jarrett, J.T., E.P. Berger, and P.T. Lansbury, Jr., *The carboxy terminus of the beta amyloid protein is critical for the seeding of amyloid formation: implications for the pathogenesis of Alzheimer's disease*. Biochemistry, 1993. **32**(18): p. 4693-7.
20. Schmechel, D.E., A.M. Saunders, W.J. Strittmatter, B.J. Crain, C.M. Hulette, S.H. Joo, M.A. Pericak-Vance, D. Goldgaber, and A.D. Roses, *Increased amyloid beta-peptide deposition in cerebral cortex as a consequence of apolipoprotein E genotype in late-onset Alzheimer disease*. Proc Natl Acad Sci U S A, 1993. **90**(20): p. 9649-53.
21. Bergem, A.L., K. Engedal, and E. Kringlen, *The role of heredity in late-onset Alzheimer disease and vascular dementia. A twin study*. Arch Gen Psychiatry, 1997. **54**(3): p. 264-70.
22. Levy, E., M.D. Carman, I.J. Fernandez-Madrid, M.D. Power, I. Lieberburg, S.G. van Duinen, G.T. Bots, W. Luyendijk, and B. Frangione, *Mutation of the Alzheimer's disease amyloid gene in hereditary cerebral hemorrhage, Dutch type*. Science, 1990. **248**(4959): p. 1124-6.
23. Van Broeckhoven, C., J. Haan, E. Bakker, J.A. Hardy, W. Van Hul, A. Wehnert, M. Vegter-Van der Vlis, and R.A. Roos, *Amyloid beta protein precursor gene and hereditary cerebral hemorrhage with amyloidosis (Dutch)*. Science, 1990. **248**(4959): p. 1120-2.
24. Coria, F., E. Castano, F. Prelli, M. Larrondo-Lillo, S. van Duinen, M.L. Shelanski, and B. Frangione, *Isolation and characterization of amyloid P component from Alzheimer's disease and other types of cerebral amyloidosis*. Lab Invest, 1988. **58**(4): p. 454-8.
25. Namba, Y., M. Tomonaga, H. Kawasaki, E. Otomo, and K. Ikeda, *Apolipoprotein E immunoreactivity in cerebral amyloid deposits and neurofibrillary tangles in Alzheimer's disease and kuru plaque amyloid in Creutzfeldt-Jakob disease*. Brain Res, 1991. **541**(1): p. 163-6.
26. McGeer, P.L., T. Kawamata, and D.G. Walker, *Distribution of clusterin in Alzheimer brain tissue*. Brain Res, 1992. **579**(2): p. 337-41.
27. Snow, A.D., J. Willmer, and R. Kisilevsky, *Sulfated glycosaminoglycans: a common constituent of all amyloids?* Lab Invest, 1987. **56**(1): p. 120-3.
28. Bernstein, H.G., S. Bruszis, D. Schmidt, B. Wiederanders, and A. Dorn, *Immunodetection of*

- cathepsin D in neuritic plaques found in brains of patients with dementia of Alzheimer type.* J Hirnforsch, 1989. **30**(5): p. 613-8.
29. Bernstein, H.G., H. Kirschke, B. Wiederanders, D. Schmidt, and A. Rinne, *Antigenic expression of cathepsin B in aged human brain.* Brain Res Bull, 1990. **24**(4): p. 543-9.
30. Abraham, C.R., D.J. Selkoe, and H. Potter, *Immunochemical identification of the serine protease inhibitor alpha 1-antichymotrypsin in the brain amyloid deposits of Alzheimer's disease.* Cell, 1988. **52**(4): p. 487-501.
31. Gollin, P.A., R.N. Kalaria, P. Eikelenboom, A. Rozemuller, and G. Perry, *Alpha 1-antitrypsin and alpha 1-antichymotrypsin are in the lesions of Alzheimer's disease.* Neuroreport, 1992. **3**(2): p. 201-3.
32. Rebeck, G.W., S.D. Harr, D.K. Strickland, and B.T. Hyman, *Multiple, diverse senile plaque-associated proteins are ligands of an apolipoprotein E receptor, the alpha 2-macroglobulin receptor/low-density-lipoprotein receptor-related protein.* Ann Neurol, 1995. **37**(2): p. 211-7.
33. Van Gool, D., B. De Strooper, F. Van Leuven, E. Triaux, and R. Dom, *alpha 2-Macroglobulin expression in neuritic-type plaques in patients with Alzheimer's disease.* Neurobiol Aging, 1993. **14**(3): p. 233-7.
34. Haan, J., M.L. Maat-Schieman, S.G. van Duinen, O. Jansson, L. Thorsteinsson, and R.A. Roos, *Co-localization of beta/A4 and cystatin C in cortical blood vessels in Dutch, but not in Icelandic hereditary cerebral hemorrhage with amyloidosis.* Acta Neurol Scand, 1994. **89**(5): p. 367-71.
35. Itoh, Y., M. Yamada, M. Hayakawa, E. Otomo, and T. Miyatake, *Cerebral amyloid angiopathy: a significant cause of cerebellar as well as lobar cerebral hemorrhage in the elderly.* J Neurol Sci, 1993. **116**(2): p. 135-41.
36. Levy, E., M. Sastre, A. Kumar, G. Gallo, P. Piccardo, B. Ghetti, and F. Tagliavini, *Codeposition of cystatin C with amyloid-beta protein in the brain of Alzheimer disease patients.* J Neuropathol Exp Neurol, 2001. **60**(1): p. 94-104.
37. Maruyama, K., S. Ikeda, T. Ishihara, D. Allsop, and N. Yanagisawa, *Immunohistochemical characterization of cerebrovascular amyloid in 46 autopsied cases using antibodies to beta protein and cystatin C.* Stroke, 1990. **21**(3): p. 397-403.
38. Vinters, H.V., G.S. Nishimura, D.L. Secor, and W.M. Pardridge, *Immunoreactive A4 and gamma-trace peptide colocalization in amyloidotic arteriolar lesions in brains of patients with Alzheimer's disease.* Am J Pathol, 1990. **137**(2): p. 233-40.
39. Forette, F., M.L. Seux, J.A. Staessen, L. Thijs, M.R. Babarskiene, S. Babeanu, A. Bossini, R. Fagard, B. Gil-Extremera, T. Laks, Z. Kobalava, C. Sarti, J. Tuomilehto, H. Vanhanen, J. Webster, Y. Yodfat, and W.H. Birkenhager, *The prevention of dementia with antihypertensive treatment: new evidence from the Systolic Hypertension in Europe (Syst-Eur) study.* Arch Intern Med, 2002. **162**(18): p. 2046-52.
40. Guo, Z., L. Fratiglioni, L. Zhu, J. Fastbom, B. Winblad, and M. Viitanen, *Occurrence and progression of dementia in a community population aged 75 years and older: relationship of antihypertensive medication use.* Arch Neurol, 1999. **56**(8): p. 991-6.
41. in't Veld, B.A., A. Ruitenberg, A. Hofman, B.H. Stricker, and M.M. Breteler, *Antihypertensive*

- drugs and incidence of dementia: the Rotterdam Study*. Neurobiol Aging, 2001. **22**(3): p. 407-12.
42. Notkola, I.L., R. Sulkava, J. Pekkanen, T. Erkinjuntti, C. Ehnholm, P. Kivinen, J. Tuomilehto, and A. Nissinen, *Serum total cholesterol, apolipoprotein E epsilon 4 allele, and Alzheimer's disease*. Neuroepidemiology, 1998. **17**(1): p. 14-20.
43. Jick, H., G.L. Zornberg, S.S. Jick, S. Seshadri, and D.A. Drachman, *Statins and the risk of dementia*. Lancet, 2000. **356**(9242): p. 1627-31.
44. Rockwood, K., S. Kirkland, D.B. Hogan, C. MacKnight, H. Merry, R. Verreault, C. Wolfson, and I. McDowell, *Use of lipid-lowering agents, indication bias, and the risk of dementia in community-dwelling elderly people*. Arch Neurol, 2002. **59**(2): p. 223-7.
45. Wolozin, B., W. Kellman, P. Ruosseau, G.G. Celesia, and G. Siegel, *Decreased prevalence of Alzheimer disease associated with 3-hydroxy-3-methylglutaryl coenzyme A reductase inhibitors*. Arch Neurol, 2000. **57**(10): p. 1439-43.
46. Simons, M., F. Schwarzler, D. Lutjohann, K. von Bergmann, K. Beyreuther, J. Dichgans, H. Wormstall, T. Hartmann, and J.B. Schulz, *Treatment with simvastatin in normocholesterolemic patients with Alzheimer's disease: A 26-week randomized, placebo-controlled, double-blind trial*. Ann Neurol, 2002. **52**(3): p. 346-50.
47. Guo, Z., L. Fratiglioni, M. Viitanen, L. Lannfelt, H. Basun, J. Fastbom, and B. Winblad, *Apolipoprotein E genotypes and the incidence of Alzheimer's disease among persons aged 75 years and older: variation by use of antihypertensive medication?* Am J Epidemiol, 2001. **153**(3): p. 225-31.
48. Myers, A., P. Holmans, H. Marshall, J. Kwon, D. Meyer, D. Ramic, S. Shears, J. Booth, F.W. DeVrieze, R. Crook, M. Hamshere, R. Abraham, N. Tunstall, F. Rice, S. Carty, S. Lillystone, P. Kehoe, V. Rudrasingham, L. Jones, S. Lovestone, J. Perez-Tur, J. Williams, M.J. Owen, J. Hardy, and A.M. Goate, *Susceptibility locus for Alzheimer's disease on chromosome 10*. Science, 2000. **290**(5500): p. 2304-5.
49. Kakuda, N., S. Funamoto, S. Yagishita, M. Takami, S. Osawa, N. Dohmae, and Y. Ihara, *Equimolar production of amyloid beta-protein and amyloid precursor protein intracellular domain from beta-carboxyl-terminal fragment by gamma-secretase*. J Biol Chem, 2006. **281**(21): p. 14776-86.
50. Sato, T., N. Dohmae, Y. Qi, N. Kakuda, H. Misonou, R. Mitsumori, H. Maruyama, E.H. Koo, C. Haass, K. Takio, M. Morishima-Kawashima, S. Ishiura, and Y. Ihara, *Potential link between amyloid beta-protein 42 and C-terminal fragment gamma 49-99 of beta-amyloid precursor protein*. J Biol Chem, 2003. **278**(27): p. 24294-301.
51. Weidemann, A., S. Eggert, F.B. Reinhard, M. Vogel, K. Paliga, G. Baier, C.L. Masters, K. Beyreuther, and G. Evin, *A novel epsilon-cleavage within the transmembrane domain of the Alzheimer amyloid precursor protein demonstrates homology with Notch processing*. Biochemistry, 2002. **41**(8): p. 2825-35.
52. Zhao, G., G. Mao, J. Tan, Y. Dong, M.Z. Cui, S.H. Kim, and X. Xu, *Identification of a new presenilin-dependent zeta-cleavage site within the transmembrane domain of amyloid precursor protein*. J Biol Chem, 2004. **279**(49): p. 50647-50.
53. Qi-Takahara, Y., M. Morishima-Kawashima, Y. Tanimura, G. Dolios, N. Hirotsani, Y. Horikoshi,

- F. Kametani, M. Maeda, T.C. Saido, R. Wang, and Y. Ihara, *Longer forms of amyloid beta protein: implications for the mechanism of intramembrane cleavage by gamma-secretase*. J Neurosci, 2005. **25**(2): p. 436-45.
54. Hebert, S.S., L. Serneels, A. Tolia, K. Craessaerts, C. Derks, M.A. Filippov, U. Muller, and B. De Strooper, *Regulated intramembrane proteolysis of amyloid precursor protein and regulation of expression of putative target genes*. EMBO Rep, 2006. **7**(7): p. 739-45.
55. Cao, X. and T.C. Sudhof, *A transcriptionally [correction of transcriptively] active complex of APP with Fe65 and histone acetyltransferase Tip60*. Science, 2001. **293**(5527): p. 115-20.
56. Minopoli, G., P. de Candia, A. Bonetti, R. Faraonio, N. Zambrano, and T. Russo, *The beta-amyloid precursor protein functions as a cytosolic anchoring site that prevents Fe65 nuclear translocation*. J Biol Chem, 2001. **276**(9): p. 6545-50.
57. Muller, T., C.G. Concannon, M.W. Ward, C.M. Walsh, A.L. Tirniceriu, F. Tribl, D. Kogel, J.H. Prehn, and R. Egensperger, *Modulation of gene expression and cytoskeletal dynamics by the amyloid precursor protein intracellular domain (AICD)*. Mol Biol Cell, 2007. **18**(1): p. 201-10.
58. Scheinfeld, M.H., S. Matsuda, and L. D'Adamio, *JNK-interacting protein-1 promotes transcription of A beta protein precursor but not A beta precursor-like proteins, mechanistically different than Fe65*. Proc Natl Acad Sci U S A, 2003. **100**(4): p. 1729-34.
59. Trommsdorff, M., J.P. Borg, B. Margolis, and J. Herz, *Interaction of cytosolic adaptor proteins with neuronal apolipoprotein E receptors and the amyloid precursor protein*. J Biol Chem, 1998. **273**(50): p. 33556-60.
60. Russo, C., V. Dolcini, S. Salis, V. Venezia, E. Violani, P. Carlo, N. Zambrano, T. Russo, and G. Schettini, *Signal transduction through tyrosine-phosphorylated carboxy-terminal fragments of APP via an enhanced interaction with Shc/Grb2 adaptor proteins in reactive astrocytes of Alzheimer's disease brain*. Ann N Y Acad Sci, 2002. **973**: p. 323-33.
61. Russo, C., V. Dolcini, S. Salis, V. Venezia, N. Zambrano, T. Russo, and G. Schettini, *Signal transduction through tyrosine-phosphorylated C-terminal fragments of amyloid precursor protein via an enhanced interaction with Shc/Grb2 adaptor proteins in reactive astrocytes of Alzheimer's disease brain*. J Biol Chem, 2002. **277**(38): p. 35282-8.
62. Scheinfeld, M.H., E. Ghersi, K. Laky, B.J. Fowlkes, and L. D'Adamio, *Processing of beta-amyloid precursor-like protein-1 and -2 by gamma-secretase regulates transcription*. J Biol Chem, 2002. **277**(46): p. 44195-201.
63. Zhang, Z., C.H. Lee, V. Mandiyan, J.P. Borg, B. Margolis, J. Schlessinger, and J. Kuriyan, *Sequence-specific recognition of the internalization motif of the Alzheimer's amyloid precursor protein by the X11 PTB domain*. Embo J, 1997. **16**(20): p. 6141-50.
64. Fiore, F., N. Zambrano, G. Minopoli, V. Donini, A. Duilio, and T. Russo, *The regions of the Fe65 protein homologous to the phosphotyrosine interaction/phosphotyrosine binding domain of Shc bind the intracellular domain of the Alzheimer's amyloid precursor protein*. J Biol Chem, 1995. **270**(52): p. 30853-6.
65. Borg, J.P., J. Ooi, E. Levy, and B. Margolis, *The phosphotyrosine interaction domains of X11 and FE65 bind to distinct sites on the YENPTY motif of amyloid precursor protein*. Mol Cell Biol, 1996. **16**(11): p. 6229-41.

66. Zambrano, N., J.D. Buxbaum, G. Minopoli, F. Fiore, P. De Candia, S. De Renzis, R. Faraonio, S. Sabo, J. Cheetham, M. Sudol, and T. Russo, *Interaction of the phosphotyrosine interaction/phosphotyrosine binding-related domains of Fe65 with wild-type and mutant Alzheimer's beta-amyloid precursor proteins*. J Biol Chem, 1997. **272**(10): p. 6399-405.
67. Duilio, A., R. Faraonio, G. Minopoli, N. Zambrano, and T. Russo, *Fe65L2: a new member of the Fe65 protein family interacting with the intracellular domain of the Alzheimer's beta-amyloid precursor protein*. Biochem J, 1998. **330 ( Pt 1)**: p. 513-9.
68. Tarr, P.E., R. Roncarati, G. Pelicci, P.G. Pelicci, and L. D'Adamio, *Tyrosine phosphorylation of the beta-amyloid precursor protein cytoplasmic tail promotes interaction with Shc*. J Biol Chem, 2002. **277**(19): p. 16798-804.
69. McLoughlin, D.M. and C.C. Miller, *The FE65 proteins and Alzheimer's disease*. J Neurosci Res, 2007.
70. Baek, S.H., K.A. Ohgi, D.W. Rose, E.H. Koo, C.K. Glass, and M.G. Rosenfeld, *Exchange of N-CoR corepressor and Tip60 coactivator complexes links gene expression by NF-kappaB and beta-amyloid precursor protein*. Cell, 2002. **110**(1): p. 55-67.
71. Kinoshita, A., C.M. Whelan, O. Berezovska, and B.T. Hyman, *The gamma secretase-generated carboxyl-terminal domain of the amyloid precursor protein induces apoptosis via Tip60 in H4 cells*. J Biol Chem, 2002. **277**(32): p. 28530-6.
72. Muresan, Z. and V. Muresan, *A phosphorylated, carboxy-terminal fragment of beta-amyloid precursor protein localizes to the splicing factor compartment*. Hum Mol Genet, 2004. **13**(5): p. 475-88.
73. Lu, D.C., S. Rabizadeh, S. Chandra, R.F. Shayya, L.M. Ellerby, X. Ye, G.S. Salvesen, E.H. Koo, and D.E. Bredesen, *A second cytotoxic proteolytic peptide derived from amyloid beta-protein precursor*. Nat Med, 2000. **6**(4): p. 397-404.
74. Podlisny, M.B., B.L. Ostaszewski, S.L. Squazzo, E.H. Koo, R.E. Rydell, D.B. Teplow, and D.J. Selkoe, *Aggregation of secreted amyloid beta-protein into sodium dodecyl sulfate-stable oligomers in cell culture*. J Biol Chem., 1995. **270**(16): p. 9564-70.
75. Walsh, D.M., B.P. Tseng, R.E. Rydel, M.B. Podlisny, and D.J. Selkoe, *The oligomerization of amyloid beta-protein begins intracellularly in cells derived from human brain*. Biochemistry., 2000. **39**(35): p. 10831-9.
76. Walsh, D.M., I. Klyubin, J.V. Fadeeva, W.K. Cullen, R. Anwyl, M.S. Wolfe, M.J. Rowan, and D.J. Selkoe, *Naturally secreted oligomers of amyloid beta protein potently inhibit hippocampal long-term potentiation in vivo*. Nature., 2002. **416**(6880): p. 535-9.
77. Walsh, D.M., I. Klyubin, J.V. Fadeeva, M.J. Rowan, and D.J. Selkoe, *Amyloid-beta oligomers: their production, toxicity and therapeutic inhibition*. Biochem Soc Trans., 2002. **30**(4): p. 552-7.
78. Kim, J., L. Onstead, S. Randle, R. Price, L. Smithson, C. Zwizinski, D.W. Dickson, T. Golde, and E. McGowan, *Abeta40 inhibits amyloid deposition in vivo*. J Neurosci, 2007. **27**(3): p. 627-33.
79. Borchelt, D.R., G. Thinakaran, C.B. Eckman, M.K. Lee, F. Davenport, T. Ratovitsky, C.M. Prada, G. Kim, S. Seekins, D. Yager, H.H. Slunt, R. Wang, M. Seeger, A.I. Levey, S.E. Gandy, N.G. Copeland, N.A. Jenkins, D.L. Price, S.G. Younkin, and S.S. Sisodia, *Familial*

- Alzheimer's disease-linked presenilin 1 variants elevate Abeta1-42/1-40 ratio in vitro and in vivo.* Neuron, 1996. **17**(5): p. 1005-13.
80. Levy-Lahad, E., E.M. Wijsman, E. Nemens, L. Anderson, K.A. Goddard, J.L. Weber, T.D. Bird, and G.D. Schellenberg, *A familial Alzheimer's disease locus on chromosome 1.* Science, 1995. **269**(5226): p. 970-3.
81. Lesne, S., M.T. Koh, L. Kotilinek, R. Kaye, C.G. Glabe, A. Yang, M. Gallagher, and K.H. Ashe, *A specific amyloid-beta protein assembly in the brain impairs memory.* Nature, 2006. **440**(7082): p. 352-7.
82. Herzig, M.C., D.T. Winkler, P. Burgermeister, M. Pfeifer, E. Kohler, S.D. Schmidt, S. Danner, D. Abramowski, C. Sturchler-Pierrat, K. Burki, S.G. van Duinen, M.L. Maat-Schieman, M. Staufenbiel, P.M. Mathews, and M. Jucker, *Abeta is targeted to the vasculature in a mouse model of hereditary cerebral hemorrhage with amyloidosis.* Nat Neurosci, 2004. **7**(9): p. 954-60.
83. Lynch, J.A., A.M. George, P.B. Eisenhauer, K. Conn, W. Gao, I. Carreras, J.M. Wells, A. McKee, M.D. Ullman, and R.E. Fine, *Insulin degrading enzyme is localized predominantly at the cell surface of polarized and unpolarized human cerebrovascular endothelial cell cultures.* J Neurosci Res, 2006. **83**(7): p. 1262-70.
84. Edland, S.D., *Insulin-degrading enzyme, apolipoprotein E, and Alzheimer's disease.* J Mol Neurosci, 2004. **23**(3): p. 213-7.
85. Perez, A., L. Morelli, J.C. Cresto, and E.M. Castano, *Degradation of soluble amyloid beta-peptides 1-40, 1-42, and the Dutch variant 1-40Q by insulin degrading enzyme from Alzheimer disease and control brains.* Neurochem Res, 2000. **25**(2): p. 247-55.
86. Tanzi, R.E. and L. Bertram, *New frontiers in Alzheimer's disease genetics.* Neuron, 2001. **32**(2): p. 181-4.
87. Citron, M., T. Oltersdorf, C. Haass, L. McConlogue, A.Y. Hung, P. Seubert, C. Vigo-Pelfrey, I. Lieberburg, and D.J. Selkoe, *Mutation of the beta-amyloid precursor protein in familial Alzheimer's disease increases beta-protein production.* Nature, 1992. **360**(6405): p. 672-4.
88. Busciglio, J., D.H. Gabuzda, P. Matsudaira, and B.A. Yankner, *Generation of beta-amyloid in the secretory pathway in neuronal and nonneuronal cells.* Proc Natl Acad Sci U S A, 1993. **90**(5): p. 2092-6.
89. Hilbich, C., B. Kisters-Woike, J. Reed, C.L. Masters, and K. Beyreuther, *Aggregation and secondary structure of synthetic amyloid beta A4 peptides of Alzheimer's disease.* J Mol Biol, 1991. **218**(1): p. 149-63.
90. Neve, R.L. and N.K. Robakis, *Alzheimer's disease: a re-examination of the amyloid hypothesis.* Trends Neurosci, 1998. **21**(1): p. 15-9.
91. Walsh, D.M. and D.J. Selkoe, *Oligomers on the brain: the emerging role of soluble protein aggregates in neurodegeneration.* Protein Pept Lett, 2004. **11**(3): p. 213-28.
92. Suzuki, N., T.T. Cheung, X.D. Cai, A. Odaka, L. Otvos, Jr., C. Eckman, T.E. Golde, and S.G. Younkin, *An increased percentage of long amyloid beta protein secreted by familial amyloid beta protein precursor (beta APP717) mutants.* Science, 1994. **264**(5163): p. 1336-40.
93. Hecimovic, S., J. Wang, G. Dolios, M. Martinez, R. Wang, and A.M. Goate, *Mutations in APP*

- have independent effects on Abeta and CTFgamma generation.* Neurobiol Dis, 2004. **17**(2): p. 205-18.
94. Hendriks, L., C.M. van Duijn, P. Cras, M. Cruts, W. Van Hul, F. van Harskamp, A. Warren, M.G. McInnis, S.E. Antonarakis, J.J. Martin, and et al., *Presenile dementia and cerebral haemorrhage linked to a mutation at codon 692 of the beta-amyloid precursor protein gene.* Nat Genet, 1992. **1**(3): p. 218-21.
95. Fryer, J.D., K. Simmons, M. Parsadanian, K.R. Bales, S.M. Paul, P.M. Sullivan, and D.M. Holtzman, *Human apolipoprotein E4 alters the amyloid-beta 40:42 ratio and promotes the formation of cerebral amyloid angiopathy in an amyloid precursor protein transgenic model.* J Neurosci, 2005. **25**(11): p. 2803-10.
96. Games, D., D. Adams, R. Alessandrini, R. Barbour, P. Berthelette, C. Blackwell, T. Carr, J. Clemens, T. Donaldson, F. Gillespie, and et al., *Alzheimer-type neuropathology in transgenic mice overexpressing V717F beta-amyloid precursor protein.* Nature, 1995. **373**(6514): p. 523-7.
97. Teller, J.K., C. Russo, L.M. DeBusk, G. Angelini, D. Zaccheo, F. Dagna-Bricarelli, P. Scartezzini, S. Bertolini, D.M. Mann, M. Tabaton, and P. Gambetti, *Presence of soluble amyloid beta-peptide precedes amyloid plaque formation in Down's syndrome.* Nat Med, 1996. **2**(1): p. 93-5.
98. Wisniewski, K.E., A.J. Dalton, C. McLachlan, G.Y. Wen, and H.M. Wisniewski, *Alzheimer's disease in Down's syndrome: clinicopathologic studies.* Neurology, 1985. **35**(7): p. 957-61.
99. Prasher, V.P., M.J. Farrer, A.M. Kessling, E.M. Fisher, R.J. West, P.C. Barber, and A.C. Butler, *Molecular mapping of Alzheimer-type dementia in Down's syndrome.* Ann Neurol, 1998. **43**(3): p. 380-3.
100. Pericak-Vance, M.A., M.L. Bass, L.H. Yamaoka, P.C. Gaskell, W.K. Scott, H.A. Terwedow, M.M. Menold, P.M. Conneally, G.W. Small, A.M. Saunders, A.D. Roses, and J.L. Haines, *Complete genomic screen in late-onset familial Alzheimer's disease.* Neurobiol Aging, 1998. **19**(1 Suppl): p. S39-42.
101. Dickson, D.W., H.A. Crystal, L.A. Mattiace, D.M. Masur, A.D. Blau, P. Davies, S.H. Yen, and M.K. Aronson, *Identification of normal and pathological aging in prospectively studied nondemented elderly humans.* Neurobiol Aging, 1992. **13**(1): p. 179-89.
102. Hsiao, K.K., D.R. Borchelt, K. Olson, R. Johannsdottir, C. Kitt, W. Yunis, S. Xu, C. Eckman, S. Younkin, D. Price, and et al., *Age-related CNS disorder and early death in transgenic FVB/N mice overexpressing Alzheimer amyloid precursor proteins.* Neuron, 1995. **15**(5): p. 1203-18.
103. Goedert, M. and R. Jakes, *Mutations causing neurodegenerative tauopathies.* Biochim Biophys Acta, 2005. **1739**(2-3): p. 240-50.
104. Andorfer, C.A. and P. Davies, *PKA phosphorylations on tau: developmental studies in the mouse.* Dev Neurosci, 2000. **22**(4): p. 303-9.
105. Wisniewski, H.M., H.K. Narang, and R.D. Terry, *Neurofibrillary tangles of paired helical filaments.* J Neurol Sci, 1976. **27**(2): p. 173-81.
106. Goedert, M., C.M. Wischik, R.A. Crowther, J.E. Walker, and A. Klug, *Cloning and sequencing of the cDNA encoding a core protein of the paired helical filament of Alzheimer disease:*

- identification as the microtubule-associated protein tau*. Proc Natl Acad Sci U S A, 1988. **85**(11): p. 4051-5.
107. Lindwall, G. and R.D. Cole, *Phosphorylation affects the ability of tau protein to promote microtubule assembly*. J Biol Chem, 1984. **259**(8): p. 5301-5.
108. Goedert, M., M.G. Spillantini, N.J. Cairns, and R.A. Crowther, *Tau proteins of Alzheimer paired helical filaments: abnormal phosphorylation of all six brain isoforms*. Neuron, 1992. **8**(1): p. 159-68.
109. Braak, H. and E. Braak, *Diagnostic criteria for neuropathologic assessment of Alzheimer's disease*. Neurobiol Aging, 1997. **18**(4 Suppl): p. S85-8.
110. Tanaka, T., K. Iqbal, E. Trenkner, D.J. Liu, and I. Grundke-Iqbal, *Abnormally phosphorylated tau in SY5Y human neuroblastoma cells*. FEBS Lett, 1995. **360**(1): p. 5-9.
111. Hanger, D.P., J.C. Betts, T.L. Loviny, W.P. Blackstock, and B.H. Anderton, *New phosphorylation sites identified in hyperphosphorylated tau (paired helical filament-tau) from Alzheimer's disease brain using nanoelectrospray mass spectrometry*. J Neurochem, 1998. **71**(6): p. 2465-76.
112. Sengupta, A., J. Kabat, M. Novak, Q. Wu, I. Grundke-Iqbal, and K. Iqbal, *Phosphorylation of tau at both Thr 231 and Ser 262 is required for maximal inhibition of its binding to microtubules*. Arch Biochem Biophys, 1998. **357**(2): p. 299-309.
113. Benneceb, M., C.X. Gong, I. Grundke-Iqbal, and K. Iqbal, *Inhibition of PP-2A upregulates CaMKII in rat forebrain and induces hyperphosphorylation of tau at Ser 262/356*. FEBS Lett, 2001. **490**(1-2): p. 15-22.
114. Li, M., A. Makkinje, and Z. Damuni, *Molecular identification of I1PP2A, a novel potent heat-stable inhibitor protein of protein phosphatase 2A*. Biochemistry, 1996. **35**(22): p. 6998-7002.
115. Singh, T.J., I. Grundke-Iqbal, W.Q. Wu, V. Chauhan, M. Novak, E. Kontzekova, and K. Iqbal, *Protein kinase C and calcium/calmodulin-dependent protein kinase II phosphorylate three-repeat and four-repeat tau isoforms at different rates*. Mol Cell Biochem, 1997. **168**(1-2): p. 141-8.
116. Alonso, A.D., T. Zaidi, M. Novak, H.S. Barra, I. Grundke-Iqbal, and K. Iqbal, *Interaction of tau isoforms with Alzheimer's disease abnormally hyperphosphorylated tau and in vitro phosphorylation into the disease-like protein*. J Biol Chem, 2001. **276**(41): p. 37967-73.
117. Woodgett, J.R., *Molecular cloning and expression of glycogen synthase kinase-3/factor A*. Embo J, 1990. **9**(8): p. 2431-8.
118. Diehl, J.A., M. Cheng, M.F. Roussel, and C.J. Sherr, *Glycogen synthase kinase-3beta regulates cyclin D1 proteolysis and subcellular localization*. Genes Dev, 1998. **12**(22): p. 3499-511.
119. Grimes, C.A. and R.S. Jope, *The multifaceted roles of glycogen synthase kinase 3beta in cellular signaling*. Prog Neurobiol, 2001. **65**(4): p. 391-426.
120. Billingsley, M.L. and R.L. Kincaid, *Regulated phosphorylation and dephosphorylation of tau protein: effects on microtubule interaction, intracellular trafficking and neurodegeneration*. Biochem J, 1997. **323** ( Pt 3): p. 577-91.
121. Imahori, K. and T. Uchida, *Physiology and pathology of tau protein kinases in relation to*

- Alzheimer's disease*. J Biochem, 1997. **121**(2): p. 179-88.
122. Johnson, G.V. and J.A. Hartigan, *Tau protein in normal and Alzheimer's disease brain: an update*. J Alzheimers Dis, 1999. **1**(4-5): p. 329-51.
123. Johnson, G.V. and S.M. Jenkins, *Tau protein in normal and Alzheimer's disease brain*. J Alzheimers Dis, 1999. **1**(4-5): p. 307-28.
124. Lovestone, S., C.L. Hartley, J. Pearce, and B.H. Anderton, *Phosphorylation of tau by glycogen synthase kinase-3 beta in intact mammalian cells: the effects on the organization and stability of microtubules*. Neuroscience, 1996. **73**(4): p. 1145-57.
125. Lovestone, S. and C.H. Reynolds, *The phosphorylation of tau: a critical stage in neurodevelopment and neurodegenerative processes*. Neuroscience, 1997. **78**(2): p. 309-24.
126. Ishiguro, K., M. Takamatsu, K. Tomizawa, A. Omori, M. Takahashi, M. Arioka, T. Uchida, and K. Imahori, *Tau protein kinase I converts normal tau protein into A68-like component of paired helical filaments*. J Biol Chem, 1992. **267**(15): p. 10897-901.
127. Mandelkow, E.M., G. Drewes, J. Biernat, N. Gustke, J. Van Lint, J.R. Vandenheede, and E. Mandelkow, *Glycogen synthase kinase-3 and the Alzheimer-like state of microtubule-associated protein tau*. FEBS Lett, 1992. **314**(3): p. 315-21.
128. Michel, G., M. Mercken, M. Murayama, K. Noguchi, K. Ishiguro, K. Imahori, and A. Takashima, *Characterization of tau phosphorylation in glycogen synthase kinase-3beta and cyclin dependent kinase-5 activator (p23) transfected cells*. Biochim Biophys Acta, 1998. **1380**(2): p. 177-82.
129. Takashima, A., H. Yamaguchi, K. Noguchi, G. Michel, K. Ishiguro, K. Sato, T. Hoshino, M. Hoshi, and K. Imahori, *Amyloid beta peptide induces cytoplasmic accumulation of amyloid protein precursor via tau protein kinase I/glycogen synthase kinase-3 beta in rat hippocampal neurons*. Neurosci Lett, 1995. **198**(2): p. 83-6.
130. Selkoe, D.J., T. Yamazaki, M. Citron, M.B. Podlisny, E.H. Koo, D.B. Teplow, and C. Haass, *The role of APP processing and trafficking pathways in the formation of amyloid beta-protein*. Ann N Y Acad Sci, 1996. **777**: p. 57-64.
131. Kim, J.W., J.E. Lee, M.J. Kim, E.G. Cho, S.G. Cho, and E.J. Choi, *Glycogen synthase kinase 3 beta is a natural activator of mitogen-activated protein kinase/extracellular signal-regulated kinase kinase kinase 1 (MEKK1)*. J Biol Chem, 2003. **278**(16): p. 13995-4001.
132. Brindle, P.K. and M.R. Montminy, *The CREB family of transcription activators*. Curr Opin Genet Dev, 1992. **2**(2): p. 199-204.
133. Alvarez, G., J.R. Munoz-Montano, J. Satrustegui, J. Avila, E. Bogonez, and J. Diaz-Nido, *Lithium protects cultured neurons against beta-amyloid-induced neurodegeneration*. FEBS Lett, 1999. **453**(3): p. 260-4.
134. Takashima, A., M. Murayama, O. Murayama, T. Kohno, T. Honda, K. Yasutake, N. Nihonmatsu, M. Mercken, H. Yamaguchi, S. Sugihara, and B. Wolozin, *Presenilin 1 associates with glycogen synthase kinase-3beta and its substrate tau*. Proc Natl Acad Sci U S A, 1998. **95**(16): p. 9637-41.
135. Hiltunen, M., A. Mannermaa, A.M. Koivisto, M. Lehtovirta, S. Helisalmi, M. Ryyanen, P. Riekkinen, Sr., and H. Soininen, *Linkage disequilibrium in the 13q12 region in Finnish late*

- onset Alzheimer's disease patients*. Eur J Hum Genet, 1999. **7**(6): p. 652-8.
136. Hiltunen, M., A. Mannermaa, D. Thompson, D. Easton, M. Pirskanen, S. Helisalimi, A.M. Koivisto, M. Lehtovirta, M. Ryyanen, and H. Soininen, *Genome-wide linkage disequilibrium mapping of late-onset Alzheimer's disease in Finland*. Neurology, 2001. **57**(9): p. 1663-8.
137. Cruts, M., C.M. van Duijn, H. Backhovens, M. Van den Broeck, A. Wehnert, S. Serneels, R. Sherrington, M. Hutton, J. Hardy, P.H. St George-Hyslop, A. Hofman, and C. Van Broeckhoven, *Estimation of the genetic contribution of presenilin-1 and -2 mutations in a population-based study of presenile Alzheimer disease*. Hum Mol Genet, 1998. **7**(1): p. 43-51.
138. Athan, E.S., J. Williamson, A. Ciappa, V. Santana, S.N. Romas, J.H. Lee, H. Rondon, R.A. Lantigua, M. Medrano, M. Torres, S. Arawaka, E. Rogaeva, Y.Q. Song, C. Sato, T. Kawarai, K.C. Fafel, M.A. Boss, W.K. Seltzer, Y. Stern, P. St George-Hyslop, B. Tycko, and R. Mayeux, *A founder mutation in presenilin 1 causing early-onset Alzheimer disease in unrelated Caribbean Hispanic families*. Jama, 2001. **286**(18): p. 2257-63.
139. Rogaev, E.I., R. Sherrington, E.A. Rogaeva, G. Levesque, M. Ikeda, Y. Liang, H. Chi, C. Lin, K. Holman, T. Tsuda, and et al., *Familial Alzheimer's disease in kindreds with missense mutations in a gene on chromosome 1 related to the Alzheimer's disease type 3 gene*. Nature, 1995. **376**(6543): p. 775-8.
140. Irizarry, R.A., Z. Wu, and H.A. Jaffee, *Comparison of Affymetrix GeneChip expression measures*. Bioinformatics, 2006. **22**(7): p. 789-94.
141. Seo, J., H. Gordish-Dressman, and E.P. Hoffman, *An interactive power analysis tool for microarray hypothesis testing and generation*. Bioinformatics, 2006. **22**(7): p. 808-14.
142. Millenaar, F.F., J. Okyere, S.T. May, M. van Zanten, L.A. Voesenek, and A.J. Peeters, *How to decide? Different methods of calculating gene expression from short oligonucleotide array data will give different results*. BMC Bioinformatics, 2006. **7**: p. 137.
143. Barash, Y., E. Dehan, M. Krupsky, W. Franklin, M. Geraci, N. Friedman, and N. Kaminski, *Comparative analysis of algorithms for signal quantitation from oligonucleotide microarrays*. Bioinformatics, 2004. **20**(6): p. 839-46.
144. Choe, S.E., M. Boutros, A.M. Michelson, G.M. Church, and M.S. Halfon, *Preferred analysis methods for Affymetrix GeneChips revealed by a wholly defined control dataset*. Genome Biol, 2005. **6**(2): p. R16.
145. Wu, Z. and R.A. Irizarry, *Preprocessing of oligonucleotide array data*. Nat Biotechnol, 2004. **22**(6): p. 656-8; author reply 658.
146. Wu, Z. and R.A. Irizarry, *Stochastic models inspired by hybridization theory for short oligonucleotide arrays*. J Comput Biol, 2005. **12**(6): p. 882-93.
147. Brazma, A., P. Hingamp, J. Quackenbush, G. Sherlock, P. Spellman, C. Stoeckert, J. Aach, W. Ansorge, C.A. Ball, H.C. Causton, T. Gaasterland, P. Glenisson, F.C. Holstege, I.F. Kim, V. Markowitz, J.C. Matese, H. Parkinson, A. Robinson, U. Sarkans, S. Schulze-Kremer, J. Stewart, R. Taylor, J. Vilo, and M. Vingron, *Minimum information about a microarray experiment (MIAME)-toward standards for microarray data*. Nat Genet, 2001. **29**(4): p. 365-71.
148. Grimm, H.S., D. Beher, S.F. Lichtenthaler, M.S. Shearman, K. Beyreuther, and T. Hartmann, *gamma-Secretase cleavage site specificity differs for intracellular and secretory amyloid beta*.

- J Biol Chem, 2003. **278**(15): p. 13077-85.
149. Lichtenthaler, S.F., G. Multhaup, C.L. Masters, and K. Beyreuther, *A novel substrate for analyzing Alzheimer's disease gamma-secretase*. FEBS Lett, 1999. **453**(3): p. 288-92.
150. Ryan, K.A. and S.W. Pimplikar, *Activation of GSK-3 and phosphorylation of CRMP2 in transgenic mice expressing APP intracellular domain*. J Cell Biol, 2005. **171**(2): p. 327-35.
151. Lu, D.C., S. Soriano, D.E. Bredesen, and E.H. Koo, *Caspase cleavage of the amyloid precursor protein modulates amyloid beta-protein toxicity*. J Neurochem, 2003. **87**(3): p. 733-41.
152. von Rotz, R.C., B.M. Kohli, J. Bosset, M. Meier, T. Suzuki, R.M. Nitsch, and U. Konietzko, *The APP intracellular domain forms nuclear multiprotein complexes and regulates the transcription of its own precursor*. J Cell Sci, 2004. **117**(Pt 19): p. 4435-48.
153. Jahn, O., D. Hesse, M. Reinelt, and H.D. Kratzin, *Technical innovations for the automated identification of gel-separated proteins by MALDI-TOF mass spectrometry*. Anal Bioanal Chem, 2006. **386**(1): p. 92-103.
154. Chu, T.M., B. Weir, and R. Wolfinger, *A systematic statistical linear modeling approach to oligonucleotide array experiments*. Math Biosci, 2002. **176**(1): p. 35-51.
155. Khalyfa, A., T. Chlon, H. Qiang, N. Agarwal, and N.G. Cooper, *Microarray reveals complement components are regulated in the serum-deprived rat retinal ganglion cell line*. Mol Vis, 2007. **13**: p. 293-308.
156. Won, J.Y., E.C. Nam, S.J. Yoo, H.J. Kwon, S.J. Um, H.S. Han, S.H. Kim, Y. Byun, and S.Y. Kim, *The effect of cellular retinoic acid binding protein-I expression on the CYP26-mediated catabolism of all-trans retinoic acid and cell proliferation in head and neck squamous cell carcinoma*. Metabolism, 2004. **53**(8): p. 1007-12.
157. Ross, A.C., *Cellular metabolism and activation of retinoids: roles of cellular retinoid-binding proteins*. Faseb J, 1993. **7**(2): p. 317-27.
158. Napoli, J.L., K.P. Posch, P.D. Fiorella, and M.H. Boerman, *Physiological occurrence, biosynthesis and metabolism of retinoic acid: evidence for roles of cellular retinol-binding protein (CRBP) and cellular retinoic acid-binding protein (CRABP) in the pathway of retinoic acid homeostasis*. Biomed Pharmacother, 1991. **45**(4-5): p. 131-43.
159. Luedi, P.P., A.J. Hartemink, and R.L. Jirtle, *Genome-wide prediction of imprinted murine genes*. Genome Res, 2005. **15**(6): p. 875-84.
160. Yoshii, A. and M. Constantine-Paton, *BDNF induces transport of PSD-95 to dendrites through PI3K-AKT signaling after NMDA receptor activation*. Nat Neurosci, 2007. **10**(6): p. 702-11.
161. Laursen, L.S., K. Kjaer-Sorensen, M.H. Andersen, and C. Oxvig, *Regulation of insulin-like growth factor (IGF) bioactivity by sequential proteolytic cleavage of IGF binding protein-4 and -5*. Mol Endocrinol, 2007. **21**(5): p. 1246-57.
162. Barnes, C.J., K. Ohshiro, S.K. Rayala, A.K. El-Naggar, and R. Kumar, *Insulin-like growth factor receptor as a therapeutic target in head and neck cancer*. Clin Cancer Res, 2007. **13**(14): p. 4291-9.
163. Slaaby, R., L. Schaffer, I. Lautrup-Larsen, A.S. Andersen, A.C. Shaw, I.S. Mathiasen, and J. Brandt, *Hybrid receptors formed by insulin receptor (IR) and insulin-like growth factor I*

- receptor (IGF-IR) have low insulin and high IGF-1 affinity irrespective of the IR splice variant.* J Biol Chem, 2006. **281**(36): p. 25869-74.
164. Denley, A., J.M. Carroll, G.V. Brierley, L. Cosgrove, J. Wallace, B. Forbes, and C.T. Roberts, Jr., *Differential activation of insulin receptor substrates 1 and 2 by insulin-like growth factor-activated insulin receptors.* Mol Cell Biol, 2007. **27**(10): p. 3569-77.
165. Denley, A., E.R. Bonython, G.W. Booker, L.J. Cosgrove, B.E. Forbes, C.W. Ward, and J.C. Wallace, *Structural determinants for high-affinity binding of insulin-like growth factor II to insulin receptor (IR)-A, the exon 11 minus isoform of the IR.* Mol Endocrinol, 2004. **18**(10): p. 2502-12.
166. Denley, A., G.V. Brierley, J.M. Carroll, A. Lindenberg, G.W. Booker, L.J. Cosgrove, J.C. Wallace, B.E. Forbes, and C.T. Roberts, Jr., *Differential activation of insulin receptor isoforms by insulin-like growth factors is determined by the C domain.* Endocrinology, 2006. **147**(2): p. 1029-36.
167. Hill, J.M., A.M. Ades, S.K. McCune, N. Sahir, E.M. Moody, D.T. Abebe, L.S. Crnic, and D.E. Brenneman, *Vasoactive intestinal peptide in the brain of a mouse model for Down syndrome.* Exp Neurol, 2003. **183**(1): p. 56-65.
168. Amour, A., P.M. Slocombe, A. Webster, M. Butler, C.G. Knight, B.J. Smith, P.E. Stephens, C. Shelley, M. Hutton, V. Knauper, A.J. Docherty, and G. Murphy, *TNF-alpha converting enzyme (TACE) is inhibited by TIMP-3.* FEBS Lett, 1998. **435**(1): p. 39-44.
169. Amour, A., C.G. Knight, A. Webster, P.M. Slocombe, P.E. Stephens, V. Knauper, A.J. Docherty, and G. Murphy, *The in vitro activity of ADAM-10 is inhibited by TIMP-1 and TIMP-3.* FEBS Lett, 2000. **473**(3): p. 275-9.
170. Allinson, T.M., E.T. Parkin, T.P. Condon, S.L. Schwager, E.D. Sturrock, A.J. Turner, and N.M. Hooper, *The role of ADAM10 and ADAM17 in the ectodomain shedding of angiotensin converting enzyme and the amyloid precursor protein.* Eur J Biochem, 2004. **271**(12): p. 2539-47.
171. Hoe, H.S., M.J. Cooper, M.P. Burns, P.A. Lewis, M. van der Brug, G. Chakraborty, C.M. Cartagena, D.T. Pak, M.R. Cookson, and G.W. Rebeck, *The metalloprotease inhibitor TIMP-3 regulates amyloid precursor protein and apolipoprotein E receptor proteolysis.* J Neurosci, 2007. **27**(40): p. 10895-905.
172. Dickson, D.W., *The pathogenesis of senile plaques.* J Neuropathol Exp Neurol, 1997. **56**(4): p. 321-39.
173. Soderberg, L., C. Dahlqvist, H. Kakuyama, J. Thyberg, A. Ito, B. Winblad, J. Naslund, and L.O. Tjernberg, *Collagenous Alzheimer amyloid plaque component assembles amyloid fibrils into protease resistant aggregates.* Febs J, 2005. **272**(9): p. 2231-6.
174. Storkebaum, E. and P. Carmeliet, *VEGF: a critical player in neurodegeneration.* J Clin Invest, 2004. **113**(1): p. 14-8.
175. Oosthuysen, B., L. Moons, E. Storkebaum, H. Beck, D. Nuyens, K. Brusselmans, J. Van Dorpe, P. Hellings, M. Gorselink, S. Heymans, G. Theilmeier, M. Dewerchin, V. Laudénbach, P. Vermylen, H. Raat, T. Acker, V. Vleminckx, L. Van Den Bosch, N. Cashman, H. Fujisawa, M.R. Drost, R. Sciot, F. Bruyninckx, D.J. Hicklin, C. Ince, P. Gressens, F. Lupu, K.H. Plate, W. Robberecht, J.M. Herbert, D. Collen, and P. Carmeliet, *Deletion of the hypoxia-response*

- element in the vascular endothelial growth factor promoter causes motor neuron degeneration.* Nat Genet, 2001. **28**(2): p. 131-8.
176. Roudabush, F.L., K.L. Pierce, S. Maudsley, K.D. Khan, and L.M. Luttrell, *Transactivation of the EGF receptor mediates IGF-1-stimulated shc phosphorylation and ERK1/2 activation in COS-7 cells.* J Biol Chem, 2000. **275**(29): p. 22583-9.
177. Gould, D.B., F.C. Phalan, S.E. van Mil, J.P. Sundberg, K. Vahedi, P. Massin, M.G. Bousser, P. Heutink, J.H. Miner, E. Tournier-Lasserre, and S.W. John, *Role of COL4A1 in small-vessel disease and hemorrhagic stroke.* N Engl J Med, 2006. **354**(14): p. 1489-96.
178. Gould, D.B., F.C. Phalan, G.J. Breedveld, S.E. van Mil, R.S. Smith, J.C. Schimenti, U. Aguglia, M.S. van der Knaap, P. Heutink, and S.W. John, *Mutations in Col4a1 cause perinatal cerebral hemorrhage and porencephaly.* Science, 2005. **308**(5725): p. 1167-71.
179. Lei, J., S. Silbiger, F.N. Ziyadeh, and J. Neugarten, *Serum-stimulated alpha 1 type IV collagen gene transcription is mediated by TGF-beta and inhibited by estradiol.* Am J Physiol, 1998. **274**(2 Pt 2): p. F252-8.
180. Brisken, C., A. Ayyannan, C. Nguyen, A. Heineman, F. Reinhardt, J. Tan, S.K. Dey, G.P. Dotto, and R.A. Weinberg, *IGF-2 is a mediator of prolactin-induced morphogenesis in the breast.* Dev Cell, 2002. **3**(6): p. 877-87.
181. Sumrejkanchanakij, P., M. Tamamori-Adachi, Y. Matsunaga, K. Eto, and M.A. Ikeda, *Role of cyclin D1 cytoplasmic sequestration in the survival of postmitotic neurons.* Oncogene, 2003. **22**(54): p. 8723-30.
182. Gossel, M.J. and P.W. Hinds, *Beyond the cell cycle: a new role for Cdk6 in differentiation.* J Cell Biochem, 2006. **97**(3): p. 485-93.
183. Matushansky, I., F. Radparvar, and A.I. Skoultchi, *CDK6 blocks differentiation: coupling cell proliferation to the block to differentiation in leukemic cells.* Oncogene, 2003. **22**(27): p. 4143-9.
184. Ericson, K.K., D. Krull, P. Slomiany, and M.J. Gossel, *Expression of cyclin-dependent kinase 6, but not cyclin-dependent kinase 4, alters morphology of cultured mouse astrocytes.* Mol Cancer Res, 2003. **1**(9): p. 654-64.
185. Ogasawara, T., M. Katagiri, A. Yamamoto, K. Hoshi, T. Takato, K. Nakamura, S. Tanaka, H. Okayama, and H. Kawaguchi, *Osteoclast differentiation by RANKL requires NF-kappaB-mediated downregulation of cyclin-dependent kinase 6 (Cdk6).* J Bone Miner Res, 2004. **19**(7): p. 1128-36.
186. Ogasawara, T., H. Kawaguchi, S. Jinno, K. Hoshi, K. Itaka, T. Takato, K. Nakamura, and H. Okayama, *Bone morphogenetic protein 2-induced osteoblast differentiation requires Smad-mediated down-regulation of Cdk6.* Mol Cell Biol, 2004. **24**(15): p. 6560-8.
187. Marine, J. and A. Winoto, *The human enhancer-binding protein Gata3 binds to several T-cell receptor regulatory elements.* Proc Natl Acad Sci U S A, 1991. **88**(16): p. 7284-8.
188. Hahne, J.C., T. Fuchs, H. El Mustapha, A.F. Okuducu, J.C. Bories, and N. Wernert, *Expression pattern of matrix metalloproteinase and TIMP genes in fibroblasts derived from Ets-1 knock-out mice compared to wild-type mouse fibroblasts.* Int J Mol Med, 2006. **18**(1): p. 153-9.

189. Toriya, M., A. Tokunaga, K. Sawamoto, K. Nakao, and H. Okano, *Distinct functions of human numb isoforms revealed by misexpression in the neural stem cell lineage in the Drosophila larval brain*. Dev Neurosci, 2006. **28**(1-2): p. 142-55.
190. Bhaumick, B. and R.M. Bala, *Parallel effects of insulin-like growth factor-II and insulin on glucose metabolism of developing mouse embryonic limb buds in culture*. Biochem Biophys Res Commun, 1988. **152**(1): p. 359-67.
191. Steen, E., B.M. Terry, E.J. Rivera, J.L. Cannon, T.R. Neely, R. Tavares, X.J. Xu, J.R. Wands, and S.M. de la Monte, *Impaired insulin and insulin-like growth factor expression and signaling mechanisms in Alzheimer's disease--is this type 3 diabetes?* J Alzheimers Dis, 2005. **7**(1): p. 63-80.
192. Morishima-Kawashima, M., M. Hasegawa, K. Takio, M. Suzuki, H. Yoshida, K. Titani, and Y. Ihara, *Proline-directed and non-proline-directed phosphorylation of PHF-tau*. J Biol Chem, 1995. **270**(2): p. 823-9.
193. Heber, S., J. Herms, V. Gajic, J. Hainfellner, A. Aguzzi, T. Rulicke, H. von Kretschmar, C. von Koch, S. Sisodia, P. Tremml, H.P. Lipp, D.P. Wolfer, and U. Muller, *Mice with combined gene knock-outs reveal essential and partially redundant functions of amyloid precursor protein family members*. J Neurosci, 2000. **20**(21): p. 7951-63.
194. Abdueva, D., D. Skvortsov, and S. Tavares, *Non-linear analysis of GeneChip arrays*. Nucleic Acids Res, 2006. **34**(15): p. e105.
195. Goodman, A.B., *Retinoid receptors, transporters, and metabolizers as therapeutic targets in late onset Alzheimer disease*. J Cell Physiol, 2006. **209**(3): p. 598-603.
196. Goodman, A.B. and A.B. Pardee, *Evidence for defective retinoid transport and function in late onset Alzheimer's disease*. Proc Natl Acad Sci U S A, 2003. **100**(5): p. 2901-5.
197. Heintz, K., M. Beck, R. Schliebs, and J.R. Perez-Polo, *Toxicity mediated by soluble oligomers of beta-amyloid(1-42) on cholinergic SN56.B5.G4 cells*. J Neurochem, 2006. **98**(6): p. 1930-45.
198. Kimberly, W.T., J.B. Zheng, S.Y. Guenette, and D.J. Selkoe, *The intracellular domain of the beta-amyloid precursor protein is stabilized by Fe65 and translocates to the nucleus in a notch-like manner*. J Biol Chem, 2001. **276**(43): p. 40288-92.
199. Walsh, D.M., J.V. Fadeeva, M.J. LaVoie, K. Paliga, S. Eggert, W.T. Kimberly, W. Wasco, and D.J. Selkoe, *gamma-Secretase cleavage and binding to FE65 regulate the nuclear translocation of the intracellular C-terminal domain (ICD) of the APP family of proteins*. Biochemistry, 2003. **42**(22): p. 6664-73.
200. Schroeter, E.H., J.A. Kisslinger, and R. Kopan, *Notch-1 signalling requires ligand-induced proteolytic release of intracellular domain*. Nature, 1998. **393**(6683): p. 382-6.
201. De Strooper, B., W. Annaert, P. Cupers, P. Saftig, K. Craessaerts, J.S. Mumm, E.H. Schroeter, V. Schrijvers, M.S. Wolfe, W.J. Ray, A. Goate, and R. Kopan, *A presenilin-1-dependent gamma-secretase-like protease mediates release of Notch intracellular domain*. Nature, 1999. **398**(6727): p. 518-22.
202. Paratore, S., R. Parenti, A. Torrisi, A. Copani, F. Cicirata, and S. Cavallaro, *Genomic profiling of cortical neurons following exposure to beta-amyloid*. Genomics, 2006. **88**(4): p. 468-79.

- 
203. Martinez, T. and A. Pascual, *Gene expression profile in beta-amyloid-treated SH-SY5Y neuroblastoma cells*. Brain Res Bull, 2007. **72**(4-6): p. 225-31.
204. Hoerndli, F.J., S. Pelech, A. Papassotiropoulos, and J. Gotz, *Abeta treatment and P301L tau expression in an Alzheimer's disease tissue culture model act synergistically to promote aberrant cell cycle re-entry*. Eur J Neurosci, 2007. **26**(1): p. 60-72.
205. Ono, K., Y. Yoshiike, A. Takashima, K. Hasegawa, H. Naiki, and M. Yamada, *Vitamin A exhibits potent anti-amyloidogenic and fibril-destabilizing effects in vitro*. Exp Neurol, 2004. **189**(2): p. 380-92.
206. Corcoran, J.P., P.L. So, and M. Maden, *Disruption of the retinoid signalling pathway causes a deposition of amyloid beta in the adult rat brain*. Eur J Neurosci, 2004. **20**(4): p. 896-902.
207. Boerwinkle, E., S. Brown, A.R. Sharrett, G. Heiss, and W. Patsch, *Apolipoprotein E polymorphism influences postprandial retinyl palmitate but not triglyceride concentrations*. Am J Hum Genet., 1994. **54**(2): p. 341-60.
208. Folin, M., S. Baiguera, L. Fioravanzo, M.T. Conconi, C. Grandi, G.G. Nussdorfer, and P.P. Parnigotto, *Caspase-8 activation and oxidative stress are involved in the cytotoxic effect of beta-amyloid on rat brain microvascular endothelial cells*. Int J Mol Med, 2006. **17**(3): p. 431-5.
209. Dixon, J.L. and D.S. Goodman, *Effects of nutritional and hormonal factors on the metabolism of retinol-binding protein by primary cultures of rat hepatocytes*. J Cell Physiol., 1987. **130**(1): p. 6-13.
210. Dixon, J.L. and D.S. Goodman, *Studies on the metabolism of retinol-binding protein by primary hepatocytes from retinol-deficient rats*. J Cell Physiol., 1987. **130**(1): p. 14-20.
211. Herbert, J., J.N. Wilcox, K.T. Pham, R.T. Freneau, Jr., M. Zeviani, A. Dwork, D.R. Soprano, A. Makover, D.S. Goodman, E.A. Zimmerman, and et al., *Transthyretin: a choroid plexus-specific transport protein in human brain. The 1986 S. Weir Mitchell award*. Neurology., 1986. **36**(7): p. 900-11.
212. Husson, M., V. Enderlin, A. Delacourte, N. Ghenimi, S. Alfos, V. Pallet, and P. Higuere, *Retinoic acid normalizes nuclear receptor mediated hypo-expression of proteins involved in beta-amyloid deposits in the cerebral cortex of vitamin A deprived rats*. Neurobiol Dis., 2006. **23**(1): p. 1-10. Epub 2006 Mar 10.
213. Bacanu, S.A., B. Devlin, K.V. Chowdari, S.T. DeKosky, V.L. Nimgaonkar, and R.A. Sweet, *Linkage analysis of Alzheimer disease with psychosis*. Neurology, 2002. **59**(1): p. 118-20.
214. Jacobs, S., D.C. Lie, K.L. DeCicco, Y. Shi, L.M. DeLuca, F.H. Gage, and R.M. Evans, *Retinoic acid is required early during adult neurogenesis in the dentate gyrus*. Proc Natl Acad Sci U S A, 2006. **103**(10): p. 3902-7.
215. Ruberte, E., P. Dolle, P. Chambon, and G. Morriss-Kay, *Retinoic acid receptors and cellular retinoid binding proteins. II. Their differential pattern of transcription during early morphogenesis in mouse embryos*. Development, 1991. **111**(1): p. 45-60.
216. Dencker, L., E. Annerwall, C. Busch, and U. Eriksson, *Localization of specific retinoid-binding sites and expression of cellular retinoic-acid-binding protein (CRABP) in the early mouse embryo*. Development, 1990. **110**(2): p. 343-52.
217. Dencker, L., A.L. Gustafson, E. Annerwall, C. Busch, and U. Eriksson, *Retinoid-binding*

- proteins in craniofacial development*. J Craniofac Genet Dev Biol, 1991. **11**(4): p. 303-14.
218. Vaessen, M.J., J.H. Meijers, D. Bootsma, and A.G. Van Kessel, *The cellular retinoic-acid-binding protein is expressed in tissues associated with retinoic-acid-induced malformations*. Development, 1990. **110**(2): p. 371-8.
219. Kane, M.A., N. Chen, S. Sparks, and J.L. Napoli, *Quantification of endogenous retinoic acid in limited biological samples by LC/MS/MS*. Biochem J, 2005. **388**(Pt 1): p. 363-9.
220. Morriss-Kay, G., *Retinoic acid and craniofacial development: molecules and morphogenesis*. Bioessays, 1993. **15**(1): p. 9-15.
221. Liu, K.X., Y. Kato, I. Kino, T. Nakamura, and Y. Sugiyama, *Ligand-induced downregulation of receptor-mediated clearance of hepatocyte growth factor in rats*. Am J Physiol, 1998. **275**(5 Pt 1): p. E835-42.
222. Kawamata, J. and S. Shimohama, *Association of novel and established polymorphisms in neuronal nicotinic acetylcholine receptors with sporadic Alzheimer's disease*. J Alzheimers Dis, 2002. **4**(2): p. 71-6.
223. Mitchell, S.J., D.P. McHale, D.A. Campbell, N.J. Lench, R.F. Mueller, S.E. Bunday, and A.F. Markham, *A syndrome of severe mental retardation, spasticity, and tapetoretinal degeneration linked to chromosome 15q24*. Am J Hum Genet, 1998. **62**(5): p. 1070-6.
224. Scott, W.K., E.R. Hauser, D.E. Schmechel, K.A. Welsh-Bohmer, G.W. Small, A.D. Roses, A.M. Saunders, J.R. Gilbert, J.M. Vance, J.L. Haines, and M.A. Pericak-Vance, *Ordered-subsets linkage analysis detects novel Alzheimer disease loci on chromosomes 2q34 and 15q22*. Am J Hum Genet, 2003. **73**(5): p. 1041-51.
225. Blacker, D., L. Bertram, A.J. Saunders, T.J. Moscarillo, M.S. Albert, H. Wiener, R.T. Perry, J.S. Collins, L.E. Harrell, R.C. Go, A. Mahoney, T. Beaty, M.D. Fallin, D. Avramopoulos, G.A. Chase, M.F. Folstein, M.G. McInnis, S.S. Bassett, K.J. Doheny, E.W. Pugh, and R.E. Tanzi, *Results of a high-resolution genome screen of 437 Alzheimer's disease families*. Hum Mol Genet, 2003. **12**(1): p. 23-32.
226. Williamson, T.L. and D.W. Cleveland, *Slowing of axonal transport is a very early event in the toxicity of ALS-linked SOD1 mutants to motor neurons*. Nat Neurosci, 1999. **2**(1): p. 50-6.
227. Sasaki, S., H. Warita, K. Abe, and M. Iwata, *Slow component of axonal transport is impaired in the proximal axon of transgenic mice with a G93A mutant SOD1 gene*. Acta Neuropathol (Berl), 2004. **107**(5): p. 452-60.
228. Shah, J.V. and D.W. Cleveland, *Slow axonal transport: fast motors in the slow lane*. Curr Opin Cell Biol, 2002. **14**(1): p. 58-62.
229. Perez-Olle, R., S.T. Jones, and R.K. Liem, *Phenotypic analysis of neurofilament light gene mutations linked to Charcot-Marie-Tooth disease in cell culture models*. Hum Mol Genet, 2004. **13**(19): p. 2207-20.
230. Gunawardena, S. and L.S. Goldstein, *Disruption of axonal transport and neuronal viability by amyloid precursor protein mutations in Drosophila*. Neuron, 2001. **32**(3): p. 389-401.
231. Kempermann, G., E.J. Chesler, L. Lu, R.W. Williams, and F.H. Gage, *Natural variation and genetic covariance in adult hippocampal neurogenesis*. Proc Natl Acad Sci U S A, 2006. **103**(3): p. 780-5.

232. Jin, K., A.L. Peel, X.O. Mao, L. Xie, B.A. Cottrell, D.C. Henshall, and D.A. Greenberg, *Increased hippocampal neurogenesis in Alzheimer's disease*. Proc Natl Acad Sci U S A, 2004. **101**(1): p. 343-7.
233. Jin, K., M. Minami, J.Q. Lan, X.O. Mao, S. Bateur, R.P. Simon, and D.A. Greenberg, *Neurogenesis in dentate subgranular zone and rostral subventricular zone after focal cerebral ischemia in the rat*. Proc Natl Acad Sci U S A, 2001. **98**(8): p. 4710-5.
234. Jin, K., V. Galvan, L. Xie, X.O. Mao, O.F. Gorostiza, D.E. Bredesen, and D.A. Greenberg, *Enhanced neurogenesis in Alzheimer's disease transgenic (PDGF-APP<sup>Sw,Ind</sup>) mice*. Proc Natl Acad Sci U S A, 2004. **101**(36): p. 13363-7.
235. Verret, L., J.L. Jankowsky, G.M. Xu, D.R. Borchelt, and C. Rampon, *Alzheimer's-type amyloidosis in transgenic mice impairs survival of newborn neurons derived from adult hippocampal neurogenesis*. J Neurosci, 2007. **27**(25): p. 6771-80.
236. Lopez-Toledano, M.A. and M.L. Shelanski, *Neurogenic effect of beta-amyloid peptide in the development of neural stem cells*. J Neurosci, 2004. **24**(23): p. 5439-44.
237. Miloso, M., D. Villa, M. Crimi, S. Galbiati, E. Donzelli, G. Nicolini, and G. Tredici, *Retinoic acid-induced neuritogenesis of human neuroblastoma SH-SY5Y cells is ERK independent and PKC dependent*. J Neurosci Res, 2004. **75**(2): p. 241-52.
238. Prinzen, C., U. Muller, K. Endres, F. Fahrenholz, and R. Postina, *Genomic structure and functional characterization of the human ADAM10 promoter*. Faseb J, 2005. **19**(11): p. 1522-4.
239. Sahin, M., S.B. Karauzum, G. Perry, M.A. Smith, and Y. Aliciguzel, *Retinoic acid isomers protect hippocampal neurons from amyloid-beta induced neurodegeneration*. Neurotox Res, 2005. **7**(3): p. 243-50.
240. Kim, S.K., J.I. Yoo, B.K. Cho, S.J. Hong, Y.K. Kim, J.A. Moon, J.H. Kim, Y.N. Chung, and K.C. Wang, *Elevation of CRABP-I in the cerebrospinal fluid of patients with Moyamoya disease*. Stroke, 2003. **34**(12): p. 2835-41.
241. Balmer, J.E. and R. Blomhoff, *Gene expression regulation by retinoic acid*. J Lipid Res, 2002. **43**(11): p. 1773-808.
242. Kaneda, A., C.J. Wang, R. Cheong, W. Timp, P. Onyango, B. Wen, C.A. Iacobuzio-Donahue, R. Ohlsson, R. Andraos, M.A. Pearson, A.A. Sharov, D.L. Longo, M.S. Ko, A. Levchenko, and A.P. Feinberg, *Enhanced sensitivity to IGF-II signaling links loss of imprinting of IGF2 to increased cell proliferation and tumor risk*. Proc Natl Acad Sci U S A, 2007. **104**(52): p. 20926-31.
243. Soroceanu, L., S. Kharbanda, R. Chen, R.H. Soriano, K. Aldape, A. Misra, J. Zha, W.F. Forrest, J.M. Nigro, Z. Modrusan, B.G. Feuerstein, and H.S. Phillips, *Identification of IGF2 signaling through phosphoinositide-3-kinase regulatory subunit 3 as a growth-promoting axis in glioblastoma*. Proc Natl Acad Sci U S A, 2007. **104**(9): p. 3466-71.
244. Morrison, K.B., C.E. Tognon, M.J. Garnett, C. Deal, and P.H. Sorensen, *ETV6-NTRK3 transformation requires insulin-like growth factor 1 receptor signaling and is associated with constitutive IRS-1 tyrosine phosphorylation*. Oncogene, 2002. **21**(37): p. 5684-95.
245. Scalia, P., E. Heart, L. Comai, R. Vigneri, and C.K. Sung, *Regulation of the Akt/Glycogen synthase kinase-3 axis by insulin-like growth factor-II via activation of the human insulin*

- receptor isoform-A*. J Cell Biochem, 2001. **82**(4): p. 610-8.
246. Dong, G., Z. Chen, Z.Y. Li, N.T. Yeh, C.C. Bancroft, and C. Van Waes, *Hepatocyte growth factor/scatter factor-induced activation of MEK and PI3K signal pathways contributes to expression of proangiogenic cytokines interleukin-8 and vascular endothelial growth factor in head and neck squamous cell carcinoma*. Cancer Res, 2001. **61**(15): p. 5911-8.
247. Fassetta, M., L. D'Alessandro, N. Coltella, M.F. Di Renzo, and A. Rasola, *Hepatocyte growth factor installs a survival platform for colorectal cancer cell invasive growth and overcomes p38 MAPK-mediated apoptosis*. Cell Signal, 2006. **18**(11): p. 1967-76.
248. Uruno, A., A. Sugawara, H. Kanatsuka, S. Arima, Y. Taniyama, M. Kudo, K. Takeuchi, and S. Ito, *Hepatocyte growth factor stimulates nitric oxide production through endothelial nitric oxide synthase activation by the phosphoinositide 3-kinase/Akt pathway and possibly by mitogen-activated protein kinase kinase in vascular endothelial cells*. Hypertens Res, 2004. **27**(11): p. 887-95.
249. Okano, J., G. Shiota, K. Matsumoto, S. Yasui, A. Kurimasa, I. Hisatome, P. Steinberg, and Y. Murawaki, *Hepatocyte growth factor exerts a proliferative effect on oval cells through the PI3K/AKT signaling pathway*. Biochem Biophys Res Commun, 2003. **309**(2): p. 298-304.
250. Su, C.C., Y.P. Lin, Y.J. Cheng, J.Y. Huang, W.J. Chuang, Y.S. Shan, and B.C. Yang, *Phosphatidylinositol 3-kinase/Akt activation by integrin-tumor matrix interaction suppresses Fas-mediated apoptosis in T cells*. J Immunol, 2007. **179**(7): p. 4589-97.
251. Chung, J., R.E. Bachelder, E.A. Lipscomb, L.M. Shaw, and A.M. Mercurio, *Integrin (alpha 6 beta 4) regulation of eIF-4E activity and VEGF translation: a survival mechanism for carcinoma cells*. J Cell Biol, 2002. **158**(1): p. 165-74.
252. Krywicki, R.F. and D. Yee, *The insulin-like growth factor family of ligands, receptors, and binding proteins*. Breast Cancer Res Treat, 1992. **22**(1): p. 7-19.
253. Blanco-Aparicio, C., O. Renner, J.F. Leal, and A. Carnero, *PTEN, more than the AKT pathway*. Carcinogenesis, 2007. **28**(7): p. 1379-86.
254. Delgado-Esteban, M., D. Martin-Zanca, L. Andres-Martin, A. Almeida, and J.P. Bolanos, *Inhibition of PTEN by peroxynitrite activates the phosphoinositide-3-kinase/Akt neuroprotective signaling pathway*. J Neurochem, 2007. **102**(1): p. 194-205.
255. Mizuno, M., K. Yamada, N. Takei, M.H. Tran, J. He, A. Nakajima, H. Nawa, and T. Nabeshima, *Phosphatidylinositol 3-kinase: a molecule mediating BDNF-dependent spatial memory formation*. Mol Psychiatry, 2003. **8**(2): p. 217-24.
256. Pearse, R.N., S.L. Swendeman, Y. Li, D. Rafii, and B.L. Hempstead, *A neurotrophin axis in myeloma: TrkB and BDNF promote tumor-cell survival*. Blood, 2005. **105**(11): p. 4429-36.
257. Fryer, R.H., D.R. Kaplan, and L.F. Kromer, *Truncated trkB receptors on nonneuronal cells inhibit BDNF-induced neurite outgrowth in vitro*. Exp Neurol, 1997. **148**(2): p. 616-27.
258. Kajimura, S., K. Aida, and C. Duan, *Insulin-like growth factor-binding protein-1 (IGFBP-1) mediates hypoxia-induced embryonic growth and developmental retardation*. Proc Natl Acad Sci U S A, 2005. **102**(4): p. 1240-5.
259. Popovici, R.M., M. Lu, S. Bhatia, G.H. Faessen, A.J. Giaccia, and L.C. Giudice, *Hypoxia regulates insulin-like growth factor-binding protein 1 in human fetal hepatocytes in primary*

- culture: suggestive molecular mechanisms for in utero fetal growth restriction caused by uteroplacental insufficiency.* J Clin Endocrinol Metab, 2001. **86**(6): p. 2653-9.
260. Dansithong, W., S. Paul, L. Comai, and S. Reddy, *MBNL1 is the primary determinant of focus formation and aberrant insulin receptor splicing in DM1.* J Biol Chem, 2005. **280**(7): p. 5773-80.
261. Barreca, A., M. Bozzola, A. Cesarone, P.H. Steenbergh, P.E. Holthuisen, F. Severi, G. Giordano, and F. Minuto, *Short stature associated with high circulating insulin-like growth factor (IGF)-binding protein-1 and low circulating IGF-II: effect of growth hormone therapy.* J Clin Endocrinol Metab, 1998. **83**(10): p. 3534-41.
262. Vu, T.H., T. Li, D. Nguyen, B.T. Nguyen, X.M. Yao, J.F. Hu, and A.R. Hoffman, *Symmetric and asymmetric DNA methylation in the human IGF2-H19 imprinted region.* Genomics, 2000. **64**(2): p. 132-43.
263. Sasaki, H., K. Ishihara, and R. Kato, *Mechanisms of Igf2/H19 imprinting: DNA methylation, chromatin and long-distance gene regulation.* J Biochem (Tokyo), 2000. **127**(5): p. 711-5.
264. Murrell, A., S. Heeson, and W. Reik, *Interaction between differentially methylated regions partitions the imprinted genes Igf2 and H19 into parent-specific chromatin loops.* Nat Genet, 2004. **36**(8): p. 889-93.
265. Mutter, G.L., C.L. Stewart, M.L. Chaponot, and R.J. Pomponio, *Oppositely imprinted genes H19 and insulin-like growth factor 2 are coexpressed in human androgenetic trophoblast.* Am J Hum Genet, 1993. **53**(5): p. 1096-102.
266. Leighton, P.A., R.S. Ingram, J. Eggenschwiler, A. Efstratiadis, and S.M. Tilghman, *Disruption of imprinting caused by deletion of the H19 gene region in mice.* Nature, 1995. **375**(6526): p. 34-9.
267. Pfeifer, K., P.A. Leighton, and S.M. Tilghman, *The structural H19 gene is required for transgene imprinting.* Proc Natl Acad Sci U S A, 1996. **93**(24): p. 13876-83.
268. Zhao, Z., G. Tavoosidana, M. Sjolinder, A. Gondor, P. Mariano, S. Wang, C. Kanduri, M. Lezcano, K.S. Sandhu, U. Singh, V. Pant, V. Tiwari, S. Kurukuti, and R. Ohlsson, *Circular chromosome conformation capture (4C) uncovers extensive networks of epigenetically regulated intra- and interchromosomal interactions.* Nat Genet, 2006. **38**(11): p. 1341-7.
269. Hatada, I. and T. Mukai, *Genomic imprinting of p57KIP2, a cyclin-dependent kinase inhibitor, in mouse.* Nat Genet, 1995. **11**(2): p. 204-6.
270. Matsuoka, S., J.S. Thompson, M.C. Edwards, J.M. Bartletta, P. Grundy, L.M. Kalikin, J.W. Harper, S.J. Elledge, and A.P. Feinberg, *Imprinting of the gene encoding a human cyclin-dependent kinase inhibitor, p57KIP2, on chromosome 11p15.* Proc Natl Acad Sci U S A, 1996. **93**(7): p. 3026-30.
271. Du, M., L.G. Beatty, W. Zhou, J. Lew, C. Schoenherr, R. Weksberg, and P.D. Sadowski, *Insulator and silencer sequences in the imprinted region of human chromosome 11p15.5.* Hum Mol Genet, 2003. **12**(15): p. 1927-39.
272. Scandura, J.M., P. Boccuni, J. Massague, and S.D. Nimer, *Transforming growth factor beta-induced cell cycle arrest of human hematopoietic cells requires p57KIP2 up-regulation.* Proc Natl Acad Sci U S A, 2004. **101**(42): p. 15231-6.

273. Ninkina, N., J. Adu, A. Fischer, L.G. Pinon, V.L. Buchman, and A.M. Davies, *Expression and function of TrkB variants in developing sensory neurons*. *Embo J*, 1996. **15**(23): p. 6385-93.
274. Ferrer, I., C. Marin, M.J. Rey, T. Ribalta, E. Goutan, R. Blanco, E. Tolosa, and E. Marti, *BDNF and full-length and truncated TrkB expression in Alzheimer disease. Implications in therapeutic strategies*. *J Neuropathol Exp Neurol*, 1999. **58**(7): p. 729-39.
275. Danzer, S.C., X. He, and J.O. McNamara, *Ontogeny of seizure-induced increases in BDNF immunoreactivity and TrkB receptor activation in rat hippocampus*. *Hippocampus*, 2004. **14**(3): p. 345-55.
276. Dugich-Djordjevic, M.M., F. Ohsawa, T. Okazaki, N. Mori, J.R. Day, K.D. Beck, and F. Hefti, *Differential regulation of catalytic and non-catalytic trkB messenger RNAs in the rat hippocampus following seizures induced by systemic administration of kainate*. *Neuroscience*, 1995. **66**(4): p. 861-77.
277. Eide, F.F., E.R. Vining, B.L. Eide, K. Zang, X.Y. Wang, and L.F. Reichardt, *Naturally occurring truncated trkB receptors have dominant inhibitory effects on brain-derived neurotrophic factor signaling*. *J Neurosci*, 1996. **16**(10): p. 3123-9.
278. Luikart, B.W., S. Nef, T. Shipman, and L.F. Parada, *In vivo role of truncated trkb receptors during sensory ganglion neurogenesis*. *Neuroscience*, 2003. **117**(4): p. 847-58.
279. Rex, C.S., C.Y. Lin, E.A. Kramar, L.Y. Chen, C.M. Gall, and G. Lynch, *Brain-derived neurotrophic factor promotes long-term potentiation-related cytoskeletal changes in adult hippocampus*. *J Neurosci*, 2007. **27**(11): p. 3017-29.
280. Santi, S., S. Cappello, M. Riccio, M. Bergami, G. Aicardi, U. Schenk, M. Matteoli, and M. Canossa, *Hippocampal neurons recycle BDNF for activity-dependent secretion and LTP maintenance*. *Embo J*, 2006. **25**(18): p. 4372-80.
281. Gooney, M., E. Messaoudi, F.O. Maher, C.R. Bramham, and M.A. Lynch, *BDNF-induced LTP in dentate gyrus is impaired with age: analysis of changes in cell signaling events*. *Neurobiol Aging*, 2004. **25**(10): p. 1323-31.
282. White, A.R., G. Multhaup, F. Maher, S. Bellingham, J. Camakaris, H. Zheng, A.I. Bush, K. Beyreuther, C.L. Masters, and R. Cappai, *The Alzheimer's disease amyloid precursor protein modulates copper-induced toxicity and oxidative stress in primary neuronal cultures*. *J Neurosci*, 1999. **19**(21): p. 9170-9.
283. Huang, X., M.P. Cuajungco, C.S. Atwood, M.A. Hartshorn, J.D. Tyndall, G.R. Hanson, K.C. Stokes, M. Leopold, G. Multhaup, L.E. Goldstein, R.C. Scarpa, A.J. Saunders, J. Lim, R.D. Moir, C. Glabe, E.F. Bowden, C.L. Masters, D.P. Fairlie, R.E. Tanzi, and A.I. Bush, *Cu(II) potentiation of alzheimer abeta neurotoxicity. Correlation with cell-free hydrogen peroxide production and metal reduction*. *J Biol Chem*, 1999. **274**(52): p. 37111-6.
284. Huang, X., C.S. Atwood, M.A. Hartshorn, G. Multhaup, L.E. Goldstein, R.C. Scarpa, M.P. Cuajungco, D.N. Gray, J. Lim, R.D. Moir, R.E. Tanzi, and A.I. Bush, *The A beta peptide of Alzheimer's disease directly produces hydrogen peroxide through metal ion reduction*. *Biochemistry*, 1999. **38**(24): p. 7609-16.
285. La Fontaine, S. and J.F. Mercer, *Trafficking of the copper-ATPases, ATP7A and ATP7B: role in copper homeostasis*. *Arch Biochem Biophys*, 2007. **463**(2): p. 149-67.

286. El Meskini, R., K.L. Crabtree, L.B. Cline, R.E. Mains, B.A. Eipper, and G.V. Ronnett, *ATP7A (Menkes protein) functions in axonal targeting and synaptogenesis*. Mol Cell Neurosci, 2007. **34**(3): p. 409-21.
287. Lutsenko, S., E.S. LeShane, and U. Shinde, *Biochemical basis of regulation of human copper-transporting ATPases*. Arch Biochem Biophys, 2007. **463**(2): p. 134-48.
288. Deibel, M.A., W.D. Ehmann, and W.R. Markesbery, *Copper, iron, and zinc imbalances in severely degenerated brain regions in Alzheimer's disease: possible relation to oxidative stress*. J Neurol Sci, 1996. **143**(1-2): p. 137-42.
289. White, A.R., R. Reyes, J.F. Mercer, J. Camakaris, H. Zheng, A.I. Bush, G. Multhaup, K. Beyreuther, C.L. Masters, and R. Cappai, *Copper levels are increased in the cerebral cortex and liver of APP and APLP2 knockout mice*. Brain Res, 1999. **842**(2): p. 439-44.
290. Bellingham, S.A., G.D. Ciccotosto, B.E. Needham, L.R. Fodero, A.R. White, C.L. Masters, R. Cappai, and J. Camakaris, *Gene knockout of amyloid precursor protein and amyloid precursor-like protein-2 increases cellular copper levels in primary mouse cortical neurons and embryonic fibroblasts*. J Neurochem, 2004. **91**(2): p. 423-8.
291. Koo, B.H., J.M. Longpre, R.P. Somerville, J.P. Alexander, R. Leduc, and S.S. Apte, *Regulation of ADAMTS9 secretion and enzymatic activity by its propeptide*. J Biol Chem, 2007. **282**(22): p. 16146-54.
292. Koo, B.H., J.M. Longpre, R.P. Somerville, J.P. Alexander, R. Leduc, and S.S. Apte, *Cell-surface processing of pro-ADAMTS9 by furin*. J Biol Chem, 2006. **281**(18): p. 12485-94.
293. Schulz, I., U. Zeitschel, T. Rudolph, D. Ruiz-Carrillo, J.U. Rahfeld, B. Gerhartz, V. Bigl, H.U. Demuth, and S. Rossner, *Subcellular localization suggests novel functions for prolyl endopeptidase in protein secretion*. J Neurochem, 2005. **94**(4): p. 970-9.
294. Rossner, S., I. Schulz, U. Zeitschel, R. Schliebs, V. Bigl, and H.U. Demuth, *Brain prolyl endopeptidase expression in aging, APP transgenic mice and Alzheimer's disease*. Neurochem Res, 2005. **30**(6-7): p. 695-702.
295. Le Goff, C., R.P. Somerville, F. Kesteloot, K. Powell, D.E. Birk, A.C. Colige, and S.S. Apte, *Regulation of procollagen amino-propeptide processing during mouse embryogenesis by specialization of homologous ADAMTS proteases: insights on collagen biosynthesis and dermatosparaxis*. Development, 2006. **133**(8): p. 1587-96.
296. Godde, N.J., G.M. D'Abaco, L. Paradiso, and U. Novak, *Efficient ADAM22 surface expression is mediated by phosphorylation-dependent interaction with 14-3-3 protein family members*. J Cell Sci, 2006. **119**(Pt 16): p. 3296-305.
297. Molinari, F., V. Meskanaite, A. Munnich, P. Sonderegger, and L. Colleaux, *Extracellular proteases and their inhibitors in genetic diseases of the central nervous system*. Hum Mol Genet, 2003. **12 Spec No 2**: p. R195-200.
298. Papassotiropoulos, A., M. Bagli, A. Kurz, J. Kornhuber, H. Forstl, W. Maier, J. Pauls, N. Lautenschlager, and R. Heun, *A genetic variation of cathepsin D is a major risk factor for Alzheimer's disease*. Ann Neurol, 2000. **47**(3): p. 399-403.
299. Eckman, E.A., M. Watson, L. Marlow, K. Sambamurti, and C.B. Eckman, *Alzheimer's disease beta-amyloid peptide is increased in mice deficient in endothelin-converting enzyme*. J Biol

- Chem, 2003. **278**(4): p. 2081-4.
300. Obholz, K.L., A. Akopyan, K.G. Waymire, and G.R. MacGregor, *FNDC3A is required for adhesion between spermatids and Sertoli cells*. Dev Biol, 2006. **298**(2): p. 498-513.
301. Li, X.F., G. Thinakaran, S.S. Sisodia, and F.S. Yu, *Amyloid precursor-like protein 2 promotes cell migration toward fibronectin and collagen IV*. J Biol Chem, 1999. **274**(38): p. 27249-56.
302. Botella-Lopez, A., F. Burgaya, R. Gavin, M.S. Garcia-Ayllon, E. Gomez-Tortosa, J. Pena-Casanova, J.M. Urena, J.A. Del Rio, R. Blesa, E. Soriano, and J. Saez-Valero, *Reelin expression and glycosylation patterns are altered in Alzheimer's disease*. Proc Natl Acad Sci U S A, 2006. **103**(14): p. 5573-8.
303. D'Arcangelo, G., G.G. Miao, S.C. Chen, H.D. Soares, J.I. Morgan, and T. Curran, *A protein related to extracellular matrix proteins deleted in the mouse mutant reeler*. Nature, 1995. **374**(6524): p. 719-23.
304. Quattrocchi, C.C., F. Wannenes, A.M. Persico, S.A. Ciafre, G. D'Arcangelo, M.G. Farace, and F. Keller, *Reelin is a serine protease of the extracellular matrix*. J Biol Chem, 2002. **277**(1): p. 303-9.
305. Trommsdorff, M., M. Gotthardt, T. Hiesberger, J. Shelton, W. Stockinger, J. Nimpf, R.E. Hammer, J.A. Richardson, and J. Herz, *Reeler/Disabled-like disruption of neuronal migration in knockout mice lacking the VLDL receptor and ApoE receptor 2*. Cell, 1999. **97**(6): p. 689-701.
306. Hiesberger, T., M. Trommsdorff, B.W. Howell, A. Goffinet, M.C. Mumby, J.A. Cooper, and J. Herz, *Direct binding of Reelin to VLDL receptor and ApoE receptor 2 induces tyrosine phosphorylation of disabled-1 and modulates tau phosphorylation*. Neuron, 1999. **24**(2): p. 481-9.
307. He, X., K. Cooley, C.H. Chung, N. Dashti, and J. Tang, *Apolipoprotein receptor 2 and X11 alpha/beta mediate apolipoprotein E-induced endocytosis of amyloid-beta precursor protein and beta-secretase, leading to amyloid-beta production*. J Neurosci, 2007. **27**(15): p. 4052-60.
308. Narindrasorasak, S., R.A. Altman, P. Gonzalez-DeWhitt, B.D. Greenberg, and R. Kisilevsky, *An interaction between basement membrane and Alzheimer amyloid precursor proteins suggests a role in the pathogenesis of Alzheimer's disease*. Lab Invest, 1995. **72**(3): p. 272-82.
309. Sawtell, N.M. and J.L. Lessard, *Cellular distribution of smooth muscle actins during mammalian embryogenesis: expression of the alpha-vascular but not the gamma-enteric isoform in differentiating striated myocytes*. J Cell Biol, 1989. **109**(6 Pt 1): p. 2929-37.
310. Yamada, H., M. Akishita, M. Ito, K. Tamura, L. Daviet, J.Y. Lehtonen, V.J. Dzau, and M. Horiuchi, *AT2 receptor and vascular smooth muscle cell differentiation in vascular development*. Hypertension, 1999. **33**(6): p. 1414-9.
311. Guo, D.C., H. Pannu, V. Tran-Fadulu, C.L. Papke, R.K. Yu, N. Avidan, S. Bourgeois, A.L. Estrera, H.J. Safi, E. Sparks, D. Amor, L. Ades, V. McConnell, C.E. Willoughby, D. Abuelo, M. Willing, R.A. Lewis, D.H. Kim, S. Scherer, P.P. Tung, C. Ahn, L.M. Buja, C.S. Raman, S.S. Shete, and D.M. Milewicz, *Mutations in smooth muscle alpha-actin (ACTA2) lead to thoracic aortic aneurysms and dissections*. Nat Genet, 2007. **39**(12): p. 1488-93.

312. Schildmeyer, L.A., R. Braun, G. Taffet, M. DeBiasi, A.E. Burns, A. Bradley, and R.J. Schwartz, *Impaired vascular contractility and blood pressure homeostasis in the smooth muscle alpha-actin null mouse*. *Faseb J*, 2000. **14**(14): p. 2213-20.
313. Aoyagi, T., T. Wada, F. Kojima, M. Nagai, S. Harada, T. Takeuchi, K. Isse, M. Ogura, M. Hamamoto, K. Tanaka, and et al., *Deficiency of fibrinolytic enzyme activities in the serum of patients with Alzheimer-type dementia*. *Experientia*, 1992. **48**(7): p. 656-9.
314. Kalaria, R.N., T. Golde, S.N. Kroon, and G. Perry, *Serine protease inhibitor antithrombin III and its messenger RNA in the pathogenesis of Alzheimer's disease*. *Am J Pathol*, 1993. **143**(3): p. 886-93.
315. Siiteri, J.E., R. Koistinen, H.T. Salem, H. Bohn, and M. Seppala, *Placental protein 5 is related to blood coagulation and fibrinolytic systems*. *Life Sci*, 1982. **30**(22): p. 1885-91.
316. Butzow, R., M.L. Huhtala, H. Bohn, I. Virtanen, and M. Seppala, *Purification and characterization of placental protein 5*. *Biochem Biophys Res Commun*, 1988. **150**(1): p. 483-90.
317. Miyagi, Y., H. Yasumitsu, H. Mizushima, N. Koshikawa, Y. Matsuda, H. Itoh, T.A. Hori, I. Aoki, K. Misugi, and K. Miyazaki, *Cloning of the cDNA encoding mouse PP5/TFPI-2 and mapping of the gene to chromosome 6*. *DNA Cell Biol*, 1996. **15**(11): p. 947-54.
318. Carter, R.E., K.M. Cerosaletti, D.J. Burkin, R.E. Fournier, C. Jones, B.D. Greenberg, B.A. Citron, and B.W. Festoff, *The gene for the serpin thrombin inhibitor (PI7), protease nexin I, is located on human chromosome 2q33-q35 and on syntenic regions in the mouse and sheep genomes*. *Genomics*, 1995. **27**(1): p. 196-9.
319. Kim, J.A., N.D. Tran, Z. Li, F. Yang, W. Zhou, and M.J. Fisher, *Brain endothelial hemostasis regulation by pericytes*. *J Cereb Blood Flow Metab*, 2006. **26**(2): p. 209-17.
320. Donovan, F.M., P.J. Vaughan, and D.D. Cunningham, *Regulation of protease nexin-1 target protease specificity by collagen type IV*. *J Biol Chem*, 1994. **269**(25): p. 17199-205.
321. Enghild, J.J., I.B. Thogersen, T.D. Oury, Z. Valnickova, P. Hojrup, and J.D. Crapo, *The heparin-binding domain of extracellular superoxide dismutase is proteolytically processed intracellularly during biosynthesis*. *J Biol Chem*, 1999. **274**(21): p. 14818-22.
322. Pietrapiana, D., M. Sala, M. Prat, and F. Sinigaglia, *Met identification on human platelets: role of hepatocyte growth factor in the modulation of platelet activation*. *FEBS Lett*, 2005. **579**(20): p. 4550-4.
323. Skovronsky, D.M., V.M. Lee, and D. Pratico, *Amyloid precursor protein and amyloid beta peptide in human platelets. Role of cyclooxygenase and protein kinase C*. *J Biol Chem*, 2001. **276**(20): p. 17036-43.
324. Henry, A., Q.X. Li, D. Galatis, L. Hesse, G. Multhaup, K. Beyreuther, C.L. Masters, and R. Cappai, *Inhibition of platelet activation by the Alzheimer's disease amyloid precursor protein*. *Br J Haematol*, 1998. **103**(2): p. 402-15.
325. Smith, R.P., D.A. Higuchi, and G.J. Broze, Jr., *Platelet coagulation factor XIa-inhibitor, a form of Alzheimer amyloid precursor protein*. *Science*, 1990. **248**(4959): p. 1126-8.
326. Oltersdorf, T., L.C. Fritz, D.B. Schenk, I. Lieberburg, K.L. Johnson-Wood, E.C. Beattie, P.J. Ward, R.W. Blacher, H.F. Dovey, and S. Sinha, *The secreted form of the Alzheimer's amyloid*

- precursor protein with the Kunitz domain is protease nexin-II*. Nature, 1989. **341**(6238): p. 144-7.
327. De Meyer, G.R., D.M. De Cleen, S. Cooper, M.W. Knaapen, D.M. Jans, W. Martinet, A.G. Herman, H. Bult, and M.M. Kockx, *Platelet phagocytosis and processing of beta-amyloid precursor protein as a mechanism of macrophage activation in atherosclerosis*. Circ Res, 2002. **90**(11): p. 1197-204.
328. Song, W.J., S.H. Chung, and D.M. Kurnit, *The murine Dyrk protein maps to chromosome 16, localizes to the nucleus, and can form multimers*. Biochem Biophys Res Commun, 1997. **231**(3): p. 640-4.
329. Becker, W. and H.G. Joost, *Structural and functional characteristics of Dyrk, a novel subfamily of protein kinases with dual specificity*. Prog Nucleic Acid Res Mol Biol, 1999. **62**: p. 1-17.
330. Altafaj, X., M. Dierssen, C. Baamonde, E. Marti, J. Visa, J. Guimera, M. Oset, J.R. Gonzalez, J. Florez, C. Fillat, and X. Estivill, *Neurodevelopmental delay, motor abnormalities and cognitive deficits in transgenic mice overexpressing Dyrk1A (minibrain), a murine model of Down's syndrome*. Hum Mol Genet, 2001. **10**(18): p. 1915-23.
331. Bigl, M., M.K. Bruckner, T. Arendt, V. Bigl, and K. Eschrich, *Activities of key glycolytic enzymes in the brains of patients with Alzheimer's disease*. J Neural Transm, 1999. **106**(5-6): p. 499-511.
332. Bigl, M., A.D. Bleyl, D. Zedlick, T. Arendt, V. Bigl, and K. Eschrich, *Changes of activity and isozyme pattern of phosphofructokinase in the brains of patients with Alzheimer's disease*. J Neurochem, 1996. **67**(3): p. 1164-71.
333. Bigl, M., J. Apelt, K. Eschrich, and R. Schliebs, *Cortical glucose metabolism is altered in aged transgenic Tg2576 mice that demonstrate Alzheimer plaque pathology*. J Neural Transm, 2003. **110**(1): p. 77-94.
334. Deak, M., A.D. Clifton, L.M. Lucocq, and D.R. Alessi, *Mitogen- and stress-activated protein kinase-1 (MSK1) is directly activated by MAPK and SAPK2/p38, and may mediate activation of CREB*. Embo J, 1998. **17**(15): p. 4426-41.
335. Herrup, K. and T. Arendt, *Re-expression of cell cycle proteins induces neuronal cell death during Alzheimer's disease*. J Alzheimers Dis, 2002. **4**(3): p. 243-7.
336. Kuan, C.Y., A.J. Schloemer, A. Lu, K.A. Burns, W.L. Weng, M.T. Williams, K.I. Strauss, C.V. Vorhees, R.A. Flavell, R.J. Davis, F.R. Sharp, and P. Rakic, *Hypoxia-ischemia induces DNA synthesis without cell proliferation in dying neurons in adult rodent brain*. J Neurosci, 2004. **24**(47): p. 10763-72.
337. Wen, Y., S. Yang, R. Liu, A.M. Brun-Zinkernagel, P. Koulen, and J.W. Simpkins, *Transient cerebral ischemia induces aberrant neuronal cell cycle re-entry and Alzheimer's disease-like tauopathy in female rats*. J Biol Chem, 2004. **279**(21): p. 22684-92.
338. Lin, P.T., J.G. Gleeson, J.C. Corbo, L. Flanagan, and C.A. Walsh, *DCAMKL1 encodes a protein kinase with homology to doublecortin that regulates microtubule polymerization*. J Neurosci, 2000. **20**(24): p. 9152-61.
339. Silverman, M.A., O. Benard, H. Jaaro, A. Rattner, Y. Citri, and R. Seger, *CPG16, a novel protein serine/threonine kinase downstream of cAMP-dependent protein kinase*. J Biol Chem,

1999. **274**(5): p. 2631-6.
340. Sontag, E., *Protein phosphatase 2A: the Trojan Horse of cellular signaling*. Cell Signal, 2001. **13**(1): p. 7-16.
341. Chao, Y., Y. Xing, Y. Chen, Y. Xu, Z. Lin, Z. Li, P.D. Jeffrey, J.B. Stock, and Y. Shi, *Structure and mechanism of the phosphotyrosyl phosphatase activator*. Mol Cell, 2006. **23**(4): p. 535-46.
342. Magnúsdóttir, A., P. Stenmark, S. Flodin, T. Nyman, M. Hammarström, M. Ehn, H.M. Bakali, H. Berglund, and P. Nordlund, *The crystal structure of a human PP2A phosphatase activator reveals a novel fold and highly conserved cleft implicated in protein-protein interactions*. J Biol Chem, 2006. **281**(32): p. 22434-8.
343. Jordens, J., V. Janssens, S. Longin, I. Stevens, E. Martens, G. Bultynck, Y. Engelborghs, E. Lescrinier, E. Waelkens, J. Goris, and C. Van Hoof, *The protein phosphatase 2A phosphatase activator is a novel peptidyl-prolyl cis/trans-isomerase*. J Biol Chem, 2006. **281**(10): p. 6349-57.
344. Hu, P., L. Yu, M. Zhang, L. Zheng, Y. Zhao, Q. Fu, and S. Zhao, *Molecular cloning and mapping of the brain-abundant B1gamma subunit of protein phosphatase 2A, PPP2R2C, to human chromosome 4p16*. Genomics, 2000. **67**(1): p. 83-6.
345. Neumann, S., S. Schobel, S. Jäger, A. Trautwein, C. Haass, C.U. Pietrzik, and S.F. Lichtenthaler, *Amyloid precursor-like protein 1 influences endocytosis and proteolytic processing of the amyloid precursor protein*. J Biol Chem, 2006. **281**(11): p. 7583-94.
346. Weber, B., C. Schaper, J. Scholz, B. Bein, C. Rodde, and H.T. P., *Interaction of the amyloid precursor like protein 1 with the alpha2A-adrenergic receptor increases agonist-mediated inhibition of adenylate cyclase*. Cell Signal, 2006. **18**(10): p. 1748-57.
347. Eggert, S., K. Paliga, P. Soba, G. Evin, C.L. Masters, A. Weidemann, and K. Beyreuther, *The proteolytic processing of the amyloid precursor protein gene family members APLP-1 and APLP-2 involves alpha-, beta-, gamma-, and epsilon-like cleavages: modulation of APLP-1 processing by n-glycosylation*. J Biol Chem, 2004. **279**(18): p. 18146-56.
348. Xu, Y., H.S. Kim, Y. Joo, Y. Choi, K.A. Chang, C.H. Park, K.Y. Shin, S. Kim, Y.H. Cheon, T.K. Baik, J.H. Kim, and Y.H. Suh, *Intracellular domains of amyloid precursor-like protein 2 interact with CP2 transcription factor in the nucleus and induce glycogen synthase kinase-3beta expression*. Cell Death Differ, 2007. **14**(1): p. 79-91.
349. Maloney, B., Y.W. Ge, N. Greig, and D.K. Lahiri, *Presence of a "CAGA box" in the APP gene unique to amyloid plaque-forming species and absent in all APLP-1/2 genes: implications in Alzheimer's disease*. Faseb J, 2004. **18**(11): p. 1288-90.
350. Siemes, C., T. Quast, C. Kummer, S. Wehner, G. Kirfel, U. Müller, and V. Herzog, *Keratinocytes from APP/APLP2-deficient mice are impaired in proliferation, adhesion and migration in vitro*. Exp Cell Res, 2006. **312**(11): p. 1939-49.
351. Araki, W. and R.J. Wurtman, *Increased expression of amyloid precursor protein and amyloid precursor-like protein 2 during trophic factor withdrawal-induced death of neuronal PC12 cells*. Brain Res Mol Brain Res, 1998. **56**(1-2): p. 169-77.
352. Cappai, R., F. Cheng, G.D. Ciccotosto, B.E. Needham, C.L. Masters, G. Multhaup, L.A.

- Fransson, and K. Mani, *The amyloid precursor protein (APP) of Alzheimer disease and its paralog, APLP2, modulate the Cu/Zn-Nitric Oxide-catalyzed degradation of glypican-1 heparan sulfate in vivo*. J Biol Chem, 2005. **280**(14): p. 13913-20.
353. Hoyer, S. and R. Nitsch, *Cerebral excess release of neurotransmitter amino acids subsequent to reduced cerebral glucose metabolism in early-onset dementia of Alzheimer type*. J Neural Transm, 1989. **75**(3): p. 227-32.
354. Canning, D.R., R.J. McKeon, D.A. DeWitt, G. Perry, J.R. Wujek, R.C. Frederickson, and J. Silver, *beta-Amyloid of Alzheimer's disease induces reactive gliosis that inhibits axonal outgrowth*. Exp Neurol, 1993. **124**(2): p. 289-98.
355. Scheff, S., *Reactive synaptogenesis in aging and Alzheimer's disease: lessons learned in the Cotman laboratory*. Neurochem Res, 2003. **28**(11): p. 1625-30.
356. Kenwrick, S., A. Watkins, and E. De Angelis, *Neural cell recognition molecule L1: relating biological complexity to human disease mutations*. Hum Mol Genet, 2000. **9**(6): p. 879-86.
357. Good, P.F., D. Alapat, A. Hsu, C. Chu, D. Perl, X. Wen, D.E. Burstein, and D.S. Kohtz, *A role for semaphorin 3A signaling in the degeneration of hippocampal neurons during Alzheimer's disease*. J Neurochem, 2004. **91**(3): p. 716-36.
358. Polleux, F., T. Morrow, and A. Ghosh, *Semaphorin 3A is a chemoattractant for cortical apical dendrites*. Nature, 2000. **404**(6778): p. 567-73.
359. Marin, O., A. Yaron, A. Bagri, M. Tessier-Lavigne, and J.L. Rubenstein, *Sorting of striatal and cortical interneurons regulated by semaphorin-neuropilin interactions*. Science, 2001. **293**(5531): p. 872-5.
360. de la Monte, S.M., S.C. Ng, and D.W. Hsu, *Aberrant GAP-43 gene expression in Alzheimer's disease*. Am J Pathol, 1995. **147**(4): p. 934-46.
361. Mi, R., W. Chen, and A. Hoke, *Pleiotrophin is a neurotrophic factor for spinal motor neurons*. Proc Natl Acad Sci U S A, 2007. **104**(11): p. 4664-9.
362. van der Voort, R., T.E. Taher, V.J. Wielenga, M. Spaargaren, R. Prevo, L. Smit, G. David, G. Hartmann, E. Gherardi, and S.T. Pals, *Heparan sulfate-modified CD44 promotes hepatocyte growth factor/scatter factor-induced signal transduction through the receptor tyrosine kinase c-Met*. J Biol Chem, 1999. **274**(10): p. 6499-506.
363. Ried, S., C. Jager, M. Jeffers, G.F. Vande Woude, H. Graeff, M. Schmitt, and E. Lengyel, *Activation mechanisms of the urokinase-type plasminogen activator promoter by hepatocyte growth factor/scatter factor*. J Biol Chem, 1999. **274**(23): p. 16377-86.
364. Delehedde, M., N. Sergeant, M. Lyon, P.S. Rudland, and D.G. Fernig, *Hepatocyte growth factor/scatter factor stimulates migration of rat mammary fibroblasts through both mitogen-activated protein kinase and phosphatidylinositol 3-kinase/Akt pathways*. Eur J Biochem, 2001. **268**(16): p. 4423-9.
365. Naim, R., R.C. Chang, S.S. Alfano, F. Riedel, C. Bayerl, H. Sadick, G. Bran, and K. Hormann, *Targeting TGF-beta1 increases hepatocyte growth factor (HGF/SF) levels in external auditory canal cholesteatoma (EACC) epithelial cell culture*. Regul Pept, 2005. **130**(1-2): p. 75-80.
366. Gutierrez, H., X. Dolcet, M. Tolcos, and A. Davies, *HGF regulates the development of cortical pyramidal dendrites*. Development, 2004. **131**(15): p. 3717-26.

367. Korhonen, L., U. Sjöholm, N. Takei, M.A. Kern, P. Schirmacher, E. Castren, and D. Lindholm, *Expression of c-Met in developing rat hippocampus: evidence for HGF as a neurotrophic factor for calbindin D-expressing neurons*. Eur J Neurosci, 2000. **12**(10): p. 3453-61.
368. Adlerz, L., M. Beckman, S. Holback, R. Tehranian, V. Cortes Toro, and K. Iverfeldt, *Accumulation of the amyloid precursor-like protein APLP2 and reduction of APLP1 in retinoic acid-differentiated human neuroblastoma cells upon curcumin-induced neurite retraction*. Brain Res Mol Brain Res, 2003. **119**(1): p. 62-72.
369. Kim, T.A., J. Lim, S. Ota, S. Raja, R. Rogers, B. Rivnay, H. Avraham, and S. Avraham, *NRP/B, a novel nuclear matrix protein, associates with p110(RB) and is involved in neuronal differentiation*. J Cell Biol, 1998. **141**(3): p. 553-66.
370. Greengard, P., F. Valtorta, A.J. Czernik, and F. Benfenati, *Synaptic vesicle phosphoproteins and regulation of synaptic function*. Science, 1993. **259**(5096): p. 780-5.
371. Mirnics, K., F.A. Middleton, A. Marquez, D.A. Lewis, and P. Levitt, *Molecular characterization of schizophrenia viewed by microarray analysis of gene expression in prefrontal cortex*. Neuron, 2000. **28**(1): p. 53-67.
372. Ho, L., Y. Guo, L. Spielman, O. Petrescu, V. Haroutunian, D. Purohit, A. Czernik, S. Yemul, P.S. Aisen, R. Mohs, and G.M. Pasinetti, *Altered expression of a-type but not b-type synapsin isoform in the brain of patients at high risk for Alzheimer's disease assessed by DNA microarray technique*. Neurosci Lett, 2001. **298**(3): p. 191-4.
373. Whitford, K.L., V. Marillat, E. Stein, C.S. Goodman, M. Tessier-Lavigne, A. Chedotal, and A. Ghosh, *Regulation of cortical dendrite development by Slit-Robo interactions*. Neuron, 2002. **33**(1): p. 47-61.
374. Stokin, G.B. and L.S. Goldstein, *Axonal transport and Alzheimer's disease*. Annu Rev Biochem, 2006. **75**: p. 607-27.
375. Vaughan, K.T. and R.B. Vallee, *Cytoplasmic dynein binds dynactin through a direct interaction between the intermediate chains and p150Glued*. J Cell Biol, 1995. **131**(6 Pt 1): p. 1507-16.
376. Yonekawa, Y., A. Harada, Y. Okada, T. Funakoshi, Y. Kanai, Y. Takei, S. Terada, T. Noda, and N. Hirokawa, *Defect in synaptic vesicle precursor transport and neuronal cell death in KIF1A motor protein-deficient mice*. J Cell Biol, 1998. **141**(2): p. 431-41.
377. Nangaku, M., R. Sato-Yoshitake, Y. Okada, Y. Noda, R. Takemura, H. Yamazaki, and N. Hirokawa, *KIF1B, a novel microtubule plus end-directed monomeric motor protein for transport of mitochondria*. Cell, 1994. **79**(7): p. 1209-20.
378. Benzi, G. and A. Moretti, *Are reactive oxygen species involved in Alzheimer's disease?* Neurobiol Aging, 1995. **16**(4): p. 661-74.
379. Fernandez-Real, J.M., J.M. Moreno, A. Lopez-Bermejo, B. Chico, J. Vendrell, and W. Ricart, *Circulating soluble transferrin receptor according to glucose tolerance status and insulin sensitivity*. Diabetes Care, 2007. **30**(3): p. 604-8.
380. Storch, S., B. Kubler, S. Honing, M. Ackmann, J. Zapf, W. Blum, and T. Bräulke, *Transferrin binds insulin-like growth factors and affects binding properties of insulin-like growth factor binding protein-3*. FEBS Lett, 2001. **509**(3): p. 395-8.
381. Manczak, M., T.S. Anekonda, E. Henson, B.S. Park, J. Quinn, and P.H. Reddy, *Mitochondria*

- are a direct site of A beta accumulation in Alzheimer's disease neurons: implications for free radical generation and oxidative damage in disease progression.* Hum Mol Genet, 2006. **15**(9): p. 1437-49.
382. Segal, A.W., I. West, F. Wientjes, J.H. Nugent, A.J. Chavan, B. Haley, R.C. Garcia, H. Rosen, and G. Scrace, *Cytochrome b-245 is a flavocytochrome containing FAD and the NADPH-binding site of the microbicidal oxidase of phagocytes.* Biochem J, 1992. **284** ( Pt 3): p. 781-8.
383. Heyworth, P.G., C.F. Shrimpton, and A.W. Segal, *Localization of the 47 kDa phosphoprotein involved in the respiratory-burst NADPH oxidase of phagocytic cells.* Biochem J, 1989. **260**(1): p. 243-8.
384. Borregaard, N., J.M. Heiple, E.R. Simons, and R.A. Clark, *Subcellular localization of the b-cytochrome component of the human neutrophil microbicidal oxidase: translocation during activation.* J Cell Biol, 1983. **97**(1): p. 52-61.
385. Garcia, R.C. and A.W. Segal, *Changes in the subcellular distribution of the cytochrome b-245 on stimulation of human neutrophils.* Biochem J, 1984. **219**(1): p. 233-42.
386. Jackson, S.H., S. Devadas, J. Kwon, L.A. Pinto, and M.S. Williams, *T cells express a phagocyte-type NADPH oxidase that is activated after T cell receptor stimulation.* Nat Immunol, 2004. **5**(8): p. 818-27.
387. Vargas, J.D., B. Herpers, A.T. McKie, S. Gledhill, J. McDonnell, M. van den Heuvel, K.E. Davies, and C.P. Ponting, *Stromal cell-derived receptor 2 and cytochrome b561 are functional ferric reductases.* Biochim Biophys Acta, 2003. **1651**(1-2): p. 116-23.
388. Linert, W., E. Herlinger, R.F. Jameson, E. Kienzl, K. Jellinger, and M.B. Youdim, *Dopamine, 6-hydroxydopamine, iron, and dioxygen--their mutual interactions and possible implication in the development of Parkinson's disease.* Biochim Biophys Acta, 1996. **1316**(3): p. 160-8.
389. Ha, C., J. Ryu, and C.B. Park, *Metal ions differentially influence the aggregation and deposition of Alzheimer's beta-amyloid on a solid template.* Biochemistry, 2007. **46**(20): p. 6118-25.
390. Riederer, P. and S. Hoyer, *From benefit to damage. Glutamate and advanced glycation end products in Alzheimer brain.* J Neural Transm, 2006. **113**(11): p. 1671-7.
391. van der Cammen, T.J., H. Tiemeier, M.J. Engelhart, and D. Fekkes, *Abnormal neurotransmitter metabolite levels in Alzheimer patients with a delirium.* Int J Geriatr Psychiatry, 2006. **21**(9): p. 838-43.
392. Mayr, A., M. Schlosser, N. Grober, H. Kenk, A.G. Ziegler, E. Bonifacio, and P. Achenbach, *GAD autoantibody affinity and epitope specificity identify distinct immunization profiles in children at risk for type 1 diabetes.* Diabetes, 2007. **56**(6): p. 1527-33.
393. Christenson, J.G., W. Dairman, and S. Udenfriend, *On the identity of DOPA decarboxylase and 5-hydroxytryptophan decarboxylase (immunological titration-aromatic L-amino acid decarboxylase-serotonin-dopamine-norepinephrine).* Proc Natl Acad Sci U S A, 1972. **69**(2): p. 343-7.
394. Ou, X.M., K. Chen, and J.C. Shih, *Monoamine oxidase A and repressor R1 are involved in apoptotic signaling pathway.* Proc Natl Acad Sci U S A, 2006. **103**(29): p. 10923-8.
395. Kuiper, M.A., T. Teerlink, J.J. Visser, P.L. Bergmans, P. Scheltens, and E.C. Wolters, *L-*

- glutamate, L-arginine and L-citrulline levels in cerebrospinal fluid of Parkinson's disease, multiple system atrophy, and Alzheimer's disease patients.* J Neural Transm, 2000. **107**(2): p. 183-9.
396. Masliah, E., M. Alford, M. Mallory, E. Rockenstein, D. Moechars, and F. Van Leuven, *Abnormal glutamate transport function in mutant amyloid precursor protein transgenic mice.* Exp Neurol, 2000. **163**(2): p. 381-7.
397. Dmitriev, L.F., *Shortage of lipid-radical cycles in membranes as a possible prime cause of energetic failure in aging and Alzheimer disease.* Neurochem Res, 2007. **32**(8): p. 1278-91.
398. Parihar, M.S. and G.J. Brewer, *Mitoenergetic failure in Alzheimer disease.* Am J Physiol Cell Physiol, 2007. **292**(1): p. C8-23.
399. Jacobs, E.H., R.J. Williams, and P.T. Francis, *Cyclin-dependent kinase 5, Munc18a and Munc18-interacting protein 1/X11alpha protein up-regulation in Alzheimer's disease.* Neuroscience, 2006. **138**(2): p. 511-22.
400. Ferrer, I., E. Marti, A. Tortosa, and J. Blasi, *Dystrophic neurites of senile plaques are defective in proteins involved in exocytosis and neurotransmission.* J Neuropathol Exp Neurol, 1998. **57**(3): p. 218-25.
401. Sommer, L., Q. Ma, and D.J. Anderson, *neurogenins, a novel family of atonal-related bHLH transcription factors, are putative mammalian neuronal determination genes that reveal progenitor cell heterogeneity in the developing CNS and PNS.* Mol Cell Neurosci, 1996. **8**(4): p. 221-41.
402. Yan, R.T., W.X. Ma, and S.Z. Wang, *neurogenin2 elicits the genesis of retinal neurons from cultures of nonneural cells.* Proc Natl Acad Sci U S A, 2001. **98**(26): p. 15014-9.
403. Scardigli, R., C. Schuurmans, G. Gradwohl, and F. Guillemot, *Crossregulation between Neurogenin2 and pathways specifying neuronal identity in the spinal cord.* Neuron, 2001. **31**(2): p. 203-17.
404. Kele, J., N. Simplicio, A.L. Ferri, H. Mira, F. Guillemot, E. Arenas, and S.L. Ang, *Neurogenin 2 is required for the development of ventral midbrain dopaminergic neurons.* Development, 2006. **133**(3): p. 495-505.
405. Miyata, T., A. Kawaguchi, K. Saito, M. Kawano, T. Muto, and M. Ogawa, *Asymmetric production of surface-dividing and non-surface-dividing cortical progenitor cells.* Development, 2004. **131**(13): p. 3133-45.
406. Ross, S.E., M.E. Greenberg, and C.D. Stiles, *Basic helix-loop-helix factors in cortical development.* Neuron, 2003. **39**(1): p. 13-25.
407. Driskell, O.J., A. Mironov, V.J. Allan, and P.G. Woodman, *Dynein is required for receptor sorting and the morphogenesis of early endosomes.* Nat Cell Biol, 2007. **9**(1): p. 113-20.
408. Castellone, M.D., H. Teramoto, B.O. Williams, K.M. Druey, and J.S. Gutkind, *Prostaglandin E2 promotes colon cancer cell growth through a Gs-axin-beta-catenin signaling axis.* Science, 2005. **310**(5753): p. 1504-10.
409. Liu, D., L. Wu, R. Breyer, M.P. Mattson, and K. Andreasson, *Neuroprotection by the PGE2 EP2 receptor in permanent focal cerebral ischemia.* Ann Neurol, 2005. **57**(5): p. 758-61.
410. Liang, X., L. Wu, T. Hand, and K. Andreasson, *Prostaglandin D2 mediates neuronal protection*

- via the DP1 receptor. *J Neurochem*, 2005. **92**(3): p. 477-86.
411. Toselli, M., L. Simoncini, V. Taglietti, and F. Tanzi, *Acetylcholine-induced currents at plasma membrane of the frog oocyte*. *Neurosci Lett*, 1985. **54**(2-3): p. 179-84.
412. Bednar, I., D. Paterson, A. Marutle, T.M. Pham, M. Svedberg, E. Hellstrom-Lindahl, M. Mousavi, J. Court, C. Morris, E. Perry, A. Mohammed, X. Zhang, and A. Nordberg, *Selective nicotinic receptor consequences in APP(SWE) transgenic mice*. *Mol Cell Neurosci*, 2002. **20**(2): p. 354-65.
413. Dineley, K.T., M. Westerman, D. Bui, K. Bell, K.H. Ashe, and J.D. Sweatt, *Beta-amyloid activates the mitogen-activated protein kinase cascade via hippocampal alpha7 nicotinic acetylcholine receptors: In vitro and in vivo mechanisms related to Alzheimer's disease*. *J Neurosci*, 2001. **21**(12): p. 4125-33.
414. Yu, W.F., Z.Z. Guan, N. Bogdanovic, and A. Nordberg, *High selective expression of alpha7 nicotinic receptors on astrocytes in the brains of patients with sporadic Alzheimer's disease and patients carrying Swedish APP 670/671 mutation: a possible association with neuritic plaques*. *Exp Neurol*, 2005. **192**(1): p. 215-25.
415. Fodero, L.R., S.S. Mok, D. Losic, L.L. Martin, M.I. Aguilar, C.J. Barrow, B.G. Livett, and D.H. Small, *Alpha7-nicotinic acetylcholine receptors mediate an Abeta(1-42)-induced increase in the level of acetylcholinesterase in primary cortical neurones*. *J Neurochem*, 2004. **88**(5): p. 1186-93.
416. Shi, S.H., Y. Hayashi, R.S. Petralia, S.H. Zaman, R.J. Wenthold, K. Svoboda, and R. Malinow, *Rapid spine delivery and redistribution of AMPA receptors after synaptic NMDA receptor activation*. *Science*, 1999. **284**(5421): p. 1811-6.
417. Song, I. and R.L. Huganir, *Regulation of AMPA receptors during synaptic plasticity*. *Trends Neurosci*, 2002. **25**(11): p. 578-88.
418. Kim, D.Y., S.H. Kim, H.B. Choi, C. Min, and B.J. Gwag, *High abundance of GluR1 mRNA and reduced Q/R editing of GluR2 mRNA in individual NADPH-diaphorase neurons*. *Mol Cell Neurosci*, 2001. **17**(6): p. 1025-33.
419. Wu, Y., A.C. Arai, G. Rumbaugh, A.K. Srivastava, G. Turner, T. Hayashi, E. Suzuki, Y. Jiang, L. Zhang, J. Rodriguez, J. Boyle, P. Tarpey, F.L. Raymond, J. Nevelsteen, G. Froyen, M. Stratton, A. Futreal, J. Gecz, R. Stevenson, C.E. Schwartz, D. Valle, R.L. Huganir, and T. Wang, *Mutations in ionotropic AMPA receptor 3 alter channel properties and are associated with moderate cognitive impairment in humans*. *Proc Natl Acad Sci U S A*, 2007. **104**(46): p. 18163-8.
420. Gecz, J., S. Barnett, J. Liu, G. Hollway, A. Donnelly, H. Eyre, H.S. Eshkevari, R. Baltazar, A. Grunn, R. Nagaraja, C. Gilliam, L. Peltonen, G.R. Sutherland, M. Baron, and J.C. Mulley, *Characterization of the human glutamate receptor subunit 3 gene (GRIA3), a candidate for bipolar disorder and nonspecific X-linked mental retardation*. *Genomics*, 1999. **62**(3): p. 356-68.
421. Micchelli, C.A., E.J. Rulifson, and S.S. Blair, *The function and regulation of cut expression on the wing margin of Drosophila: Notch, Wingless and a dominant negative role for Delta and Serrate*. *Development*, 1997. **124**(8): p. 1485-95.
422. Eiraku, M., A. Tohgo, K. Ono, M. Kaneko, K. Fujishima, T. Hirano, and M. Kengaku, *DNER*

- acts as a neuron-specific Notch ligand during Bergmann glial development.* Nat Neurosci, 2005. **8**(7): p. 873-80.
423. Guarnaccia, C., A. Pintar, and S. Pongor, *Exon 6 of human Jagged-1 encodes an autonomously folding unit.* FEBS Lett, 2004. **574**(1-3): p. 156-60.
424. Loomes, K.M., D.B. Taichman, C.L. Glover, P.T. Williams, J.E. Markowitz, D.A. Piccoli, H.S. Baldwin, and R.J. Oakey, *Characterization of Notch receptor expression in the developing mammalian heart and liver.* Am J Med Genet, 2002. **112**(2): p. 181-9.
425. Zhang, Y., Z. Wang, F. Ahmed, S. Banerjee, Y. Li, and F.H. Sarkar, *Down-regulation of Jagged-1 induces cell growth inhibition and S phase arrest in prostate cancer cells.* Int J Cancer, 2006. **119**(9): p. 2071-7.
426. Yvon, E.S., S. Vigouroux, R.F. Rousseau, E. Biagi, P. Amrolia, G. Dotti, H.J. Wagner, and M.K. Brenner, *Overexpression of the Notch ligand, Jagged-1, induces alloantigen-specific human regulatory T cells.* Blood, 2003. **102**(10): p. 3815-21.
427. LaVoie, M.J. and D.J. Selkoe, *The Notch ligands, Jagged and Delta, are sequentially processed by alpha-secretase and presenilin/gamma-secretase and release signaling fragments.* J Biol Chem, 2003. **278**(36): p. 34427-37.
428. Artavanis-Tsakonas, S., K. Matsuno, and M.E. Fortini, *Notch signaling.* Science, 1995. **268**(5208): p. 225-32.
429. Liu, Y., G. Dehni, K.J. Purcell, J. Sokolow, M.L. Carcangiu, S. Artavanis-Tsakonas, and S. Stifani, *Epithelial expression and chromosomal location of human TLE genes: implications for notch signaling and neoplasia.* Genomics, 1996. **31**(1): p. 58-64.
430. Sestan, N., S. Artavanis-Tsakonas, and P. Rakic, *Contact-dependent inhibition of cortical neurite growth mediated by notch signaling.* Science, 1999. **286**(5440): p. 741-6.
431. Tang, L.S., H.M. Alger, and F.A. Pereira, *COUP-TFI controls Notch regulation of hair cell and support cell differentiation.* Development, 2006. **133**(18): p. 3683-93.
432. Radtke, F., A. Wilson, G. Stark, M. Bauer, J. van Meerwijk, H.R. MacDonald, and M. Aguet, *Deficient T cell fate specification in mice with an induced inactivation of Notch1.* Immunity, 1999. **10**(5): p. 547-58.
433. Koch, U., T.A. Lacombe, D. Holland, J.L. Bowman, B.L. Cohen, S.E. Egan, and C.J. Guidos, *Subversion of the T/B lineage decision in the thymus by lunatic fringe-mediated inhibition of Notch-1.* Immunity, 2001. **15**(2): p. 225-36.
434. Pui, J.C., D. Allman, L. Xu, S. DeRocco, F.G. Karnell, S. Bakkour, J.Y. Lee, T. Kadesch, R.R. Hardy, J.C. Aster, and W.S. Pear, *Notch1 expression in early lymphopoiesis influences B versus T lineage determination.* Immunity, 1999. **11**(3): p. 299-308.
435. Wilson, A., H.R. MacDonald, and F. Radtke, *Notch 1-deficient common lymphoid precursors adopt a B cell fate in the thymus.* J Exp Med, 2001. **194**(7): p. 1003-12.
436. Deftos, M.L., E. Huang, E.W. Ojala, K.A. Forbush, and M.J. Bevan, *Notch1 signaling promotes the maturation of CD4 and CD8 SP thymocytes.* Immunity, 2000. **13**(1): p. 73-84.
437. Mousseau, D.D., S. Chapelsky, G. De Crescenzo, M.D. Kirkitadze, J. Magoon, S. Inoue, D.B. Teplow, and M.D. O'Connor-McCourt, *A direct interaction between transforming growth factor (TGF)-betas and amyloid-beta protein affects fibrillogenesis in a TGF-beta receptor-*

- independent manner*. J Biol Chem, 2003. **278**(40): p. 38715-22.
438. Buckwalter, M., J.P. Pepper, R.F. Gaertner, D. Von Eeuw, P. Lacombe, and T. Wyss-Coray, *Molecular and functional dissection of TGF-beta1-induced cerebrovascular abnormalities in transgenic mice*. Ann N Y Acad Sci, 2002. **977**: p. 87-95.
439. Wyss-Coray, T., C. Lin, F. Yan, G.Q. Yu, M. Rohde, L. McConlogue, E. Masliah, and L. Mucke, *TGF-beta1 promotes microglial amyloid-beta clearance and reduces plaque burden in transgenic mice*. Nat Med, 2001. **7**(5): p. 612-8.
440. Chaudhry, S.S., S.A. Cain, A. Morgan, S.L. Dallas, C.A. Shuttleworth, and C.M. Kielty, *Fibrillin-1 regulates the bioavailability of TGFbeta1*. J Cell Biol, 2007. **176**(3): p. 355-67.
441. Okamoto, O., S. Fujiwara, M. Abe, and Y. Sato, *Dermatopontin interacts with transforming growth factor beta and enhances its biological activity*. Biochem J, 1999. **337** ( Pt 3): p. 537-41.
442. Caricasole, A., A. Copani, F. Caraci, E. Aronica, A.J. Rozemuller, A. Caruso, M. Storto, G. Gaviraghi, G.C. Terstappen, and F. Nicoletti, *Induction of Dickkopf-1, a negative modulator of the Wnt pathway, is associated with neuronal degeneration in Alzheimer's brain*. J Neurosci, 2004. **24**(26): p. 6021-7.
443. Benhaj, K., K.C. Akcali, and M. Ozturk, *Redundant expression of canonical Wnt ligands in human breast cancer cell lines*. Oncol Rep, 2006. **15**(3): p. 701-7.
444. Topol, L., X. Jiang, H. Choi, L. Garrett-Beal, P.J. Carolan, and Y. Yang, *Wnt-5a inhibits the canonical Wnt pathway by promoting GSK-3-independent beta-catenin degradation*. J Cell Biol, 2003. **162**(5): p. 899-908.
445. Katoh, Y. and M. Katoh, *Comparative genomics on DKK2 and DKK4 orthologs*. Int J Mol Med, 2005. **16**(3): p. 477-81.
446. Katoh, M., *WNT antagonist, DKK2, is a Notch signaling target in intestinal stem cells: augmentation of a negative regulation system for canonical WNT signaling pathway by the Notch-DKK2 signaling loop in primates*. Int J Mol Med, 2007. **19**(1): p. 197-201.
447. Emilsson, L., P. Saetre, and E. Jazin, *Low mRNA levels of RGS4 splice variants in Alzheimer's disease: association between a rare haplotype and decreased mRNA expression*. Synapse, 2006. **59**(3): p. 173-6.
448. Muma, N.A., R. Mariyappa, K. Williams, and J.M. Lee, *Differences in regional and subcellular localization of G(q/11) and RGS4 protein levels in Alzheimer's disease: correlation with muscarinic M1 receptor binding parameters*. Synapse, 2003. **47**(1): p. 58-65.
449. Blalock, E.M., J.W. Geddes, K.C. Chen, N.M. Porter, W.R. Markesbery, and P.W. Landfield, *Incipient Alzheimer's disease: microarray correlation analyses reveal major transcriptional and tumor suppressor responses*. Proc Natl Acad Sci U S A, 2004. **101**(7): p. 2173-8.
450. Buckholtz, J.W., A. Meyer-Lindenberg, R.A. Honea, R.E. Straub, L. Pezawas, M.F. Egan, R. Vakkalanka, B. Kolachana, B.A. Verchinski, S. Sust, V.S. Mattay, D.R. Weinberger, and J.H. Callicott, *Allelic variation in RGS4 impacts functional and structural connectivity in the human brain*. J Neurosci, 2007. **27**(7): p. 1584-93.
451. Lu, Y., Q.B. Tian, S. Endo, and T. Suzuki, *A role for LRP4 in neuronal cell viability is related to apoE-binding*. Brain Res, 2007. **1177**: p. 19-28.

452. Pietrzik, C.U., I.S. Yoon, S. Jaeger, T. Busse, S. Weggen, and E.H. Koo, *FE65 constitutes the functional link between the low-density lipoprotein receptor-related protein and the amyloid precursor protein*. J Neurosci, 2004. **24**(17): p. 4259-65.
453. Kinoshita, A., T. Shah, M.M. Tangredi, D.K. Strickland, and B.T. Hyman, *The intracellular domain of the low density lipoprotein receptor-related protein modulates transactivation mediated by amyloid precursor protein and Fe65*. J Biol Chem, 2003. **278**(42): p. 41182-8.
454. Guenette, S.Y., Y. Chang, B.T. Hyman, R.E. Tanzi, and G.W. Rebeck, *Low-density lipoprotein receptor-related protein levels and endocytic function are reduced by overexpression of the FE65 adaptor protein, FE65L1*. J Neurochem, 2002. **82**(4): p. 755-62.
455. Youn, H.D., L. Sun, R. Prywes, and J.O. Liu, *Apoptosis of T cells mediated by Ca<sup>2+</sup>-induced release of the transcription factor MEF2*. Science, 1999. **286**(5440): p. 790-3.
456. Wang, H.G., N. Pathan, I.M. Ethell, S. Krajewski, Y. Yamaguchi, F. Shibasaki, F. McKeon, T. Bobo, T.F. Franke, and J.C. Reed, *Ca<sup>2+</sup>-induced apoptosis through calcineurin dephosphorylation of BAD*. Science, 1999. **284**(5412): p. 339-43.
457. Youn, D.H., G. Royle, M. Kolaj, B. Vissel, and M. Randic, *Enhanced LTP of primary afferent neurotransmission in AMPA receptor GluR2-deficient mice*. Pain, 2007.
458. Jia, Z., N. Agopyan, P. Miu, Z. Xiong, J. Henderson, R. Gerlai, F.A. Taverna, A. Velumian, J. MacDonald, P. Carlen, W. Abramow-Newerly, and J. Roder, *Enhanced LTP in mice deficient in the AMPA receptor GluR2*. Neuron, 1996. **17**(5): p. 945-56.
459. Gerlai, R., J.T. Henderson, J.C. Roder, and Z. Jia, *Multiple behavioral anomalies in GluR2 mutant mice exhibiting enhanced LTP*. Behav Brain Res, 1998. **95**(1): p. 37-45.
460. Bellone, C. and C. Luscher, *mGluRs induce a long-term depression in the ventral tegmental area that involves a switch of the subunit composition of AMPA receptors*. Eur J Neurosci, 2005. **21**(5): p. 1280-8.
461. Colvin, R.A., N. Davis, A. Wu, C.A. Murphy, and J. Levensgood, *Studies of the mechanism underlying increased Na<sup>+</sup>/Ca<sup>2+</sup> exchange activity in Alzheimer's disease brain*. Brain Res, 1994. **665**(2): p. 192-200.
462. Blanchard, B.J., G. Konopka, M. Russell, and V.M. Ingram, *Mechanism and prevention of neurotoxicity caused by beta-amyloid peptides: relation to Alzheimer's disease*. Brain Res, 1997. **776**(1-2): p. 40-50.
463. Hotte, M., S. Thuault, K.T. Dineley, H.C. Hemmings, Jr., A.C. Nairn, and T.M. Jay, *Phosphorylation of CREB and DARPP-32 during late LTP at hippocampal to prefrontal cortex synapses in vivo*. Synapse, 2007. **61**(1): p. 24-8.
464. Kocher, O., A. Yesilaltay, C. Cirovic, R. Pal, A. Rigotti, and M. Krieger, *Targeted disruption of the PDZK1 gene in mice causes tissue-specific depletion of the high density lipoprotein receptor scavenger receptor class B type I and altered lipoprotein metabolism*. J Biol Chem, 2003. **278**(52): p. 52820-5.
465. Ikemoto, M., H. Arai, D. Feng, K. Tanaka, J. Aoki, N. Dohmae, K. Takio, H. Adachi, M. Tsujimoto, and K. Inoue, *Identification of a PDZ-domain-containing protein that interacts with the scavenger receptor class B type I*. Proc Natl Acad Sci U S A, 2000. **97**(12): p. 6538-43.
466. Kim, S.K. and R.J. MacDonald, *Signaling and transcriptional control of pancreatic*

- organogenesis*. *Curr Opin Genet Dev*, 2002. **12**(5): p. 540-7.
467. Kim, S.K., L. Selleri, J.S. Lee, A.Y. Zhang, X. Gu, Y. Jacobs, and M.L. Cleary, *Pbx1 inactivation disrupts pancreas development and in *lpf1*-deficient mice promotes diabetes mellitus*. *Nat Genet*, 2002. **30**(4): p. 430-5.
468. Qin, P., J.M. Haberbush, K.J. Soprano, and D.R. Soprano, *Retinoic acid regulates the expression of *PBX1*, *PBX2*, and *PBX3* in *P19* cells both transcriptionally and post-translationally*. *J Cell Biochem*, 2004. **92**(1): p. 147-63.
469. Wu, Y.H., M.G. Feenstra, J.N. Zhou, R.Y. Liu, J.S. Torano, H.J. Van Kan, D.F. Fischer, R. Ravid, and D.F. Swaab, *Molecular changes underlying reduced pineal melatonin levels in Alzheimer disease: alterations in preclinical and clinical stages*. *J Clin Endocrinol Metab*, 2003. **88**(12): p. 5898-906.
470. Ross, R.A., B.A. Spengler, and J.L. Biedler, *Coordinate morphological and biochemical interconversion of human neuroblastoma cells*. *J Natl Cancer Inst*, 1983. **71**(4): p. 741-7.
471. Biedler, J.L., S. Roffler-Tarlov, M. Schachner, and L.S. Freedman, *Multiple neurotransmitter synthesis by human neuroblastoma cell lines and clones*. *Cancer Res*, 1978. **38**(11 Pt 1): p. 3751-7.
472. Ida, N., T. Hartmann, J. Pantel, J. Schroder, R. Zerfass, H. Forstl, R. Sandbrink, C.L. Masters, and K. Beyreuther, *Analysis of heterogeneous A4 peptides in human cerebrospinal fluid and blood by a newly developed sensitive Western blot assay*. *J Biol Chem*, 1996. **271**(37): p. 22908-14.
473. Tuschl, T., *Functional genomics: RNA sets the standard*. *Nature*, 2003. **421**(6920): p. 220-1.
474. Elbashir, S.M., W. Lendeckel, and T. Tuschl, *RNA interference is mediated by 21- and 22-nucleotide RNAs*. *Genes Dev*, 2001. **15**(2): p. 188-200.
475. Elbashir, S.M., J. Harborth, W. Lendeckel, A. Yalcin, K. Weber, and T. Tuschl, *Duplexes of 21-nucleotide RNAs mediate RNA interference in cultured mammalian cells*. *Nature*, 2001. **411**(6836): p. 494-8.
476. Fire, A., S. Xu, M.K. Montgomery, S.A. Kostas, S.E. Driver, and C.C. Mello, *Potent and specific genetic interference by double-stranded RNA in *Caenorhabditis elegans**. *Nature*, 1998. **391**(6669): p. 806-11.
477. Tuschl, T., J.B. Thomson, and F. Eckstein, *RNA cleavage by small catalytic RNAs*. *Curr Opin Struct Biol*, 1995. **5**(3): p. 296-302.
478. Tuschl, T., P.D. Zamore, R. Lehmann, D.P. Bartel, and P.A. Sharp, *Targeted mRNA degradation by double-stranded RNA in vitro*. *Genes Dev*, 1999. **13**(24): p. 3191-7.
479. Tuschl, T., *Expanding small RNA interference*. *Nat Biotechnol*, 2002. **20**(5): p. 446-8.
480. Lipshutz, R.J., S.P. Fodor, T.R. Gingeras, and D.J. Lockhart, *High density synthetic oligonucleotide arrays*. *Nat Genet*, 1999. **21**(1 Suppl): p. 20-4.

## 9 Acknowledgements

First of all I would like to thank Tobias Hartmann and Konrad Beyreuther for the confidence they placed in me, for giving me the freedom to work as I liked and for the generous financial support of my work. Furthermore, I am grateful that I had the opportunity to work on a very interesting and exciting scientific subject.

I am very thankful to Peter Prior for his help and advice. Thanks Peter especially for your famous “Prior-Jokes”. Many thanks to Laura Busia for creating a really nice working atmosphere and for the joy we had to work together. Thanks Laura, even after coming to the lab with the Italian flag after Italy had won the football world cup..... I would like to thank Çağla Defterali for a really great summer 2006, recalling our funny journey home from a wine festival, which makes me laugh each time thinking about it. Many thanks to Tomas Grübl for his friendship and work outs in the gym. I would like to thank Patricia Rusu for the nicesquash matches making me feeling relaxed during the final period of my thesis. I am grateful to Peter Soba and Stefan Kins for scientific and non-scientific discussions.

I would like to thank the whole bunch of people working in the lab 128, namely Anita Szodorai, Nadine Lauther, Marcus Heinzmann, Tweety Kuan, Simone Back, Annette Trutzel, Ronny Stahl, Katja Wagner, Simone Eggert and Frank Harder. Moreover, I am thankful to the whole lab 129, especially to Jakob Tschäpe, Endré Högyes, Inge Tomic, Anke Diehlmann and Sandra Kühl.

Many thanks to all the people of the DKFZ lab, in which I could perform the data analysis, especially to Yuri Knyazev, Annette Weninger and Monica Hollstein. Thanks Yuri also for the coffee breaks. I would like to thank Kamran Honarnejad for a relaxed working atmosphere. Moreover, I am grateful to Verena Wiedmann for supporting my fight with an incredible amount of data. Many thanks to Carina Ittrich for a plenty of helpful discussions about biostatistics. I am thankful to Christian Beisel for useful information and giving me access to the Agilent Bioanalyzer. Furthermore I would like to thank Ulrike Müller and Christoph Schuster for their readiness to act as examiners for my defense. Thanks also to Frank Peter for many Sunday morning brunches and to Vincent Beuger for helpful discussions.

Last, but definitely not least, I am most thankful to my mother and my sisters Petra and Gabi for supporting everything I have done during my thesis, not only financially, but also morally.

## 10 Abbreviations

A	absorption
aa	amino acids
A $\beta$	amyloid- $\beta$ peptide
ACTA2	actin alpha 2 smooth muscle aorta
ACTN1	actinin alpha 1
AD	Alzheimer's disease
ADAM	a disintegrin-like and metalloprotease
ADAMTS3	a disintegrin-like and metalloprotease (reprolysin type) with thrombospondin type 1 motif 3
ADAMTS9	a disintegrin-like and metalloprotease (reprolysin type) with thrombospondin type 1 motif 9
ADRB1	adrenergic, beta-1-receptor
AICD	APP intracellular domain
AKT1	v-akt murine thymoma viral oncogene homolog 1
AMPA2	glutamate receptor ionotropic AMPA 2 (synonym: <i>gria2</i> )
AMPA3	glutamate receptor ionotropic AMPA 3 (synonym: <i>gria3</i> )
APLP	amyloid precursor like protein
APLP1	amyloid beta (A4) precursor-like protein 1
APLP2	amyloid beta (A4) precursor-like protein 2
APP	amyloid precursor protein (synonym: A $\beta$ PP)
ASS	argininosuccinate synthase
ATP7A	ATPase, Cu <sup>2+</sup> transporting, alpha polypeptide (Menkes syndrome)
BAMBI	BMP and activin membrane-bound inhibitor
BCA	bicinchinonic acid
BDNF	brain-derived neurotrophic factor
BMP7	bone morphogenetic protein 7 (osteogenic protein 1)
bp	base pairs
BSA	bovine serum albumin
b-561	cytochrome b-561 (CYB561)
b-245	cytochrome b-245, alpha polypeptide (CYBA)
C99	C-terminal fragment of APP comprising 99 aa
CCND1	cyclin D1 (synonym: PRAD1, parathyroid adenomatosis 1)
CDK6	cyclin-dependent kinase 6
CDKL1	cyclin-dependent kinase-like 1 (CDC2-related kinase)
CDKL5	cyclin-dependent kinase-like 5
CDKN1A	cyclin-dependent kinase inhibitor 1A (synonym: p21, Cip1)
CHRNA7	cholinergic receptor nicotinic alpha polypeptide 7
COL4A1	collagen type IV alpha 1
COL4A2	collagen type IV alpha 2
CRABP1	cellular retinoic acid binding protein 1
CREB1	cAMP responsive element binding protein 1
CSF	cerebro spinal fluid
CTF	C-terminal fragment
CTSD	cathepsin D (lysosomal aspartyl protease)
CUTL2	cut-like 2 ( <i>Drosophila</i> )
DAPI	4', 6'-diamidino-2-phenylindole dihydrochloride
DCAMKL1	DCAMKL1, doublecortin and CaM kinase-like 1
DDC	dopa decarboxylase (aromatic L-amino acid decarboxylase)
DKK2	dickkopf homolog 2 ( <i>Xenopus laevis</i> )
DKK4	dickkopf homolog 4 ( <i>Xenopus laevis</i> )
DMEM	Dulbecco's minimal essential medium
DNA	deoxyribonucleic acid
DNase	deoxyribonuclease

DNCL12	dynein cytoplasmic light intermediate polypeptide 2
DNER	delta-notch-like EGF repeat-containing transmembrane
dNTPs	2'-deoxyribonucleoside-5'-triphosphates
DS	Down's syndrome
DTT	dithiothreitol
DYRK1	dual-specificity tyrosine-(Y)-phosphorylation regulated kinase 1B
ECEL1	endothelin converting enzyme-like 1
EDTA	ethylene diamine tetra acetic acid
EGFR	epidermal growth factor receptor (erythroblastic leukemia viral (v-erb-b) oncogene homolog, avian)
ERK1	extracellular regulated protein-serine kinase 1 (p44 MAP kinase)
et al.	et alii, and others
FAD	familial AD
FBS	fetal bovine serum
FCS	fetal calf serum
FGB	fibrinogen B beta polypeptide
GABRB3	$\gamma$ -aminobutyric acid (GABA) A receptor beta 3
GAD1	glutamate decarboxylase 1 (brain 67kDa)
GATA3	GATA binding protein 3
GC-RMA	robust multichip averaging, regarding GC content
GLRB	glycine receptor, beta
GLS	glutaminase
GLUL	glutamine synthase (synonym: Glutamate-ammonia ligase)
GRIA2	synonym: glutamate receptor, ionotropic, AMPA 2
GRIA3	synonym: glutamate receptor, ionotropic, AMPA 3
GRM7	glutamate receptor, metabotropic 7
GRM8c	glutamate receptor, metabotropic 8c
GSK3 $\beta$	glycogen synthase kinase 3 $\beta$
H19	H19 imprinted maternally expressed untranslated mRNA
HCHWAD	hereditary cerebral hemorrhages with amyloidosis
HGF	hepatocyte growth factor (hepapoietin A; scatter factor)
HMP19	HMP19 protein (LOC51617)
HRP	horse radish peroxidase
HS3ST2	heparan sulfate (glucosamine) 3-O-sulfotransferase 2
IDE	insulin degrading enzyme
IGF1R	insulin-like growth factor 1 receptor
IGF2	insulin-like growth factor 2 (somatomedin A)
IGFBP5	insulin-like growth factor binding protein 5
ITGB5	integrin $\beta$ 5
JAG1	jagged 1
JNK	c-Jun amino-terminal kinase
kb	kilobase pair
kDa	kilodalton
L1CAM	L1 cell adhesion molecule
LB	Luria-Bertani medium
LOAD	late onset Alzheimer's disease
LOD Score	logarithm of the odds score
LRP4	low density lipoprotein receptor-related protein 4
LTP	long-term potentiation
MAPT	microtubule-associated protein tau (synonym: Tau)
MEK1	MAPK/ERK protein-serine kinase 1 (synonym: MKK1)
MEM	minimal essential medium
MES	2-morpholinoethane-sulfonic acid
min	minute

MMP8	matrix metalloproteinase 8 (neutrophil collagenase)
MOPS	3-(N-morpholino) propane-sulfonic acid
MT	microtubule
NDUFB9	NADH dehydrogenase (ubiquinone) 1 beta subcomplex
NFTs	neuro fibrillary tangles
NGF	nerve growth factor
NP-40	nonidet P-40
NSAIDS	non steroidal anti-inflammatory drugs
NTRK2	neurotrophic tyrosine kinase receptor type 2
PAGE	polyacrylamide gel electrophoresis
PBS	phosphate buffered saline
PBX1	pre-B-cell leukemia transcription factor 1
PD	Parkinson's disease
PDZK1	PDZ domain containing 1
PFA	paraformaldehyde
PFKP	phosphofructokinase platelet
PI3K	phosphoinositide-3-kinase
PKC	protein kinase C
PLAT	plasminogen activator tissue
PLIER	probe logarithmic intensity error
PLL	poly-L-Lysine
PREP	prolyl endopeptidase
PRSS12	protease serine 12 (neurotrypsin, motopsin)
PS	presenilin
PTGER2,	prostaglandin E receptor 2 (subtype EP2), 53kDa
PTN	pleiotrophin (heparin binding growth factor 8, neurite growth-promoting factor 1)
RA	retinoic acid
RELN	reelin
RGS4	regulator of G-protein signaling 4
RMA	robust multichip average
RNA	ribonucleic acid
RNase	ribonuclease
rpm	revolutions per minute
RT	room temperature
SD	standard deviation
SDS	sodium dodecyl sulphate
SEMA3A	sema domain, immunoglobulin domain (Ig), short basic domain, secreted, (semaphorin) 3A
SEMA3C	sema domain, immunoglobulin domain (Ig), short basic domain, secreted, (semaphorin) 3C
SERPINE2	serine proteinase inhibitor clade E member 2
SERPINF1	serine proteinase inhibitor clade F member 1
SGK	serum/glucocorticoid regulated kinase
SHOX2	short stature homeobox 2
siRNA	small interfering RNA
SLIT1	slit homolog 1 (Drosophila)
STX3A	syntaxin 3A
SYN2	synapsin 2
TAE	tris acetate EDTA buffer
tau	microtubule-associated protein tau (synonym : MAPT)
TBE	tris borate EDTA buffer
TFPI2	tissue factor pathway inhibitor 2
TGFB2	transforming growth factor, beta 2
TGFB2	transforming growth factor, beta receptor 2 (70/80kDa)

## Abbreviations

---

TIMP1	tissue inhibitor of metalloproteinase 1 (erythroid potentiating activity collagenase inhibitor)
TIMP3	tissue inhibitor of metalloproteinase 3 (Sorsby fundus dystrophy pseudoinflammatory)
TLE1	transducin-like enhancer of split 1 (E(sp1) homolog <i>Drosophila</i> )
TLE2	transducin-like enhancer of split 2 (E(sp1) homolog <i>Drosophila</i> )
Tris	tris (hydroxymethyl) aminomethane
TRKB	tyrosine kinase receptor B, synonym: NTRK2
3'-UTR	3-prime untranslated region
5'-UTR	5-prime untranslated region
v/v	volume per volume
VEGF	vascular endothelial growth factor
VMP	vesicular membrane protein p24
w/v	weight per volume
WNT	composition of Wingless und Int1
WT	wild type

## 11 Declaration

Ich erkläre hiermit, dass ich die vorgelegte Dissertation selbst verfasst und mich dabei keiner anderen als der von mir ausdrücklich bezeichneten Quellen und Hilfen bedient habe. Ich erkläre, dass ich an keiner anderen Stelle ein Prüfungsverfahren beantragt bzw. die Dissertation in dieser oder anderer Form bereits anderweitig als Prüfungsarbeit verwendet oder einer anderen Fakultät als Dissertation vorgelegt habe.

.....  
Markus Uhrig

## 12 Supplementary Information

### 12.1 Preface

All the data were calculated with three different normalisation algorithms (PLIER, GC-RMA, MAS 5). The thresholds for the p-values were adjusted to  $p < 0.05$  (PLIER), to  $p < 0.005$  (GC-RMA) and to  $p < 0.05$  (MAS 5). However, data slightly greater than these thresholds (for instance  $p = 0.058$ , when the threshold was  $p < 0.05$ ) are also listed here (the exact p-value is given in the tables), if they might have crucial biological functions. P-values were calculated from three independent single clones. For some genes no gene symbols, titles or locations are shown, because this information is not available for all probes (for instance for expressed sequence tags) on the Chip. Instead, only the probe set ID is shown allowing to get information from public databases.

### 12.2 Genes identified using different algorithms

#### 12.2.1 Genes identified using the PLIER-algorithm (Array Assist, Stratagene)

**Table 12.1 Most up and down-regulated genes derived from the comparison C99I45F/C99WT1 ( $A\beta_{42}/A\beta_{40}\uparrow$ ,  $n=3$ ,  $p < 0.05$ , C99WT1 was the baseline experiment)**

Position	Probe Set ID	p-value	Fold change C99I45F/C99WT1	Gene Symbol	Title	Location
1	218623_at	0.0030	3.0	HMP19	HMP19 protein (LOC51617)	chr5q35.2
2	239293_at	0.0055	2.8	VMP	vesicular membrane protein p24	chr6p22.2
3	205358_at	0.0331	2.7	GRIA2	glutamate receptor ionotropic AMPA 2	chr4q32-q33
4	223672_at	0.0189	2.7	DKFZp761D221	hypothetical protein DKFZp761D221	chr1p31.2
5	205113_at	0.0441	2.6	NEF3	neurofilament 3 (150kDa medium)	chr8p21
6	227690_at	0.0256	2.6	GABRB3	Gamma-aminobutyric acid (GABA) A receptor beta 3	chr15q11.2-q12
7	228010_at	0.0201	2.4	PPP2R2C	protein phosphatase 2 (formerly 2A) regulatory subunit B (PR 52) gamma isoform	chr4p16.1
8	227830_at	0.0076	2.4	GABRB3	Gamma-aminobutyric acid (GABA) A receptor beta 3	chr15q11.2-q12
9	226281_at	0.0048	2.3	DNER	delta-Notch-like EGF repeat-containing transmembrane	chr2q36.3
10	201939_at	0.0415	2.3	PLK2	polo-like kinase 2	chr5q12.1-q13.2

Supplementary Information

					(Drosophila)	
11	226086_at	0.0309	2.3	SYT13	synaptotagmin XIII	chr11p12-p11
12	227210_at	0.0414	2.3	SFMBT2	Scm-like with four mbt domains 2	chr10p14
13	201341_at	0.0079	2.2	ENC1	ectodermal-neural cortex (with BTB-like domain)	chr5q12-q13.3
14	221916_at	0.0430	2.2	NEFL	Neurofilament light polypeptide 68kDa	chr8p21
15	221796_at	0.0231	2.2	NTRK2	neurotrophic tyrosine kinase receptor type 2, non-catalytic isoform	chr9q22.1
16	225111_s_at	0.0157	2.1	NAPB	N-ethylmaleimide-sensitive factor attachment protein beta	chr20p12.3-p11.21
17	209755_at	0.0289	2.1	NMNAT2	nicotinamide nucleotide adenyltransferase 2	chr1q25
18	212096_s_at	0.0170	2.1	MTUS1	mitochondrial tumor suppressor 1	chr8p22
19	212314_at	0.0388	2.1	KIAA0746	KIAA0746 protein	chr4p15.2
20	234904_x_at	0.0226	2.1	ELAVL4	ELAV (embryonic lethal abnormal vision Drosophila)-like 4 (Hu antigen D)	chr1p34
21	206502_s_at	0.0356	2.0	INSM1	insulinoma-associated 1	chr20p11.2
22	206002_at	0.0076	2.0	GPR64	G protein-coupled receptor 64	chrXp22.13
23	209591_s_at	0.0114	2.0	BMP7	bone morphogenetic protein 7 (osteogenic protein 1)	chr20q13
24	204396_s_at	0.0167	2.0	GRK5	G protein-coupled receptor kinase 5	chr10q24-qter
25	213338_at	0.0400	2.0	RIS1	Ras-induced senescence 1	chr3p21.3
26	229724_at	0.0462	2.0	GABRB3	gamma-aminobutyric acid (GABA) A receptor beta 3	chr15q11.2-q12
27	226814_at	0.0032	2.0	ADAMTS9	a disintegrin-like and metalloprotease (reprolysin type) with thrombospondin type 1 motif 9	chr3p14.3-p14.2
28	213802_at	0.0008	2.0	PRSS12	Protease serine 12 (neurotrypsin motopsin)	chr4q28.1
29	223500_at	0.0297	2.0	CPLX1	complexin 1	chr4p16.3
30	226560_at	0.0541	2.0	SGPP2	Sphingosine-1-phosphate phosphatase 2	chr2q36.1
31	203329_at	0.0189	1.9	PTPRM	protein tyrosine phosphatase receptor type M	chr18p11.2
32	201621_at	0.0015	1.9	NBL1	neuroblastoma suppression of tumorigenicity 1	chr1p36.13-p36.11
33	221801_x_at	0.0297	1.9	NEFL	neurofilament light polypeptide 68kDa	chr8p21
34	221933_at	0.0300	1.9	NLGN4X	neuroligin 4 X-linked	chrXp22.32-p22.31
35	228347_at	0.0304	1.9	SIX1	Sine oculis homeobox homolog 1 (Drosophila)	chr14q23.1
36	203789_s_at	0.0106	1.9	SEMA3C	sema domain immunoglobulin domain (Ig) short basic domain secreted (semaphorin) 3C	chr7q21-q31
37	212658_at	0.0180	1.9	LHFPL2	lipoma HMGIC fusion partner-like 2	chr5q14.1
38	223143_s_at	0.0275	1.9	C6orf166	chromosome 6 open reading frame 166	chr6q15
39	230112_at	0.0199	1.9	C3HC4	membrane-associated ring finger (C3HC4) 4	chr2q35

Supplementary Information

40	219926_at	0.0134	1.8	POPDC3	popeye domain containing 3	chr6q21
41	205348_s_at	0.0111	1.8	DNC11	dynein cytoplasmic intermediate polypeptide 1	chr7q21.3-q22.1
42	210108_at	0.0454	1.8	CACNA1D	calcium channel voltage-dependent L type alpha 1D subunit	chr3p14.3
43	205515_at	0.0132	1.8	PRSS12	protease serine 12 (neurotrypsin motopsin)	chr4q28.1
44	201645_at	0.0492	1.8	TNC	tenascin C (hexabrachion)	chr9q33
45	205068_s_at	0.0093	1.8	ARHGAP26	Rho GTPase activating protein 26	chr5q31
46	209590_at	0.0190	1.8	BMP7	Bone morphogenetic protein 7 (osteogenic protein 1)	chr20q13
47	201037_at	0.0022	1.8	PFKP	phosphofructokinase platelet	chr10p15.3-p15.2
48	206577_at	0.0361	1.8	VIP	vasoactive intestinal peptide	chr6q25
49	213273_at	0.0053	1.8	ODZ4	odz odd Oz/ten-m homolog 4 (Drosophila)	chr11q14.1
50	219825_at	0.0123	1.8	CYP26B1	cytochrome P450 family 26 subfamily B polypeptide 1	chr2p13.2
51	219225_at	0.0068	1.8	PGBD5	piggyBac transposable element derived 5	chr1q42.13
52	204465_s_at	0.0376	1.8	INA	internexin neuronal intermediate filament protein alpha	chr10q24.33
53	224940_s_at	0.0504	1.8	PAPPA	pregnancy-associated plasma protein A pappalysin 1	chr9q33.2
54	203030_s_at	0.0414	1.8	PTPRN2	protein tyrosine phosphatase receptor type N polypeptide 2	chr7q36
55	229576_s_at	0.0514	1.8	TBX3	T-box 3 (ulnar mammary syndrome)	chr12q24.1
56	241872_at	0.0323	1.8	DKFZp761D221	Hypothetical protein DKFZp761D221	chr1p31.2
57	209295_at	0.0220	1.8	TNFRSF10B	tumor necrosis factor receptor superfamily member 10b	chr8p22-p21
58	203788_s_at	0.0319	1.8	SEMA3C	sema domain immunoglobulin domain (Ig) short basic domain secreted (semaphorin) 3C	chr7q21-q31
59	204319_s_at	0.0195	1.8	RGS10	regulator of G-protein signaling 10	chr10q25
60	205373_at	0.0114	1.7	CTNNA2	catenin (cadherin-associated protein) alpha 2	chr2p12-p11.1
61	212841_s_at	0.0271	1.7	PPFIBP2	PTPRF interacting protein binding protein 2 (liprin beta 2)	chr11p15.4
62	202507_s_at	0.0236	1.7	SNAP25	synaptosomal-associated protein 25kDa	chr20p12-p11.2
63	219697_at	0.0116	1.7	HS3ST2	heparan sulfate (glucosamine) 3-O-sulfotransferase 2	chr16p12
64	213689_x_at	0.0540	1.7	LOC388650	Hypothetical LOC388650	chr1p22.1
65	212095_s_at	0.0198	1.7	MTUS1	mitochondrial tumor suppressor 1	chr8p22
66	212311_at	0.0332	1.7	KIAA0746	KIAA0746 protein	chr4p15.2
67	212328_at	0.0003	1.7	KIAA1102	KIAA1102 protein	chr4p13
68	213478_at	0.0021	1.7	KIAA1026	KIAA1026 protein	chr1p36.21
69	202508_s_at	0.0235	1.7	SNAP25	synaptosomal-associated	chr20p12-p11.2

Supplementary Information

					protein 25kDa	
70	221558_s_at	0.0364	1.7	LEF1	lymphoid enhancer-binding factor 1	chr4q23-q25
71	212843_at	0.0016	1.7	NCAM1	neural cell adhesion molecule 1	chr11q23.1
72	203029_s_at	0.0530	1.7	PTPRN2	protein tyrosine phosphatase receptor type N polypeptide 2	chr7q36
73	205143_at	0.0112	1.7	CSPG3	chondroitin sulfate proteoglycan 3 (neurocan)	chr19p12
74	201150_s_at	0.0263	1.7	TIMP3	tissue inhibitor of metalloproteinase 3 (Sorsby fundus dystrophy pseudoinflammatory)	chr22q12.1-q13.2 22q12.3
75	203130_s_at	0.0109	1.7	KIF5C	kinesin family member 5C	chr2q23.1
76	213411_at	0.0074	1.7	ADAM22	A disintegrin and metalloproteinase domain 22	chr7q21
77	37005_at	0.0038	1.7	NBL1	neuroblastoma suppression of tumorigenicity 1	chr1p36.13-p36.11
78	212327_at	0.0069	1.7	KIAA1102	KIAA1102 protein	chr4p13
79	206014_at	0.0521	1.6	ACTL6B	actin-like 6B	chr7q22
80	215740_at	0.0083	1.6	PTPRN2	Protein tyrosine phosphatase receptor type N polypeptide 2	chr7q36
81	205117_at	0.0201	1.6	FGF1	fibroblast growth factor 1 (acidic)	chr5q31
82	219610_at	0.0496	1.6	RGNEF	Rho-guanine nucleotide exchange factor	chr5q13.2
83	212325_at	0.0079	1.6	KIAA1102	KIAA1102 protein	chr4p13
84	217028_at	0.0523	1.6	CXCR4	chemokine (C-X-C motif) receptor 4	chr2q21
85	219277_s_at	0.0133	1.6	OGDHL	oxoglutarate dehydrogenase-like	chr10q11.23
86	204412_s_at	0.0384	1.6	NEFH	neurofilament heavy polypeptide 200kDa	chr22q12.2
87	211160_x_at	0.0045	1.6	ACTN1	actinin alpha 1	chr14q24.1-q24.2 14q24 14q22-q24
88	205721_at	0.0332	1.6	GFRA2	GDNF family receptor alpha 2	chr8p21
89	219837_s_at	0.0378	1.6	CYTL1	cytokine-like 1	chr4p16-p15
90	212093_s_at	0.0088	1.6	MTUS1	mitochondrial tumor suppressor 1	chr8p22
91	203037_s_at	0.0192	1.6	MTSS1	metastasis suppressor 1	chr8p22
92	202920_at	0.0014	1.6	ANK2	ankyrin 2 neuronal	chr4q25-q27
93	204117_at	0.0025	1.6	PREP	prolyl endopeptidase	chr6q22
94	214875_x_at	0.0179	1.6	APLP2	amyloid beta (A4) precursor-like protein 2	chr11q23-q25 11q24
95	209234_at	0.0371	1.6	KIF1B	kinesin family member 1B	chr1p36.2
96	206290_s_at	0.0062	1.5	RGS7	regulator of G-protein signaling 7	chr1q43 1q23.1 according to Sierra (Transcriptomics 79; 177; 2002) [AFS]
97	216672_s_at	0.0332	1.5	MYT1L	myelin transcription factor 1-like	chr2p25.3
98	37950_at	0.0002	1.5	PREP	prolyl endopeptidase	chr6q22
99	203640_at	0.0370	1.5	MBNL2	muscleblind-like 2 (Drosophila)	chr13q32.1

Supplementary Information

100	215955_x_at	0.0074	1.5	ARHGAP26	Rho GTPase activating protein 26	chr5q31
21	204314_s_at	0.0072	-1.1	CREB1	cAMP responsive element binding protein 1	chr2q34
20	214080_x_at	0.0471	-1.1	PRKCSH	protein kinase C substrate 80K-H	chr19p13.2
19	204313_s_at	0.0144	-1.1	CREB1	cAMP responsive element binding protein 1	chr2q34
18	201337_s_at	0.0327	-1.1	VAMP3	vesicle-associated membrane protein 3 (cellubrevin)	chr1p36.23
17	221745_at	0.0406	-1.1	HAN11	WD-repeat protein	chr17q23.3
16	201259_s_at	0.0297	-1.2	SYPL	synaptophysin-like protein	chr7q22.3
15	206848_at	0.0149	-1.2	HOXA7	homeo box A7	
14	220138_at	0.0277	-1.3	HAND1	heart and neural crest derivatives expressed 1	chr5q33
13	207966_s_at	0.0106	-1.3	GLG1	golgi apparatus protein 1	chr16q22-q23
12	201726_at	0.0162	-1.3	ELAVL1	ELAV (embryonic lethal abnormal vision Drosophila)-like 1 (Hu antigen R)	chr19p13.2
11	200879_s_at	0.0127	-1.4	EPAS1	endothelial PAS domain protein 1	chr2p21-p16
10	203590_at	0.0066	-1.5	DNCL12	dynein cytoplasmic light intermediate polypeptide 2	chr16q22.1
9	200878_at	0.0404	-1.6	EPAS1	endothelial PAS domain protein 1	chr2p21-p16
8	210816_s_at	0.0343	-1.6	CYB561	cytochrome b-561	chr17q11-qter
7	202291_s_at	0.0246	-1.7	MGP	matrix Gla protein	chr12p13.1-p12.3
6	217200_x_at	0.037	-1.7	CYB561	cytochrome b-561	chr17q11-qter
5	214020_x_at	0.0446	-1.9	ITGB5	Integrin beta 5	chr3q21.2
4	201125_s_at	0.0477	-2	ITGB5	integrin beta 5	chr3q21.2

3	204337_at	0.0124	-2.2	RGS4	regulator of G-protein signaling 4	chr1q23.3
2	204339_s_at	0.0068	-2.6	RGS4	regulator of G-protein signaling 4	chr1q23.3
1	204338_s_at	0.0176	-2.7	RGS4	regulator of G-protein signaling 4	chr1q23.3

**Table 12.1 Most up and down-regulated genes derived from the comparison C99145F/C99WT1 (n=3, p<0.05), analyzed with the Array Assist software and the PLIER algorithm.**

**Table 12.2 Most up and down-regulated genes derived from the comparison C99V50F/C99WT1 ( $A\beta_{42}/A\beta_{40}\downarrow$ , n=3, p<0.05, C99WT1 was the baseline experiment)**

Position	Probe Set ID	p-value	Fold change C99V50F/C99WT1	Gene Symbol	Title	Location
1	209291_at	0.0153	3.0	ID4	inhibitor of DNA binding 4, dominant negative helix-loop-helix protein	chr6p22-p21
2	212092_at	0.0173	2.7	PEG10	paternally expressed 10	chr7q21
3	209278_s_at	0.0272	2.6	TFPI2	tissue factor pathway inhibitor 2	chr7q22
4	209277_at	0.0186	2.5	TFPI2	Tissue factor pathway inhibitor 2	chr7q22
5	202479_s_at	0.0217	2.3	TRIB2	tribbles homolog 2 (Drosophila)	chr2p24.3
6	205113_at	0.0374	2.3	NEF3	neurofilament 3 (150kDa medium)	chr8p21
7	212094_at	0.0077	2.3	PEG10	paternally expressed 10	chr7q21
8	215411_s_at	0.0258	2.2	TRAF3IP2	TRAF3 interacting protein 2	chr6q21
9	221916_at	0.0315	2.2	NEFL	Neurofilament, light polypeptide 68kDa	chr8p21
10	202478_at	0.0285	2.2	TRIB2	tribbles homolog 2 (Drosophila)	chr2p24.3
11	221805_at	0.0425	2.1	NEFL	neurofilament, light polypeptide 68kDa	chr8p21
12	218623_at	0.0139	2.1	HMP19		chr5q35.2
13	209293_x_at	0.0141	2.1	ID4	inhibitor of DNA binding 4, dominant negative helix-loop-helix protein	chr6p22-p21
14	202284_s_at	0.0453	2.0	CDKN1A	cyclin-dependent kinase inhibitor 1A (p21, Cip1)	chr6p21.2
15	205586_x_at	0.0375	2.0	VGF	VGF nerve growth factor inducible	chr7q22
16	201739_at	0.0420	1.9	SGK	serum/glucocorticoid regulated kinase	chr6q23
17	219914_at	0.0368	1.9	ECEL1	endothelin converting enzyme-like 1	chr2q36-q37
18	203304_at	0.0150	1.9	BAMBI	BMP and activin membrane-bound inhibitor	chr10p12.3-p11.2
19	221801_x_at	0.0384	1.9	NEFL	neurofilament, light polypeptide 68kDa	chr8p21
20	206631_at	0.0111	1.8	PTGER2	prostaglandin E receptor 2 (subtype	chr14q22

Supplementary Information

					EP2), 53kDa	
21	213894_at	0.0474	1.8	KIAA0960	KIAA0960 protein	chr7p21.3
22	209292_at	0.0233	1.8	ID4	Inhibitor of DNA binding 4, dominant negative helix-loop-helix protein	chr6p22-p21
23	204688_at	0.0183	1.8	SGCE	sarcoglycan, epsilon	chr7q21-q22
24	203685_at	0.0291	1.7	BCL2	B-cell CLL/lymphoma 2	chr18q21.33 18q21.3
25	209462_at	0.0188	1.7	APLP1	amyloid beta (A4) precursor-like protein 1	chr19q13.1
26	206478_at	0.0104	1.7	KIAA0125	KIAA0125	chr14q32.33
27	219093_at	0.0482	1.7	FLJ20701	hypothetical protein FLJ20701 /// hypothetical protein FLJ20701	chr2q36.3
28	203662_s_at	0.0065	1.7	TMOD1	tropomodulin 1	chr9q22.3
29	201341_at	0.0089	1.7	ENC1	ectodermal-neural cortex (with BTB-like domain)	chr5q12-q13.3
30	201939_at	0.0299	1.6	PLK2	polo-like kinase 2 (Drosophila)	chr5q12.1-q13.2
31	205399_at	0.0459	1.6	DCAMKL1	doublecortin and CaM kinase-like 1	chr13q13
32	213260_at	0.0428	1.6	FOXC1	Forkhead box C1	chr6p25
33	220386_s_at	0.0224	1.6	EML4	echinoderm microtubule associated protein like 4	chr2p22-p21
34	203661_s_at	0.0308	1.6	TMOD1	tropomodulin 1	chr9q22.3
35	205373_at	0.0079	1.5	CTNNA2	catenin (cadherin-associated protein), alpha 2	chr2p12-p11.1
36	207260_at	0.0246	1.5	FEV	FEV (ETS oncogene family)	chr2q36
37	202517_at	0.0422	1.5	CRMP1	collapsin response mediator protein 1	chr4p16.1-p15
38	213601_at	0.0484	1.5	MEGF4		
39	214508_x_at	0.0312	1.5	CREM	cAMP responsive element modulator	chr10p11.21
40	210829_s_at	0.0086	1.5	SSBP2	single-stranded DNA binding protein 2	chr5q14.1
41	204471_at	0.0409	1.5	GAP43	growth associated protein 43	chr3q13.1-q13.2
42	208070_s_at	0.0244	1.5	REV3L	REV3-like, catalytic subunit of DNA polymerase zeta (yeast)	chr6q21
43	205068_s_at	0.0199	1.5	ARHGAP26	Rho GTPase activating protein 26	chr5q31
44	203787_at	0.0031	1.5	SSBP2	single-stranded DNA binding protein 2	chr5q14.1
45	204134_at	0.0490	1.5	PDE2A	phosphodiesterase 2A, cGMP-stimulated	chr11q13.4
46	209967_s_at	0.0461	1.5	CREM	cAMP responsive element modulator	chr10p11.21
47	208712_at	0.0249	1.5	CCND1	cyclin D1 (PRAD1: parathyroid adenomatosis 1)	chr11q13
48	214326_x_at	0.0350	1.5	JUND	jun D proto-oncogene	chr19p13.2
49	200672_x_at	0.0037	1.5	SPTBN1	spectrin, beta, non-erythrocytic 1	chr2p21
50	200671_s_at	0.0015	1.5	SPTBN1	spectrin, beta, non-erythrocytic 1	chr2p21
51	212843_at	0.0089	1.4	NCAM1	neural cell adhesion molecule 1	chr11q23.1
52	211160_x_at	0.0171	1.4	ACTN1	actinin, alpha 1	chr14q24.1-q24.2

Supplementary Information

53	209197_at	0.0280	1.4	SYT11	synaptotagmin XI	chr1q21.2
54	213093_at	0.0291	1.4	PRKCA	protein kinase C, alpha	chr17q22-q23.2
55	208637_x_at	0.0141	1.4	ACTN1	actinin, alpha 1	chr14q24.1-q24.2
56	208978_at	0.0179	1.4	CRIP2	cysteine-rich protein 2	chr14q32.3
57	201954_at	0.0145	1.4	ARPC1B	actin related protein 2/3 complex, subunit 1B, 41kDa	chr7q22.1
58	214839_at	0.0398	1.4	LOC157627	hypothetical protein LOC157627	chr8p23.1
59	218773_s_at	0.0106	1.4	MSRB2	methionine sulfoxide reductase B2	chr10p12
60	220377_at	0.0079	1.4	C14orf110	chromosome 14 open reading frame 110	chr14q32.33
61	219451_at	0.0202	1.4	MSRB2	methionine sulfoxide reductase B2	chr10p12
62	210078_s_at	0.0416	1.4	KCNAB1	potassium voltage-gated channel, shaker-related subfamily, beta member 1	chr3q26.1
63	216963_s_at	0.0473	1.4	GAP43	growth associated protein 43	chr3q13.1-q13.2
64	208729_x_at	0.0124	1.4	HLA-B	major histocompatibility complex, class I, B	chr6p21.3
65	212328_at	0.0260	1.4	KIAA1102	KIAA1102 protein	chr4p13
66	215678_at	0.0016	1.4	LOC440792	similar to proline dehydrogenase (oxidase) 1; tumor protein p53 inducible protein 6; p53 induced protein; proline oxidase 2; proline dehydrogenase (proline oxidase )	chr22q11.21
67	213013_at	0.0352	1.3	MAPK8IP1	mitogen-activated protein kinase 8 interacting protein 1	chr11p12-p11.2
68	207353_s_at	0.0017	1.3	HMX1	homeo box (H6 family) 1	chr4p16.1
69	212878_s_at	0.0271	1.3	KNS2	kinesin 2 60/70kDa	chr14q32.3
70	202177_at	0.0146	1.3	GAS6	growth arrest-specific 6	chr13q34
71	212325_at	0.0394	1.3	KIAA1102	KIAA1102 protein	chr4p13
72	204099_at	0.0104	1.3	SMARCD3	SWI/SNF related, matrix associated, actin dependent regulator of chromatin, subfamily d, member 3	chr7q35-q36
73	219327_s_at	0.0329	1.3	GPRC5C	G protein-coupled receptor, family C, group 5, member C	chr17q25
74	218876_at	0.0089	1.3	CGI-38	brain specific protein /// brain specific protein	chr16q22.1
75	208636_at	0.0266	1.3	ACTN1	Actinin, alpha 1	chr14q24.1-q24.2
76	203409_at	0.0086	1.3	DDB2 /// LHX3	damage-specific DNA binding protein 2, 48kDa /// LIM homeobox 3	chr11p12-p11 /// chr9q34.3
77	212803_at	0.0164	1.3	NAB2	NGFI-A binding protein 2 (EGR1 binding protein 2)	chr12q13.3-q14.1
78	214781_at	0.0061	1.3	DKFZp761P19121		
79	211530_x_at	0.0271	1.3	HLA-G	HLA-G histocompatibility antigen, class I, G	chr6p21.3
80	200852_x_at	0.0180	1.3	GNB2	guanine nucleotide binding protein (G	chr7q21.3-q22.1 7q22

Supplementary Information

					protein), beta polypeptide 2	
81	203752_s_at	0.0430	1.3	JUND	jun D proto-oncogene	chr19p13.2
82	1598_g_at	0.0391	1.3	GAS6	growth arrest-specific 6	chr13q34
83	206397_x_at	0.0325	1.3	GDF1 /// LASS1	growth differentiation factor 1 /// LAG1 longevity assurance homolog 1 (S. cerevisiae)	chr19p12
84	204608_at	0.0021	1.3	ASL	argininosuccinate lyase	chr7cen-q11.2
85	204806_x_at	0.0134	1.3	HLA-F	major histocompatibility complex, class I, F	chr6p21.3
86	203149_at	0.0137	1.3	PVRL2	poliovirus receptor-related 2 (herpesvirus entry mediator B)	chr19q13.2-q13.4
87	207788_s_at	0.0145	1.3	SCAM-1	vinexin beta (SH3-containing adaptor molecule-1)	chr8p21.3
88	211911_x_at	0.0365	1.3	HLA-B	major histocompatibility complex, class I, B /// major histocompatibility complex, class I, B	chr6p21.3
89	222240_s_at	0.0049	1.3	ISYNA1	myo-inositol 1-phosphate synthase A1	chr19p13.11
90	200710_at	0.0107	1.3	ACADVL	acyl-Coenzyme A dehydrogenase, very long chain	chr17p13-p11
91	212935_at	0.0380	1.3	MCF2L	MCF.2 cell line derived transforming sequence-like	chr13q34
92	212071_s_at	0.0077	1.3	SPTBN1	spectrin, beta, non-erythrocytic 1	chr2p21
93	209855_s_at	0.0103	1.3	KLK2	kallikrein 2, prostatic	chr19q13.41
94	207469_s_at	0.0428	1.3	PIR	pirin (iron-binding nuclear protein)	chrXp22.2
95	213201_s_at	0.0216	1.3	TNNT1	troponin T1, skeletal, slow	chr19q13.4
96	202786_at	0.0016	1.3	STK39	serine threonine kinase 39 (STE20/SPS1 homolog, yeast)	chr2q24.3
97	213423_x_at	0.0286	1.2	TUSC3	tumor suppressor candidate 3	chr8p22
98	208874_x_at	0.0069	1.2	PPP2R4	protein phosphatase 2A, regulatory subunit B' (PR 53)	chr9q34
99	200989_at	0.0048	1.2	HIF1A	hypoxia-inducible factor 1, alpha subunit (basic helix-loop-helix transcription factor)	chr14q21-q24
100	221875_x_at	0.0439	1.2	HLA-F	major histocompatibility complex, class I, F	chr6p21.3
50	203804_s_at	0.0491	-1.2	CROP	cisplatin resistance-associated overexpressed protein	chr17q21.33
49	222018_at	0.0465	-1.2	NACA	nascent-polypeptide-associated complex alpha polypeptide	chr12q23-q24.1
48	209081_s_at	0.0027	-1.2	COL18A1	collagen, type XVIII, alpha 1	chr21q22.3
47	210387_at	0.0306	-1.2	HIST1H2BG	histone 1, H2bg	chr6p21.3
46	206848_at	0.0234	-1.2			

Supplementary Information

45	204030_s_at	0.0445	-1.2	SCHIP1	schwannomin interacting protein 1	chr3q25.32-q25.33
44	209082_s_at	0.0421	-1.2	COL18A1	collagen, type XVIII, alpha 1	chr21q22.3
43	215338_s_at	0.0173	-1.2	NKTR	natural killer-tumor recognition sequence	chr3p23-p21
42	214469_at	0.045	-1.2	HIST1H2AE	histone 1, H2ae	chr6p22.2-p21.1
41	213902_at	0.0345	-1.2	ASAH1	N-acylsphingosine amidohydrolase (acid ceramidase) 1	chr8p22-p21.3
40	204635_at	0.018	-1.2	RPS6KA5	ribosomal protein S6 kinase, 90kDa, polypeptide 5	chr14q31-q32.1
39	215919_s_at	0.0206	-1.2	MRPS11	mitochondrial ribosomal protein S11	chr15q25
38	214805_at	0.0293	-1.2	EIF4A1	Eukaryotic translation initiation factor 4A, isoform 1	chr17p13
37	209007_s_at	0.0163	-1.2	NPD014	NPD014 protein	chr1p36.13-p35.1
36	202202_s_at	0.0231	-1.2	LAMA4	laminin, alpha 4	chr6q21
35	203989_x_at	0.0266	-1.2	F2R	coagulation factor II (thrombin) receptor	chr5q13
34	210523_at	0.0234	-1.2	BMPR1B	bone morphogenetic protein receptor, type IB	chr4q22-q24
33	203781_at	0.0264	-1.2	MRPL33	mitochondrial ribosomal protein L33	chr2p21
32	213410_at	0.0343	-1.2	C10orf137	chromosome 10 open reading frame 137	chr10q26.13-q26.2
31	206653_at	0.031	-1.2	POLR3G	Polymerase (RNA) III (DNA directed) polypeptide G (32kD)	chr5q14.3
30	202127_at	0.0061	-1.3	PRPF4B	PRP4 pre-mRNA processing factor 4 homolog B (yeast)	chr6p25.2
29	203259_s_at	0.0351	-1.3	C6orf74	chromosome 6 open reading frame 74	chr6q13-q24.3
28	201578_at	0.0458	-1.3	PODXL	podocalyxin-like	chr7q32-q33
27	204702_s_at	0.0381	-1.3	NFE2L3	nuclear factor (erythroid-derived 2)-like 3	chr7p15-p14
26	234729_at	0.0441	-1.3	PHKG1	phosphorylase kinase gamma 1 (muscle)	chr7p12-q21
25	209957_s_at	0.0488	-1.3	NPPA	natriuretic peptide precursor A	chr1p36.21
24	212179_at	0.0259	-1.3	C6orf111	chromosome 6 open reading frame 111	chr6q16.3
23	203790_s_at	0.0448	-1.4	HRSP12	heat-responsive protein 12	chr8q22
22	213701_at	0.019	-1.4	DKFZp434N2030	hypothetical protein DKFZp434N2030	chr12q21.33
21	203726_s_at	0.046	-1.4	LAMA3	laminin, alpha 3	chr18q11.2
20	208691_at	0.0361	-1.4	TFRC	transferrin receptor (p90, CD71) /// transferrin receptor (p90, CD71)	chr3q29
19	241271_at	0.0215	-1.4	PKN2	Protein kinase N2	chr1p22.2
18	212382_at	0.0467	-1.4	TCF4	Transcription factor 4	chr18q21.1
17	213245_at	0.0426	-1.5	ADCY1	adenylate cyclase 1 (brain)	chr7p13-p12
16	209220_at	0.0057	-1.6	GPC3	glypican 3	chrXq26.1
15	202669_s_at	0.0168	-1.7	EFNB2	ephrin-B2	chr13q33
14	235957_at	0.0374	-1.7		transcribed locus	
13	206673_at	0.0372	-1.7	GPR	putative G protein coupled receptor	chr15q14-q15.1

12	209238_at	0.0438	-1.8	STX3A	syntaxin 3A	chr11q12.1
11	202283_at	0.0266	-1.8	SERPINF1	serine (or cysteine) proteinase inhibitor, clade F (alpha-2 antiplasmin, pigment epithelium derived factor), member 1	chr17p13.1
10	222288_at	0.0164	-1.8		Similar to CG9996-PA	chr3p13
9	209757_s_at	0.0242	-1.9	MYCN	v-myc myelocytomatosis viral related oncogene, neuroblastoma derived (avian)	chr2p24.1
8	242385_at	0.049	-2	RORB	RAR-related orphan receptor B	chr9q22
7	218330_s_at	0.0348	-2	NAV2	neuron navigator 2	chr11p15.1
6	214596_at	0.0359	-2	CHRM3	cholinergic receptor, muscarinic 3	chr1q41-q44
5	228978_at	0.0027	-2.2	LOC440450	LOC440450	chr17q23.2
4	207401_at	0.0303	-2.2	PROX1	prospero-related homeobox 1	chr1q32.2-q32.3
3	212713_at	0.047	-2.3	MFAP4	microfibrillar-associated protein 4	chr17p11.2
2	243808_at	0.0408	-2.5	CDK6	Cyclin-dependent kinase 6	chr7q21-q22
1	215632_at	0.0162	-2.5	NEUROG2	neurogenin 2	chr4q25

**Table 12.2 Most up and down-regulated genes derived from the comparison C99V50F/C99WT1 (n=3, p<0.05), analyzed with the Array Assist software and the PLIER algorithm.**

**Table 12.3 Most up and down-regulated genes derived from the comparison C99WT1/mock (n=3, p<0.05, mock was the baseline experiment)**

Position	Probe Set ID	P-value	Fold change C99WT1/mock	Gene Symbol	Title	Location
1	204239_s_at	0.0079	17.2	NNAT	neuronatin	chr20q11.2-q12
2	214953_s_at	0.0011	11.2	APP <sup>13</sup>	amyloid beta (A4) precursor protein (protease nexin-II Alzheimer disease)	chr21q21.2 21q21.3
3	215632_at	0.0127	4.6	NEUROG2	neurogenin 2	chr4q25
4	214596_at	0.0014	4.2	CHRM3	cholinergic receptor muscarinic 3	chr1q41-q44
5	212713_at	0.0053	3.6	MFAP4	microfibrillar-associated protein 4	chr17p11.2
6	221796_at	0.0111	3.3	NTRK2	neurotrophic tyrosine kinase receptor type 2, non-catalytic isoform	chr9q22.1
7	210414_at	0.0165	2.9	FLRT1	fibronectin leucine rich transmembrane protein 1	chr11q12-q13
8	207401_at	0.0258	2.7	PROX1	prospero-related homeobox 1	chr1q32.2-q32.3
9	221795_at	0.0038	2.7	NTRK2	neurotrophic tyrosine kinase receptor type 2, non-catalytic isoform	chr9q22.1
10	212226_s_at	0.0140	2.5	PPAP2B	phosphatidic acid phosphatase type 2B	chr1pter-p22.1

<sup>13</sup> APP appears as up-regulated. However the over-expressed C99 most probably leads to this effect. C99 and APP are both recognized by the same probe set on the Chip. Since the probe set for APP detection is taken from the 3' end by Affymetrix, the C-terminus of APP (C99) is recognized as well. Detection of the strongly up-regulated C99 (second most up-regulated transcript out of approximately 44,000) is an indicator that overexpressed and hence up-regulated transcripts are recognized correctly. A simultaneous detection of putative up-regulated APP cannot be completely excluded.

Supplementary Information

11	223940_x_at	0.0520	2.3	MALAT1	metastasis associated lung adenocarcinoma transcript 1 (non-coding RNA)	chr11q13.1
12	209355_s_at	0.0311	2.3	PPAP2B	phosphatidic acid phosphatase type 2B	chr1pter-p22.1
13	202669_s_at	0.0282	2.1	EFNB2	ephrin-B2	chr13q33
14	221310_at	0.0142	2.1	FGF14	fibroblast growth factor 14	chr13q34
15	213593_s_at	0.0075	2.1	TRA2A	Transformer-2 alpha	chr7p15.3
16	211600_at	0.0059	2.0			
17	213742_at	0.0003	2.0	SFRS11	splicing factor arginine/serine-rich 11	chr1p31
18	222344_at	0.0011	2.0	C5orf13	Chromosome 5 open reading frame 13	chr5q22.1
19	213517_at	0.0077	2.0	PCBP2	Poly(rC) binding protein 2	chr12q13.12-q13.13
20	217853_at	0.0196	2.0	TENS1	tensin-like SH2 domain containing 1	chr7p13-p12.3
21	217813_s_at	0.0245	2.0	SPIN	spindlin	chr9q22.1-q22.3
22	211454_x_at	0.0511	2.0			
23	214577_at	0.0454	1.9	MAP1B	microtubule-associated protein 1B	chr5q13
24	221019_s_at	0.0125	1.9	COLEC12	collectin sub-family member 12 /// collectin sub-family member 12	chr18pter-p11.3
25	242488_at	0.0401	1.9		CDNA FLJ38396 fis clone FEBRA2007957	
26	222272_x_at	0.0320	1.9	SCIN	scinderin	chr7p21.3
27	212230_at	0.0169	1.9	PPAP2B	phosphatidic acid phosphatase type 2B	chr1pter-p22.1
28	217342_x_at	0.0043	1.9	FLJ11292	hypothetical protein FLJ11292	chr5q14.3
29	238549_at	0.0136	1.9	CBFA2T2	core-binding factor runt domain alpha subunit 2; translocated to 2	chr20q11
30	211127_x_at	0.0047	1.9	EDA	ectodysplasin A	chrXq12-q13.1
31	210511_s_at	0.0050	1.9	INHBA	inhibin beta A (activin A activin AB alpha polypeptide)	chr7p15-p13
32	208120_x_at	0.0235	1.9			
33	217321_x_at	0.0009	1.8	ATXN3	Ataxin 3	chr14q24.3-q32.2
34	209144_s_at	0.0309	1.8	CBFA2T2	core-binding factor runt domain alpha subunit 2; translocated to 2	chr20q11
35	213229_at	0.0110	1.8	DICER1	Dicer1 Dcr-1 homolog (Drosophila)	chr14q32.13
36	219697_at	0.0143	1.8	HS3ST2	heparan sulfate (glucosamine) 3-O-sulfotransferase 2	chr16p12
37	221234_s_at	0.0327	1.8	BACH2	BTB and CNC homology 1 basic leucine zipper transcription factor 2 /// BTB and CNC homology 1 basic leucine zipper transcription factor 2	chr6q15
38	214902_x_at	0.0086	1.8	FLJ42393	FLJ42393 protein	chr3q27.3
39	201309_x_at	0.0549	1.8	C5orf13	chromosome 5 open reading frame 13	chr5q22.1
40	228656_at	0.0289	1.8	PROX1	Prospero-related homeobox 1	chr1q32.2-q32.3
41	211571_s_at	0.0065	1.8	CSPG2	chondroitin sulfate proteoglycan 2 (versican)	chr5q14.3
42	203628_at	0.0274	1.8	IGF1R	insulin-like growth factor 1 receptor	chr15q26.3
43	207115_x_at	0.0057	1.8	MBTD1	mbt domain containing 1	chr17q21.33
44	205168_at	0.0199	1.8	DDR2	discoidin domain receptor family member 2	chr1q12-q23
45	212385_at	0.0177	1.8	TCF4	Transcription factor 4	chr18q21.1
46	214761_at	0.0046	1.8	ZNF423	zinc finger protein 423	chr16q12
47	219647_at	0.0245	1.8	POPDC2	popeye domain containing 2	chr3q13.33
48	206056_x_at	0.0003	1.8	SPN	sialophorin (gpL115 leukosialin CD43)	chr16p11.2
49	203002_at	0.0003	1.8	AMOTL2	angiomin like 2	chr3q21-q22

Supplementary Information

50	211304_x_at	0.0005	1.8	KCNJ5	potassium inwardly-rectifying channel subfamily J member 5	chr11q24
51	218330_s_at	0.0056	1.7	NAV2	neuron navigator 2	chr11p15.1
52	202379_s_at	0.0028	1.7	NKTR	natural killer-tumor recognition sequence	chr3p23-p21
53	212151_at	0.0299	1.7	PBX1	Pre-B-cell leukemia transcription factor 1	chr1q23
54	209757_s_at	0.0223	1.7	MYCN	v-myc myelocytomatosis viral related oncogene neuroblastoma derived (avian)	chr2p24.1
55	215063_x_at	0.0074	1.7	FLJ20331	hypothetical protein FLJ20331	chr1p31.1
56	215615_x_at	0.0216	1.7	RERE	Arginine-glutamic acid dipeptide (RE) repeats	chr1p36.1-p36.2
57	227671_at	0.0360	1.7			
58	219206_x_at	0.0002	1.7	CGI-119	CGI-119 protein	chr12q14.1-q15
59	200879_s_at	0.0119	1.7	EPAS1	endothelial PAS domain protein 1	chr2p21-p16
60	210368_at	0.0016	1.7	PCDHGB4 /// PCDHGA8	protocadherin gamma subfamily B 4 /// protocadherin gamma subfamily A 8	chr5q31
61	213956_at	0.0484	1.7	CAP350	centrosome-associated protein 350	chr1p36.13-q41
62	204913_s_at	0.0105	1.7	SOX11	SRY (sex determining region Y)-box 11	chr2p25
63	222358_x_at	0.0102	1.7		Transcribed locus weakly similar to XP_517655.1 similar to KIAA0825 protein [Pan troglodytes]	
64	208238_x_at	0.0146	1.7			
65	211704_s_at	0.0435	1.7	SPIN2 /// SPIN-2	spindlin family member 2 /// spindlin family member 2 /// spindlin-like protein 2 /// spindlin-like protein 2	chrXp11.1
66	206061_s_at	0.0048	1.7	DICER1	Dicer1 Dcr-1 homolog (Drosophila)	chr14q32.13
67	217586_x_at	0.0076	1.7			
68	209584_x_at	0.0044	1.7	APOBEC3C	apolipoprotein B mRNA editing enzyme catalytic polypeptide-like 3C	chr22q13.1-q13.2
87	211160_x_at	0.0045	1.6	ACTN1	actinin alpha 1	chr14q24.1-q24.2 14q24 14q22-q24
70	210525_x_at	0.0008	1.7	C14orf143	chromosome 14 open reading frame 143	chr14q32.11
71	207117_at	0.0473	1.6	H-plk	Krüppel-related zinc finger protein	chr7q11.21
72	212966_at	0.0263	1.6	HIC2	hypermethylated in cancer 2	chr22q11.21
73	211936_at	0.0277	1.6	HSPA5	heat shock 70kDa protein 5 (glucose-regulated protein 78kDa)	chr9q33-q34.1
74	210172_at	0.0246	1.6	SF1	splicing factor 1	chr11q13
75	235716_at	0.0456	1.6	TRA2A	Transformer-2 alpha	chr7p15.3
76	221387_at	0.0278	1.6	GPR147	G protein-coupled receptor 147	chr10q21-q22
77	213575_at	0.0217	1.6	TRA2A	Transformer-2 alpha	chr7p15.3
78	217536_x_at	0.0267	1.6		Transcribed locus weakly similar to NP_055301.1 neuronal thread protein AD7c-NTP [Homo sapiens]	
79	212468_at	0.0342	1.6	SPAG9	sperm associated antigen 9	chr17q21.33
80	214329_x_at	0.0254	1.6	TNFSF10	Tumor necrosis factor (ligand) superfamily member 10 /// Tumor necrosis factor (ligand) superfamily member 10	chr3q26
81	235060_at	0.0311	1.6	LOC23117	KIAA0220-like protein /// Similar to PI-3-kinase-related kinase SMG-1 isoform 1; lambda/iota protein kinase C-interacting protein; phosphatidylinositol 3-kinase-related protein kinase	chr16p12.2 /// chr16p12.1
82	209638_x_at	0.0256	1.6	RGS12	regulator of G-protein signaling 12	chr4p16.3

Supplementary Information

83	223287_s_at	0.0446	1.6	FOXP1	forkhead box P1	chr3p14.1
84	214707_x_at	0.0080	1.6	ALMS1	Alstrom syndrome 1	chr2p13
85	207365_x_at	0.0037	1.6	USP34	ubiquitin specific protease 34	chr2p15
86	200920_s_at	0.0137	1.6	BTG1	B-cell translocation gene 1 anti-proliferative	chr12q22
87	220071_x_at	0.0112	1.6	C15orf25	chromosome 15 open reading frame 25	chr15q15.1
88	206551_x_at	0.0301	1.6	DRE1	DRE1 protein	chr3q27.1
89	216882_s_at	0.0512	1.6	NEBL	nebullette	chr10p12
90	207625_s_at	0.0473	1.6	CBFA2T2	core-binding factor runt domain alpha subunit 2; translocated to 2	chr20q11
91	215179_x_at	0.0082	1.6	PGF	Placental growth factor vascular endothelial growth factor-related protein	chr14q24-q31
92	214594_x_at	0.0467	1.6	ATP8B1	ATPase Class I type 8B member 1	chr18q21-q22 18q21.31
93	202971_s_at	0.0075	1.6	DYRK2	dual-specificity tyrosine-(Y)-phosphorylation regulated kinase 2	chr12q15
94	216459_x_at	0.0272	1.6			
95	206792_x_at	0.0122	1.6	PDE4C	phosphodiesterase 4C cAMP-specific (phosphodiesterase E1 dunce homolog Drosophila)	chr19p13.11
96	205347_s_at	0.0003	1.6	TMSL8	thymosin-like 8	chrXq21.33-q22.3
97	207186_s_at	0.0547	1.6	FALZ	fetal Alzheimer antigen	chr17q24.3
98	203308_x_at	0.0006	1.6	HPS1	Hermansky-Pudlak syndrome 1	chr10q23.1-q23.3
99	232168_x_at	0.0244	1.6	MACF1	microtubule-actin crosslinking factor 1	chr1p32-p31
100	210508_s_at	0.0159	1.6	KCNQ2	potassium voltage-gated channel KQT-like subfamily member 2	chr20q13.3
101	214989_x_at	0.0002	1.6	PLEKHA5	Pleckstrin homology domain containing family A member 5	chr12p12
102	205572_at	0.0450	1.6	ANGPT2	angiopoietin 2	chr8p23.1
103	207164_s_at	0.0103	1.6	ZNF238	zinc finger protein 238	chr1q44-qter
104	207173_x_at	0.0418	1.6	CDH11	cadherin 11 type 2 OB-cadherin (osteoblast)	chr16q22.1
105	221728_x_at	0.0101	1.6			
106	208404_x_at	0.0170	1.6			
107	203627_at	0.0007	1.6	IGF1R	Insulin-like growth factor 1 receptor	chr15q26.3
108	214683_s_at	0.0478	1.6	CLK1	CDC-like kinase 1	chr2q33
109	60815_at	0.0212	1.6	MGC13098	hypothetical protein MGC13098	chr7p13
110	219437_s_at	0.0332	1.6	ANKRD11	ankyrin repeat domain 11	chr16q24.3
110	226101_at	0.0491	-1.9	PRKCE	protein kinase C epsilon	chr2p21
109	203303_at	0.0010	-2.0	TCTE1L	t-complex-associated-testis-expressed 1-like	chrXp21
108	217763_s_at	0.0436	-2.0	RAB31	RAB31 member RAS oncogene family	chr18p11.3
107	207620_s_at	0.0018	-2.0	CASK	calcium/calmodulin-dependent serine protein kinase (MAGUK family)	chrXp11.4
106	208700_s_at	0.0377	-2.0	TKT	transketolase (Wernicke-Korsakoff syndrome)	chr3p14.3
105	202016_at	0.0192	-2.0	MEST	mesoderm specific transcript homolog (mouse)	chr7q32
104	226614_s_at	0.0342	-2.0	C8orf13	chromosome 8 open reading frame 13	chr8p23-p22
103	225817_at	0.0285	-2.0	CGNL1	cingulin-like 1	chr15q21.3
102	207447_s_at	0.0537	-2.0	GNTIVH	UDP-N-acetylglucosamine:a-1 3-D-mannoside beta-1 4-N-acetylglucosaminyltransferase IV	chr12q21
101	201744_s_at	0.0090	-2.0	LUM	lumican	chr12q21.3-q22

Supplementary Information

100	213787_s_at	0.0325	-2.0	EBP	emopamil binding protein (sterol isomerase)	chrXp11.23-p11.22
99	214527_s_at	0.0019	-2.0	PQBP1	polyglutamine binding protein 1	chrXp11.23
98	205324_s_at	0.0108	-2.0	FTSJ1	FtsJ homolog 1 (E. coli)	chrXp11.23
97	236236_at	0.0350	-2.0		CDNA FLJ30437 fis clone BRACE2009045	
96	223051_at	0.0221	-2.0	HSPC182	HSPC182 protein	chr1p36.33
95	209170_s_at	0.0041	-2.0	GPM6B	glycoprotein M6B	chrXp22.2
94	206631_at	0.0102	-2.0	PTGER2	prostaglandin E receptor 2 (subtype EP2) 53kDa	chr14q22
93	201037_at	0.0339	-2.0	PFKP	phosphofructokinase platelet	chr10p15.3-p15.2
92	209191_at	0.0068	-2.1	TUBB6	tubulin beta 6	chr18p11.21
91	230547_at	0.0212	-2.1		CDNA FLJ42249 fis clone TKIDN2007667	
90	204134_at	0.0181	-2.1	PDE2A	phosphodiesterase 2A cGMP-stimulated	chr11q13.4
89	203304_at	0.0308	-2.1	BAMBI	BMP and activin membrane-bound inhibitor	chr10p12.3-p11.2
88	206233_at	0.0125	-2.1	B4GALT6	UDP-Gal:betaGlcNAc beta 1 4-galactosyltransferase polypeptide 6	chr18q11
87	222138_s_at	0.0086	-2.1	WDR13	WD repeat domain 13	chrXp11.23
86	205656_at	0.0197	-2.1	PCDH17	protocadherin 17	chr13q21.1
85		0.0461	-2.1			
84	223313_s_at	0.0403	-2.1	MAGED4	melanoma antigen family D 4	
83	221910_at	0.0354	-2.1	LOC221810	hypothetical protein LOC221810	chr7p21.3
82	206837_at	0.0005	-2.1	CART1	cartilage paired-class homeoprotein 1	chr12q21.3-q22
81	212457_at	0.0040	-2.1	TFE3	transcription factor binding to IGHM enhancer 3	chrXp11.22
80	206478_at	0.0006	-2.1	KIAA0125	KIAA0125	chr14q32.33
79	205068_s_at	0.0104	-2.1	ARHGAP26	Rho GTPase activating protein 26	chr5q31
78	218532_s_at	0.0120	-2.2	FLJ20152	hypothetical protein FLJ20152	chr5p15.1
77	228010_at	0.0198	-2.2	PPP2R2C	protein phosphatase 2 (formerly 2A) regulatory subunit B (PR 52) gamma isoform	chr4p16.1
76	243610_at	0.0000	-2.2	LOC138255	OTTHUMP00000021439	chr9q21.11
75	214913_at	0.0475	-2.2	ADAMTS3	a disintegrin-like and metalloprotease (reprolysin type) with thrombospondin type 1 motif 3	chr4q13.3
74	202284_s_at	0.0192	-2.2	CDKN1A	cyclin-dependent kinase inhibitor 1A (p21 Cip1)	chr6p21.2
73	229110_at	0.0228	-2.2		CDNA clone IMAGE:4794876 partial cds	
72	205857_at	0.0392	-2.2			
71	229576_s_at	0.0257	-2.2	TBX3	T-box 3 (ulnar mammary syndrome)	chr12q24.1
70	216963_s_at	0.0182	-2.2	GAP43	growth associated protein 43	chr3q13.1-q13.2
69	217764_s_at	0.0514	-2.2	RAB31	RAB31 member RAS oncogene family	chr18p11.3
68	219073_s_at	0.0226	-2.2	OSBPL10	oxysterol binding protein-like 10	chr3p22.3
67	223193_x_at	0.0250	-2.2	E2IG5	growth and transformation-dependent protein	chr3q21.1
66	233337_s_at	0.0337	-2.3	SEZ6L2	seizure related 6 homolog (mouse)-like 2	chr16p11.2
65	33767_at	0.0456	-2.3	NEFH	neurofilament heavy polypeptide 200kDa	chr22q12.2
64	204723_at	0.0470	-2.3	SCN3B	sodium channel voltage-gated type III beta	chr11q24.1
63	216047_x_at	0.0098	-2.3	SEZ6L	seizure related 6 homolog (mouse)-like	chr22q12.1
62	225029_at	0.0206	-2.3		CDNA clone IMAGE:4686928 partial cds	

Supplementary Information

61	224345_x_at	0.0485	-2.3	E2IG5	growth and transformation-dependent protein /// growth and transformation-dependent protein	chr3q21.1
60	239352_at	0.0121	-2.3	SLC6A15	solute carrier family 6 member 15	chr12q21.3
59	210319_x_at	0.0139	-2.3	MSX2	msh homeo box homolog 2 (Drosophila)	chr5q34-q35
58	225081_s_at	0.0282	-2.4	RAM2	transcription factor RAM2	chr7p15.3
57	204412_s_at	0.0207	-2.4	NEFH	neurofilament heavy polypeptide 200kDa	chr22q12.2
56	209120_at	0.0362	-2.4	NR2F2	nuclear receptor subfamily 2 group F member 2	chr15q26
55	221914_at	0.0349	-2.4			
54		0.0190	-2.4			
53	230896_at	0.0490	-2.4		CDNA FLJ35632 fis clone SPLEN2011678	
52	218623_at	0.0249	-2.5			
51	213664_at	0.0109	-2.5	SLC1A1	solute carrier family 1 (neuronal/epithelial high affinity glutamate transporter system Xag) member 1	chr9p24
50	219230_at	0.0215	-2.5	FLJ10970	hypothetical protein FLJ10970	chr17q23.1
49	213200_at	0.0139	-2.5	SYP	synaptophysin	chrXp11.23-p11.22
48	203329_at	0.0013	-2.5	PTPRM	protein tyrosine phosphatase receptor type M	chr18p11.2
47	221288_at	0.0118	-2.6	GPR22	G protein-coupled receptor 22	chr7q22-q31.1
46	225516_at	0.0156	-2.6	SLC7A2	solute carrier family 7 (cationic amino acid transporter y+ system) member 2	chr8p22-p21.3
45	203430_at	0.0033	-2.6	HEBP2	heme binding protein 2	chr6q24
44	206376_at	0.0049	-2.7	SLC6A15	solute carrier family 6 member 15	chr12q21.3
43	238600_at	0.0339	-2.7	MARLIN1	multiple coiled-coil GABABR1-binding protein	chr4p16.1
42	235333_at	0.0312	-2.7			
41	226281_at	0.0427	-2.7	DNER	delta-Notch-like EGF repeat-containing transmembrane	chr2q36.3
40	212192_at	0.0094	-2.8	KCTD12	potassium channel tetramerisation domain containing 12	chr13q22.3
39	221801_x_at	0.0384	-2.8	NEFL	neurofilament light polypeptide 68kDa	chr8p21
38	209755_at	0.0433	-2.9	NMNAT2	nicotinamide nucleotide adenyltransferase 2	chr1q25
37	221916_at	0.0453	-2.9	NEFL	Neurofilament light polypeptide 68kDa	chr8p21
36	225544_at	0.0205	-2.9	TBX3	T-box 3 (ulnar mammary syndrome)	chr12q24.1
35	212094_at	0.0130	-3	PEG10	paternally expressed 10	chr7q21
34	230112_at	0.0214	-3	-	membrane-associated ring finger (C3HC4) 4	chr2q35
33	209278_s_at	0.0153	-3	TFPI2	tissue factor pathway inhibitor 2	chr7q22
32	219682_s_at	0.0105	-3	TBX3	T-box 3 (ulnar mammary syndrome)	chr12q24.1
31	221805_at	0.0385	-3	NEFL	neurofilament light polypeptide 68kDa	chr8p21
30	209291_at	0.0355	-3	ID4	inhibitor of DNA binding 4 dominant negative helix-loop-helix protein	chr6p22-p21
29	227289_at	0.0389	-3.1	LOC144997	hypothetical protein LOC144997	chr13q14.3
28	215411_s_at	0.0066	-3.1	TRAF3IP2	TRAF3 interacting protein 2	chr6q21
27	203824_at	0.0433	-3.1	TSPAN8	tetraspanin 8	chr12q14.1-q21.1
26	204471_at	0.0094	-3.2	GAP43	growth associated protein 43	chr3q13.1-q13.2
25	202242_at	0.0038	-3.2	TSPAN7	tetraspanin 7	chrXp11.4
24	213609_s_at	0.0063	-3.3	SEZ6L	seizure related 6 homolog (mouse)-like	chr22q12.1

23	209277_at	0.0052	-3.3	TFPI2	Tissue factor pathway inhibitor 2	chr7q22
22	227198_at	0.0402	-3.4	LAF4	Lymphoid nuclear protein related to AF4	chr2q11.2-q12
21	225996_at	0.0533	-3.4		CDNA FLJ36725 fis clone UTERU2012230	
20	218858_at	0.0026	-3.4	DEPDC6	DEP domain containing 6	chr8q24.12
19	206137_at	0.0014	-3.4	RIMS2	regulating synaptic membrane exocytosis 2	chr8q22.3
18	205113_at	0.0236	-3.4	NEF3	neurofilament 3 (150kDa medium)	chr8p21
17	229823_at	0.0020	-3.4		Transcribed locus	
16	204869_at	0.0104	-3.5	PCSK2	proprotein convertase subtilisin/kexin type 2	chr20p11.2
15	228863_at	0.0353	-3.5	PCDH17	Hypothetical protein LOC144997	chr13q21.1
14	212096_s_at	0.0028	-3.5	MTUS1	mitochondrial tumor suppressor 1	chr8p22
13	210839_s_at	0.0185	-3.6	ENPP2	ectonucleotide pyrophosphatase/phosphodiesterase 2 (autotaxin)	chr8q24.1
12	205305_at	0.0010	-3.6	FGL1	fibrinogen-like 1	chr8p22-p21.3
11	221245_s_at	0.0207	-4	C2orf31	chromosome 2 open reading frame 31 /// chromosome 2 open reading frame 31	chr2q34
10	204035_at	0.0092	-4.1	SCG2	secretogranin II (chromogranin C)	chr2q35-q36
9	204389_at	0.0035	-4.3	MAOA	monoamine oxidase A	chrXp11.4-p11.3
8	206805_at	0.0153	-4.3	SEMA3A	sema domain immunoglobulin domain (lg) short basic domain secreted (semaphorin) 3A	chr7p12.1
7	209392_at	0.0081	-4.5	ENPP2	ectonucleotide pyrophosphatase/phosphodiesterase 2 (autotaxin)	chr8q24.1
6	209205_s_at	0.0131	-4.6	LMO4	LIM domain only 4	chr1p22.3
5	212741_at	0.0098	-4.6	MAOA	monoamine oxidase A	chrXp11.4-p11.3
4	204388_s_at	0.0077	-4.7	MAOA	monoamine oxidase A	chrXp11.4-p11.3
3	213847_at	0.0334	-4.9	PRPH	peripherin	chr12q12-q13
2	204870_s_at	0.0019	-9.2	PCSK2	proprotein convertase subtilisin/kexin type 2	chr20p11.2
1	201739_at	0.0023	-10.1	SGK	serum/glucocorticoid regulated kinase	chr6q23

**Table 12.3** Most up and down-regulated genes derived from the comparison C99WT1/mock (n=3, p<0.05), analyzed with the Array Assist software and the PLIER algorithm.

## 12.2.2 Genes identified using the GC-RMA algorithm (Language R, Bioconductor)

**Table 12.4 Most up and down-regulated genes derived from the comparison C99I45F/C99WT1 ( $A\beta_{42}/A\beta_{40}\uparrow$ , n=3, p<0.005, fold change of expression >2.0, C99WT1 was the baseline experiment)**

Position	Probe Set ID	p-value	Fold change C99I45F/C99WT1	Gene Symbol	Gene Title	Chromosomal Location
1	205358_at	0.00034	8.7	GRIA2	glutamate receptor, ionotropic, AMPA 2	chr4q32-q33
2	213920_at	0.00426	6.9	CUTL2	cut-like 2 (Drosophila)	chr12q24.13
3	209591_s_at	0.00005	6.2	BMP7	bone morphogenetic protein 7 (osteogenic protein 1)	chr20q13
4	221933_at	0.00007	5.0	NLGN4X	neuroligin 4, X-linked	chrxp22.32-p22.31
5	212096_s_at	0.00100	5.0	MTUS1	mitochondrial tumor suppressor 1	chr8p22
6	206502_s_at	0.00291	5.0	INSM1	insulinoma-associated 1	chr20p11.2
7	218623_at	0.00288	4.9			
8	203329_at	0.00139	4.4	PTPRM	protein tyrosine phosphatase, receptor type, M	chr18p11.2
9	213338_at	0.00352	4.3	RIS1	Ras-induced senescence 1	chr3p21.3
10	203973_s_at	0.00372	3.9	CEBPD	CCAAT/enhancer binding protein (C/EBP), delta	chr8p11.2-p11.1
11	209590_at	0.00110	3.8	BMP7	bone morphogenetic protein 7 (osteogenic protein 1)	chr20q13
12	201645_at	0.00210	3.7	TNC	tenascin C (hexabrachion)	chr9q33
13	210108_at	0.00113	3.7	CACNA1D	calcium channel, voltage-dependent, L type, alpha 1D subunit	chr3p14.3
14	205348_s_at	0.00176	3.4	DNC11	dynein, cytoplasmic, intermediate polypeptide 1	chr7q21.3-q22.1
15	206290_s_at	0.00135	3.2	RGS7	regulator of G-protein signaling 7	chr1q43
16	219225_at	0.00201	3.0	PGBD5	piggyBac transposable element derived 5	chr1q42.13
17	219825_at	0.00262	3.0	CYP26B1	cytochrome P450, family 26, subfamily B, polypeptide 1	chr2p13.2
18	201341_at	0.00116	2.8	ENC1	ectodermal-neural cortex (with BTB-like domain)	chr5q12-q13.3
19	212658_at	0.00112	2.8	LHFPL2	lipoma HMGIC fusion partner-like 2	chr5q14.1
20	207076_s_at	0.00470	2.6	ASS	argininosuccinate synthetase	chr9q34.1
21	201621_at	0.00002	2.6	NBL1	neuroblastoma, suppression of tumorigenicity 1	chr1p36.13-p36.11
22	212538_at	0.00343	2.6	DOCK9	dedicator of cytokinesis 9	chr13q32.3
23	213273_at	0.00476	2.6	ODZ4	odz, odd Oz/ten-m homolog 4 (Drosophila)	chr11q14.1
24	37005_at	0.00003	2.5	NBL1	neuroblastoma, suppression of tumorigenicity 1	chr1p36.13-p36.11
25	213744_at	0.00138	2.4	ATRNL1	attractin-like 1	chr10q26
26	205003_at	0.00244	2.4	DOCK4	dedicator of cytokinesis 4	chr7q31.1
27	219277_s_at	0.00124	2.3	OGDHL	oxoglutarate dehydrogenase-like	chr10q11.23
28	37950_at	0.00090	2.2	PREP	prolyl endopeptidase	chr6q22
29	213802_at	0.00035	2.2			
30	211259_s_at	0.00481	2.1	BMP7	bone morphogenetic protein 7 (osteogenic protein 1)	chr20q13
31	205515_at	0.00486	2.1	PRSS12	protease, serine, 12 (neurotrypsin, motopsin)	chr4q28.1

32	205279_s_at	0.00018	2.1	GLRB	glycine receptor, beta	chr4q31.3
33	204140_at	0.00210	2.1	TPST1	tyrosylprotein sulfotransferase 1	chr7q11.21
34	212325_at	0.00380	2.1	KIAA1102	KIAA1102 protein	chr4p13
35	201037_at	0.00230	2.1	PFKP	phosphofructokinase, platelet	chr10p15.3-p15.2
36	218899_s_at	0.00240	2.0	BAALC	brain and acute leukemia, cytoplasmic	chr8q22.3
23	212057_at	0.00110	-2.0	KIAA0182	KIAA0182 protein	chr16q24.1
22	221605_s_at	0.00494	-2.1	PIPOX	pipecolic acid oxidase	chr17q11.2
21	219031_s_at	0.00246	-2.1			
20	208424_s_at	0.00433	-2.1	CIAPIN1	cytokine induced apoptosis inhibitor 1	chr16q13-q21
19	211671_s_at	0.00129	-2.2	NR3C1	nuclear receptor subfamily 3, group C, member 1 (glucocorticoid receptor)	chr5q31
18	207966_s_at	0.00288	-2.3	GLG1	golgi apparatus protein 1	chr16q22-q23
17	206848_at	0.00007	-2.3			
16	217200_x_at	0.00034	-2.3			
15	218354_at	0.00424	-2.3	HSPC176	hematopoietic stem/progenitor cells 176	chr16q24.3
14	209163_at	0.00333	-2.3	CYB561	cytochrome b-561	chr17q11-qter
13	209560_s_at	0.00430	-2.4	DLK1	delta-like 1 homolog (Drosophila)	chr14q32
12	203028_s_at	0.00028	-2.5	CYBA	cytochrome b-245, alpha polypeptide	chr16q24
11	202765_s_at	0.00105	-2.6			
10	219437_s_at	0.00033	-2.6	ANKRD11	ankyrin repeat domain 11	chr16q24.3
9	40837_at	0.00253	-2.8	TLE2	transducin-like enhancer of split 2 (E(sp1) homolog, Drosophila)	chr19p13.3
8	209164_s_at	0.00129	-2.8	CYB561	cytochrome b-561	chr17q11-qter
7	214347_s_at	0.00496	-3.1	DDC	dopa decarboxylase (aromatic L-amino acid decarboxylase)	chr7p11
6	201667_at	0.00243	-3.5	GJA1	gap junction protein, alpha 1, 43kDa (connexin 43)	chr6q21-q23.2
5	210816_s_at	0.00018	-4.8	CYB561	cytochrome b-561	chr17q11-qter
4	207074_s_at	0.00199	-5.1	SLC18A1	solute carrier family 18 (vesicular monoamine), member 1	chr8p21.3
3	208443_x_at	0.00439	-6.1	SHOX2	short stature homeobox 2	chr3q25-q26.1
2	201028_s_at	0.00403	-12.6	CD99	CD99 antigen	chrxp22.32; yp11.3
1	201029_s_at	0.00363	-15.7	CD99	CD99 antigen	chrxp22.32; yp11.3

**Table 12.4 Most up and down-regulated genes derived from the comparison C99I45F/C99WT1, (n=3, p<0.005, fold change of expression >2.0, C99WT1 was the baseline experiment), analyzed with the Language R software and the GC-RMA algorithm.**

**Table 12.5 Most up and down-regulated genes derived from the comparison C99V50F/C99WT1 ( $A\beta_{42}/A\beta_{40}\downarrow$ , n=3, p<0.005, fold change of expression >2.0, C99WT1 was the baseline experiment)**

Position	Probe Set ID	p-value	Fold change C99V50F/C99WT1	Gene Symbol	Gene Title	Chromosomal Location
1	206478_at	0.00142	5.3	KIAA0125	KIAA0125	chr14q32.33
2	208603_s_at	0.00191	2.5	MAPK8IP2	mitogen-activated protein kinase 8 interacting protein 2	chr22q13.33
3	200974_at	0.00115	2.2	ACTA2	actin, alpha 2, smooth muscle, aorta	chr10q23.3
4	216963_s_at	0.00449	2.2	GAP43	growth associated protein 43	chr3q13.1-q13.2
5	201860_s_at	0.00477	2.1	PLAT	plasminogen activator, tissue	chr8p12
6	206397_x_at	0.00269	2.1	GDF1	growth differentiation factor 1	chr19p12
7	204471_at	0.00190	2.1	GAP43	growth associated protein 43	chr3q13.1-q13.2
7	220287_at	0.00110	-2.0	ADAMTS9	a disintegrin-like and metalloprotease (reprolysin type) with thrombospondin type 1 motif, 9	chr3p14.3-p14.2
6	209220_at	0.00089	-2.5	GPC3	glypican 3	chrxq26.1
5	212148_at	0.00288	-2.8	PBX1	pre-B-cell leukemia transcription factor 1	chr1q23
4	209757_s_at	0.00416	-3.0	MYCN	v-myc myelocytomatosis viral related oncogene, neuroblastoma derived (avian)	chr2p24.1
3	202283_at	0.00362	-3.1	SERPINF1	serine (or cysteine) proteinase inhibitor, clade F (alpha-2 antiplasmin, pigment epithelium derived factor), member 1	chr17p13.1
2	209238_at	0.00268	-3.7	STX3A	syntaxin 3A	chr11q12.1
1	215632_at	0.00166	-12.5	NEUROG2	neurogenin 2	chr4q25

**Table 12.5 Most up and down-regulated genes derived from the comparison C99V50F/C99WT1 (p<0.005, n=3), analyzed with the Language R software and the GC-RMA algorithm.**

**Table 12.6 Most up and down-regulated genes derived from the comparison C99WT1/mock (n=3, p<0.005, fold change of expression >2.0, mock was the baseline experiment)**

Position	Probe Set ID	p-value	Fold change C99WT1/mock	Gene Symbol	Gene Title	Chromosomal Location
1	204239_s_at	0.00161	32.1	NNAT	neuronatin	chr20q11.2-q12
2	215632_at	0.00083	15.8	NEUROG2	neurogenin 2	chr4q25
3	214953_s_at	0.00000	12.1	APP	amyloid beta (A4) precursor protein (protease nexin-II, Alzheimer disease)	chr21q21.3
4	212713_at	0.00367	8.0	MFAP4	microfibrillar-associated protein 4	chr17p11.2
5	221796_at	0.00051	7.7	NTRK2	neurotrophic tyrosine kinase, receptor, type 2, non-catalytic isoform	chr9q22.1
6	214596_at	0.00006	6.1	CHRM3	cholinergic receptor, muscarinic 3	chr1q41-q44
7	212226_s_at	0.00031	5.7	PPAP2B	phosphatidic acid phosphatase type 2B	chr1pter-p22.1
8	222344_at	0.00048	4.6			
9	210414_at	0.00244	4.5	FLRT1	fibronectin leucine rich transmembrane protein 1	chr11q12-q13
10	221310_at	0.00074	4.1	FGF14	fibroblast growth factor 14	chr13q34
11	217996_at	0.00026	4.0	PHLDA1	pleckstrin homology-like domain, family A, member 1	chr12q15
12	213742_at	0.00041	3.8	SFRS11	splicing factor, arginine/serine-rich 11	chr1p31
13	213593_s_at	0.00062	3.4	TRA2A	transformer-2 alpha	chr7p15.3
14	215164_at	0.00120	3.4		MRNA; cDNA DKFZp564I083 (from clone DKFZp564I083)	
15	213517_at	0.00396	3.2	PCBP2	poly(rC) binding protein 2	chr12q13.12-q13.13
16	209144_s_at	0.00244	3.0	CBFA2T2	core-binding factor, runt domain, alpha subunit 2; translocated to, 2	chr20q11
17	212230_at	0.00025	2.8	PPAP2B	phosphatidic acid phosphatase type 2B	chr1pter-p22.1
18	222214_at	0.00289	2.8		CDNA: FLJ21335 fis, clone COL02546	
19	221234_s_at	0.00120	2.8	BACH2	BTB and CNC homology 1, basic leucine zipper transcription factor 2 /// BTB and CNC homology 1, basic leucine zipper transcription factor 2	chr6q15
20	209750_at	0.00392	2.6	NR1D2	nuclear receptor subfamily 1, group D, member 2	chr3p24.2
21	201294_s_at	0.00392	2.5	WSB1	WD repeat and SOCS box-containing 1	chr17q11.1
22	212966_at	0.00003	2.4	HIC2	hypermethylated in cancer 2	chr22q11.21
23	60815_at	0.00432	2.4	MGC13098	hypothetical protein MGC13098	chr7p13
24	213575_at	0.00016	2.4	TRA2A	transformer-2 alpha	chr7p15.3
25	212151_at	0.00074	2.4	PBX1	pre-B-cell leukemia transcription factor 1	chr1q23
26	207598_x_at	0.00393	2.4	XRCC2	X-ray repair complementing defective repair in Chinese hamster cells 2	chr7q36.1
27	205168_at	0.00392	2.4	DDR2	discoidin domain receptor family, member 2	chr1q12-q23
28	214251_s_at	0.00467	2.4	NUMA1	nuclear mitotic apparatus protein 1	chr11q13
29	213956_at	0.00095	2.3	CAP350	centrosome-associated protein 350	chr1p36.13-q41
30	206848_at	0.00009	2.2			
31	211466_at	0.00445	2.2	NFIB	nuclear factor I/B	chr9p24.1
32	211600_at	0.00438	2.1	PTPRO	protein tyrosine phosphatase, receptor type, O /// protein tyrosine phosphatase, receptor type, O	chr12p13.3-p13.2
33	214683_s_at	0.00344	2.1	CLK1	CDC-like kinase 1	chr2q33
34	210655_s_at	0.00406	2.1	FOXO3A	forkhead box O3A	chr6q21

Supplementary Information

35	208120_x_at	0.00427	2.1			
36	201309_x_at	0.00370	2.1	C5orf13	chromosome 5 open reading frame 13	chr5q22.1
37	207605_x_at	0.00479	2.1	H-plk	Krueppel-related zinc finger protein	chr7q11.21
38	222366_at	0.00497	2.1			
39	211571_s_at	0.00447	2.1	CSPG2	chondroitin sulfate proteoglycan 2 (versican)	chr5q14.3
40	213649_at	0.00353	2.1	SFRS7	splicing factor, arginine/serine-rich 7, 35kDa	chr2p22.1
41	219206_x_at	0.00250	2.0	CGI-119	CGI-119 protein	chr12q14.1-q15
42	218066_at	0.00125	2.0	SLC12A7	solute carrier family 12 (potassium/chloride transporters), member 7	chr5p15
104	213079_at	0.00080	-2.0	DT1P1A10	hypothetical protein DT1P1A10	chrxp11.22
103	201673_s_at	0.00357	-2.0	GYS1	glycogen synthase 1 (muscle)	chr19q13.3
102	205541_s_at	0.00002	-2.0	GSPT2	G1 to S phase transition 2	chrxp11.23-p11.21
101	207769_s_at	0.00001	-2.0	PQBP1	polyglutamine binding protein 1	chrxp11.23
100	209216_at	0.00307	-2.0	WDR45	WD repeat domain 45	chrxp11.23
99	203814_s_at	0.00003	-2.0	NQO2	NAD(P)H dehydrogenase, quinone 2	chr6pter-q12
98	208700_s_at	0.00021	-2.1	TKT	transketolase (Wernicke-Korsakoff syndrome)	chr3p14.3
97	203617_x_at	0.00002	-2.1	ELK1	ELK1, member of ETS oncogene family	chrxp11.2
96	219188_s_at	0.00377	-2.1	LRP16	LRP16 protein	chr11q11
95	204639_at	0.00054	-2.1	ADA	adenosine deaminase	chr20q12-q13.11
94	213744_at	0.00485	-2.1	ATRNL1	attractin-like 1	chr10q26
93	218532_s_at	0.00140	-2.1	FLJ20152	hypothetical protein FLJ20152	chr5p15.1
92	218935_at	0.00078	-2.1	EHD3	EH-domain containing 3	chr2p21
91	207447_s_at	0.00064	-2.1	HGNT-IV-H	UDP-N-acetylglucosamine:a-1,3-D-mannoside beta-1,4-N-acetylglucosaminyltransferase IV	chr12q21
90	203629_s_at	0.00007	-2.1	COG5	component of oligomeric golgi complex 5	chr7q22-q31
89	218826_at	0.00180	-2.1	SLC35F2	solute carrier family 35, member F2	chr11q22.3
88	218251_at	0.00014	-2.1	MID1IP1	MID1 interacting protein 1 (gastrulation specific G12-like (zebrafish))	chrxp11.4
87	203458_at	0.00072	-2.1	SPR	sepiapterin reductase (7,8-dihydrobiopterin:NADP+ oxidoreductase)	chr2p14-p12
86	204866_at	0.00005	-2.1	PHF16	PHD finger protein 16	chrxp11.3
85	201895_at	0.00003	-2.1	ARAF1	v-raf murine sarcoma 3611 viral oncogene homolog 1	chrxp11.4-p11.2
84	219959_at	0.00403	-2.1	MOCOS	molybdenum cofactor sulfurase	chr18q12
83	205324_s_at	0.00000	-2.1	FTSJ1	FtsJ homolog 1 (E. coli)	chrxp11.23
82	206339_at	0.00017	-2.1	CART	cocaine- and amphetamine-regulated transcript	chr5q13.2
81	221524_s_at	0.00092	-2.1	RRAGD	Ras-related GTP binding D	chr6q15-q16
80	200632_s_at	0.00450	-2.2	NDRG1	N-myc downstream regulated gene 1	chr8q24.3
79	218625_at	0.00027	-2.2	NRN1	neuritin 1	chr6p25.1
78	212916_at	0.00005	-2.2	PHF8	PHD finger protein 8	chrxp11.22
77	202504_at	0.00405	-2.2	TRIM29	tripartite motif-containing 29	chr11q22-q23
76	212063_at	0.00006	-2.2	CD44	CD44 antigen (homing function and Indian blood group system)	chr11p13
75	204412_s_at	0.00087	-2.2			
74	201136_at	0.00064	-2.2	PLP2	proteolipid protein 2 (colonic epithelium-enriched)	chrxp11.23
73	211896_s_at	0.00100	-2.2	DCN	decorin	chr12q13.2
72	211894_x_at	0.00079	-2.3	SEZ6L	seizure related 6 homolog (mouse)-like /// seizure related 6 homolog (mouse)-like	chr22q12.1
71	213200_at	0.00149	-2.3	SYP	synaptophysin	chrxp11.23-p11.22
70	204513_s_at	0.00192	-2.3	ELMO1	engulfment and cell motility 1 (ced-12 homolog, C. elegans)	chr7p14.1

Supplementary Information

69	218501_at	0.00087	-2.3	ARHGEF3	Rho guanine nucleotide exchange factor (GEF) 3	chr3p21-p13
68	213358_at	0.00097	-2.3	KIAA0802	KIAA0802	chr18p11.22
67	203303_at	0.00184	-2.3	TCTE1L	t-complex-associated-testis-expressed 1-like	chrxp21
66	203320_at	0.00003	-2.3	LNK	lymphocyte adaptor protein	chr12q24
65	218603_at	0.00015	-2.3	HECA	headcase homolog (Drosophila)	chr6q23-q24
64	213107_at	0.00119	-2.3	TNIK	TRAF2 and NCK interacting kinase	chr3q26.31
63	208690_s_at	0.00468	-2.3	PDLIM1	PDZ and LIM domain 1 (elfin)	chr10q22-q26.3
62	222138_s_at	0.00002	-2.3	WDR13	WD repeat domain 13	chrxp11.23
61	217763_s_at	0.00408	-2.4	RAB31	RAB31, member RAS oncogene family	chr18p11.3
60	206016_at	0.00037	-2.4	CXorf37	chromosome X open reading frame 37	chrxp11.23
59	203386_at	0.00154	-2.4	TBC1D4	TBC1 domain family, member 4	chr13q21.33
58	213787_s_at	0.00183	-2.4	EBP	emopamil binding protein (sterol isomerase)	chrxp11.23-p11.22
57	214527_s_at	0.00000	-2.4	PQBP1	polyglutamine binding protein 1	chrxp11.23
56	205433_at	0.00002	-2.4	BCHE	butyrylcholinesterase	chr3q26.1-q26.2
55	39966_at	0.00322	-2.5	CSPG5	chondroitin sulfate proteoglycan 5 (neuroglycan C)	chr3p21.3
54	209191_at	0.00239	-2.5	MGC4083	tubulin beta MGC4083	chr18p11.21
53	219855_at	0.00000	-2.5	NUDT11	nudix (nucleoside diphosphate linked moiety X)-type motif 11	chrxp11.22
52	212573_at	0.00198	-2.5	KIAA0830	KIAA0830 protein	chr11q21
51	33767_at	0.00270	-2.5	NEFH	neurofilament, heavy polypeptide 200kDa	chr22q12.2
50	203387_s_at	0.00298	-2.6	TBC1D4	TBC1 domain family, member 4	chr13q21.33
49	205857_at	0.00003	-2.6	SLC18A2	solute carrier family 18 (vesicular monoamine), member 2	chr10q25
48	213937_s_at	0.00000	-2.6	FTSJ1	FtsJ homolog 1 (E. coli)	chrxp11.23
47	200974_at	0.00024	-2.6	ACTA2	actin, alpha 2, smooth muscle, aorta	chr10q23.3
46	218619_s_at	0.00107	-2.7	SUV39H1	suppressor of variegation 3-9 homolog 1 (Drosophila)	chrxp11.23
45	210319_x_at	0.00183	-2.8			
44	205651_x_at	0.00000	-2.9	RAPGEF4	Rap guanine nucleotide exchange factor (GEF) 4	chr2q31-q32
43	212730_at	0.00016	-2.9	DMN	desmuslin	chr15q26.3
42	207813_s_at	0.00027	-3.0	FDXR	ferredoxin reductase	chr17q24-q25
41	221914_at	0.00194	-3.0	SYN1	synapsin I	chrxp11.23
40	202735_at	0.00262	-3.1	EBP	emopamil binding protein (sterol isomerase)	chrxp11.23-p11.22
39	212457_at	0.00000	-3.1	TFE3	transcription factor binding to IGHM enhancer 3	chrxp11.22
38	217764_s_at	0.00193	-3.1	RAB31	RAB31, member RAS oncogene family	chr18p11.3
37	203430_at	0.00347	-3.2	HEBP2	heme binding protein 2	chr6q24
36	219073_s_at	0.00008	-3.2	OSBPL10	oxysterol binding protein-like 10	chr3p22.3
35	204955_at	0.00054	-3.2	SRPX	sushi-repeat-containing protein, X-linked	chrxp21.1
34	206187_at	0.00026	-3.3	PTGIR	prostaglandin I2 (prostacyclin) receptor (IP)	chr19q13.3
33	210997_at	0.00204	-3.4	HGF	hepatocyte growth factor (hepapoietin A; scatter factor)	chr7q21.1
32	204471_at	0.00002	-3.4	GAP43	growth associated protein 43	chr3q13.1-q13.2
31	217762_s_at	0.00180	-3.4	RAB31	RAB31, member RAS oncogene family	chr18p11.3
30	205230_at	0.00343	-3.4	RPH3A	rabphilin 3A homolog (mouse)	chr12q24.13
29	207620_s_at	0.00001	-3.4	CASK	calcium/calmodulin-dependent serine protein kinase (MAGUK family)	chrxp11.4
28	205656_at	0.00340	-3.5	PCDH17	protocadherin 17	chr13q21.1
27	216963_s_at	0.00011	-3.5	GAP43	growth associated protein 43	chr3q13.1-q13.2
26	221288_at	0.00174	-3.6	GPR22	G protein-coupled receptor 22	chr7q22-q31.1

25	206837_at	0.00012	-3.6	CART1	cartilage paired-class homeoprotein 1	chr12q21.3-q22
24	205068_s_at	0.00326	-3.6	ARHGAP26	Rho GTPase activating protein 26	chr5q31
23	218424_s_at	0.00003	-3.6	TSAP6	dudulin 2	chr2q14.2
22	210519_s_at	0.00066	-3.8	NQO1	NAD(P)H dehydrogenase, quinone 1	chr16q22.1
21	209627_s_at	0.00153	-4.0	OSBPL3	oxysterol binding protein-like 3	chr7p15
20	219271_at	0.00131	-4.0	GALNT14	UDP-N-acetyl-alpha-D-galactosamine:polypeptide N-acetylgalactosaminyltransferase 14 (GalNAc-T14)	chr2p23.1
19	206376_at	0.00482	-4.3	SLC6A15	solute carrier family 6 (neurotransmitter transporter), member 15	chr12q21.3
18	210675_s_at	0.00160	-4.4	PTPRR	protein tyrosine phosphatase, receptor type, R	chr12q15
17	205305_at	0.00000	-4.5	FGL1	fibrinogen-like 1	chr8p22-p21.3
16	213664_at	0.00000	-4.9	SLC1A1	solute carrier family 1 (neuronal/epithelial high affinity glutamate transporter, system Xag), member 1	chr9p24
15	213620_s_at	0.00001	-5.2	ICAM2	intercellular adhesion molecule 2	chr17q23-q25
14	206478_at	0.00103	-5.7	KIAA0125	KIAA0125	chr14q32.33
13	204035_at	0.00055	-5.9	SCG2	secretogranin II (chromogranin C)	chr2q35-q36
12	213609_s_at	0.00005	-6.2	SEZ6L	seizure related 6 homolog (mouse)-like	chr22q12.1
11	212741_at	0.00017	-6.5	MAOA	monoamine oxidase A	chrxp11.4-p11.3
10	204389_at	0.00001	-6.5	MAOA	monoamine oxidase A	chrxp11.4-p11.3
9	202242_at	0.00021	-6.9	TM4SF2	transmembrane 4 superfamily member 2	chrxp11.4
8	204388_s_at	0.00008	-7.0	MAOA	monoamine oxidase A	chrxp11.4-p11.3
7	221245_s_at	0.00019	-7.1	C2orf31	chromosome 2 open reading frame 31 /// chromosome 2 open reading frame 31	chr2q34
6	210839_s_at	0.00000	-7.1	ENPP2	ectonucleotide pyrophosphatase/phosphodiesterase 2 (autotaxin)	chr8q24.1
5	212096_s_at	0.00017	-7.2	MTUS1	mitochondrial tumor suppressor 1	chr8p22
4	218858_at	0.00001	-7.9	DEPDC6	DEP domain containing 6	chr8q24.12
3	213847_at	0.00050	-10.4	PRPH	peripherin	chr12q12-q13
2	209392_at	0.00000	-17.3	ENPP2	ectonucleotide pyrophosphatase/phosphodiesterase 2 (autotaxin)	chr8q24.1
1	201739_at	0.00184	-21.8	SGK	serum/glucocorticoid regulated kinase	chr6q23

**Table 12.6** Most up and down-regulated genes derived from the comparison C99WT1/mock (n=3, p≤0.005), analyzed with the Language R software and the GC-RMA algorithm.

### 12.2.3 Genes identified using the MAS 5 algorithm (Array Assist, Stratagene)

**Table 12.7 Most up and down-regulated genes derived from the comparison C99I45F/C99WT1 ( $A\beta_{42}/A\beta_{40}\uparrow$ , n=3, p<0.05, C99WT1 was the baseline experiment)**

Position	Probe Set ID	p-value	Fold Change C99I45F/C99WT1	Gene Symbol	Gene Title	Chromosomal Location
1	215168_at	0.00653	8.0	TIMM17A	translocase of inner mitochondrial membrane 17 homolog A (yeast)	chr1q32.1
2	238368_at	0.00132	6.3	PVT1	Pvt1 oncogene homolog, MYC activator (mouse)	chr8q24
3	240106_at	0.00132	6.3	MGC4170	MGC4170 protein	chr12q23.3
4	241040_at	0.00132	6.3		Transcribed locus	
5	213174_at	0.00313	6.3	TTC9	tetratricopeptide repeat domain 9	chr14q24.2
6	213338_at	0.03347	6.3	RIS1	Ras-induced senescence 1	chr3p21.3
7	207860_at	0.00219	5.0	NCR1	natural cytotoxicity triggering receptor 1	chr19q13.42
8	217085_at	0.00219	5.0	SLC14A2	Solute carrier family 14 (urea transporter), member 2	chr18q12.1-q21.1
9	217394_at	0.00219	5.0	TRA@	T cell receptor alpha locus	chr14q11.2
10	232825_s_at	0.00219	5.0	C18orf4	chromosome 18 open reading frame 4	chr18q22.1
11	242758_x_at	0.00219	5.0	JMJD1A	Jumonji domain containing 1A	chr2p11.2
12	243169_at	0.00219	5.0		Transcribed locus	
13	227342_s_at	0.02322	5.0	MYEOV	myeloma overexpressed gene (in a subset of t(11;14) positive multiple myelomas)	chr11q13
14	205220_at	0.02490	5.0	GPR109B	G protein-coupled receptor 109B /// G protein-coupled receptor 109B	chr12q24.31
15	211341_at	0.02490	5.0	POU4F1	POU domain, class 4, transcription factor 1	chr13q21.1-q22
16	239776_at	0.02490	5.0		MRNA; cDNA DKFZp686G0585	
17	242003_at	0.02490	5.0	LOC157697	Hypothetical protein LOC157697	chr8p23.3
18	244261_at	0.02490	5.0	IL28RA	interleukin 28 receptor, alpha (interferon, lambda receptor)	chr1p36.11
19	209909_s_at	0.00219	4.0	TGFB2	transforming growth factor, beta 2	chr1q41
20	216994_s_at	0.00219	4.0	RUNX2	runt-related transcription factor 2	chr6p21
21	219949_at	0.00219	4.0	LRRC2	leucine rich repeat containing 2	chr3p21.31
22	220190_s_at	0.00219	4.0	ALF /// SALF	TFIIA-alpha/beta-like factor /// stoned B/TFIIA-alpha/beta-like factor	chr2p16.3
23	206575_at	0.02490	4.0	CDKL5	cyclin-dependent kinase-like 5	chrXp22
24	241177_at	0.02490	4.0		Transcribed locus	
25	242708_at	0.02490	4.0	PEX1	Peroxisome biogenesis factor 1	chr7q21-q22
26	212942_s_at	0.02572	4.0	KIAA1199	KIAA1199	chr15q24
27	214343_s_at	0.02572	4.0	ATXN7L1	ataxin 7-like 1 /// ataxin 7-like 4	chr7q22.1 /// chr7q22.3
28	215559_at	0.02572	4.0	ABCC6	ATP-binding cassette, sub-family C (CFTR/MRP), member 6	chr16p13.1
29	216191_s_at	0.02572	4.0	TRA@ /// TRD@	T cell receptor alpha locus /// T cell receptor delta locus	chr14q11.2
30	221182_at	0.02572	4.0	FLJ23550	hypothetical protein FLJ23550	chr1q24.3
31	224506_s_at	0.02572	4.0	C9orf67	chromosome 9 open reading frame 67 /// chromosome 9 open reading frame 67	chr9q34.13
32	228054_at	0.02572	4.0	TMEM44	transmembrane protein 44	chr3q29
33	233314_at	0.02572	4.0	PTEN	phosphatase and tensin homolog (mutated in multiple advanced cancers 1)	chr10q23.3
34	241051_at	0.02572	4.0			

Supplementary Information

35	243847_at	0.02572	4.0	CLIC4	Chloride intracellular channel 4	chr1p36.11
36	244604_at	0.02572	4.0	LOC340171	hypothetical LOC340171	chr6q14.1
37	201645_at	0.00749	3.2	TNC	tenascin C (hexabrachion)	chr9q33
38	205302_at	0.00749	3.2	IGFBP1	insulin-like growth factor binding protein 1	chr7p13-p12
39	206856_at	0.00749	3.2	LILRB5	leukocyte immunoglobulin-like receptor, subfamily B (with TM and ITIM domains), member 5	chr19q13.4
40	213317_at	0.00749	3.2	CLIC5	Chloride intracellular channel 5	chr6p12.1-21.1
41	215351_at	0.00749	3.2	RTCD1	RNA terminal phosphate cyclase domain 1	chr1p21.3
42	215653_at	0.00749	3.2		Clone IMAGE:205688, mRNA sequence	
43	216541_x_at	0.00749	3.2	IGHG1 /// IGHG3 /// MGC27165	immunoglobulin heavy constant gamma 1 (G1m marker) /// immunoglobulin heavy constant gamma 3 (G3m marker) /// hypothetical protein MGC27165	chr14q32.33
44	217006_x_at	0.00749	3.2			
45	220996_s_at	0.00749	3.2	C1orf14	chromosome 1 open reading frame 14 /// chromosome 1 open reading frame 14	chr1q25
46	223045_at	0.00749	3.2	EGLN1	egl nine homolog 1 (C. elegans)	chr1q42.1
47	223694_at	0.00749	3.2	TRIM7	tripartite motif-containing 7	chr5q35.3
48	231797_at	0.00749	3.2	SIX4	sine oculis homeobox homolog 4 (Drosophila)	chr14q23
49	234531_at	0.00749	3.2		CDNA FLJ13378 fis, clone PLACE1000931	
50	235519_at	0.00749	3.2			
51	236538_at	0.00749	3.2	GRIA2	glutamate receptor, ionotropic, AMPA 2	chr4q32-q33
52	238825_at	0.00749	3.2	ACRC	acidic repeat containing	chrXq13.1
53	240459_at	0.00749	3.2	YT521	splicing factor YT521-B	chr4q13.2
54	242223_at	0.00749	3.2	MCCC1	Methylcrotonoyl-Coenzyme A carboxylase 1 (alpha)	chr3q27
55	244399_at	0.00749	3.2	STAB2	Stabilin 2	chr12q23.3
56	244528_at	0.00749	3.2	ARMC8	Armadillo repeat containing 8	chr3q22.3
57	244611_at	0.00749	3.2	THRAP1	Thyroid hormone receptor associated protein 1	chr17q22-q23
58	206838_at	0.01324	3.2	TBX19	T-box 19	chr1q23-q24
59	225864_at	0.01324	3.2	NSE2	breast cancer membrane protein 101	chr8q24.21
60	226560_at	0.01324	3.2	SGPP2	Sphingosine-1-phosphate phosphatase 2	chr2q36.1
61	228018_at	0.01324	3.2			
62	230394_at	0.01324	3.2	TCP10L	t-complex 10 (mouse)-like	chr21q22.11
63	233908_x_at	0.01324	3.2		CDNA FLJ12050 fis, clone HEMBB1002002	
64	233927_at	0.01324	3.2		CDNA FLJ11919 fis, clone HEMBB1000274	
65	241154_x_at	0.01324	3.2	MTSS1	Metastasis suppressor 1	chr8p22
66	241265_x_at	0.01324	3.2	TINP1	TGF beta-inducible nuclear protein 1	chr5q13.3
67	241793_at	0.01324	3.2	ZMYND17	zinc finger, MYND domain containing 17	chr10q22.2
68	242299_at	0.01324	3.2		Transcribed locus	
69	204988_at	0.01613	2.5	FGB	fibrinogen, B beta polypeptide	chr4q28
70	206490_at	0.01613	2.5	DLGAP1	discs, large (Drosophila) homolog-associated protein 1	chr18p11.3
71	206619_at	0.01613	2.5	DKK4	dickkopf homolog 4 (Xenopus laevis)	chr8p11.2-p11.1
72	206699_x_at	0.01613	2.5	NPAS1	neuronal PAS domain protein 1	chr19q13.2-q13.3
73	206814_at	0.01613	2.5	NGFB	nerve growth factor, beta polypeptide	chr1p13.1
74	207766_at	0.01613	2.5	CDKL1	cyclin-dependent kinase-like 1 (CDC2-related kinase)	chr14q21.3
75	208007_at	0.01613	2.5			
76	209689_at	0.01613	2.5	FLJ10996	hypothetical protein FLJ10996	chr2q14.1
77	211128_at	0.01613	2.5	EDA	ectodysplasin A	chrXq12-q13.1
78	217199_s_at	0.01613	2.5	STAT2	signal transducer and activator of transcription 2, 113kDa	chr12q13.3
79	217523_at	0.01613	2.5	CD44	CD44 antigen (homing function and Indian blood group system)	chr11p13
80	219059_s_at	0.01613	2.5	XLKD1	extracellular link domain containing 1	chr11p15
81	221667_s_at	0.01613	2.5	HSPB8	heat shock 22kDa protein 8	chr12q24.23

Supplementary Information

82	223316_at	0.01613	2.5	CCDC3	coiled-coil domain containing 3	chr10p13
83	223574_x_at	0.01613	2.5	PPP2R2C	protein phosphatase 2 (formerly 2A), regulatory subunit B (PR 52), gamma isoform	chr4p16.1
84	224274_at	0.01613	2.5	C14orf155	chromosome 14 open reading frame 155	chr14q21.2
85	224300_x_at	0.01613	2.5	FTCD	formiminotransferase cyclodeaminase	chr21q22.3
86	226220_at	0.01613	2.5	DREV1	DORA reverse strand protein 1	chr16p13-p12
87	226281_at	0.01613	2.5	DNER	delta-Notch-like EGF repeat-containing transmembrane	chr2q36.3
88	227276_at	0.01613	2.5	PLXDC2	plexin domain containing 2	chr10p12.31
89	228590_at	0.01613	2.5	FLJ20758	FLJ20758 protein	chr2p11.2
90	232729_at	0.01613	2.5	FBXO32	F-box protein 32	chr8q24.13
91	234261_at	0.01613	2.5	EB-1	E2a-Pbx1-associated protein	chr12q23.1
92	234717_at	0.01613	2.5			
93	234826_at	0.01613	2.5	LOC375295	Hypothetical gene supported by BC013438	chr2q31.1
94	234924_s_at	0.01613	2.5	KIAA1441	KIAA1441 protein	chr1q21.2
95	236316_at	0.01613	2.5	FAM3C	family with sequence similarity 3, member C	chr7q22.1-q31.1
96	236991_at	0.01613	2.5		Transcribed locus	
97	237273_at	0.01613	2.5	KCNU1	potassium channel, subfamily U, member 1	chr8p11.22
98	237469_at	0.01613	2.5	TOP2A	Topoisomerase (DNA II) alpha 170kDa	chr17q21-q22
99	238977_at	0.01613	2.5	MCM6	MCM6 minichromosome maintenance deficient 6 (MIS5 homolog, <i>S. pombe</i> ) ( <i>S. cerevisiae</i> )	chr2q21
100	239064_at	0.01613	2.5		CDNA FLJ36582 fis, clone TRACH2013081	
100	232391_at	0.00749	-3.2	GIOT-1	gonadotropin inducible transcription repressor 1	chr19q13.12
99	237820_at	0.00749	-3.2			
98	239337_at	0.00749	-3.2			
97	240300_at	0.00749	-3.2	TK2	Thymidine kinase 2, mitochondrial	chr16q22-q23.1
96	241092_at	0.00749	-3.2	BBX	Bobby sox homolog ( <i>Drosophila</i> )	chr3q13.1
95	241139_at	0.00749	-3.2		Transcribed locus	
94	243353_at	0.00749	-3.2	PDCD8	Programmed cell death 8 (apoptosis-inducing factor)	chrXq25-q26
93	206701_x_at	0.02572	-3.2	EDNRB	endothelin receptor type B	chr13q22
92	207652_s_at	0.02572	-3.2	CMKLR1	chemokine-like receptor 1	chr12q24.1
91	210584_s_at	0.02572	-3.2	POLDIP3 /// dJ222E13.2	polymerase (DNA-directed), delta interacting protein 3 /// similar to CGI-96	chr22q13.2
90	213277_at	0.02572	-3.2	ZFP36L1	Zinc finger protein 36, C3H type-like 1	chr14q22-q24
89	214131_at	0.02572	-3.2	CYorf15B	chromosome Y open reading frame 15B	chrYq11.222
88	214374_s_at	0.02572	-3.2	PPFIBP1	PTPRF interacting protein, binding protein 1 (liprin beta 1)	chr12p11.23-p11.22
87	216039_at	0.02572	-3.2	PMS2L1	postmeiotic segregation increased 2-like 1	chr7q22.1
86	221026_s_at	0.02572	-3.2	SCRT1	scratch homolog 1, zinc finger protein ( <i>Drosophila</i> ) /// scratch homolog 1, zinc finger protein ( <i>Drosophila</i> )	chr8q24.3
85	223620_at	0.02572	-3.2	GPR34	G protein-coupled receptor 34	chrXp11.4-p11.3
84	223815_at	0.02572	-3.2	LOC90799	hypothetical protein BC009518	chr17q24.2
83	228533_at	0.02572	-3.2	FNDC3A	fibronectin type III domain containing 3A	chr13q14.2
82	228575_at	0.02572	-3.2	FNDC6	fibronectin type III domain containing 6	chr3q22.3
81	229972_at	0.02572	-3.2			
80	230385_at	0.02572	-3.2	LOC153277	hypothetical protein LOC153277	chr5q23.3
79	230451_at	0.02572	-3.2			
78	230534_at	0.02572	-3.2	MGC15634	hypothetical protein MGC15634	chr1q42.13
77	232688_at	0.02572	-3.2	BMP2K	BMP2 inducible kinase	chr4q21.21
76	233703_x_at	0.02572	-3.2	FLJ42117	FLJ42117 protein	chr3p14.2
75	233714_at	0.02572	-3.2	ARNT	Aryl hydrocarbon receptor nuclear translocator	chr1q21
74	233997_at	0.02572	-3.2		Hypothetical LOC388790	chr20p11.23
73	235592_at	0.02572	-3.2	ELL2	Elongation factor, RNA polymerase II, 2	chr5q15

Supplementary Information

72	236783_at	0.02572	-3.2	KCNIP4	Kv channel interacting protein 4	chr4p15.31
71	239849_at	0.02572	-3.2	EMCN	Endomucin	chr4q24
70	239862_at	0.02572	-3.2	TPD52	Tumor protein D52	chr8q21
69	240936_at	0.02572	-3.2	RARRES1	Retinoic acid receptor responder (tazarotene induced) 1	chr3q25.32
68	241088_at	0.02572	-3.2	MGC14816	Hypothetical protein MGC14816	chr1p21.3
67	242542_at	0.02572	-3.2	PHACTR2	Phosphatase and actin regulator 2	chr6q24.2
66	242815_x_at	0.02572	-3.2		CDNA FLJ32308 fis, clone PROST2002906	
65	242921_at	0.02572	-3.2	RUTBC2	RUN and TBC1 domain containing 2	chr22q11.23
64	244231_at	0.02572	-3.2			
63	203556_at	0.00219	-5.0	ZHX2	zinc fingers and homeoboxes 2	chr8q24.13
62	207329_at	0.00219	-5.0	MMP8	matrix metalloproteinase 8 (neutrophil collagenase)	chr11q22.3
61	213094_at	0.00219	-5.0	GPR126	G protein-coupled receptor 126	chr6q24.1
60	214648_at	0.00219	-5.0	GPX5	Glutathione peroxidase 5 (epididymal androgen-related protein)	chr6p22.1
59	220674_at	0.00219	-5.0	FLJ22814	hypothetical protein FLJ22814	chr19q13.13
58	224021_at	0.00219	-5.0	RP1	retinitis pigmentosa 1 (autosomal dominant)	chr8q11-q13
57	236419_at	0.00219	-5.0	TGFBR2	Transforming growth factor, beta receptor II (70/80kDa)	chr3p22
56	237314_at	0.00219	-5.0	C10orf63	chromosome 10 open reading frame 63	chr10p12.1
55	243268_at	0.00219	-5.0	UNQ3112	LVL3112	chr11q24.2
54	240853_at	0.00219	-5.0			
53	221433_at	0.01324	-5.0	FGF21	fibroblast growth factor 21	chr19q13.1-qter
52	234861_at	0.01324	-5.0	LOC93463	hypothetical protein LOC93463	chr2q37.3
51	236293_at	0.01324	-5.0	RHOH	Ras homolog gene family, member H	chr4p13
50	236606_at	0.01324	-5.0	SAV1	Salvador homolog 1 (Drosophila)	chr14q13-q23
49	237216_at	0.01324	-5.0	GARNL1	GTPase activating Rap/RanGAP domain-like 1	chr14q13.2
48	237429_at	0.01324	-5.0		Transcribed locus	
47	242892_at	0.01324	-5.0	PER2	Period homolog 2 (Drosophila)	chr2q37.3
46	243247_at	0.01324	-5.0	MGC27434	Hypothetical LOC401477	chr8q24.21
45	244318_at	0.01324	-5.0	KIAA0241	KIAA0241 protein	chr7p14.3
44	AFFX-r2-Bs-dap-M_at	0.01324	-5.0			
43	241098_at	0.01324	-5.0			
42	208525_s_at	0.02490	-5.0	OR2F1 /// OR2F2	olfactory receptor, family 2, subfamily F, member 1 /// olfactory receptor, family 2, subfamily F, member 2	chr7q35
41	217655_at	0.02490	-5.0	FXVD5	FXVD domain containing ion transport regulator 5	chr19q12-q13.1
40	224095_at	0.02490	-5.0		PRO2591	
39	225453_x_at	0.02490	-5.0	LOC115098	Hypothetical protein BC013949	chr19p13.11
38	232415_at	0.02490	-5.0	PCDHB13	protocadherin beta 13	chr5q31
37	236401_at	0.02490	-5.0			
36	240782_at	0.02490	-5.0		Transcribed locus	
35	241256_at	0.02490	-5.0			
34	211811_s_at	0.00132	-5.0	PCDHA6	protocadherin alpha 6	chr5q31
33	215325_x_at	0.00132	-5.0	C19orf26	chromosome 19 open reading frame 26	chr19p13.3
32	228356_at	0.00132	-5.0	ANKRD11	Ankyrin repeat domain 11	chr16q24.3
31	232958_at	0.00132	-5.0		CDNA FLJ13595 fis, clone PLACE1009595	
30	236399_at	0.00132	-5.0		Homo sapiens, clone IMAGE:3896086, mRNA	
29	236469_at	0.00132	-5.0		MRNA full length insert cDNA clone EUROIMAGE 110216	
28	238808_at	0.00132	-5.0	HOXA13	Homeo box A13	chr7p15-p14
27	241113_at	0.00132	-5.0	C14orf125	Chromosome 14 open reading frame 125	chr14q12
26	242893_at	0.00132	-5.0			
25	217267_s_at	0.00776	-5.0			
24	219584_at	0.00776	-5.0	PLA1A	phospholipase A1 member A	chr3q13.13-q13.2

23	238878_at	0.00776	-5.0	ARX	aristaless related homeobox	chrXp22.1-p21.3
22	234764_x_at	0.01613	-5.0	IGLC2	Ig lambda chain V-region (VL-AIG) /// Immunoglobulin lambda variable 3-21	chr22q11.2
21	244306_at	0.01613	-5.0		Transcribed locus	
20	203726_s_at	0.03517	-5.0	LAMA3	laminin, alpha 3	chr18q11.2
19	240156_at	0.03517	-5.0	RFX2	Regulatory factor X, 2 (influences HLA class II expression)	chr19p13.3-p13.2
18	223596_at	0.03902	-5.0	SLC12A6	solute carrier family 12 (potassium/chloride transporters), member 6	chr15q13-q15
17	230951_at	0.03902	-5.0	EPB41L5	Erythrocyte membrane protein band 4.1 like 5	chr2q14.2
16	223374_s_at	0.00653	-8.0	B3GALT3	UDP-Gal:betaGlcNAc beta 1,3-galactosyltransferase, polypeptide 3	chr3q25
15	242105_at	0.00653	-8.0	CCNE1	Cyclin E1	chr19q12
14	243528_at	0.00653	-8.0	ZDHHC2	Zinc finger, DHHC domain containing 2	chr8p21.3-p22
13	240408_at	0.01613	-8.0	TBC1D14	TBC1 domain family, member 14	chr4p16.1
12	241502_x_at	0.01613	-8.0	MRPS22	Mitochondrial ribosomal protein S22	chr3q23
11	207430_s_at	0.00056	-8.0	MSMB	microseminoprotein, beta-	chr10q11.2
10	243602_at	0.00056	-8.0		Transcribed locus	
9	216045_at	0.00749	-8.0	KIAA0565	KIAA0565 gene product	chr17p11.2
8	210705_s_at	0.01580	-8.0	TRIM5	tripartite motif-containing 5	chr11p15
7	214488_at	0.01944	-8.0	RAP2B	RAP2B, member of RAS oncogene family	chr3q25.2
6	217050_at	0.02322	-8.0	EPAG	early lymphoid activation protein	
5	238237_at	0.02322	-8.0		Transcribed locus, weakly similar to NP_064698.1 a disintegrin and metalloprotease domain 3 (cyritestin) [Rattus norvegicus]	
4	233297_s_at	0.00039	-8.0			
3	241855_s_at	0.01417	-8.0	CUL3	Cullin 3	chr2q36.3
2	241532_at	0.01944	-8.0			
1	239200_at	0.03800	-8.0			

**Table12.7 Most up and down-regulated genes derived from the comparison C99I45F/C99WT1 (n=3, p<0.05), analyzed with the Array Assist software and the MAS 5 algorithm.**

**Table 12.8 Most up and down-regulated genes derived from the comparison C99V50F/C99WT1 ( $A\beta_{42}/A\beta_{40}\downarrow$ , n=3, p<0.05, C99WT1 was the baseline experiment)**

Position	Probe Set ID	p-value	Fold Change C99V50F/ C99WT1	Gene Symbol	Gene Title	Gene Location
1	226757_at	0.01613	16.0	IFIT2	interferon-induced protein with tetratricopeptide repeats 2	chr10q23-q25
2	231644_at	0.00749	10.1		Transcribed locus	
3	225664_at	0.00653	8.0	COL12A1	collagen, type XII, alpha 1	chr6q12-q13
4	242271_at	0.00653	8.0	SLC26A9	solute carrier family 26, member 9	chr1q31-q32
5	241833_at	0.00749	8.0		Full length insert cDNA clone YY86C01	
6	241436_at	0.03411	8.0	SCNN1G	sodium channel, nonvoltage-gated 1, gamma	chr16p12
7	205414_s_at	0.00132	6.3	KIAA0672	KIAA0672 gene product	chr17p12
8	211667_x_at	0.00132	6.3		T-cell receptor alpha chain	
9	217394_at	0.00132	6.3	TRA@	T cell receptor alpha locus	chr14q11.2
10	230643_at	0.00132	6.3	WNT9A	Wingless-type MMTV integration site family, member 9A	chr1q42
11	244399_at	0.00132	6.3	STAB2	Stabilin 2	chr12q23.3
12	233499_at	0.01580	6.3			
13	204908_s_at	0.01613	6.3	BCL3	B-cell CLL/lymphoma 3	chr19q13.1-q13.2
14	224506_s_at	0.01613	6.3	C9orf67	chromosome 9 open reading frame 67 /// chromosome 9 open reading frame 67	chr9q34.13
15	225288_at	0.01613	6.3	COL27A1	Collagen, type XXVII, alpha 1	chr9q32
16	237193_s_at	0.01613	6.3			
17	243530_at	0.01613	6.3	CPSF6	Cleavage and polyadenylation specific factor 6, 68kDa	chr12q15
18	237874_at	0.03347	6.3	RNF150	Ring finger protein 150	chr4q31.21
19	241756_at	0.03347	6.3	SMARCA2	SWI/SNF related, matrix associated, actin dependent regulator of chromatin, subfamily a, member 2	chr9p22.3
20	239776_at	0.03902	6.3		MRNA; cDNA DKFZp686G0585	
21	205829_at	0.00219	5.0	HSD17B1	hydroxysteroid (17-beta) dehydrogenase 1	chr17q11-q21
22	206229_x_at	0.00219	5.0	PAX2	paired box gene 2	chr10q24
23	234531_at	0.00219	5.0		CDNA FLJ13378 fis, clone PLACE1000931	
24	244480_at	0.00219	5.0		Transcribed locus	
25	244604_at	0.00219	5.0	LOC340171	hypothetical LOC340171	chr6q14.1
26	206670_s_at	0.00481	5.0	GAD1	glutamate decarboxylase 1 (brain, 67kDa)	chr2q31
27	216994_s_at	0.00481	5.0	RUNX2	runt-related transcription factor 2	chr6p21
28	202404_s_at	0.02322	5.0	COL1A2	collagen, type I, alpha 2	chr7q22.1
29	224213_at	0.02322	5.0	C14orf91	chromosome 14 open reading frame 91	chr14q22.1-q23.3
30	232656_at	0.02322	5.0		CDNA FLJ11692 fis, clone HEMBA1004983	
31	243103_at	0.02322	5.0	TK1	Thymidine kinase 1, soluble	chr17q23.2-q25.3
32	220551_at	0.02490	5.0	SLC17A6	solute carrier family 17 (sodium-dependent inorganic phosphate cotransporter), member 6	chr11p14.3
33	221134_at	0.02490	5.0	ANGPT4	angiopoietin 4	chr20p13
34	230516_at	0.02490	5.0	C7orf30	Chromosome 7 open reading frame 30	chr7p15.3
35	232729_at	0.02490	5.0	FBXO32	F-box protein 32	chr8q24.13

Supplementary Information

36	237641_at	0.02490	5.0	LOC388563	hypothetical LOC388563	chr19q13.42
37	237785_at	0.02490	5.0	ASB14	Ankyrin repeat and SOCS box-containing 14	chr3p21.1
38	240341_at	0.02490	5.0	LOC339529	Hypothetical protein LOC339529	chr1q44
39	241051_at	0.02490	5.0			
40	241834_at	0.02490	5.0	PAR1	Prader-Willi/Angelman region-1	chr15q11.2
41	209909_s_at	0.00219	4.0	TGFB2	transforming growth factor, beta 2	chr1q41
42	220077_at	0.00219	4.0	FLJ22349	hypothetical protein FLJ22349	chr22q13.2
43	220474_at	0.00219	4.0	SLC25A21	solute carrier family 25 (mitochondrial oxodicarboxylate carrier), member 21	chr14q11.2
44	232277_at	0.00219	4.0	SLC28A3	Solute carrier family 28 (sodium-coupled nucleoside transporter), member 3	chr9q22.2
45	226959_at	0.02490	4.0	LOC283070	Hypothetical protein LOC283070	chr10p14
46	233084_s_at	0.02490	4.0	C10orf94	chromosome 10 open reading frame 94	chr10q26.3
47	237488_at	0.02490	4.0	HNRPC	Heterogeneous nuclear ribonucleoprotein C (C1/C2)	chr14q11.2
48	238289_at	0.02490	4.0	RPGR	Retinitis pigmentosa GTPase regulator	chrXp11.4
49	240643_at	0.02490	4.0	TTBK1	tau tubulin kinase 1	chr6p21.1
50	240711_at	0.02490	4.0	MGC12197	Arginine/serine-rich coiled-coil 1	chr3q25.32
51	241363_at	0.02490	4.0	FLJ20433	Hypothetical protein FLJ20433	chr9q34.3
52	242202_at	0.02490	4.0		Hypothetical LOC402532	chr7
53	242708_at	0.02490	4.0	PEX1	Peroxisome biogenesis factor 1	chr7q21-q22
54	244163_at	0.02490	4.0	SEMA3A	Sema domain, immunoglobulin domain (Ig), short basic domain, secreted, (semaphorin) 3A	chr7p12.1
55	244548_at	0.02490	4.0	ARHGAP26	Rho GTPase activating protein 26	chr5q31
56	202600_s_at	0.02572	4.0	NRIP1	nuclear receptor interacting protein 1	chr21q11.2
57	206805_at	0.02572	4.0	SEMA3A	sema domain, immunoglobulin domain (Ig), short basic domain, secreted, (semaphorin) 3A	chr7p12.1
58	207178_s_at	0.02572	4.0	FRK	fyn-related kinase	chr6q21-q22.3
59	214146_s_at	0.02572	4.0	PPBP	pro-platelet basic protein (chemokine (C-X-C motif) ligand 7)	chr4q12-q13
60	214708_at	0.02572	4.0	SNTB1	syntrophin, beta 1 (dystrophin-associated protein A1, 59kDa, basic component 1)	chr8q23-q24
61	214781_at	0.02572	4.0			
62	216140_at	0.02572	4.0			
63	217085_at	0.02572	4.0	SLC14A2	Solute carrier family 14 (urea transporter), member 2	chr18q12.1-q21.1
64	219327_s_at	0.02572	4.0	GPRC5C	G protein-coupled receptor, family C, group 5, member C	chr17q25
65	223858_at	0.02572	4.0	ESRRB	estrogen-related receptor beta	chr14q24.3
66	224012_at	0.02572	4.0	ANKRD20	ankyrin repeat domain 20A	chr9q12 /// chr9p11.2
67	228146_at	0.02572	4.0	LOC339263	hypothetical protein LOC339263	chr17p11.2
68	228644_s_at	0.02572	4.0	SLC12A4	Solute carrier family 12 (potassium/chloride transporters), member 4	chr16q22.1
69	229880_at	0.02572	4.0		Full-length cDNA clone CS0DD009YF23	
70	229999_at	0.02572	4.0			
71	232024_at	0.02572	4.0	GIMAP2	GTPase, IMAP family member 2	chr7q36.1
72	232993_at	0.02572	4.0	SYNJ1	Synaptojanin 1	chr21q22.2
73	233753_at	0.02572	4.0	SFRS15	splicing factor, arginine/serine-rich 15	chr21q22.1
74	234283_at	0.02572	4.0	HSPC117	Hypothetical protein HSPC117	chr22q12
75	235655_at	0.02572	4.0			
76	235995_at	0.02572	4.0	LOC442009	similar to solute carrier family 7 member 8 (53.8 kD) (4K364)	chr2p24.1

Supplementary Information

77	236295_s_at	0.02572	4.0	NOD3	NOD3 protein	chr16p13.3
78	238368_at	0.02572	4.0	PVT1	Pvt1 oncogene homolog, MYC activator (mouse)	chr8q24
79	238825_at	0.02572	4.0	ACRC	acidic repeat containing	chrXq13.1
80	239310_at	0.02572	4.0	DDB2	Damage-specific DNA binding protein 2, 48kDa	chr11p12-p11
81	241103_at	0.02572	4.0			
82	242173_at	0.02572	4.0			
83	243091_at	0.02572	4.0	CRYZL1	Crystallin, zeta (quinone reductase)-like 1	chr21q21.3
84	243919_at	0.02572	4.0			
85	244060_at	0.02572	4.0	ADD2	Adducin 2 (beta)	chr2p14-p13
86	244528_at	0.02572	4.0	ARMC8	Armadillo repeat containing 8	chr3q22.3
87	241673_x_at	0.03902	4.0			
88	206155_at	0.00749	3.2	ABCC2	ATP-binding cassette, sub-family C (CFTR/MRP), member 2	chr10q24
89	207147_at	0.00749	3.2	DLX2	distal-less homeo box 2	chr2q32
90	207355_at	0.00749	3.2	SLC1A7	solute carrier family 1 (glutamate transporter), member 7	chr1p32.3
91	211635_x_at	0.00749	3.2			
92	215496_at	0.00749	3.2	SAMD4	sterile alpha motif domain containing 4	chr14q22.2
93	220416_at	0.00749	3.2	ATP8B4	ATPase, Class I, type 8B, member 4	chr15q21.2
94	224043_s_at	0.00749	3.2	UPB1	ureidopropionase, beta	chr22q11.2
95	226646_at	0.00749	3.2	KLF2	Kruppel-like factor 2 (lung)	chr19p13.13-p13.11
96	227371_at	0.00749	3.2	BAIAP2L1	BAI1-associated protein 2-like 1	chr7q21.3-q22.1
97	228434_at	0.00749	3.2	BTNL9	butyrophilin-like 9	chr5q35.3
98	228599_at	0.00749	3.2	MS4A1	Membrane-spanning 4-domains, subfamily A, member 1	chr11q12
99	228761_at	0.00749	3.2	DKFZp547F072	hypothetical protein DKFZp547F072	chr8q24.3
100	229910_at	0.00749	3.2	LOC126669	hypothetical protein LOC126669	chr1q21.3
101	230034_x_at	0.00749	3.2	MRPL41	Mitochondrial ribosomal protein L41	chr9q34.3
102	230462_at	0.00749	3.2	NUMB	numb homolog (Drosophila)	chr14q24.3
101	238647_at	0.01613	-2.5	C14orf28	chromosome 14 open reading frame 28	chr14q21.2
100	238815_at	0.01613	-2.5	LRRTM1	leucine rich repeat transmembrane neuronal 1	chr2p12
99	239632_at	0.01613	-2.5			
98	239666_at	0.01613	-2.5	PYGO2	Pygopus homolog 2 (Drosophila)	chr1q22
97	240138_at	0.01613	-2.5			
96	240695_at	0.01613	-2.5	SH2D3C	SH2 domain containing 3C	chr9q34.11
95	241312_at	0.01613	-2.5			
94	241423_at	0.01613	-2.5			chr5q13.3
93	242281_at	0.01613	-2.5	GLUL	Glutamate-ammonia ligase (glutamine synthase)	chr1q31
92	242445_at	0.01613	-2.5	FGD4	FYVE, RhoGEF and PH domain containing 4	chr12p11.21
91	243122_at	0.01613	-2.5	PACRG	PARK2 co-regulated	chr6q26
90	243334_at	0.01613	-2.5	CACNA1D	Calcium channel, voltage-dependent, L type, alpha 1D subunit	chr3p14.3
89	243559_at	0.01613	-2.5	ZNF148	Zinc finger protein 148 (pHZ-52)	chr3q21
88	244669_at	0.01613	-2.5	C6orf160	LOC441164	chr6q14.3
87	238308_at	0.01613	-2.5			
86	238311_at	0.01613	-2.5			
85	206466_at	0.00749	-3.2			
84	206761_at	0.00749	-3.2	CD96	CD96 antigen	chr3q13.13-q13.2

Supplementary Information

83	207324_s_at	0.00749	-3.2	DSC1	desmocollin 1	chr18q12.2 18q12.1
82	207977_s_at	0.00749	-3.2	DPT	dermatopontin	chr1q12-q23
81	208350_at	0.00749	-3.2	CSN1S1	casein alpha s1	chr4q21.1
80	217203_at	0.00749	-3.2			
79	221996_s_at	0.00749	-3.2	CLTB	Clathrin, light polypeptide (Lcb)	chr4q2-q3
78	224851_at	0.00749	-3.2	CDK6	cyclin-dependent kinase 6	chr7q21-q22
77	225590_at	0.00749	-3.2	SH3MD2	SH3 multiple domains 2	chr4q32.3-q33
76	226613_at	0.00749	-3.2	TBC1D10A	TBC1 domain family, member 10A	chr22q12.1-qter
75	228624_at	0.00749	-3.2	FLJ11155	hypothetical protein FLJ11155	chr4q32.1
74	229134_at	0.00749	-3.2			
73	229706_at	0.00749	-3.2	TCERG1	transcription elongation regulator 1	chr5q31
72	230051_at	0.00749	-3.2	C10orf47	chromosome 10 open reading frame 47	chr10p14
71	230395_at	0.00749	-3.2	DREV1	DORA reverse strand protein 1	chr16p13-p12
70	232562_at	0.00749	-3.2	CDNA FLJ11554		
69	232903_at	0.00749	-3.2	CDNA: FLJ21199		
68	235401_s_at	0.00749	-3.2	FREB	Fc receptor homolog expressed in B cells	chr1q23.3
67	235574_at	0.00749	-3.2	GBP4	guanylate binding protein 4	chr1p22.2
66	236410_x_at	0.00749	-3.2	LOC387593	TPTE/TPIP pseudogene	chr22q13
65	238752_at	0.00749	-3.2	MRS2L	MRS2-like, magnesium homeostasis factor (S. cerevisiae)	chr6p22.3-p22.1
64	238898_at	0.00749	-3.2			
63	239169_at	0.00749	-3.2	RAD52B	RAD52 homolog B (S. cerevisiae)	chr17q11.2
62	239299_at	0.00749	-3.2	DDI1	DNA-damage inducible protein 1	
61	241057_x_at	0.00749	-3.2	DDX26	DEAD/H (Asp-Glu-Ala-Asp/His) box polypeptide 26	chr13q14.12-q14.2
60	241113_at	0.00749	-3.2	C14orf125	Chromosome 14 open reading frame 125	chr14q12
59	241270_at	0.00749	-3.2	RHBDL6	Rhomboid, veinlet-like 6 (Drosophila)	chr17q25.1
58	243184_at	0.00749	-3.2	TJP1	Tight junction protein 1 (zona occludens 1)	chr15q13
57	243636_s_at	0.00749	-3.2	EVE1	SH3 domain protein D19	chr4q31.3
56	240921_at	0.00749	-3.2			
55	240910_at	0.00749	-3.2			
54	206145_at	0.04742	-3.2	RHAG	Rhesus blood group-associated glycoprotein	chr6p21.1-p11
53	207008_at	0.04742	-3.2	IL8RB	interleukin 8 receptor, beta	chr2q35
52	207221_at	0.04742	-3.2	F2RL3	coagulation factor II (thrombin) receptor-like 3	chr19p12
51	208536_s_at	0.04742	-3.2	BCL2L11	BCL2-like 11 (apoptosis facilitator)	chr2q13
50	214342_at	0.04742	-3.2	ATXN7L1 /// ATXN7L4	ataxin 7-like 1 /// ataxin 7-like 4	chr7q22.1 /// chr7q22.3
49	214460_at	0.04742	-3.2	LSAMP	limbic system-associated membrane protein	chr3q13.2-q21
48	214680_at	0.04742	-3.2	NTRK2	neurotrophic tyrosine kinase, receptor, type 2, non-catalytic isoform	chr9q22.1
47	216131_at	0.04742	-3.2	FRMD4B	FERM domain containing 4B	chr3p14.1
46	216558_x_at	0.04742	-3.2			
45	221790_s_at	0.04742	-3.2	LDLRAP1	low density lipoprotein receptor adaptor protein 1	chr1p36-p35
44	229554_at	0.04742	-3.2	LUM	Lumican	chr12q21.3-q22
43	230752_at	0.04742	-3.2	CBX5	Chromobox homolog 5 (HP1 alpha homolog, Drosophila)	chr12q13.13
42	231699_at	0.04742	-3.2	NFKBIA	Nuclear factor of kappa light polypeptide gene enhancer in B-cells inhibitor, alpha	chr14q13
41	231709_x_at	0.04742	-3.2	MYR8	Myosin heavy chain Myr 8	chr13q33.3

40	237640_at	0.04742	-3.2	C14orf138	chromosome 14 open reading frame 138	chr14q21.3
39	237841_at	0.04742	-3.2	C9orf5	Chromosome 9 open reading frame 5	chr9q31
38	238170_at	0.04742	-3.2	Cep63	Centrosome protein Cep63	chr3q22.1
37	239022_at	0.04742	-3.2	SDHAL2	Succinate dehydrogenase complex, subunit A, flavoprotein-like 2	chr3q29
36	239837_at	0.04742	-3.2	ADAM11	A disintegrin and metalloproteinase domain 11	chr17q21.3
35	244323_at	0.04742	-3.2	BHLHB5	basic helix-loop-helix domain containing, class B, 5	chr8q13
34	237009_at	0.04742	-3.2			
33	241104_at	0.04742	-3.2			
32	210096_at	0.00749	-4.0	CYP4B1	cytochrome P450, family 4, subfamily B, polypeptide 1	chr1p34-p12
31	202307_s_at	0.02572	-4.0	TAP1	transporter 1, ATP-binding cassette, sub-family B (MDR/TAP)	chr6p21.3
30	208170_s_at	0.02572	-4.0	TRIM31	tripartite motif-containing 31	chr6p21.3
29	210525_x_at	0.02572	-4.0	C14orf143	chromosome 14 open reading frame 143	chr14q32.11
28	211907_s_at	0.02572	-4.0	PARD6B	par-6 partitioning defective 6 homolog beta (C. elegans)	chr20q13.13 chr20p11.21-p11.1
27	215487_x_at	0.02572	-4.0			
26	217584_at	0.02572	-4.0	NPC1	Niemann-Pick disease, type C1	chr18q11-q12
25	220931_at	0.02572	-4.0	MGC5590	hypothetical protein MGC5590	chr13q14.11
24	221928_at	0.02572	-4.0	ACACB	acetyl-Coenzyme A carboxylase beta	chr12q24.11
23	222272_x_at	0.02572	-4.0	SCIN	scinderin	chr7p21.3
22	223582_at	0.02572	-4.0	MASS1	monogenic, audiogenic seizure susceptibility 1 homolog (mouse)	chr5q13
21	229261_at	0.02572	-4.0	SOS1	Son of sevenless homolog 1 (Drosophila)	chr2p22-p21
20	236399_at	0.02572	-4.0			
19	240242_at	0.02572	-4.0			
18	240421_x_at	0.02572	-4.0			
17	242321_at	0.02572	-4.0			
16	243660_at	0.02572	-4.0	CHD9	Chromodomain helicase DNA binding protein 9	chr16q12.2
15	202235_at	0.00219	-5.0	SLC16A1	solute carrier family 16 (monocarboxylic acid transporters), member 1	chr1p12
14	206715_at	0.00219	-5.0	TFEC	transcription factor EC	chr7q31.2
13	207430_s_at	0.00219	-5.0	MSMB	microseminoprotein, beta-	chr10q11.2
12	203902_at	0.01324	-5.0	HEPH	hephaestin	chrXq11-q12
11	214479_at	0.01324	-5.0	GFRA3	GDNF family receptor alpha 3	chr5q31.1-q31.3
10	214826_at	0.01324	-5.0	2'-PDE	2'-phosphodiesterase	chr3p14.3
9	233305_at	0.01324	-5.0	EFCBP1	EF hand calcium binding protein 1	chr8q21.3
8	238555_at	0.01324	-5.0	MRPS31	Mitochondrial ribosomal protein S31	chr13q14.11
7	234945_at	0.02490	-5.0	FAM54A	family with sequence similarity 54, member A	chr6q23.3
6	240894_at	0.02490	-5.0			
5	205380_at	0.00132	-6.3	PDZK1	PDZ domain containing 1	chr1q21
4	234344_at	0.00132	-6.3	RAP2C	RAP2C, member of RAS oncogene family	chrXq25
3	214488_at	0.01613	-6.3	RAP2B	RAP2B, member of RAS oncogene family	chr3q25.2
2	244749_at	0.01613	-6.3			
1	240850_at	0.03517	-6.3	DYRK1A	Dual-specificity tyrosine-(Y)-phosphorylation regulated kinase 1A	chr21q22.13

**Table 12.8 Most up and down-regulated genes derived from the comparison C99V50F/C99WT1 (n=3, p<0.05), analyzed with the Array Assist software and the MAS 5 algorithm.**

**Table 12.9 Most up and down-regulated genes derived from the comparison C99WT1/mock (n=3, p<0.05, mock was the baseline experiment)**

Position	Probe Set ID	p-value	Fold change C99WT1/mock	Gene Symbol	Gene Title	Chromosomal Location
1	219691_at	0.00015	25.4	SAMD9	sterile alpha motif domain containing 9	chr7q21.2
2	244621_x_at	0.00039	12.7		Transcribed locus	
3	244820_at	0.00582	12.7	ZNRF3	Zinc and ring finger 3	chr22q12.1
4	238237_at	0.01417	12.7		Transcribed locus, weakly similar to NP_064698.1 a disintegrin and metalloprotease domain 3 (cyritestin) [Rattus norvegicus]	
5	240146_at	0.00056	10.1	CAPZA2	Capping protein (actin filament) muscle Z-line, alpha 2	chr7q31.2-q31.3
6	221795_at	0.00793	10.1	NTRK2	neurotrophic tyrosine kinase, receptor, type 2, non-catalytic isoform	chr9q22.1
7	204239_s_at	0.01944	10.1	NNAT	neuronatin	chr20q11.2-q12
8	242631_x_at	0.03411	10.1			
9	214953_s_at	0.00056	8.0	APP	amyloid beta (A4) precursor protein (protease nexin-II, Alzheimer disease)	chr21q21.2 21q21.3
10	219584_at	0.00653	8.0	PLA1A	phospholipase A1 member A	chr3q13.13-q13.2
11	237462_at	0.00653	8.0	MGC40405	Hypothetical protein MGC40405	chr7q21.2
12	201789_at	0.00132	6.3	DHRS7	dehydrogenase/reductase (SDR family) member 7	chr14q23.1
13	206142_at	0.00132	6.3	ZNF135	zinc finger protein 135 (clone pHZ-17)	chr19q13.4
14	211466_at	0.00132	6.3	NFIB	nuclear factor I/B	chr9p24.1
15	215632_at	0.00132	6.3	NEUROG2	neurogenin 2	chr4q25
16	218113_at	0.00132	6.3	TMEM2	transmembrane protein 2	chr9q13-q21
17	229723_at	0.00132	6.3	TAGAP	T-cell activation GTPase activating protein	chr6q25.3
18	231281_at	0.00132	6.3		CDNA FLJ13469 fis, clone PLACE1003528	
19	236484_at	0.00132	6.3	STARD7	START domain containing 7	chr2q11.2
20	237383_at	0.00132	6.3		Transcribed locus	
21	237656_at	0.00132	6.3	BOMB	BH3-only member B protein	chr4q35.1
22	238332_at	0.00132	6.3	ANKRD29	ankyrin repeat domain 29	chr18q11.2
23	240327_at	0.00132	6.3	SEPT6	Septin 6	chrXq24
24	240472_at	0.00132	6.3		MRNA; cDNA DKFZp761N2217 (from clone DKFZp761N2217)	
25	242036_x_at	0.00132	6.3	ATP2B3	ATPase, Ca++ transporting, plasma membrane 3	chrXq28
26	239465_at	0.00132	6.3			
27	204320_at	0.00313	6.3	COL11A1	collagen, type XI, alpha 1	chr1p21
28	242433_at	0.00313	6.3			
29	227344_at	0.01613	6.3	ZNFN1A1	Zinc finger protein, subfamily 1A, 1 (Ikaros)	chr7p13-p11.1
30	233295_at	0.01613	6.3		Pheromone receptor (PHRET) pseudogene, partial mRNA sequence	
31	238635_at	0.01613	6.3	FLJ21657	hypothetical protein FLJ21657	chr5p12
32	240906_at	0.01613	6.3	MRPS36	Mitochondrial ribosomal protein S36	chr5q13.2
33	243838_at	0.01613	6.3	ATXN2	Ataxin 2	chr12q24.1
34	233172_at	0.03902	6.3		CDNA FLJ13313 fis, clone OVARC1001489	
35	215188_at	0.00219	5.0	STK24	serine/threonine kinase 24 (STE20 homolog, yeast)	chr13q31.2-q32.3
36	215824_at	0.00219	5.0	NUDT7	nudix (nucleoside diphosphate linked moiety X)-type motif 7	chr16q23.1
37	227266_s_at	0.00219	5.0	FYB	FYN binding protein (FYB-120/130)	chr5p13.1
38	229162_s_at	0.00219	5.0	ABTB1	Ankyrin repeat and BTB (POZ) domain containing 1	chr3q21

Supplementary Information

39	233243_at	0.00219	5.0	CBFA2T2	Core-binding factor, runt domain, alpha subunit 2; translocated to, 2	chr20q11
40	234344_at	0.00219	5.0	RAP2C	RAP2C, member of RAS oncogene family	chrXq25
41	238481_at	0.00219	5.0	MGP	matrix Gla protein	chr12p13.1-p12.3
42	238932_at	0.00219	5.0		CDNA FLJ41867 fis, clone OCBBF2005546	
43	239712_at	0.00219	5.0	C9orf93	Chromosome 9 open reading frame 93	chr9p22.3
44	244478_at	0.00219	5.0		Transcribed locus, weakly similar to XP_515998.1 similar to SLC39A10 protein [Pan troglodytes]	
45	236653_at	0.00481	5.0			
46	236791_at	0.00481	5.0	AMMECR1	Hypothetical protein LOC286505	chrXq22.3
47	243195_s_at	0.00481	5.0	ZNF551	zinc finger protein 551	chr19q13.43
48	244148_at	0.00481	5.0		Similar to 40S ribosomal protein S20	chr2q23.1
49	244434_at	0.00481	5.0			
50	210697_at	0.02322	5.0	ZNF257	zinc finger protein 257	chr19q13
51	227070_at	0.02322	5.0	GLT8D2	glycosyltransferase 8 domain containing 2	chr12q
52	236293_at	0.02322	5.0	RHOH	Ras homolog gene family, member H	chr4p13
53	243325_at	0.02322	5.0	GSTK1	Glutathione S-transferase kappa 1	
54	203902_at	0.02490	5.0	HEPH	hephaestin	chrXq11-q12
55	206392_s_at	0.02490	5.0	RARRES1	retinoic acid receptor responder (tazarotene induced) 1	chr3q25.32
56	215558_at	0.02490	5.0	UBR2	Ubiquitin protein ligase E3 component n-recogin 2	chr6p21.1
57	216766_at	0.02490	5.0	PRKCE	Protein kinase C, epsilon	chr2p21
58	228496_s_at	0.02490	5.0	CRIM1	Cysteine-rich motor neuron 1	chr2p21
59	232343_at	0.02490	5.0		CDNA FLJ12138 fis, clone MAMMA1000331	
60	232473_at	0.02490	5.0	PRPF18	PRP18 pre-mRNA processing factor 18 homolog (yeast)	chr10p13
61	232502_at	0.02490	5.0	FLJ34077	weakly similar to zinc finger protein 195	chr10q23-q24
62	236523_at	0.02490	5.0	LOC285556	hypothetical protein LOC285556	chr4q23
63	236892_s_at	0.02490	5.0			
64	243421_at	0.02490	5.0			
65	243436_at	0.03347	5.0		Transcribed locus	
66	239938_x_at	0.04742	5.0	MEF2C	MADS box transcription enhancer factor 2, polypeptide C (myocyte enhancer factor 2C)	chr5q14
67	214488_at	0.00219	4.0	RAP2B	RAP2B, member of RAS oncogene family	chr3q25.2
68	219955_at	0.00219	4.0			
69	220521_s_at	0.00219	4.0	APG16L	APG16 autophagy 16-like (S. cerevisiae)	chr2q37.1 chr10q26.13-q26.3
70	232930_at	0.00219	4.0	DOCK1	Dedicator of cytokinesis 1	chr13q12.11
71	236837_x_at	0.00219	4.0		Hypothetical LOC387904	
72	243602_at	0.00219	4.0		Transcribed locus	
73	206443_at	0.02490	4.0	RORB	RAR-related orphan receptor B	chr9q22
74	208577_at	0.02490	4.0	HIST1H3C	histone 1, H3c	chr6p21.3
75	210426_x_at	0.02490	4.0	RORA	RAR-related orphan receptor A	chr15q21-q22
76	214680_at	0.02490	4.0	NTRK2	neurotrophic tyrosine kinase, receptor, type 2, non-catalytic isoform	chr9q22.1
77	219211_at	0.02490	4.0	USP18	ubiquitin specific protease 18	chr22q11.21
78	220609_at	0.02490	4.0	LOC441118	similar to FLJ44216 protein; similar to cell surface antigen	chr5q35.3
79	227803_at	0.02490	4.0	ENPP5	ectonucleotide pyrophosphatase/phosphodiesterase 5 (putative function)	chr6p21.1-p11.2
80	233717_x_at	0.02490	4.0	SMO	Smoothened homolog (Drosophila)	chr7q32.3
81	235593_at	0.02490	4.0	ZFX1B	zinc finger homeobox 1b	chr2q22
82	237491_at	0.02490	4.0	MYH10	Myosin, heavy polypeptide 10, non-muscle	chr17p13
83	237951_at	0.02490	4.0	FLJ21628	Hypothetical protein FLJ21628	chr5q35.3
84	243332_at	0.02490	4.0			
85	244050_at	0.02490	4.0			

Supplementary Information

86	205703_at	0.02572	4.0	ATP6V0A2	ATPase, H+ transporting, lysosomal V0 subunit a isoform 2	chr12q24.31
87	208011_at	0.02572	4.0	PTPN22	protein tyrosine phosphatase, non-receptor type 22 (lymphoid)	chr1p13.3-p13.1
88	214712_at	0.02572	4.0			
89	215213_at	0.02572	4.0	NUP54	nucleoporin 54kDa	chr4q21.1
90	216157_at	0.02572	4.0		CDNA FLJ14169 fis, clone NT2RP2002056	
91	222966_at	0.02572	4.0			
92	226701_at	0.02572	4.0	GJA5	gap junction protein, alpha 5, 40kDa (connexin 40)	chr1q21.1
93	228884_at	0.02572	4.0	LOC440010	similar to leucine rich repeat containing 27	chr10q26.3
94	231145_at	0.02572	4.0	SLC25A21	Solute carrier family 25 (mitochondrial oxodicarboxylate carrier), member 21	chr14q11.2
95	231357_at	0.02572	4.0	UNQ5782	macrophage antigen h	chr12p13.31
96	233548_at	0.02572	4.0		Clone IMAGE:35115, mRNA sequence	
97	235438_at	0.02572	4.0		MRNA; cDNA DKFZp686E22185 (from clone DKFZp686E22185)	
98	239270_at	0.02572	4.0	PLCXD3	phosphatidylinositol-specific phospholipase C, X domain containing 3	chr5p13.1
99	239448_at	0.02572	4.0			
100	239619_at	0.02572	4.0	ZNF395	Zinc finger protein 395	chr8p21.1
100	229823_at	0.00749	-3.2		Transcribed locus	
99	230398_at	0.00749	-3.2	CTEN	C-terminal tensin-like	chr17q21.2
98	232533_at	0.00749	-3.2		CDNA FLJ31054 fis, clone HSYRA2000706	
97	235108_at	0.00749	-3.2	KCNK3	Potassium channel, subfamily K, member 3	chr2p23
96	235655_at	0.00749	-3.2		Transcribed locus	
95	235900_at	0.00749	-3.2	MGC29671	hypothetical protein MGC29671	chr17p13.2
94	236652_at	0.00749	-3.2	LOC149703	hypothetical protein LOC149703	chr20q13.12
93	237608_at	0.00749	-3.2			
92	237631_at	0.00749	-3.2		Transcribed locus	
91	238600_at	0.00749	-3.2	MARLIN1	multiple coiled-coil GABABR1-binding protein	chr4p16.1
90	240483_at	0.00749	-3.2	LOC377064	kruppel-like zinc finger factor X17	chr3p12.3
89	242003_at	0.00749	-3.2	LOC157697	Hypothetical protein LOC157697	chr8p23.3
88	200872_at	0.04742	-3.2	S100A10	S100 calcium binding protein A10 (annexin II ligand, calpactin I, light polypeptide (p11))	chr1q21
87	202910_s_at	0.04742	-3.2	CD97	CD97 antigen	chr19p13
86	205856_at	0.04742	-3.2	SLC14A1	solute carrier family 14 (urea transporter), member 1 (Kidd blood group)	chr18q11-q12
85	206136_at	0.04742	-3.2	FZD5	frizzled homolog 5 (Drosophila)	chr2q33-q34
84	207860_at	0.04742	-3.2	NCR1	natural cytotoxicity triggering receptor 1	chr19q13.42
83	207864_at	0.04742	-3.2	SCN7A	sodium channel, voltage-gated, type VII, alpha	chr2q21-q23
82	210181_s_at	0.04742	-3.2	CABP1	calcium binding protein 1 (calbrain)	chr12q24.31
81	218484_at	0.04742	-3.2	LOC56901	NADH:ubiquinone oxidoreductase MLRQ subunit homolog	chr12q13.3
80	219478_at	0.04742	-3.2	WFDC1	WAP four-disulfide core domain 1	chr16q24.3
79	219772_s_at	0.04742	-3.2	SMPX	small muscle protein, X-linked	chrXp22.1
78	221312_at	0.04742	-3.2	GLP2R	glucagon-like peptide 2 receptor	chr17p13.3
77	221667_s_at	0.04742	-3.2	HSPB8	heat shock 22kDa protein 8	chr12q24.23
76	222963_s_at	0.04742	-3.2	IL1RAPL1	interleukin 1 receptor accessory protein-like 1	chrXp22.1-p21.3
75	227910_at	0.04742	-3.2	LOC63929	hypothetical protein LOC63929	chr22q13.31-q13.33
74	228590_at	0.04742	-3.2	FLJ20758	FLJ20758 protein	chr2p11.2
73	231760_at	0.04742	-3.2	C20orf51	chromosome 20 open reading frame 51	chr20q13.33
72	235943_at	0.04742	-3.2	FLJ13197	Hypothetical LOC401126	chr4p14
71	236151_at	0.04742	-3.2	KIAA1853	KIAA1853 protein	chr12q24.23
70	236638_at	0.04742	-3.2		Transcribed locus	

Supplementary Information

69	238133_at	0.04742	-3.2		Transcribed locus	
68	239108_at	0.04742	-3.2	MLSTD1	Male sterility domain containing 1	chr12p11.22
67	239218_at	0.04742	-3.2		CDNA FLJ43039 fis, clone BRTHA3003023	
66	241756_at	0.04742	-3.2	SMARCA2	SWI/SNF related, matrix associated, actin dependent regulator of chromatin, subfamily a, member 2	chr9p22.3
65	242192_at	0.04742	-3.2			
64	242963_at	0.04742	-3.2	MGC26963	hypothetical protein MGC26963	chr4q25
63	233418_at	0.00749	-4.0	LOC91450	hypothetical protein LOC91450	chr15q24.1
62	240858_at	0.00749	-4.0	LTBP1	Latent transforming growth factor beta binding protein 1	chr2p22-p21 chrXp11.4-p11.3
61	204388_s_at	0.02572	-4.0	MAOA	monoamine oxidase A	
60	206670_s_at	0.02572	-4.0	GAD1	glutamate decarboxylase 1 (brain, 67kDa)	chr2q31
59	209167_at	0.02572	-4.0	GPM6B	glycoprotein M6B	chrXp22.2
58	209392_at	0.02572	-4.0	ENPP2	ectonucleotide pyrophosphatase/phosphodiesterase 2 (autotaxin)	chr8q24.1
57	211324_s_at	0.02572	-4.0	RANBP2L1	RAN binding protein 2-like 1	chr2q13
56	212942_s_at	0.02572	-4.0	KIAA1199	KIAA1199	chr15q24
55	218858_at	0.02572	-4.0	DEPDC6	DEP domain containing 6	chr8q24.12
54	221245_s_at	0.02572	-4.0	C2orf31	chromosome 2 open reading frame 31 /// chromosome 2 open reading frame 31	chr2q34
53	223719_s_at	0.02572	-4.0	RTBDN	retbindin	chr19p12
52	223783_s_at	0.02572	-4.0	GEMIN4	Gem (nuclear organelle) associated protein 4	chr17p13
51	226088_at	0.02572	-4.0	ZDHHC12	zinc finger, DHHC domain containing 12	chr9q34.11
50	226281_at	0.02572	-4.0	DNER	delta-Notch-like EGF repeat-containing transmembrane	chr2q36.3 chr2q11.2-q12
49	227198_at	0.02572	-4.0	LAF4	Lymphoid nuclear protein related to AF4	
48	229197_at	0.02572	-4.0	ING5	inhibitor of growth family, member 5	chr2q37.3
47	230547_at	0.02572	-4.0		CDNA FLJ42249 fis, clone TKIDN2007667	
46	235180_at	0.02572	-4.0	STYX	serine/threonine/tyrosine interacting protein	
45	240129_at	0.02572	-4.0	UBE2V1	Ubiquitin-conjugating enzyme E2 variant 1	chr20q13.2 chr17q23.2-q25.3
44	243103_at	0.02572	-4.0	TK1	Thymidine kinase 1, soluble	
43	243994_at	0.02572	-4.0			
42	244465_at	0.02572	-4.0		Transcribed locus	
41	237219_at	0.02572	-4.0			
40	AFFX-HUMRGE/M10098_M_at	0.02572	-4.0			
39	221134_at	0.00219	-5.0	ANGPT4	angiopoietin 4	chr20p13
38	222061_at	0.00219	-5.0	CD58	CD58 antigen, (lymphocyte function-associated antigen 3)	chr1p13 chr9q12 /// chr9p11.2
37	224012_at	0.00219	-5.0	ANKRD20	ankyrin repeat domain 20A	
36	231849_at	0.00219	-5.0	LOC144501	hypothetical protein LOC144501	chr12q13.13
35	240106_at	0.00219	-5.0	MGC4170	MGC4170 protein	chr12q23.3
34	243232_at	0.00219	-5.0			
33	244261_at	0.00219	-5.0	IL28RA	interleukin 28 receptor, alpha (interferon, lambda receptor)	chr1p36.11
32	204803_s_at	0.01324	-5.0	RRAD	Ras-related associated with diabetes	chr16q22
31	211642_at	0.01324	-5.0		Rheumatoid factor RF-ET11 /// Rheumatoid factor RF-ET11	
30	219607_s_at	0.01324	-5.0	MS4A4A	membrane-spanning 4-domains, subfamily A, member 4	chr11q12
29	229471_s_at	0.01324	-5.0	SRP46	Splicing factor, arginine/serine-rich, 46kD	chr11q22
28	238419_at	0.01324	-5.0	PHLDB2	pleckstrin homology-like domain, family B, member 2	chr3q13.2
27	241765_at	0.01324	-5.0	CPM	carboxypeptidase M	chr12q14.3

26	204389_at	0.02490	-5.0	MAOA	monoamine oxidase A	chrXp11.4-p11.3
25	211667_x_at	0.02490	-5.0		T-cell receptor alpha chain (TCRAV2S1J22) /// T-cell receptor alpha chain (TCRAV2S1J22)	
24	213174_at	0.02490	-5.0	TTC9	tetratricopeptide repeat domain 9	chr14q24.2
23	214562_at	0.02490	-5.0	HIST1H4L	histone 1, H4I	chr6p22-p21.3
22	213620_s_at	0.02490	-5.0			
21	224162_s_at	0.02490	-5.0	FBXO31	F-box protein 31	chr16q24.2
20	227229_at	0.02490	-5.0		Homo sapiens, clone IMAGE:5303499, mRNA	
19	243610_at	0.02490	-5.0	LOC138255	OTTHUMP00000021439	chr9q21.11
18	207178_s_at	0.00132	-6.3	FRK	fyn-related kinase	chr6q21-q22.3
17	225664_at	0.00776	-6.3	COL12A1	collagen, type XII, alpha 1	chr6q12-q13
16	229070_at	0.00776	-6.3	C6orf105	chromosome 6 open reading frame 105	chr6p24.1
15	209309_at	0.01613	-6.3	AZGP1	alpha-2-glycoprotein 1, zinc	chr7q22.1
14	208791_at	0.03902	-6.3	CLU	clusterin (complement lysis inhibitor, SP-40,40, sulfated glycoprotein 2, testosterone-repressed prostate message 2, apolipoprotein J)	chr8p21-p12
13	209120_at	0.03902	-6.3	NR2F2	nuclear receptor subfamily 2, group F, member 2	chr15q26
12	237193_s_at	0.03902	-6.3			
11	242939_at	0.03902	-6.3	TFDP1	transcription factor Dp-1	chr13q34
10	204908_s_at	0.00653	-8.0	BCL3	B-cell CLL/lymphoma 3	chr19q13.1-q13.2
9	225516_at	0.00653	-8.0	SLC7A2	solute carrier family 7 (cationic amino acid transporter, y+ system), member 2	chr8p22-p21.3
8	209357_at	0.01613	-8.0	CITED2	Cbp/p300-interacting transactivator, with Glu/Asp-rich carboxy-terminal domain, 2	chr6q23.3
7	244849_at	0.02131	-8.0	SEMA3A	Sema domain, immunoglobulin domain (Ig), short basic domain, secreted, (semaphorin) 3A	chr7p12.1
6	220884_at	0.02490	-8.0			
5	215161_at	0.00056	-10.1	CAMK1G	calcium/calmodulin-dependent protein kinase IG	chr1q32-q41
4	224506_s_at	0.00749	-10.1	C9orf67	chromosome 9 open reading frame 67 /// chromosome 9 open reading frame 67	chr9q34.13
3	240724_at	0.01417	-12.7		Transcribed locus	
2	201739_at	0.02572	-16.0	SGK	serum/glucocorticoid regulated kinase	chr6q23
1	204870_s_at	0.01235	-32.0	PCSK2	proprotein convertase subtilisin/kexin type 2	chr20p11.2

**Table 12.9** Most up and down-regulated genes derived from the comparison C99WT1/mock (n=3, p<0.05), analyzed with the Array Assist software and the MAS 5 algorithm.

## 12.3 Gene annotations

### 12.3.1 Preface

Information about genes is taken and modified from several databases (<http://harvester.embl.de>, [www.ncbi.nlm.nih.gov/omim](http://www.ncbi.nlm.nih.gov/omim), [www.ncbi.nlm.nih.gov/sites/entrez?db=gene](http://www.ncbi.nlm.nih.gov/sites/entrez?db=gene), [www.ihop-net.org](http://www.ihop-net.org) and others). Due to the inherent properties of such databases, which are updated regularly, the given information is what was available when the databases were last accessed (August 2007-January 2008). It is important to look for the latest information updates from time to time. Some data are managed automatically and extracted by specialized computer programs and consequently a reference is not provided for all information, but can be obtained from the databases mentioned above.

### 12.3.2 Annotations for differentially expressed genes (volcano plots)

See results, Chapter 5.4.4, volcano plots, Fig. 5.5

#### Selection of down-regulated genes, C99I45F/C99WT1 (volcano plot)

Gene Symbol	Gene Name	Chromosomal Location	Annotations
DOK4	DOCKING PROTEIN 4	chr16q13	Cai et al. (2003) found that both DOK4 and DOK5 are tyrosine-phosphorylated in response to insulin and insulin-like growth factor-1 (IGF1) in transfected cells. DOK4 is rapidly and heavily phosphorylated in response to insulin and, once phosphorylated, binds a set of SH2 domain proteins, including RasGAP, CRK and the nonreceptor tyrosine kinases SRS and FYN. DOK4 also activates MAPK in cells.
ADAMTS3	disintegrin-like and metalloprotease (reprolysin	chr4q13.3	The protein encoded by this gene is the major procollagen II N-propeptidase.
CD99	CD99 antigen	chrXp22.32; Yp11.3	Putative single-pass type I membrane protein involved in cell adhesion and leukocyte transendothelial migration.
CHRM3	cholinergic receptor muscarinic 3	chr1q41-q44	The muscarinic cholinergic receptors belong to a larger family of G protein-coupled receptors. The functional diversity of these receptors is defined by the binding of acetylcholine and includes cellular responses such as adenylate cyclase inhibition, phosphoinositide degeneration, and potassium channel mediation. Muscarinic receptors influence many effects of acetylcholine in the central and peripheral nervous system.

CCND1	cyclin D1 (PRAD1; parathyroid adenomatosis 1)	chr11q13	The protein encoded by this gene belongs to the highly conserved cyclin family, whose members are characterized by a strong periodicity in protein abundance throughout the cell cycle. Cyclins function as regulators of CDK kinases. Different cyclins exhibit distinct expression and degradation patterns which contribute to the temporal coordination of each mitotic event. This cyclin forms a complex with, and functions as, a regulatory subunit of CDK4 or CDK6, whose activity is required for cell cycle G1/S transition. This protein has been shown to interact with tumor suppressor protein Rb and the expression of this gene is regulated positively by Rb. Mutations, amplification and overexpression of this gene, which alters cell cycle progression, are observed frequently in a variety of tumors and may contribute to tumorigenesis. Brisken et al. (2002) found that prolactin induced Igf2 mRNA and Igf2 induced cyclin D1 protein expression in mouse mammary epithelial cultures.
CDKN1C	cyclin-dependent kinase inhibitor 1C (p57 Kip2)	chr11p15.5	Cyclin-dependent kinase inhibitor 1C is a tight-binding inhibitor of several G1 cyclin/Cdk complexes and a negative regulator of cell proliferation. Hatada and Mukai (1995) showed that a mouse homolog of p57(KIP2) is genomically imprinted. Matsuoka et al. (1996) demonstrated that the p57(KIP2) gene is imprinted in humans as well. Upregulation of p57 mRNA and protein occurred before TGF-beta-induced G1 cell cycle arrest, required transcription, and was mediated via a highly conserved region of the proximal p57 promoter.
CYB561	cytochrome b-561	chr17q11-qter	Cytochrome b561 is a major transmembrane protein that is specific to catecholamine and neuropeptide secretory vesicles of the adrenal medulla, pituitary gland, and other neuroendocrine tissues. This 30kD cytochrome is present in both the small synaptic vesicles and the large dense core vesicles (chromaffin granules) of the tissues. Its role is to supply reducing equivalents to 2 monooxygenases, dopamine beta-hydroxylase in chromaffin granules and peptidylglycine monooxygenase in neurosecretory vesicles. The cytochrome fulfills this role by catalyzing the transfer of electrons from a cytoplasmic donor, ascorbate, across a phospholipid bilayer to the luminal acceptor, semidehydroascorbate, in the interior of the vesicles. The continuously regenerated ascorbate within these vesicles is the immediate donor for the monooxygenases within the neuroendocrine secretory vesicles. Thus, cytochrome b561 is a transmembrane electron channel. b561 is assumed to binds 2 heme groups non-covalently.
DDC	dopa decarboxylase (aromatic L-amino acid decarboxylase)	chr7p11	DDC catalyzes the decarboxylation of l-3,4- dihydroxyphenylalanine (dopa) to dopamine, l-5-hydroxytryptophan to serotonin and l-tryptophan to tryptamine. Defects in DDC are the cause of aadc (aromatic L-amino acid decarboxylase deficiency). Aadc deficiency is an inborn error in neurotransmitter metabolism that leads to combined serotonin and catecholamine deficiency. it causes developmental and psychomotor delay, poor feeding, lethargy, ptosis, intermittent hypothermia, gastrointestinal disturbances. The onset is early in infancy and inheritance is autosomal recessive. DOPA decarboxylase (EC 4.1.1.28) is an enzyme implicated in 2 metabolic pathways, synthesizing 2 important neurotransmitters, dopamine and serotonin (Christenson et al., 1972). Following the hydroxylation of tyrosine to form L-dihydroxyphenylalanine (L-DOPA), catalyzed by tyrosine hydroxylase (TH), DDC decarboxylates L-DOPA to form dopamine. This neurotransmitter is found in different areas of the brain and is particularly abundant in basal ganglia. Dopamine is also produced by DDC in the sympathetic nervous system and is the precursor of the catecholaminergic hormones, noradrenaline and adrenaline in the adrenal medulla. In the nervous system, tryptophan hydroxylase produces 5-OH tryptophan, which is decarboxylated by DDC, giving rise to serotonin. DDC is a homodimeric, pyridoxal phosphate-dependent enzyme. Ichinose et al. (1989) prepared a cDNA clone for the coding region of human aromatic L-amino acid decarboxylase by screening a human pheochromocytoma cDNA library with an oligonucleotide probe that corresponded to a partial amino acid sequence of the enzyme purified from the tumor. The cDNA clone encoded a protein of 480 amino acids, with a calculated molecular mass of 53.9 kD. The amino acid sequence asn-phe-asn-pro-his-lys-trp around a possible pyridoxal phosphate cofactor binding site was shown to be identical in human, Drosophila, and pig enzymes. The protein encoded by hepatoma cells is the same as that encoded by adrenal chromaffin-derived pheochromocytoma cells. De Luca et al. (2003) found that variation in the dopa decarboxylase gene is related to longevity in Drosophila. They pointed out that DDC is only one of the enzymes in the biosynthetic pathways for bioamines and catecholamines. A polymorphism in tyrosine hydroxylase, the rate-limiting enzyme in the synthesis of catecholamines, is associated with variation in human longevity (De Benedictis et al., 1998; De Luca et al., 2001).
DNCL12	dynein cytoplasmic light intermediate polypeptide 2	chr16q22.1	DNCL12 may play a role in regulating interactions between dynein and p150-glued, and the cellular substrates for dynein- mediated motility (such as organelles).

FBN1	fibrillin 1 (Marfan syndrome)	chr15q21.1	Fibrillins are structural components of 10-12 nm extracellular calcium-binding microfibrils, which occur either in association with elastin or in elastin-free bundles. Fibrillin-1 containing microfibrils provide long-term force bearing structural support. The FBN1 gene encodes a member of the fibrillin family. The encoded protein is a large, extracellular matrix glycoprotein that serves as a structural component of 10-12 nm calcium-binding microfibrils. These microfibrils provide force bearing structural support in elastic and non-elastic connective tissue throughout the body. Mutations in this gene are associated with Marfan syndrome, isolated ectopia lentis, autosomal dominant Weill-Marchesani syndrome, MASS syndrome, and Shprintzen-Goldberg craniosynostosis syndrome. Fibrillin-1 sequence encoded by exons 44-49 releases endogenous TGFbeta1, thereby stimulating TGFbeta receptor-mediated Smad2 signaling (J Cell Biol. 2007 Jan 29;176(3):355-67).
GATA3	GATA binding protein 3	chr10p15	Transcriptional activator which binds to the enhancer of the t-cell receptor alpha and delta genes. Binds to the consensus sequence 5'-agatag-3'. Fields et al. (2002) noted that high levels of histone acetylation at particular loci correlate with transcriptional activity, whereas reduced levels correlate with silencing. GATA3 regulated FUT7 transcription by recruiting histone deacetylase-3 (HDAC3) and HDAC5 in a phosphorylation-dependent manner, and by competing with CBP (CREBBP)/p300 (EP300) in binding to the N terminus of TBET. Maximal expression of FUT7 and sialyl Lewis x in T cells was obtained by ROG (ZBTB32)-mediated suppression of GATA3. Chen et al. (2006) concluded that the GATA3/TBET transcription factor complex regulates cell lineage-specific expression of lymphocyte homing receptors and that glycoconjugates are regulated by this complex to attain cell lineage-specific expression in Th1 and Th2 lymphocyte subsets. Zhu et al. (2004) generated mice with a conditional deletion of Gata3 and Gata3-deficient mouse T-cell lines and found that both IL4-dependent and -independent Th2 differentiation was diminished, permitting Th1 differentiation in the absence of IFNγ and IL12. Deletion of Gata3 from established Th2 cells stopped production of IL5 and IL13, but not of IL4. Mice lacking Gata3 produced IFNγ rather than Th2 cytokines in response to infection with <i>Nippostrongylus brasiliensis</i> . Zhu et al. (2004) concluded that Gata3 serves as a principal switch in determining Th1-Th2 responses.
H19	H19 imprinted maternally expressed untranslated mRNA	chr11p15.5	The human H19 gene is 2.7 kb long and includes 4 small introns. Zhang and Tycko (1992) found restriction site polymorphisms in the human H19 gene and, by examination of the representation of these polymorphisms in cDNAs from fetal organs, demonstrated that H19 expression was largely or exclusively from a single allele. The H19 gene and 2 other genes, insulin-like growth factor II (IGF2) and insulin-like growth factor II receptor, show monoallelic expression in mice. IGF2 is, like H19, located in 11p15. Zhang and Tycko (1992) commented that if IGF2 also shows monoallelic expression, it may indicate that that region is a 'hotspot' for this phenomenon. Mutter et al. (1993) found that normal gestations only express H19 from the maternal allele and express IGF2 from the paternal allele, whereas neither is expressed from the maternal genome of gynogenetic gestations, and both are expressed from the paternal genome of androgenetic gestations. The imprinted H19 gene, which encodes an untranslated RNA, lies at the end of a cluster of imprinted genes. Imprinted genes are expressed from only 1 of the parental alleles and are marked epigenetically by DNA methylation and histone modifications. The paternally expressed gene Igf2 is separated by approximately 100 kb from the maternally expressed noncoding gene H19 on mouse distal chromosome 7. Differentially methylated regions in Igf2 and H19 contain chromatin boundaries, silencers, and activators, and regulate the reciprocal expression of the 2 genes in a methylation-sensitive manner.
HSBP1	heat shock factor binding protein 1	chr16q23.3	Negative regulator of the heat shock response. Negatively affects HSF1 DNA-binding activity. May have a role in the suppression of the activation of the stress response during the aging process.

HGF	hepatocyte growth factor	chr7q21.1	<p>Hepatocyte growth factor regulates cell growth, cell motility, and morphogenesis by activating a tyrosine kinase signaling cascade after binding to the proto-oncogenic c-Met receptor. Hepatocyte growth factor is secreted by mesenchymal cells and acts as a multi-functional cytokine on cells of mainly epithelial origin. Its ability to stimulate mitogenesis, cell motility, and matrix invasion gives it a central role in angiogenesis, tumorigenesis and tissue regeneration. It is secreted as a single inactive polypeptide and is cleaved by serine proteases into a 69-kDa alpha-chain and 34-kDa beta-chain. A disulfide bond between the alpha and beta chains produces the active, heterodimeric molecule. The protein belongs to the plasminogen subfamily of S1 peptidases but has no detectable protease activity. Alternative splicing of this gene produces multiple transcript variants encoding different isoforms. The cytokine hepatocyte growth factor/scatter factor inhibits apoptosis and enhances DNA repair by a common mechanism involving signaling through phosphatidylinositol 3-kinase-, HGF/SF induced the phosphorylation of c-Akt (protein kinase-B), a PI3K substrate implicated in apoptosis inhibition; HGF/SF activates a cell survival and DNA repair pathway that involves signaling through PI3K and c-Akt and stabilization of the expression of Bcl-XL; and they implicate Bcl-XL in the DNA repair process (Oncogene. 2000 Apr 27;19(18):2212-23). Scatter factor/hepatocyte growth factor protects against cytotoxic death in human glioblastoma via phosphatidylinositol 3-kinase- and AKT-dependent pathways (Cancer Res. 2000 Aug 1;60(15):4277-83). Anti-apoptotic signaling by hepatocyte growth factor/Met via the phosphatidylinositol 3-kinase/Akt and mitogen-activated protein kinase pathways (Proc Natl Acad Sci U S A. 2001 Jan 2;98(1):247-52). Neuroprotection by scatter factor/hepatocyte growth factor and FGF-1 in cerebellar granule neurons is phosphatidylinositol 3-kinase/akt-dependent and MAPK/CREB-independent (J Neurochem. 2002 Apr;81(2):365-78).The receptor tyrosine kinase Met and its ligand hepatocyte growth factor are clustered at excitatory synapses and can enhance clustering of synaptic proteins (Cell Cycle. 2006 Jul;5(14):1560-8). Heparan sulfate-modified CD44 promotes hepatocyte growth factor/scatter factor-induced signal transduction through the receptor tyrosine kinase c-Met (J Biol Chem. 1999 Mar 5;274(10):6499-506). Activation mechanisms of the urokinase-type plasminogen activator promoter by hepatocyte growth factor/scatter factor (J Biol Chem. 1999 Jun 4;274(23):16377-86). Gene transfer of hepatocyte growth factor gene into rat brains improves learning and memory in the chronic stage of cerebral infarction; immunohistochemical analysis for Cdc42 and synaptophysin in the peri-infarct region revealed that HGF enhanced the neurite extension and increased the number of synapses. These data demonstrated that HGF plays a pivotal role in the functional recovery after cerebral infarction through neuritogenesis, improved microcirculation, and the prevention of gliosis (Eur J Biochem. 2001 Aug;268(16):4423-9). Hepatocyte growth factor/scatter factor (HGF/SF) antagonizes TGF-beta1 by stabilizing SMAD transcriptional co-repressor TGIF (Regul Pept. 2005 Aug 15;130(1-2):75-80). Human platelets express HGF receptor, the tyrosine kinase encoded by c-MET gene. At physiological concentrations HGF was found to inhibit both glycoprotein (alpha)IIb(beta)3 activation and thrombin-dependent platelet aggregation in a dose- and time-dependent manner. These results suggest that circulating HGF may counteract thrombogenesis by negatively modulating platelet functions (FEBS Lett. 2005 Aug 15;579(20):4550-4). Exogenous HGF promoted a highly significant increase in dendritic growth and branching of layer 2 pyramidal neurons, whereas inactivation of endogenous HGF with function-blocking, anti-HGF antibody caused a marked reduction in size and complexity of the dendritic arbors of these neurons. Likewise, pyramidal neurons transfected with an MET dominant-negative mutant receptor had much smaller and less complex dendritic arbors than control transfected neurons did. These results indicate that HGF plays a role in regulating dendritic morphology in the developing cerebral cortex (Development. 2004 Aug;131(15):3717-26.). Expression of c-Met in developing rat hippocampi: evidence for HGF as a neurotrophic factor for calbindin D-expressing neurons (Eur J Neurosci. 2000 Oct;12(10):3453-61). It is known that HGF/SF induces in vitro expression of vascular endothelial growth factor (VEGF), a key agonist of tumor angiogenesis; by contrast, thrombospondin 1 (TSP-1) is a negative regulator of angiogenesis. It was shown that in the very same tumor cells, in addition to inducing VEGF expression, HGF/SF dramatically down-regulates TSP-1 expression. These studies identify HGF/SF as a key switch for turning on angiogenesis (Proc Natl Acad Sci U S A. 2003 Oct 28;100(22):12718-23). Autocrine and/or paracrine trophic support of the HGF-c-Met system contributes to the attenuation of the degeneration of residual anterior horn cells in ALS, while disruption of the neuronal HGF-c-Met system at an advanced disease stage accelerates cellular degeneration and/or the process of cell death (Acta Neuropathol (Berl). 2003 Aug;106(2):112-20). PKC, p42/44 MAPK and p38 MAPK regulate hepatocyte growth factor secretion from human astrocytoma cells (Brain Res Mol Brain Res. 2002 Jun 15;102(1-2):73-82). It was reported that APP level, soluble APP (sAPP) secretion, and A beta production in HEK293 cells transfected with either wild-type APP(751) or APP(751) carrying the Swedish mutation are all elevated by hepatocyte growth factor (HGF) (Exp Cell Res. 2003 Jul 15;287(2):387-96).</p>
-----	--------------------------	-----------	--

IGF2	insulin-like growth factor 2 (somatomedin A)	chr11p15.5	This gene encodes a member of the insulin family of polypeptide growth factors that is involved in development and growth. It is an <i>imprinted</i> gene and is expressed only from the paternally inherited allele. Interaction of insulin-like growth factor II (IGF-II) with multiple plasma proteins: high affinity binding of plasminogen to IGF-II and IGF-binding protein-3 (Biol Chem. 2005 Mar 18;280(11):9994-10000). Transferrin binds insulin-like growth factors and affects binding properties of insulin-like growth factor binding protein-3 (FEBS Lett. 2001 Dec 14;509(3):395-8).
INSM2	insulinoma-associated 2	chr14q13.2	Transcription corepressor activity, zinc ion binding. Insulinoma-associated protein-2 is a major autoantigen in type 1 diabetes that occurs through autoimmune-mediated beta-cell destruction (Diabetes. 2007 Jan;56(1):41-8).
ITGB5	integrin beta 5	chr3q21.2	Membrane; single-pass type I membrane protein. Heterodimer of an alpha and a beta subunit. Beta-5 associates with alpha-v. Integrin alpha-v/beta-5 is a receptor for fibronectin. It recognizes the sequence r-g-d in its ligand.
NEBL	nebulette	chr10p12	Millevoi et al. (1998) showed that nebulette binds to actin and plays an important role in the assembly of the Z-disc.
NELL1	NEL-like 1 (chicken)	chr11p15.2-p15.1	This gene encodes a cytoplasmic protein that contains epidermal growth factor (EGF)-like repeats. The encoded heterotrimeric protein may be involved in cell growth regulation and differentiation. It is believed to be a secreted protein and to bind to pkc beta-1.
PDLIM3	PDZ and LIM domain 3	chr4q35	Cytoskeletal protein that may act as an adapter that brings other proteins (like kinases) to the cytoskeleton. It is thought to interact with alpha-actinins 1, 2 and 4. It has 1 lim zinc-binding domain. The ZASP-like motif in actinin-associated LIM protein is required for interaction with the alpha-actinin rod and for targeting to the muscle Z-line (J Biol Chem. 2004 Jun 18;279(25):26402-10). The Z-line is a specialized structure connecting adjacent sarcomeres in muscle cells. Alpha-Actinin cross-links actin filaments in the Z-line. Several PDZ-LIM domain proteins localize to the Z-line and interact with alpha-actinin. Actinin-associated LIM protein (ALP), C-terminal LIM domain protein (CLP36), and Z band alternatively spliced PDZ-containing protein (ZASP) have a conserved region named the ZASP-like motif (ZM) between PDZ and LIM domains. It is suggested that the two interaction sites of ALP (PDZ domain and ZM motif) would stabilize certain conformations of alpha-actinin 2 that would strengthen the Z-line integrity.
POU3F3	POU domain class 3 transcription factor 3	chr2q12.1	POU3F3 is a member of the class III POU family of transcription factors (see POU3F1; 602479) that are expressed in the central nervous system. The POU domain in these proteins is required for high affinity binding to octamer DNA sequences (Sumiyama et al. (1996)). Overexpression experiments in vivo indicate that Brn2 (a POU protein), like Mash1, regulates additional aspects of neurogenesis, including the division of progenitors and the differentiation and migration of neurons.
PROX1	Prospero-related homeobox 1	chr1q32.2-q32.3	Prox1 is a transcription factor with two highly conserved domains, a homeobox and a prospero domain. Dyer et al. (2003) found that the Prox1 regulates the exit of progenitor cells from the cell cycle in the embryonic mouse retina. Cells lacking Prox1 are less likely to stop dividing, and ectopic expression of Prox1 forces progenitor cells to exit the cell cycle. Other observations indicated that Prox1 activity is both necessary and sufficient for progenitor-cell proliferation and cell-fate determination in the vertebrate retina. Prox1 inactivation caused abnormal cellular proliferation, down-regulated expression of the cell cycle inhibitors Cdkn1b and Cdkn1c, misexpression of E-cadherin, and inappropriate apoptosis.
PTPRK	protein tyrosine phosphatase receptor type K	chr6q22.2-23.1	The protein encoded by this gene is a member of the protein tyrosine phosphatase (PTP) family. PTPs are known to be signaling molecules that regulate a variety of cellular processes including cell growth, differentiation, mitotic cycle, and oncogenic transformation. This PTP possesses an extracellular region, a single transmembrane region, and two tandem catalytic domains, and thus represents a receptor-type PTP. The extracellular region contains a meprin-A5 antigen-PTP mu (MAM) domain, an Ig-like domain and four fibronectin type III-like repeats. This PTP was shown to mediate homophilic intercellular interaction, possibly through the interaction with beta- and gamma-catenin at adherens junctions. Expression of this gene was found to be stimulated by TGF-beta 1, which may be important for the inhibition of keratinocyte proliferation.
LOC492304	putative insulin-like growth factor II associated protein	chr11p15.5	This gene encodes a member of the insulin family of polypeptide growth factors that is involved in development and growth. It is an <i>imprinted</i> gene and is expressed only from the paternally inherited allele. It is a candidate gene for eating disorders. There is a read-through, INS-IGF2, which aligns to this gene at the 3' region and to the upstream INS gene at the 5' region. Two alternatively spliced transcript variants encoding the same protein have been found for this gene.

RGS4	regulator of G-protein signaling 4	chr1q23.3	Regulator of G protein signaling (RGS) family members are regulatory molecules that act as GTPase activating proteins (GAPs) for G alpha subunits of heterotrimeric G proteins. RGS proteins are able to deactivate G protein subunits of the Gi alpha, Go alpha and Gq alpha subtypes. They drive G proteins into their inactive GDP-bound forms. Regulator of G protein signaling 4 belongs to this family. All RGS proteins share a conserved 120-amino acid sequence termed the RGS domain. Regulator of G protein signaling 4 protein is 37% identical to RGS1 and 97% identical to rat Rgs4. This protein negatively regulates signaling upstream or at the level of the heterotrimeric G protein and is localized in the cytoplasm. In AD parietal cortex, total levels of G(q/11) and RGS4 proteins were significantly lower than age-matched control cases by 40% and 53% respectively (Synapse. 2003 Jan;47(1):58-65). DNA microarray studies of postmortem brain samples have shown RGS4 underexpression in the dorsolateral prefrontal cortex, motor and visual cortices in schizophrenia patients relative to control subjects (Mol Psychiatry. 2005 Feb;10(2):213-9). Support for RGS4 as a susceptibility gene for schizophrenia (Biol Psychiatry. 2004 Jan 15;55(2):192-5).
SERPINE2	serine (or cysteine) proteinase inhibitor clade E (nexin) plasminogen activator inhibitor type 1 member 2	chr2q33-q35	Synonyms: glial-derived neurite promoting factor p, protease nexin I, protease inhibitor 7. Protease nexin I (PN-I) is a 44-kD thrombin and urokinase inhibitor released by human foreskin fibroblasts. PN-I shares several features with antithrombin III, an abundant plasma thrombin inhibitor. Both PN-I and AT-III have high affinities for heparin, and heparin accelerates their rate of thrombin inhibition. In addition, the published sequence of 28 amino acids at the N-terminus of PN-I is identical to the N-terminal amino acid sequence of a glial-derived neurite promoting factor. Protease nexin I is the most important physiologic regulator of alpha-thrombin in tissues (Carter et al., 1995). PN1 is highly expressed and developmentally regulated in the nervous system where it is concentrated at neuromuscular junctions and also central synapses in the hippocampus and striatum. Approximately 10% of identified proteins at mammalian neuromuscular junctions are serine protease inhibitors, consistent with their central role in balancing serine protease activity to develop, maintain, and remodel synapses. Pericyte expression of protease nexin 1 may provide endogenous <i>anticoagulant activity</i> (J Cereb Blood Flow Metab. 2006 Feb;26(2):209-17). Protease nexin 1 is a potent urinary plasminogen activator inhibitor in the presence of collagen type IV. Protease nexin 1 (PN1) in solution forms inhibitory complexes with thrombin or urokinase, which have <i>opposing effects on the blood coagulation cascade</i> . An initial report supported the idea that PN1 target protease specificity is under the influence of collagen type IV (1). Although collagen type IV demonstrated no effect on the association rate between PN1 and thrombin, the study reported that the association rate between PN1 and urokinase was allosterically reduced 10-fold. This has led to the generally accepted idea that the primary role of PN1 in the brain is to act as a rapid thrombin inhibition and clearance mechanism during trauma and loss of vascular integrity. In studies to identify the structural determinants of PN1 that mediate the allosteric interaction with collagen type IV, it was found that protease specificity was only affected after transient exposure of PN1 to acidic conditions that mimic the elution protocol from a monoclonal antibody column. Because PN1 used in previous studies was purified over a monoclonal antibody column, it was proposed that the allosteric regulation of PN1 target protease specificity by collagen type IV is a result of the purification protocol. Both biochemical and kinetic data support this conclusion. This finding is significant because it implies that PN1 may play a much larger role in the modeling and remodeling of brain tissues during development and is not simply a thrombin clearance mechanism as previously suggested (J Biol Chem. 2002 Dec 6;277(49):47285-91).
SHOX2	short stature homeobox 2	chr3q25-q26.1	This gene is a member of the homeo box family of genes that encode proteins containing a 60-amino acid residue motif that represents a DNA binding domain. Homeo box genes have been characterized extensively as transcriptional regulators involved in pattern formation in both invertebrate and vertebrate species. Several human genetic disorders are caused by aberrations in human homeo box genes. SHOX is a pseudoautosomal homeo box gene that is thought to be responsible for idiopathic short stature and implicated to play a role in the short stature phenotype of Turner syndrome patients. This gene is considered to be a candidate gene for Cornelia de Lange syndrome.
TFPI2	tissue factor pathway inhibitor 2	chr7q22	Tissue factor pathway inhibitor is an important regulator of the extrinsic pathway of blood coagulation through its ability to inhibit factor Xa and factor VIIa-tissue factor activity. It was originally identified by Siiteri et al. (1982) and Butzow et al. (1988) as a placental glycoprotein that inhibits plasmin, trypsin, and thrombin (Miyagi et al., 1996). Sprecher et al. (1994) described the molecular cloning and expression of a full-length cDNA that encodes a molecule, designated TFPI2 that has a similar overall domain organization and considerable primary amino acid sequence homology to TFPI. After a 22-residue signal peptide, the mature TFPI2 protein contains 213 amino acids with 18 cysteines and 2 canonical N-linked glycosylation sites. The deduced sequence of mature TFPI2 revealed a short acidic N-terminal region, 3 tandem Kunitz-type domains, and a C-terminal tail highly enriched in basic amino acids. It may play a role in the regulation of plasmin-mediated matrix remodeling.

TIMP1	tissue inhibitor of metalloproteinase 1 (erythroid potentiating activity collagenase inhibitor)	chrXp11.3-p11.23	Synonym: Collagenase inhibitor. This gene belongs to the TIMP gene family. The proteins encoded by this gene family are natural inhibitors of the matrix metalloproteinases (MMPs), a group of peptidases involved in degradation of the extracellular matrix. In addition to its inhibitory role against most of the known MMPs, the encoded protein is able to promote cell proliferation in a wide range of cell types, and may also have an anti-apoptotic function. Transcription of this gene is highly inducible in response to many cytokines and hormones. In addition, the expression from some but not all inactive X chromosomes suggests that this gene inactivation is polymorphic in human females. This gene is located within intron 6 of the synapsin I gene and is transcribed in the opposite direction.
TLE4	transducin-like enhancer of split 4 (E(sp1) homolog)	chr9q21.31	Synonym: enhancer of split groucho 4, transcriptional corepressor that binds to a number of transcription factors. Inhibits the transcriptional activation mediated by pax5, and by ctnnb1 and tcf family members in wnt signaling.

### Selection of up-regulated genes, C99V50F/C99WT1 (volcano plot)

Gene Symbol	Gene Name	Chromosomal Location	Annotations
ADAMTS9	a disintegrin-like and metalloprotease (reprolysin type) with thrombospondin type 1 motif 9	chr3p14.3-p14.2	This gene encodes a member of the ADAMTS ( <i>a disintegrin and metalloproteinase with thrombospondin motifs</i> ) protein family. Members of this family share several distinct protein modules, including a propeptide region, a <i>metalloproteinase domain</i> , a disintegrin-like domain, and a <i>thrombospondin type 1 (TS) motif</i> . Individual members of this family differ in the number of C-terminal TS motifs, and some have unique C-terminal domains. Members of the ADAMTS family have been implicated in the <i>cleavage of proteoglycans</i> , the control of organ shape during development, and the <i>inhibition of angiogenesis</i> . <i>Knockdown of ADAMTS9</i> resulted in <i>diminished production of collagen</i> in A549 cells exposed to TGF-beta1. ADAMTS9 is a secreted, cell-surface-binding metalloprotease that cleaves the proteoglycans versican and aggrecan. Unlike most precursor proteins, the ADAMTS9 zymogen (pro-ADAMTS9) is resistant to intracellular processing. Instead, pro-ADAMTS9 is processed by furin at the cell surface. Observations suggest that, unlike other metalloproteases, furin processing of the ADAMTS9 propeptide reduces its catalytic activity. Observations suggest that the propeptide is a key functional domain of ADAMTS9, mediating an unusual regulatory mechanism that may have evolved to ensure maximal activity of this protease at the cell surface. ADAMTS proteins are structurally homologous to ADAM proteins, but they also contain at least 1 C-terminal thrombospondin type 1 (TSP1) repeat and are secreted rather than membrane bound.
APLP2	amyloid beta (A4) (reprolysin type) with thrombospondin type precursor-like protein 2	chr11q23-q25 11q24	The human amyloid precursor-like protein APLP2 is a highly conserved homolog of a sequence-specific DNA-binding mouse protein with an important function in the cell cycle. It may play a role in the regulation of hemostasis, may have inhibitory properties towards coagulation factors and may interact with cellular G-protein signaling pathways. APLP2 interact with CP2 transcription factor in the nucleus and induce glycogen synthase kinase-3beta expression Cell Death Differ. 2007 Jan;14(1):79-91, FASEB J. 2004 Aug;18(11):1288-90.
ARHGAP26	Rho and Rho and metalloproteases 1 motif GTPase activating protein 26	chr5q31	The avian ARHGAP26 protein binds to the C-terminal domain of pp125, one of the tyrosine kinases predicted to be a critical component of the integrin signaling transduction pathway in an SH3 domain-dependent manner and stimulates the GTPase activity of the GTP-binding protein RhoA. Thus, ARHGAP26 acts as a negative regulator of RhoA.
BMP7	bone morphogenetic protein 7 (osteogenic protein 1)	chr20q13	The bone morphogenetic proteins are members of the transforming growth factor-beta superfamily. BMP7 induced SMAD1, both of which were inhibited by follistatin. Transfection with antisense SMAD2/SMAD3 prevented activin-induced expression and accumulation of alpha-smooth muscle actin.

CACNA1B	Calcium channel voltage-dependent L type alpha 1B subunit	chr9q34	Voltage-dependent Ca(2+) channels are multisubunit complexes found in the membrane of many excitable cells that regulate calcium entry. N-type calcium channels, which control neurotransmitter release from neurons, are dihydropyridine-insensitive and omega-conotoxin-insensitive. The alpha-1 subunit forms the pore through which calcium enters the cell, and is encoded by a family of at least 5 genes. Using binding and immunoprecipitation assays on adult rat cortical tissue, Maeno-Hikichi et al. (2003) showed that the enigma-like LIM domain protein (ENH) interacts specifically with protein kinase C-epsilon (PRKCE) and the C terminus of CACNA1B to form a macromolecular complex. Functional studies in <i>Xenopus</i> oocytes indicated that expression of ENH resulted in increased rapid and specific modulation of N-type calcium channels by PKCE. The authors concluded that through interactions with a common adaptor protein, the formation of a kinase-substrate complex is the molecular basis for the specificity and efficiency of cellular signaling.
CACNA1D	calcium channel voltage-dependent L type alpha 1D subunit	chr3p14.3	Davare et al. (2001) found that the beta-2 adrenergic receptor is directly associated with one of its ultimate effectors, CACNA1D. This complex also contains a G protein, an adenylyl cyclase, cAMP-dependent kinase, and the counterbalancing phosphatase PP2A. Davare et al. (2001) used electrophysiologic recordings from hippocampal neurons to demonstrate highly localized signal transduction from the receptor to the channel. The assembly of this signaling complex provides a mechanism that ensures specific and rapid signaling by a G protein-coupled receptor.
CEBPD	CCAAT/enhancer binding protein (C/EBP) delta	chr8p11.2-p11.1	Transcriptional activator; activity is stimulated by sepsis, keratinocyte growth factor, and may be involved in glucose-mediated regulation of iNOS.
CHRNA7	Cholinergic receptor nicotinic alpha polypeptide 7	chr15q14	The nicotinic acetylcholine receptors (nAChRs) are members of a superfamily of ligand-gated ion (Na <sup>+</sup> , K <sup>+</sup> , Ca <sup>2+</sup> ) channels that mediate fast signal transmission at synapses. The nAChRs are thought to be hetero-pentamers composed of homologous subunits. The proposed structure for each subunit is a conserved N-terminal extracellular domain followed by three conserved transmembrane domains, a variable cytoplasmic loop, a fourth conserved transmembrane domain, and a short C-terminal extracellular region. The protein encoded by this gene forms a homo-oligomeric channel, displays marked <i>permeability to calcium ions</i> and is a major component of brain nicotinic receptors that are blocked by, and highly sensitive to, alpha-bungarotoxin. <i>Once this receptor binds acetylcholine, it undergoes an extensive change in conformation that affects all subunits and leads to opening of an ion-conducting channel across the plasma membrane. Significant increases in the total numbers of astrocytes and of astrocytes expressing the alpha7 nAChR subunit, along with significant decreases in the levels of alpha7 and alpha4 nAChR subunits on neurons, were observed in the hippocampus and temporal cortex of both APPSwe and sporadic AD brains. Both of these phenomena were more pronounced in APPSwe than sporadic AD cases. The increase in the level of expression of alpha7 nAChR on astrocytes was positively correlated with the extent of neuropathological alternations, especially the number of neuritic plaques, in the AD brain. The elevated expression of alpha7 nAChR on astrocytes might participate in causing Abeta cascade and formation of neuritic plaques, thereby playing an important role in the pathogenesis of AD.</i>
CRMP1	collapsin response mediator protein 1	chr4p16.1-p15	This gene encodes a member of a family of cytosolic phosphoproteins expressed exclusively in the nervous system. The encoded protein is thought to be a part of the <i>semaphorin signal transduction pathway implicated in semaphorin-induced growth cone collapse during neural development</i> . Alternative splicing results in multiple transcript variants. Synonym: Dihydropyrimidinase-related protein 1 (DRP-1). CRMP1 is a predicted functional partner of CDK5.
CTNNA2	catenin (cadherin-associated protein) alpha 2	chr2p12-p11.1	Cell-cell and cell-matrix adhesions involve transmembrane glycoproteins such as cell adhesion molecules and integrins, which are thought to function via interactions of their cytoplasmic domains with proteins associated with the cytoskeleton. Vinculin and talin are examples. The activity of cadherins, which mediate homophilic cell-cell Ca <sup>2+</sup> -dependent association, depends on their anchorage to cytoskeleton via proteins termed catenins.
CUTL2	cut-like 2 (Drosophila)	chr12q24.11-q24.12	Homeobox protein cut-like 2 (Cux2). In <i>Drosophila</i> it may act as a transcription factor involved in neural specification. Binds to DNA in a sequence-specific manner. CUX2 is a potential regulator of NCAM expression: Genomic characterization and analysis as a positional candidate susceptibility gene for bipolar disorder.
DKK2	dickkopf homolog 2 ( <i>Xenopus laevis</i> )	chr4q25	This gene encodes a protein that is a member of the <i>dickkopf family</i> . The <i>secreted</i> protein contains two cysteine rich regions and is involved in embryonic development through its <i>interactions with the Wnt signaling pathway. It can act as either an agonist or antagonist of Wnt/beta-catenin signaling, depending on the cellular context and the presence of the co-factor kremen 2. Activity of this protein is also modulated by binding to the Wnt co-receptor LDL-receptor related protein 6 (LRP6).</i>

DNC1	dynein cytoplasmic intermediate polypeptide 1	chr7q21.3-q22.1	Belongs to the dynein intermediate chain family. The intermediate chains seem to help dynein bind to dynactin 150 kDa component. May play a role in mediating the interaction of cytoplasmic dynein with membranous organelles and kinetochores.
DNER	delta-Notch-like EGF repeat-containing transmembrane	chr2q36.3	DNER was identified as a new epidermal growth factor (EGF)-like repeat-containing single-pass <i>transmembrane protein</i> that is specifically expressed in the developing and mature central nervous system. Sequence analysis revealed that the 10 EGF-like repeats in the extracellular domain are closely related to those of the developmentally important receptor Notch and its ligand Delta. Thus it was named Delta/Notch-like EGF-related receptor (DNER). DNER protein is strongly expressed in several types of post-mitotic neurons, including cortical and hippocampal pyramidal neurons, cerebellar granule cells, and Purkinje cells. DNER protein is localized to the <i>dendritic</i> plasma membrane and endosomes and is <i>excluded from the axons, even when overexpressed</i> . The tyrosine-based sorting motif in the cytoplasmic domain is required for dendritic targeting of DNER. DNER contains an N-terminal signal sequence and 10 distinct EGF-like motifs. The final EGF-like repeat displays a typical signature of a calcium-binding domain important for molecular orientation. DNER also has a single transmembrane region and an intracellular C-terminal region containing potential tyrosine kinase phosphorylation sites, a typical tyrosine-based sorting signal (YEEF), and a dileucine-type sorting signal (LI). Using coimmunoprecipitation techniques, it was found to bind directly between DNER and the clathrin coat-associated protein complex Ap1, and Dner and Ap1 were found to be colocalized within mouse Purkinje cells. Eiraku et al. (2002) concluded that DNER undergoes Ap1-dependent sorting to the somatodendritic compartments from the trans-Golgi network. Differentiation of glia in the central nervous system is regulated by Notch signaling through neuron-glia interaction. Eiraku et al. (2005) identified DNER as a ligand of Notch during cellular morphogenesis of Bergmann glia in the mouse cerebellum. Dner bound to Notch1 at cell-cell contacts and activated Notch signaling in vitro. In the developing cerebellum, Dner was highly expressed in Purkinje cell dendrites, which were tightly associated with radial fibers of Bergmann glia expressing Notch. Dner specifically bound to Bergmann glia in culture and induced process extension by activating gamma-secretase and Dtx1-dependent Notch signaling. Inhibition of Dtx1-dependent but not Rbpj (RBPSUH)-dependent Notch signaling in Bergmann glia suppressed formation and maturation of radial fibers in organotypic slice cultures. Additionally, deficiency of DNER retarded the formation of radial fibers and resulted in abnormal arrangement of Bergmann glia.
ENC1	ectodermal-neural cortex (with BTB-like domain)	chr5q12-q13.3	Synonym: p53-induced gene 10. DNA damage and/or hyperproliferative signals activate wildtype p53 tumor suppressor protein (TP53), inducing cell cycle arrest or apoptosis. Mutations that inactivate p53 occur in 50% of all tumors. Polyak et al. (1997) used serial analysis of gene expression (SAGE) to evaluate cellular mRNA levels in a colorectal cancer cell line transfected with p53. Of 7,202 transcripts identified, only 14 were expressed at levels more than 10-fold higher in p53-expressing cells than in control cells. Polyak et al. (1997) termed these genes 'p53-induced genes,' or PIGs, several of which were predicted to encode redox-controlling proteins. They noted that reactive oxygen species (ROS) are potent inducers of apoptosis. Flow cytometric analysis showed that p53 expression induces ROS production, which increases as apoptosis progresses under some conditions. The authors stated that the PIG10 gene, also called ENC1, encodes an actin-binding protein.
FLJ35632	-	-	Not annotated
GABRB3	Gamma-aminobutyric acid (GABA) A receptor beta 3	chr15q11.2-q12	This gene encodes a member of the ligand-gated ionic channel family. The encoded protein is one of at least 13 distinct subunits of a multisubunit <i>chloride</i> channel that serves as the receptor for gamma-aminobutyric acid, the major <i>inhibitory</i> transmitter of the nervous system. This gene is located on the long arm of chromosome 15 in a cluster with two genes encoding related subunits of the family. Mutations in this gene may be associated with the pathogenesis of Angelman syndrome, Prader-Willi syndrome, and autism. Alternatively spliced transcript variants encoding isoforms with distinct signal peptides have been described.
GPR64	G protein-coupled receptor 64	chrXp22.13	G-protein-coupled receptor proteolytic site domain

GRIA2	glutamate receptor ionotropic AMPA 2	chr4q32-q33	Glutamate receptors sensitive to alpha-amino-3-hydroxy-5-methyl-4-isoxazolpropionate (AMPA) are ligand-activated cation channels that mediate the fast component of excitatory postsynaptic currents in neurons of the central nervous system. These channels are assembled from 4 related subunits, GLURA (GRIA1; 138248), GLURB (GRIA2), GLURC (GRIA3), GLURD (GRIA4), with the GLURB subunit rendering the channel almost impermeable to Ca <sup>2+</sup> (Hollmann et al., 1991). <i>Long-term depression</i> was absent in cultured cerebellar Purkinje cells from mutant mice lacking the AMPAR GluR2 subunit and <i>could be rescued by transient transfection with the wildtype GluR2 subunit</i> . Transfection with GluR2 carrying a point mutation that eliminated PKC phosphorylation of ser880 in the carboxy-terminal PDZ ligand of GluR2 failed to restore long-term depression. In contrast, transfection with GluR2 carrying a point mutation that mimicked phosphorylation on ser880 occluded subsequent long-term depression. Thus, PKC phosphorylation of GluR2 on ser880 is a critical event in the induction of cerebellar long-term depression. Passafaro et al. (2003) demonstrated that overexpression of GLUR2 increases dendritic spine size and density in hippocampal neurons, and more remarkably, induces spine formation in GABA-releasing interneurons that normally lack spines. The extracellular N-terminal domain of GLUR2 is responsible for this effect, and heterologous fusion proteins of the N-terminal domain of GLUR2 inhibit spine morphogenesis. Passafaro et al. (2003) proposed that the N-terminal domain of GLUR2 functions at the cell surface as part of a receptor-ligand interaction that is important for spine growth and/or stability.
GRK5	G protein-coupled receptor kinase 5	chr10q24-qter	This gene encodes a member of the guanine nucleotide-binding protein (G protein)-coupled receptor kinase subfamily of the Ser/Thr protein kinase family. The protein phosphorylates the activated forms of G protein-coupled receptors, thus initiating their deactivation. It has also been shown to play a role in regulating the motility of polymorphonuclear leukocytes (PMNs).
HS3ST2	heparan sulfate (glucosamine) 3-O-sulfotransferase 2	chr16p12	Heparan sulfate biosynthetic enzymes are key components in generating a myriad of distinct heparan sulfate fine structures that carry out multiple biological activities. The enzyme encoded by this gene is a member of the heparan sulfate biosynthetic enzyme family. It is a type II integral membrane protein and possesses heparan sulfate glucosaminyl 3-O-sulfotransferase activity. This gene is expressed predominantly in the brain and may play a role in the nervous system.
INA	interneuron neuronal intermediate filament protein alpha	chr10q24.33	Class-IV neuronal intermediate filament that is able to self-assemble. It is involved in the morphogenesis of neurons. It may form an independent structural network without the involvement of other neurofilaments or it may cooperate with NF-L to form the filamentous backbone to which NF-M and NF-H attach to form the cross-bridges. Abnormal neuronal intermediate filament (IF) inclusions immunopositive for the type IV IF alpha-internexin have been identified as the pathological hallmark of neuronal intermediate filament inclusion disease (NIFID) (Eur J Neurol. 2006 May;13(5):528-32). Abnormal neuronal aggregates of alpha-internexin and the three neurofilament (NF) subunits, NF-L, NF-M, and NF-H have recently been identified as the pathological hallmarks of neuronal intermediate filament (IF) inclusion disease (NIFID), an early onset neurological disease with a variable clinical phenotype including frontotemporal dementia, pyramidal and extrapyramidal signs (Acta Neuropathol (Berl). 2004 Sep;108(3):213-23).
INSM1	insulinoma-associated 1	chr20p11.2	Insulinoma-associated 1 (INSM1) gene is intronless and encodes a protein containing both a zinc finger DNA-binding domain and a putative prohormone domain. This gene is a sensitive marker for neuroendocrine differentiation of human lung tumors. Coimmunoprecipitation assays of mammalian cells revealed that INSM1 interacted with HDAC1 and HDAC3 and that the interaction was mediated through cyclin D1. Cyclin D1 cooperated with INSM1 to suppress Neurod1 promoter activity, and overexpression of cyclin D1 and HDAC3 significantly enhanced the transcriptional repression activity of INSM1 on the Neurod1 promoter. A chromatin immunoprecipitation assay showed that HDAC3 occupied the same region of the Neurod1 promoter by forming a transcription complex with INSM1. Liu et al. (2006) concluded that INSM1 recruits cyclin D1 and HDACs, which confer transcriptional repressor activity.
KIAA1102	KIAA1102 protein	chr4p13	Genes encodes a protein with LIM domain. Actin binding, zinc ion binding. The LIM domain is a cysteine and histidine rich, zinc-coordinating domain composed of two tandemly repeated zinc fingers. The domain consists of two orthogonally arranged antiparallel beta-sheets with the carboxy-terminal zinc finger motif terminated by an alpha helix. The two zinc fingers pack together via a hydrophobic interface formed by conservatively substituted residues
KIF1A	kinesin family member 1A	chr2q37.3	The protein encoded by this gene is a member of the kinesin family. This protein is very similar to mouse heavy chain kinesin member 1A protein which is an anterograde motor protein transporting membranous organelles along axonal microtubules. It is thought that this protein may play a critical role in the development of axonal neuropathies resulting from impaired axonal transport. There are multiple polyadenylation sites found in this gene.
KIF21A	kinesin family member 21A	chr12q12	Marszalek et al. (1999) demonstrated that mouse Kif21a bound strongly to microtubules in the presence of a nonhydrolyzable ATP analog. They found that Kif21a accumulated on the proximal side of a sciatic nerve ligation, consistent with Kif21a being a plus end-directed motor.

MTUS1	mitochondrial tumor suppressor 1	chr9p22	This gene encodes a protein which contains a C-terminal domain able to interact with the angiotension II (AT2) receptor and a large coiled-coil region allowing dimerization. Multiple alternatively spliced transcript variants encoding different isoforms have been found for this gene. One of the transcript variants has been shown to encode a mitochondrial protein that acts as a tumor suppressor and participates in AT2 signaling pathways. Other variants may encode nuclear or transmembrane proteins but it has not been determined whether they also participate in AT2 signaling pathways.
NBL1	neuroblastoma suppression of tumorigenicity 1	chr1p36.13-p36.11	The protein encoded by this gene is a transcription factor that may function as an inhibitor or repressor in cell growth and/or maintenance, and plays a role in the negative regulation of the cell cycle. It has a possible tumor suppressive activity when over expressed. Alternative splicing occurs at this locus and two transcript variants encoding the same protein have been identified. These proteins are secreted, and act as BMP (bone morphogenetic protein) antagonists by binding to BMPs and preventing them from interacting with their receptors. Thus they may play an important role during growth and development. Alternatively spliced transcript variants encoding distinct isoforms have been identified for this gene. <i>NBL1 was identified as a binding partner for APP (770aa) and ubiquilin-1 (UBQLN1). (UBQLN1 modulates amyloid precursor protein trafficking and Abeta secretion.</i>
NEF3	neurofilament 3 (150kDa medium)	chr8p21	Synonym: Neurofilament, medium polypeptide. Kinesin participates in axonal transport of neurofilaments (NFs). It was indicated that phosphorylation of NF-H dissociates NFs from kinesin and provides a mechanism by which NF-H phosphorylation can contribute to the slowing of NF axonal transport (Brain Res Mol Brain Res. 2005 Nov 30;141(2):151-5). The high molecular weight subunits of neurofilaments, NF-H and NF-M, have distinctive long carboxyl-terminal domains that become highly phosphorylated after newly formed neurofilaments enter the axon (J Cell Biol. 1994 Aug;126(4):1031-46).
NEFL	neurofilament light polypeptide 68kDa	chr8p21	Neurofilaments usually contain three intermediate filament proteins: L, M, and H, which are involved in the maintenance of neuronal caliber. Accumulations of neurofilaments are a pathological feature of several neurodegenerative diseases, including amyotrophic lateral sclerosis (ALS), Alzheimer's disease, Parkinson's disease, dementia with Lewy bodies, and diabetic neuropathy. The authors concluded that their results demonstrated that aberrant neurofilament assembly and transport can induce neurologic disease and further implicated defective neurofilament metabolism in the pathogenesis of human neurodegenerative diseases.
NLGN4X	neuroligin 4 X-linked	chrXp22.32-p22.31	This gene encodes a member of a family of neuronal cell surface proteins. Members of this family may act as splice site-specific ligands for beta-neurexins and may be involved in the formation and remodeling of central nervous system synapses. The encoded protein interacts with discs, large (Drosophila) homolog 4 (DLG4). Mutations in this gene have been associated with autism and Asperger syndrome. Two transcript variants encoding the same protein have been identified for this gene.
NTRK2 (non-catalytic isoform)	neurotrophic tyrosine kinase receptor type 2	chr9q22.1	The gene (for the full length receptor) encodes a member of the neurotrophic tyrosine receptor kinase (NTRK) family. This kinase is a membrane-bound receptor that, upon neurotrophin binding, phosphorylates itself and members of the MAPK pathway. <i>Signaling through this kinase leads to cell differentiation.</i> Alternate transcriptional splice variants encoding different isoforms have been found for this gene, but only two of them have been characterized to date. Receptor for brain-derived neurotrophic factor (BDNF), neurotrophin-3 and neurotrophin-4/5 but not nerve growth factor (NGF). Known substrates for the Trk receptors are shc1, pi-3 kinase, and plc-gamma-1.
PFKP	phosphofructokinase platelet	chr10p15.3-p15.2	PFK catalyzes the irreversible conversion of fructose-6-phosphate to fructose-1,6-bisphosphate and is a key regulatory enzyme in glycolysis. PFK is found in platelets, brain and fibroblasts.
PLCB1	Phospholipase C beta 1 (phosphoinositide-specific)	chr20p12	The protein encoded by this gene catalyzes the formation of inositol 1,4,5-trisphosphate and diacylglycerol from phosphatidylinositol 4,5-bisphosphate. This reaction uses calcium as a cofactor and plays an important role in the intracellular transduction of many extracellular signals. This gene is activated by two G-protein alpha subunits, alpha-q and alpha-11. Two transcript variants encoding different isoforms have been found for this gene.
PLK2	polo-like kinase 2 (Drosophila)	chr5q12.1-q13.2	Serum-inducible kinase is a member of the 'polo' family of serine/threonine protein kinases that have a role in normal cell division.

PPP2R2C	protein phosphatase 2 (formerly 2A) regulatory subunit B (PR 52) gamma isoform	chr4p16.1	The product of this gene belongs to the phosphatase 2 regulatory subunit B family. Protein phosphatase 2 is one of the four major Ser/Thr phosphatases, and it is implicated in the negative control of cell growth and division. It consists of a common heteromeric core enzyme, which is composed of a catalytic subunit and a constant regulatory subunit which associates with a variety of regulatory subunits. The B regulatory subunit might modulate substrate selectivity and catalytic activity. This gene encodes a gamma isoform of the regulatory subunit B55 subfamily. Alternatively spliced transcript variants encoding different isoforms have been identified. PP2a consists of a common heterodimeric core enzyme, composed of a 36 kDa catalytic subunit (subunit c) and a 65 kDa constant regulatory subunit (pr65 or subunit a) that associates with a variety of regulatory subunits. Proteins that associate with the core dimer include three families of regulatory subunits b (the r2/b/pr55/b55, r3/b''/pr72/pr130/pr59 and r5/b'/b56 families), the 48 kDa variable regulatory subunit, viral proteins, and cell signaling molecules.
PREP	prolyl endopeptidase	chr6q22	The protein encoded by this gene is a cytosolic prolyl endopeptidase that cleaves peptide bonds on the C-terminal side of prolyl residues within peptides that are up to approximately 30 amino acids long. Prolyl endopeptidases have been reported to be involved in the maturation and degradation of peptide hormones and neuropeptides. PREP is believed to deactivate neuropeptides that are present in the extracellular space. However, the intracellular localization of PREP suggests additional, as yet unidentified physiological functions for this enzyme. Immunocytochemical double-labelling procedures and localization of PREP-enhanced green fluorescent protein fusion proteins that PREP is mainly localized to the perinuclear space, and is associated with the microtubulin cytoskeleton in human neuroblastoma and glioma cell lines. Disassembly of the microtubules by nocodazole treatment disrupts both the fibrillar tubulin and PREP labelling. Furthermore, in a two-hybrid screen, PREP was identified as a binding partner of tubulin. These findings indicate novel functions for PREP in axonal transport and/or protein secretion. In the brains of young APP transgenic Tg2576 mice, hippocampal PREP activity was increased compared to wild-type littermates in the pre-plaque phase, but not in aged mice with beta-amyloid plaque pathology. This "accelerated aging" with regard to hippocampal PREP expression in young APP transgenic mice might be one factor contributing to the observed cognitive deficits in these mice in the pre-plaque phase and could also explain, in part, the cognition-enhancing effects of PREP inhibitors in several experimental paradigms (Neurochem Res. 2005 Jun-Jul;30(6-7):695-702). Prolyl endopeptidase (PREP) is a proline-specific oligopeptidase with a reported effect on learning and memory in different rat model systems. Measuring different second-messenger concentrations revealed an inverse correlation between inositol 1,4,5-triphosphate [Ins(1,4,5)P3] concentration and PREP expression.
PRSS12	Protease serine 12 (neurotrypsin motopsin)	chr4q28.1	This gene encodes a member of the trypsin family of secreted serine proteases. Studies in mice suggest that the encoded enzyme may be involved in structural reorganizations associated with learning and memory. Plays a role in neuronal plasticity and the proteolytic action may subserve structural reorganizations associated with learning and memory operations. Defects in prss12 are a cause of autosomal recessive nonsyndromic mental retardation. This kind of mental retardation is a mental disorder characterized by significantly subaverage general intellectual functioning associated with impairments in adaptive behavior and manifested during the developmental period.
PTPRM	protein tyrosine phosphatase receptor type M	chr18p11.2	The protein encoded by this gene is a member of the protein tyrosine phosphatase (PTP) family and a membrane single-pass type I membrane protein. PTPs are known to be signaling molecules that regulate a variety of cellular processes including cell growth, differentiation, mitotic cycle, and oncogenic transformation. PTPRM possesses an extracellular region, a single transmembrane region, and two tandem catalytic domains, and thus represents a receptor-type PTP. The extracellular region contains a meprin-A5 antigen-PTP mu (MAM) domain, an Ig-like domain and four fibronectin type III-like repeats. PTPRM has been shown to mediate cell-cell aggregation through the interaction with another molecule of this PTP on an adjacent cell. PTPRM can interact with scaffolding protein RACK1/GNB2L1, which may be necessary for the downstream signaling in response to cell-cell adhesion.
PTPRN2	protein tyrosine phosphatase receptor type N polypeptide 2	chr7q36	The protein encoded by this gene is a member of the protein tyrosine phosphatase (PTP) family. PTPs are known to be signaling molecules that regulate a variety of cellular processes including cell growth, differentiation, mitotic cycle, and oncogenic transformation. This PTP possesses an extracellular region, a single transmembrane region, and a single intracellular catalytic domain, and thus represents a receptor-type PTP. The catalytic domain of this PTP is most closely related to PTPRN/IA-2beta. This PTP and PTPRN are both found to be major autoantigens associated with insulin-dependent diabetes mellitus. Three alternatively spliced transcript variants of this gene encoding different proteins have been reported.

RELN	reelin	chr7q22	This gene encodes a large <i>secreted extracellular matrix protein</i> thought to control cell-cell interactions critical for cell positioning and neuronal migration during brain development. This protein may be involved in schizophrenia, autism, bipolar disorder, major depression and in migration defects associated with temporal lobe epilepsy. Mutations of this gene are associated with autosomal recessive lissencephaly with cerebellar hypoplasia. Two transcript variants encoding distinct isoforms have been identified for this gene. Other transcript variants have also been described. Extracellular matrix serine protease that plays a role in layering of neurons in the cerebral cortex and cerebellum. Regulates microtubule function in neurons and neuronal migration. Affects migration of sympathetic preganglionic neurons in the spinal cord, where it seems to act as a barrier to neuronal migration. Enzymatic activity is important for the modulation of cell adhesion. Binding to the extracellular domains of lipoprotein receptors VLDLR and APOER2 induces tyrosine phosphorylation of dab1 and modulation of tau phosphorylation. Abundantly produced during brain ontogenesis by the Cajal-retzius cells and other pioneer neurons located in the telencephalic marginal zone and by granule cells of the external granular layer of the cerebellum. In adult brains, RELN is preferentially expressed in gabaergic interneurons of prefrontal cortices, temporal cortices, hippocampi and glutamatergic granule cells of cerebellum. Also expressed in fetal and adult livers.
RIS1	Ras-inducible senescence 1	chr3p21.3	Transmembrane protein.
SEMA6D	sema domain transmembrane domain (TM) and cytoplasmic domain (semaphorin) 6D	15q21.1	Semaphorins are a large family, including both secreted and membrane associated proteins, many of which have been implicated as inhibitors or chemorepellents in axon pathfinding, fasciculation and branching, and target selection. All semaphorins possess a semaphorin (Sema) domain and a PSI domain (found in plexins, semaphorins and integrins) in the N-terminal extracellular portion. Additional sequence motifs C-terminal to the semaphorin domain allow classification into distinct subfamilies. Results demonstrate that transmembrane semaphorins, like the secreted ones, can act as repulsive axon guidance cues. This gene encodes a class 6 vertebrate transmembrane semaphorin that demonstrates alternative splicing. Six transcript variants have been identified and expression of the distinct encoded isoforms is thought to be regulated in a tissue- and development-dependent manner. Qu et al. (2002) exposed chicken embryo dorsal root ganglion explants and neonatal rat cortical and hippocampal neurons to SEMA6D secreted from transfected COS-7 cells and found that <i>SEMA6D induced growth cone collapse. SEMA6D also inhibited axonal extension in a nerve growth factor (NGF)-differentiated rat pheochromocytoma cell line.</i>
SEMA3C	sema domain immunoglobulin domain	chr7q21-q31	Semaphorins, or collapsins, constitute a family characterized by the presence of a conserved semaphorin domain at the N terminus. Secreted protein, may be involved in diverse cell survival mechanisms. All glioma cell lines express SEMA3A and SEMA3C and exhibit SEMA3A binding sites.
SNAP25	synaptosomal-associated protein 25kDa	chr20p12-p11.2	Synaptic vesicle membrane docking and fusion is mediated by SNAREs (soluble N-ethylmaleimide-sensitive factor attachment protein receptors) located on the vesicle membrane (v-SNAREs) and the target membrane (t-SNAREs). The assembled v-SNARE/t-SNARE complex consists of a bundle of four helices, one of which is supplied by v-SNARE and the other three by t-SNARE. For t-SNAREs on the plasma membrane, the protein syntaxin supplies one helix and the protein encoded by this gene contributes the other two. Therefore, this gene product is a presynaptic plasma membrane protein involved in the regulation of neurotransmitter release. Two alternative transcript variants encoding different protein isoforms have been described for this gene. Elevated cerebrospinal fluid SNAP-25 in schizophrenia (Biol Psychiatry. 2003 Jun 15;53(12):1132-7). Increased RNA levels of the 25 kDa synaptosomal associated protein in brain samples of adult patients with Down Syndrome (Neurosci Lett. 2003 Jan 16;336(2):77-80). The heavy chain of kinesin interacts with the SNARE proteins SNAP25 and SNAP23 (Biochemistry. 2002 Dec 17;41(50):14906-15).
SGPP2	Sphingosine-1-phosphate phosphatase	chr2q36.1	Sphingosine-1-phosphatase is an intracellular enzyme located in the endoplasmic reticulum, which regulates the level of sphingosine-1-phosphate (S1P), a bioactive lipid.
SYT13	synaptotagmin XIII	chr11p12-p11	SYT13 belongs to the large synaptotagmin protein family. All synaptotagmins show type I membrane topology, with an extracellular N terminus, a single transmembrane region, and a cytoplasmic C terminus containing tandem C2 domains. Major functions of synaptotagmins include vesicular traffic, exocytosis, and secretion.
TNC	tenascin C (hexabrachion)	chr9q33	TenascinC is part of a specialized extracellular matrix in the region of the horizontal myoseptum (in zebrafish) that influences the growth of motor axons. In situ hybridization and immunocytochemistry experiments revealed that tenascin-C, one candidate molecule which was suspected to be involved in neonatal learning, is expressed in the forebrain of domestic chicks around the sensitive period during which auditory filial imprinting takes place (Neuroscience. 2006 Sep 15;141(4):1709-19).

TNFRSF10B	tumor necrosis factor receptor superfamily member 10b	chr9p22-p21	The protein encoded by this gene is a member of the TNF-receptor superfamily, and contains an intracellular death domain. This receptor can be activated by tumor necrosis factor-related apoptosis inducing ligand (TNFSF10/TRAIL/APO-2L), and transduces apoptosis signal. Studies with FADD-deficient mice suggested that FADD, a death domain containing adaptor protein, is required for the apoptosis mediated by this protein. Receptor for the cytotoxic ligand TNFSF10/TRAIL. The adapter molecule FADD recruits caspase-8 to the activated receptor. The resulting death-inducing signaling complex (disc) performs caspase-8 proteolytic activation which initiates the subsequent cascade of caspases (aspartate-specific cysteine proteases) mediating apoptosis. Promotes the activation of NF- kappa-b.
VMP	vesicular membrane protein 24	chr6p22.2	VMP contains two putative membrane spanning domains and a hydrophilic tail homologous to the microtubule-binding domain of MAPs. So it is speculated that VMP may associate with microtubules through its C-terminal and plays an important role in vesicular organelles transport and nerve signals.
WNT5A	wingless-type MMTV integration site family member 5A	chr3p21-p14	The WNT gene family consists of structurally related genes which encode secreted signaling proteins. These proteins have been implicated in oncogenesis and in several developmental processes, including regulation of cell fate and patterning during embryogenesis. This gene is a member of the WNT gene family. It encodes a protein which shows 98%, 98% and 87% amino acid identity to the mouse, rat and the xenopus Wnt5A protein, respectively. The experiments performed in Xenopus laevis embryos identified that human frizzled-5 (hFz5) is the receptor for the Wnt5A ligand and the Wnt5A/hFz5 signaling mediates axis induction. <i>Wnt-5a inhibits the Wnt pathway</i> by promoting GSK-3-independent beta-catenin degradation. The Wnt antagonist DICKKOPF-1 gene is a downstream target of beta-catenin/TCF and is down-regulated in human colon cancer (Oncogene. 2005 Feb 3;24(6):1098-103).
-	HMP19 protein (LOC51617)	chr5q35.2	D1 dopamine receptor-interacting protein.

### Selection of down-regulated genes, C99V50F/C99WT1 (volcano plot):

ADAMTS9	a disintegrin-like and metalloprotease (reprolysin type) with thrombospondin type 1 motif 9	chr3p14.3-p14.2	Previously described in Chapter 12.3
ADCY1	adenylate cyclase 1 (brain)	chr7p13-p12	ADCY1 is the founding member of the adenylate cyclase (EC 4.6.1.1) family of enzymes responsible for the synthesis of cAMP (Ludwig and Seuwen, 2002). In transgenic mice with specific overexpression of Adcy1 in the forebrain, Wang et al. (2004) found a tendency towards increased long-term potentiation, increased memory for object recognition, and slower rates of loss of contextual memory compared to wildtype mice.
CTSD	cathepsin D (lysosomal aspartyl protease)	chr11p15.5	The protein encoded by this gene is a lysosomal aspartyl protease composed of a dimer of disulfide-linked heavy and light chains, both produced from a single protein precursor. This proteinase is a member of the peptidase C1 family. Transcription of this gene is initiated from several sites, including one which is a start site for an estrogen-regulated transcript. Mutations in this gene are involved in the pathogenesis of several diseases, including breast cancer and possibly Alzheimer's disease. Acid protease active in intracellular protein breakdown. involved in the pathogenesis of several diseases such as breast cancer and possibly Alzheimer's disease. Localized in lysosomes. The val-58 allele is significantly overrepresented in demented patients (11.8%) compared with nondemented controls (4.9%). Carriers of the val-58 allele have a 3.1-fold increased risk for developing AD than noncarriers.
CHRM3	cholinergic receptor, muscarinic 3	chr1q41-q44	The muscarinic cholinergic receptors belong to a larger family of G protein-coupled receptors. The functional diversity of these receptors is defined by the binding of acetylcholine and includes cellular responses such as adenylate cyclase inhibition, phosphoinositide degeneration, and potassium channel mediation. Muscarinic receptors influence many effects of acetylcholine in the central and peripheral nervous system. The muscarinic acetylcholine receptor mediates various cellular responses, including inhibition of adenylate cyclase, breakdown of phosphoinositides and modulation of potassium channels through the action of G proteins.

CDK6	cyclin-dependent kinase 6	chr7q21-q22	The cyclin-dependent protein kinases (CDKs) regulate major cell cycle transitions in eukaryotic cells. In primary T cells that were stimulated to enter the cell cycle, cellular CDK6 kinase activity first appeared in mid-G1, prior to the activation of any previously characterized CDK. Meyerson and Harlow (1994) suggested that CDK6, and the homologous CDK4, link growth factor stimulation with the onset of cell cycle progression. Guan et al. (1994) proposed that CDK4 and CDK6 are physiologic RB1 kinases that are inhibited by the p14 (600431), p16 (600160), and p18 (603369) CDK inhibitors. This inhibition prevents the phosphorylation of RB1 and keeps RB1 in its active growth-suppressing state.
CDKN1C	cyclin-dependent kinase inhibitor 1C (p57, Kip2)	chr11p15.5	Previously described in Chapter 12.3
DYRK2	dual-specificity tyrosine-(Y)-phosphorylation regulated kinase 2	chr12q15	DYRK2 belongs to a family of protein kinases whose members are presumed to be involved in cellular growth and/or development. The family is defined by structural similarity of their kinase domains and their capability to autophosphorylate on tyrosine residues. DYRK2 has demonstrated tyrosine autophosphorylation and catalyzed phosphorylation of histones H3 and H2B in vitro. DYRK2 is targeted to the nucleus and controls p53 via Ser46 phosphorylation in the apoptotic response to DNA damage (Mol Cell. 2007 Mar 9;25(5):725-38). Taira et al. (2007) found that DYRK2 phosphorylated p53 (TP53) on ser46 in vitro and in human cells. Upon exposure to genotoxic stress, DYRK2 translocated into the nucleus and phosphorylated p53 on ser46, inducing P53AIP1 expression and apoptosis in a ser46 phosphorylation-dependent manner. Taira et al. (2007) concluded that DYRK2 regulates p53 to induce apoptosis in response to DNA damage.
EFNB2	ephrin-B2	chr13q33	This gene encodes a member of the ephrin (EPH) family. The ephrins and EPH-related receptors comprise the largest subfamily of receptor protein-tyrosine kinases and have been implicated in mediating developmental events, especially in the nervous system and in erythropoiesis. Based on their structures and sequence relationships, ephrins are divided into the ephrin-A (EFNA) class, which are anchored to the membrane by a glycosylphosphatidylinositol linkage, and the ephrin-B (EFNB) class, which are transmembrane proteins. This gene encodes an EFNB class ephrin which binds to the EPHB4 and EPHA3 receptors. EFNB2 binds to the receptor tyrosine kinases ephb4 and epha3 and may play a role in constraining the orientation of longitudinally projecting axons.
GFRA3	GDNF family receptor alpha 3	chr5q31.1-q31.3	Glial cell line-derived neurotrophic factor receptor alpha-3. The protein encoded by this gene is a glycosylphosphatidylinositol(GPI)-linked cell surface receptor and a member of the GDNF receptor family. It forms a signaling receptor complex with RET tyrosine kinase receptor and binds the ligand artemin. Glial cell line-derived neurotrophic factor (GDNF) and neurturin (NRTN) promote the survival and maintenance of different neuronal cell types. GDNF signals through a receptor complex composed of a GDNF family receptor and the membrane-bound protein tyrosine-kinase receptor RET.
GPC3	glypican 3	chrXq26.1	Cell surface heparan sulfate proteoglycans are composed of a membrane-associated protein core substituted with a variable number of heparan sulfate chains. Members of the glypican-related integral membrane proteoglycan family (GRIPS) contain a core protein anchored to the cytoplasmic membrane via a glycosyl phosphatidylinositol linkage. These proteins may play a role in the control of cell division and growth regulation. Deletion mutations in this gene are associated with Simpson-Golabi-Behmel syndrome. Cell surface proteoglycan that bears heparan sulfate may be involved in the suppression/modulation of growth in the predominantly mesodermal tissues and organs. May play a role in the modulation of IGF2 interactions with its receptor and thereby modulate its function. May regulate growth and tumor predisposition. Predicted functional partners are IGF2, Insulin precursor, WNT5A, CDKN1C, WNT3A, WNT7B.
INSM2	insulinoma-associated 2	chr14q13.2	Insulinoma-associated protein-2 is a major autoantigen in type 1 diabetes that occurs through autoimmune-mediated beta-cell destruction (Diabetes. 2007 Jan;56(1):41-8).
LRP4	low density lipoprotein receptor-related protein 4	chr11p11.2-p12	Potential cell surface endocytic receptor, which binds and internalizes extracellular ligands for degradation by lysosomes.
MFAP4	microfibrillar-associated protein 4	chr17p11.2	This gene encodes a protein with similarity to a bovine microfibril-associated protein. The protein has binding specificities for both collagen and carbohydrate. It is thought to be an extracellular matrix protein which is involved in cell adhesion or intercellular interactions. The gene is located within the Smith-Magenis syndrome region. Although the precise function of this protein is not known, it has been suggested that it could be a Ca <sup>2+</sup> -dependent adhesive protein that is associated with elastin (ELN) microfibrils in the extracellular matrix. MFAP4 has a fibrinogen-like domain. The N-terminus of the protein contains an arg-gly-asp sequence that serves as the ligand motif for cell surface receptor integrin.

NNAT	neuronatin	chr20q11.2-q12	The protein encoded by this gene is a proteolipid that may be involved in the regulation of ion channels during brain development. The encoded protein may also play a role in forming and maintaining the structure of the nervous system. This gene is found within an intron of the BLCAP gene, but on the opposite strand. This gene is imprinted and is expressed only from the paternal allele, while BLCAP is not imprinted. Two transcript variants encoding two different isoforms have been found for this gene. The NNAT gene contains in its 5-prime flanking region a neural restrictive silencer element that was thought to govern neuron-specific expression. The deduced protein is a proteolipid that may function as a regulator of ion channels during brain development.
PROX1	Prospero-related homeobox 1	chr1q32.2-q32.3	Previously described in Chapter 12.3
GPR176	putative G protein coupled receptor	chr15q14-q15.1	Belongs to the G-protein coupled receptor 1 family. Orphan receptor. Membrane; multi-pass membrane protein.
SERPINF1	serine (or cysteine) proteinase inhibitor, clade F (alpha-2 antiplasmin, pigment epithelium derived factor), member 1	chr17p13.1	Neurotrophic protein; induces extensive neuronal differentiation in retinoblastoma cells. Potent inhibitor of angiogenesis. As it does not undergo the s (stressed) to r (relaxed) conformational transition characteristic of active serpins, it exhibits no serine protease inhibitory activity expressed in quiescent cells. The N-terminal (aa 44-121) exhibits neurite outgrowth-inducing activity. The C-terminal exposed loop (aa 382-418) is essential for serpin activity, secreted protein. Natural inhibitors of angiogenesis are able to block pathologic neovascularization without harming the pre-existing vasculature. Volpert et al. (2002) demonstrated that 2 such inhibitors, thrombospondin I and SERPINF1, derive specificity for remodeling vessels from their dependence on Fas/Fas ligand (FasL)-mediated apoptosis to block angiogenesis. Both inhibitors up-regulated FasL on endothelial cells. Expression of the essential partner of FasL, Fas receptor, was low on quiescent endothelial cells and vessels but greatly enhanced by inducers of angiogenesis, thereby specifically sensitizing the stimulated cells to apoptosis by inhibitor-generated FasL. The antiangiogenic activity of thrombospondin I and SERPINF1 both in vitro and in vivo was dependent on this dual induction of Fas and FasL and the resulting apoptosis. Volpert et al. (2002) concluded that this example of cooperation between pro- and antiangiogenic factors in the inhibition of angiogenesis provides one explanation for the ability of inhibitors to select remodeling capillaries for destruction.
STX3A	syntaxin 3A	chr11q12.1	Potentially involved in docking of synaptic vesicles at presynaptic active zones, contains 1 t-snare coiled-coil homology domain.
TFRC	transferrin receptor (p90, CD71) /// transferrin receptor (p90, CD71)	chr3q29	Cellular uptake of iron occurs via receptor-mediated endocytosis of ligand-occupied transferrin receptor into specialized endosomes, endosomal acidification leads to iron release. The apotransferrin-receptor complex is then recycled to the cell surface with a return to neutral pH and the concomitant loss of affinity of apotransferrin for its receptor. Transferrin receptor (TFR) is necessary for development of erythrocytes and the nervous system. The relationships between iron metabolism and type 2 diabetes are bidirectional: Iron affects glucose metabolism and glucose metabolism impinges on several iron metabolic pathways. Both insulin sensitivity and glucose tolerance status are strongly associated with serum TFR concentrations (Diabetes Care. 2007 Mar;30(3):604-8). The early endosome is organised into domains to ensure the separation of cargo. Activated mitogenic receptors, such as the epidermal growth factor (EGF) receptor, are concentrated into vesicles enriched for the small GTPase Rab5, which progressively exclude nutrient receptors, such as transferrin receptor, into neighbouring tubules. These vesicles become enlarged, increase their content of intraluminal vesicles as EGF receptors are sorted from the limiting membrane, and eventually mature to late endosomes. Maturation is governed by the loss of Rab5 and is accompanied by the movement of endosomes along microtubules towards the cell centre. It has been shown that EGF relocates to the cell centre in a dynein-dependent fashion, concomitant with the sorting away of transferrin receptors, although it remains in Rab5-positive early endosomes. When dynein function is acutely disrupted, efficient recycling of transferrin from EGF-containing endosomes is retarded, loss of Rab5 is slowed and endosome enlargement is reduced (Nat Cell Biol. 2007 Jan;9(1):113-20). Transferrin receptor 1 is required for iron delivery from transferrin to cells. It was established as a gatekeeper for regulating iron uptake by most cells. TFRC is regulated by cellular iron levels through binding of the iron regulatory proteins, IRP1 and IRP2, to iron-responsive elements in the 3'-utr. Up-regulated upon mitogenic stimulation.

MYCN	v-myc myelocytomatous viral related oncogene, neuroblastoma derived (avian)	chr2p24.1	This gene is a member of the MYC family and encodes a protein with a basic helix-loop-helix (bHLH) domain. This protein is located in the nucleus and must dimerize with another bHLH protein in order to bind DNA. Amplification of this gene is associated with a variety of tumors, most notably neuroblastomas.
------	---	-----------	---

### Selection of up-regulated genes, C99V50F/C99WT1 (volcano plot):

ID4	inhibitor of DNA binding 4, dominant negative helix-loop-helix protein	chr6p22-p21	Transcription factors containing a basic helix-loop-helix (bHLH) motif regulate expression of tissue-specific genes in a number of mammalian and insect systems. DNA-binding activity of the bHLH proteins is dependent on formation of homo- and/or heterodimers. Dominant-negative HLH proteins encoded by Id-related genes (inhibitor of DNA binding), such as ID4, also contain the HLH-dimerization domain but lack the DNA-binding basic domain. Consequently, Id proteins inhibit binding to DNA and transcriptional transactivation by heterodimerization with bHLH proteins (Pagliuca et al., 1995). Downregulation of ID4 by promoter hypermethylation in gastric adenocarcinoma (Oncogene. 2003 Oct 9;22(44):6946-53). HLH proteins lack a basic DNA-binding domain but are able to form heterodimers with other hhl proteins, thereby inhibiting DNA binding.
SEMA3A	sema domain, immunoglobulin domain (Ig), short basic domain, secreted, (semaphorin) 3A	chr7p12.1	This gene is a member of the semaphorin family and encodes a protein with an Ig-like C2-type (immunoglobulin-like) domain, a PSI domain and a Sema domain. This secreted protein can function as a chemoattractive agent, stimulating the growth of apical dendrites. The protein is vital for normal neuronal pattern development. Also, aberrant release of this protein is associated with the progression of Alzheimer's disease. SEMA3A is a secreted protein and could serve as a ligand that guides specific growth cones by a motility-inhibiting mechanism. It binds to the complex neuropilin-1/plexin-1. Polleux et al. (2000) demonstrated that the growth of apical dendrites toward the pial surface is regulated by a diffusible chemoattractant present at high levels near the marginal zone. A major component of the signal is SEMA3A, which was previously characterized as a chemorepellant for cortical axons. Soluble guanylate cyclase is asymmetrically localized to the developing apical dendrite, and is required for the chemoattractive effect of SEMA3A. Thus, the asymmetric localization of soluble guanylate cyclase confers distinct SEMA3A responses to axons and dendrites. Polleux et al. (2000) concluded that these observations reveal a mechanism by which a single chemotropic signal can pattern both axons and dendrites during development. Loss of neuropilin function increases the number of interneurons that migrate into the striatum. Marin et al. (2001) concluded that their observations reveal a mechanism by which neuropilins mediate sorting of distinct neuronal populations into different brain structures, and provide evidence that, in addition to guiding axons, these receptors also control neuronal migration in the central nervous system.
PEG10	paternally expressed 10	chr7q21	This gene includes two overlapping reading frames of the same transcript encoding distinct isoforms. The shorter isoform has a CCHC-type zinc finger motif containing a sequence characteristic of gag proteins of most retroviruses and some retrotransposons, and it functions in part by interacting with members of the TGF-beta receptor family. The longer isoform has the active-site DSG consensus sequence of the protease domain of pol proteins. The longer isoform is the result of -1 translational frameshifting that is also seen in some retroviruses. Expression of these two isoforms only comes from the paternal allele due to imprinting. Increased gene expression (as observed by an increase in mRNA levels) is associated with hepatocellular carcinomas. By yeast 2-hybrid analysis and coimmunoprecipitation experiments, Lux et al. (2005) determined that human PEG10-RF1 and PEG10-RF1/RF2 interacted with the cytoplasmic domain of ALK1, a TGF-beta (TGFB1) receptor.
TFPI2	tissue factor pathway inhibitor 2	chr7q22	Previously described in Chapter 12.3
NFASC	neurofascin	chr1q32.1	Neurofascin is an L1 family immunoglobulin cell adhesion molecule (see L1CAM) involved in axon subcellular targeting and synapse formation during neural development (Ango et al., 2004).

NEF3	neurofilament 3 (150kDa medium)	chr8p21	Previously described in Chapter 12.3
PCSK2	proprotein convertase subtilisin/kexin type 2	chr20p11.2	The protein encoded by this gene belongs to the subtilisin-like proprotein convertase family. The members of this family are proprotein convertases that process latent precursor proteins into their biologically active products. This encoded protein is a proinsulin-processing enzyme that plays a key role in regulating insulin biosynthesis. It is also known to cleave proopiomelanocortin, proenkephalin, prodynorphin and proluteinizing-hormone-releasing hormone. The use of alternate polyadenylation sites has been found for this gene. The proprotein convertase PC2 is involved in the maturation of prosomatostatin to somatostatin-14 but not in the somatostatin deficit in Alzheimer's disease (Neuroscience. 2003;122(2):437-47).
TRAF3IP2	TRAF3 interacting protein 2	chr6q21	This gene encodes a protein involved in regulating responses to cytokines by members of the Rel/NF-kappaB transcription factor family. These factors play a central role in innate immunity in response to pathogens, inflammatory signals and stress. This gene product interacts with TRAF proteins (tumor necrosis factor receptor-associated factors) and either I-kappaB kinase or MAP kinase to activate either NF-kappaB or Jun kinase. Two alternative transcripts encoding different proteins have been identified. A third transcript, which does not encode a protein and is transcribed in the opposite orientation, has also been identified. Overexpression of this transcript has been shown to reduce expression of at least one of the protein encoding transcripts, suggesting it has a regulatory role in the expression of this gene.
NEFL	Neurofilament, light polypeptide 68kDa	chr8p21	Previously described in Chapter 12.3
NEFL	neurofilament, light polypeptide 68kDa	chr8p21	Previously described in Chapter 12.3
TBX3	T-box 3 (ulnar mammary syndrome)	chr12q24.1	Tbx3 impinges on the p53 pathway to suppress apoptosis, facilitate cell transformation and block myogenic differentiation (Oncogene. 2002 May 30;21(24):3827-35).

CDKN1A	cyclin-dependent kinase inhibitor 1A (p21, Cip1)	chr6p21.2	<p>This gene encodes a potent cyclin-dependent kinase inhibitor. The encoded protein binds to and inhibits the activity of cyclin CDK2 or -CDK4 complexes, and thus functions as a regulator of cell cycle progression at G1. The expression of this gene is tightly controlled by the tumor suppressor protein p53, through which this protein mediates the p53-dependent cell cycle G1 phase arrest in response to a variety of stress stimuli. This protein can interact with proliferating cell nuclear antigen (PCNA), a DNA polymerase accessory factor, and plays a regulatory role in S phase DNA replication and DNA damage repair. This protein was reported to be specifically cleaved by CASP3-like caspases, which thus leads to a dramatic activation of CDK2, and may be instrumental in the execution of apoptosis following caspase activation. Two alternatively spliced variants, which encode an identical protein have been reported. This gene encodes a potent cyclin-dependent kinase inhibitor. The encoded protein binds to and inhibits the activity of cyclin CDK2 or -CDK4 complexes, and thus functions as a regulator of cell cycle progression at G1. The expression of this gene is tightly controlled by the tumor suppressor protein p53, through which this protein mediates the p53-dependent cell cycle G1 phase arrest in response to a variety of stress stimuli. This protein can interact with proliferating cell nuclear antigen (PCNA), a DNA polymerase accessory factor, and plays a regulatory role in S phase DNA replication and DNA damage repair. This protein was reported to be specifically cleaved by CASP3-like caspases, which thus leads to a dramatic activation of CDK2, and may be instrumental in the execution of apoptosis following caspase activation. Two alternatively spliced variants, which encode an identical protein have been reported. Transforming growth factor-beta (TGF-beta) inhibits epithelial cell growth, in part via transcriptional induction of the cell cycle inhibitor p21(WAF1/Cip1) (p21). It has been shown that bone morphogenetic protein (BMP)-7 induces higher p21 expression than TGF-beta1 in various epithelial cells. Despite this, BMP-7 only weakly suppresses epithelial cell proliferation, as Id2, a cell cycle-promoting factor, becomes concomitantly induced by BMP-7. Signaling studies with all type I receptors of the TGF-beta superfamily show that BMP receptors induce higher p21 expression than TGF-beta/activin receptors. Smad4 is essential for p21 regulation by all receptor pathways. Based on the previously known ability of c-Myc to block p21 expression and epithelial growth arrest in response to TGF-beta1, it has been demonstrated that ectopic c-Myc expression can abrogate Smad-mediated p21 induction by all TGF-beta and BMP receptors. Furthermore, p21 induction by all receptor pathways can be blocked by the natural inhibitors of the TGF-beta superfamily, p21 is a common target of all TGF-beta superfamily pathways. (J Cell Physiol. 2005 Jul;204(1):260-72).</p>
VGF	VGF nerve growth factor inducible	chr7q22	<p>This gene is specifically expressed in a subpopulation of neuroendocrine cells, and is up-regulated by nerve growth factor. The structural organization of this gene is similar to that of the rat gene, and both the translated and the untranslated regions show a high degree of sequence similarity to the rat gene. The encoded secretory protein also shares similarities with the secretogranin/chromogranin family, however, its exact function is not known. VGF levels were found to be significantly lower in the CSF from patients with ALS and suggested as biomarkers (in combination with others) for ALS (amyotrophic lateral sclerosis). VGF may be involved in the regulation of cell-cell interactions or in synaptogenesis during the maturation of the nervous system and may be stored in secretory vesicles and then secreted. Targeted deletion of the Vgf gene indicates that the encoded secretory peptide precursor plays a role in the regulation of energy balance (Neuron 23: 537-548, 1999).</p>
NELL2	NEL-like 2 (chicken) /// NEL-like 2 (chicken)	chr12q13.11-q13.12	<p>This gene encodes a cytoplasmic protein that contains epidermal growth factor (EGF) -like repeats. The encoded heterotrimeric protein may be involved in cell growth regulation and differentiation. Secreted protein, binds to pkc beta-1.</p>

SGK	serum/glucocorticoid regulated kinase	chr6q23	Transforming growth factor-beta (TGFB1) participates in the pathophysiology of diabetic complications. Lang et al. (2000) demonstrated markedly enhanced transcription of SGK in diabetic nephropathy, with particularly high expression in mesangial cells, interstitial cells, and cells in the thick ascending limbs of the loop of Henle and distal tubules. The enhanced SGK transcription, which results from excessive extracellular glucose concentrations, stimulates renal tubular Na <sup>+</sup> transport. These observations disclosed an additional element in the pathophysiology of diabetic nephropathy. Gamper et al. (2002) found that expression of SGK1, SGK2, and SGK3 in human embryonic kidney cells and <i>Xenopus</i> oocytes significantly stimulated voltage-gated K <sup>+</sup> channels. Arteaga et al. (2006) found that mouse SGK1 is a short-lived protein with a significantly shorter half-life than SGK2 or Akt. SGK1 was ubiquitinated and degraded at the endoplasmic reticulum (ER) membrane by the action of the ER-associated ubiquitin-conjugating enzymes Ubc6 and Ubc7 and the ligase Hrd1. A hydrophobic alpha helix located within the N terminus of SGK1 serves as the signal for targeting the protein to the ER for ubiquitination and subsequent degradation. This kinase has been shown to be important in activating certain potassium, sodium, and chloride channels. Expression of this gene in hepatocytes is stimulated by transforming growth factor-beta (TGF-beta) which participates in the pathophysiology of diabetic complications. Since both TGF-beta expression and SGK expression are elevated in diabetic nephropathy, this suggests an involvement of SGK in the development of this condition. Mediates cell survival signals. SGK phosphorylates and negatively regulates pro-apoptotic foxo3a. SGK is induced by serum and/or glucocorticoids, by excessive extracellular glucose and by tgf-beta, in cultured cells. It is regulated by phosphorylation: phosphoinositide 3-kinase (PI3K-kinase) pathway promotes phosphorylation on ser-422 which in turn increases the phosphorylation of thr-256 by pdpk1. Ubiquitinated by nedd4l, which promotes proteasomal degradation.
ECEL1	endothelin converting enzyme-like 1	chr2q36-q37	This gene encodes a member of the neutral endopeptidase (NEP)-related family. It is expressed specifically in the nervous system. It may contribute to the degradation of peptide hormones and be involved in the inactivation of neuronal peptides. It is assumed to bind 1 zinc ion. The gene disruption in mouse embryonic stem cells results in neonatal mortality due to respiratory failure shortly after birth. Based on the specific expression of this gene and the phenotype of the gene deficiency in mouse embryos, it is suggested that the protein encoded by this gene plays a critical role in the nervous regulation of the respiratory system.
BAMBI	BMP and activin membrane-bound inhibitor	chr10p12.3-p11.2	This gene encodes a transmembrane glycoprotein related to the type I receptors of the transforming growth factor-beta (TGF-beta) family, whose members play important roles in signal transduction in many developmental and pathological processes. The encoded protein However, is a pseudoreceptor, lacking an intracellular serine/threonine kinase domain required for signaling. Similar proteins in frog, mouse and zebrafish function as negative regulators of TGF-beta, which has led to the suggestion that the encoded protein may function to limit the signaling range of the TGF-beta family during early embryogenesis. Negatively regulates tgf-beta signaling.
DGKB	diacylglycerol kinase, beta 90kDa	chr7p21.3	Diacylglycerol kinases (DGKs) are regulators of the intracellular concentration of the second messenger diacylglycerol (DAG) and thus play a key role in cellular processes. Nine mammalian isotypes have been identified, which are encoded by separate genes. Mammalian DGK isozymes contain a conserved catalytic (kinase) domain and a cysteine-rich domain (CRD). The protein encoded by this gene is a diacylglycerol kinase, beta isotype. Two alternatively spliced transcript variants have been found for this gene. Diacylglycerol kinases (DGKs) are regulators of the intracellular concentration of the second messenger diacylglycerol (DAG) and thus play a key role in cellular processes. Nine mammalian isotypes have been identified, which are encoded by separate genes. Mammalian DGK isozymes contain a conserved catalytic (kinase) domain and a cysteine-rich domain (CRD). The protein encoded by this gene is a diacylglycerol kinase, beta isotype.
NEFL	neurofilament, light polypeptide 68kDa	chr8p21	Previously described in Chapter 12.3

L1CAM	L1 cell adhesion molecule	chrXq28	Membrane; single-pass type I membrane protein. The protein encoded by this gene is an axonal glycoprotein belonging to the immunoglobulin supergene family. The ectodomain, consisting of several immunoglobulin-like domains and fibronectin-like repeats (type III), is linked via a single transmembrane sequence to a conserved cytoplasmic domain. This cell adhesion molecule plays an important role in nervous system development, including neuronal migration and differentiation. L1CAM is a cell adhesion molecule with an important role in the development of the nervous system. Involved in neuron-neuron adhesion, neurite fasciculation, outgrowth of neurites, etc.. Binds to axonin on neurons. Mutations in the gene cause three X-linked neurological syndromes known by the acronym CRASH (corpus callosum hypoplasia, retardation, aphasia, spastic paraplegia and hydrocephalus). Defects in Hydrocephalus due to stenosis of the aqueduct of sylvius is characterized by mental retardation and enlarged brain ventricles. Kenwrick et al. (2000) reviewed the various functions of L1CAM, including guidance of neurite outgrowth in development, neuronal cell migration, axon bundling, synaptogenesis, myelination, neuronal cell survival, and long-term potentiation. On differentiated neurons, L1 is found at regions of contact between neighbouring axons and on the growth cones, the structures at the leading tip of axons that are responsible for sensing extracellular growth and guidance cues. This distribution supports the suggestion from in vitro studies that L1 adhesive interactions may mediate axon bundling (fasciculation) (6,7) and that L1 acts as a growth cone receptor for signals that induce the extension of processes (neurites) from neurons in culture (8). Neurite outgrowth is likened to axon growth and is taken as evidence that L1 may be involved in axon growth during development (Human Molecular Genetics, 2000, Vol. 9, No. 6, 879-886).
NRCAM	neuronal cell adhesion molecule	chr7q31.1-q31.2	Cell adhesion molecules (CAMs) are members of the immunoglobulin superfamily. This gene encodes a neuronal cell adhesion molecule with multiple immunoglobulin-like C2-type domains and fibronectin type-III domains. This ankyrin-binding protein is involved in neuron-neuron adhesion and promotes directional signaling during axonal cone growth. This gene is also expressed in non-neural tissues and may play a general role in cell-cell communication via signaling from its intracellular domain to the actin cytoskeleton during directional cell migration. Allelic variants of this gene have been associated with autism and addiction vulnerability.
PTGER2	prostaglandin E receptor 2 (subtype EP2), 53kDa	chr14q22	Receptor for prostaglandin e2. The activity of this receptor is mediated by g(s) proteins that stimulate adenylate cyclase. The subsequent raise in intracellular camp is responsible for the relaxing effect of this receptor on smooth muscle. How cyclooxygenase-2 (COX-2) and its proinflammatory metabolite prostaglandin E2 (PGE2) enhance colon cancer progression remains poorly understood. It has been shown that PGE2 stimulates colon cancer cell growth through its heterotrimeric guanine nucleotide-binding protein (G protein)-coupled receptor, EP2, by a signaling route that involves the activation of phosphoinositide 3-kinase and the protein kinase Akt by free G protein beta/gamma subunits and the direct association of the G protein alphas subunit with the regulator of G protein signaling (RGS) domain of axin. This leads to the inactivation and release of glycogen synthase kinase 3beta from its complex with axin, thereby relieving the inhibitory phosphorylation of beta-catenin and activating its signaling pathway (Science. 2005 Dec 2;310(5753):1504-10). Recent studies suggest a neuroprotective function of the PGE2 EP2 receptor in excitotoxic neuronal injury. The function of the EP2 receptor was examined at time points after excitotoxicity in an organotypic hippocampal model of N-methyl-D-aspartate (NMDA) challenge and in a permanent model of focal forebrain ischemia. Activation of EP2 led to significant neuroprotection in hippocampal slices up to 3 hours after a toxic NMDA stimulus. Genetic deletion of EP2 resulted in a marked increase in the number of strokes in the permanent middle cerebral artery occlusion model. These findings support further investigation into therapeutic strategies targeting the EP2 receptor in strokes (Ann Neurol. 2005 May;57(5):758-61). Neuroprotective function of the PGE2 EP2 receptor was observed in cerebral ischemia (J Neurosci. 2004 Jan 7;24(1):257-68). Cyclo-oxygenases (COXs) catalyze the first committed step in the synthesis of the prostaglandins PGE(2), PGD(2), PGF(2alpha), PGI(2) and thomboxane A(2). Expression and enzymatic activity of COX-2, the inducible isoform of COX, are observed in several neurological diseases and result in significant neuronal injury. The neurotoxic effect of COX-2 is believed to occur through downstream effects of its prostaglandin products. In this study, the function of PGD(2) and its two receptors DP1 and chemoattractant receptor-homologous molecule expressed on Th2 cells (CRTH2) (DP2) was examined in neuronal survival. PGD(2) is the most abundant prostaglandin in the brain and regulates sleep, temperature and nociception. It signals through two distinct G protein-coupled receptors, DP1 and DP2 that have opposite effects on cyclic AMP (cAMP) production. Physiological concentrations of PGD(2) potently and unexpectedly rescued neurons in paradigms of glutamate toxicity in cultured hippocampal neurons and organotypic slices (J Neurochem. 2005 Feb;92(3):477-86).
KIAA0960	KIAA0960 protein	chr7p21.3	Synonym: THSD7A thrombospondin, type I, domain containing 7A. Membrane; single-pass type I membrane protein.

PRPH	peripherin	chr12q12-q13	This gene encodes a cytoskeletal protein found in neurons of the peripheral nervous system. The encoded protein is a type III intermediate filament protein with homology to other cytoskeletal proteins such as desmin, and is a different protein than the peripherin found in photoreceptors. Mutations in this gene have been associated with susceptibility to amyotrophic lateral sclerosis. Peripherin overexpression in transgenic mice can cause defective transport of type IV neurofilament proteins, a phenomenon that may account for the progressive formation of amyotrophic lateral sclerosis-like spheroids in axons (J Neurochem. 2006 Aug;98(3):926-38).
BCL2	B-cell CLL/lymphoma 2	chr18q21.33 18q21.3	This gene encodes an integral outer mitochondrial membrane protein that blocks the apoptotic death of some cells such as lymphocytes. It suppresses apoptosis in a variety of cell systems including factor-dependent lymphohematopoietic and neural cells. Regulates cell death by controlling the mitochondrial membrane permeability. Appears to function in a feedback loop system with caspases. Inhibits caspase activity either by preventing the release of cytochrome c from the mitochondria and/or by binding to the apoptosis-activating factor (apaf-1). Forms homodimers, and heterodimers with bax, bad, bak and bcl-x(l). Heterodimerization with bax requires intact bh1 and bh2 motifs, and is necessary for anti-apoptotic activity. Phosphorylation/dephosphorylation on ser-70 regulates bcl2 anti-apoptotic activity. Growth factor-stimulated phosphorylation on ser-70 by pkc is required for the anti-apoptosis activity and occurs during the g2/m phase of the cell cycle. In the absence of growth factors, bcl2 appears to be phosphorylated by other protein kinases such as ERKS and stress-activated kinases. Dephosphorylated by protein phosphatase 2a (pp2a). BCL2 is proteolytically cleaved by caspases during apoptosis. The cleaved protein, lacking the bh4 motif, has pro-apoptotic activity and causes the release of cytochrome c into the cytosol, promoting further caspase activity. Farlie et al. (1995) reported observations in transgenic mice expressing BCL2 under the control of the neuron-specific enolase promoter, suggesting that the role of BCL2 is wider than merely its role in lymphocytes. Sensory neurons isolated from dorsal ganglia of newborn mice normally require nerve growth factor for their survival in culture, but those from the BCL2 transgenic mice showed enhanced survival in its absence. Furthermore, apoptotic death of motor neurons after axotomy of the sciatic nerve was inhibited in these mice. The number of neurons in the 2 neuronal populations from the central and peripheral nervous system was increased by 30%, indicating that BCL2 expression can protect neurons from cell death during development. Thus, BCL2 may play an important role in survival of neurons both during development and throughout adult life.
APLP1	amyloid beta (A4) precursor-like protein 1	chr19q13.1	This gene encodes a member of the highly conserved amyloid precursor protein gene family. The encoded protein is a membrane-associated glycoprotein that is cleaved by secretases in a manner similar to amyloid beta A4 precursor protein cleavage. This cleavage liberates an intracellular cytoplasmic fragment that may act as a transcriptional activator. The encoded protein may also play a role in synaptic maturation during cortical development. APLP1 may interact with cellular G-protein signaling pathways. It can regulate neurite outgrowth through binding to components of the extracellular matrix such as heparin and collagen I. See Discussion for further information.
KIAA0125	KIAA0125	chr14q32.3	This gene localizes to the immunoglobulin heavy chain locus (IGH@) on chromosome 14. The function of its protein product has not been determined.
TMOD1	tropomodulin 1	chr9q22.3	TMOD1 binds to the n-terminus of isoforms 2/3 of tpm3 and to actin. Blocks the elongation and depolymerization of the actin filaments at the pointed end. The TMOD/TM complex contributes to the formation of the short actin protofilament, which in turn defines the geometry of the membrane skeleton. May play an important role in regulating the organization of actin filaments by preferentially binding to a specific tropomyosin isoform at its N-terminus.
GNG11	guanine nucleotide binding protein (G protein), gamma 11	chr7q31-q32	This gene is a member of the guanine nucleotide-binding protein (G protein) gamma family and encodes a lipid-anchored, cell membrane protein. As a member of the heterotrimeric G protein complex, this protein plays a role in this transmembrane signaling system.
STRA6	(mouse) /// stimulated by retinoic acid gene 6 homolog (mouse)	chr15q24.1	Similar to Collagen alpha-1(I) chain [Precursor]

SCN3B	sodium channel, voltage-gated, type III, beta	chr11q24.1	Voltage-gated sodium channels are transmembrane glycoprotein complexes composed of a large alpha subunit and one or more regulatory beta subunits. They are responsible for the generation and propagation of action potentials in neurons and muscle. This gene encodes one member of the sodium channel beta subunit gene family, and influences the inactivation kinetics of the sodium channel. SCN3B association with neurofascin may target the sodium channels to the nodes of Ranvier of developing axons and retain these channels at the nodes in mature myelinated axons.
ENC1	ectodermal-neural cortex (with BTB-like domain)	chr5q12-q13.3	ENC1 expression increased dramatically in a neuroblastoma cell line undergoing retinoic acid-induced differentiation. By differential display, Zhao et al. (2000) identified rat Enc1 as a transcript associated with differentiation of rat preadipocytes in primary culture. Kim et al. (1998) showed that expression of ENC1 induced neuronal process formation, whereas antisense treatment inhibited neurite development. Immunoblot analysis showed that ENC1 is a nuclear matrix protein, can be phosphorylated and binds to the functionally active hypophosphorylated form of the nuclear matrix protein RB1 during neuronal differentiation. Using primary cell culture of rat stroma-vascular cells, Zhao et al. (2000) found that transient early expression of Enc1 preceded the conversion of the fibroblastic preadipocytes to mature adipose. Enc1 expression also preceded expression of adipocyte-specific markers, including transcription factors known to activate adipocyte genes. Antisense transfection blocked differentiation to the mature adipocyte morphology.
BASP1	brain abundant, membrane attached signal protein 1	chr5p15.1-p14	This gene encodes a membrane bound protein with several transient phosphorylation sites and PEST motifs. Conservation of proteins with PEST sequences among different species supports their functional significance. PEST sequences typically occur in proteins with high turnover rates. Immunological characteristics of this protein are species specific. This protein also undergoes N-terminal myristoylation. Intercellular signaling and nerve outgrowth are influenced by a number of proteins expressed at nerve endings and synapses. GAP43 (162060) is a determinant of neurite outgrowth and plasticity. The rat 22-kD neuronal tissue-enriched acidic protein (Nap22, synonym:BASP1), like GAP43, binds calmodulin, is phosphorylated by protein kinase C, and is expressed specifically in nervous tissue.
INA	interneuron intermediate filament protein, alpha	chr10q24.3	Previously described in Chapter 12.3
PLK2	polo-like kinase 2 (Drosophila)	chr5q12.1-q13.2	Previously described in Chapter 12.3
NR2F1	nuclear receptor subfamily 2, group F, member 1	chr5q14	NR2F1 belongs to the nuclear hormone receptor family. Coup (chicken ovalbumin upstream promoter) transcription factor binds to the ovalbumin promoter and, in conjunction with another protein (TFIIB) stimulates initiation of transcription. Binds to both direct repeats and palindromes of the 5'-aggTca-3' motif. The transcription factor NR2F1, an orphan member of the nuclear receptor superfamily, is an important regulator of neurogenesis, cellular differentiation and cell migration. NR2F1 is required for proper axonal growth and guidance of all major forebrain commissures. Moreover, hippocampal neurons lacking COUP-TFI have a defect in neurite outgrowth and show an abnormal axonal morphology. Armentano et al., Development (2006). Suppression of Notch signaling by the COUP-TFI transcription factor (NR2F2) regulates vein identity (Nature. 2005 May 5;435(7038):98-104). COUP-TFI (NR2F1) controls Notch regulation of hair cell and support cell differentiation. Notch regulation of hair cell differentiation in COUP-TFI(-/-) mice was investigated and misregulation of Notch signaling components was confirmed. Reduced Notch signaling correlated with increased hair cell differentiation. (Development. 2006 Sep;133(18):3683-93).
DCAMKL1	doublecortin and CaM kinase-like 1	chr13q13	DCAMKL1 belongs to the ser/thr protein kinase family, this kinase is probably involved in a calcium-signaling pathway controlling neuronal migration in the developing brain. DCAMKL1 is a microtubule-associated protein that phosphorylates itself and myelin basic protein (MBP). DCAMKL1 has microtubule polymerizing activity that is independent of its protein kinase activity (Lin et al., 2000). It may also participate in functions of the mature nervous system. DCAMKL1 contains 2 doublecortin and 1 protein kinase domains. Purified DCAMKL1 associates with microtubules and stimulates polymerization of purified tubulin and the formation of aster-like microtubule structures. Overexpressed DCAMKL1 leads to striking microtubule bundling in cell lines and cultured primary neural cells. (J Neurosci. 2000 Dec 15;20(24):9152-61).
RIMS2	regulating synaptic membrane exocytosis 2	chr8q22.3	Rim is a putative Rab3 effector in regulating synaptic-vesicle fusion (Nature. 1997 Aug 7;388(6642):593-8). Binding to Rab3A-interacting molecule RIM regulates the presynaptic recruitment of Munc13-1 and ubMunc13-2. Transmitter release at synapses between nerve cells is spatially restricted to active zones, where synaptic vesicle docking, priming, and Ca <sup>2+</sup> -dependent fusion take place in a temporally highly coordinated manner. Munc13s are essential for priming synaptic vesicles to a fusion competent state, and their specific active zone localization contributes to the active zone restriction of transmitter release and the speed of excitation-secretion coupling. (J Biol Chem. 2006 Jul 14;281(28):19720-31. Epub 2006 May 1).

PCDH17	protocadherin 17	chr13q21.1	This gene belongs to the protocadherin gene family, a subfamily of the cadherin superfamily. The encoded protein contains six extracellular cadherin domains, a transmembrane domain, and a cytoplasmic tail differing from those of the classical cadherins. The encoded protein may play a role in the establishment and function of specific cell-cell connections in the brain.
PTN	pleiotrophin (heparin binding growth factor 8, neurite growth-promoting factor 1)	chr7q33-q34	Synonym: neurite growth-promoting factor 1, pleiotrophin (Ptn). Ptn is a heparin binding mitogenic protein. It has neurite extension activity. Heparin-binding neurite outgrowth-promoting factor is a member of a highly conserved human gene family of proteins. It exhibits neurite outgrowth-promoting activity and may play a role in nervous tissue development and/or maintenance. Expression of this factor is developmentally regulated, increasing in the brain during embryogenesis and reaching its maximum expression at the time of birth. The gene codes for a 168-residue protein that is a precursor for a previously described brain-derived heparin-binding protein of 136 amino acids (Eddy et al., 1991). Using cDNA microarray analysis, Mi et al. (2007) found that Ptn mRNA was up-regulated in acutely denervated rat Schwann cells from sciatic nerve. High levels of Ptn mRNA peaked at day 7 but were not maintained, returning to baseline levels by 3 months. In a spinal cord explant system, Ptn caused increased outgrowth of spinal motor axons and protected spinal motor neurons against chronic excitotoxic injury. In neonatal mice, Ptn protected facial motor neurons against cell death induced by deprivation of growth factors. In adult rats, Ptn enhanced regeneration of myelinated axons across a graft in transected sciatic nerve. Further studies suggested that Alk may mediate trophic activities of Ptn. The findings indicated that Ptn has a neurotrophic role in peripheral nerves. Pleiotrophin is a neurotrophic factor for spinal motor neurons (Proc Natl Acad Sci U S A. 2007 Mar 13;104(11):4664-9).
SCG2	secretogranin II (chromogranin C)	chr2q35-q36	Secretogranin II belongs to a class of secretory proteins contained in large dense core vesicles of many endocrine cells and neurons (Kirchmair et al., 1993). A 33-amino acid neuropeptide derived from secretogranin II, termed secretoneurin, is involved in chemotaxis of monocytes and endothelial cells and in regulation of endothelial cell proliferation (Dunzendorfer et al., 1998). Kirchmair et al. (2004) found that secretoneurin had potent angiogenic activity in vivo in a mouse cornea model of neovascularization. Treatment of human umbilical vein endothelial cells (HUVECs) with secretoneurin inhibited apoptosis, stimulated proliferation. Stimulation of HUVECs with secretoneurin led to activation of ERK and, to a lesser extent, AKT, and inhibition of these pathways abrogated the effects of secretoneurin. Studies in rodents suggest that the full length protein, secretogranin II, is involved in the packaging or sorting of peptide hormones and neuropeptides into secretory vesicles. Secretogranin-2 is a neuroendocrine secretory granule protein, which is the precursor for biologically active peptides.
EML4	echinoderm microtubule associated protein like 4	chr2p22-p21	Transient transfection of a fusion construct of full-length mouse Eml4 with green fluorescent protein (GFP-Eml4) into Cos7 and HeLa cells resulted in colocalization of GFP-Eml4 with microtubules. This colocalization was observed both with microtubules of non-dividing cells and with the mitotic spindle of dividing cells. In addition, transient overexpression of GFP-Eml4 in Cos7 cells resulted in microtubules that were resistant to nocodazole treatment suggesting that Eml4 stabilizes microtubules (Houtman SH, Rutteman M, De Zeeuw CI, French PJ). Eml4 belongs to the wd repeat map family.
PTPRN2	protein tyrosine phosphatase, receptor type, N polypeptide 2	chr7q36	Synonym: IA-2beta. The protein encoded by this gene is a member of the protein tyrosine phosphatase (PTP) family. PTPs are known to be signaling molecules that regulate a variety of cellular processes including cell growth, differentiation, mitotic cycle, and oncogenic transformation. This PTP possesses an extracellular region, a single transmembrane region, and a single intracellular catalytic domain, and thus represents a receptor-type PTP. The catalytic domain of this PTP is most closely related to PTPRN/IA-2beta. This PTP and PTPRN are both found to be major autoantigens associated with insulin-dependent diabetes mellitus. Three alternatively spliced transcript variants of this gene, which encode distinct proteins, have been reported. Targeted disruption of the IA-2beta gene causes glucose intolerance and impairs insulin secretion but does not prevent the development of diabetes in NOD mice. Diabetes. 2004 Jul;53(7):1684-91. Protein tyrosine phosphatases (PTP) catalyze the dephosphorylation of phosphotyrosine peptides; they regulate phosphotyrosine levels in signal transduction pathways.

STX1A	syntaxin 1A (brain)	<p>chr7q11.23</p> <p>Synaptic vesicles store neurotransmitters that are released during calcium-regulated exocytosis. The specificity of neurotransmitter release requires the localization of both synaptic vesicles and calcium channels to the presynaptic active zone. Syntaxins function in this vesicle fusion process. Syntaxins also serve as a substrate for botulinum neurotoxin type C, a metalloprotease that blocks exocytosis and has high affinity for a molecular complex that includes the alpha-latrotoxin receptor which produces explosive exocytosis (Zhang et al., 1995). Bennett et al. (1992) identified two 35-kD proteins (p35 or syntaxins) that interact with synaptic vesicle protein p65 (synaptotagmin; 185605). The p35 proteins are expressed only in the nervous system. The 2 proteins are 84% identical, include C-terminal membrane anchors, and are concentrated on the plasma membrane at synaptic sites. The authors speculated that the p35 proteins may function in docking synaptic vesicles near calcium channels at presynaptic active zones. The priming step of synaptic vesicle exocytosis is thought to require the formation of the SNARE complex, which comprises the proteins synaptobrevin, SNAP25, and syntaxin. In solution, syntaxin adopts a default, closed configuration that is incompatible with formation of the SNARE complex. Specifically, the amino terminus of syntaxin binds the SNARE motif and occludes interactions with the other SNARE proteins. The N terminus of syntaxin also binds the presynaptic protein UNC13 (605836). Studies in mouse, <i>Drosophila</i>, and <i>Caenorhabditis elegans</i> suggest that UNC13 functions at a post-docking step of exocytosis, most likely during synaptic vesicle priming. Therefore, UNC13 binding to the N terminus of syntaxin may promote the open configuration of syntaxin. To test this model, Richmond et al. (2001) engineered mutations into <i>C. elegans</i> syntaxin that caused the protein to adopt the open configuration constitutively. Richmond et al. (2001) demonstrated that the open form of syntaxin can bypass the requirement for UNC13 in synaptic vesicle priming. Thus, Richmond et al. (2001) concluded that it is likely that UNC13 primes synaptic vesicles for fusion by promoting the open configuration of syntaxin. Neuronal exocytosis is triggered by calcium and requires 3 SNARE proteins: synaptobrevin on the synaptic vesicle, and syntaxin and SNAP25 on the plasma membrane.</p>
STX1A	syntaxin 1A (brain)	<p>chr7q11.23</p> <p>Neuronal SNARE proteins form a parallel 4-helix bundle that is thought to drive the fusion of opposing membranes. Hu et al. (2002) demonstrated that whereas syntaxin and SNAP25 in target membranes are freely available for SNARE complex formation, availability of synaptobrevin on synaptic vesicles is very limited. Calcium at micromolar concentrations triggers SNARE complex formation and fusion between synaptic vesicles and reconstituted target membranes. Although calcium does promote interaction of SNARE proteins between opposing membranes, it does not act by releasing synaptobrevin from synaptic vesicle restriction. Hu et al. (2002) concluded that their data suggests a mechanism in which calcium-triggered membrane apposition enables syntaxin and SNAP25 to engage synaptobrevin, leading to membrane fusion. SNARE proteins normally face the cytoplasm, within which their helical domains can pair to link membranes for fusion. To ascertain whether SNAREs can fuse cells, Hu et al. (2003) flipped their orientation and engineered cognate cells to express either the v or t-SNAREs. Hu et al. (2003) found that cells expressing the interacting domains of v (VAMP2) and t-SNAREs (syntaxin 1A and SNAP25) on the cell surface fused spontaneously, demonstrating that SNAREs are sufficient to fuse biological membranes. Tucker et al. (2004) investigated the effect of synaptotagmin I (SYT1) on membrane fusion mediated by neuronal SNARE proteins SNAP25, syntaxin, and synaptobrevin, which were reconstituted into vesicles. In the presence of calcium, the cytoplasmic domain of SYT1 strongly stimulated membrane fusion when synaptobrevin densities were similar to those found in native synaptic vesicles. The calcium dependence of SYT1-stimulated fusion was modulated by changes in lipid composition of the vesicles and by a truncation that mimics cleavage of SNAP25 by botulinum neurotoxin A. Stimulation of fusion was abolished by disrupting the calcium-binding activity, or by severing the tandem C2 domains, of SYT1. Thus, SYT1 and SNAREs are likely to represent the minimal protein complement for calcium-triggered exocytosis. Syntaxin-1A plays a central role in neurotransmitter release through multiple protein-protein interactions. To investigate the 3-dimensional structure Fernandez et al. (1998) used nuclear magnetic resonance spectroscopy and identified an autonomously folded N-terminal domain in syntaxin-1A. This 120-residue N-terminal domain is conserved in plasma membrane syntaxins but not in other syntaxins, indicating a specific role in exocytosis. The domain contains 3 long alpha helices that form an up-and-down bundle with a left-handed twist. A striking residue conservation is observed throughout a long groove that is likely to provide a specific surface for protein-protein interactions. A highly acidic region binds to the C(2)A domain of synaptotagmin-1 in a Ca<sup>2+</sup>-dependent interaction that may serve as an electrostatic switch in neurotransmitter release. The dopamine transporter (DAT) regulates the extent and duration of dopamine receptor activation through sodium-dependant reuptake of dopamine into presynaptic neurons, resulting in termination of dopaminergic neurotransmission. Using the yeast two-hybrid system, new interactions between DAT, the SNARE protein syntaxin 1A, and the receptor for activated C kinases (RACK1) have been identified (Neurochem Res. 2004 Jul;29(7):1405-9). Association between schizophrenia and the syntaxin 1A gene has been shown (Biol Psychiatry. 2004 Jul 1;56(1):24-9).</p>

GDF15	growth differentiation factor 15	chr19p13.1-13.2	Synonym: Bone morphogenetic protein, placental TGF-beta. Bone morphogenetic proteins are members of the transforming growth factor-beta superfamily and regulate tissue differentiation and maintenance. They are synthesized as precursor molecules that are processed at a dibasic cleavage site to release C-terminal domains containing a characteristic motif of 7 conserved cysteines in the mature protein. GDF15 is a secreted homodimeric protein that is disulfide-linked. GDF15 is not expressed in undifferentiated cells but is progressively up-regulated upon differentiation with retinoic acid followed by phorbol ester or cytokine treatment. Exposure of macrophages to MIC1 or TGFB1, followed by stimulation with lipopolysaccharide, suppressed the production of TNFA
KIAA0746	KIAA0746 protein	chr4p15.2	Potential single-pass type I membrane protein, may play a role in Notch signaling. It has 27% similarity with SEL-1 homolog precursor (Mus musculus). It contains one fibronectin type-II domain. SEL-1 functions as a negative regulator of the LIN-12/GLP-1 Notch-like signaling pathway in <i>C. elegans</i> .
CTNNA2	catenin (cadherin-associated protein), alpha 2	chr2p12-p11.1	Previously described in Chapter 12.3
GAD1	glutamate decarboxylase 1 (brain, 67kDa)	chr2q31	Glutamate decarboxylase (GAD; L-glutamate-1-carboxylase; EC 4.1.1.15) catalyzes the conversion of glutamic acid to gamma-aminobutyric acid (GABA), the major inhibitory neurotransmitter in the vertebral central nervous system. This gene encodes one of several forms of glutamic acid decarboxylase, identified as a major autoantigen in insulin-dependent diabetes. The enzyme encoded is responsible for catalyzing the production of gamma-aminobutyric acid from L-glutamic acid. A pathogenic role for this enzyme has been identified in the human pancreas since it has been identified as an autoantigen and an autoreactive T cell target in insulin-dependent diabetes. This gene may also play a role in the stiff man syndrome. Deficiency in this enzyme has been shown to lead to pyridoxine dependency with seizures. Alternative splicing of this gene results in two products, the predominant 67-kD form and a less-frequent 25-kD form. Autoantibodies to insulin and GAD are features of preclinical type 1 diabetes in children. For insulin autoantibodies, the antibody affinity and epitope specificity predict which children progress to diabetes (Diabetes. 2007 Jun; 56(6):1527-33). Its phosphorylation by protein kinase C correlates with long-term potentiation.
GAP43	growth associated protein 43	chr3q13.1-q13.2	The protein encoded by this gene has been termed a 'growth' or 'plasticity' protein because it is expressed at high levels in neuronal growth cones during development and axonal regeneration. This encoded protein is considered a crucial component of an effective regenerative response in the nervous system. GAP43 binds calmodulin with a greater affinity in the absence of $Ca^{2+}$ than in its presence. Phosphorylation of this protein by protein kinase c is specifically correlated with certain forms of synaptic plasticity.

### 12.3.3 Annotations for inversely regulated genes

See results, Chapter 5.6

Gene symbol	Gene name	Annotations
ADAMTS9	a disintegrin-like and metalloprotease with thrombospondin type motif 9	Previously described in Chapter 12.3
KIAA1573	KIAA1573 protein	Synonym: von Willebrand factor type A and cache domain containing 1, calcium channel protein which plays an important role in excitation-contraction coupling. The L-type calcium channel is supposed to be composed of several subunits. Alpha-2 and delta subunits form heterodimers that are disulfide-linked. Alpha-2 and delta subunits are supposed to be proteolytically processed from a precursor form .
BOC	brother of CDO	BOC is a cell surface receptor of the immunoglobulin (Ig)/fibronectin type III repeat family involved in myogenic differentiation.
RAM2	transcription factor RAM2	Monoamine oxidase A (MAO A) degrades serotonin, norepinephrine, and dopamine and produces reactive oxygen that may cause neuronal cell death. The transcription factor R1 (RAM2/CDC47L/JPO2) inhibits the MAO A promoter and enzymatic activities. Using R1 overexpression, R1 small interfering RNA, and a MAO A inhibitor, it was found that R1 and MAO A act upstream of cyclin D1 and E2F1. In summary, this study demonstrated the functions of MAO A and its repressor R1 in apoptotic signaling pathways (Proc Natl Acad Sci U S A. 2006 Jul 18;103(29):10923-8).
NTRK2	neurotrophic tyrosine kinase receptor type 2, non-catalytic isoform	Previously described in Chapter 12.3
CNTN3	contactin 3 (plasmacytoma associated)	Contactins mediate cell surface interactions during nervous system development. CNTN3 is assumed to have neurite outgrowth-promoting activity. CNTN3 contains 4 fibronectin type-iii domains. It contains 6 ig-like c2-type (immunoglobulin-like) domains.
LOC440450	LOC440450	A gene in close vicinity to LOC440450 (chr. 17q23) is for instance: APPBP2 (amyloid beta precursor protein binding protein 2) on chr. 17q21-q23.
DNAJC12	DnaJ (Hsp40) homolog subfamily C member 12	This gene encodes a member of a subclass of the HSP40/DnaJ protein family. Members of this family of proteins are associated with complex assembly, protein folding, and export.
C9orf105	chromosome 9 (Hsp40) open reading frame 105	-
NDUFB9	NADH dehydrogenase (ubiquinone) 1 beta subcomplex 9, 22kDa	NDUFB9 transfers electrons from NADH to the respiratory chain. The immediate electron acceptor for the enzyme is believed to be ubiquinone, mitochondrion; mitochondrial inner membrane; matrix side. NADH + ubiquinone = NAD <sup>+</sup> + ubiquinol.

LOC143903	layilin	Layilin, a novel integral membrane protein, is a hyaluronan receptor. Layilin's ability to bind hyaluronan, a ubiquitous extracellular matrix component, reveals an interesting parallel between layilin and CD44, because both can bind to cytoskeleton-membrane linker proteins through their cytoplasmic domains and to hyaluronan through their extracellular domains. This parallelism suggests a role for layilin in cell adhesion and motility (Bono P, Rubin K, Higgins JM, Hynes RO, Mol. Biol. Cell (2001)).
HOXD10	homeobox D10	This gene is a member of the Abd-B homeobox family and encodes a protein with a homeobox DNA-binding domain. It is included in a cluster of homeobox D genes located on chromosome 2. The encoded nuclear protein functions as a sequence-specific transcription factor that is expressed in the developing limb buds and is involved in differentiation and limb development. Mutations in this gene have been associated with Wilm's tumor and congenital vertical talus (also known as "rocker-bottom foot" deformity or congenital convex pes valgus) and/or a foot deformity resembling that seen in Charcot-Marie-Tooth disease.
DKFZp761D221	Hypothetical protein DKFZp761D221	Synonym: SH3-domain GRB2-like (endophilin) interacting protein 1, belongs to the family of fibril-associated collagens with interrupted helices. Has 28% similarity to Collagen alpha-1(XII) chain. type xii collagen interacts with type I collagen- containing fibrils
NLGN4X	neurigin 4 X-linked	Previously described in Chapter 12.3
LOC285878	hypothetical protein LOC285878	Unknown function, hypothetical protein MGC33530 (V-set and transmembrane domain containing 2), 23% similarity to T-cell receptor alpha chain, protein coding.
LOC440731	LOC440731	Unknown function
GALNT13	UDP-N-acetyl-alpha-D-galactosamine: polypeptide N-acetylgalactosaminyltransferase 13	The GALNT13 protein is a member of the UDP-N-acetyl-alpha-D-galactosamine-polypeptide N-acetylgalactosaminyltransferase (GalNAcT; EC 2.4.1.41) family, which initiates O-linked glycosylation of mucins by the initial transfer of N-acetylgalactosamine (GalNAc) with an alpha-linkage to a serine or threonine residue, localized in the golgi apparatus.
HS3ST2	heparan sulfate (glucosaminide) 3-O-sulfotransferase 2	Previously described in Chapter 12.3
MASK	Mst3 and SOK1-related kinase // Mst3 and SOK1-related kinase	MASK is a protein kinase, potential mediator of cell growth and is pro-apoptotic, localized in the cytoplasm and golgi apparatus. Interaction with golgi matrix protein golga2 leading to autophosphorylation on thr-178, possibly as a consequence of stabilization of dimer formation. May also be activated by C- terminal cleavage.
STX3A	syntaxin 3A	Previously described in Chapter 12.3
PAG	phosphoprotein associated with glycosphingolipid-enriched microdomains	The protein encoded by this gene is a type III transmembrane adaptor protein that binds to the tyrosine kinase csk protein. It is thought to be involved in the regulation of T cell activation. Negatively regulates TCR (T-cell antigen receptor)- mediated signaling in T-cells and FCER1 (high affinity immunoglobulin epsilon receptor)-mediated signaling in mast cells. Promotes CSK activation and recruitment to lipid rafts, which results in LCK inhibition. Inhibits immunological synapse formation by preventing dynamic arrangement of lipid raft proteins. May be involved in cell adhesion signaling. Subunit interacts with FYN. Phosphorylated by FYN on Tyr-317 in resting T-cells; which promotes interaction with CSK. Dephosphorylated by PTPRC/CD45 upon TCR activation; which leads to CSK dissociation. May also be dephosphorylated by PTPN11. Hyperphosphorylated in mast cells upon FCER1 activation.
CHRNA7	cholinergic receptor nicotinic alpha polypeptide 7	Previously described in Chapter 12.3
MBNL2	muscleblind-like 2 (Drosophila)	This gene encodes a C3H-type zinc finger protein, which is similar to the Drosophila melanogaster muscleblind B protein. Drosophila muscleblind is a gene required for photoreceptor differentiation. MBNL proteins regulate alternative splicing of two pre-mRNAs that are misregulated in myotonic dystrophy, cardiac troponin T (cTNT) and insulin receptor (IR).

KIAA0644	KIAA0644 gene product	Strong similarity to Insulin-like growth factor-binding protein complex acid labile chain precursor, may have an important role in regulating the access of circulating insulin growth factors to the tissues. KIAA0644 is assumed to form a ternary complex of about 140 to 150 kDa with IGF2 or IGFBP-3.
NTRK2	neurotrophic tyrosine kinase receptor type 2, non-catalytic isoform	Previously described in Chapter 12.3
PDZK1	PDZ domain containing 1	PDZK1, a multi-PDZ domain containing adaptor protein, interacts with various membrane proteins, including the high density lipoprotein (HDL) receptor scavenger receptor class B type I (SR-BI). Targeted disruption of the PDZK1 gene in mice causes tissue-specific depletion of the high density lipoprotein receptor scavenger receptor class B type I, and an altered lipoprotein metabolism (J Biol Chem. 2003 Dec 26;278(52):52820-5). The scavenger receptor class B type I (SRBI or CD36L1), mediates the selective uptake of cholesteryl esters from high density lipoprotein and cholesterol secretion into bile in the liver. By coexpressing SRBI with PDZK1 in Chinese hamster ovary cells, Ikemoto et al. (2000) observed an increase in the expression level of SRBI, a reduction in the deacylation rate of the cholesteryl esters taken up from HDL, and a change in the intracellular distribution of a fluorescent lipid taken up from HDL. Taken together, these data suggested that PDZK1 is associated with SRBI in the liver sinusoidal plasma membranes and may modulate intracellular transport and metabolism of cholesteryl esters taken up from HDL.
PBX1	Pre-B-cell leukemia transcription factor 1	In vitro studies have shown that PBX1 regulates the activity of IPF1 (insulin promoter factor 1, IPF1; IPF1 is a para-Hox homeodomain transcription factor required for the development and function of the pancreas in mice and humans). To investigate in vivo roles of PBX1 in pancreatic development and function, Kim et al. (2002) examined pancreatic Pbx1 expression, and morphogenesis, cell differentiation, and function in mice deficient for Pbx1. Pbx1 <sup>-/-</sup> embryos had pancreatic hypoplasia and marked defects in exocrine and endocrine cell differentiation prior to death at embryonic day 15 or 16. In these embryos, expression of Isl1 and Atoh5, essential regulators of pancreatic morphogenesis and differentiation, was severely reduced. Pbx1 <sup>+/-</sup> adults had pancreatic islet malformations, impaired glucose tolerance, and hypoinsulinemia. Thus, Kim et al. (2002) concluded that PBX1 is essential for normal pancreatic development and function. Analysis of trans-heterozygous Pbx1 <sup>+/-</sup> and Ipf1 <sup>+/-</sup> mice revealed in vivo genetic interactions between Pbx1 and Ipf1 that are essential for postnatal pancreatic function. Trans-heterozygous mice developed age-dependent overt diabetes mellitus, unlike Pbx1 <sup>+/-</sup> or Ipf1 <sup>+/-</sup> mice. Mutations affecting the Ipf1 protein promote diabetes mellitus in mice and humans. Kim et al. (2002) concluded that perturbation of PBX1 activity may also promote susceptibility to diabetes mellitus. Retinoic acid regulates the expression of PBX1, PBX2, and PBX3 in P19 cells both transcriptionally and post-translationally (J Cell Biochem. 2004 May 1;92(1):147-63).
OSAP	ovary-specific acidic protein	OSAP is a hypothetical conserved protein with strong similarity to cell death 8 (apoptosis-inducing factor).
DPT	dermatopontin	Dermatopontin is an extracellular (secreted) matrix protein with possible functions in cell-matrix interactions and matrix assembly. The protein is found in various tissues and many of its tyrosine residues are sulphated. Dermatopontin is postulated to modify the behavior of TGF-beta through interaction with decorin. Seems to mediate adhesion by cell surface integrin binding, DPT may serve as a communication link between the dermal fibroblast cell surface and its extracellular matrix environment. Dermatopontin, a recently found low-molecular-mass component of the extracellular matrix, was studied for its interaction with decorin and transforming growth factor beta (TGF-beta) and its influence on TGF-beta bioactivity. Dermatopontin reacted with decorin with an apparent Kd of 100 nM in a solid-phase assay. Dermatopontin inhibited the formation of the decorin-TGF-beta1 complex. Decorin also competed with dermatopontin for the binding of this cytokine. The dermatopontin-decorin complex bound 3 times more TGF-beta1 than each individual component did, and binding was more strongly inhibited by decorin pre-incubated with dermatopontin than by dermatopontin or decorin alone. Dermatopontin augmented the biological activity of TGF-beta1, as analysed by the expression of luciferase in mink lung epithelial cells transfected with a plasminogen activator inhibitor-promoter-luciferase construct, although dermatopontin itself did not show apparent induction of luciferase. Dermatopontin showed weak inhibitory activity on the proliferation of mink lung epithelial cells, and it enhanced the growth-inhibitory activity of TGF-beta on these cells. Thus dermatopontin increases the cellular response to TGF-beta. These findings strongly suggest that dermatopontin modifies the behaviour of TGF-beta through interaction with decorin in the microenvironment of the extracellular matrix in vivo (Dermatopontin interacts with transforming growth factor beta and enhances its biological activity." Biochem J, 1999).

FLJ10094	hypothetical protein FLJ10094	Synonyms: Proliferation-inducing protein 38, ecto-NOX disulfide-thiol exchanger 1, candidate growth-related and time keeping constitutive hydroquinone (NADH) oxidase with a strong similarity to tumor-associated hydroquinone oxidase, hydroquinone [NADH] oxidase and protein disulfide-thiol oxidoreductase isoform 2. The cytochrome bc complexes found in mitochondria, chloroplasts and many bacteria play critical roles in their respective electron transport chains. The quinol oxidase (Q(o)) site in this complex oxidizes a hydroquinone (quinol), reducing two one-electron carriers, a low potential cytochrome b heme and the "Rieske" iron-sulfur cluster. The overall electron transfer reactions are coupled to transmembrane translocation of protons via a "Q-cycle" mechanism, which generates proton motive force for ATP synthesis. Since semiquinone intermediates of quinol oxidation are generally highly reactive, one of the key questions in this field is how does the Q (o) site oxidize quinol without the production of harmful side reactions including superoxide production? Similar transition states mediate the Q-cycle and superoxide production by the cytochrome bc1 complex (J Biol Chem. 2006 Dec 15;281(50):38459-65).
STX3A	syntaxin 3A	Previously described in Chapter 12.3
SYN2	synapsin II	This gene is a member of the synapsin gene family. Synapsins encode neuronal phosphoproteins which associate with the cytoplasmic surface of synaptic vesicles. Family members are characterized by common protein domains, and they are implicated in synaptogenesis and the modulation of neurotransmitter release, suggesting a potential role in several neuropsychiatric diseases. The synapsins are a family of 4 synaptic vesicle-associated proteins, synapsins Ia, Ib, IIa, and IIb that have been implicated in modulation of neurotransmitter release and in synaptogenesis (Greengard et al., 1993). They are products from alternative splicing of 2 distinct genes, SYN1 and SYN2. SYN2 encodes a neuron-specific phosphoprotein that selectively binds to small synaptic vesicles in the presynaptic nerve terminal. The TIMP4 gene is located within an intron of this gene and is transcribed in the opposite direction. Mutations in this gene may be associated with abnormal presynaptic function and schizophrenia. Alternative splicing of this gene results in two transcripts. SYN2 is a neuronal phosphoprotein that coats synaptic vesicles, binds to the cytoskeleton, and is believed to function in the regulation of neurotransmitter release. By use of microarray expression profiling of prefrontal cortex from matched pairs of patients with schizophrenia and control subjects and hierarchical data analysis, Mirmics et al. (2000) found that levels of transcripts encoding proteins involved in the regulation of presynaptic function were decreased in all subjects with schizophrenia. Genes of presynaptic function showed different combinations of decreased expressions across subjects. Over 250 other gene groups did not show altered expression. Selected presynaptic function gene microarray observations were verified by in situ hybridization. Two of the most consistently changed transcripts in the presynaptic functional gene group, N-ethylmaleimide-sensitive factor and synapsin-2, were decreased in 10 out of 10 and 9 out of 10 subjects with schizophrenia respectively. The combined data suggested that subjects with schizophrenia share a common abnormality in presynaptic function. Predicted Functional Partners:TIMP2, 3 and 4. Using a cDNA microarray representing 6794 distinct human genes, candidate genes whose expression is altered in cerebral cortex of cases of early Alzheimer's disease (AD) were identified; among these was the synaptic vesicle protein synapsin II, which plays an important role in neurotransmitter release. A selective decrease in the expression of the synapsin splice variants I-III of the a-type isoform in the entorhinal but not in the visual cortex of cases characterized by the earliest clinically detectable stage of AD was found. In contrast, no changes in synapsin splice variant II of the b-type isoform was found. Alteration of synapsin expression at the earliest clinical stage of AD may suggest new strategies for improved treatment (Ho et al., Neurosci. Lett. (2001).

JAG1	jagged 1 (Alagille syndrome)	<p>The jagged 1 protein encoded by JAG1 is the human homolog of the Drosophila jagged protein. Human jagged 1 is the ligand for the receptor Notch 1, the latter a human homolog of the Drosophila jagged receptor Notch. Mutations that alter the jagged 1 protein cause Alagille syndrome. Jagged 1 signaling through Notch 1 has also been shown to play a role in hematopoiesis. Jagged-1 is a ligand of the Notch receptor and its binding triggers a cascade of proteolytic cleavage that eventually leads to the release of the intracellular part of the receptor from the membrane, allowing it to translocate to the nucleus and activate transcription factors that play key roles in cell differentiation and morphogenesis (Guarnaccia et al., 2004). Loomes et al. (2002) found that JAG1 is expressed in cells adjacent to those expressing Notch2, suggesting a possible ligand receptor interaction. Guarnaccia et al. (2004) stated that JAG1 is a type I, membrane- anchored, multidomain protein. The extracellular part is made of a DSL domain, followed by a series of 16 EGF-like repeats, and a von Willebrand factor type C domain. Li et al. (2006) found that Jag1 activated Notch signaling in rats and enhanced the differentiation of mesenchymal stem cells into cardiomyocytes. Wild-type JAG1 is inhibitory for HGF expression and mutant JAG1s relieve the inhibition. AG1 controls HGF expression by a dosage-dependent regulation and Notch2 signaling seems to mediate JAG1 function. Given that HGF plays a critical role in differentiation of hepatic stem cells, overexpression of HGF acts on off-balanced cell fate determination in AGS (Alagille syndrome) patients. Downregulation of Jagged-1 induces cell growth inhibition and S phase arrest in prostate cancer cells (Int J Cancer. 2006 Nov 1;119(9):2071-7). Downregulation of Notch-1, Delta-like-1, or Jagged-1 by RNA interference induces apoptosis and inhibits proliferation in multiple glioma cell lines (Cancer Res. 2005 Mar 15;65(6):2353-63). The soluble form of Jagged1 when present in the cell culture medium, was sufficient to induce keratinocyte differentiation (J Cell Biochem. 2004 Aug 15;92(6):1271-81). Jagged1-selective Notch signaling induces smooth muscle differentiation via a RBP-Jkappa-dependent pathway (J Biol Chem. 2006 Sep 29;281(39):28555-64). Overexpression of the Notch ligand Jagged-1 induces alloantigen-specific human regulatory T cells (Blood. 2003 Nov 15;102(10):3815-21). Induction of antigen-specific regulatory T cells following overexpression of a Notch ligand by human B lymphocytes (J Virol. 2003 Oct;77(20):10872-80).The Notch ligands jagged and delta, are sequentially processed by alpha-secretase and presenilin/gamma-secretase and release signaling fragments (J Biol Chem. 2003 Sep 5;278(36):34427-37.). The Notch ligand Jagged-1 is able to induce maturation of monocyte-derived human dendritic cells (J Immunol. 2002 Oct 15;169(8):4273-8). Jagged-1 mediated activation of Notch signaling induces complete maturation of human keratinocytes through NF-kappaB and PPARgamma (Cell Death Differ. 2002 Aug;9(8):842-55). Jagged1 was expressed at high levels by hypertrophic astrocytes. Experiments in vitro showed that Jagged1 signaling inhibited process outgrowth from primary human oligodendrocytes (Nat Med. 2002 Oct;8(10):1075-6).</p>
------	------------------------------	---

### 12.3.4 Annotations for clustered genes

#### C99WT1, C99I45F, C99V50F:

Gene Symbol or Probe Set ID	Gene Name	Chromosomal Location (human)	Annotations
nlgn4x	neuroligin 4, X-linked	Xp22.32-p22.31	This gene encodes a member of a family of neuronal cell surface proteins. Members of this family may act as splice site-specific ligands for beta-neurexins and may be involved in the formation and remodeling of central nervous system synapses. The encoded protein interacts with discs, large (Drosophila) homolog 4 (DLG4). Mutations in this gene have been associated with autism and Asperger's syndrome. Two transcript variants encoding the same protein have been identified for this gene.
gria2	glutamate receptor, ionotropic, AMPA 2	4q32-q33	Glutamate receptors are the predominant excitatory neurotransmitter receptors in the mammalian brain and are activated in a variety of normal neurophysiologic processes. This gene product belongs to a family of glutamate receptors that are sensitive to alpha-amino-3-hydroxy-5-methyl-4-isoxazole propionate (AMPA), and function as ligand-activated cation channels. These channels are assembled from 4 related subunits, GRIA1-4. The subunit encoded by this gene (GRIA2) is subject to RNA editing (CAG->CGG; Q->R) within the second transmembrane domain, which is thought to <i>render the channel impermeable to Ca<sup>2+</sup></i> . Human and animal studies suggest that pre-mRNA editing is essential for brain function, and defective GRIA2 RNA editing at the Q/R site may be relevant to <i>amyotrophic lateral sclerosis (ALS)</i> etiology. Alternative splicing has been noted for this gene resulting in transcript variants encoding different isoforms, including the generation of flip and flop isoforms that vary in their signal transduction properties.
vmp	vesicular membrane protein p24;	6p22.2	Neuro-p24/Neurensin-1, a protein containing a <i>microtubule-associated domain</i> at the carboxyl-terminus and exclusively localized to small vesicles of neurons. Neurensin-1 was found mainly in neuritic processes.
bmp7	bone morphogenetic protein 7	20q13	The bone morphogenetic proteins (BMPs) are a family of secreted signaling molecules that can induce ectopic bone growth. Many BMPs are part of the <i>transforming growth factor-beta (TGFB) superfamily</i> . BMPs were originally identified by the ability of demineralized bone extract to induce endochondral osteogenesis in vivo in an extraskeletal site. Based on its expression early in embryogenesis, the BMP encoded by this gene has a proposed role in early development.
flj13710	thrombospondin type 1 domain	15q23	Uncharacterized gene, 37% similarity to ADAMTS-1 precursor (Rattus norvegicus): ADAMTS-1 precursor cleaves aggrecan, a cartilage proteoglycan, and may be involved in its turnover. Flj13710 is expected to have angiogenic inhibitor activity. Active metalloprotease, which may be associated with various inflammatory processes.
prep	prolyl endopeptidase	6q22	Previously described in Chapter 12.3

		nbl1		Previously described in Chapter 12.3
	237563_s_at	hypothetical neuroblastoma, LOC440731	1q42.2	Protein coding, unknown function.
	gIrb	glycine receptor, beta	4q31.3	The inhibitory glycine receptor mediates <i>postsynaptic inhibition</i> in the spinal cord and other regions of the central nervous system. It is a pentameric receptor composed of alpha (GLRA1, GLRA2) and beta subunits.
	213802_at	serine, protease, (neurotrypsin, motopsin)	4q28.1	This gene encodes a member of the trypsin family of <i>serine proteases</i> . A 4-base pair deletion in the neuronal serine protease neurotrypsin gene was associated with autosomal recessive nonsyndromic <i>mental retardation</i> (MR). In situ hybridization experiments on human fetal brains showed that neurotrypsin was highly expressed in brain structures involved in learning and memory. Immunoelectron microscopy on adult human brain sections revealed that neurotrypsin is located in <i>presynaptic nerve endings</i> , particularly over the presynaptic membrane lining the synaptic cleft. These findings suggest that neurotrypsin-mediated proteolysis is required for normal synaptic function and suggest potential association with mental retardation.
	ankrd11	ankyrin repeat domain 11	16q24.3	ANKRD11 is a 9kb gene encoding nuclear-located protein with ankyrin domains. May recruit histone deacetylases to the p160 coactivators/nuclear receptor complex to inhibit ligand-dependent transactivation.
	217200_x_at	cytochrome b-561 (CYB561) ferric-chelate reductase 2	17q11-qter	Cytochrome b561 is a major <i>transmembrane protein</i> that is specific to <i>catecholamine and neuropeptide secretory vesicles</i> of the adrenal medulla, pituitary gland, and other neuroendocrine tissues. This 30-kD <i>cytochrome</i> is present in both the small <i>synaptic vesicles</i> and the large dense core vesicles (chromaffin granules) of the tissues. Its role is to <i>supply reducing equivalents to 2 monooxygenases, dopamine beta-hydroxylase</i> in chromaffin granules and <i>peptidylglycine monooxygenase</i> in neurosecretory vesicles. The cytochrome fulfills this role by <i>catalyzing the transfer of electrons from a cytoplasmic donor, ascorbate, across a phospholipid bilayer to the luminal acceptor, semidehydroascorbate, in the interior of the vesicles. The continuously regenerated ascorbate within these vesicles is the immediate donor for the monooxygenases within the neuroendocrine secretory vesicles. Thus, cytochrome b561 is a transmembrane electron channel.</i>
	206848_at	homeobox A7 (HOXA7)	7p15-p14	In vertebrates, the genes encoding the class of transcription factors called homeobox genes are found in clusters named A, B, C, and D on four separate chromosomes. Expression of these proteins is spatially and temporally regulated during embryonic development. This gene is part of the A cluster on chromosome 7 and encodes a <i>DNA-binding transcription factor which may regulate gene expression, morphogenesis, and differentiation</i> . For example, the encoded protein represses the transcription of differentiation-specific genes during keratinocyte proliferation, but this repression is then overcome by differentiation signals. This gene is very similar to the antennapedia (Antp) gene of <i>Drosophila</i> .
	cyba	cytochrome b245, alpha polypeptide	16q24	<i>Cytochrome b</i> is comprised of a light chain (alpha) and a heavy chain (beta). This gene encodes the <i>light, alpha subunit</i> which has been proposed as a primary component of the <i>microbicidal oxidase system of phagocytes</i> . Mutations in this gene are associated with autosomal recessive chronic granulomatous disease (CGD) that is characterized by the <i>failure of activated phagocytes to generate superoxide</i> , important for the microbicidal activity of these cells.
cyb561	cytochrome b561 (CYB561)		17q11-qter	Refer to 217200_x_at, same transcript detected by a different probe set.

## C99WT2, C99I45F, C99V50F:

Gene Symbol	Gene Name	Chromosomal location (human)	Annotation
sept6	septin 6	Xq24	The conserved septin protein family was first identified in yeast and subsequently shown to play an important role in <i>cytoskeletal organization</i> and cytokinesis. This gene is a member of the septin family of <i>GTPases</i> . Members of this family are required for <i>cytokinesis</i> . This gene encodes four transcript variants encoding three distinct isoforms. An additional transcript variant has been identified, but its biological validity has not been determined.
lhfp12	lipoma HMGIC fusion partner-like 2	5q14.1	This gene is a member of the lipoma HMGIC fusion partner (LHFP) gene family, which is a subset of the superfamily of tetraspan transmembrane protein encoding genes. Mutations in one LHFP-like gene result in deafness in humans and mice, and a second LHFP-like gene is fused to a high-mobility group gene in a translocation-associated lipoma. Alternatively spliced transcript variants have been found, but their biological validity has not been determined.
atrn1	attractin-like 1	10q26	Involved in the initial immune cell clustering during inflammatory response and may regulate chemotactic activity of chemokines. Low-affinity receptor for agouti, has a <i>critical role in normal myelination in the central nervous system</i> .
calb1	calbindin 1	8q21.3-q22.1	Calbindin is a <i>calcium-binding protein</i> belonging to the troponin C superfamily. It was originally described as a 27-kD protein induced by vitamin D in the duodenum of the chick. In the brain, its synthesis is independent of vitamin-D-derived hormones. <i>Calbindin contains 4 active calcium-binding domains</i> , and 2 modified domains that presumably have lost their calcium-binding capacity. <i>The neurons in brains of patients with Huntington's disease are calbindin-depleted</i> .
traf5	TNF receptor-associated factor 5	1q32	The <i>scaffold protein</i> encoded by this gene is a member of the <i>tumor necrosis factor receptor-associated factor (TRAF)</i> protein family and contains a meprin and TRAF homology (MATH) domain, a RING-type zinc finger, and two TRAF-type zinc fingers. TRAF proteins are associated with, and <i>mediate signal transduction from, members of the TNF receptor superfamily</i> . This protein is one of the components of a multiple protein complex which binds to tumor necrosis factor (TNF) receptor cytoplasmic domains and mediates TNF-induced activation. Alternate transcriptional splice variants have been characterized.
cyr61	cysteine-rich, angiogenic inducer, 61	1p31-p22	CYR61 is a <i>secreted, cysteine-rich, heparin-binding protein</i> encoded by a <i>growth factor-inducible immediate-early gene</i> . Acting as an <i>extracellular, matrix-associated signaling molecule</i> , CYR61 promotes the adhesion of endothelial cells through interaction with integrin and augments growth factor-induced DNA synthesis in the same cell type.
adamts9	ADAM metalloproteinase with thrombospondin type 1 motif, 9	3p14.3-p14.2	Previously described in Chapter 12.3
boc	brother of CDO	3q13.2	BOC is a cell surface receptor of the immunoglobulin (Ig)/fibronectin type III repeat family involved in myogenic differentiation.
hoxd	homeobox D10	2q31.1	This gene is a member of the Abd-B homeobox family and encodes a protein with a homeobox DNA-binding domain. It is included in a cluster of homeobox D genes located on chromosome 2. The encoded nuclear protein functions as a sequence-specific transcription factor that is expressed in the developing limb buds and is involved in differentiation and limb development. Mutations in this gene have been associated with Wilm's tumor and congenital vertical talus (also known as "rocker-bottom foot" deformity or congenital convex pes valgus) and/or a foot deformity resembling that seen in Charcot-Marie-Tooth disease.

dnci1	dynein, cytoplasmic 1, intermediate chain 1	7q21.3-q22.1	The intermediate chains seem to <i>help dynein bind to dynactin 150 kDa component</i> . May play a role in <i>mediating the interaction of cytoplasmic dynein with membranous organelles and kinetochores</i> . There is experimental evidence of an association between <i>dnci1</i> and <i>internexin neuronal intermediate filament protein, alpha (INA)</i> .
flj14721	chromosome 12 open reading frame 34 (C12orf34)	12q24.11	Conserved hypothetical protein. This amino acid sequence is of soluble protein.
intrk2	neurotrophic tyrosine kinase, type 2 receptor, non-(TRKB), non-catalytic isoform	9q22.1	Previously described in Chapter 12.3
popdc3	popeye domain containing 3	6q21	This gene encodes a member of the POP family of proteins containing three putative transmembrane domains. This gene is expressed in cardiac and skeletal muscles and may play an important role in these tissues during development.
hs3st2	heparan sulfate (glucosamine 3-O-sulfotransferase 2	16p12	Previously described in Chapter 12.3
cutl2	cut-like 2 (Drosophila) (Cux-2)	12q24.11-q24.12	Cux-1 and Cux-2 represent early markers of <i>neuronal differentiation</i> ; both genes are expressed in postmitotic cortical neurons, from embryonic stages to adulthood and in the <i>proliferative</i> regions of the developing cortex. Cux-2 mRNA expression is also found in the embryonic SVZ ( <i>subventricular zone</i> ), overlapping with BrdU-positive <i>dividing precursors</i> , but it is not expressed in the VZ (ventricular zone). Cux2 is an ortholog of the Drosophila cut gene, which encodes a homeodomain protein involved in neuronal specification. During cortical development Cux2 identifies two subpopulations with different spatial origins, migratory behaviours and phenotypic characteristics: 1. A population of interneurons, which invades the pallium from the subpallium; 2. A neuronal population produced in the pallium around embryonic day 11.5 (in mice), which divides in the SVZ and accumulates in the intermediate zone (IZ). Subsequently, Cux2 is a marker of upper cortical layers. Using different molecular markers and Pax6-deficient mice, data were provided suggesting relationship between the early-determined Cux2-positive neuronal precursors in the SVZ/IZ and upper layer neurons. This suggests that laminar determination of upper cortical layer neurons occurs during the earliest stages of corticogenesis.
tle2	transducin-like enhancer of split 2 (E(sp1) homolog, Drosophila)	19p13.3	The <i>Notch signaling pathway controls cellular interactions important for the specification of a variety of fates</i> in both invertebrates and vertebrates. The <i>TLE genes are human homologs of the Drosophila 'groucho' gene and their products belong to this pathway</i> . Analysis of mutant alleles of members of the Notch cascade showed that Notch signaling extends the differentiation-competent state of developmentally immature precursor cells, thereby preventing or delaying their differentiation until the correct morphogenetic signals become available (reviewed by Artavanis-Tsakonas et al., 1995). A number of pathologies resulting from incomplete cellular differentiation due to this general inhibitory action during cell determination were shown to be the result of alterations in Notch signaling, including both lymphoblastic and epithelial neoplasms. Liu et al. (1996) studied the expression of individual TLE genes during epithelial differentiation. By a combination of in situ hybridization and immunohistochemical studies, they showed that <i>TLE1, TLE2 and TLE3 are coexpressed in a number of tissues</i> . Moreover, they showed that the expression is elevated in cervical squamous <i>metaplasias and carcinomas</i> .
213158_at	cDNA DKFZp586B211	-	EST, unknown function
mgc15429	abhydrolase domain containing 14B (ABHD14B)	3p21.1	Uncharacterized gene, belongs to the AB hydrolase superfamily
glg1	golgi apparatus protein 1	16q22-q23	Synonyms: membrane sialoglycoprotein of the Golgi apparatus, cysteine-rich fibroblast growth factor receptor, unknown function.

pctp	phosphatidylcholine transfer protein	17q21-q24	Phosphatidylcholine (PC) transfer protein (PCTP) is a cytosolic protein first purified from bovine and rat liver that catalyzes intermembrane transfer of PC. In mammalian cells, these insoluble molecules are transferred between membranes by a highly specific phosphatidylcholine transfer protein (PC-TP) belonging to the steroidogenic acute regulatory protein related transfer (START) domain superfamily of hydrophobic ligand-binding proteins.
tle1	transducin-like enhancer of split 1 (E(sp1) homolog, Drosophila)	9q21.32	The <i>transcription co-repressor TLE1</i> interacts with the intracellular region of gpl30 through its Q domain. The transcription factor <i>Groucho/TLE1 (TLE1)</i> is expressed in virtually all major cortical subdivisions, hippocampus, amygdala, and thalamus, as well as in the cerebellum of the adult rat brain. In both neocortex and subcortical structures, TLE1 expression was mostly localized to neurons. Transcriptional corepressors of the Groucho (Gro)/TLE family play important roles during a variety of developmental pathways, including neuronal differentiation. In particular, they <i>act as negative regulators of neurogenesis</i> , together with Hairy/Enhancer of split (Hes) DNA-binding proteins. The interaction with Hes1 leads to Gro/TLE hyperphosphorylation and increased transcription repression activity in mammalian cells, but the underlying molecular mechanisms are poorly characterized. Gro/TLE1 is phosphorylated in vivo by protein kinase CK2. This phosphorylation occurs at serine 239 within the conserved CcN domain present in all Gro/TLE family members. Mutation of serine 239 into alanine decreases Hes1-induced hyperphosphorylation of Gro/TLE1 and also reduces its nuclear association and transcription repression activity. It was further demonstrated that Gro/TLE1 inhibits the transition of cortical neural progenitors into neurons and that its antineurogenic activity is inhibited by a serine-239-alanine mutation, but not by a serine-239-glutamate mutation. These results suggest that CK2 phosphorylation of serine 239 of Gro/TLE1 is important because of its function during neuronal differentiation.

## 12.4 Mathematical background

### 12.4.1 Preface

Microarray analysis provides the possibility of measuring several thousands of transcripts in parallel. Analyzing such a large number of transcripts simultaneously provides information about the interplay between genes. Processing such an amount of data is accompanied by difficulties in its interpretation. There are features which have to be considered in the context of the whole experiment to obtain reliable results, such as: Quality control of Chips and target-RNA, normalisation algorithms, suitable statistical methods and filtering of data. Here, the most important background information is presented. For detailed information refer to the “Statistical Algorithms Description Document” at [www.affymetrix.com](http://www.affymetrix.com).

### 12.4.2 Background calculation

Background and noise are distinct phenomena which are calculated separately by the Gene Chip software. The background calculation is a measurement of the intensity of the autofluorescence of the array surface and of the non-specific binding of target or stain molecules (streptavidin-phycoerythrin). The calculation is performed as follows:

The array is divided into sectors (16 by default)

The software ranks probe cells by fluorescence intensity, identifies the *lowest* 2% (by default) for each sector and calculates their average (=sector's background)

The sector's background is *subtracted* from the average intensities of all probe cells within that sector. This subtraction here is described simplified.

### 12.4.3 Noise calculation

Noise (Q) results from small variations in the digitized signal observed by the scanner as it scans the probe array's surface. The level of noise is calculated and then used as one of the parameters in determining the significance of differences in probe set intensities across two probe arrays. Noise is the extent of pixel to pixel variation of the signal intensities. It is calculated using the standard deviations of pixel intensities of the background probe cells. The noise is scaled or normalized along with the rest of the data according to the following equation:

$$Q = \frac{1}{N} \left( \sum_i^N \frac{stdev_i}{\sqrt{pixel_i}} \right) \times SF \times NF$$

Q= noise for a given probe array

N= total number of background cells for an array

stdev<sub>*i*</sub>= standard deviation of the intensities of the pixels making up background cell *i*

pixel<sub>*i*</sub>= total number of pixels in cell *i*

SF= scaling factor

NF= normalization factor

Noise Q is not used anywhere in the statistical algorithm. However, since it is based on pixels it provides a *useful quality measure* of how well the grid was placed on the array to calculate the CEL file. *All other calculations are derived from the CEL files. Hence, if errors occur at this step (which can be recognized by increased noise or an increased scale factor), this error can systematically influence the entire following data analysis (systematic bias leads to systematic error).*

#### 12.4.4 Match/Mismatch system™ of Affymetrix

A specific feature of Affymetrix microarrays are the so-called MisMatch (MM) probes<sup>14</sup>. Each of the 16-20 probe pairs (ten of those are shown in Figure 12.1) in a probe set has a Perfect Match (PM) and a MisMatch probe. One probe set is designed to detect one kind of transcript. Its probe pairs are distributed randomly over the microarray (although in Figure 12.1 they are shown adjacent to each other), however, PM and MM are located next to each other on the microarray. The PM probes are designed to bind perfectly to the transcript of interest and the MM probes have a mismatching base at position 13 (of a 25 oligomer, not shown in Figure 12.1) with the intention of measuring non-specific binding [480].

<sup>14</sup> Information is mainly based on [www.Affymetrix.com](http://www.Affymetrix.com) and modified.

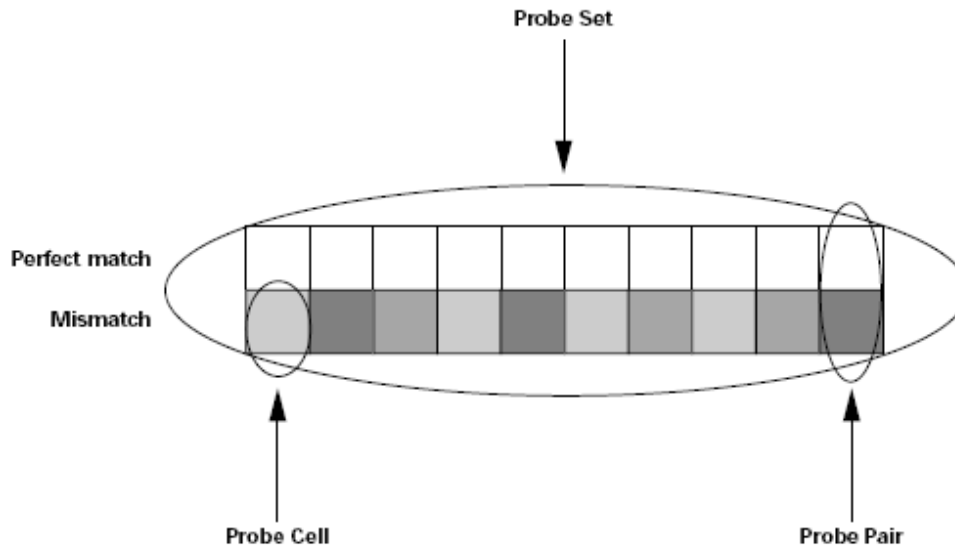


**Figure. 12.1 Match/Mismatch System (Affymetrix).** A complete probe set is designed to detect one kind of transcript and consists of 16-20 probe pairs (here a probe set of 10 probe pairs is shown). A probe cell is a square-shaped feature with a unique sequence. Its size ranges from 18-50  $\mu\text{m}$  per side, depending on the array type. Each of the probe pairs has a Perfect Match (PM) and a MisMatch (MM) probe. The probes are 25-mer oligonucleotides. MM probes have a mismatching base at position 13 with the intention of measuring non-specific binding. (Figure taken from [www.affymetrix.com](http://www.affymetrix.com)).

## 12.4.5 Normalisation algorithms

### 12.4.5.1 Absolute analysis algorithms

#### Signal algorithm

Signal is a *quantitative* metric calculated for each probe set, which *represents the relative level of expression of a transcript*. Signal is calculated using the One-Step Tukey's Biweight Estimate which yields a robust weighted mean that is relatively insensitive to outliers. The MisMatch intensity is used to estimate stray signal. *The real signal is estimated by taking the log of the Perfect Match intensity after subtracting the stray signal estimate.*

The Signal value is calculated from the combined, background-adjusted PM and MM values of the probe set. *It represents the amount of transcript in solution.*

Signal is calculated as follows:

1. Cell intensities are pre-processed for global background.
2. An ideal MisMatch value is calculated and subtracted to adjust the PM intensity.

3. The adjusted PM intensities are log-transformed to stabilize the variance.
4. The biweight estimator is used to provide a robust mean of the resulting values. Signal is output as the antilog of the resulting value.
5. Finally, signal is scaled using a trimmed mean.

#### Detection algorithm

The detection algorithm assesses probe pair saturation, uses probe pair intensities to generate a *detection p-value*<sup>15</sup> and assign a *Present, Marginal, or Absent* call. Each probe pair in a probe set is considered as having a potential vote in determining whether the measured transcript is *detected (Present)* or not *detected (Absent)*. The vote is described by a value called the discrimination score [R]. The discrimination score is a basic property of a probe pair that describes its ability to detect its intended target. It measures the target-specific intensity difference of the probe pair (PM-MM) relative to its overall hybridization intensity (PM+MM):  $R = (PM - MM) / (PM + MM)$ .

For example, if the PM is much larger than the MM, the discrimination score for that probe pair will be close to 1.0. If the discrimination scores are close to 1.0 for the majority of the probe pairs, the calculated detection *p-value* will be lower (more significant). A lower *p-value* is a reliable indicator that the result is valid and that the probability of error in the calculation is small. Conversely, if the MM is larger than or equal to the PM, then the discrimination score for that probe pair will be negative or zero. If the discrimination scores are low for the majority of the probe pairs, the calculated detection *p-value* will be higher (less significant).

#### Detection calls:

1. Saturated probe pairs are removed.
2. Discrimination scores are calculated (this gives information about how different the PM and MM cells are).
3. The Wilcoxon's rank test is used to calculate a detection *p-value* (this gives information about how confident one can be that a transcript is really absent/present).
4. The detection *p-value* is compared with a preset significance level to make the decision.

---

<sup>15</sup> The *detection p-value* must not be mixed up with the *statistical p-value* which is calculated at later steps.

If a MisMatch cell is saturated, the corresponding probe pair is excluded from further data analysis.

### 12.4.5.2 Relative analysis algorithms

Previously mentioned in the Introduction, Chapter 3.6.

### 12.4.6 Derivation of the $2^{-\Delta\Delta C_T}$ Method

*Relative quantification* with data from the ABI PRISM<sup>®</sup> 5700 Sequence Detection System was performed with the comparative method (the  $2^{-\Delta\Delta C_T}$  Method).

This method is a convenient way of analyzing the relative changes in gene expression from real-time quantitative PCR experiments. *For the  $\Delta\Delta C_T$  calculation to be valid, the amplification efficiencies of the target and reference must be approximately equal.* A sensitive method for assessing if two amplicons have the same efficiency is to look at how  $\Delta C_T$  varies with the template dilution. Therefore, standard curves were established for calculating the efficiency of amplification.

The equation that describes the exponential amplification of PCR is given by

$$X_n = X_o \times (1 + E_x)^n, \quad [1]$$

where  $X_n$  is the number of target molecules at cycle  $n$  of the reaction,  $X_o$  is the initial number of target molecules.  $E_x$  is the efficiency of target amplification, and  $n$  is the number of cycles. The threshold cycle ( $C_T$ ) indicates the fractional cycle number at which the amount of amplified target reaches a fixed threshold.

Thus,

$$X_T = X_o \times (1 + E_x)^{C_{T,x}} = K_x \quad [2]$$

where  $X_T$  is the threshold number of target molecules,  $C_{T,x}$  is the threshold cycle for target amplification, and  $K_x$  is a constant.

A similar equation for endogenous reference (internal control gene) reaction is given by

$$R_T = R_O \times (1 + E_R)^{C_{T,R}} = K_R \quad [3]$$

where  $R_T$  is the threshold number of reference molecules,  $R_O$  is the initial number of reference molecules,  $E_R$  is the efficiency of reference amplification,  $C_{T,R}$  is the threshold cycle for reference amplification, and  $K_R$  is a constant.

Dividing  $X_T$  by  $R_T$  gives the expression

$$\frac{X_T}{R_T} = \frac{X_O \times (1 + E_X)^{C_{T,X}}}{R_O \times (1 + E_R)^{C_{T,R}}} = \frac{K_X}{K_R} = K \quad [4]$$

For real-time amplification using TaqMan probes, the exact values of  $X_T$  and  $R_T$  depend on a number of factors including the reporter dye used in the probe, the sequence context effects on the fluorescence properties of the probe cleavage, purity of the probe, and setting of the fluorescence threshold.

Therefore, the constant  $K$  does not have to be equal to one.

*Assuming efficiencies of the target and the reference are the same,*

$$E_X = E_R = E$$

$$\frac{X_O}{R_O} \times (1 + E)^{C_{T,X} - C_{T,R}} = K, \quad [5]$$

or

$$X_N \times (1 + E)^{\Delta C_T} = K, \quad [6]$$

Where  $X_N$  is equal to the normalized amount of target  $(C_{T,X} - C_{T,R})$ .

Rearranging gives the expression

$$X_N = K \times (1 + E)^{-\Delta C_T}. \quad [7]$$

The final step is to divide the  $X_N$  for any sample  $q$  by the  $X_N$  for the calibrator ( $cb$ ):

$$\frac{X_{N,q}}{X_{N,cb}} = \frac{K \times (1 + E)^{-\Delta C_{T,q}}}{K \times (1 + E)^{-\Delta C_{T,cb}}} = (1 + E)^{-\Delta \Delta C_T} \quad [8]$$

Here  $-\Delta \Delta C_T = -(\Delta C_{T,q} - \Delta C_{T,cb})$ .

For amplicons designed to be less than 150 bp and for which the primer and  $Mg^{2+}$  concentrations have been properly optimized, the *efficiency is close to one*.

Therefore, the amount of target, normalized to an endogenous reference and relative to calibrator, is given by

$$\text{Amount of target} = 2^{-\Delta \Delta C_T}. \quad [9]$$

*For the  $\Delta \Delta C_T$  calculation to be valid, the amplification efficiencies of the target and reference must be approximately equal.*

A sensitive method for assessing if two amplicons have the same efficiency is to look at how  $\Delta C_T$  varies with the template dilution.

### **Standard deviation calculation using the comparative method**

The  $\Delta C_T$  value is determined by subtracting the average of the endogenous control gene  $C_T$  values from the average of the gene of interest  $C_T$  values.

The standard deviation of the difference is calculated from the standard deviations of the gene of interest and endogenous control gene values using the following formula:

$$\sigma = \sqrt{\sigma_1^2 + \sigma_2^2}$$

Where:

$\sigma$  = std dev

The fold change of gene expression is calculated as follows:

The  $\Delta C_T$  value is determined by subtracting the average of the endogenous control gene  $C_T$  value from the average of the gene of interest  $C_T$  value. The same is done for a so-called calibrator (this is for instance a user-defined baseline experiment)

$\Delta C_{T1}$  =  $C_T$  gene of interest -  $C_T$  endogenous control (calibrator=baseline experiment,  
for instance wildtype)

$\Delta C_{T2}$  =  $C_T$  gene of interest -  $C_T$  endogenous control (for instance mutant)

The fold change (fc) of gene expression is:

$$fc = 2^{-(\Delta C_{T2} - \Delta C_{T1})}$$

This is the amount of target, normalized to an endogenous reference and relative to a calibrator (baseline experiment).

## **12.5 Quality control**

### **12.5.1 Quality control of cells, target-RNA and arrays**

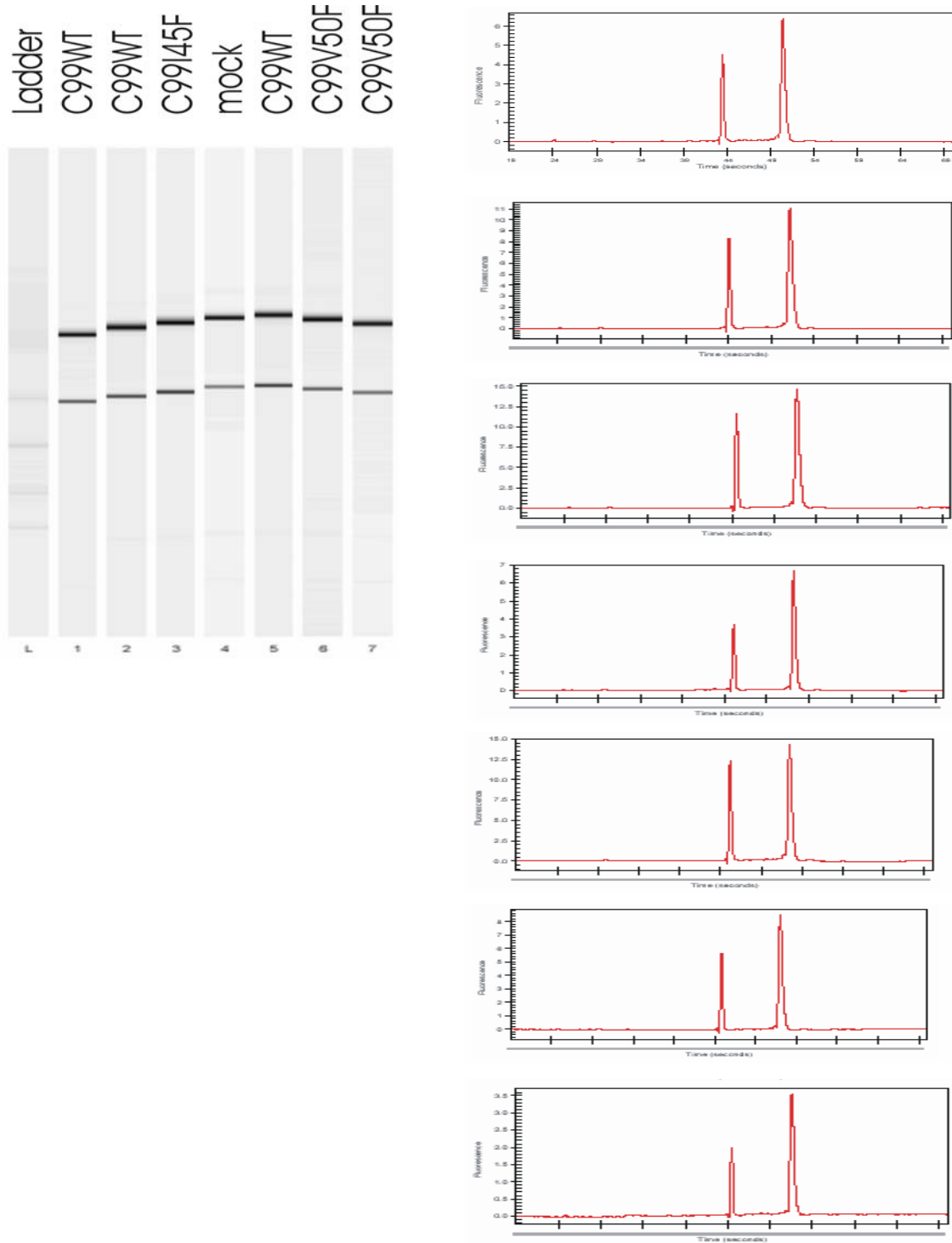
Each sample was screened and found to be free from mycoplasma contamination. The 260 nm/280 nm ratio for total-RNA was between 1.9-2.1 for Chip experiments and 1.8-2.1 for quantitative real-time PCR. Total-RNA and unfragmented cRNA was checked with a Bioanalyzer 2100™. For total-RNA, two distinct bands (28s and 18s ribosomal RNA) were detected with the 28 s band approximately twice as strong as the 18 s band. For unfragmented cRNA a distribution of bands representing the different m-RNAs, was detected with an accumulation in the centre of each lane. For fragmented cRNA, bands corresponding to a size of 35-200 bases were detected. After scanning, array images were assessed by eye to confirm the absence of bubbles or scratches. The mean of all Chips are shown, the highest and lowest value is indicated in brackets. Target intensities of 100 (HG-U133 A Chip) and 20 (HG-U133 B Chip) were used. Only Chips with equal target intensities were compared to each other (using Affymetrix MAS 5.0 array analysis software and Gene Chip operating software GCOS). Scaling factors for A-Chips were within acceptable limits 0,91 (0.8-1.4), as were background 75,1(60.7-97.7), noise (rawQ) 2,7 (2.4-3.3) and number of present transcripts 51% (47,4-52.9%). 3'/5' ratios for GAPDH and  $\beta$ -actin were confirmed to be within acceptable limits (GAPDH: 0.92 (0,79-1.81),  $\beta$ -actin: 1.26 (1.03-2.29), and BioB spike controls were found to be present on 100% of all the Chips, with BioC, BioD and CreX also present in increasing intensity. Scaling factors for all B-Chips were within acceptable limits 1.24 (0.9-1.6), as were background 63.87 (43.9-112), noise (raw Q) 2.6 (2.0-3.6) and number of present transcripts (30% (14.3-38,4%). 3'/5' ratios for GAPDH and  $\beta$ -actin were confirmed to be within acceptable limits (GAPDH: 1.1 (0.88-2.03),  $\beta$ -actin: 1.3 (0.92-2.95), and BioB spike controls were found to be present on 95% of all the Chips, with BioC, BioD and CreX also present in increasing intensity.

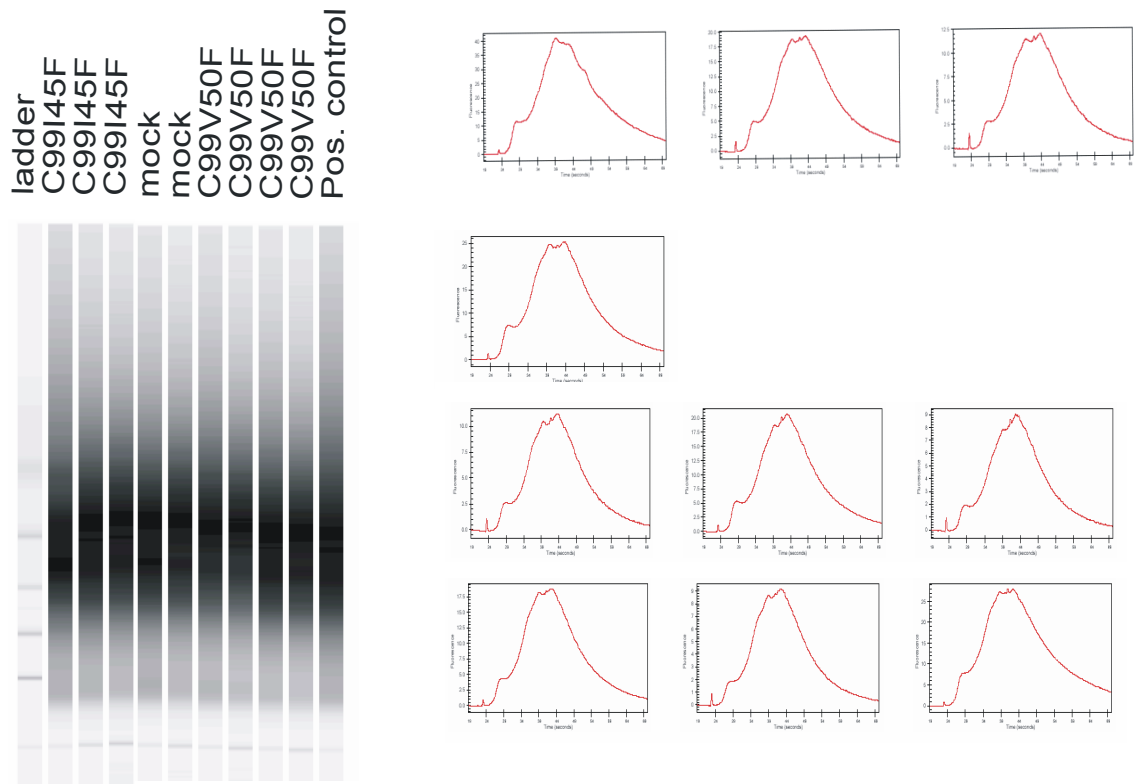
### **12.5.2 Quality control of RNA by a test Chip prior to the whole genome Chip**

Prior to using the whole genome array, a test array had been used, in order to check sample quality. Parameters like scaling factors, background, noise, number of present transcripts, 3'/5' ratios for GAPDH and beta-actin and detection of Bio spike controls were evaluated. If these parameters were in a suitable range, the same sample was used for whole genome arrays.

12.5.3 RNA-quality assessed using the Agilent 2100 Bioanalyzer

**A**

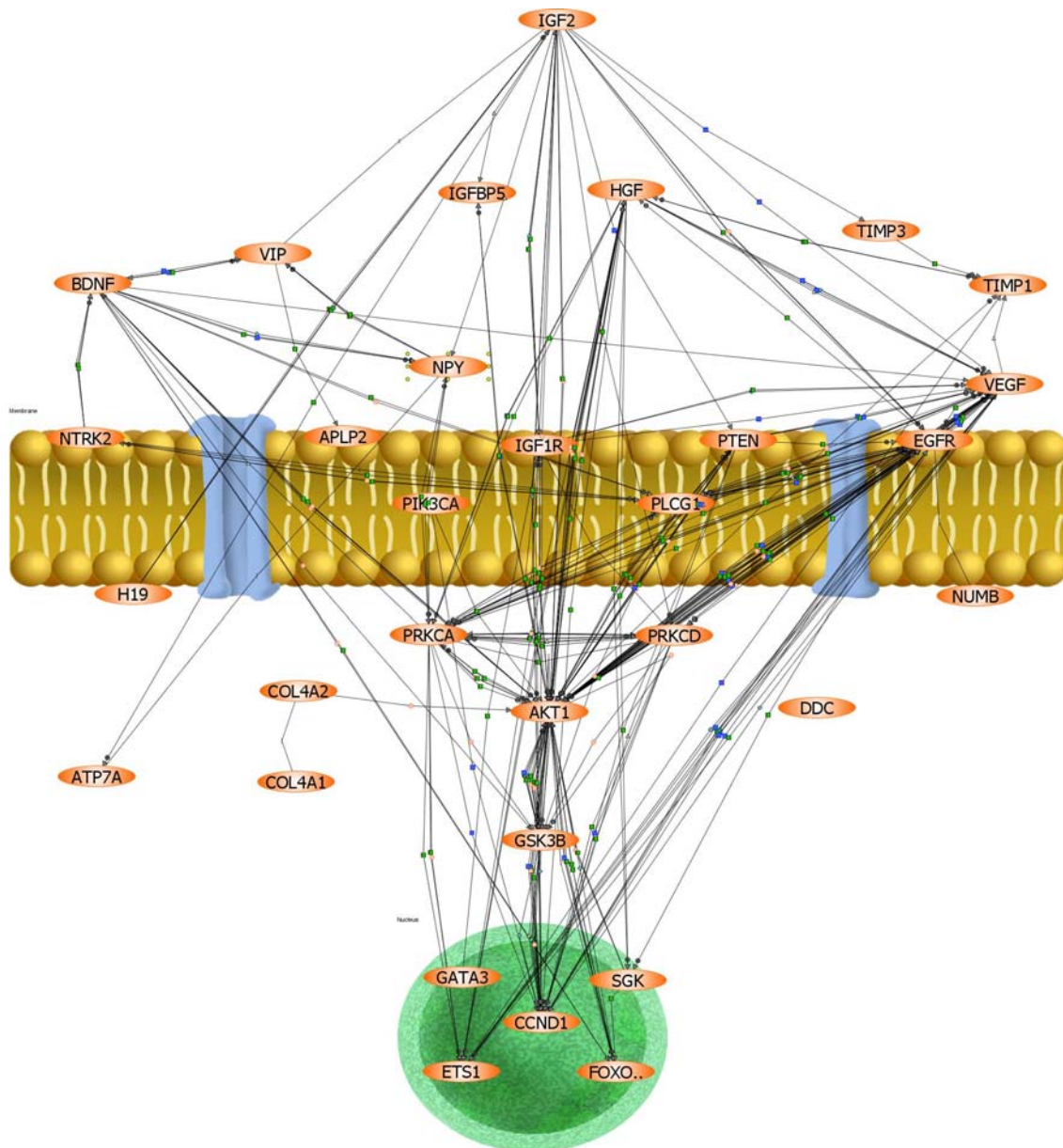


**B**

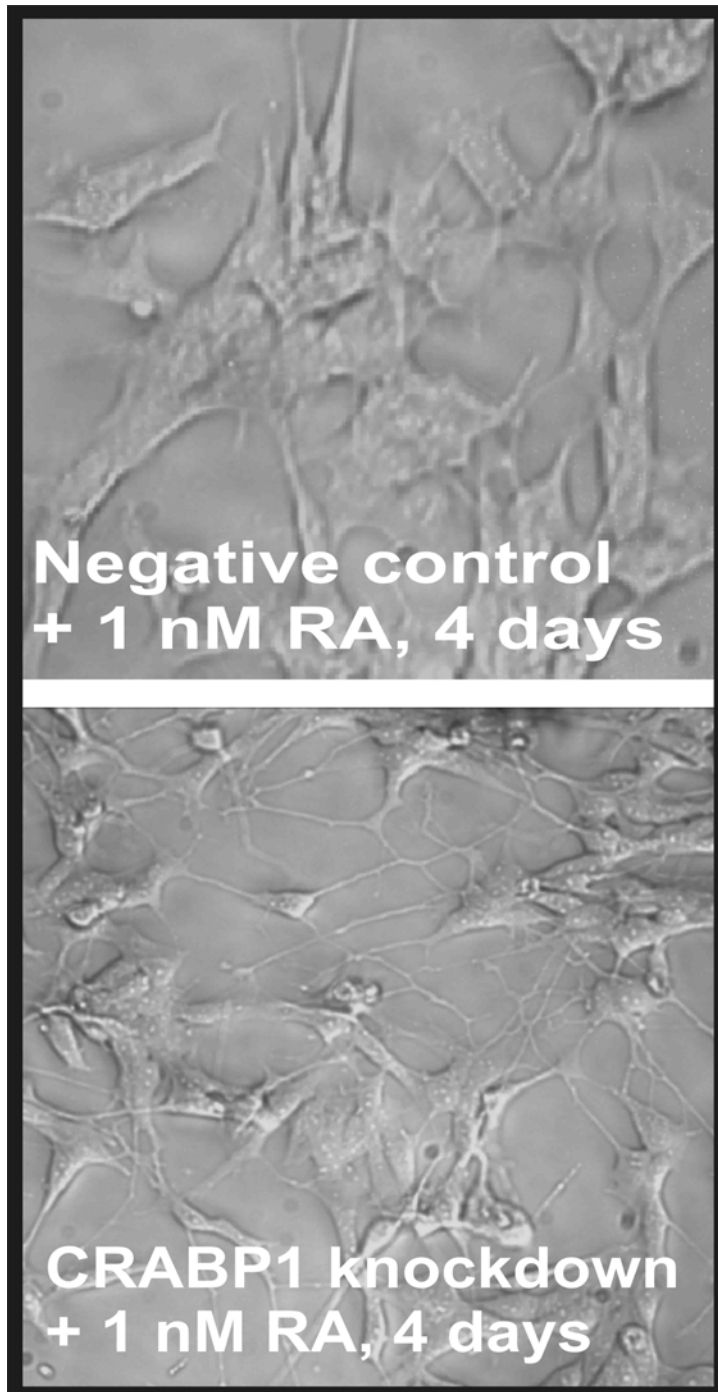
**Figure 12.2 Total-RNA (A) and unfragmented cRNA (B) were checked with a Bioanalyzer 2100™ (Agilent).** The Bioanalyzer generates an artificial gel and electropherograms, providing information about RNA quality. A) For total-RNA, two distinct bands (28s and 18s ribosomal RNA) were detected with the 28 s band approximately twice as strong as the 18 s band. The two distinct bands appear slightly shifted from lane to lane due to an unfixed Bioanalyzer or software problem but this does not affect the quality of information. B) For unfragmented cRNA a distribution of bands representing the different mRNAs, was detected with an accumulation in the center of each lane. Notice the wide range of size distribution in each lane showing unfragmented cRNA and the characteristic curves of the electropherograms. Only samples satisfying the highest quality standards (a selection of such samples is shown here) were used for analysis.

## 12.6

## Extended view of connectivities



**Figure 12.3 Extended view of interconnectivities created with Pathway Architect (Stratagene).** Pathway Architect is a literature mining program used to build biological interaction networks among genes/proteins of interest. It accesses over 2 million biological facts from the current literature. IGF2/IGF1R/PKC and PI3K/AKT signaling were influenced by an altered  $A\beta_{42}/A\beta_{40}$  ratio. Crucial differentially expressed genes (transcripts and partially proteins, if protein information was available) were selected and integrated into the Pathway Architect software. By a complex filtering procedure this pathway was created, in which all transcripts (except for DDC) were found to be connected in a network. Nodes (transcripts and/or proteins, orange-coloured) are connected via interconnectivities (lines). These lines represent direct interactions, regulatory processes or other kinds of associations that have been published.

**12.7 CRABP1 knockdown, larger scale of Figure 5.9 D**

**Figure 12.4 Phase contrast images showing living human neuroblastoma cells (SH-SY5Y, mutant C99I45F,  $A\beta_{42}/A\beta_{40}\uparrow$ ), grown on collagen coated glass cover slips and treated with 1 nM RA. Differentiation was evaluated by the number, shape and length of outgrowing protrusions. 30 nM siRNA was administered to the cells for 24 h in combination with a treatment of 1 nM RA for 4 days. After 4 days, the effects of >50% knockdown of CRABP1 was compared to a nonsense sequence (negative control).**